INVESTIGATION OF THE ROLE OF DIVALENT IRON COMPLEXES OF AMINO ACIDS AND SUGARS IN CONTROLLING THE PATHWAYS OF THE MAILLARD REACTION NETWORK

EUN SIL KIM

Department of Food Science and Agricultural Chemistry
McGill University, Montreal

2023

A thesis submitted to McGill University in partial fulfilment of the requirements of the degree of Doctor in Philosophy

SUGGESTED SHORT TITLE:

Controlling the Maillard Reaction Network by Fe^{2}

ABSTRACT

Thermally induced chemical transformations of amino acids and sugars via the Maillard reaction are generally controlled by parameters, such as the temperature, time, pH, and nature, of the initial reactants. However, minor components in food such as metal ions can also play a critical role as catalysts, in regulating this reaction owing to their high binding affinities toward amino acids and reducing sugars through their redox activity. Hence, to study the role of divalent metal ions in the Maillard reaction, a glucose/alanine model system was investigated in the presence and absence of divalent iron chloride ($FeCl_2$) heated at 110 °C for 2 h. The reactivity of metal ions towards sugar-derived short chain enediol moieties formed during the reaction was exploited to develop a convenient analytical procedure for their profiling through complexation combined with electrospray ionization/quadrupole time-of-flight mass spectrometry (ESI/qTOF/MS). Excess $FeCl_2$ was added to glucose or glucose [^{13}C-U] solutions in methanol either before or after heating at 110 °C, and the samples were analyzed by tandem mass spectrometry (MS/MS). The results indicated the formation of various sugar degradation products as positively charged mono- and *bis*-sugar iron complexes in the form of $[M + H]^+$, $[M + Na]^+$, $[M + K]^+$, $[M + Fe^{35}Cl]^+$, and $[M + Fe^{37}Cl]^+$, as well as by charge localization on iron, $[M]^+$. Metal ions are also known to influence the course of the Maillard reaction by forming various complexes such as *bis*(amino acids); these complexes undergo a more facile reaction with sugars. Due to this enhanced reactivity, the possible formation of diglycated amino acids was investigated in this model system using isotope labelling in conjunction with ESI/qTOF/MS/MS. Forty-seven derivatives of *bis*[*N*,*N'*-diglycated alanine]iron(II) complexes were tentatively identified. These complexes incorporated one iron atom, two [^{13}C-3] atoms from alanine, and up to 24 carbon atoms from glucose [^{13}C-U]. MS/MS analysis of the diglycated alanines indicated that they followed similar fragmentation pathways as the Amadori product of alanine. Furthermore, in this thesis, *N*,*N*-diglycated alanine derivatives were generated *in situ* through the dissociation of their stable precursors, *bis*[*N*,*N'*-diglycated alanine]iron(II) complexes, formed in an alanine/glucose/$FeCl_2$ model system and their reactivity was investigated. Three intramolecular cyclization reactions between the sugar rings were identified: one was initiated by 1,2-enolization on one of the sugar moieties followed by cyclization at the carbonyl group of the neighboring sugar to form 4*H*-1,4-oxazine derivatives, the second was initiated by the formation of an Amadori moiety on one of the sugars and its subsequent cyclization with the carbonyl group of the adjacent sugar, leading to dihydro-1,4-diazine

structures. Generally, the interaction between amino groups and carbonyl compounds generates Schiff bases. They can be stabilized through different mechanisms such as Amadori rearrangement, complexation with metal ions or through intramolecular cyclization of the carboxylate ion with Schiff bases to form more stable oxazolidin-5-one Schiff base isomers. High-resolution mass spectrometry (HRMS) and isotope labelling techniques were used to identify the oxazolidin-5-one derivatives in the above model systems. Experiments using standard aldehydes, such as formaldehyde, acetaldehyde, and glycolaldehyde, further confirmed the identity of the oxazolidin-5-ones observed at *m/z* 102, *m/z* 116, and *m/z* 132, respectively. Data analysis indicated that 4-methyl-oxazolidin-5-one, which was formed initially from the interaction of alanine and formaldehyde, served as a molecular scaffold, from which different oligomers were generated through the interaction of its amino group with three different aldehydes, generating three different iminium ion derivatives of the 4-methyl-oxazolidin-5-one. Although polymerization reactions are generally unexplored in the Maillard reaction, each of these derivatives served as a branching point for the formation of different oligomeric structures using similar chemical transformations, such as aldol-type addition, Amadori rearrangement, and Schiff base formation, each of which followed a different sequence of reactions to form new dimeric, trimeric, or higher-order oxazolidin-5-one oligomers. Twelve different reaction sequences were tentatively identified, generating more than 200 oxazolidin-5-one oligomers. The data from the HRMS, isotope labelling using [^{13}C-3] alanine and [^{13}C-U] glucose, and MS/MS analyses all justified the proposed pathways and structures in this study.

RESUMÉ

Les transformations chimiques induites thermiquement des acides aminés et des sucres via la réaction de Maillard sont généralement contrôlées par des paramètres tels que la température, le temps, le pH et la nature des réactifs initiaux. Cependant, des composants mineurs dans les aliments, tels que les ions métalliques, peuvent également jouer un rôle essentiel en tant que catalyseurs dans la régulation de cette réaction en raison de leurs affinités de liaison élevées envers les acides aminés et les sucres réducteurs grâce à leur activité redox. Ainsi, pour étudier le rôle des ions métalliques divalents dans la réaction de Maillard, un système modèle glucose/alanine a été étudié en présence et en l'absence de fer divalent ($FeCl_2$) chauffé à 110 °C pendant 2 h. La réactivité des ions métalliques vis-à-vis des fragments d'ènediol à chaîne courte dérivés du sucre formés au cours de la réaction a été exploitée pour développer une procédure analytique pratique pour leur profilage par complexation combinée à l'ionisation par électrospray/spectrométrie de masse à temps de vol quadripolaire (ESI/qTOF/MS). Un excès de $FeCl_2$ a été ajouté à des solutions de glucose ou de glucose [1^3C-U] dans du méthanol avant ou après chauffage à 110 °C, et les échantillons ont été analysés par spectrométrie de masse en tandem (MS/MS). Les résultats ont indiqué la formation de divers produits de dégradation des sucres sous forme de complexes de fer mono- et bis-sucre chargés positivement sous la forme de $[M + H]^+$, $[M + Na]^+$, $[M + K]^+$, $[M + Fe^{35}Cl]^+$, and $[M + Fe^{37}Cl]^+$, ainsi que par localisation de charge sur le fer, $[M]^+$. Les ions métalliques sont également connus pour influencer le cours de la réaction de Maillard en formant divers complexes tels que les bis (acides aminés); ces complexes subissent une réaction plus facile avec les sucres. En raison de cette réactivité accrue, la formation possible d'acides aminés diglycés a été étudiée dans ce système modèle en utilisant le marquage isotopique en conjonction avec ESI/qTOF/MS/MS. Quarante-sept dérivés de complexes *bis*[*N*,*N'*-alanine diglycée]fer(II) ont été provisoirement identifiés. Ces complexes incorporaient un atome de fer, deux atomes de [^{13}C-3] d'alanine et jusqu'à 24 atomes de carbone de glucose [^{13}C-U]. L'analyse MS/MS des alanines diglycées a indiqué qu'elles suivaient des voies de fragmentation similaires à celles du produit Amadori de l'alanine. De plus, dans cette thèse, des dérivés d'alanine *N*,*N*-diglycatée ont été générés in situ par la dissociation de leurs précurseurs stables, les complexes *bis*[*N*,*N*'-alanine diglycatée]fer(II), formés dans un modèle alanine/glucose/$FeCl_2$ système et leur réactivité a été étudiée. Trois réactions de cyclisation intramoléculaire entre les cycles de sucre ont été identifiées: l'une a été initiée par une 1,2-énolisation sur l'un des fragments de sucre suivie d'une cyclisation

au niveau du groupe carbonyle du sucre voisin pour former des dérivés de 4H-1,4-oxazine, la seconde a été initiée par la formation d'un fragment Amadori sur l'un des sucres et sa cyclisation ultérieure avec le groupe carbonyle du sucre adjacent, conduisant à des structures dihydro-1,4-diazine. Généralement, l'interaction entre les groupes amino et les composés carbonyle génère des bases de Schiff. Ils peuvent être stabilisés par différents mécanismes tels que le réarrangement d'Amadori, la complexation avec des ions métalliques ou par la cyclisation intramoléculaire de l'ion carboxylate avec des bases de Schiff pour former des isomères de base de Schiff oxazolidine-5-one plus stables. La spectrométrie de masse à haute résolution (HRMS) et les techniques de marquage isotopique ont été utilisées pour identifier les dérivés d'oxazolidine-5-one dans les systèmes modèles ci-dessus. Des expériences utilisant des aldéhydes standard, tels que le formaldéhyde, l'acétaldéhyde et le glycolaldéhyde, ont en outre confirmé l'identité des oxazolidine-5-ones observées à *m/z* 102, *m/z* 116 et *m/z* 132, respectivement. L'analyse des données a indiqué que la 4-méthyl-oxazolidine-5-one, qui s'est formée initialement à partir de l'interaction de l'alanine et du formaldéhyde, a servi d'échafaudage moléculaire, à partir duquel différents oligomères ont été générés par l'interaction de son groupe amino avec trois aldéhydes différents, générant trois dérivés d'ions iminium différents de la 4-méthyl-oxazolidine-5-one. Bien que les réactions de polymérisation soient généralement inexplorées dans la réaction de Maillard, chacun de ces dérivés a servi de point de ramification pour la formation de différentes structures oligomères utilisant des transformations chimiques similaires telles que l'addition de type aldol, le réarrangement d'Amadori et la formation de bases de Schiff, chacune d'entre elles ayant suivi une séquence différente de réactions pour former de nouveaux oligomères dimériques, trimériques ou d'oxazolidine-5-one d'ordre supérieur. Douze séquences de réaction différentes ont été provisoirement identifiées, générant plus de 200 oligomères d'oxazolidine-5-one. Les données du HRMS, le marquage isotopique à l'aide d'alanine [^{13}C-3] et de glucose [^{13}C-U] et les analyses MS/MS ont toutes justifié les voies et structures proposées dans cette étude.

STATEMENT FROM THE THESIS OFFICE

In accordance with the regulation of Graduate and Postdoctoral Studies of McGill University, the following statement from the Guidelines for Thesis Preparation in included:

Candidates have the option of including, as part of the thesis, the text of one or more papers submitted, or to be submitted, for publication, or the clearly-duplicated text of one or more published papers. These texts must conform to the "Guidelines for Thesis Preparation" and must be bound together as an integral part of the thesis.

The thesis must be more than a collection of manuscripts. All components must be integrated into a cohesive unit with a logical progression from one chapter to the next. In order to ensure that the thesis has continuity, connecting texts that provide logical bridge between the different papers are mandatory.

The thesis must conform to all other requirements of the "Guidelines for Thesis Preparation" in addition to the manuscripts.

As manuscripts for publication are frequently very concise documents, where appropriate, additional material must be provided in sufficient detail to allow a clear and precise judgement to be made of the importance and originality of the research reported in the thesis.

In general, when co-authored papers are included in a thesis, the candidate must have made a substantial contribution to all papers included in the thesis. In addition, the candidate is required to make an explicit statement in the thesis as to who contributed to such work and to what extent. This statement should appear in a single section entitled "Contribution of Authors" as a preface of the thesis.

When previously published copyright material is presented in a thesis, the candidate must obtain, if necessary, signed waivers from the co-authors and publishers and submit these to the Thesis Office with the final deposition.

CONTRIBUTION OF AUTHORS

This thesis is presented in a manuscript format and consists of nine chapters. Chapter 1 briefly introduces the role of metal ions in the Maillard reaction and presents the rationale, research hypothesis, experimental methodology, objectives, and significance of the study. Chapter 2 presents a current literature review on the various roles of metal ions in the Maillard reaction. In addition, it provides an understanding of the interaction with reactants or food components. Chapters 3 to 8 are drawn based on published or submitted manuscripts and are bridged logically and sequentially via connecting paragraphs. Finally, chapter 9 presents a brief conclusion and the contributions of this investigation to knowledge. This dissertation follows guidelines for thesis preparation as published by the Faculty of Graduate Studies and Research of McGill University.

The present author was responsible for the concepts, design of experiments, experimental work, and manuscript preparation in all the published and submitted papers. Dr. Varoujan Yaylayan, the thesis supervisor, had direct advisory input into the work as it progressed and, as manuscript co-author, critically edited the dissertation prior to its submission.

PUBLICATIONS

Kim, E. S. and Yaylayan, V. Formation of Oligomeric Oxazolidin-5-ones in Alanine/Glucose/Fe^{2+} Model System. Manuscript in preparation.

Kim, E. S. and Yaylayan, V. Intramolecular Cyclization and Amadori rearrangement of *N*,*N*-diglycated alanine derivatives. Manuscript in preparation.

Kim, E. S. and Yaylayan, V. (2023). Amino-Acid-Derived Oxazolidin-5-Ones as Chemical Marker for Schiff Base Formation in Glycation Reactions. *Applied Science*. 13(3). 7658. doi.org/10.3390/app13137658

Kim, E. S. and Yaylayan, V. (2022). *Bis*(alaninato)iron(II) complexes as molecular scaffolds for the generation of *N*,*N*-di-glycated alanine derivatives in the presence of glucose. *Food Chemistry*, 374(2022), 131815. doi.org/10.1016/j.foodchem.2021.131815

Kim, E. S. and Yaylayan, V. (2021). Identification of the Maillard reaction intermediates as divalent iron complexes in alanine/glucose/$FeCl_2$ model system using ESI/qTOF/MS/MS and isotope labelling technique. *Current Research in Food Science*, 4(2021), 287–294. doi.org/10.1016/j.crfs.2021.04.003

Kim, E. S. and Yaylayan, V. (2020). Profiling of sugar degradation products through complexation with divalent Metal ions coupled with ESI/qTOF/MS/MS analysis. *Current Research in Food Science*, 3(2020), 268–274. doi.org/10.1016/j.crfs.2020.10.001

ACKNOWLEDGEMENTS

First, I express my deepest gratitude and appreciation toward my supervisor Dr. Varoujan Yaylayan for his guidance, inspiration, encouragement, and financial support that made my Ph.D. experience a reality. Ever since I started my Ph.D. to study a new academic topic in a different language, Dr. Varoujan Yaylayan has been a compass along every path of this long journey. I am extraordinarily fortunate to have him as my mentor. I appreciate his patience, persistence, and understanding, which gave me the opportunity to learn and practice the new area of food chemistry.

Thank you to my family for believing in me, helping me pursue my life goals, and upholding my core values. I would like to express my sincere gratitude toward my mother, Kyung Hee Kim, for her perseverance and unconditional love. Her very existence gives me strength and stops me from giving up.

A special thanks to my lifelong friends Dr. Hyekyung Yang, Dr. Yangsun. Kim, and Dr. Choong Je Ma, as well as Miae, Jinjoo, Sei-eun, Hyeri, Chanyoung, Mijin, Hyerim, and my pals Kaka and Vini for their support, consideration, and understanding. Your involvement in this long journey for a Ph.D. has turned this into a fantasy adventure, just like a movie. My profound gratitude goes to the late Dr. Sang Hyun Sung, who introduced and provided the opportunity for me to advance in the academic field. Dr. Youn-bong Ku and Dr. Kwang-Hyun Baek encouraged me to pursue a Ph.D. in Canada and gave me sound advice when I doubted myself.

A big thanks to my lab mates Raheleh, Haoran, and Carolyne for making the campus life at Macdonald full of joy. I would also like to thank Dr. Alexander Wahba from the Mass Spectrometry laboratory of the department of chemistry (McGill University) for his prompt service and technical support throughout this Ph.D. program, as well as the administrative support staff, especially Ms. Erin Minnett, who always assisted me in a variety of ways.

I also gratefully acknowledge the Pilarczyk Fellowship and the Natural Sciences and Engineering Research Council of Canada (NSERC) for their generous financial support. Last but certainly not least, I am grateful toward Drs. Ashraf Ismail, Yixiang Wang, Idaresit Ekaette, and Micheal Murkovic members of the thesis advisory committee, for their time, feedback, and support for this study.

TABLE OF CONTENTS

LIST OF TABLES

LIST OF FIGURES

ABBREVIATIONS

AA	Amino acid
AGE	Advanced glycation end products
Ala	Alanine
$(Ala)_2Cu$	*Bis*(alaninato)copper(II)
$(Ala)_2Fe$	*Bis*(alaninato)iron(II)
amu	Atomic mass unit
ARPs	Amadori rearrangement products
Ca	Calcium
COSY	Correlational spectroscopy
Cd	Cadmium
CD	Circular dichroism
Cl	Chloride
Cu	Copper
DTPA	Diethylenetriaminepentaacetic acid
DG	Deoxyglucosone
ESI/qTOF/MS	Electrospray ionization quadrupole time of flight mass spectrometry
EDTA	Ethylenediaminetetraacetic acid
Fe	Iron
FeH_2	Iron Hydride
$Fe(OH)_2$	Iron Hydroxide
FTIR	Fourier-transform infrared spectroscopy
GC/MS	Gas chromatography mass spectrometry
Glu	Glucose
$(Glu)_2Fe$	*Bis*(gluconato)iron(II)
Gly	Glycine
$(Gly)_2Cu$	*Bis*(glycinato)copper(II)
HPAEC	High-performance anion-exchange chromatography
HPLC	High-performance liquid chromatography
HRMS	High-resolution mass spectrometry
K	Potassium
LC/MS	Liquid chromatography mass spectrometry
M	Methanol
Mg	Magnesium
Mn	Manganese
MR	Maillard reaction
MRIs	Maillard reaction intermediates
MRPs	Maillard reaction products
MS/MS	Tandem mass spectrometry

m/z	Mass to charge
Na	Sodium
NMR	Nuclear magnetic resonance
NOESY	Nuclear overhauser enhancement spectroscopy
ppm	Parts per million
Py	Pyrolysis
qTOF	quadrupole time of flight
Ser	Serine
$(Ser)_2Fe$	*Bis*(serinato)iron(II)
SDP	Sugar degradation product
TIC	Total ion chromatogram
W	Water
Zn	Zinc

CHAPTER 1

INTRODUCTION

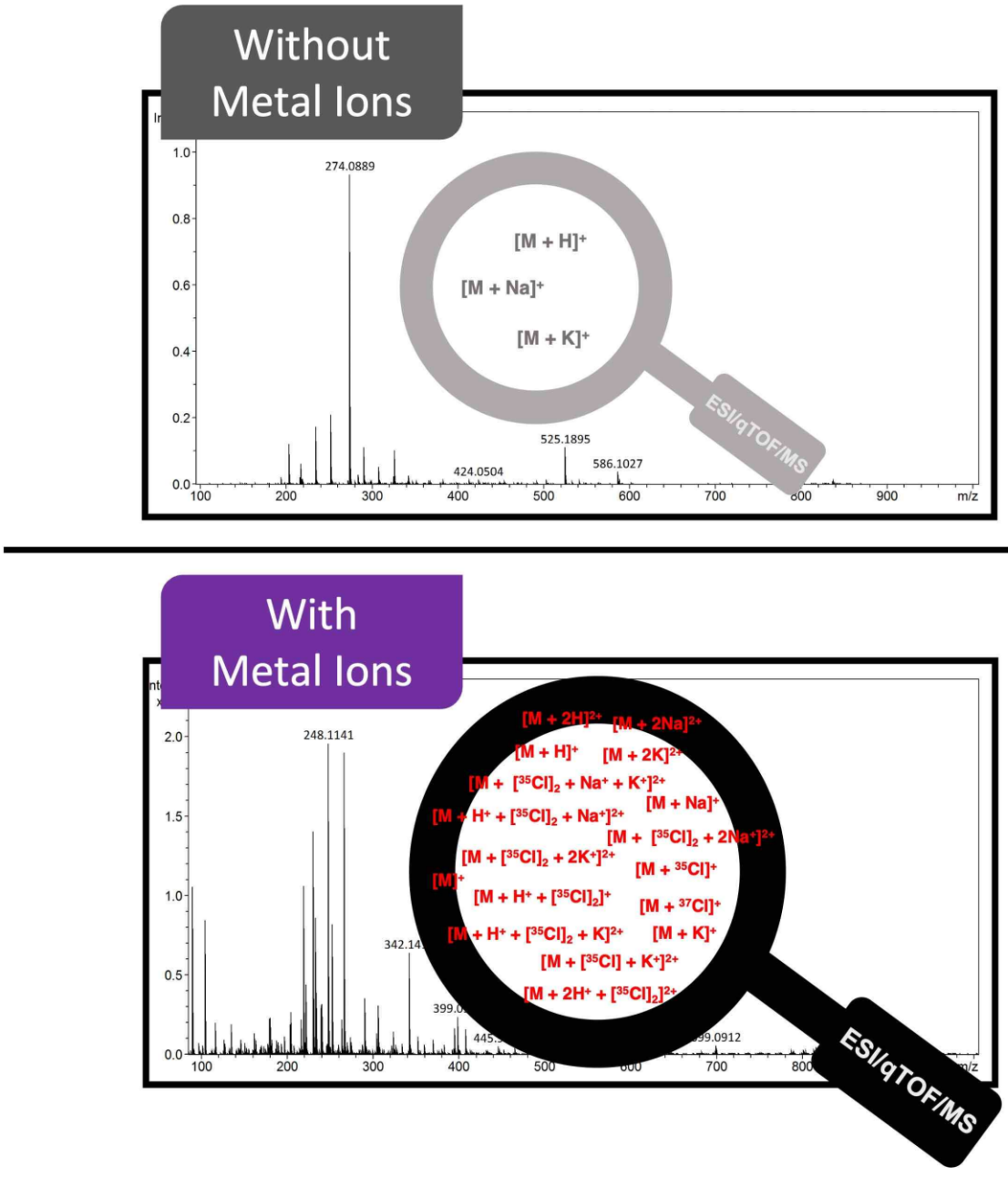

1.1. GENERAL INTRODUCTION

The Maillard reaction is considered as one of the most important chemical transformations during food processing; it is in responsible for the generation of the precursors of aroma and flavour active compounds. This thermally initiated process produces sugar amino acid adducts by the reaction of the carbonyl groups of reducing sugars with the amino groups of amino acids (Yaylayan, 1997). As the reaction progresses, it causes significant structural and functional changes that affect the colour, flavour, safety, and protein digestibility of foods (Lund and Ray, 2017). Numerous attempts have been made to control the reaction pathways and, hence, promote or inhibit the Maillard rection to achieve desirable food flavours, aromas, and colour profiles or to reduce the toxic load of foods (Paravisini and Peterson, 2019). Various parameters have been found to influence the Maillard reaction rates, such as temperature/time combinations, pH, and water activity (Nursten, 2005). The formation pattern of the Maillard reaction products have been shown to be influenced by non-thermal processing parameters, such as high hydrostatic pressure (Devi *et al*., 2015; Ramirez-Suarez and Morrissey, 2005) and pulsed electrical field applications (Aguilo-Aguayo *et al*., 2009). However, the Maillard reaction cannot be completely controlled by manipulating external parameters. For example, the nature of the initial reactants (the type of amino acids and carbohydrates) controls the rate of formation of the Amadori rearrangement product and cannot be easily manipulated in food. In several recent studies, transition-metal ions have been shown to affect the Maillard reaction through their catalytic role in generating oxidative pathways and their ability to form sugar/metal, amino acid/metal, or sugar-conjugated amino acid metal complexes (Nashalian and Yaylayan, 2014, 2015a; Ramnonaitytė *et al*., 2009). When compared with control substances, these complexes have been suggested to promote different reaction pathways, such as oxidative decarboxylation of amino acids, and regulating the release of important intermediates (e.g., Strecker aldehydes and Amadori rearrangement products) (Nashalian and Yaylayan, 2014; 2015b). Metal cations have been shown to promote the formation of 1,2-dicarbonyl compounds—important precursors of various heterocyclic compounds—from gloucose (Gensberge-Reigl, *et al*., 2020) and to produce more volatiles and ninhydrin-active components form amino acid metal complexes in otherwise similar systems, e.g. the *bis*(glycinato)copper(II)/glucose model system and the glycine/glucose system (Nashalian and Yaylayan, 2015b).

1.2. RATIONALE AND RESEARCH OBJECTIVES

All foods contain various metal ions in catalytic amounts that will ultimately influence the outcome of the Maillard reaction when thermally processed. However, in most so called "model studies" designed to explore the Maillard reaction pathways, do not include metal ions and consequently are not realistic representations of the conditions of the Maillard reaction in food systems. Such ions have high affinity to form stable coordination complexes with amino acids, sugar enediols, and their degradation products, influencing the aroma or flavour profile of the food. The mechanisms through which these metal ions influence the Maillard reaction pathways have not been elucidated yet. Hence, the primary goal of this thesis was to investigate how the divalent metal ion complexes using iron as an example, react with critical components of the Maillard reaction and what are their impact on the profile of the various products formed. The main objective of this study was to identify target substrates of the metal ions in the Maillard reaction and identify such metal ion complexes in heated sugar or sugar amino acid mixtures and follow their fate in the reaction mixtures using high-resolution electrospray ionization quadrupole time-of-flight mass spectrometry (ESI/qTOF/MS), isotope labelling strategy, and tandem mass spectrometry (MS/MS) based techniques.

Following are the specific objectives of this study:

1. To investigate the use of divalent iron as a convenient analytical tool for profiling various reactive sugar intermediates using their more stable divalent iron complexes as targets in combination with high resolution ESI/qTOF/MS/MS and isotope labelling techniques.
2. To verify the applicability of the above approach for identifying Maillard reaction intermediates.
3. To explore the generation of *N,N*-diglycated alanine derivatives predicted to be released from *bis*[*N,N'*-diglycated alanine]iron(II) complexes and study their degradation products as precursors of flavour under Maillard reaction conditions.
4. To investigate the fate of oxazolidin-5-one intermediates observed as one of the degradation products of diglycated amino acids.
5. To investigate the role of divalent iron in the formation and reactions of oxazolidin-5-one moieties.

1.3. EXPERIMETAL APPROACH

1.3.1. Sample preparation

Test model systems were prepared by adding glucose (18 mg) and/or alanine (9 mg), and $FeCl_2$ (6.4 mg) to methanol (1 mL) and heating in sealed stainless-steel reactors at 110 ℃ for 2 h, followed by evaporation of the solvent for 30 min. The control model system was prepared similarly by heating glucose (18 mg) and/or alanine (9 mg) in methanol (1 mL) in stainless-steel reactors at 110 ℃ for 2 h in the absence of $FeCl_2$. All samples were analyzed at least in two replicates.

Synthesis of *bis*(serinato)iron(II). *Bis*(serinato)iron(II) was prepared by dissolving serine (1.05 g) in methanol (10 mL) in the presence of KOH (0.05 g), followed by the addition of $FeCl_2$ (0.64 g). The dark reddish precipitate was filtered, washed with methanol, and dried in a vacuum oven at room temperature. The obtained solid was analyzed by high-resolution electrospray ionization quadrupole time-of-flight mass spectrometry (HR/ESI/qTOF/MS), which generated a major ion at $[M + H]^+ = 265.0109$ corresponding to the elemental composition of $[C_6H_{13}FeN_2O_6]^+$ with – 2.07 ppm of error (Nashalian and Yaylayan, 2015a).

***Bis*(serinato)iron(II) interaction with free alanine.** The *bis*(serinato)iron(II) (26.5 mg) and alanine (9 mg) were mixed in methanol or water (1 mL), and heated in a stainless-steel reactor at 110 ℃ for 2 h, followed by evaporation of the solvent for 30 min.

Spiked model systems with selected aldehydes. The selected Strecker aldehydes were conducted using excess (~ 1:10 w/wt) aldehydes (paraformaldehyde, acetaldehyde and glycolaldehyde), individually or all three, relative to alanine and glucose in the presence and absence of $FeCl_2$.

1.3.2. Analysis of the metal complexes and Maillard reaction products

The profile of the metal complexes, Maillard reaction intermediates, and Maillard reaction products were analyzed by HR/ESI/qTOF/MS and MS/MS. To identify the influence of divalent iron on the Maillard reaction, all model systems were analyzed in the absence and presence of divalent iron in solution. The samples were dissolved in liquid chromatography (LC)-grade methanol at a 1 mg/mL concentration. The samples were then diluted 10-fold in 10% methanol prior to analysis by HR/ESI/qTOF/MS in positive ion mode. The ESI/qTOF/MS system comprised a Bruker Maxis Impact quadrupole-time-of-flight mass spectrometer (Bruker Daltonics, Bremen, Germany) operated in positive ion mode. The samples (1 μL) were directly injected into the

ESI/qTOF/MS system. Instrument calibration was performed using sodium formate clusters. The electrospray interface settings were as follows: nebulizer pressure, 0.6 bar; drying gas, 4 L/min; temperature, 180 ℃; and capillary voltage, 4500 V. The scan range was from *m*/*z* 100 to 1000. Molecular formulae were assigned to all the observed peaks based on their exact *m/z* values using "ChemCalc" software (Institute of Chemical Sciences and Engineering, Lausanne, Switzerland) (Patiny and Borel, 2013). The reaction intermediates were detected as singly or doubly charged ions in various ionic forms such as $[M + H^+]^+$ or $[M + 2H + 2Cl]^{2+}$, etc., in addition to their hydrated, dehydrated or methanolated forms. Doubly charged ions were confirmed through the observation of isotopic spacing of 0.5 amu and mono- and dichlorinated ions were confirmed through observation of appropriate isotope abundance ratios.

1.3.3. Model systems with glucose [^{13}C-U] and alanine [^{13}C-3]

Model systems conjugated with glucose [^{13}C-U] and alanine [^{13}C-3] were prepared by adding glucose [^{13}C-U] (18.6 mg) and/or alanine [^{13}C-3] (9.2 mg), and $FeCl_2$ (6.4 mg) to methanol (1 mL) and heating in stainless-steel reactors at 110 ℃ for 2 h, followed by evaporation of the solvent for 30 min. The obtained solid was analyzed by HR/ESI/qTOF/MS, which generated a major ion, Amadori compound, at $[M + H]^+$ = 258.1266 and 253.1099 corresponding to the elemental composition of $[C_3[^{13}C]_6H_{18}NO_7]^+$ with – 5.06 ppm of error and $[C_8[^{13}C]H_{18}NO_7]^+$ with – 4.87 ppm of error, respectively. All samples were analyzed at least in two replicates.

1.3.4. Structural elucidation

Evidence for the proposed structures was provided through ESI/qTOF/MS analysis of their elemental composition, analysis of their MS/MS fragmentation patterns, and isotope-labelling studies using glucose [^{13}C-U] and alanine [^{13}C-3], in addition to the proposed structures were based on well-known glucose degradation products.

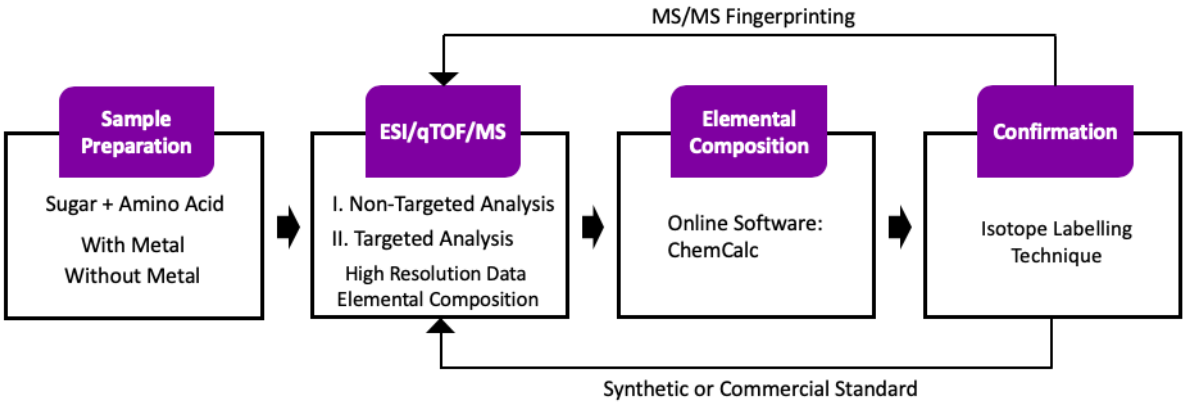

Figure 1.1. Analytical strategy for the identification of Maillard reaction products

1.4. SIGNIFICANCE OF THE PROPOSED RESEARCH

Although metal ions are ubiquitously distributed in food and are essential and reactive components, research carried out regarding the mechanism of the Maillard reaction mainly neglected their influence on the reaction. Consequently, in the absence of metal ions, the research outcomes and conclusions arrived at the need to accurately reflect the actual reaction environment in the food and arguably had diminished predictive value. The proposed research in its attempt to bridge the research gaps **1)** in developing analytical methodologies for the study of the role of metal ions in the Maillard reaction, **2)** in a comprehensive understanding of the molecular mechanism of their interference in the Maillard reaction, and **3)** in the identification of specific metal complexed intermediates and their fate in the Maillard reaction, can have a significant impact on improving the predictive value of research on the Maillard reaction during food processing; such as in the formation of process-induced toxicants or the extent of browning and the type and profile of flavour active compounds generated. In addition, all these factors are critical contributors to food quality parameters.

1.5. REFERENCES

Aguilo-Aguayo, L., Soliva-Fortuny, R., Martin-Belloso, O. (2009). Avoiding non-enzymatic browning by high-intensity pulsed electric fields in strawberry, tomato and watermelon juices. *Journal of Food Engineering*, 92(1), 37–43.

Devi, A. F., Buchow, R., Singh, T., Hemar. Y., Kasapis, S. (2015). Colour change and proteolysis of skim milk during high pressure thermal-processing. *Journal of Food Engineering*, 147, 102–110.

Gensberger-Reigl, S., Auditore, A., Huppert, J., Pischetsrieder, M. (2021) Metal cations promote α-dicarbonyl formation in glucose-containing peritoneal dialysis fluids. *Glycoconjugate Journal*, 38: 319–329.

Lund, M. N. and Ray, C. A. (2017). Control of Maillard Reaction in Foods: Strategies and Chemical Mechanisms. *Journal of Agricultural and Food Chemistry*, 65, 4537–4552.

Nashalian, O. and Yaylayan, V. A. (2014). Thermally induced oxidative decarboxylation of copper complexes of amino acids and formation of Strecker Aldehyde. *Journal of Agricultural and Food Chemistry*, 62, 8518–8523.

Nashalian, O. and Yaylayan, V. A. (2015a). De Novo Synthesis of Amino Acids during the Maillard Reaction: qTOF/ESI Mass Spectrometric Evidence for the Mechanism of Akabori Transformation. *Journal of Agricultural and Food Chemistry*, 63, 328–334.

Nashalian, O. and Yaylayan, V. A. (2015b). Sugar-conjugated Bis(glycinato)copper (II) Complexes and Their Modulating Influence on the Maillard Reaction. *Journal of Agricultural and Food Chemistry*, 63, 4353–4360.

Nursten, H. E. (2005). The Chemistry of Non Enzymatic Browning. The Maillard reaction: Chemistry, Biochemistry and Implications. Cambridge, UK: *The Royal Society of Chemistry*, 5–29.

Paravisini, L. and Peterson, D. G. (2019) Reactive carbonyl species as key control point for optimization of reaction flavors. *Food Chemistry*, 274, 71–78.

Ramirez-Suarez, J. C. and Morrissey, M. T. (2005). Effect of high pressure processing (HPP) on shelf life of albacore tuna (*Thunnus alalonga*) minced muscle. *Innovative Food Science and Emerging Technologies*, 7, 19–27.

Ramonaitytė, D. T., Keršienė, M., Adams, A., Tehrani, K. A., Kimpe, N. D. (2009). The interaction of metal ions with Maillard reaction products in a lactose-glycine model system. *Food Research International*, 42, 331−336.

Yaylayan, V. A. (1997). Classification of the Maillard reaction: A conceptual approach. *Trends in Food Science & Technology*, 8, 13−18.

CHAPTER 2

LITERATURE REVIEW

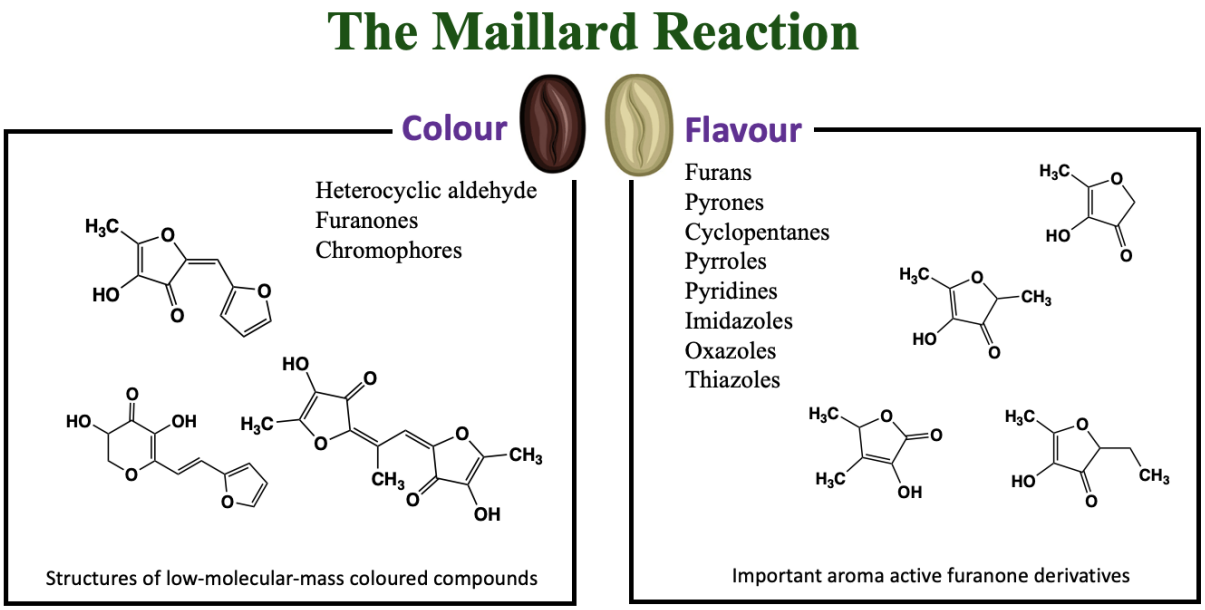

2.1. HISTORICAL PERSPECTIVE OF THE MAILLARD REACTION

The Maillard reaction can be considered as a cascade type reaction initiated by an amino group reacting with the α-hydroxy carbonyl moiety of a reducing sugar (Yaylayan, 1997). It was first observed in 1912 by Louis Camille Maillard (1878–1936) while heating free amino acids in glycerol (Finot, 2005). Maillard was investigating peptide synthesis and his serendipitous discovery triggered significant interest in food chemistry research, considering nutritional, toxicological, and physiological aspects of the reaction. Before Maillard, Schiff (1866) and Fischer (1886) described the reaction between sugars with amino compounds. Schiff revealed the formation of imines via the reaction of aldehydes and amino acids, whereas Fischer explored the synthesis of sugars and peptides using glycerol. In particular, the discovery by Fischer inspired Maillard to examine the reaction of sugars with amino acids (Maillard, 1912). Over the century, several studies have been conducted to further understand the detailed mechanism of the Maillard reaction and reveal its pathways. In the 1920s, Amadori identified *N*-glycosides as labile isomers of Schiff bases. Later, the "Amadori products" were identified as the first stable products of the Maillard reaction (Amadori, 1925; Yaylayan and Huyghues-Despointes, 1994). Heyns observed the formation of D-glucosamine during the reaction of fructose with ammonia (Hellwing and Henle, 2014). Subsequently, Heyns *et al*. (1952) identified the formation of aldose derivatives from amino acids and ketoses known as the "Heyns product", which is similar to the Amadori product (Hellwing and Henle, 2014). Since the late 1930s, various studies have demonstrated the formation of reaction products that generate colour and flavour. Doob *et al*. (1942) examined the formation of aldehydes during the Maillard reaction. This decomposition reaction was named as "Strecker degradation" after the discovery of Adolph Strecker (Strecker, 1850; 1854; Schönberg and Moubacher, 1951). Although numerous studies were conducted on this subject, this network of reactions remained complicated. In 1953, John Hodge reviewed the Maillard reaction and attempted to simplify it by constructing a diagram, which was divided into three stages; initial, intermediate, and final stages, and it remains a suitable description of this reaction. During 1973–1975, Namiki *et al*. studied the free radical formation from the reducing sugars in the intermediate stage of the Maillard reaction (Namiki, 1988). In 1986, Nursten proposed the new Hodge's diagram by adding Namiki's pathway into the intermediate stage of the Maillard reaction (Nursten, 2005). Until the 1980s, the majority of studies focused on the flavour, colour, texture, digestibility, and nutritional value of foods (Zhang *et al*., 2010). Subsequently, several researchers started

investigating the undesirable aspects of the Maillard reaction. Koschinsky *et al.* (1997) introduced the term "glycotoxin." They suggested that the process of degradation of tissue-bound advanced glycation end-products can generate a new pool of reactive intermediates. Tareke *et al*. (2002) revealed the existence of acrylamide (type 2A carcinogen) in fried potato products, which triggered worldwide investigations on the origin and mechanism of its formation (Figure 2.1).

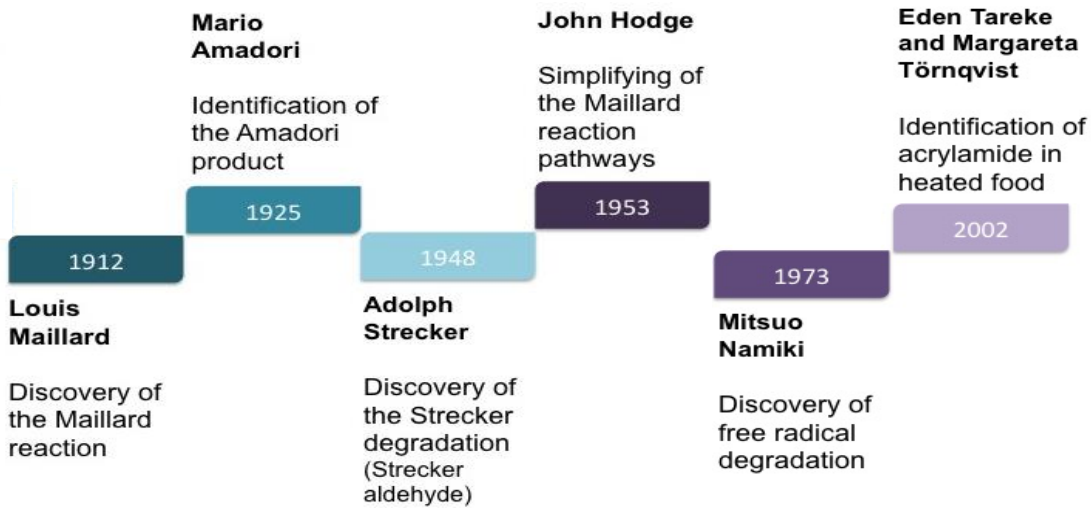

Figure 2.1. Infographics of the discoveries related to the Maillard reaction.

2.2. CHEMISTRY OF THE MAILLARD REACTION

The Maillard reaction starts with a simple nucleophilic attack by an amino group onto an electrophilic center such as the carbonyl moiety of the open form of sugars. In due course, this reaction forms various reactive intermediates and Maillard reaction products that leads to the formation of colour, flavour, texture, and taste in processed food (Martins, 2001). However, potentially harmful products, such as heterocyclic amines, furans, and acrylamides, are also formed by this reaction (Tareke *et al*., 2002; Zadeh and Yaylayan, 2020). A typical Maillard reaction can be divided into three main stages that were simplified by Hodge in 1953: initial, intermediate, and final stages. In the initial stage, the carbonyl groups of sugars undergo a reversible reaction with the amino group of amino acids via condensation to form a Schiff base. Depending on the reaction conditions, this base can either cyclize into 5-oxazolidinone or

glycosylamine through the carboxylate anion of the amino acid or the sugar hydroxyl groups, respectively, or spontaneously rearrange into the more stable 1-amino-1-deoxy-2-ketose (Amadori product) (Figure 2.2) (Chu and Yaylayan; 2008). The intermediate stage of the Maillard reaction involves various chemical reactions, such as aldol reactions, retro-aldol reactions, enolizations, decarboxylations, dehydrations, and Michael additions (Nursten, 2005). The Amadori products are degraded via 1,2- and 2,3-enolization pathways. For example, in acidic solutions (at pH $\leq$ 5.0), the degradation involves 1,2-enolization to afford a furfural compound. The formation of reactive carbonyl and dicarbonyl compounds involves sugar fragmentations, which primarily occur through a retro-aldol reaction (Yaylayan and Keyhani, 2000). Fission products are formed from sugars, such as acetol, diacetyl, and pyruvaldehyde, and react with amino acids followed by the production of Strecker aldehydes from the amino acids and aminoketones. The aminoketones subsequently condense to form pyrazines. The Strecker aldehydes and aminocarbonyl compounds are the main contributors to the formation of aromas, and these can be generated through the pathways established for Strecker degradation (Yaylayan, 2003). The final stage is mainly characterized by the polymerization of various Maillard intermediates, leading to the aldol condensation of the furfurals and aldehydes (Nursten, 2005). The Maillard reaction proceeds to completion, with the formation of "brown, nitrogenous polymers and copolymers" known as melanoidins (Hodge, 1953) (Figure 2.3).

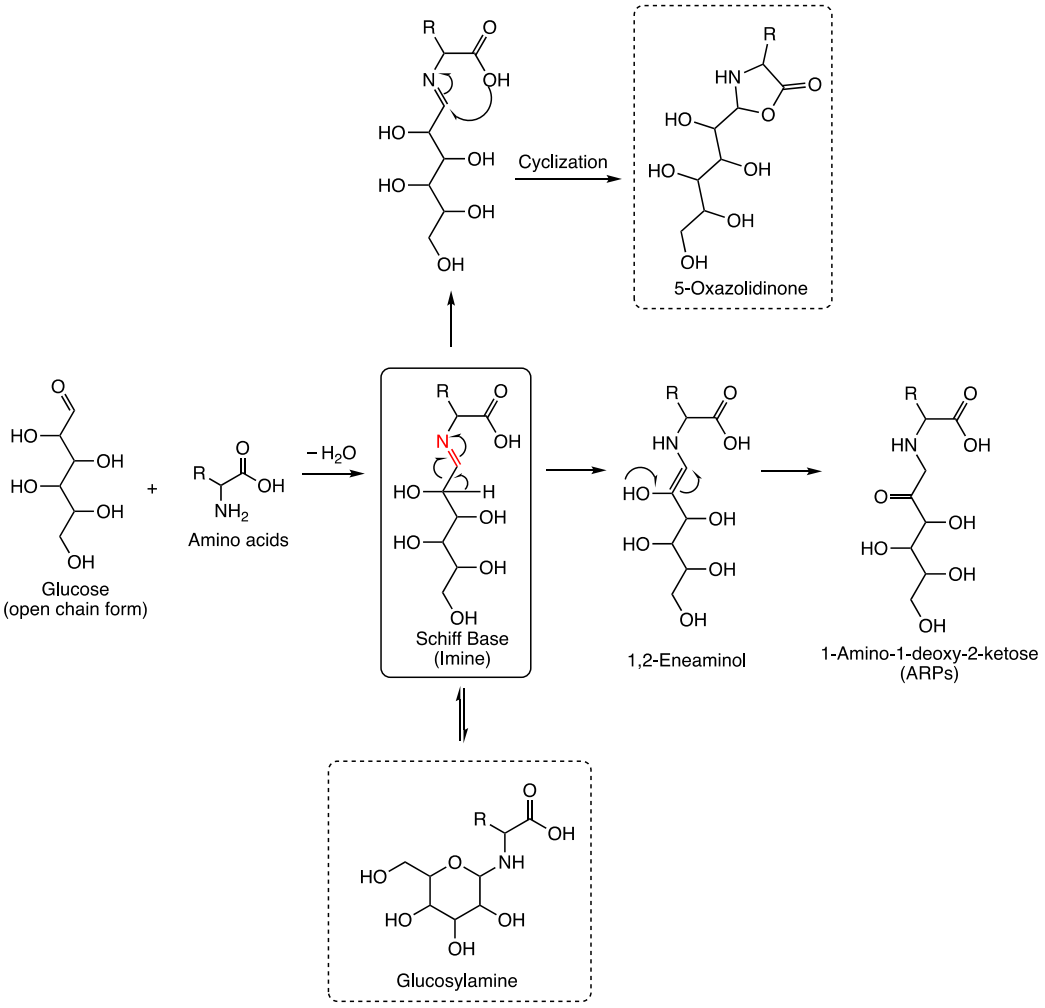

Figure 2.2. Synthetic pathway of the Amadori rearrangement product (ARP), glycosylamine, and oxazolidinone via Schiff base, employing the carbonyl groups of sugars and the amino groups of amino acids

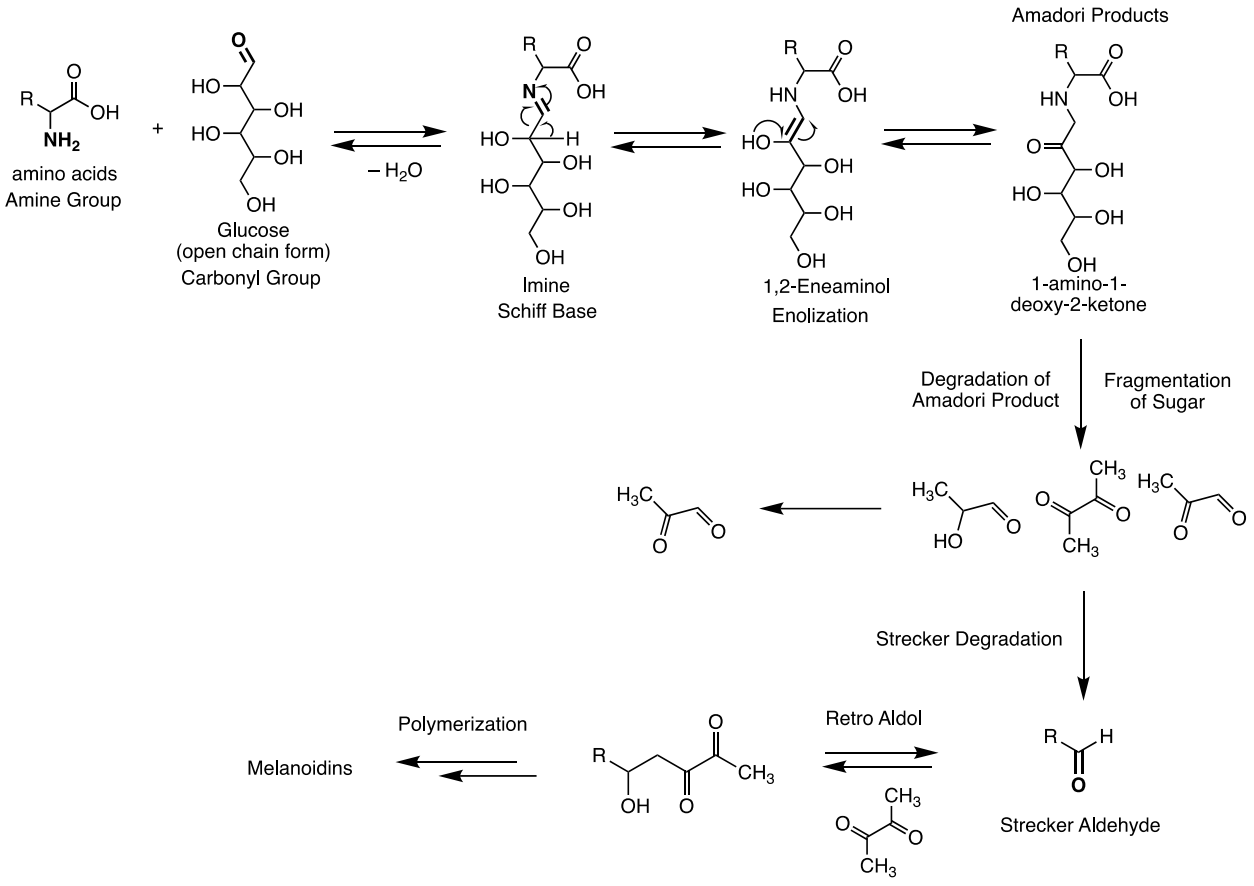

Figure 2.3. Synthetic pathways involved in the Maillard reaction

2.3. METAL IONS IN FOOD: HEME IRON AND NONHEME IRON

Generally, metals are naturally present in different food products (Table 2.1) (Marles, 2017), or they are added during food processing for various reasons. For example, iron is a natural food ingredient (Figure 2.4), and it is present in vital tissues, such as liver and muscle, and in biomolecules such as hemoglobin. Iron is also added during food processing to products, such as flour, grains, or dairy products (Coates *et al*., 2017). Dietary iron contains both heme and nonheme iron. Heme iron consists of a tetrapyrrole ring system known as protoporphyrin IX iron complex, and it is generally acquired from the hemoglobin (tetrameric protein) of animal flesh (West and Oates, 2008). However, several plants contain heme iron, known as leghemoglobin (monomeric

protein), which is mainly found in the root nodule of leguminous plants (Figure 2.5). Nonheme iron can be derived from all types of plant- and animal-based foods (Jin *et al*., 2018).

Table 2.1. Range of the mineral nutrient content (mg/100 g dry weight) in grains, vegetables, and fruits adapted and reproduced from Marles (2017)

Units are mg/100 g dry weight

n/a: not available

Crop	Ca	K	Mg	Cu	Fe	Mn	Zn
Wheat	8 – 80	280 – 730	20 – 220	0.1 – 1.4	1.6 – 16.3	1.0 – 9.0	1.5 – 10.2
Rice (brown)	10 – 60	70 – 320	20 – 170	0.1 – 0.7	0.2 – 6.0	0.2 – 4.2	0.7 – 3.3
Maize (sweet)	8.3 – 69	9000 – 1560	106 – 281	0.08 – 0.25	1.6 – 3.1	n/a	1.9 – 6.25
Barley	40 – 70	300 – 590	90 – 150	n/a	n/a	n/a	n/a
Common bean	9 – 425	1300 – 2490	100 – 326	< 0.04 – 1.4	3.14 – 12.07	0.0009 – 2.63	1.89 – 6.24
Soybean	120 – 320	1800 – 2320	220 – 310	0.11 – 1.98	6.0 – 20.0	< 2.75 – 5.9	1.09 – 6.77
Sweet potato (raw peeled)	79.0 – 147.4	724.0 – 1454	73.7 – 87.6	0.5 – 0.7	2.1 – 6.4	1.3 – 2.6	0.6 – 1.2
Broccoli	170 – 510	n/a	160 – 370	n/a	n/a	n/a	n/a
Tomato (red ripe raw)	145.2 – 181.8	3600 – 4833	116.7 – 206.9	0.67 – 1.07	4.91 – 8.33	1.83 – 2.07	1.50 – 3.09
Papaya (ripe)	57.93 – 285.9	1238 – 2309	89.53 – 29.6	0.12 – 0.83	0.9 – 14.81	0.081 – 0.24	0.39 – 2.80

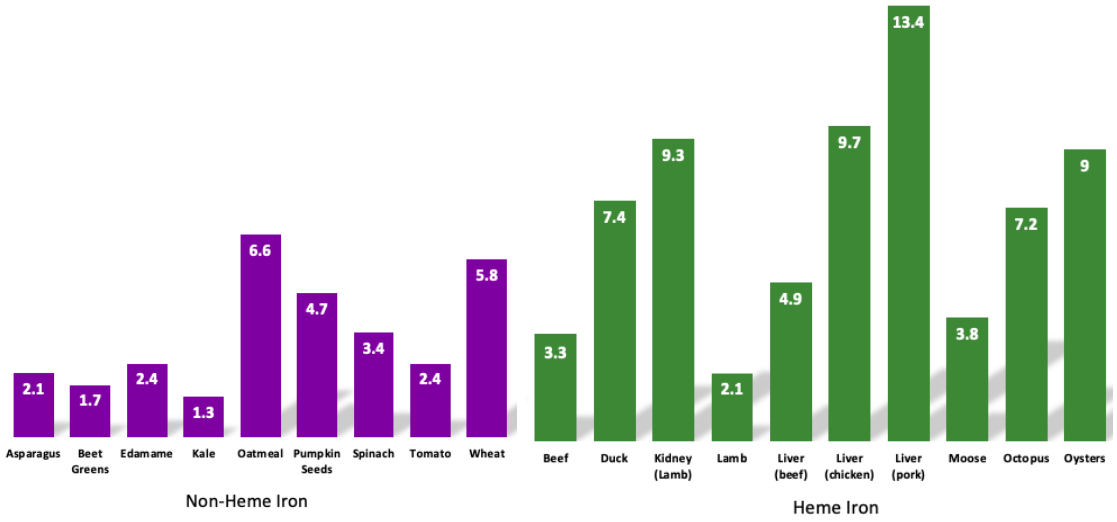

Units are mg of nonheme Iron /125 mL (½ cup) and mg of heme Iron /75 g (2 ½ oz)

Figure 2.4 Iron content (mg of nonheme iron/125 mL (½ cup) and mg of heme iron/75 g (2 ½ oz)) of common foods (adapted and reproduced from Canadian Nutrient File (2015)): www.hc-sc-gc.ca/fn-an;nutrition/fiche-nutri-data/index-eng.php

Studying the effects of metals on the Maillard reaction is important from various perspectives. For instance, heme iron is an essential catalyst for the chemical transformation of various reactants into complex flavour precursors that can define the characteristic flavour of meat (Jin *et al*., 2018). Fraser *et al*. (2017) patented their method of generating the characteristic meaty flavours and/or aromas during the thermal processing of food products (US Patent No. 9700067 B2). Their method involved the chemical reaction of various flavour precursors or compositions catalyzed by the presence of a highly conjugated heterocyclic ring-iron complex, such as a heme-, corrinoid-, and chlorin-iron complexes, which were detected using gas chromatography mass spectrometry (GC/MS) and evaluated by sensory panels. Their studies involved the creation of a meaty flavour or aroma using a mixture of leghemoglobin and reactants, such as amino acids and sugars, which was labelled the "magic mix." However, they did not report the associated structures or mechanisms affording any flavour precursors.

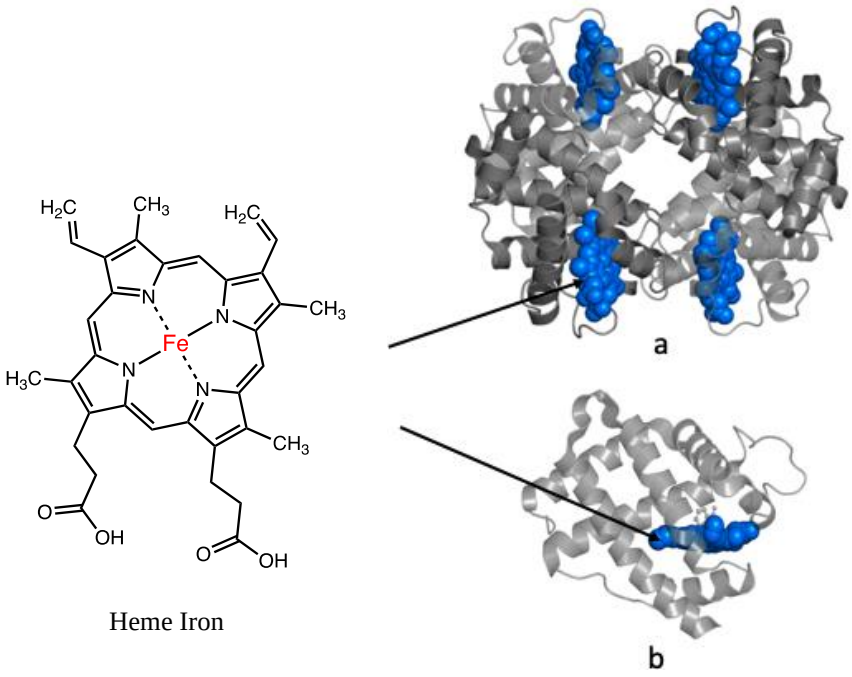

Figure 2.5 Structures of (a) heme iron (protoporphyrin IX iron complex), tetrameric human hemoglobin (PDB code: 6nbd) and (b) monomeric *lupinus luteus* (European yellow lupine) leghemoglobin (PDB code: 21h6) adapted and reproduced from Protein Data Bank in Europe (PDBe)

2.4. METAL IONS AFFECTING THE MAILLARD REACTION INTERMEDIATES

Although the exact mechanism of the effects of metal ions on the Maillard reaction is not clear, metal ions have been studied for their potential in controlling the Maillard reaction, such as accelerating the reaction rates, complexing with the reactants, and even mitigating the formation of the undesired Maillard reaction intermediates. Among the Maillard reaction components, amino acids are the ideal ligands for metal complexation (Beck, 2009; 2011) due to their affinity to bind via amino and carboxylate groups. Owing to such complexation, the amino acid-metal complexes play a key role in the oxidative decarboxylation (Yablokov *et al.*, 2014) and conversion of one amino acid into another through the Akabori reaction (Akabori *et al.*, 1959; Otani and Winitz, 1960). Similarly, the serine-copper(II) complex can also undergo an Akabori reaction via Schiff

base formation and generate the corresponding Akabori amino acid hydroxymethyl-serine, as reported by Nashalian and Yaylayan (2015a). In this study, the key intermediates double Schiff base-copper complex and α-hydroxymethyl-serine complex, are essential for the formation of unconventional amino acids through the Maillard reaction (Figure 2.6).

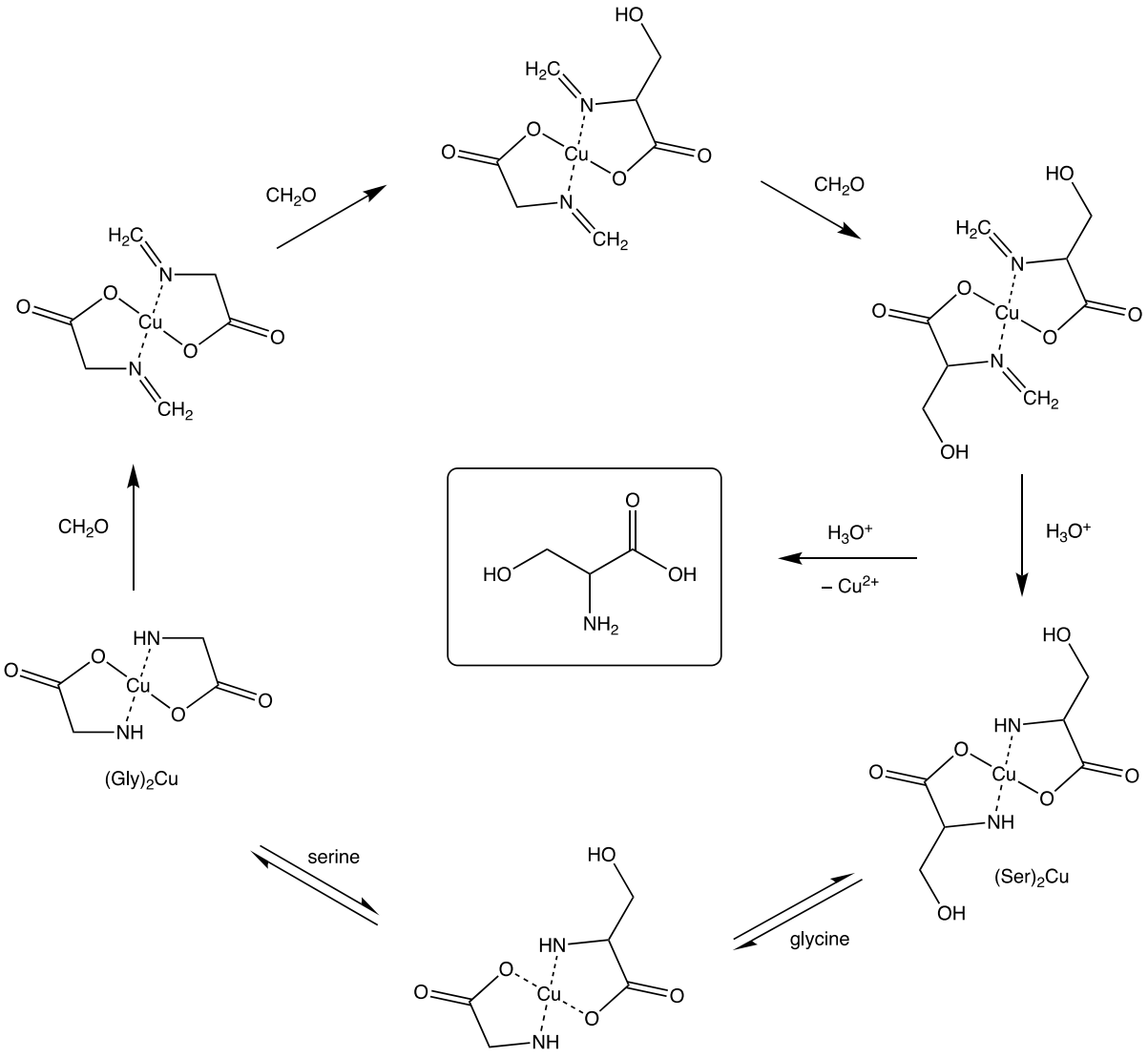

Figure 2.6 Mechanism of the Akabori reaction and the generation of serine in the presence of formaldehyde. $[M + 1]^+$ values represent the theoretical masses of formaldehyde adapted from Nashalian and Yaylayan (2015a)

2.4.1. Effect of Metals on the Formation of the ARPs

The ARPs are indicative of the Maillard reaction (Hodge, 1953; Harohally *et al*., 2014), and they are reported as the precursors or the desirable compounds for the browning or aroma/flavour of foods. To reveal the precise conditions for controlling the formation of the Amadori or Heyn products, various parameters, such as temperature and pH, have been studied. Furthermore, researchers have focused on forming complexes of the Amadori products as a catalytic method for the synthesis of the ARP. For example, Tonkovic *et al*. (1997) synthesized metal complexes with Amadori products and trivalent iron, which were characterized using Fourier transform infrared (FTIR) and nuclear magnetic resonance (NMR) spectroscopy. Gyurcsik *et al*. (1993) also reported complexes of the Amadori compounds with divalent copper and nickel, which were analyzed by infrared (IR) and circular dichroism (CD) spectrometry.

Degraded ARPs have also been reported, such as the *n*-butylamine/glucose Amadori copper complex, which undergoes oxidative degradation to generate hydroxyl radicals and various dicarbonyl products faster than its free counterpart (Horikawa *et al.*, 2002). Cheng and Kawakishi (1994) reported the oxidative decomposition of the Amadori products catalyzed by copper. Lewis acid metals have been regarded as effective catalysts to accelerate the formation of ARP. Studies showed that the addition of divalent zinc to the Amadori rearrangement reaction on α-hydroxyl groups afforded the formation of a complex with a Schiff base (Hofmann and Schieberle, 2000). Harohally *et al*. (2014) reported a zinc-mediated practical protocol for the synthesis of an Amadori ketose under different solvent conditions. Moreover, the $Zn(OAc)_2$ complex acts as a Lewis acid catalyst for the formation of the Amadori and Heyns products in the presence of reducing sugars in their acyclic form that is crucial for catalytic Maillard reaction intermediates (Chanda and Harohally, 2018). Nashalian and Yaylayan (2015; 2016; 2017) studied the role of metals and metal-amino acid complexes in the Maillard reaction. They used pyrolysis gas chromatography mass spectrometry (Py/GC-MS) and electrospray ionization quadruple time-of-flight mass spectrometry (ESI/qTOF/MS) and examined the modulation of the Maillard reaction by the amino acid-copper complexes. Specifically, they showed that copper promoted the oxidative decarboxylation of sugar-conjugated amino acid-copper complexes and controlled the release of the two most important intermediates of the Maillard reaction: Strecker aldehydes and Amadori products.

2.4.2. Effect of Metals on the Formation of Strecker Aldehydes

Before the discovery of the Maillard reaction, the Strecker reaction (Strecker, 1850;1854) was known for affording the precursors of flavour in foods, such as phenylacetaldehyde (honey aroma) from the corresponding amino acids and α-dicarbonyl compounds (Hofman and Schieberle, 2000; Yaylayan, *et al*., 2003). Oxidizing agents, such as copper, are expected to enhance oxidative decarboxylation reactions and contribute to the pool of aroma-active aldehydes (Fitzpatrick and Hopgood, 1974). However, the oxidative decomposition of sugars leads to the formation of α-dicarbonyl compounds, such as glucosone and deoxyglucosone, that can trigger the Strecker reaction of amino acids (Yaylayan and Keyhani, 2000). Similarly, Hofman and Schieberle (2000) demonstrated that the Strecker aldehyde can be produced during the Maillard reaction through the oxidative degradation of the Amadori compounds, catalyzed by transition metal ions (i.e., copper) in the presence of oxygen. The ARP transforming into the imine form is the key step of this reaction. The contribution of these aldehydes and enhancement of their generation pathways could be key factors in controlling the overall flavour of food. Metal salts, such as those of copper, can enhance oxidative decarboxylation reactions owing to their oxidation capacity. Nashalian and Yaylayan (2014) reported the formation of Schiff bases and Strecker aldehydes after the pyrolysis of *bis*(alaninato)copper(II). These findings clearly indicated that certain amino acids can undergo thermally induced oxidative decarboxylation and generate Strecker aldehydes in the absence of 1,2-dicarbonyl compounds. However, in the presence of divalent copper or trivalent iron, this ability is significantly enhanced by these metal complexes. Other metals, such as calcium and zinc, can also complex with amino acids. However, when copper(II) or iron(III) chloride was replaced by calcium(II) or zinc(II) chlorides, the formation of the Strecker aldehyde was not promoted (Figure 2.7).

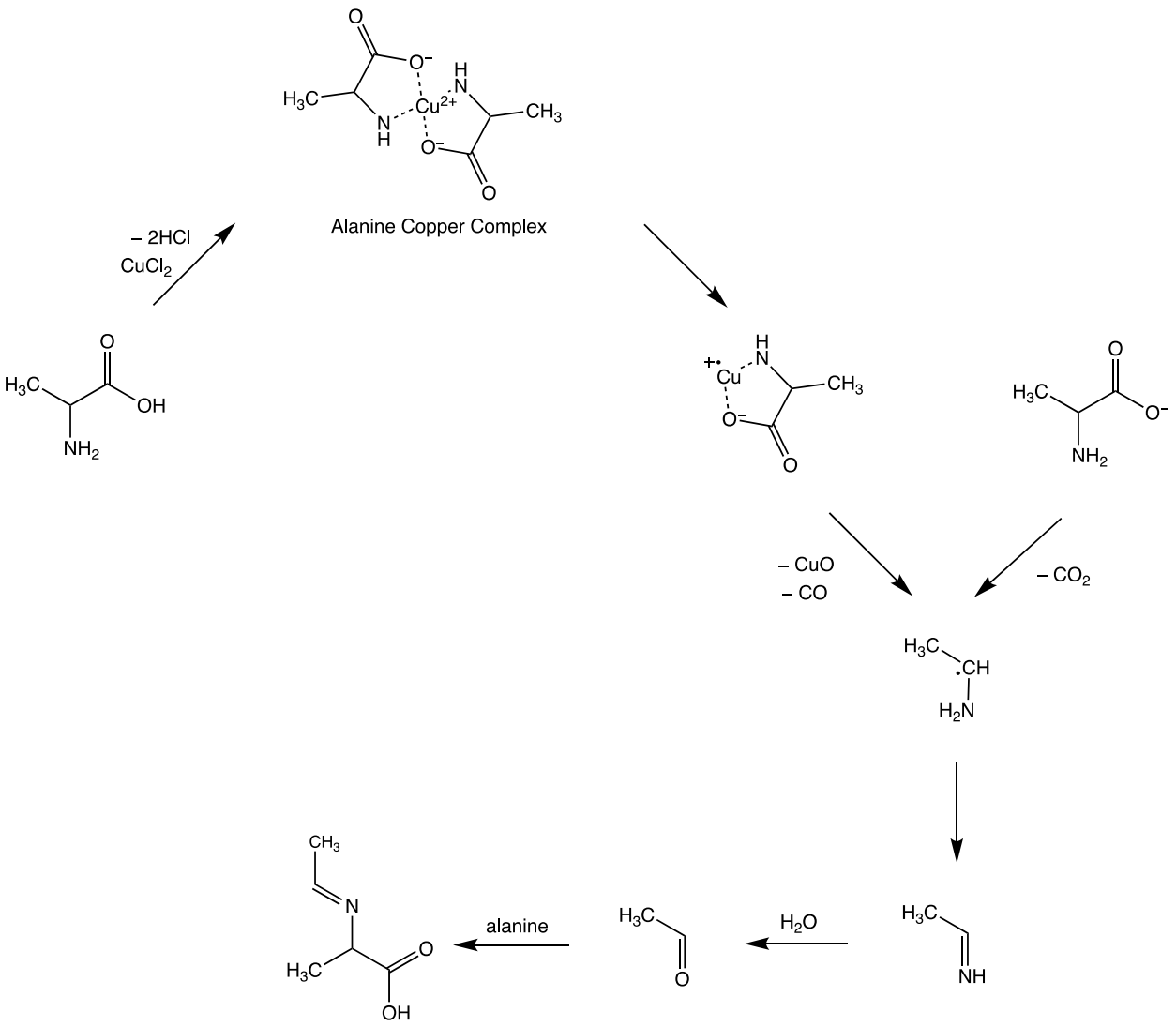

Figure 2.7 Proposed mechanism of the copper-assisted thermal decarboxylation of alanine and the formation of acetaldehyde adapted from Nashalian and Yaylayan (2014)

2.5. METAL IONS AFFECTING THE MAILLARD BROWNING

ARPs have been considered as key Maillard intermediates as well as attractive flavour enhancers and browning precursors. The creation of stable intermediates is an important parameter for the slow generation of flavouring/browning compounds, preventing their rapid loss over the course of the Maillard reactions. Browning is also an essential reaction in food processing and storage because it can positively and negatively affect food quality. Various factors, such as the heating time and water activity, were examined to regulate the formation of colour via Maillard chemistry

for the food industry. Rendleman and Inglett (1990) reported that divalent copper affected the colour development by accelerating the rate of the reaction in a glucose and glycine model system. Similarly, Hayase *et al*. (1996) demonstrated that transition metal ions can accelerate the formation of the Maillard intermediates such as ARPs. They can also affect polymerization in the final stage through thermal treatment and form browning products, such as fluorescent compounds or melanoidins. Furthermore, the browning reaction rate of the Amadori products was measured in solution through the number of metal ions and cations (Bertelli *et al*., 1996) due to the release of protons from the individual metal ions such as cupric ions (Rendleman and Inglett, 1990). Nursten (2005) reported that divalent copper and trivalent iron can promote Maillard browning, whereas ethylenediaminetetraacetic acid (EDTA) and diethylenetriaminepentaacetic acid (DTPA) exhibited the opposite effect. Metal ions, such as divalent copper, iron, and zinc, influenced the intensity of the Maillard browning of different fractions, depending on the time of heat treatment and the nature and concentration of the incorporated metals (Kwak and Lim, 2004; Ramonaitytė *et al*., 2009). Kocadağlı and Gökmen (2014) examined the development of browning in food model systems, such as cookies. Based on their model systems, NaCl, KCl, and $CaCl_2$ improved the browning of cookies by increasing the formation of furfurals; however, these salts decreased the browning intensity in a glucose/glycine system during thermal reactions. Kinetic analyses through multi-response data modeling showed that 3-deoxyosone was the key precursor in the formation of carbohydrate fragments such as α-dicarbonyl compounds responsible for the browning formation (Martins and Van Boekel, 2003; Cui *et al*., 2021). Although glucosamine can increase the intensity of browning, the presence of divalent zinc in the reaction mixture was significant for generating browning products during the entire heating (100 °C) period (Ramonaityte *et al*., 2009; Wu *et al*., 2018).

2.6. REFERENCES

Amadori, M. (1925). Products of condensation between glucose and p-phenetidine. *Atti Della Accademia Nazionale Dei Lincei*, 6(2), 337–342.

Akabori, S., Otani, T. T., Marshall, R., Winitz, M., Greenstein, J. P. (1959). A synthesis and resolution of DL-serine. *Archives of Biochemistry and Biophysics,* 83(1), 1–9.

Beck, W. (2009). Metal Complexes of Biologically Important Ligands, CLXXII [1]. Metal Ions and Metal Complexes as Protective Groups of Amino Acids and Peptides- Reactions at Coordinated Amino Acids. *Zeitschrift für Naturforschung* A, 64B, 1221–1245.

Beck, W. (2011). Metal Complexes of Biologically Important Ligands, CLXXVI [1]. Formation of Peptides within the Coordination Sphere of Metal Ions and of Classical and Organometallic Complexes and Some Aspects of Prebiotic Chemistry. *Zeitschrift für Anorganische und Allgemeine Chemi*e, 637, 1647–1672.

Bertelli, L., Torregiani, D., Bertolo, G. (1996). Non-enzymatic browning in hydrolysed concentrated cheese whey permeates. *Food Chemistry,* 55, 353–358.

Chanda D. and Harohally, N. V (2018). Revisiting Amadori and Heyns synsthesis: Ciritical percentage of acyclic form play the trick in addition to catalyst. *Tetrahedron Letters*, 59(31) 2983–2988.

Cheng, R. and Kawakishi, S. (1994). Novel decomposition of Amadori compound catalyzed by copper ion. *Journal of Agriculture and Food Chemistry, 42*, 700–703.

Chu, F.L. and Yaylayan, V. A. (2008). Post-schiff chemistry of the Maillard reaction. *Annals of the New York Academy of Science*, 1126, 30–37.

Coates, A., Mountihoy, M.,Burr, J. (2017). Incidence of Iron Deficiency and Iron Deficient Anemia in Elite Runners and Triathletes. *Clinical Journal of Sport Medicine*. 27(5), 493–498.

Cui, H., Yu, J., Zhai, Y., Feng, L., Chen, P., Hayat, K., Xu, Y., Zhang, X., Ho, C.T. (2021). Formatio and fate of Amadori rearrangement products in Maillard reaction. *Trend in Food Science & Technology*, 115(2021), 391–408.

Doob, H., Willmann, A., Sharp P.F. (1942). Influence of moisture on browning of dried whey and skim milk. *Industrial & Engineering Chemistry, 34*, 1460–1468.

Finot, P. A. (2005). Historical Perspective of the Maillard Reaction in Food Science. *Annals of the New York Academy of Sciences,* 1043(1), 1–8.

Fitzpatrick, J. H. and Hopgood, D. (1974). Metal ion catalyzed decarboxylation. Kinetics and mechanism of the oxidative decarboxylation of copper(II) complexes of aminomalonic acid in aqueous solution. *Inorganic Chemistry*, 13, 568–574.

Fraser, R., Brwon, P. O., Karr, J., Holz-Schietinger, C., Cohn, E., (2017). Methods and Compositions for affecting the flavor and aroma profile of consumables. United States Patent. US 9,700.067 B2.

Gyurcsik, B., Gajda, T., Nagy, L., Burger, K., Rockenbauer, A., Korecz Jr. L. (1993). Proton, copper(II) and nickel(II) complexes of some Amadori rearrangement products of D-glucose and amino acids. *Inoranica Chimica Acta, 214*, 57–66.

Harohally, N. V., Srinivas, S. M, Umesh, S. (2014). ZnCl2-mediated practical protocol for the synthesis of Amadori ketose. *Food Chemistry*, 158(1), 340–344.

Hayase, F., Shibuya, T., Sato, J., Yamamoto, M. (1996). Effects of Oxygen and Transition Metals on the Advanced Maillard Reaction of Proteins with Glucose. *Bioscience, Biotechnology, and Biochemistry*, 60(11), 1820–1825.

Hellwig, M. and Henle, T. (2014). Baking, Ageing, Diabetes: A Short History of the Maillard reaction. Angewandte Chemie International Edition. 53, 10316–10329.

Heyns, K. and Koch, W. Z. (1952). Über die bildung eines aminozuckers ausd-fruktose und ammoniak. Zeitshrift für Naturforschung B, 7B, 486–488.

Hodge, J. E. (1953). Chemistry of Browning Reactions in Model Systems. *Journal of Agricultural and Food Chemistry*, 1(15), 928–943.

Hofmann, T. and Schieberle, P. (2000). Formation of Aroma-Active Strecker-Aldehydes by a Direct Oxidative Degradation of Amadori Compounds. *Journal of Agricultural and Food Chemistry*, *48*(9), 4301–4305.

Horikawa, H., Okada, M., Nakamura, Y., Sato, A., Iwamoto, N. (2002). Production of hydroxyl radicals and α-dicarbonyl compounds associated with Amadori compound–Cu^{2+} complex degradation. *Free Radical Research*, 36, 1059–1065.

Jin, Y., He, X., Andoh-Kumi, K., Fraser, R. Z., Lu, M., Goodman, R. E. (2018). Evaluating Potential Risks of Food Allergy and Toxicity of Soy Leghemoglobin Expressed in Pichia pastoris. *Molecular Nutrition,* 62, 1–13.

Jin, Y., He, X., Andoh-Kumi, K., Fraser, R. Z., Lu, M., Goodman, R. E. (2018). Evaluating Potential Risks of Food Allergy and Toxicity of Soy Leghemoglobin Expressed in Pichia pastoris. *Molecular Nutrition*, 62, 1–13.

Kocadagli, T. and Gokmen, V. (2016) Multiresponse kinetic modelling of Maillard reaction and caramelization in a heated glucose/wheat flour system. *Food Chemistry*, 211(15), 892–902.

Koschinsky, T., He, C. J., Mitsuhashi, T., Bucala, R., Liu, C., Buenting, C., Heitmann, K., Vlassara, H. (1997). Orally absorbed reactive glycation products (glycotoxins): An environmental risk factor in diabetic nephropathy. *Proceedings of the National Academy of Science of the United States of America*, 94, 6474–6479.

Kwak, E. J. and Lim, S. I. (2004). The effect of sugar, amino acid, metal ion, and NaCl on model Maillard reaction under pH control. *Amino Acids*, 27, 85–90.

Maillard, L. C. (1911). Synthese des peptides inferieurs par une methods nouvelle et directe, voisine des reaction biolgique. C. R. Hebd. *Seances Mem. Soc. Biol*., 71, 546–9

Marles, R. J. (2017). Mineral nutrient composition of vegetables, fruits and grains: The context of reports of apparent historical declines. *Journal of Food Composition and Analysis*, 56(2017) 93–103.

Martins S. I. F. S. and Boekel M. A. J. S. (2003) Melanoidins extinction coefficient in the glucose/glycine Maillard reaction, *Food Chemistry*, 83(1), 135–142.

Martins, S. I. F. S., Jongen, W. M. F. and Boekel, M. A. J. S. V. (2001). A review of Maillard reaction in food and implications to kinetic modelling. *Trends in Food Science & Technology*, 11(2001), 346–373.

Namiki, M. (1988). Chemistry of Maillard reactions: Recent studies on the browning reaction mechanism and the development of antioxidants and mutagens. *Advances in Food Research*, 32, 115–183.

Nashalian, O. and Yaylayan, V. A. (2014). Thermally induced oxidative decarboxylation of copper complexes of amino acids and formation of Strecker Aldehyde. *Journal of Agricultural and Food Chemistry*, 62, 8518–8523.

Nashalian, O. and Yaylayan, V. A. (2015a). De Novo Synthesis of Amino Acids during the Maillard Reaction: qTOF/ESI Mass Spectrometric Evidence for the Mechanism of Akabori Transformation. *Journal of Agricultural and Food Chemistry*, 63, 328–334.

Nashalian, O. and Yaylayan, V. A. (2015b). Sugar-conjugated *Bis*(glycinato)copper (II) Complexes and Their Modulating Influence on the Maillard Reaction. *Journal of Agricultural and Food Chemistry*, 63, 4353–4360.

Nashalian, O. and Yaylayan, V. A. (2016a). In situ formation of the amino sugars 1-amino-deoxy-frutosoe and 2-amino-2-deoxy-glucose under Maillard reaction conditions in the absence of ammonia. *Food Chemistry*, 197, Part A, 489–495.

Nursten, H. E. (2005). The Chemistry of Non Enzymatic Browning. The Maillard reaction: Chemistry, Biochemistry and Implications. Cambridge, UK: *The Royal Society of Chemistry*, 5-29.

Otani, T. T. and Winitz, M. (1960). Studies on hydroxyamino acids. I. Synthesis of some α-alkylated serines. *Archives of Biochemistry and Biophysics, 90*, 254–259.

Ramonaityte, D. T., Keršiene M., Adams A, Tehrani K. A. (2009). The interaction of metal ions with Maillard reaction products in a lactose-glycine model system. *Food Research International*, 42(2009) 3331–3336.

Rendleman, J. A. and Inglett, G. E. (1990). The influence of Cu^{2+} in the Maillard reaction. *Carbohydrate Research*, 201, 311–326.

Schönberg, A. and Moubacher, R. (1951). The Strecker Degradation of α-Amino Acids. *Chemical Reviews*. 50(2), 261–277.

Strecker, A. (1850). Ueber die kūnstliche Bildung der Milchsäure und einen neuen, dem Glycocoll homologen Körper. *Annalen der Chemie und Pharmacie*. 75(1), 27–45.

Strecker, A. (1854). Ueber einen neuen aus Aldehyd-Ammoniak und Blausäure entstehenden Körper. *Justus Liebigs Annalen der Chemie*. 91(3), 349–351.

Tareke, E., Rydberg, P., Karlsson, P., Eriksson, S., Törnqvist, M. (2002). Analysis of Acrylamide, a Carcinogen Formed in Heated Foodstuffs. *Journal of Agricultural and Food Chemistry*. 50, 4998–5006.

Tonkovicc, M., Jakas, A., Horvat, S. (1997). Preparation and properties of an Fe(III)-complex with an Amadori compound derived from L-tyrosine. *Biometals, 10*, 55–59.

West, A. R. and Oates, P. S. (2008). Mechanisms of heme iron absorption: Current questions and controversies. *World Journal of Gastroenterology*, 14(26), 4104–4110.

Wu, S., Dai, X., Shilong, F., Zhu, M., Shen, X., Zhang, K., Li, S. (2018). Antimicrobial and antioxidant capacity of glucosamine-zinc(II) complex via non-enzymatic browning reaction. *Food Science and Biotechnology* 27(1), 1–7.

Yablokov, V. A., Smel'tsova, I. L., Faerman, V. I. (2014). Kinetics of Heat-Induced Transformation of Copper Complexes with Amino Acids. *Russian Journal of General Chemistry*. 84(3), 568–570.

Yaylayan, V. A. (1997). Classification of the Maillard reaction: A conceptual approach. *Trends in Food Science & Technology*, 8, 13–18.

Yaylayan, V. A. (2003). Recent Advances in the Chemistry of Strecker Degradation and Amadori Rearrangement: Implications to Aroma and Color Formation. *Food Science and Technology Research*, 9(1):1–6.

Yaylayan, V. A. and Keyhani, A. (2000). Origin of Carbohydrate Degradation Products in L-Alanine/D-[^{13}C] Glucose Model Systems. *Journal of Agricultural and Food Chemistry*, 48, 2415–2419.

Yaylayan, V. A., Huyghues-Despointes A. (1994). Chemistry of Amadori Rearrangement Products: Analysis, Synthesis, Kinetics, Reactions, and Spectroscopic Properties. *Critical Reviews in Food Science and Nutrition*, 34(4), 321–369.

Zhang, Y., Ren, Y., Zhang, Y. (2010). New Research Development on Acrylamide: Analytical Chemistry, Formation Mechanism, and Mitigation Recipes. *Chemical Reviews*, 109(9), 4375–4397.

Zhdeh, R. G. and Yaylayan, V. (2020). Monitoring of methylglyoxal/indole interaction by ATR-FTIR spectroscopy and qTOF/MS/MS analysis. *Current Research in Food Science*, 3, 67–72.

CONNECTING PARAG RAPH

Chapter 2 provided an overview of the critical aspects of the Mallard reaction and presented a review of the role of metal ions based on the literature recently reported. In addition, it provided a systematic investigation of the chemical characteristics of amino acid-metal ions interactions. **Chapter 3** introduces a convenient analytical tool for hard-to-detect sugar degradation products through their complexation and stabilization as bidentate ligands with divalent iron ($FeCl_2$) and proposes a mechanistic interpretation for their formation. **Chapter 3** was published in the *Current Research in Food Science*: Kim, E. S. and Yaylayan, V. (2020). Profiling of sugar degradation products through complexation with divalent Metal ions coupled with ESI/qTOF/MS/MS analysis, 3(2020), 268–274.

CHAPTER 3

PROFILING OF GLUCOSE DEGRADATION PRODUCTS THROUGH COMPLEXATION WITH DIVALENT METAL IONS COUPLED WITH ESI/QTOF/MS/MS ANALYSIS

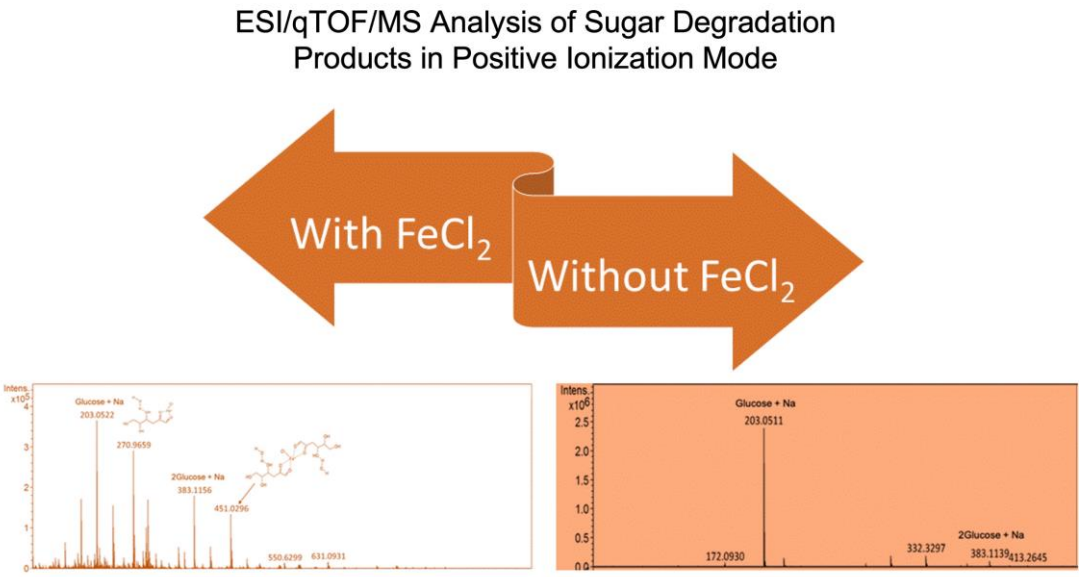

3.1. ABSTRACT

Sugar degradation products generated through thermal treatment of foods are considered the key precursors for various flavor compounds, toxicants, and browning, but their high reactivity makes their detection difficult. In this study, a convenient analytical procedure for profiling of various reactive sugar intermediates having enediol or α-dicarbonyl moieties through complexation with divalent metal ions combined with electrospray ionization/quadrupole time-of-flight mass spectrometry was developed. Excess divalent iron chloride ($FeCl_2$) was added to glucose or ^{13}U6-[glucose] solutions in methanol either before or after heating at 110 °C for 2 h, and the samples were analyzed by tandem mass spectrometry. The results indicated the formation of ethylene glycol, glycolaldehyde, glyceraldehyde, glycerol, methylglyoxal, glyoxylic acid, erythrose, erythrosone, 3-deoxy-erythrosone, erythritol, ribose, ribosone, 3-deoxy-ribose, ribitol, 3-deoxy-glucosone, and rhamnose. These sugars and sugar degradation products acting as bidentate ligands were detected as positively charged mono- and *bis*-sugar iron complexes in the form of $[M + H]^+$, $[M + Na]^+$, $[M + K]^+$, $[M + Fe^{35}Cl]^+$, and $[M + Fe^{37}Cl]^+$, as well as by charge localization on iron, $[M]^+$. The divalent metal complexation technique was applied for the profiling of sugar degradation products in aged manuka honey.

KEYWORDS: Sugar iron complexes, Qualitative profiling of sugar degradation products, ESI/qTOF/MS

3.2. INTRODUCTION

During the thermal treatment of food, reducing sugars undergo a complex reaction cascade that leads to the formation of various reactive sugar intermediates and degradation products, such as α-dicarbonyl, α-hydroxy-carbonyl, deoxyosones, and α-hydroxy acids (Davídek *et al*., 2006a). In the context of the Maillard reaction, these intermediates constitute the "sugar fragmentation pool" that provides important precursors necessary for the formation of heterocyclic aromatic compounds (Yaylayan, 1997). Some of these reactive sugar intermediates form independently through acid- or base-catalyzed sugar degradation reactions, while others form interactively

through reactions with amino acids or proteins. The ability to profile such reaction mixtures for reactive sugar intermediates or sugar degradation products (SDP) poses an analytical challenge due to their high reactivity and transient nature, which allows them to form and react before detection. Although there are numerous quantitative analytical techniques based on chemical derivatization using silylating agents (Davídek *et al*., 2006a; 2006b; Paravisini and Peterson, 2019; Usui *et al*., 2007; Yaylayan, 1997; Zheng *et al*., 2019). There are no methods reported so far for the fast detection of such sugar degradation products. Chemical derivatization is usually employed in conjunction with various chromatographic and mass spectrometric techniques, such as gas chromatography mass spectrometry (GC/MS) and liquid chromatography mass spectrometry (LC/MS) (Page and Conacher, 1982). Taking advantage of the ease of complexation of divalent metal ions such as copper(II) (Nashalian and Yaylayan, 2015) with not only α-dicarbonyl compounds but also many of the shorter-chain sugar fragments formed during the Maillard reaction, and their subsequent stabilization, we propose the utilization of divalent metal ions as suitable fast trapping agents for profiling of such reactive SDP as metal complexes in conjunction with electrospray ionization/quadrupole time-of-flight mass spectrometry (ESI/qTOF/MS) analysis.

3.3. MATERIRALS AND METHODS

3.3.1. Materials and Reagents

Iron(II) chloride ($FeCl_2$) (99%) and D-glucose were purchased from Sigma-Aldrich Chemical Co. (Oakville, Ontario, Canada). [$^{13}C_6$-U] glucose (99%) was purchased from Cambridge Isotope Laboratories (Andover, MI). Liquid chromatography-mass spectrometry (LC-MS) grade methanol (OmniSolv, > 99%) was obtained from VWR International (Mississauga, Ontario, Canada). Manuka honey used in this study was purchased from a local store in 2009 and aged at room temperature.

3.3.2. Sample Preparation

Test model systems were prepared by adding $FeCl_2$ (6.4 mg) either before or after heating glucose (18 mg) in methanol (1 mL) using sealed stainless-steel reactors at 110 °C for 2 h followed by evaporation of the solvent at 75 °C for 5 min. The samples were kept frozen until analysis. To

see the effect of storage temperatures on the profile, the same samples were also stored for 15 days at room and at refrigerated temperatures. Control model systems were prepared by heating glucose (18 mg) in methanol (1 mL) at 110 °C for 2 h without the addition of $FeCl_2$ or by adding $FeCl_2$ (6.4 mg) to an unheated glucose (18 mg) in methanol (1 mL). Aged manuka honey (2 mg) was dissolved in methanol (2 mL) and then $FeCl_2$ (0.02 mg) was added and analyzed after storage at refrigerated conditions for 15 days. All samples were analyzed at least in two replicates as indicated in Table 3.1.

Table 3.1. Composition of the model systems studied[a]

Model System	
Control Model Systems	Glucose solution heated in the absence of $FeCl_2$ kept at room temperature (RT) for 15 days until analyzed - **[Glu]**[b] $FeCl_2$ added to a glucose solution at RT analyzed after storage at RT for 15 days - **Glu/$FeCl_2$**
Test Model Systems	$FeCl_2$ added to heated glucose solution kept in the freezer for 15 days until analyzed - **[Glu]$FeCl_2$ I** $FeCl_2$ added to heated glucose solution kept at RT for 15 days until analyzed - **[Glu]$FeCl_2$ II** Glucose solution heated in the presence of $FeCl_2$ kept at RT for 15 days until analyzed - **[Glu/$FeCl_2$]**
Food Model Systems	Methanolic manuka honey solution was kept in the refrigerator for 15 days until analyzed - **Honey** $FeCl_2$ was added to a methanolic solution of manuka honey and kept in the refrigerator for 15 days until analyzed - **Honey/$FeCl_2$**

[a]All model systems were analyzed minimum in two replicates.

[b]Square brackets indicate heating at 110 °C for 2 h in methanol by using sealed stainless-steel reactors.

3.3.3. ESI/qTOF/MS Analysis

The dry reaction mixtures were dissolved in liquid chromatography (LC)-grade methanol to a concentration of 1 mg/mL. The samples were then diluted 10-fold in 10% methanol prior to analysis by ESI/qTOF/MS in positive mode. The ESI/qTOF/MS system was comprised of a Bruker Maxis Impact quadrupole-time-of-flight mass spectrometer (Bruker Daltonics, Bremen, Germany) operated in positive-ion mode. This system was permitted a high resolution with ~ 60,000 full

sensitivity resolution and mass accuracy of 1 ppm. Samples (1 μL) were injected directly into ESI/qTOF/MS. Instrument calibration was performed using sodium formate clusters. The electrospray interface settings were the following: nebulizer pressure, 0.6 bar; drying gas, 4 L/min; temperature, 180 °C; and capillary voltage, 4500 V. The scan range was from *m*/*z* 100 to 1000. Molecular formulae were assigned to all the observed peaks based on their exact *m/z* values by using the online software "ChemCalc" (Institute of Chemical Sciences and Engineering, Lausanne, Switzerland) (Patiny and Borel, 2014). ESI/qTOF/MS/MS was carried out in multiple reaction monitoring (MRM) mode using 20.0 eV collision energy for the ions at *m/z* 270, 284, and 295.

3.3.4. Structural Elucidation

Evidence for the proposed structures of SDP was provided through ESI/qTOF/MS analysis of their elemental composition, MS/MS, and isotope-labelling studies using $^{13}C_6$-U glucose. In addition, the proposed structures were based on well-known glucose degradation products. Furthermore, the incorporation of chlorine from $FeCl_2$ in the identified complexes was confirmed through detection of the isotopic signature of chlorine at M + 2 peaks *ca*. 25% relative intensity of M ion. Isotope labelling techniques were used to confirm the elemental composition and the MS/MS fragmentation mechanisms using corresponding isotopically labelled counterparts generated from $^{13}C_6$-U labelled glucose.

The proposed structures represent only one possible isomer or stereoisomer out of many possibilities for a particular nominal molecular weight. Those structures are the most commonly reported in the literature.

3.4. RESULTS AND DISCUSSION

To develop a convenient technique for profiling SDP formed during the Maillard reaction or thermal processing of foods, a method based on the known and observed ease of complexation of Maillard reaction intermediates with divalent metal ions (Nashalian and Yaylayan, 2015) was investigated using $FeCl_2$. In this study, glucose was degraded by heating at 110 °C for 2 h in methanol and excess $FeCl_2$ was added either before ([Glu/$FeCl_2$]) or after the degradation reaction ([Glu]/$FeCl_2$) and analyzed using ESI/qTOF/MS. Heated glucose in the absence of $FeCl_2$ was also

analyzed ([Glu]) as a control (see Table 3.1). The control system without addition of the metal salt did not display any detectable low-molecular-weight SDP in the positive ionization mode. All other model systems, however, generated metal complexes with various sugar fragments, which are listed in Table 3.2 (see also Figures S3.1 and S3.2). In these model systems, the glucose degradation products acted as bidentate ligands and were detected as positively charged mono- and *bis*-sugar iron complexes such as $[M + H]^+$, $[M + Na]^+$, $[M + K]^+$, $[M + Fe^{35}Cl]^+$, and $[M + Fe^{37}Cl]^+$ in addition to charge localization on iron $[M]^+$ (see Figure 3.1). Moreover, some ions were associated with more than one solvent molecule (water and methanol), and some also showed dehydration products. The data indicated that the iron(II) complexes were stable enough to be detected by MS. The iron in these complexes assumed different charged states of 0, +1, and +2 depending on the number and type of bonding (covalent or coordinate) and simultaneously formed up to four bonds, two covalent and two coordinate, allowing for the binary complexes to be detected as protonated, sodiated, chlorinated, or potassiated ions as shown in Figure 3.1.

Table 3.2. Observed SDP following the method of complexation with $FeCl_2$[a]

	SDP[b] of glucose	SDP in aged manuka
C2	Ethylene Glycol and Glycolaldehyde	Not detected
C3	Glycerol, Glyceraldehyde and Methylglyoxal	Glyceraldehyde
C4	Erythrose, 3-Deoxyerythrosone, 3-Deoxyerythrose, Erythrosone, and Erythritol	Erythrose, 3-Deoxyerythrosone, 3-Deoxyerythrose, Erythrosone, and Erythrisol
C5	Ribose, Ribosone, 3-Deoxyribosone, 3-Deoxypentosulose, and Ribitol	Ribose, Ribosone, and 3-Deoxyribosone
C6	3-Deoxyglucosone, Glucosone, 3,4-Dideoxyglucosone, and Rhamnose	3-Deoxyglucosone

[a]See Table S3.1 for their various mono-, *bis*(sugar) metal complexes, and hydrates observed (reported names represent the most common isomer).

[b]Dehydrated and methanolated counterparts are not listed (see Table S3.1).

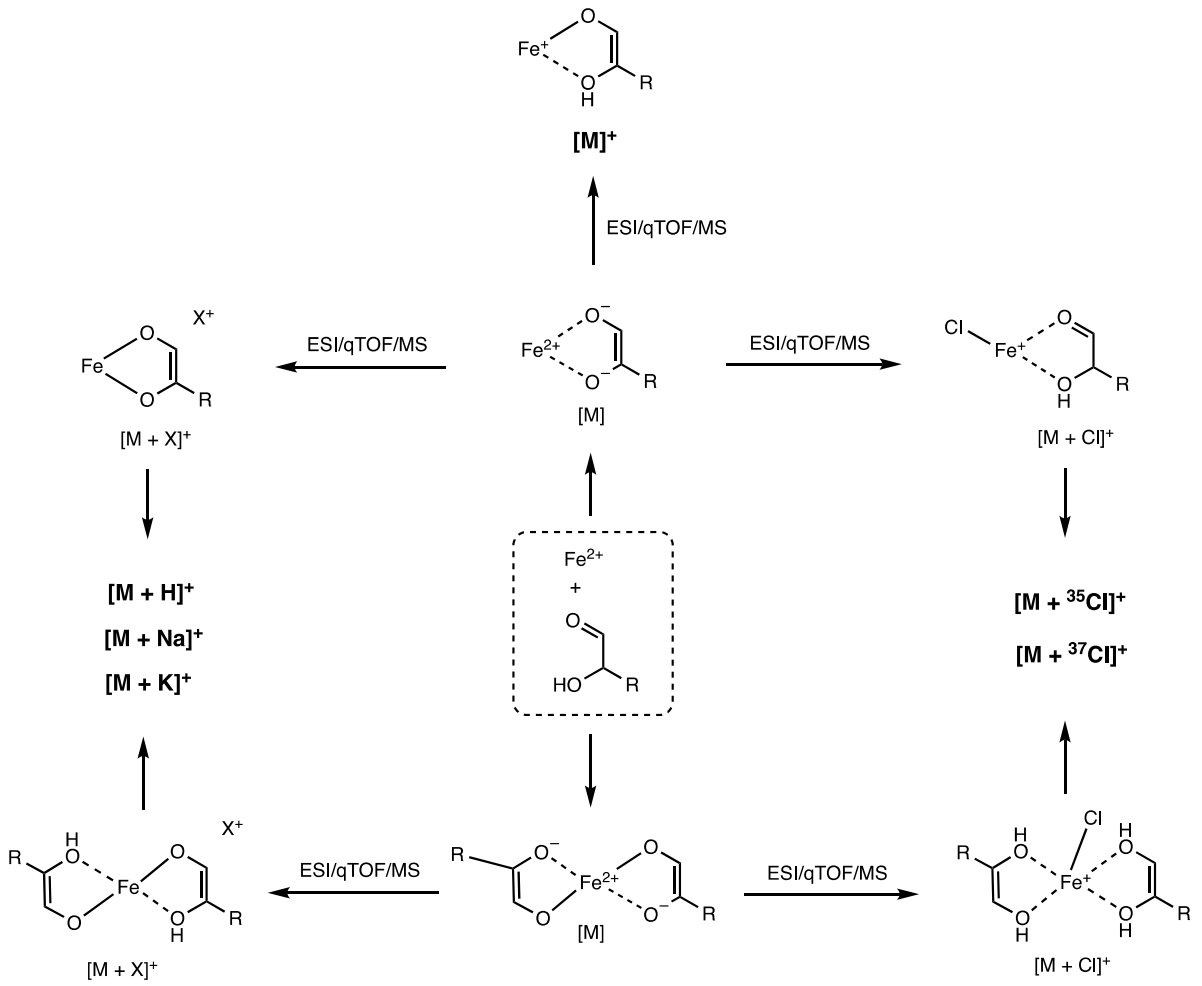

Figure 3.1. SDP can form single and/or *bis*(1,2-enediol) complexes of iron (II) and can be detected through various ionizations processes to form positively charged species such as $[M]^+$, $[M + H]^+$, $[M + Na]^+$, $[M + K]^+$, $[M + {}^{35}Cl]^+$, and $[M + {}^{37}Cl]^+$. The 1, 2-dicarbonyl type degradation products can also form single or *bis*(1,2-dicarbonyl) iron complexes of the type $[M + {}^{35}Cl]^+$ and $[M + {}^{37}Cl]^+$ (Not shown).

3.4.1. Profiling of Glucose Degradation Products via Iron(II) Complexation as Determined by ESI/qTOF/MS and ESI/qTOF/MS/MS

ESI/qTOF/MS analysis (positive ionization mode) of the different model systems listed in Table 3.1, indicated that in the absence of metal salts, only few low-molecular-weight SDP and some high-molecular-weight products in addition to unreacted glucose could be positively charged and detected (see Figures S3.1 and S3.2). However, in the model systems with metal ions, the enhanced intensity of the SDP was observed due to their complexation with the metal ions (see Table S3.1). This can be attributed to the increased stability of the metal complexes versus free SDP. These complexes can prevent their decomposition/polymerization and, at the same time, can provide structural features (see Figure 3.1) that are lacking in SDP for the development and stabilization of positive charges necessary for their detection under positive ionization mode of ESI-qTOF/MS system.

Storing the samples at room temperature before analysis did not significantly alter their sugar degradation profile, although some enhanced peak intensities were observed in the room temperature stored samples but those were not statistically significant and were within the experimental error of calculated average peak intensities. Furthermore, room temperature storage may encourage binary complex formation between two SDP. No new products were observed in [Glu/$FeCl_2$] relative to [Glu]/$FeCl_2$. Only enhanced intensities of some peaks, indicating that heating the sample in the presence of $FeCl_2$ enhances the signals of low intensity degradation products, which can aid in their profiling. It is important to caution the formation of some low intensity sugar alcohols such as ethylene glycol, glycerol, erythrol, and ribitol as artifacts during this procedure (see section 3.4.2).

The detailed glucose degradation products listed in Table S3.1 were categorized below based on the number of sugar carbon atoms incorporated in the observed degradation products as confirmed by isotope labelling technique.

C2 sugar degradation products

Ethylene glycol and glycolaldehyde were categorized as C2 sugar fragments (see Table S3.1). The former was detected as $[M]^+$ at *m/z* 116.9638 ($C_2H_5FeO_2$), presumed to be formed by the reduction

of glycolaldehyde (see section 3.2) which was observed as both $[M + Fe^{35}Cl]^+$ at *m/z* 150.9247 ($C_2H_4[^{35}Cl]FeO_2$) and $[M + Fe^{37}Cl]^+$ at *m/z* 152.922 ($C_2H_4[^{37}Cl]FeO_2$). Both C2 SDP were detected in all the model systems, with higher peak intensities when samples were heated with $FeCl_2$.

C3 sugar degradation products

Glycerol, methylglyoxal, and glyceraldehyde were categorized as C3 sugar fragments (see Table S3.1). Glycerol was observed as iron(II) complex in the form of $[M]^+$ at *m/z* 146.9742 ($C_3H_7FeO_3$). Methylglyoxal, one of the most important 1,2-dicarbonyl compounds, was detected as a binary (enediol) iron(II) complex, was observed as $[M + Fe^{35}Cl]^+$and $[M + Fe^{37}Cl]^+$ at *m/z* 234.9464 ($C_6H_8[^{35}Cl]FeO_4$) and *m/z* 236.9441 ($C_6H_8[^{37}Cl]FeO_4$) (see Figure 3.1). The *bis*-methylglyoxal iron(II) complexes were observed in all the model systems. Glyceraldehyde was also observed in all the model systems as a mono-chlorinated iron complexes $[M + Fe^{35}Cl]^+$ and $[M + Fe^{37}Cl]^+$ at *m/z* 180.9355 ($C_3H_6[^{35}Cl]FeO_3$) and *m/z* 182.336 ($C_3H_6[^{37}Cl]FeO_3$), respectively, as well as charge localized iron complex, $[M]^+$ at *m/z* 144.9585 ($C_3H_5FeO_3$).

C4 sugar degradation products

Various C4 SDP were observed including mono- and bis-3-deoxyerythrosone, erythrose, erythritol complexed with dehydrated erythrosone and iron, and hydrated erythrosone (see Table S3.1). Erythrose and its derivatives were detected as various mono and binary iron(II) complexes shown in Figure 3.1, such as $[M + H]^+$, $[M + K]^+$, $[M + Na]^+$, $[M + Fe^{35}Cl]^+$, $[M + Fe^{37}Cl]^+$, and $[M]^+$. The 3-deoxyerythrosone was conjugated with iron(II) in mono-, bis- and as methanolated 3-deoxyerythrosone iron(II) complexes.

Mono 3-deoxyerythrosone was observed at *m/z* 158.9743 ($C_4H_7FeO_3$) and its dehydration product was detected at *m/z* 158.9743 ($C_4H_5FeO_2$). It was also detected as $[M + Fe^{35}Cl]^+$ at *m/z* 194.9505 ($C_4H_8[^{35}Cl]FeO_3$) and $[M + Fe^{37}Cl]^+$ at *m/z* 196.9493 ($C_4H_8[^{37}Cl]FeO_3$) as shown in Table S3.1. Furthermore, 3-deoxyerythrosone was also detected as the potassiated dimer at *m/z* 300.9784 ($C_8H_{14}FeKO_6$), and as well as the counter ligand in various complexes with other glucose degradation products such as glycolaldehyde at *m/z* 265.0019 ($C_7H_{13}FeO_7$), and glyoxylic acid at *m/z* 280.9962 ($C_7H_{13}FeO_8$). The proposed erythrosone derivatives were further confirmed through

isotope labelling technique which indicated the incorporation of four carbon atoms from [$^{13}C_6$-U] glucose. Erythrose was observed in various charged states such as the ions at *m/z* 174.9694 ($C_4H_7FeO_4$), $[M + Fe^{35}Cl]^+$, *m/z* 210.9465 ($C_4H_8[^{35}Cl]FeO_4$), and $[M + Fe^{37}Cl]^+$ at *m/z* 212.9445 ($C_4H_8[^{37}Cl]FeO_4$). In addition, erythritol was detected as an artifact (see section 3.2) at *m/z* 176.9839 ($C_4H_9FeO_4$) and only in [Glu/$FeCl_2$] model system. Erythrosone on the other hand, was detected in the monohydrated form at *m/z* 190.9645 ($C_4H_7FeO_5$) and as the counter ligand of a binary complex with erythritol observed at *m/z* 295.0119 ($C_8H_{15}FeO_8$), as well as its dehydration product $[M + H]^+$ at *m/z* 277.0015 ($C_8H_{13}FeO_7$).

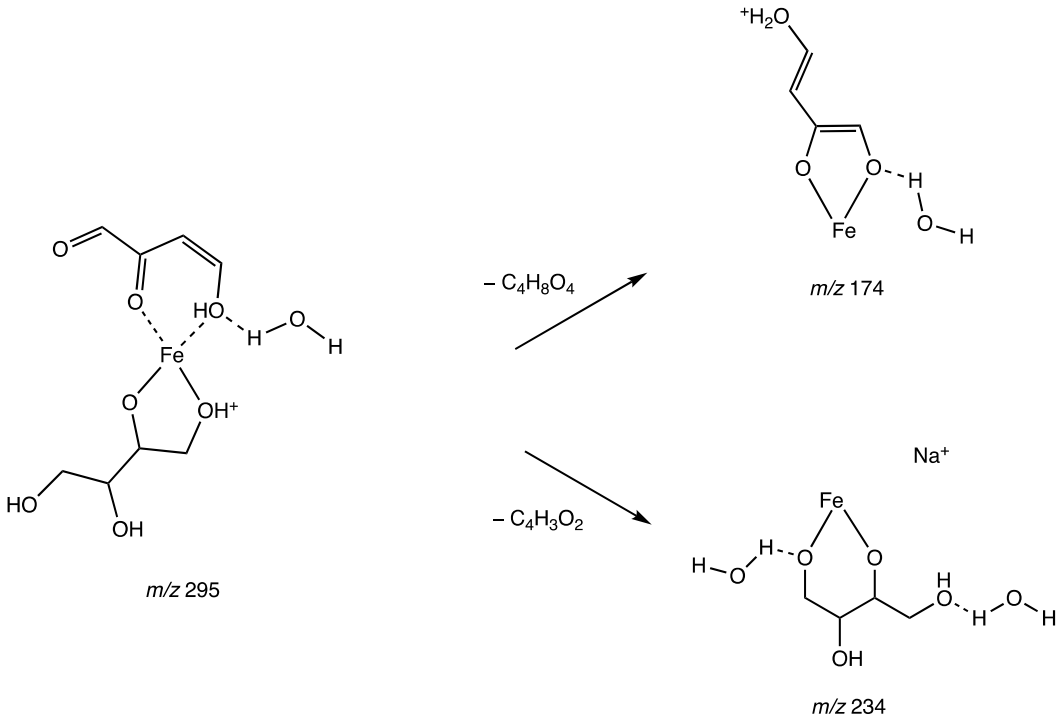

Figure 3.2. Proposed MS/MS fragmentations of the ion at *m/z* 295 observed in the [Glu/$FeCl_2$] model system (see Table 3.3)

Table 3.3. MS/MS fragmentations of the ion at *m/z* 295 ($C_8H_{15}FeO_8$) generated in the [Glu/$FeCl_2$] model system (see Figures. 3.2 and 3.3)

m/z 295	*m/z*	Intensity (%)	Elemental composition	Error ppm[a]	^{13}C-U	Elemental composition	Error ppm
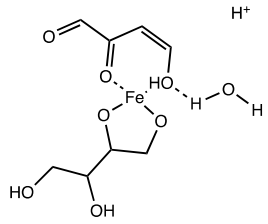	174.9685[b]	100	$C_4H_7FeO_4$	− 4.97	4	$[^{13}C]_4H_7FeO_4$	− 7.2
	234.9888	51.4	$C_4H_{12}FeNaO_6$	3.01	4	$[^{13}C]_4H_{12}FeNaO_6$	37.18
	295.0129	89.3	$C_8H_{15}FeO_8$	4.31	8	$[^{13}C]_8H_{15}FeO_8$	6.49
$[M + H]^+$							

[a]Error (in ppm) in calculating the elemental composition

[b]Base peak

The proposed binary complex observed at *m/z* 295.0119 ($C_8H_{15}FeO_8$) was further studied through analysis of its MS/MS fragmentations as shown in Table 3.3 and Figure 3.2. The predicted erythrosone moiety at $[M]^+$ *m/z* 174.9685 was the base peak and erythritol appeared at *m/z* 234.9888 (51.4%). The proposed MS/MS fragmentation of the ion at *m/z* 295.0119 is shown in Figure 3.3 and the structural information was based on the isotope labelling studies and MS/MS fragmentations. As shown in Table 3.3 both fragments incorporated four carbon atoms from glucose. The proposed mechanism of formation of erythritol is further discussed in section 3.3.2 below.

C5 sugar degradation products

The C5 SDP, ribose, ribosone, and dideoxypentosulose were observed in the form of mono- and binary iron(II) complexes (see Table S3.1). Ribose was detected as a mono iron(II) complex at *m/z* 204.9803 ($C_5H_9FeO_5$), and its dehydration reaction generated the ion at *m/z* 186.9696. In addition, the ribose binary iron (II) complex was found as $[M + H]^+$ at *m/z* 355.0334 ($C_{10}H_{19}FeO_{10}$), as well as its dehydration product $[M + H]^+$ at *m/z* 337.0228 ($C_{10}H_{17}FeO_9$). Ribosone and dideoxypentosulose were detected as their hydrated forms in all the model systems studied. Hydrated ribose was found at *m/z* 220.975 ($C_5H_9FeO_6$) and its dehydration product at *m/z* 202.9647

($C_5H_7FeO_5$). The hydrated dideoxypentosulose was detected as $[M + {}^{35}Cl]^+$ at *m/z* 224.9618 ($C_5H_{10}[{}^{35}Cl]FeO_4$), and as $[M + {}^{37}Cl]^+$ at *m/z* 226.9594 ($C_5H_{10}[{}^{37}Cl]FeO_4$), the latter was also observed at *m/z* 188.9849 ($C_5H_9FeO_4$) and as its dehydration product at *m/z* 170.9743 ($C_5H_9FeO_4$). In terms of the reduced ribose adduct, ribitol, was detected at *m/z* 206.9956.

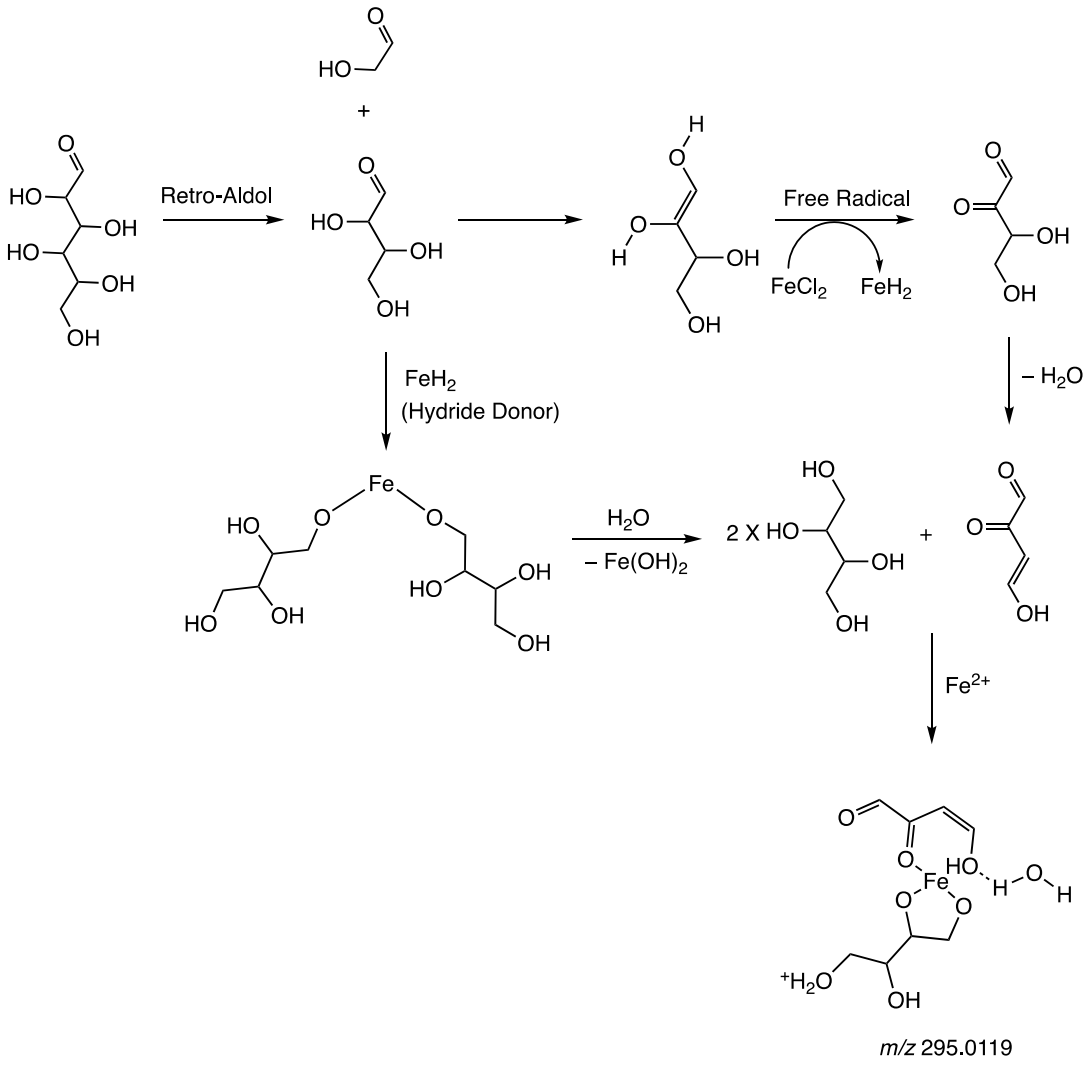

Figure 3.3. Proposed mechanism of formation of erythritol detected as bis (sugar) iron(II) complex at *m/z* 295 (see Table 3.4 and Figure 3.2)

C6 sugar degradation products

The C6 SDP were observed as the most diversified species (see Table S3.1). The 3-deoxyglucosone was the dominant ion in all model systems in the form of various iron(II) complexes. In particular, it was associated with solvent molecules, water and/or methanol, and also afforded dehydration products. The dominant ion peaks were found at *m/z* 270.9677 and *m/z* 272.9648 corresponding to $[M + Fe^{35}Cl]^+$ ($C_6H_{12}[^{35}Cl]FeO_6$) and $[M + Fe^{37}Cl]^+$ ($C_6H_{12}[^{37}Cl]FeO_6$), respectively, and both underwent dehydration to generate ions at *m/z* 252.9569 as $[M + Fe^{35}Cl]^+$ ($C_6H_{10}[^{35}Cl]FeO_5$) and *m/z* 254.9543 as $[M + Fe^{37}Cl]^+$ ($C_6H_{10}[^{37}Cl]FeO_5$). Moreover, 3-deoxyglucosone was detected as a monohydrated iron (II) complex at *m/z* 234.9907 ($C_6H_{11}FeO_6$) and as dehydrated ion at *m/z* 216.9802 ($C_6H_{11}FeO_6$) and also as $[M - 2H_2O]^+$ at *m/z* 198.9695 ($C_6H_9FeO_5$). Furthermore, 3-deoxyglucosone was detected as chlorinated binary iron(II) complexes at *m/z* 451.032 ($C_{12}H_{24}[^{35}Cl]FeO_{12}$) and at *m/z* 453.0276 ($C_{12}H_{24}[^{37}Cl]FeO_{12}$), as well as $[M + H]^+$ at *m/z* 415.0548 ($C_{12}H_{23}FeO_{12}$) in addition to its dehydration products $[M + Fe^{35}Cl - H_2O]^+$ at *m/z* 433.0211 ($C_{12}H_{22}[^{35}Cl]FeO_{11}$), $[M + Fe^{37}Cl - H_2O]^+$ at *m/z* 435.0167 ($C_{12}H_{22}[^{37}Cl]FeO_{11}$), $[M + H - H_2O]^+]^+$ at *m/z* 397.0445 ($C_{12}H_{21}FeO_{11}$), and $[M + H - 2H_2O]^+$ at *m/z* 379.0335 ($C_{12}H_{19}FeO_{10}$).

Mono- and bis-3-deoxyglucosone iron(II) complexes were also observed as various derivatives generated from further dehydration, hydration, and methanolation reactions as mentioned previously. Monomethanolated 3-deoxylglucosone was detected as $[M + Fe^{35}Cl]^+$ at *m/z* 284.9833 ($C_7H_{14}[^{35}Cl]FeO_6$) and $[M + Fe^{37}Cl]^+$ at *m/z* 286.9805 ($C_7H_{14}[^{37}Cl]FeO_6$). Monohydrated and methanolated 3-deoxylglucosone was found to form iron(II) complex at *m/z* 267.0169 ($C_7H_{15}FeO_7$), followed by dehydration steps to form two ions as $[M - H_2O]^+$ at *m/z* 249.0064 ($C_7H_{13}FeO_6$) and $[M - 2H_2O]^+$ at *m/z* 230.9951 ($C_7H_{11}FeO_5$). Dimethanolated adducts of 3-deoxylglucosone were also detected at *m/z* 317.0086 ($C_8H_{18}[^{35}Cl]FeO_7$). Methanolated 3-deoxyglucosone was also observed as binary iron (II) complexes associated with different sugar derivatives. For example, methanolated 3-deoxyglucosone conjugated with a hydrated 3-deoxyglucosone iron(II) complex was detected at *m/z* 465.0476 ($C_{13}H_{26}[^{35}Cl]FeO_{12}$) and at *m/z* 467.0432 ($C_{13}H_{26}[^{37}Cl]FeO_{12}$), along with its dehydration products at *m/z* 447.0364 ($C_{13}H_{24}[^{35}Cl]FeO_{11}$) and at *m/z* 449.0334 ($C_{13}H_{24}[^{37}Cl]FeO_{11}$), respectively. *Bis*-methanolated 3-deoxyglucosone was also observed at *m/z* 479.063 ($C_{14}H_{28}[^{35}Cl]FeO_{12}$), *m/z* 481.057 ($C_{14}H_{28}[^{37}Cl]FeO_{12}$), and *m/z* 443.0862 ($C_{14}H_{27}FeO_{12}$). Hydrated 3-deoxyglucosone associated

with hydrated glucosone as iron(II) complex was also detected at *m/z* 453.0297 ($C_{12}H_{22}FeNaO_{13}$) with its dehydration product observed at *m/z* 435.0201 ($C_{12}H_{20}FeNaO_{12}$). Finally, rhamnose was observed as an iron complex conjugated with glycolaldehyde at *m/z* 309.0276 ($C_9H_{17}FeO_8$).

Comparison of the MS/MS fragmentations of the hydrated (m/z 270) and methanolated (m/z 284) 3-deoxyglucosone iron complexes using 20 eV collision energy

The difference between these two sugar iron complexes is the presence of non-covalently attached solvent molecules, and it is expected that their MS/MS fragmentations to be very similar as shown in Table 3.4 and in Figure S3.3. The data has indeed indicated that in these molecules, 3-deoxyglucosone can be regenerated by the loss of water or methanol as shown in Figure S3.3, which then can undergo further degradation to form reactive C2, C3, C4, and C5 sugar intermediates. These results are consistent with the proposed structure of these ions.

3.4.2. Formation of Sugar Alcohols as Artifacts through Redox Reaction Promoted by $FeCl_2$

In this procedure, sugar alcohol intermediates, such as ethylene glycol, glycerol, erythritol, and ribitol were observed as artifacts of using $FeCl_2$. Of particular interest was the ion observed at $[M + H]^+ = 295$. ESI/qTOF/MS/MS analysis of this ion indicated it was composed of iron complex of erythritol and dehydrated erythrosone as shown in Figure 3.3. A proposed mechanism of formation of erythritol is shown in Figure 3.3. According to this figure $FeCl_2$ through free radical mechanism can oxidize erythrose into eryhthrosone and in the process be converted into iron hydride (FeH_2), the latter, can reduce erythrose into erythritol through hydride transfer mechanism. Iron hydroxide [$Fe(OH)_2$] which is the predicted by- product of this reaction was observed in the reaction mixtures at $[M + H]^+ = 90.9475$ with elemental composition H_3FeO_2 (– 8.1 ppm error).

Table 3.4. Comparison of elemental composition and accurate masses of product ions of *m/z* 270.9663 and *m/z* 284.9883 generated in MRM mode using 20 eV collision energy

Product ions of *m/z* 270.9663						Product ions of *m/z* 284.9883					
m/z	Elemental composition	Error ppm[a]	^{13}C-U	Elemental composition[b]	Intensity (%)	*m/z*	Elemental composition	Error ppm	^{13}C-U	Elemental composition	Intensity (%)
127.0388	$C_6H_7O_3$	− 5.66	6	$[^{13}C]_6H_7O_3$	16	127.0395	$C_6H_7O_3$	− 0.15	6	$[^{13}C]_6H_7O_3$	10.6
145.0492	$C_6H_9O_4$	− 6.09	6	$[^{13}C]_6H_9O_4$	23.4						
150.9243	$C_2H_4[^{35}Cl]FeO_2$	− 4.1	2	$[^{13}C]_2H_4[^{35}Cl]FeO_2$	18.5	150.9237	$C_2H_4[^{35}Cl]FeO_2$	− 8.07	2	$[^{13}C]_2H_4[^{35}Cl]FeO_2$	24.7
						158.9742	$C_4H_7FeO_3$	− 1.61	4	$[^{13}C]_4H_7FeO_3$	11.7
162.969	$C_3H_7FeO_4$	− 2.27	3	$[^{13}C]_3H_7FeO_4$	7.8						
168.9346	$C_2H_6[^{35}Cl]FeO_3$	− 5.23	2	$[^{13}C]_2H_6[^{35}Cl]FeO_3$	40.3	168.935	$C_2H_6[^{35}Cl]FeO_3$	− 2.86	2	$[^{13}C]_2H_6[^{35}Cl]FeO_3$	49.7
174.9685	$C_4H_7FeO_4$	− 4.97	4	$[^{13}C]_4H_7FeO_3$	15.2	174.9689	$C_4H_7FeO_4$	− 2.69	4	$[^{13}C]_4H_7FeO_3$	10.7
						176.984	$C_4H_9FeO_4$	− 5.76	nd[d]	nd	16.1
180.9347	$C_3H_6[^{35}Cl]FeO_3$	− 4.33	3	$[^{13}C]_3H_6[^{35}Cl]FeO_3$	47.7	180.9344	$C_3H_6[^{35}Cl]FeO_3$	− 5.99	3	$[^{13}C]_3H_6[^{35}Cl]FeO_3$	13.8
						184.9291	$C_2H_6[^{35}Cl]FeO_4$	− 7.02	nd	nd	9.8
186.9684	$C_5H_7FeO_4$	− 5.19	5	$[^{13}C]_5H_7FeO_4$	58.9						
192.9347	$C_4H_6[^{35}Cl]FeO_3$	− 4.06	4	$[^{13}C]_4H_6[^{35}Cl]FeO_3$	21.5	192.9347	$C_4H_6[^{35}Cl]FeO_3$	− 4.06	4	$[^{13}C]_4H_6[^{35}Cl]FeO_3$	16.1
198.9454[c]	$C_3H_8[^{35}Cl]FeO_4$	− 3.26	3	$[^{13}C]_3H_8[^{35}Cl]FeO_4$	100	198.9454	$C_3H_8[^{35}Cl]FeO_4$	− 3.26	3	$[^{13}C]_3H_8[^{35}Cl]FeO_4$	15
						198.9695	$C_6H_7FeO_4$	0.65	6	$[^{13}C]_6H_7FeO_4$	21
204.9346	$C_5H_6ClFeO_3$	− 4.31	5	$[^{13}C]_5H_6[^{35}Cl]FeO_3$	7.6						
204.9792	$C_5H_9FeO_5$	− 3.58	5	$[^{13}C]_5H_9FeO_5$	22.3						
210.9454	$C_4H_8ClFeO_4$	− 3.07	4	$[^{13}C]_4H_8[^{35}Cl]FeO_4$	57.2	210.9454[c]	$C_4H_8[^{35}Cl]FeO_4$	− 3.07	4	$[^{13}C]_4H_8[^{35}Cl]FeO_4$	100
						212.961	$C_4H_{10}[^{35}Cl]FeO_4$	− 3.28	nd	nd	9.7
216.9792	$C_6H_9FeO_5$	− 3.39	6	$[^{13}C]_6H_9FeO_5$	24.9	216.9793	$C_6H_9FeO_5$	− 2.93	6	$[^{13}C]_6H_9FeO_5$	24.6
222.9452	$C_5H_8[^{35}Cl]FeO_4$	− 3.8	5	$[^{13}C]_5H_8ClFeO_4$*	3.9						
228.9553	$C_4H_{10}[^{35}Cl]FeO_5$	− 5.73	4	$[^{13}C]_4H_{10}ClFeO_5$	25.7	228.9553	$C_4H_{10}ClFeO_5$	− 5.73	4	$[^{13}C]_4H_{10}[^{35}Cl]FeO_5$	45.3

234.9457	$C_6H_8[^{35}Cl]FeO_4$	− 1.48	6	$[^{13}C]_6H_8ClFeO_4$	10.5	234.9453	$C_6H_8ClFeO_4$	− 3.18	6	$[^{13}C]_6H_8[^{35}Cl]FeO_4$	13.1
234.9892	$C_6H_{11}FeO_6$	− 5.53	6	$[^{13}C]_6H_{11}FeO_6$	26.7	234.9897	$C_6H_{11}FeO_6$	− 3.4	6	$[^{13}C]_6H_{11}FeO_6$	36.7
252.9558	$C_6H_{10}[^{35}Cl]FeO_5$	− 3.21	6	$[^{13}C]_6H_{10}ClFeO_5$	84	252.956	$C_6H_{10}ClFeO_5$	− 2.42	6	$[^{13}C]_6H_{10}[^{35}Cl]FeO_5$	70.9
270.9663	$C_6H_{12}[^{35}Cl]FeO_6$	− 3.24	6	$[^{13}C]_6H_{12}ClFeO_6$	77.9	270.9667	$C_6H_{12}ClFeO_6$	− 1.76	6	$[^{13}C]_6H_{12}[^{35}Cl]FeO_6$	26.5
						284.9823	$C_7H_{14}ClFeO_6$	− 1.85	6	$C[^{13}C]_6H_{14}[^{35}Cl]FeO_6$	53.8

[a]Error (in ppm) in calculating the elemental composition

[b]Error in the calculation of elemental formulas ($^{13}C_6$-U) ranged between 1.23 to 8.15 ppm except for the ion indicated by asterisks where the error was 12.63 ppm

[c]Base peak

[d]nd: not detected

3.4.3. Detection of SDP in Aged Manuka Honey

To confirm the applicability of this fast detection technique in profiling SDP in processed food, manuka honey was chosen as an example. Manuka honey is known to contain various SDP such as α-dicarbony compounds (Yan *et al*., 2019; Marceau and Yaylayan, 2009). Manuka honey was diluted in methanol and mixed with $FeCl_2$ as indicated in the experimental section and analyzed without heating by ESI/qTOF/MS. Most of the SDP identified in aged manuka honey were also reported in the literatures (Marceau and Yaylayan, 2009; Silva *et al*., 2016). Various reactive sugar intermediates with different charge localizations were observed in the manuka honey model system, and the detected metal complexes conjugated with SDP from three to six carbons in length are discussed below and listed in Table S3.2 and Table 3.2.

C3 sugar degradation products

Glyceraldehyde, the only C3 sugar fragment observed in the manuka honey, was detected at *m/z* 144.958 ($C_3H_5FeO_3$) and at *m/z* 180.9354 ($C_3H_6[^{35}Cl]FeO_3$).

C4 sugar degradation products

Eythrose, 3-deoxythrosone, 3-deoxyerythorose, erythritol, and dehydrated erythrosone were observed as C4 sugar degradation products. Erythrose, 3-deoxythreosone, and 3-deoxyerythorose were found as mono iron(II) complexes in the form of $[M]^+$ at *m/z* 174.9683 ($C_4H_7FeO_4$), *m/z* 156.9598 ($C_4H_5FeO_3$), and *m/z* 158.975 ($C_4H_7FeO_3$). Erythritol was detected as a conjugated complex with dehydrated erythrosone at *m/z* 295.0095 ($C_8H_{15}FeO_8$). The details of this ion were discussed above.

C5 sugar degradation products

Ribosone and ribose were observed as the only C5 SDP. Ribosone was detected as a mono iron complex at *m/z* 202.9633 ($C_5H_7FeO_5$). Ribose was found as both mono- and binary iron(II) complexes at *m/z* 204.9785 ($C_5H_9FeO_5$) and at *m/z* 355.0307 ($C_{10}H_{19}FeO_{10}$) including its dehydration product at *m/z* 337.0228 ($C_{10}H_{17}FeO_9$).

C6 sugar degradation products

The 3-deoxyglucosone was detected in the form of mono- and binary iron(II) complexes. Mono-3-deoxyglucosone iron complexes were observed at *m/z* 270.9658 ($C_6H_{12}[^{35}Cl]FeO_6$), *m/z* 272.9635 ($C_6H_{12}[^{37}Cl]FeO_6$) and *m/z* 234.9891 ($C_6H_{11}FeO_6$), along with their dehydration products such as $[M + Fe^{35}Cl - H_2O]^+$ at *m/z* 252.9551 ($C_6H_{10}[^{35}Cl]FeO_5$), $[M + Fe^{37}Cl - H_2O]^+$ at *m/z* 254.9561 ($C_6H_{10}[^{37}Cl]FeO_5$), $[M - H_2O]^+$ at *m/z* 216.9786 ($C_6H_{11}FeO_6$), and $[M - 2H_2O]^+$ at *m/z* 198.9679 ($C_6H_9FeO_4$). The *bis*-(3-DG) hydrated iron complex was detected at *m/z* 451.0275 ($C_{12}H_{24}[^{35}Cl]FeO_{12}$) and at *m/z* 453.0196 ($C_{12}H_{24}[^{37}Cl]FeO_{12}$), along with their dehydration products at *m/z* 433.018 ($C_{12}H_{22}[^{35}Cl]FeO_{11}$) and at *m/z* 415.0514 ($C_{12}H_{23}FeO_{12}$). The 3-deoxyglucosone associated peaks were present at relatively high intensities in the honey model system, followed by ribose adducts and C4 sugar fragments.

3.5. CONCLUSION

Reactive SDP acting as bidentate ligands were converted into stable metal complexes and were easily detected by electrospray ionization/quadrupole time-of-flight mass spectrometry in the positive ion mode. The formation of metal complexes prevented the degradation or polymerization of these reactive SDP and at the same time provided structural features (see Figure 3.1) that were lacking in the free SDP for the development and stabilization of positive charges necessary for their detection under positive ionization mode of ESI-qTOF/MS system.

3.6. REFERENCES

Davídek, T., Robert, F., Devaud, S., Vera, F. A., Blank, I. (2006a). Sugar Fragmentation in the Maillard Reaction Cascade: Formation of Short-Chain Carboxylic Acids, by a New Oxidative α-Dicarbonyl Cleavage Pathway. *Journal of Agricultural and Food chemistry*, 54, 6677–6684.

Davídek, T., Robert, F., Devaud, S., Vera, F. A., Blank, I. (2006b). Sugar Fragmentation in the Maillard Reaction Cascade: Isotope Labeling Studies on the Formation of Acetic Acid by a Hydrolytic β-Dicarbonyl Cleavage Mechanism. *Journal of Agricultural and Food chemistry*, 54, 6667–6676.

Marceau, E. and Yaylayan, V. A. (2009). Profiling of α-Dicarbonyl Content of Commercial Honeys from Different Botanical Origins: Identification of 3,4-Dideoxyglucosone-3-ene (3,4-DGE) and Related Compounds. *Journal of Agricultural and Food chemistry*, 57, 10837–10844.

Nashalian, O. and Yaylayan, V. A. Sugar-conjugated Bis(glycinato)copper (II) Complexes and Their Modulating Influence on the Maillard Reaction. *Journal of Agricultural and Food chemistry*, 63 (2015) 4353–4360.

Page, B. D. and Conacher, B. S. The Pros and Cons of Derivatization in the Chromatographic Determination of Food Additives, in: R. W. Frei (Eds.), Chemical Derivatization in Analytical Chemistry, Springer, US, 1982, pp. 243–292.

Paravisini, L. and Peterson, D. G. (2019). Reactive carbonyl species as key control point for optimization of reaction flavors. *Food chemistry*, 274, 71–78.

Patiny, L. and Borel, A. (2013). ChemCals: A Building Block for Tomorrow's Chemical Infrastructure. *Journal of chemical Information and Modeling*, 53(5), 1223–1228.

Silva, P. M., Gauche, C., Gonzaga, L. V., Costa, A. C. O., Fett, R. (2016). Honey: Chemical composition, stability and authenticity. *Food Chemistry*, 196, 309–323.

Usui, T., Yanagisawa, S., Ohguchi, M., Yoshino, M., Kawabata, R., Kishimoto, J., Arai, Y., Watanabe, H., Hayase, F. (2007). Identification and determination of α-Dicarbonyl Compounds Formed in the Degradation of Sugars. *Bioscience, Biotechnology, and Biochemistry*, 71(10), 2465–2472.

Yaylayan, V. A. (1997). Classification of the Maillard reaction: A conceptual approach. *Trends in Food Science and Technology*, 8, 13–18.

Yan, S., Sun, M., Zhao, L., Wang, K., Fang, X., Wu, L., Xue, X. (2019). Comparison of Differences of α-Dicarbonyl Compounds between Naturally Matured and Artificially Heated Acacia Honey: Their Application to Determine Honey Quality. *Journal of Agricultural and Food chemistry*, 67(46), 12885–12894.

Zheng, J., Ou, J., Ou, S. Alpha-Dicarbonyl Compounds, in: S. Wang (Eds.), Chemical Hazards in Thermal-Processed Foods, Springer, Nature Singapore Pte Ltd., 2019, pp.19–46.

3.7. SUPPLEMENTARY DATA

Table S3.1. Sugar degradation products observed in the [Glu/$FeCl_2$], [Glu]$FeCl_2$ I, [Glu]$FeCl_2$ II, and Glu/$FeCl_2$ model systems[a]

	Structure	$[M]^+/[M + X]^+$ (*m/z*)	Elemental Composition	Error ppm[b]	^{13}C-U	Elemental Composition[c]	Content (%)			
							[Glu/$FeCl_2$]	[Glu]$FeCl_2$ I	[Glu]$FeCl_2$II	Glu/$FeCl_2$
C2	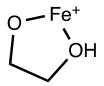 $[M]^+$ Ethylene Glycol	116.9638	$C_2H_5FeO_2$	– 0.78	2	$[^{13}C]_2H_5FeO_2$	0.1 ± 0.03	0.19 ± 0.08	0.22 ± 0.13	0.03
	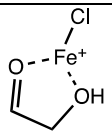 $[M + Cl]^+$ Glycoaldehyde	150.9247	$C_2H_4[^{35}Cl]FeO_2$	1.486	2	$[^{13}C]_2H_4[^{35}Cl]FeO_2$	0.43 ± 0.02	0.15 ± 0.01	0.37 ± 0.19	0.1 ± 0.03
		152.922	$C_2H_4[^{37}Cl]FeO_2$[d]	0.21	2	$[^{13}C]_2H_4[^{37}Cl]FeO_2$	0.13 ± 0.02	0.04 ± 0.01	0.12 ± 0.06	0.03
	Total Content						0.56 ± 0.04	0.19 ± 0.02	0.49 ± 0.26	0.11 ± 0.05
C3	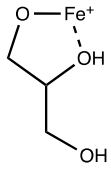 $[M]^+$ Glycerol	146.9742	$C_3H_7FeO_3$	1.777	3	$[^{13}C]_3H_7FeO_3$	0.16 ± 0.02	0.11 ± 0.03	0.23 ± 0.14	0.02
	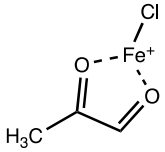	162.925	$C_3H_4[^{35}Cl]FeO_2$	0.465	3	$[^{13}C]_3H_4[^{35}Cl]FeO_2$	0.18 ± 0.08	nd	0.1 ± 0.04	nd[e]

	[M + Cl]$^+$									
	Methyglyoxal									
	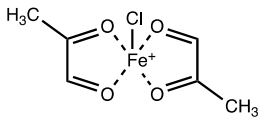	234.9464	$C_6H_8[^{35}Cl]FeO_4$	1.474	6	$[^{13}C]_6H_8[^{35}Cl]FeO_4$	0.24 ± 0.05	0.16 ± 0.03	0.24 ± 0.06	0.16 ± 0.03
		236.9441	$C_6H_8[^{37}Cl]FeO_4$	4.206	6	$[^{13}C]_6H_8[^{37}Cl]FeO_4$	0.12 ± 0.01	0.06 ± 0.01	0.08 ± 0.02	0.06
	[M + Cl]$^+$									
	Bis Methyglyoxal									
	Total Content						0.39 ± 0.01	0.21 ± 0.04	0.32 ± 0.08	0.19 ± 0.06
	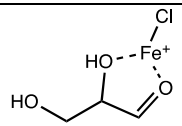	180.9355	$C_3H_6[^{35}Cl]FeO_3$	0.061	3	$[^{13}C]_3H_6[^{35}Cl]FeO_3$	1.01 ± 0.14	0.57 ± 0.16	0.92 ± 0.31	0.44 ± 0.12
		182.9336	$C_3H_6[^{37}Cl]FeO_3$	5.801	3	$[^{13}C]_3H_6[^{37}Cl]FeO_3$	0.32 ± 0.04	0.18 ± 0.04	0.32 ± 0.09	0.16 ± 0.03
	[M + Cl]$^+$									
	Glyceraldehyde									
	[M]$^+$	144.9585	$C_3H_5FeO_3$	2.146	3	$[^{13}C]_3H_5FeO_3$	0.27 ± 0.02	0.38 ± 0.13	0.37 ± 0.14	0.22 ± 0.03
	Total Content						1.6 ± 0.16	1.12 ± 0.07	1.62 ± 0.54	0.83 ± 0.12
C4	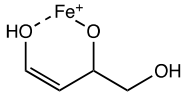	158.9743	$C_4H_7FeO_3$	1.014	4	$[^{13}C]_4H_7FeO_3$	0.57 ± 0.08	0.37 ± 0.1	0.51 ± 0.03	0.34 ± 0.05
	[M]$^+$									
	3-Deoxyerythrosone									
	[M – H_2O]$^+$	140.9627	$C_4H_5FeO_2$	8.488	-	$[^{13}C]_4H_5FeO_2$	0.12 ± 0.03	nd	0.11	0.11 ± 0.02
	[M + Cl]$^+$	194.9505	$C_4H_8[^{35}Cl]FeO_3$	3.278	4	$[^{13}C]_4H_8[^{35}Cl]FeO_3$*	0.28 ± 0.1	nd	0.2	nd
		196.9493	$C_4H_8[^{37}Cl]FeO_3$	5.642	4	$[^{13}C]_4H_8[^{37}Cl]FeO_3$	0.16		0.17	
	Total Content						1.09 ± 0.06	0.37 ± 0.1	0.74 ± 0.09	0. 45 ± 0.07

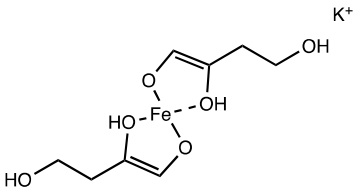 [M + K]⁺ Bis 3-Deoxyerythrosone	300.9784	$C_8H_{14}FeKO_6$	2.368	8	$[^{13}C]_8H_{14}FeKO_6$	0.66 ± 0.14	nd	1.28 ± 0.52	0.7 ± 0.25
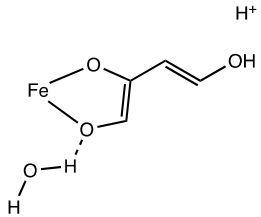 [M + H]⁺ Erythrose	174.9694	$C_4H_7FeO_4$	0.138	4	$[^{13}C]_4H_7FeO_4$	4.98 ± 0.77	9.27 ± 1.74	11.09 ± 1.47	10.78 ± 2.59
[M + Cl]⁺	210.9465	$C_4H_8[^{35}Cl]FeO_4$	2.116	4	$[^{13}C]_4H_8[^{35}Cl]FeO_4$	2.22 ± 0.37	0.48 ± 0.11	0.94 ± 0.3	0.51 ± 0.12
	212.9445	$C_4H_8[^{37}Cl]FeO_4$	6.558	4	$[^{13}C]_4H_8[^{37}Cl]FeO_4$	0.65 ± 0.12	0.16 ± 0.03	0.3 ± 0.1	0.16 ± 0.03
Total Content						7.85 ± 0.58	9.95 ± 1.63	12.34 ± 1.87	11.45 ± 2.44
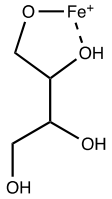 [M]⁺ Erythritol	176.9839	$C_4H_9FeO_4$	– 6.33	nd	nd	0.2 ± 0.3	0.2 ± 0.04	nd	nd

	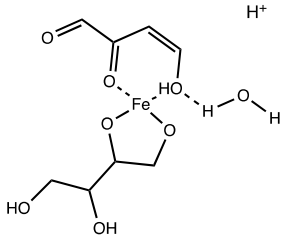	295.0119	$C_8H_{15}FeO_8$	0.9	8	$[^{13}C]_8H_{15}FeO_8$	3.73 ± 1.14	6.15 ± 1.7	9.73 ± 2	9.28 ± 1.5
	$[M + H]^+$									
	Erythritol + Dehydrated Erythrosone									
	$[M + H - H_2O]^+$	277.0015	$C_8H_{13}FeO_7$	1.553	8	$[^{13}C]_8H_{13}FeO_7$	1.61 ± 0.68	1.71 ± 0.6	2.21 ± 0.29	2.7 ± 0.46
	Total Content						4.8 ± 0.64	7.86 ± 2.3	11.94 ± 2.29	11.98 ± 1.97
	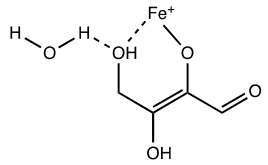	190.9645	$C_4H_7FeO_5$	1.097	4	$[^{13}C]_4H_7FeO_5$	0.1 ± 0.03	nd	0.12 ± 0.06	nd
	$[M]^+$									
	Hydrated Erythrosone									
C5	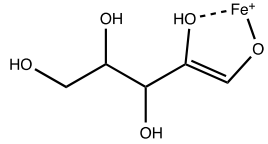	204.9803	$C_5H_9FeO_5$	1.754	5	$[^{13}C]_5H_9FeO_5$	0.91 ± 0.26	0.97 ± 0.43	1.4	1.17 ± 0.19
	$[M]^+$									
	Ribose									
	$[M-H_2O]^+$	186.9696	$C_5H_7FeO_4$	1.199	5	$[^{13}C]_5H_7FeO_4$	1.75 ± 0.28	1.77 ± 0.2	2.17 ± 0.22	1.95 ± 0.12
	Total Content						2.66 ± 0.35	2.73 ± 0.63	2.87 ± 0.48	3.11 ± 0.31
	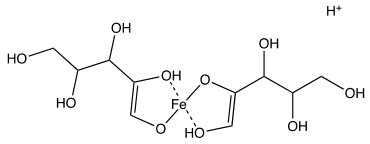	355.0334	$C_{10}H_{19}FeO_{10}$	1.792	10	$[^{13}C]_{10}H_{19}FeO_{10}$	2.13 ± 0.59	5.08 ± 1.13	4.23 ± 0.35	5.29 ± 0.98
	$[M + H]^+$									

Bis Ribose									
$[M + H - H_2O]^+$	337.0228	$C_{10}H_{17}FeO_9$	1.782	10	$[^{13}C]_{10}H_{17}FeO_9$	1.26 ± 0.5	0.84 ± 0.25	0.64± 0.03	0.99 ± 0.24
Total Content						3.39 ± 0.65	5.92 ± 1.38	4.87 ± 0.38	6.28 ± 1.21
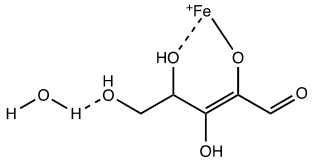	220.975	$C_5H_9FeO_6$	0.656	5	$[^{13}C]_5H_9FeO_6$	0.28 ± 0.11	0.12 ± 0.01	0.29 ± 0.03	0.16 ± 0.09
$[M]^+$									
Hydrated Ribosone									
$[M - H_2O]^+$	202.9647	$C_5H_7FeO_5$	2.018	5	$[^{13}C]_5H_7FeO_5$	0.28 ± 0.09	nd	0.56 ± 0.09	0.26
Total Content						0.55 ± 0.2		0.85 ± 0.12	0.41 ± 0.09
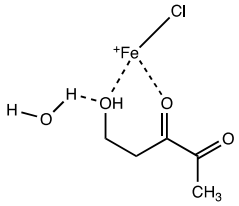	224.9618 226.9594	$C_5H_{10}[^{35}Cl]FeO_4$ $C_5H_{10}[^{37}Cl]FeO_4$	0.428 2.87	5	$[^{13}C]_5H_{10}[^{35}Cl]FeO_4$* nd	0.34 ± 0.21 0.42 ± 0.16	nd	0.23 nd	0.05 ± 0.02 nd
$[M + Cl]^+$									
Hydrated Dideoxypentosulose									
$[M]^+$	188.9849	$C_5H_9FeO_4$	0.666	5	$[^{13}C]_5H_9FeO_4$*	0.32 ± 0.08	0.11 ± 0.03	0.19 ± 0.02	0.1 ± 0.03
$[M - H_2O]^+$	170.9743	$C_5H_7FeO_3$	0.943	5	$[^{13}C]_5H_7FeO_3$	0.2 ± 0.03	0.13 ± 0.04	0.13 ± 0.03	0.13
Total Content						0.94 ± 0.33	0.25 ± 0.09	0.51 ± 0.19	0.27 ± 0.05
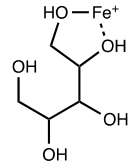	206.9956	$C_5H_{11}FeO_5$	0.07	nd	nd	0.14 ± 0.01	0.06 ± 0.04	0.09	nd
$[M]^+$									
Ribitol									

C6	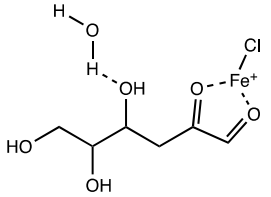	270.9677	$C_6H_{12}[^{35}Cl]FeO_6$	1.908	6	$[^{13}C]_6H_{12}[^{35}Cl]FeO_6$	12.69 ± 1.29	23.25 ± 3.75	23.87 ± 2.4	23.86 ± 4.67
		272.9648	$C_6H_{12}[^{37}Cl]FeO_6$	2.078	6	$[^{13}C]_6H_{12}[^{37}Cl]FeO_6$	3.43 ± 0.27	6.11 ± 0.78	6.48 ± 0.32	6.22 ± 0.93
	$[M + Cl]^+$									
	Hydrated 3-Deoxyglucosone									
	$[M + Cl - H_2O]^+$	252.9569	$C_6H_{10}[^{35}Cl]FeO_5$	1.114	6	$[^{13}C]_6H_{10}[^{35}Cl]FeO_5$	1.95 ± 0.51	1.5 ± 0.31	1.65 ± 0.34	1.26 ± 0.35
		254.9543	$C_6H_{10}[^{37}Cl]FeO_5$	2.478	6	$[^{13}C]_6H_{10}[^{37}Cl]FeO_5$	0.6 ± 0.13	0.47 ± 0.1	0.54 ± 0.16	0.38 ± 0.12
	$[M]^+$	234.9907	$C_6H_{11}FeO_6$	0.829	6	$[^{13}C]_6H_{11}FeO_6$	4.61 ± 1.87	5.06 ± 1.77	5.01 ± 0.41	6.9± 1.32
	$[M - H_2O]^+$	216.9802	$C_6H_9FeO_5$	1.196	6	$[^{13}C]_6H_9FeO_5$	2.39 ± 0.45	1.51 ± 0.32	2.15 ± 0.1	2.3 ± 0.09
	$[M - 2H_2O]^+$	198.9695	$C_6H_7FeO_4$	0.624	6	$[^{13}C]_6H_7FeO_4$	1.73 ± 0.13	1.05 ± 0.27	1.47 ± 0.01	1.63 ± 0.05
	Total Content						27.31 ± 0.74	38.96 ± 2.58	41.11 ± 2.78	42.6 ± 4.61
	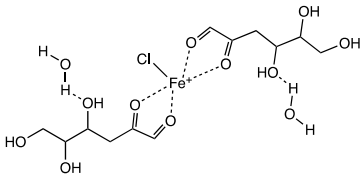	451.032	$C_{12}H_{24}ClFeO_{12}$	3.168	12	$[^{13}C]_{12}H_{24}ClFeO_{12}$	5.46 ± 2.06	19.13 ± 5.61	10.97 ± 1.1	12.4 ± 1.74
		453.0276	$C_{12}H_{24}[^{37}Cl]FeO_{12}$	- 0.03		$[^{13}C]_{12}H_{24}[^{37}Cl]FeO_{12}$	2.07 ± 0.3	5.48 ± 1.44	3.43 ± 0.01	3.71 ± 0.29
	$[M +Cl]^+$									
	Bis Hydrated 3-Deoxyglucosone									
	$[M + Cl - H_2O]^+$	433.0211	$C_{12}H_{22}[^{35}Cl]FeO_{11}$	2.526	12	$[^{13}C]_{12}H_{22}[^{35}Cl]FeO_{11}$	2.43 ± 1.83	nd	nd	nd
		435.0167	$C_{12}H_{22}[^{37}Cl]FeO_{11}$	- 0.81		$[^{13}C]_{12}H_{22}[^{37}Cl]FeO_{11}$	0.96 ± 0.77			
	$[M + H]^+$	415.0548	$C_{12}H_{23}FeO_{12}$	2.184	12	$[^{13}C]_{12}H_{23}FeO_{12}$	1.72 ± 0.68	2.39 ± 1.14	1.61 ± 0.11	2.26 ± 0.78
	$[M + H - H_2O]^+$	397.0445	$C_{12}H_{21}FeO_{11}$	2.95	12	$[^{13}C]_{12}H_{21}FeO_{11}$	1.01 ± 0.39	0.5 ± 0.15	0.32 ± 0.01	0.46 ± 0.12
	$[M +H - 2H_2O]^+$	379.0335	$C_{12}H_{19}FeO_{10}$	1.942	12	$[^{13}C]_{12}H_{19}FeO_{10}$	0.28 ± 0.03	0.28 ± 0.09	0.2 ± 0.01	0.35 ± 0.1
	Total Content						13.16 ± 0.73	27.8 ± 5.68	16.84 ± 0.92	19.19 ± 1.03
		284.9833	$C_7H_{14}[^{35}Cl]FeO_6$	1.639	6	$C[^{13}C]_6H_{14}[^{35}Cl]FeO_6$	14.94 ± 0.18	0.06 ± 0.02	0.63 ± 0.19	0.59 ± 0.01
		286.9805	$C_7H_{14}[^{37}Cl]FeO_6$	2.15	6	$C[^{13}C]_6H_{14}[^{37}Cl]FeO_6$	4.16 ± 0.06	0.09 ± 0.02	0.27 ± 0.05	0.24 ± 0.02

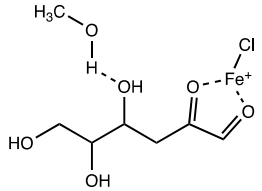									
[M + Cl]⁺									
Methanolated 3-Deoxyglucosone									
Total Content							19.1 ± 0.24	0.15 ± 0.04	0.89 ± 0.24	0.83 ± 0.01
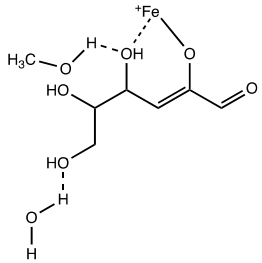									
[M]⁺	267.0169	$C_7H_{15}FeO_7$	0.674	6	$C[^{13}C]_6H_{15}FeO_7$	0.69 ± 0.09	nd	0.17 ± 0.05	0.13
Methanolated and Hydrated 3-Deoxyglucosone									
$[M - H_2O]^+$	249.0064	$C_7H_{13}FeO_6$	0.983	6	$C[^{13}C]_6H_{13}FeO_6$	0.55 ± 0.18	nd	nd	nd
$[M - 2H_2O]^+$	230.9951	$C_7H_{11}FeO_5$	2.124	6	$C[^{13}C]_6H_{11}FeO_5$	0.14 ± 0.01	nd	0.12	0.03
Total Content						1.31 ± 0.16		1.12 ± 0.25	0.08 ± 0.05
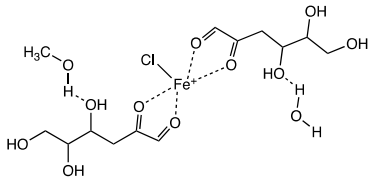	465.0476	$C_{13}H_{26}[^{35}Cl]FeO_{12}$	2.965	12	$C[^{13}C]_{12}H_{26}[^{35}Cl]FeO_{12}$	1.27 ± 0.05	nd	0.232	0.19
	467.0432	$C_{13}H_{26}[^{37}Cl]FeO_{12}$	- 0.14	12	$C[^{13}C_{12}]H_{26}[^{37}Cl]FeO_{12}$	0.44 ± 0.02		0.09 ± 0.03	0.06 ± 0.01
[M + Cl]⁺									
Methanolated 3-Deoxyglucosone + Hydrated 3-Deoxyglucosone									
$[M + Cl - H_2O]^+$	447.0364	$C_{13}H_{24}[^{35}Cl]FeO_{11}$	1.68	12	$C[^{13}C]_{12}H_{24}[^{35}Cl]FeO_{11}$	0.8 ± 0.64	nd	0.29	nd

		449.0334	$C_{13}H_{24}[^{37}Cl]FeO_{11}$	1.545	12	$C[^{13}C]_{12}H_{24}[^{37}Cl]FeO_{11}$	0.54 ± 0.14		0.55 ± 0.01	0.57 ± 0.01
	$[M]^+$	429.0705	$C_{13}H_{25}FeO_{12}$	2.23	12	$C[^{13}C]_{12}H_{25}FeO_{12}$	0.5 ± 0.1	nd	nd	0.06
	Total Content						4.74 ± 1.03		0.7 ± 0.11	0.83 ± 0.01
	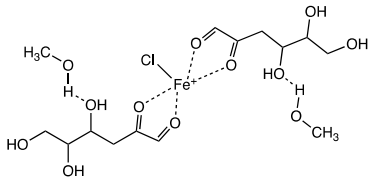	479.063 481.057	$C_{14}H_{28}[^{35}Cl]FeO_{12}$ $C_{14}H_{28}[^{37}Cl]FeO_{12}$	2.356 - 3.98	12	$C_2[^{13}C]_{12}H_{28}[^{35}Cl]FeO_{12}$ nd	0.57 ± 0.23 0.37 ± 0.12	nd	nd	nd
	$[M + Cl]^+$									
	Bis Methanolated 3-Deoxyglucosone									
	$[M + H]^+$	443.0862	$C_{14}H_{27}FeO_{12}$	2.272	12	$C_2[^{13}C]_{12}H_{27}FeO_{12}$	0.72 ± 0.14	nd	nd	nd
	Total Content						1.54 ± 0.49		nd	nd
C4 + C3	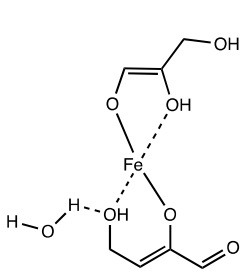	265.0019	$C_7H_{13}FeO_7$	3.132	7	$[^{13}C]_7H_{13}FeO_7$	0.17 ± 0.01	0.16 ± 0.08	0.49 ± 0.17	0.26 ± 0.07
	$[M + H]^+$									
	Hydrated 3-Deoxyerythrosone +									
	Glycoaldehyde									
	$[M + H - H_2O]^+$	246.9911	$C_7H_{11}FeO_6$	2.43	7	$[^{13}C]_7H_{11}FeO_6$	0.19 ± 0.02	0.13 ± 0.04	0.31 ± 0.01	0.21 ± 0.05
	Total Content						0.36 ± 0.03	0.28 ± 0.12	0.41 ± 0.11	0.46 ± 0.12

C6	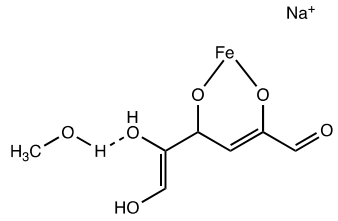	268.9714	$C_7H_{10}FeNaO_6$	3.903	6	$C[^{13}C]_6H_{10}FeNaO_6$	0.63 ± 0.03	1.07 ± 0.09	0.88 ± 0.23	1.05 ± 0.08
	[M + Na]⁺									
	Methanolated 3,4-Dideoxyglycosone-3-ene									
	[M + Na – H_2O]⁺	250.9622	$C_7H_8FeNaO_5$	1.255	6	$C[^{13}C]_6H_8FeNaO_5$	0.1 ± 0.05	0.09 ± 0.02	nd	0.08 ± 0.01
	Total Content						0.72 ± 0.07	1.16 ± 0.11	0.88 ± 0.23	1.13 ± 0.1
C4 + C2	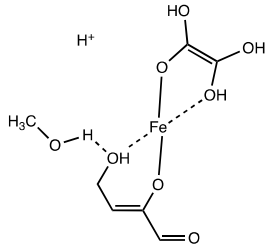	280.9962	$C_7H_{13}FeO_8$	0.767	6	$C[^{13}C]_6H_{13}FeO_8$	0.26 ± 0.1	0.19 ± 0.05	0.26 ± 0.06	0.26
	[M + H]⁺									
	Methanolated 3-Deoxyerythrosone + Glyoxylic Acid									
	[M + H – H_2O]⁺	262.9858	$C_7H_{11}FeO_7$	1.446	6	$C[^{13}C]_6H_{11}FeO_7$	0.1 ± 0.05	0.06 ± 0.01	0.28 ± 0.05	0.18 ± 0.02
	Total Content						0.36 ± 0.06	0.25 ± 0.06	0.54 ± 0.11	0.43 ± 0.02
C6	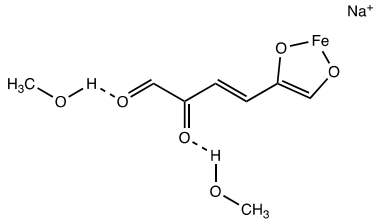	282.9872	$C_8H_{12}FeNaO_6$	3.18	6	$C_2[^{13}C]_6H_{12}FeNaO_6$	0.42 ± 0.12	nd	nd	nd
	[M + Na]⁺									

	Dimethanolated 3,4-Dideoxyglucosone-3,5-diene									
	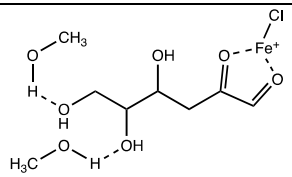 [M + Cl]⁺ Dimethanolated 3-Deoxyglucosone Total Content	317.0086 319.008	$C_8H_{18}[^{35}Cl]FeO_7$ $C_8H_{18}[^{37}Cl]FeO_7$	1.412 5.98	6 6	$C_2[^{13}C]_6H_{18}[^{35}Cl]FeO_7$ $C_2[^{13}C]_6H_{18}[^{37}Cl]FeO_7$	0.66 ± 0.15 0.34 ± 0.01 1.01 ± 0.18	nd	nd	nd
C6 + C3	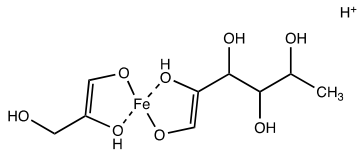 [M + H]⁺ Glycealdehyde + Rhamnose	309.0276	$C_9H_{17}FeO_8$	1.02	9	$[^{13}C]_9H_{17}FeO_8$	1.47 ± 0.29	nd	nd	0.21 ± 0.05
C6 + C4	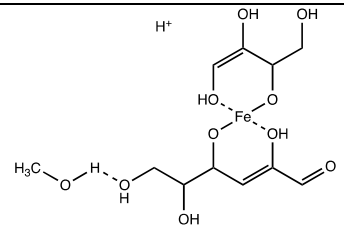 [M + H]⁺ Methanolated 3-Deoxyglucosone + Erythrosone	369.0493	$C_{11}H_{21}FeO_{10}$	2.401	10	$C[^{13}C]_{11}H_{21}FeO_{10}$	0.73 ± 0.14	nd	0.13 ± 0.02	0.11 ± 0.02

C6 + C6	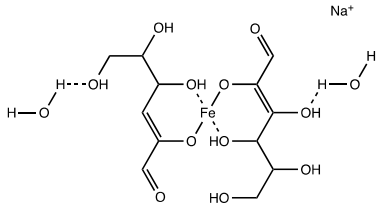	453.0297	$C_{12}H_{22}FeNaO_{13}$	2.323	12	$[^{13}C]_{12}H_{22}FeNaO_{13}$	1.72 ± 0.41	nd	3.35 ± 0.09	3.71 ± 0.29
	[M + Na]$^+$									
	Hydrated 3-Deoxyglucosone + Hydrated Glucosone									
	[M + Na – H_2O]$^+$	435.0201	$C_{12}H_{20}FeNaO_{12}$	0.19	12	$[^{13}C]_{12}H_{20}FeNaO_{12}$	0.96 ± 0.77	nd	0.09	nd
	Total Content						2.36 ± 0.19		3.39 ± 0.14	3.71 ± 0.29

[a]See Table 3.1

[b]Error (ppm) in calculating the elemental composition

[c]Error in the calculation of elemental formulas (^{13}C-U) ranged between 1.64 to 14.4 ppm except for ions indicated by asterisks where the error ranged between 20.56 to 29.08

[d][M + 2] represents chlorine isotopes ^{37}Cl

[e]nd: not detected

Table S3.2. Sugar degradation products identified in aged manuka honey through complexation with $FeCl_2$

	Structure	$[M]^+/[M + X]^+$ (*m/z*)	Elemental Composition	Error ppm[a]
C3	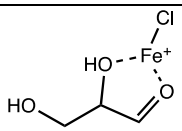	180.9354	$C_3H_6[^{35}Cl]FeO_3$	– 0.46
	$[M + Cl]^+$			
	Glyceraldehyde			
	$[M]^+$	144.958	$C_3H_5FeO_3$	5.596
C4	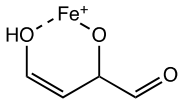	156.9598	$C_4H_5FeO_3$	6.3
	$[M]^+$			
	3-Deoxythreosone			
	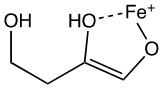	158.975	$C_4H_7FeO_3$	3.389
	$[M]^+$			
	3-Deoxyerythrose			
	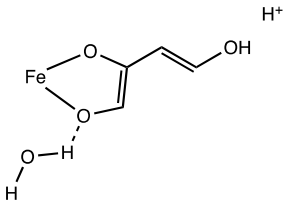	174.9683	$C_4H_7FeO_4$	– 6.12
	$[M + H]^+$			
	Erythrose			
C5	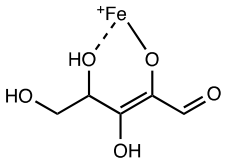	202.9633	$C_5H_7FeO_5$	– 4.85
	$[M]^+$			
	Ribosone			

	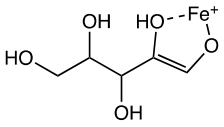	204.9785	$C_5H_9FeO_5$	– 7.00
	$[M]^+$			
	Ribose			
	$[M - H_2O]^+$	186.968	$C_5H_7FeO_4$	– 7.33
C6	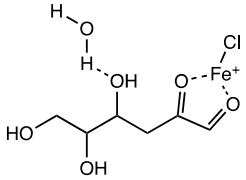	270.9658	$C_6H_{12}[^{35}Cl]FeO_6$	– 5.08
		272.9635	$C_6H_{12}[^{37}Cl]FeO_6$[b]	– 2.66
	$[M + Cl]^+$			
	Hydrated 3-Deoxyglucosone			
	$[M + Cl - H_2O]^+$	252.9551	$C_6H_{10}[^{35}Cl]FeO_5$	– 5.98
		254.9561	$C_6H_{10}[^{37}Cl]FeO_5$	9.56
	$[M]^+$	234.9891	$C_6H_{11}FeO_6$	– 5.96
	$[M - H_2O]^+$	216.9786	$C_6H_9FeO_5$	– 6.15
	$[M - 2H_2O]^+$	198.9679	$C_6H_7FeO_4$	– 7.39
C4 + C4	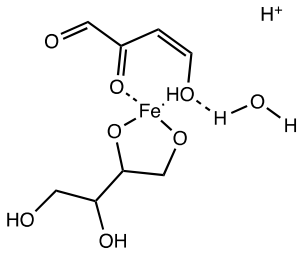	295.0095	$C_8H_{15}FeO_8$	– 7.22
	$[M + H]^+$			
	Erythritol + Dehydrated Erythrosone			
C5 + C5	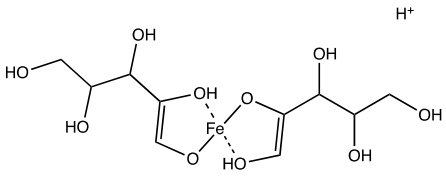	355.0307	$C_{10}H_{19}FeO_{10}$	– 5.80
	$[M + H]^+$			
	Bis Ribose			
	$[M + H - H_2O]^+$	337.0228	$C_{10}H_{17}FeO_9$	1.78

C6 + C6	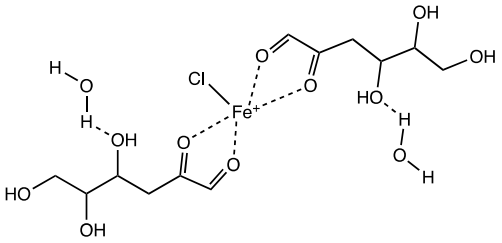	451.0275 453.0196	$C_{12}H_{24}[^{35}Cl]FeO_{12}$ $C_{12}H_{24}[^{37}Cl]FeO_{12}$	– 6.80 – 17.69
	$[M + Cl]^+$			
	Bis Hydrated 3-Deoxyglucosone			
	$[M + Cl - H_2O]^+$	433.018	$C_{12}H_{22}[^{35}Cl]FeO_{11}$	– 4.62
	$[M + H]^+$	415.0514	$C_{12}H_{23}FeO_{12}$	– 5.99

[a]Error (in ppm) in calculating the elemental composition

[b][M + 2] represents chlorine isotope ^{37}Cl

(A) The mass spectrum of glucose solution heated alone and analyzed after addition of $FeCl_2$ - [Glu]$FeCl_2$ II

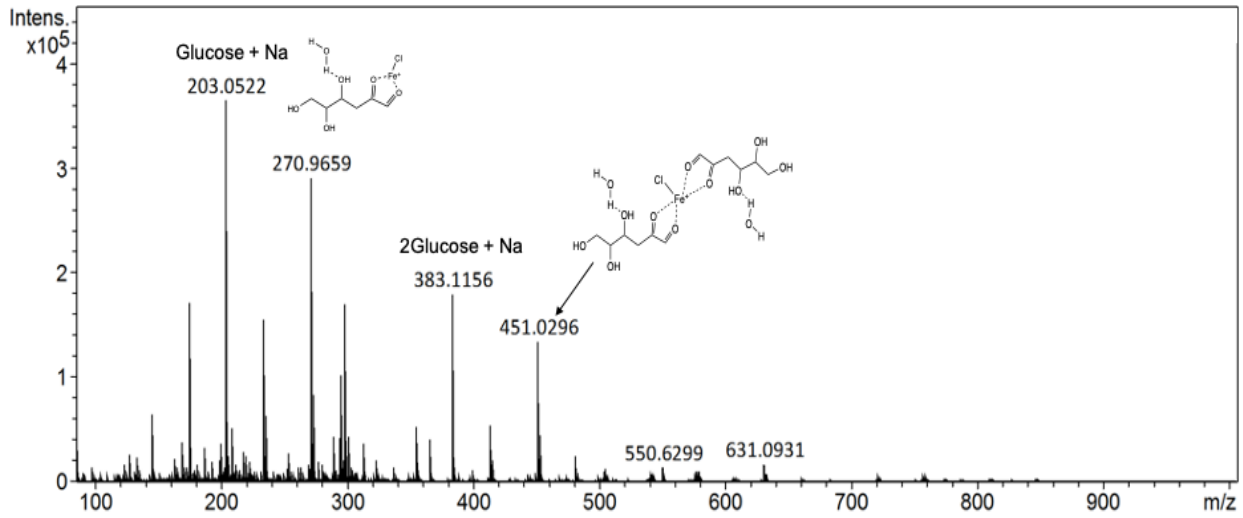

(B) The mass spectrum of heated glucose solution in the presence of $FeCl_2$ - [Glu/$FeCl_2$]

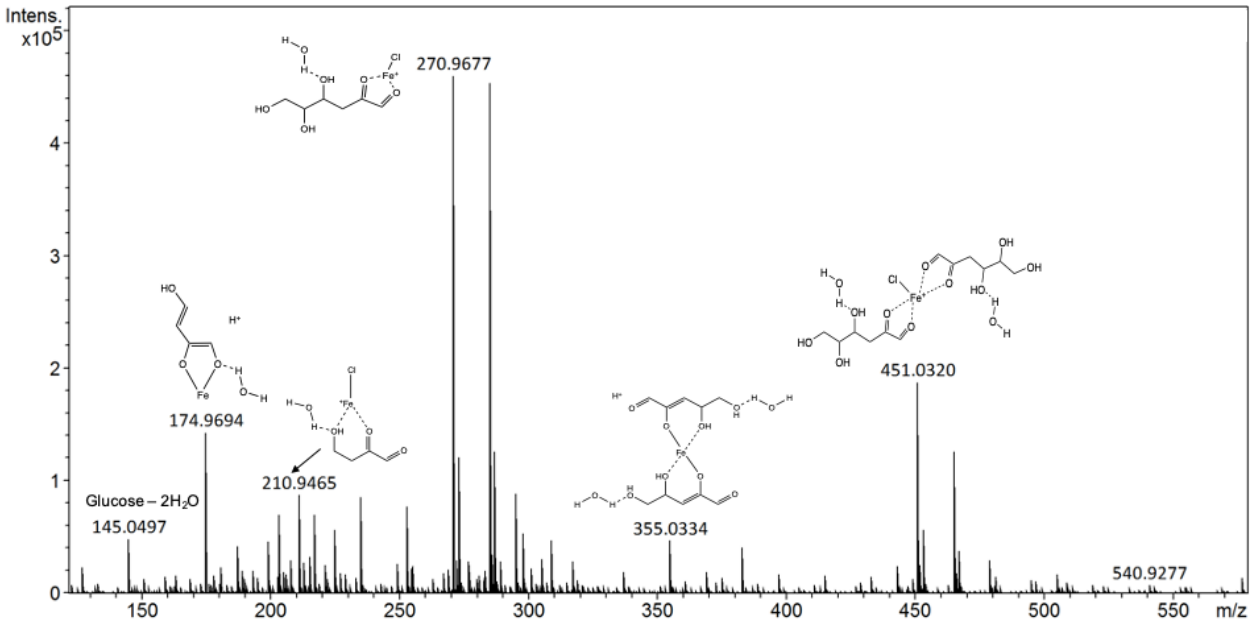

Figure S3.1. ESI/qTOF/MS spectra: (A) Glucose solution heated alone and analyzed after addition of $FeCl_2$ - [Glu]$FeCl_2$ and (B) Heated glucose solution in the presence of $FeCl_2$ - [Glu/$FeCl_2$]

(A) The mass spectrum of heated glucose in the absence of $FeCl_2$ - [Glu]

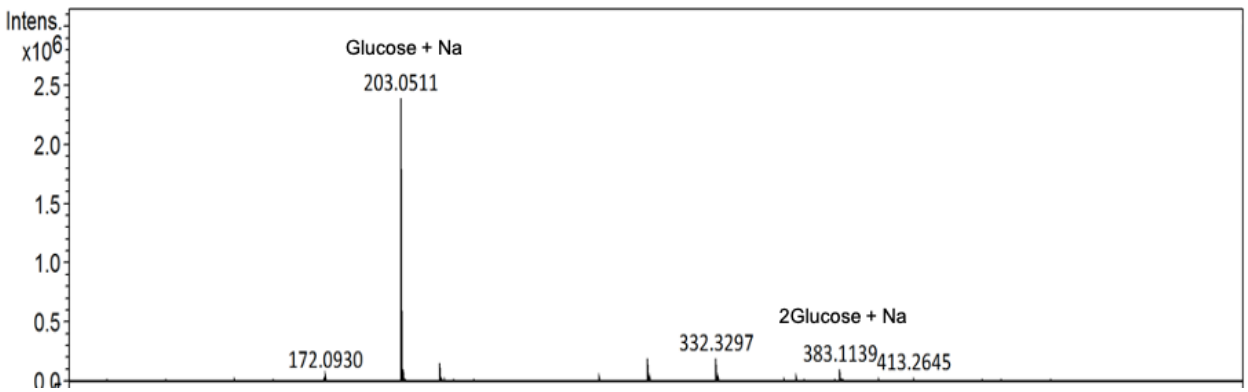

(B) The mass spectrum of unheated glucose in the presence of $FeCl_2$ - Glu/$FeCl_2$

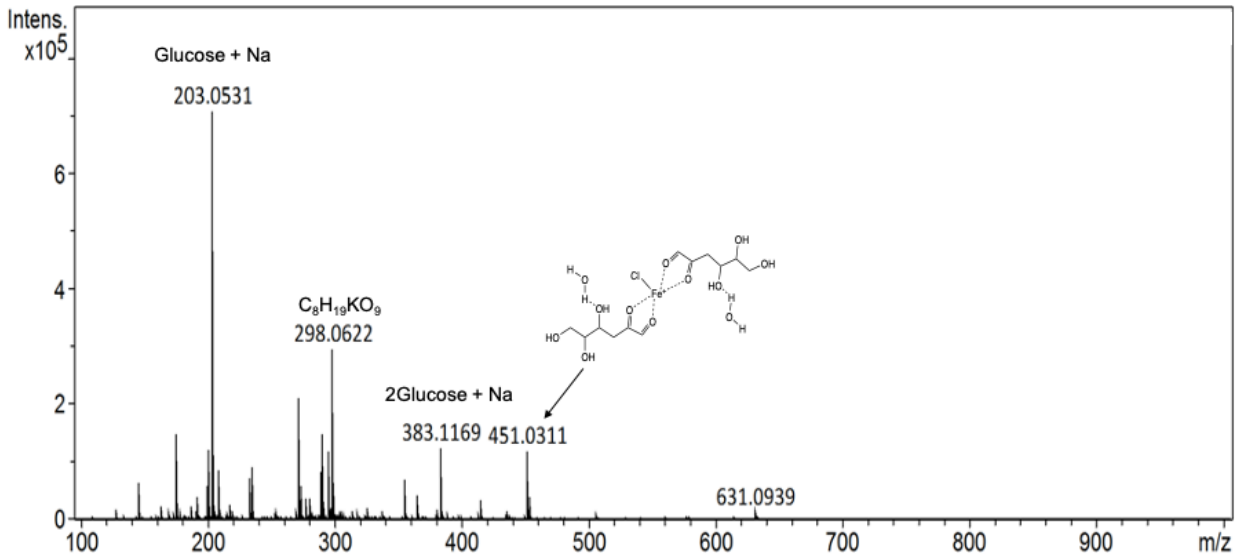

Figure S3.2. ESI/qTOF/MS spectra: (A) Heated glucose in the absence of $FeCl_2$ - [Glu] and (B) Unheated glucose in the presence of $FeCl_2$ - Glu/$FeCl_2$

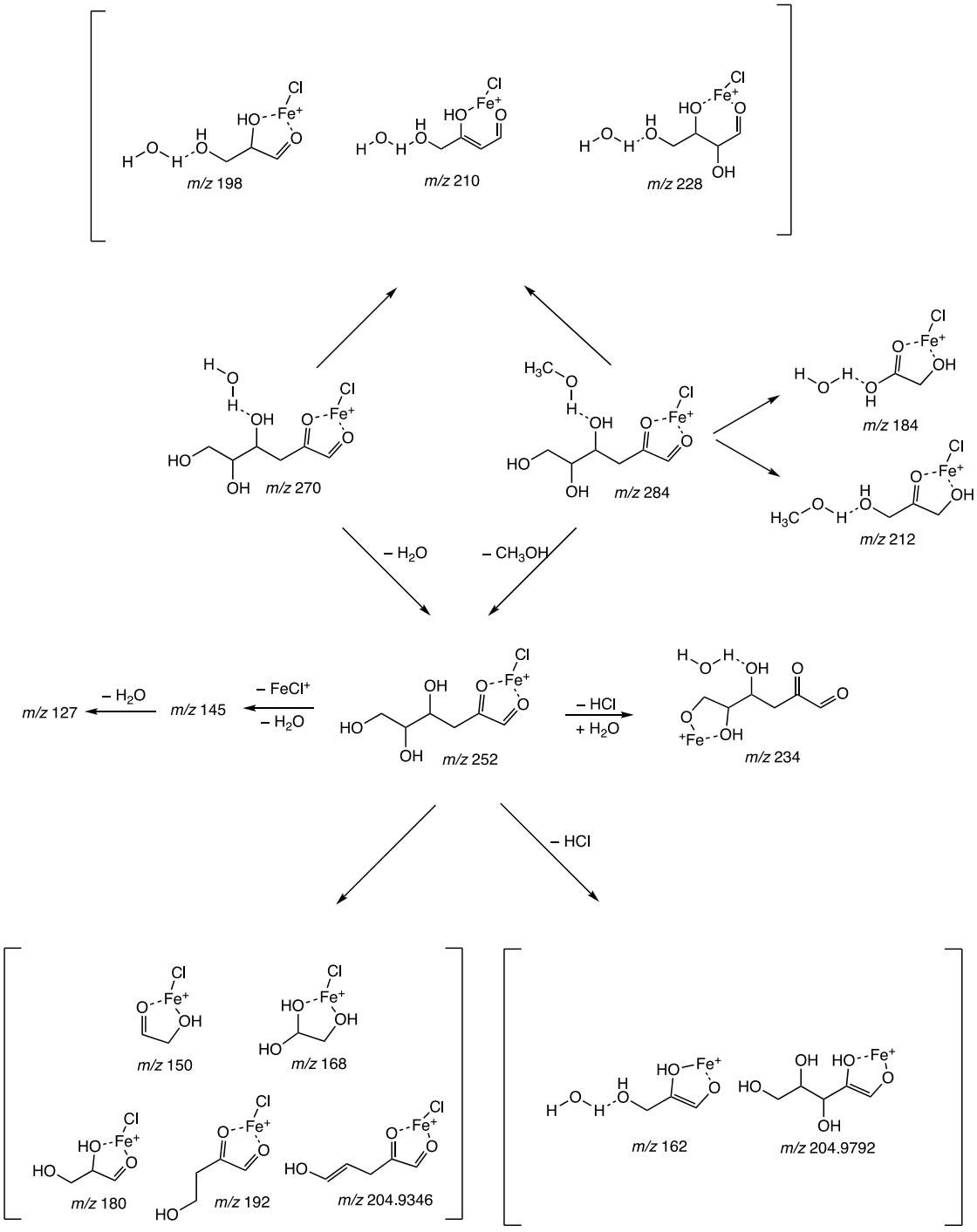

Figure S3.3. Proposed MS/MS fragmentation pathways of the ions at *m/z* 270 and *m/z* 284 (3-deoxyglurcosones) generated in the [Glu/$FeCl_2$] model system (see Table 3.4)

CONNECTING PARAGRAPH

In **chapter 3**, a convenient analytical procedure was developed for profiling of a variety of reactive sugar intermediates or their thermal degradation products having an enediol or α-dicarbonyl moieties complexed with divalent iron using high-resolution electrospray ionization mass spectrometry. In addition, the divalent iron complex technique was utilized for the profiling of sugar degradation products in honey. In **chapter 4**, we further apply this method for the detection of Maillard reaction intermediates in heated alanine and glucose mixture in the presence of divalent iron under the Maillard reaction condition (110 °C, 2 h). **Chapter 4** was published in the *Current Research in Food Science*: Kim, E. S. and Yaylayan, V. (2021). Identification of the Maillard reaction Intermediates as Divalent Iron Complexes in Alanine/Glucose/$FeCl_2$ Model System Using ESI/qTOF/MS/MS and Isotope Labelling Technique, 4(2021), 287−294.

CHAPTER 4

IDENTIFICATION OF THE MAILLARD REACTION INTERMEDIATES AS DIVALENT IRON COMPLEXES IN ALANINE/GLUCOSE/FECL2 MODEL SYSTEM USING ESI/QTOF/MS/MS AND ISOTOPE LABELLING TECHNIQUE

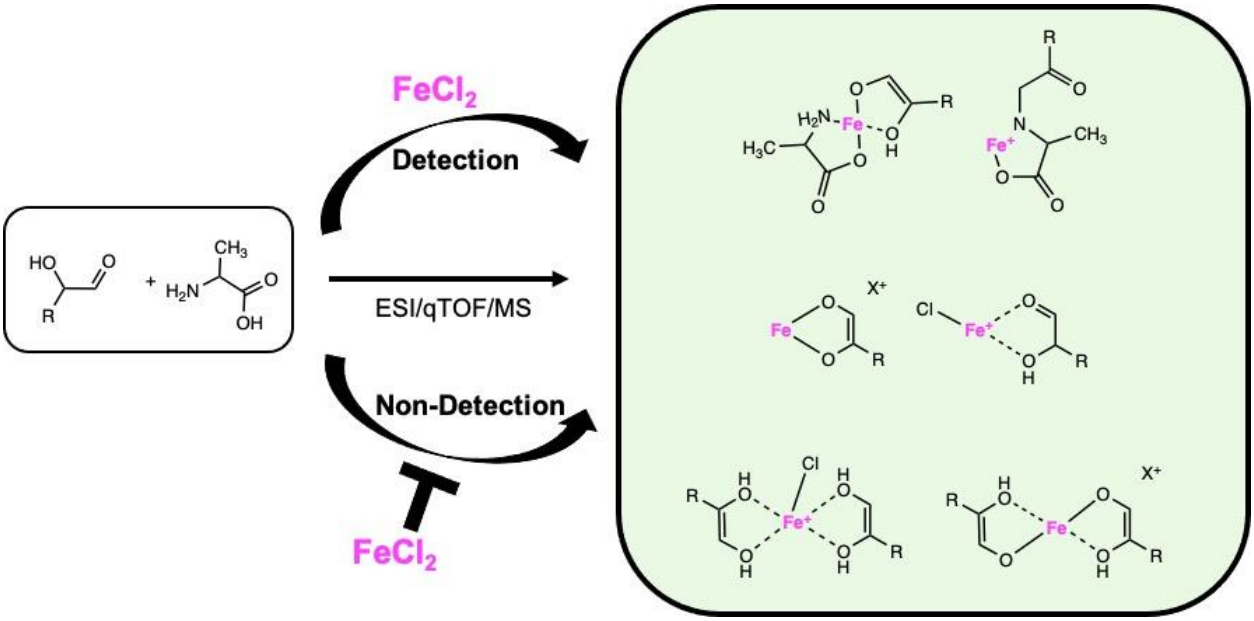

4.1. ABSTRACT

Due to their high reactivities and short half-lives, the detection of Maillard reaction intermediates is relatively difficult to achieve in a single analytical run. In this study, the formation of Maillard reaction intermediates from heated alanine/glucose mixtures (110 °C for 2 h) was investigated through their complexation with divalent iron using electrospray ionization/quadrupole time-of-flight mass spectrometry and isotope labeling techniques. Analysis of the mixtures indicated that this approach allows the simultaneous detection of many important labile and reactive Maillard reaction intermediates along with unreacted alanine and glucose in addition to various other Maillard reaction products, such as glyceraldehyde, erythrose, ribose, acetol, glycolaldehyde, fructosamine, glucosone, osones, deoxyosones, and Amadori products. Some osones and deoxyosones also formed their corresponding Schiff bases with alanine. The above mentioned Maillard reactions intermediates were detected either as binary metal complexes with alanine or with other enediol generating species, including self-complexation adducts and they formed positively charged ions, such as $[M + H]^+$, $[M + Na]^+$, $[M + K]^+$, $[M + Fe^{35}Cl]^+$, and $[M + Fe^{37}Cl]^+$, that can be detected using the positive ionization mode.

KEYWORDS: Amadori rearrangement products, Maillard reaction intermediates, Metal complex, Sugar degradation products, Isotope labelling, ESI/qTOF/MS

4.2. INTRODUCTION

In the thermal processing of food, Maillard reaction intermediates (MRIs), resulting from the degradation of sugars and Amadori rearrangement products (ARPs) are considered important precursors for the development of colour, flavour, and thermally generated toxicants (Yaylayan, 1997).

Analysis of the MRIs and sugar degradation products (SDPs) has been achieved through the use of a range of time-consuming analytical technique (Davidek *et al*., 2002; Gensberger *et al*, 2013; Yaylayan and Huyghues-Despointes, 1994) that required elaborate procedures. Thus, various

systems have been developed for the discrimination and determination of MRIs and ARPs. For example, volatile Maillard reaction products, including ARPs were analyzed by gas chromatography (GC) after derivatization step; however, this system has achieved limited success in analysis of the MRIs and their degradation products due to their low volatility (Yaylayan and Huyghues-Despointes, 1994). High-performance liquid chromatography (HPLC) and high-performance anion-exchange chromatography (HPAEC) based methods reported in the literature (Davidek *et al*., 2002; Gensberger *et al*, 2013) have been focused on the detection of nonvolatile water-soluble compounds of the Maillard products by using either refractive index or UV detection (Davidek *et al*., 2002; Gensberger *et al*, 2013). However, chemical derivatization steps (Davidek *et al*., 2002; Gensberger *et al*, 2013; Page and Conacher, 1982) are essential for their analysis. Infrared (IR) spectroscopy was applied to quantify the open chain or *keto* forms of ARPs (Tamic and Hartman, 1983). In addition, Fourier transformed infrared (FTIR) spectroscopy has provided a more useful method to study the effect of environmental factors, such as pH and temperature, on the concentration of the *keto* form (Wnorowski and Yaylayan, 2003). Furthermore, nuclear magnetic resonance (NMR) spectroscopy, including 1D-^{1}H NMR, ^{13}C-NMR, DEPT-2D ^{1}H-^{1}H and ^{13}C-^{1}H correlational spectroscopy (COSY), and 2D nuclear overhauser enhancement spectroscopy (NOESY) has also been employed for structural elucidation of the ARPs (Kim and Yaylayan, 2020; Li *et al*, 2014).

However, rapid analytical procedures for the simultaneous profiling of MRIs and SDPs have yet to be reported in the literature. In a previous study (Kim and Yaylayan, 2020), a convenient analytical procedure for profiling of SDPs through complexation with divalent metal ions combined with ESI/qTOF/MS was developed and applied for the analysis of honey. Here, we demonstrate the utility of this technique to detect iron (II) catalyzed Maillard reaction intermediates of alanine and glucose using a methodology that most researchers already utilize, the qTOF/LC/MS with additional step of adding metal salts to the solution being analyzed. This step facilitates the detection of not only hard-to-identify and labile products, but at the same time enhances the detection of nitrogen containing MRIs due to the ability of metal ions to coordinate equally with nitrogen and oxygen atoms.

4.3. MATERIALS AND METHODS

4.3.1. Materials and Reagents

L-Alanine (98%), D-glucose, copper(II) chloride ($CuCl_2$) (99.9%) and iron(II) chloride ($FeCl_2$) (99%) were purchased from Sigma-Aldrich Chemical Co. (Oakville, Ontario, Canada). Alanine-3-^{13}C ($^{13}CH_3CH(NH_2)CO_2H$) (98%) and glucose ^{13}C-U ($^{13}C_6H_{12}O_6$) (99%) were purchased from Cambridge Isotope Laboratories (Andover, MI). Liquid chromatography-mass spectrometry (LC-MS)-grade water and methanol (OmniSolv, > 99%) were obtained from VWR International (Mississauga, Ontario, Canada).

4.3.2. Sample Preparation

Test model systems were prepared by heating glucose (18 mg), alanine (9 mg), and $FeCl_2$ (6.4 mg) in methanol or water (1 mL) in tightly closed stainless-steel reactors at 110 ℃ for 2 h. Control model systems were prepared by heating glucose (18 mg) and alanine (9 mg) with or without $CuCl_2$ (5.6 mg) in methanol at 110 ℃ for 2 h. All samples were analyzed at least in two replicates, as indicated in Table 4.1.

Table 4.1. Composition of the model systems[a]

	Model System
Control Model System	Alanine was added to glucose solution and heated in the absence of metal ions - **Ala/Glu**
	Alanine was added to glucose solution and heated in the presence of $CuCl_2$ - **Ala/Glu/$CuCl_2$**
Test Model System	Alanine was added to glucose solution and heated in the presence of $FeCl_2$ - **Ala/Glu/$FeCl_2$**
Isotope Labelling Model System	Alanine was added to glucose ^{13}C-U solution and heated in the presence of $FeCl_2$ - **Ala/Glu[^{13}C-U]/$FeCl_2$**
	Alanine-3-^{13}C was added to glucose solution and heated in the presence of $FeCl_2$ - **Ala[^{13}C-3]/Glu/$FeCl_2$**

[a]All the Model systems were prepared in 1:1 molar ratio and heated at 110 ℃ for 2 h in water or methanol by using a sealed stainless-steel reactor and analyzed in at least two replicates.

4.3.3. ESI/qTOF/MS

The dry reaction mixtures were dissolved in liquid chromatography (LC)-grade methanol to a concentration of 1 mg/mL. The samples were then diluted 10-fold in 10% methanol prior to analysis by ESI/qTOF/MS in positive mode. The ESI/qTOF/MS system was comprised of a Bruker Maxis Impact quadrupole-time-of-flight mass spectrometer (Bruker Daltonics, Bremen, Germany) operated in positive ion mode. Samples (1 μL) were injected directly into ESI/qTOF/MS. Instrument calibration was performed using sodium formate clusters. The electrospray interface settings were the following: nebulizer pressure, 0.6 bar; drying gas, 4 L/min; temperature, 180 °C; and capillary voltage, 4500 V. The scan range was from *m/z* 90 to 1000. Molecular formulae were assigned to all the observed peaks based on their exact *m/z* values by using the online software "ChemCalc" (Institute of Chemical Sciences and Engineering, Lausanne, Switzerland) (Patiny and Borel, 2013). ESI/qTOF/MS/MS was carried out in the multiple reaction monitoring (MRM) mode using a collision energy of 10.0 eV for the ions at *m/z* 252, 342, and 395.

4.3.4. Structural Elucidation

Evidence for the proposed structures was provided through ESI/qTOF/MS analysis of their elemental composition, MS/MS analysis, and isotope-labeling. Furthermore, the incorporation of chlorine and copper in the identified complexes was also confirmed through the detection of their specific isotopic signatures; for chlorine the [M + 2] peaks accounted for ~ 25% of the peak intensity for the M ions, while for copper, the [M + 2] peaks accounted for ~ 30% of the peak intensity. Isotope labelling techniques were also used to generate the corresponding isotopically-labelled counterparts from [^{13}C-U]-labelled glucose and [^{13}C-3]-labelled alanine. The proposed structures represent only one possible isomeric form out of many possible forms for a particular nominal molecular weight, and are based on the most commonly reported structures in the literature.

4.4. RESULTS AND DISCUSSION

Sugar degradation products formed during the Maillard reaction are normally more amenable for analysis under negative ionization mode when analyzed by mass spectrometry (Figure S4.1).

However, the addition of metal ions prior to analysis allows these mixtures to be analyzed in the positive ionization mode (Kim and Yaylayan, 2020) where nitrogen-containing MRPs are also readily detectable (Figure S4.2). Furthermore, the formation of metal complexes can prevent the degradation or further reactions of these reactive intermediates, while at the same time providing structural features for the development of the positive charge necessary for their detection under the positive ionization mode of the ESI/qTOF/MS system (Kim and Yaylayan, 2020). In the presence of metal ions, sugars, amino acids, MRIs (i.e., ARPs), and SDPs (i.e., 3-deoxyglucosone (3-DG), α-hydroxyl carbonyl, and α-dicarbonyl compounds) have the ability to undergo self- or random complexations to generate various metal-centered binary complexes, as listed in Table 4.2. In this study, the alanine/glucose model system was heated at 110 ℃ for 2 h in the presence of metal ions ($FeCl_2$ or $CuCl_2$) in water or methanol and analyzed by ESI/qTOF/MS in the positive ionization mode. The heating of glucose and alanine in the absence of metal ions was also performed as a control, and it was found that the control system also produced alanine Amadori compound with glucose as the dominant product, but with reduced formation of other MRPs, as analyzed under positive ionization mode.

4.4.1. Identification of the Maillard Reaction Intermediates through Complexation with Iron(II) using ESI/qTOF/MS and ESI/qTOF/MS/MS Analysis

The Maillard reaction intermediates obtained (see Tables S4.1 and S4.2) in all the model systems heated at 110 ℃ for 2 h could be categorized into four groups **(1)** metal complexes with free amino acids/and or intact sugars, **(2)** ARPs and their corresponding metal complexes, **(3)** amino sugars and their corresponding metal complexes, and **(4)** reactive SDPs and their metal complexes. Table 4.2 shows selected examples of the above complexes. Previously (Kim and Yaylayan, 2020), we demonstrated that SDPs acting as bidentate ligands were converted into stable metal complexes and were easily profiled by ESI/qTOF/MS in the positive ionization mode. In this study, the alanine/glucose model system was reacted in the presence or absence of $FeCl_2$ or $CuCl_2$ as metal catalysts to enhance the formation of MRPs, and at the same time to provide the metal ions needed for the formation of stable binary complexes for detection by ESI/qTOF/MS in positive ionization mode.

Table 4.2. Possible binary complexes of divalent metal ions with Maillard reaction precursors and intermediates[a]

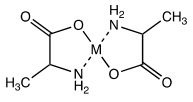 AA-AA	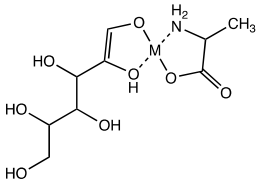 AA-S	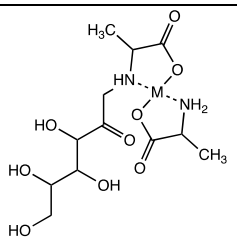 AA-ARP
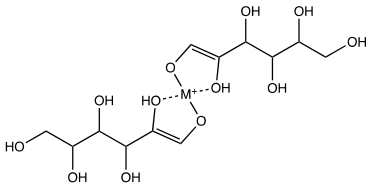 S-S	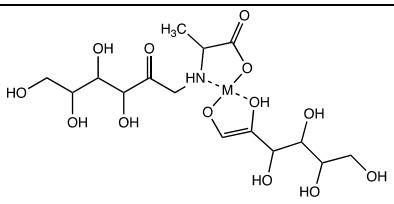 S-ARP	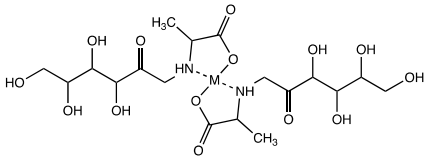 ARP-ARP
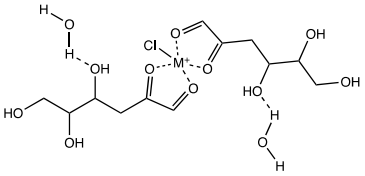 3DG-3DG		

[a]Metal ion = M; Amino acid = AA; Sugar = S; Amadori arrangement product = ARP; 3-deoxyglucosone = 3DG

4.4.2. Detection of intact amino acid and intact sugar metal complexes

The amino acid metal complexes were detected as mono(alaninate)- and *bis*(alaninato)iron(II) complexes and were observed as $[M]^+$ ions at *m/z* values of 143.9744 ($C_3H_6FeNO_2$) and 233.0224 ($C_6H_{13}FeN_2O_4$), respectively. These structures were confirmed by observing the incorporation of one or two carbon atoms from [^{13}C-3] alanine, but no carbon atoms from [^{13}C-U] glucose. Furthermore, mono(alaninate)iron(II) was found to conjugate with glucose to give a signal as $[M + H]^+$ at *m/z* 324.0378 ($C_9H_{18}FeNO_8$) that was found to incorporate six carbon atoms from [^{13}C-U] glucose and one C-3 atom from [^{13}C-3] alanine. The ions corresponding to the free alanine or

glucose were observed as $[M + H]^+$ ions at *m/z* 90.055 ($C_3H_9NO_2$) or $[M + K]^+$ ions at *m/z* 219.0266 ($C_6H_{12}KO_6$) not shown in Tables 2 and S1.

4.4.3. Detection of Amadori rearrangement products

The Amadori product of alanine with glucose, namely *N*-(1-deoxy-D-fructose-1-yl)-L-alanine, was observed as the dominant peak in both the Ala/Glu and the Ala/Glu/$FeCl_2$ model systems, being detected in its free form $[M]^+$ at *m/z* 252.1074 ($C_9H_{18}NO_7$). It was also detected as $[M + Na]^+$ at *m/z* 274.0891 ($C_9H_{17}NNaO_7$) and $[M + K]^+$ at *m/z* 290.0662 ($C_9H_{17}NKO_7$). All structures were confirmed by observing the incorporation of six carbon atoms from [^{13}C-U] glucose and one C-3 atom from [^{13}C-3] alanine. The Amadori product was observed to undergo three dehydration reactions generating $[M - H_2O]^+$ at *m/z* 234.0967 ($C_9H_{16}NO_6$) and $[M - 2H_2O]^+$ at *m/z* 216.0863 ($C_9H_{14}NO_5$), and $[M - 3H_2O]^+$ at *m/z* 198.0755 ($C_9H_{12}NO_4$). In addition, the hydrated form $[M + H_2O]^+$ appeared at *m/z* 270.1175 ($C_9H_{20}NO_8$). All three dehydrated ions and the hydrated ion were found to incorporate six carbon atoms from [^{13}C-U] glucose and one carbon atom from [^{13}C-3] alanine. Furthermore, the ARP was also observed as a *bis*-ARP iron(II) complex as $[M + H]^+$ at *m/z* 557.1295 ($C_{18}H_{33}FeN_2O_{14}$), where twelve carbon atoms from glucose and two C-3 atoms from alanine were incorporated in the structure. In addition, the ARP was able to form iron complexes with alanine at *m/z* 395.0752 ($C_{12}H_{23}FeN_2O_9$) and with glucose at *m/z* 486.0917 ($C_{15}H_{28}FeNO_{13}$), wherein the former was confirmed by detecting the incorporation of six carbons from [^{13}C-U] glucose and two C-3 atoms from [^{13}C-3] alanine, while the latter contained twelve carbon atoms from [^{13}C-U] glucose and one C-3 atoms from [^{13}C-3] alanine (see Tables S1 and 2). In methanol, the methyl ester of the ARP was also observed as the second dominant peak in the form of $[M + H]^+$ at *m/z* 266.1229 ($C_{10}H_{20}NO_7$), as well as $[M + Na]^+$ at *m/z* 288.1059 ($C_{10}H_{19}NNaO_7$). These structures were confirmed by observing the incorporation of six carbon atoms from [^{13}C-U] glucose and one C-3 atom from [^{13}C-3] alanine, respectively. Dehydrated ARP esters were detected as $[M + H - H_2O]^+$ at *m/z* 248.1125 ($C_{10}H_{18}NO_6$) and $[M + H - 2H_2O]^+$ at *m/z* 230.1019 ($C_{10}H_{16}NO_5$) (see Tables 3 and S1). Both dehydrated ions were found to incorporate six carbon atoms from [^{13}C-U] glucose and one carbon atom from [^{13}C-3] alanine.

In addition to glucose, smaller sugars, such as glycolaldehyde, glyceraldehyde, and erythrose, were also found to form Amadori products with alanine as either free or as mono(alaninate)iron(II)

complexes. More specifically, the free glycolaldehyde Amadori compound was observed as $[M + H]^+$ at *m/z* 132.0656 ($C_5H_{10}NO_3$) and the iron complex was observed as $[M]^+$ at *m/z* 185.9848 ($C_5H_8FeNO_3$). Both structures incorporated two carbon atoms from glucose and one C-3 atom from alanine. Similarly, the glyceraldehyde and acetol Amadori compounds of mono(alaninate)iron(II) were observed at *m/z* 215.9958 ($C_6H_{10}FeNO_4$) and *m/z* 200.001 ($C_6H_{10}FeNO_3$), respectively, where three carbon atoms from glucose and one C-3 atom from alanine were incorporated in both structures. Moreover, the erythrose Amadori compound of alanine was also observed at *m/z* 246.0064 ($C_7H_{12}FeNO_5$), which was found to incorporate four carbon atoms from glucose and one C-3 atom from alanine. Interestingly, 3-deoxyerythrosone was observed as the mono(alaninate)iron(II) complex of its Schiff base as $[M]^+$ at *m/z* 227.9968 ($C_7H_{10}FeNO_4$), whereas, 3-deoxyerythrose was observed at *m/z* 230.0117 ($C_7H_{12}FeNO_4$) most likely as the Amadori compound. These structures were confirmed by detecting the incorporation of four carbon atoms from [^{13}C-U] glucose and one C-3 atom from [^{13}C-3] alanine. Similar to the case of 3-deoxyerythrosone, glycerosone (hydroxymethylglyoxal) was also observed as the mono(alaninate)iron(II) complex of its Schiff base at *m/z* 231.9913 ($C_6H_{10}FeNO_5$), where three carbon atoms from glucose and one C-3 atom from alanine were found incorporated. Furthermore, the Schiff base of glucosone with methyl ester of alanine was detected as $[M + H]^+$ at *m/z* 264.1085 ($C_{10}H_{18}NO_7$) along with its dehydrated form $[M + H - H_2O]^+$ at *m/z* 246.0979 ($C_{10}H_{16}NO_6$). Both structures incorporated six carbon atoms from glucose and one C-3 atom from alanine.

Table 4.3. Elemental composition and/or isotope incorporation of the common Maillard reaction intermediates obtained in the Ala/Glu/$CuCl_2$ and Ala/Glu/$FeCl_2$ model system in methanol (see Table S4.1)

Ala/Glu/$CuCl_2$			Ala/Glu/$FeCl_2$			Ala/Glu[^{13}C-U]/$FeCl_2$			Ala[^{13}C-3]/Glu/$FeCl_2$		
[M + X]	Elemental Composition[a]	Error ppm[b]	[M + X]	Elemental Composition	Error ppm	[M + X]	Elemental Composition	Error ppm	[M + X]	Elemental Composition	Error ppm
127.0386	$C_6H_7O_3$	7.235	127.0389	$C_6H_7O_3$	4.873	133.0585	$[^{13}C]_6H_7O_3$	8.629	127.0384	$C_6H_7O_3$	8.809
nd[c]			143.9744	$C_3H_6FeNO_2$	2.747	143.9741	$C_3H_6FeNO_2$	4.831	144.9769	$C_2[^{13}C]H_6FeNO_2$	8.625
180.0862	$C_6H_{14}NO_5$	5.539	180.0867	$C_6H_{14}NO_5$	2.763	186.1058	$[^{13}C]_6H_{14}NO_5$	8.203	180.0857	$C_6H_{14}NO_5$	8.316
162.0757	$C_6H_{12}NO_4$	5.756	162.0761	$C_6H_{12}NO_4$	2.671	168.0952	$[^{13}C]_6H_{12}NO_4$	9.292	162.0751	$C_6H_{12}NO_4$	9.458
144.0645	$C_6H_{10}NO_3$	10.885	144.0656	$C_6H_{10}NO_3$	4.638	150.085	$[^{13}C]_6H_{10}NO_3$	7.977	144.0644	$C_6H_{10}NO_3$	11.579
126.0545	$C_6H_8NO_2$	7.961	126.0543	$C_6H_8NO_2$	3.994	132.0751	$[^{13}C]_6H_8NO_2$	4.032	126.0544	$C_6H_8NO_2$	8.754
202.0701	$C_6H_{13}NNaO_5$	4.74	202.071	$C_6H_{13}NNaO_5$	9.194	nd			202.068	$C_6H_{13}NNaO_5$	5.653
206.1018	$C_8H_{16}NO_5$	5.083	206.102	$C_8H_{16}NO_5$	4.113	212.1201	$C_2[^{13}C]_6H_{16}NO_5$	13.56	207.1042	$C_7[^{13}C]H_{16}NO_5$	9.669
188.0914	$C_8H_{14}NO_4$	4.694	188.0917	$C_8H_{14}NO_4$	3.099	194.1109	$C_2[^{13}C]_6H_{14}NO_4$	7.789	189.0939	$C_7[^{13}C]H_{14}NO_4$	9.19
240.0159	$C_6H_{13}[^{63}Cu]N_2O4$	5.137	233.0224	$C_6H_{13}FeN_2O_4$	0.318	233.0205	$C_6H_{13}FeN_2O_4$	8.471	235.0253	$C_4[^{13}C]_2H_{13}FeN_2O_4$	16.524
242.013	$C_6H_{13}[^{65}Cu]N_2O_4$[d]	9.609	na[e]			na			na		
nd			234.9907	$C_6H_{11}FeO_6$	0.85	241.0089	$[^{13}C]_6H_{11}FeO_6$	7.196	234.9897	$C_6H_{11}FeO_6$	3.427
nd			216.9802	$C_6H_9FeO_5$	1.196	222.9981	$[^{13}C]_6H_9FeO_5$	8.832	nd		
nd			198.9686	$C_6H_7FeO_4$	3.899	204.9872	$[^{13}C]_6H_7FeO_4$	11.24	198.9668	$C_6H_7FeO_4$	12.946
nd			270.9673	$C_6H_{12}[^{35}Cl]FeO_6$	0.45	276.9861	$[^{13}C]_6H_{12}[^{35}Cl]FeO_6$	4.157	270.9652	$C_6H_{12}[^{35}Cl]FeO_6$	− 7.3

nd			272.9646	$C_6H_{12}[^{37}Cl]FeO_6$[f]	1.37	278.983	$[^{13}C]_6H_{12}[^{37}Cl]FeO_6$	− 4.86	272.9629	$C_6H_{12}[^{37}Cl]FeO_6$	− 4.86
252.1074	$C_9H_{18}NO_7$	3.677	252.1082	$C_9H_{18}NO_7$	1.297	258.1266	$C_3[^{13}C]_6H_{18}NO_7$	7.19	253.1099	$C_8[^{13}C]H_{18}NO_7$	7.039
234.0967	$C_9H_{16}NO_6$	4.538	234.0976	$C_9H_{16}NO_6$	1.547	240.1161	$C_3[^{13}C]_6H_{16}NO_6$	7.46	235.0994	$C_8[^{13}C]H_{16}NO_6$	7.304
216.0863	$C_9H_{14}NO_5$	4.154	216.087	$C_9H_{14}NO_5$	1.84	222.1056	$C_3[^{13}C]_6H_{14}NO_6$	7.774	nd[c]		
198.0755	$C_9H_{12}NO_4$	5.719	198.0765	$C_9H_{12}NO_4$	1.68	204.0963	$C_3[^{13}C]_6H_{12}NO_4$	2.263	199.077	$C_8[^{13}C]H_{12}NO_4$	15.008
270.1175	$C_9H_{20}NO_8$	5.152	270.1188	$C_9H_{20}NO_8$	1.08	296.0822	$C_3[^{13}C]_6H_{20}NO_8$	7.22	271.1204	$C_8[^{13}C]H_{20}NO_8$	6.81
274.0891	$C_9H_{17}NNaO_7$	4.274	274.0908	$C_9H_{17}NNaO_7$	0.626	276.1391	$C_3[^{13}C]_6H_{17}NnaO_7$	0.287	275.0087	$C_8[^{13}C]H_{17}NnaO_7$	7.366
290.0662	$C_9H_{17}KNO_7$	6.865	290.0673	$C_9H_{17}KNO_7$	10.657	280.1084	$C_3[^{13}C]_6H_{17}NKO_7$	7.142	291.0641	$C_8[^{13}C]H_{17}NKO_7$	11.9
266.1229	$C_{10}H_{20}NO_7$	4.047	266.1237	$C_{10}H_{20}NO_7$	1.041	272.1423	$C_4[^{13}C]_6H_{20}NO_7$	6.636	267.1255	$C_9[^{13}C]H_{20}NO_7$	6.858
248.1125	$C_{10}H_{18}NO_6$	3.677	248.1132	$C_{10}H_{18}NO_6$	0.856	nd			249.115	$C_9[^{13}C]H_{18}NO_6$	7.094
230.1019	$C_{10}H_{16}NO_5$	4.118	230.1026	$C_{10}H_{16}NO_5$	1.076	236.1213	$C_4[^{13}C]_6H_{16}NO_5$	7.101	231.1046	$C_9[^{13}C]H_{16}NO_5$	6.934
288.1059	$C_{10}H_{19}NNaO_7$	0.075	288.1071	$C_{10}H_{19}NNaO_7$	4.09	294.1239	$C_4[^{13}C]_6H_{19}NnaO_7$	7.312	289.1074	$C_9[^{13}C]H_{19}NnaO_7$	6.491
nd			284.9825	$C_7H_{14}[^{35}Cl]FeO_6$	− 1.15	291.0013	$C[^{13}C]_6H_{14}[^{35}Cl]O_6$	− 5.69	284.9819	$C_7H_{14}[^{35}Cl]FeO_6$	− 3.25
nd			286.9816	$C_7H_{14}[^{37}Cl]FeO_6$	6	nd			nd		
331.0317	$C_9H_{18}[^{63}Cu]NO_8$	3.452	324.0378	$C_9H_{18}FeNO_8$	1.184	330.0561	$C_3[^{13}C]_6H_{18}FeNO_8$	6.704	325.0384	$C_8[^{13}C]H_{18}FeNO_8$	9.656
333.0304	$C_9H_{18}[^{65}Cu]NO_8$	− 1.9	na			na			na		
360.1468	$C_{12}H_{26}NO_{11}$	10.511	360.1503	$C_{12}H_{26}NO_{11}$	0.793	372.1868	$[^{13}C]_{12}H_{26}NO_{11}$	10.87	360.1483	$C_{12}H_{26}NO_{11}$	6.346
342.1387	$C_{12}H_{24}NO_{10}$	3.861	342.14	$C_{12}H_{24}NO_{10}$	0.061	354.1779	$[^{13}C]_{12}H_{24}NO_{10}$	6.717	342.1381	$C_{12}H_{24}NO_{10}$	5.615
324.1281	$C_{12}H_{22}NO_9$	4.184	324.1292	$C_{12}H_{22}NO_9$	0.791	336.1675	$[^{13}C]_{12}H_{22}NO_8$	6.587	324.1275	$C_{12}H_{22}NO_9$	6.036
306.1176	$C_{12}H_{20}NO_8$	4.219	306.1188	$C_{12}H_{20}NO_8$	0.299	318.157	$[^{13}C]_{12}H_{20}NO_7$	6.757	306.1172	$C_{12}H_{20}NO_8$	5.526

nd			288.107	$C_{12}H_{18}NO_7$	4.606	300.1432	$[^{13}C]_{12}H_{18}NO_6$	17.94	288.1051	$C_{12}H_{18}NO_7$	11.2
402.0686	$C_{12}H_{23}[^{63}Cu]N_2O_9$	3.374	395.0752	$C_{12}H_{23}FeN_2O_9$	0.247	401.0928	$C_6[^{13}C]_6H_{23}FeN_2O_9$	6.548	397.0789	$C_{10}[^{13}C]_2H_{23}FeN_2O_9$	7.825
386.058	$C_{12}H_{21}[^{65}Cu]N_2O_8$	1.09	na			na			na		
424.0504	$C_{12}H_{22}[^{63}Cu]N_2NaO_9$	3.54	417.0581	$C_{12}H_{22}FeN_2NaO_9$	2.057	nd			419.0609	$C_{12}[^{13}C]_2H_{21}FeN_2O_9$	13.022
426.0495	$C_{12}H_{22}[^{65}Cu]N_2NaO_8$	– 1.38	na			na			na		
nd			415.054	$C_{12}H_{23}FeO_{12}$	0.257	427.0929	$[^{13}C]_{12}H_{23}FeO_{12}$	2.93	415.0516	$C_{12}H_{23}FeO_{12}$	5.525
nd			451.0306	$C_{12}H_{24}[^{35}Cl]FeO_{12}$	0.63	463.0713	$[^{13}C]12H_{24}[^{35}Cl]FeO_{12}$	1.03	451.0283	$C_{12}H_{24}[^{35}Cl]FeO_{12}$	– 5.02
nd			453.0294	$C_{12}H_{24}[^{37}Cl]FeO_{12}$	3.94	465.0634	$C_{12}H_{24}[^{37}Cl]FeO_{12}$	– 9.62	453.0289	$C_{12}H_{24}[^{37}Cl]FeO_{12}$	2.84
493.0852	$C_{15}H_{28}[^{63}Cu]NO_{13}$	0.945	486.0917	$C_{15}H_{28}FeNO_{13}$	1.425	498.1289	$C_3[^{13}C]_{12}H_{28}FeNO_{13}$	4.748	487.0918	$C_{14}[^{13}C]H_{28}FeNO_{13}$	5.26
495.0837	$C_{15}H_{28}[^{65}Cu]NO_{13}$	0.321	na			na			na		
475.0761	$C_{15}H_{26}[^{63}Cu]NO_{12}$	2.102	468.0798	$C_{15}H_{26}FeNO_{12}$	0.2	480.116	$C_3[^{13}C]_{12}H_{26}FeNO_{12}$	9.79	nd		
564.121	$C_{18}H_{33}[^{63}Cu]N_2O_{14}$	3.155	557.1295	$C_{18}H_{33}FeN_2O_{14}$	2.475	569.1658	$C_6[^{13}C]_{12}H_{33}FeN_2O_{14}$	4.531	559.1323	$C_{16}[^{13}C]_2H_{33}FeN_2O_{14}$	4.526
566.1197	$C_{18}H_{33}[^{65}Cu]N_2O_{14}$	2.248	na			na			na		

[a]All of the ions listed in Table S4.1 are included in this table

[b]Error (in ppm) in calculating the elemental composition

[c]nd: not detected

[d]$[\mathbf{M} + 2]$ represents copper isotopes ^{65}Cu

[e]na: not available

[f]$[\mathbf{M} + 2]$ represents chlorine isotopes ^{37}Cl

4.4.3.1. MS/MS fragmentations of the Amadori product (*m/z* 252), the Amadori product-iron complex (*m/z* 395), and Amadori product of fructosamine (*m/z* 342) using a collision energy of 10 eV

To further confirm the structures of the glucose/alanine Amadori products, the free ARP, the Amadori product of fructosamine, and the ARP(alaninate)iron(II) complex observed at *m/z* 252, 342, and 395, respectively, were analyzed using ESI/qTOF/MS/MS, and the MS/MS fragmentations are shown in Figure 1. It was found that the free ARP and the Amadori product of fructosamine formed with glucose generated a greater number of fragment ions under a 10 eV ionization energy compared to the ARP(alaninate)iron(II) complex (*m/z* 395), which generated only four fragment ions, thereby indicating the stability imparted by metal ion complexation to the Amadori product (see Table 4.4). As shown in Figure 1, the fragment ions are consistent with the proposed structures, and the MS/MS fragmentations of the free ARP (Figure 1A) generated the expected diagnostic ions at *m/z* 88 and 97 (Xing *et al*., 2020) in addition to dehydrated ions at *m/z* 234 and 216 characteristic of the Amadori compounds in positive ionization mode. (Xing *et al*., 2020).

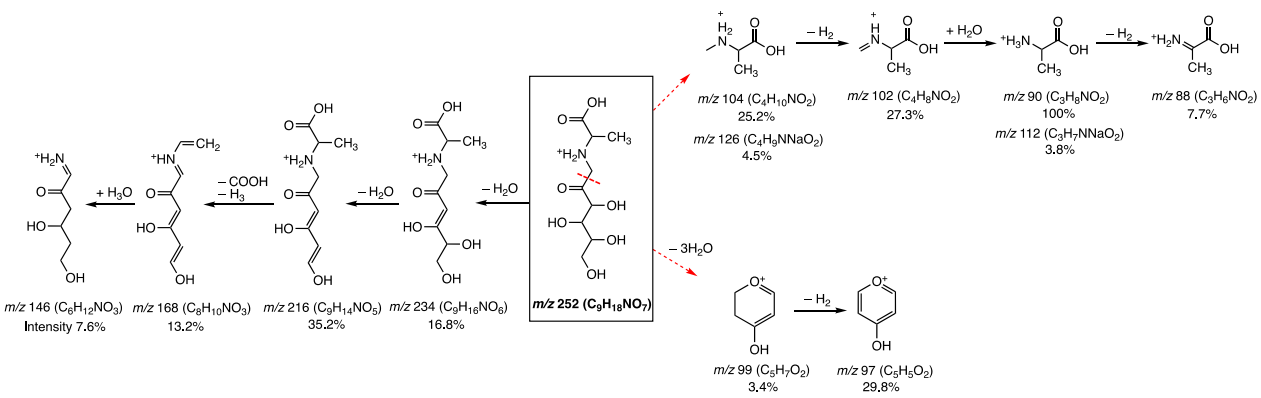

(A) Proposed MS/MS fragmentation pathways of the ions at *m/z* 252

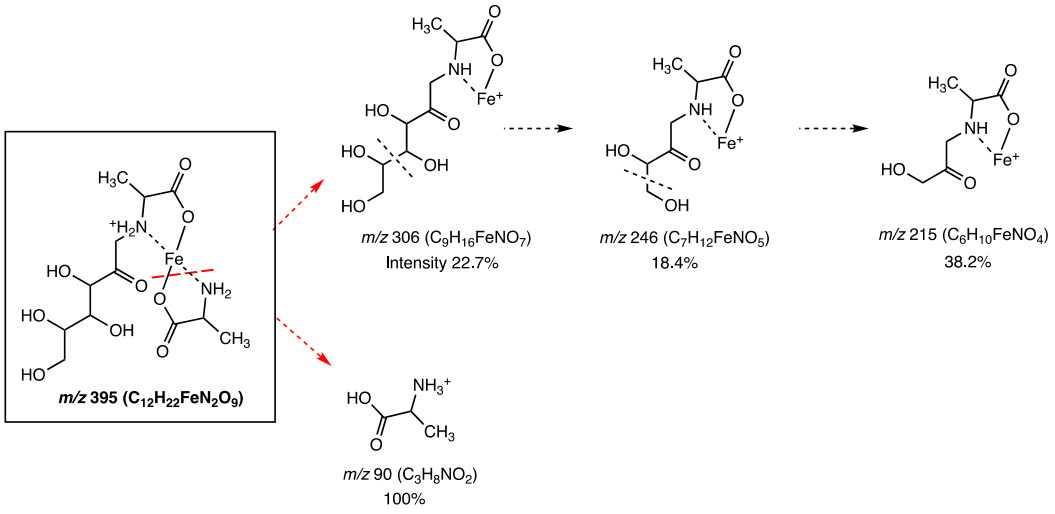

(B) Proposed MS/MS fragmentation pathways of the ions at *m/z* 395

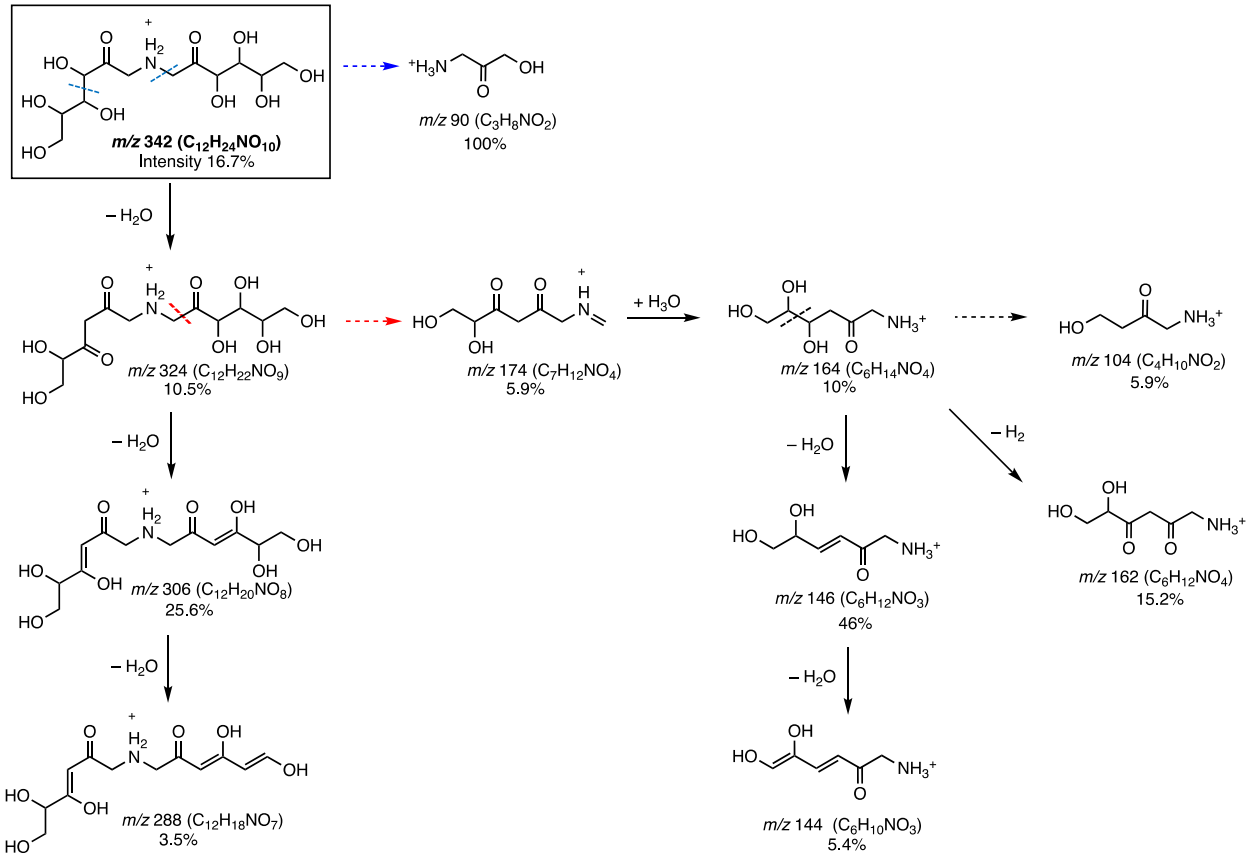

(C) Proposed MS/MS fragmentation pathways of the ions at *m/z* 342

Figure 4.1. Proposed MS/MS fragmentation pathways of **(A)** Amadori products (*m/z* 252), **(B)** Amadori product conjugated (alaninate)iron(II) their derivatives (*m/z* 395), and **(C)** glucose conjugated amino sugar (*m/z* 342) in the Ala/Glu/$FeCl_2$ model system

Table 4.4. MS/MS fragmentations of the ions observed at *m/z* 252, 342, and 395 generated in the Ala/Glu/$FeCl_2$ model system using 10 eV collision energy (see Figure 4.1)

Product ions of *m/z* 252							
Structure	*m/z*	Elemental composition[a]	Error ppm[b]	Glu [^{13}C-U]	Error ppm	Ala [^{13}C-3]	Error ppm
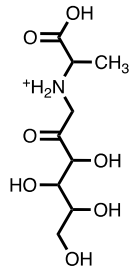	88.0386	$C_3H_6NO_2$	– 14.24	0	– 14.24	nd[c]	
	90.0547[d]	$C_3H_8NO_2$	– 8.92	0	– 8.92	1	9.426
	97.028	$C_5H_5O_2$	– 9.84	5	– 6.16	0	– 9.84
	99.0439	$C_5H_7O_2$	– 7.11	nd		0	– 7.11
	102.0546	$C_4H_8NO_2$	– 8.85	1	8.329	1	7.358
	104.0705	$C_4H_{10}NO_2$	– 6.28	1	– 26.73	1	7.694
	112.0386	$C_3H_7NNaO_2$	10.28	0	– 4.89	1	– 7.10
	126.0546	$C_4H_9NNaO_2$	11.92	nd		nd	
$[M + H]^+ = 252$	146.0804	$C_6H_{12}NO_3$	– 9.02	6	8.2	0	8.34
	168.0651	$C_8H_{10}NO_3$	– 5.76	6	24.72	1	10.332
	216.0866	$C_9H_{14}NO_5$	– 2.77	6	7.774	1	14.68
	234.0984	$C_9H_{16}NO_6$	2.72	6	7.46	1	7.304
Product ions of *m/z* 342							
Structure	*m/z*	Elemental composition	Error ppm	Glu [^{13}C-U]	Error ppm	Ala [^{13}C-3]	Error ppm[a]
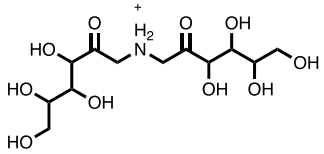	90.0548[d]	$C_3H_8NO_2$	– 7.81	3	28.281	0	8.922
	104.0703	$C_4H_{10}NO_2$	– 8.2	nd		0	8.202
	144.0659	$C_6H_{10}NO_3$	– 1.17	6	7.977	0	11.579
	146.0812	$C_6H_{12}NO_3$	– 3.55	6	8.2	0	8.34
	162.0762	$C_6H_{12}NO_4$	– 2.67	6	9.292	0	9.458
	164.0921	$C_6H_{14}NO_4$	– 1.11	6	– 10.06	0	– 10.26
	174.077	$C_7H_{12}NO_4$	2.11	7	– 16.66	0	2.68
$[M + H]^+ = 342$	288.1094	$C_{12}H_{18}NO_7$	3.72	12	17.941	0	11.2
	306.1207	$C_{12}H_{20}NO_8$	5.91	12	6.757	0	5.526
	324.1319	$C_{12}H_{22}NO_9$	7.54	12	6.587	0	6.036
	342.1424	$C_{12}H_{24}NO_{10}$	6.95	12	6.717	0	5.615
Product ions of *m/z* 395							

Structure	*m/z*	Elemental composition	Error ppm	Glu [^{13}C-U]	Error ppm	Ala [^{13}C-3]	Error ppm[a]
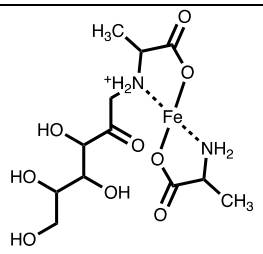	90.0552[d]	$C_3H_8NO_2$	– 3.37	0	8.922	1	9.426
	215.9955	$C_6H_{10}FeNO_4$	– 1.94	3	3.148	1	12.81
	246.0074	$C_7H_{12}FeNO_5$	3.72	4	– 7.61	1	– 6.63
	306.0292	$C_9H_{16}FeNO_7$	5.19	6	7.204	1	8.383
$[M + H]^+ = 395$							

[a]All of the ions listed in Figure 4.1 are included in this table

[b]Error (in ppm) in calculating the elemental composition

[c]nd: not detected

[d]Base peak

4.4.4. Detection of amino sugars and their complexes

Amino sugars, such as fructosamine, are known to be formed in Maillard model systems containing metal ions (Nashalian, O. and Yaylayan, 2015). They originate from the oxidative decarboxylation of glucose-conjugated *bis*(amino acid) metal complexes. As expected, fructosamine was observed only in the metal ion containing model systems, and was detected in the form of $[M + H]^+$ at *m/z* 180.0867 ($C_6H_{14}NO_5$) or as $[M + Na]^+$ at *m/z* 202.071 ($C_6H_{13}NNaO_5$). This ion, which is considered to the Amadori product of ammonia, underwent three characteristic dehydration reactions, generating $[M + H - H_2O]^+$ at *m/z* 162.0757 ($C_6H_{12}NO_4$), $[M + H - 2H_2O]^+$ at *m/z* 144.0645 ($C_6H_{10}NO_3$), and $[M + H - 3H_2O]^+$ at *m/z* 126.0543 ($C_6H_8NO_2$). All of the above ions incorporated six carbon atoms from glucose and no C-3 atoms from alanine, further supporting the proposed structures. Furthermore, the Schiff base formed between fructosamine and the Strecker aldehyde of alanine (acetaldehyde) along with its dehydration product were also observed at *m/z* 206.102 ($C_8H_{16}NO_5$) and *m/z* 188.0917 ($C_8H_{14}NO_4$), respectively. In the iron(II)-containing model systems (see Tables 4.3 and S4.1), both of the above ions incorporated six carbon atoms from glucose and one C-3 atom from alanine. In addition, the Amadori product formed between fructosamine and glucose was observed at *m/z* 342.14 ($C_{12}H_{24}NO_{10}$), along with its three dehydration products at *m/z* 324.1292 ($C_{12}H_{22}NO_9$), *m/z* 306.1188 ($C_{12}H_{20}NO_8$), and *m/z* 288.107

($C_{12}H_{18}NO_7$). Moreover, the monohydrated product $[M + H + H_2O]^+$ was also detected at *m/z* 360.1503 ($C_{12}H_{26}NO_{11}$) (Table 4.3). All the five ions, including the three dehydrated ions and one hydrated ion, were found to incorporate twelve carbon atoms from glucose and no C-3 atoms from alanine.

4.4.5. Detection of iron (II) complexes of sugar degradation products

The formation pathways of the reactive sugar degradation products, such as glyoxal and methylglyoxal, have been previously reported in the literature (Hodge, 1999; Kerler *et al*., 2010) and these compounds are up to 20,000-fold more reactive than glucose (Hofmann, 1999; Usui, 2007). As a result, they have been widely studied in model systems (Marceau and Yaylayan, 2009; Scalone *et al*., 2015; Thornalley, 2005; Wang and Ho, 2012; Yan, *et al*., 2019); however, the profiling of SDPs is complicated due to their high reactivities and their ability to undergo further reactions prior to detection. In this study, it was found that these reactive intermediates, when generated in the presence of metal ions, can act as bidentate ligands and be converted into stable metal complexes that can be easily profiled by ESI/qTOF/MS. Furthermore, the ability of various SDPs to undergo self- or random complexations with other SDPs can generate multiple metal-centered binary complexes of the same SDPs; for example, 3-DG was found to form metal complexes with alanine and with itself, thereby providing several opportunities for their identification. In the absence of metal ions, no SDPs were detected due to their high reactivities. A total of 37 degradation products of the MRIs (including their dehydration products) were detected, as confirmed by isotope labelling experiments (see Tables 4.3 and S4.2). In this context, alanine was able to form iron(II) complexes with SDPs, such as glycolaldehyde, acetol, glyceraldehyde, 3-deoxyerythrose, and erythrose, which were observed at *m/z* 203.9955 ($C_5H_{10}FeNO_4$), *m/z* 218.011 ($C_6H_{12}FeNO_4$), *m/z* 234.0079 ($C_6H_{12}FeNO_5$), *m/z* 248.0247 ($C_7H_{14}FeNO_5$), and *m/z* 264.0162 ($C_7H_{12}FeNO_6$), respectively. Supporting evidence for these structures were provided by observing the incorporation of expected number of carbon atoms from [^{13}C-U] glucose and [^{13}C-3] alanine. For example, the binary complex of glycolaldehyde with alanine was found to incorporate two carbon atoms from glucose and one C-3 atom from alanine, while acetol and glyceraldehyde complexes incorporated three carbon atoms from glucose, and 3-deoxyerythrose and erythrose complexes incorporated four carbon atoms from glucose with one C-3 atom originating from alanine. Glyceraldehyde and erythrose were also observed as their

respective iron(II) complexes. More specifically, the glyceraldehyde complex was detected as $[M]^+$ at *m/z* 144.9585 ($C_3H_5FeO_3$) and erythrose was observed in the form of $[M]^+$, $[M + {}^{35}Cl]^+$, and $[M + {}^{37}Cl]^+$, at *m/z* 174.969 ($C_4H_7FeO_4$), 210.9473 ($C_4H_8[{}^{35}Cl]FeO_4$), and 212.9434 ($C_4H_8[{}^{37}Cl]FeO_4$), respectively. All structures were confirmed by detecting the incorporation of expected number of carbon atoms from [^{13}C-U] glucose. For example, glyceraldehyde and erythrose incorporated three and four carbon atoms from [^{13}C-U] glucose, respectively, but no C-3 carbon atom from alanine. Other SDPs, such as dideoxypentosone, erythritol, 3-deoxy-glucoson-5-one, rhamnose, and ribose were also observed as their corresponding iron(II) complexes. Some of these SDPs, such as dideoxypentosone and 3-deoxy-glucoson-5-one, were associated with solvent molecules, i.e., water or methanol. More specifically, the former was detected in its hydrated form associated with an iron(II) complex to give $[M]^+$ at *m/z* 188.9843 ($C_5H_9FeO_4$), where five carbon atoms from glucose were incorporated, while the latter was observed in its methanolated form complexed with iron(II) to give $[M + Na]^+$ at *m/z* 268.9734 ($C_7H_{10}FeNaO_6$), where six carbon atoms from glucose and no C-3 carbon atoms from alanine were incorporated in the structure. In addition, erythritol was observed as an iron complex with dehydrated erythrosone at *m/z* 295.0113 ($C_8H_{15}FeO_8$). Supporting information was provided by observing the incorporation of eight carbon atoms from [^{13}C-U] glucose (Kim and Yaylayan, 2020). Furthermore, rhamnose was found to form an iron complex with glyceraldehyde and was detected as $[M + H]^+$ at *m/z* 309.0278 ($C_9H_{17}FeO_8$), where nine carbon atoms from glucose was incorporated in the structure. Moreover, pentose was detected as a binary iron(II) complex i.e., $[M + H]^+$ at *m/z* 355.0327 ($C_{10}H_{19}FeO_{10}$), with its dehydrated form $[M + H - H_2O]^+$ at *m/z* 337.0247 ($C_{10}H_{17}FeO_9$). All of the above ions incorporated as expected ten carbon atoms from glucose and no C-3 atoms from alanine (Table S4.2).

Along with ARP, the 3-DG was also found to be one of the highest intensity peaks, and was associated with solvent molecules (i.e., water and/or methanol) in the forms of $[M + Fe^{35}Cl]^+$, $[M + Fe^{37}Cl]^+$, and $[M + H]^+$ in the Ala/Glu/$FeCl_2$ system. The monohydrated 3-DG iron(II) complex was detected in the form of $[M + Fe^{35}Cl]^+$ at *m/z* 270.9673 ($C_6H_{12}[{}^{35}Cl]FeO_6$) and $[M + Fe^{37}Cl]^+$ at *m/z* 272.9646 ($C_6H_{12}[{}^{37}Cl]FeO_6$), and also in the form of $[M + H]^+$ at *m/z* 234.9907 ($C_6H_{11}FeO_6$) (Kim and Yaylayan, 2020). Furthermore, its dehydration peaks were observed as $[M + H - H_2O]^+$ at *m/z* 216.9802 ($C_6H_9FeO_5$) and $[M + H - 2H_2O]^+$ at *m/z* 198.9686 ($C_6H_7FeO_4$) (Table 4.3). All

the five ions corresponding to 3-DG were found to incorporate six carbon atoms form glucose and no carbon atoms from alanine. In addition, 3-DG was detected as a binary iron(II) complex in the form of $[M + Fe^{35}Cl]^+$ at *m/z* 451.0306 ($C_{12}H_{24}[^{35}Cl]FeO_{12}$) and $[M + Fe^{37}Cl]^+$ at *m/z* 453.0294 ($C_{12}H_{24}[^{37}Cl]FeO_{12}$), as well as $[M + H]^+$ at *m/z* 415.054 ($C_{12}H_{23}FeO_{12}$). These structures were found to incorporate twelve carbon atoms from glucose, but no carbon atoms from alanine. Furthermore, 3-DG was also detected as methanolated iron(II) complex corresponding to $[M + Fe^{35}Cl]^+$ at *m/z* 284.9825 ($C_7H_{14}[^{35}Cl]FeO_6$) and $[M + Fe^{37}Cl]^+$ at *m/z* 286.9816 ($C_7H_{14}[^{37}Cl]FeO_6$). These hydrated- and methanolated 3-DG iron(II) complexes were confirmed based on their MS/MS fragmentations (Kim and Yaylayan, 2020), and by observing the incorporation of six carbon atoms from glucose. Moreover, Hydroxymethylfurfural (HMF) was detected as $[M + H]^+$ at *m/z* 127.0389 ($C_6H_7O_3$); both in the presence and absence of iron(II). The peak intensity of HMF in the Ala/Glu/$FeCl_2$ system was at least 2-fold higher than in the Ala/Glu model system (Table 4.3). As expected, the ion observed at *m/z* 127.0389 incorporated six carbon atoms from glucose. Finally, 3-DG was detected also as alanine-iron(II) complex $[M + H]^+$ at *m/z* 306.0274 ($C_9H_{16}FeNO_7$), in addition to its corresponding dehydrated product $[M + H - H_2O]^+$ at *m/z* 288.0174 ($C_9H_{14}FeNO_6$) and $[M + H - 2H_2O]^+$ at *m/z* 270.0067 ($C_9H_{12}FeNO_5$). Furthermore, 3-DG conjugated with mono(alaninate)iron(II) was also observed at *m/z* 342.0044 and *m/z* 344.0026, corresponding to $[M + Fe^{35}Cl]^+$ ($C_9H_{17}Fe[^{35}Cl]NO_7$) and $[M + Fe^{37}Cl]^+$ ($C_9H_{17}Fe[^{37}Cl]NO_7$), respectively (Table S4.2). All the five ions corresponding to 3-DG conjugated with mono(alaninate)iron(II) were found to incorporate six carbon atoms from glucose and one C-3 carbon atom from alanine.

4.5. CONCLUSION

The addition of metal ions to Maillard model systems before heating not only enhances the reaction and generates metal specific products, such as fructosamine, but also stabilizes many of the reactive enediol-containing moieties through the formation of binary metal complexes, which renders them easily detectable by electrospray ionization/quadrupole time-of-flight mass spectrometry (ESI/qTOF/MS).

4.6. REFERENCES

Davidek, T., Clety, N., Aubin, S., Blank, I. (2002). Degradation of the Amadori Compound *N*-(1-Deoxy-D-frutos-1-yl)glycine in Aqueous Model Systems. *Journal of Agricultural and Food chemistry*, 50, 5472–5479.

Hodge, J. E. (1953). Chemistry of Browning Reactions in Model Systems *Journal of Agricultural and Food chemistry*, 1(15), 928–943.

Hofmann, T. (1999). Quantitative studies on the role of browning precursors in the Maillard reaction of pentoses and hexoses with L-alanine. *European Food Research and Technology*, 209, 113–121.

Gensberger, S., Glomb, M. A., Pischetsrider, M. (2013). Analysis of Sugar Degradation Products with α-Dicarbonyl Structure in Carbonated Soft Drinks by UHPLC-DAD-MS/MS. *Journal of Agricultural and Food chemistry*, 61(43), 10238–10245.

Kaufmann, M., Meissner, P. M., Pelke, D., Mügge C., Kroh, L. W. (2016). Structure–reactivity relationship of *Amadori* rearrangement products compared to related ketoses. *Carbohydrate Research*, 428(16), 87–99.

Kerler, J., Winkel, C., Davidek, T., Blank, I. Food Flavour Technology; Basic chemistry and process conditions for reaction flavours with particular focus on Maillard-type reactions (eds Taylor, A. J. and Linforth, S. T., John Wiley & Sons, Wiley-Blackwell, 2010, pp. 51–88.

Kim, E. S. and Yaylayan, V. (2020), Profiling of sugar degradation products through Complexation with Divalent Metal ions coupled with ESI/qTOF/MS/MS analysis. *Current research in food Science*, 3, 268–274.

Nashalian, O. and Yaylayan, V. A. (2015). Sugar-conjugated Bis(glycinato)copper (II) Complexes and Their Modulating Influence on the Maillard Reaction *Journal of Agricultural and Food chemistry*, 63, 4353–4360.

Li, C., Wang, H., Juárez, M., Ruan, E. D. (2014). Structural Characterization of Amadori Rearrangement Product of Glucosylated N^{α}-Acetyl-Lysine by Nuclear Magnetic Resonance Spectroscopy. *International Journal of Spectroscopy*, 1–6.

Page, B. D. and Conacher, B. S. The Pros and Cons of Derivatization in the Chromatographic Determination of Food Additives, in: R. W. Frei (Eds.), Chemical Derivatization in Analytical Chemistry, Springer, US, 1982, pp. 243–292.

Patiny, L. and Borel, A. (2013). ChemCals: A Building Block for Tomorrow's Chemical Infrastructure. *Journal of Chemical Information and Modeling*, 53(5), 1223–1228.

Tamic L. A. and Hartman, K. A. (1983). The Infrared Spectra and Structure of the Amadori Product Formed from Glucose and Glycine. Appl. Spectrosc. 39(4), 591–594.

Wnorowski, A. and Yaylayan, V. A. (2003). Monitoring Carbonyl-Amine Reaction between Pyruvic Acid and α-Amino Alcohols by FTIR Spectroscopy-A Possible Route To Amadori Products. *Journal of Agricultural and Food chemistry*, 51(22), 6537–6543.

Xing, H., Mossine, V. V., Yaylayan, V. (2020). Diagnostic MS/MS fragmentation patterns for the discrimination between Schiff bases and their Amadori or Heyns rearrangement products. *Carbohydrate Research*, 491, 107985–107985.

Usui, T., Yanagisawa, S., Ohguchi, M., Yoshino, M., Kawabata, R., Kishimoto, J., Arai, Y., Watanabe H., Hayase, F. (2007). Identification and determination of α-Dicarbonyl Compounds Formed in the Degradation of Sugars. *Bioscience, Biotechology, and Biochemistry*, 71(10), 2465–2472.

Marceau E. and Yaylayan, V. A. (2009). Profiling of α-Dicarbonyl Content of Commercial Honeys from Different Botanical Origins: Identification of 3,4-Dideoxyglucosone-3-ene (3,4-DGE) and Related Compounds. *Journal of Agricultural and Food chemistry*, 57, 10837–10844.

Scalone, G. L. L., Cucu, T., Kimpe, N. D., Meulenaer, B. D. (2015). Influence of Free Amino Acids, Oligopeptides, and Polypeptides on the Formation of Pyrazines in Maillard Model Systems. Journal of Agricultural and Food chemistry, 63(22), 5364–5373.

Thornalley, P. J. (2005). Dicarbonyl Intermediates in the Maillard Reaction. The New York Academy of Science, 1043, 111–117.

Yan, S., Sun, M., Zhao, L., Wang, K., Fang, X., Wu, L., Xue, X. (2019). Comparison of Differences of α-Dicarbonyl Compounds between Naturally Matured and Artificially Heated Acacia Honey: Their Application to Determine Honey Quality. *Journal of Agricultural and Food chemistry*, 67(46), 12885–12894.

Yaylayan, V. A. (1997). Classification of the Maillard reaction: A conceptual approach. *Trends Food Science and Technology*, 8, 13–18.

Yaylayan, V. A. and Huyghues-Despointes, A. (1994). Chemistry of Amadori Rearrangement Products: Analysis, Synthesis, Kinetics, Reactions, and Spectroscopic Properties. *Critical Reviews in Food Science and Nutrition,* 34(4), 321–369.

Wang Y. and Ho, C. T. (2012). Flavour chemistry of methylglyoxal and glyoxal. *Chemical Society Reviews*, 41, 4140–4149.

4.7. SUPPLEMENTARY DATA

Table S4.1. Common Maillard reaction intermediates obtained in the Ala/Glu, Ala/Glu/$CuCl_2$, and Ala/Glu/$FeCl_2$ model system[a] (see Table 4.3)

Structure	Elemental Composition[b]	Relative Intensity (%)			
		Ala/Glu	Ala/Glu/$CuCl_2$	Ala/Glu/$FeCl_2$	
		Methanol	Methanol	Methanol	Water
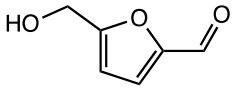 $[M^c + H]^+ = 127$	$C_6H_7O_3$	1.5	2.3 ± 0.55	3.8 ± 0.8	3.05 ± 1.45
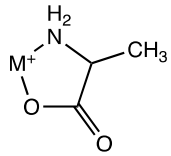 $[M]^+ = 143$	$C_3H_6M^dNO_2$	na[e]	nd[f]	0.65 ± 0.15	0.7 ± 0.5
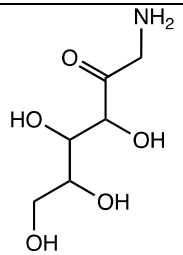 $[M + H]^+ = 180$	$C_6H_{14}NO_5$	nd	1.8 ± 0.45	8.75 ± 2.05	1.5 ± 0.5
$[M + H - H_2O]^+ = 162$	$C_6H_{12}NO_4$	nd	2 ± 0.95	5.75 ± 0.45	1.9 ± 0.9

$[M + H - 2H_2O]^+ = 144$	$C_6H_{10}NO_3$	nd	0.7 ± 0.35	1 ± 0.2	0.75 ± 0.35
$[M + H - 3H_2O]^+ = 126$	$C_6H_8NO_2$	nd	0.7 ± 0.25	0.85 ± 0.05	0.4 ± 0.2
$[M + Na]^+ = 202$	$C_6H_{13}NNaO_5$	nd	0.5 ± 0.1	0.35 ± 0.05	nd
Total Relative Intensity			5.5 ± 1.4	16.7 ± 2.3	4.55 ± 1.95
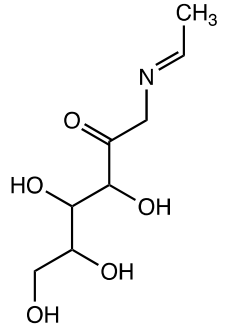	$C_8H_{16}NO_5$	nd	1.9 ± 0.65	0.6 ± 0.1	2.35 ± 0.65
$[M + H]^+ = 206$					
$[M + H]^+ - H_2O = 188$	$C_8H_{14}NO_4$	nd	6.1 ± 4.05	3.25 ± 1.05	8 ± 2.3
Total Relative Intensity			7.9 ± 4.7	3.85 ± 1.15	10.35 ± 2.95
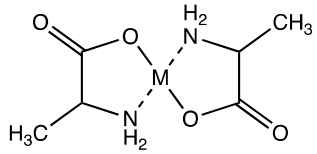	$C_6H_{13}MN_2O_4$	na	0.5 ± 0.1	3.8 ± 0.5	2.8 ± 1.5
$[M + H]^+$ (Fe = 233, ^{63}Cu = 240)					
$[M + H]^+ = 242$	$C_6H_{13}[^{65}Cu]N_2O_4$[g]	na	0.4 ± 0.05	na	na
Total Relative Intensity			0.9 ± 0.15	3.8 ± 0.5	2.8 ± 1.5

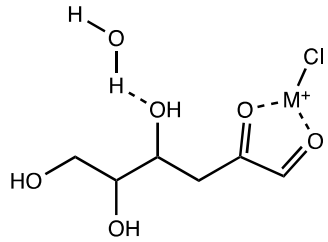	$C_6H_{12}[^{35}Cl]MO_6$	na	nd	7.2 ± 1.1	6.7 ± 1.7
$[M + {}^{35}Cl]^+ = 270$					
$[M + {}^{37}Cl]^+ = 272$	$C_6H_{12}[^{37}Cl]MO_6$[h]	na	nd	2.4 ± 0.5	2 ± 0.4
$[M + H]^+ = 234$	$C_6H_{11}MO_6$	na	nd	4.8 ± 0.2	7.3 ± 1.6
$[M + H - H_2O]^+ = 216$	$C_6H_9MO_5$	na	nd	1.65 ± 0.35	4.3 ± 1.2
$[M + H - 2H_2O]^+ = 198$	$C_6H_7MO_4$	na	nd	1.25 ± 0.15	2.1 ± 0.6
Total Relative Intensity				17.3 ± 0.9	22.4 ± 1.3
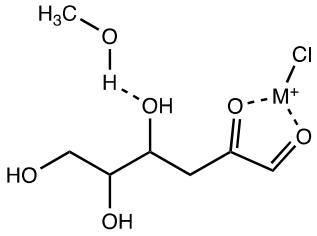	$C_7H_{14}[^{35}Cl]MO_6$	na	nd	0.25 ± 0.5	nd
$[M + {}^{35}Cl]^+ = 284$					
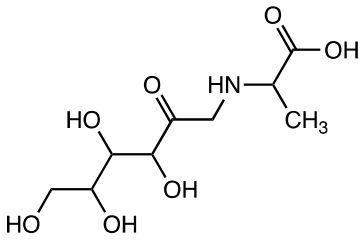	$C_9H_{18}NO_7$	100	84.9 ± 15.1	32.6 ± 1.3	93.45 ± 6.55
$[M + H]^+ = 252$					

$[M + H - H_2O]^+ = 234$	$C_9H_{16}NO_6$	71.7	87.5 ± 12.5	22.5 ± 10.25	81.15 ± 18.85
$[M + H - 2H_2O]^+ = 216$	$C_9H_{14}NO_5$	27	20.1 ± 10.1	14 ± 5.6	29.1 ± 6.9
$[M + H - 3H_2O]^+ = 198$	$C_9H_{12}NO_4$	0.8	0.7 ± 0.5	0.6 ± 0.05	3.25 ± 1.35
$[M + H + H_2O]^+ = 270$	$C_9H_{20}NO_8$	0.2	1.6	16.2 ± 1.1	5.65 ± 0.45
$[M + Na]^+ = 274$	$C_9H_{17}NNaO_7$	51	19.5 ± 10.7	1.5	12.85 ± 9.65
$[M + K]^+ = 290$	$C_9H_{17}KNO_7$	4	4.3 ± 3.35	0.3 ± 0.1	2.65 ± 2.15
Total Relative Intensity		254.7	217.7 ± 0.5	87.6 ± 18.1	228.1 ± 31.9
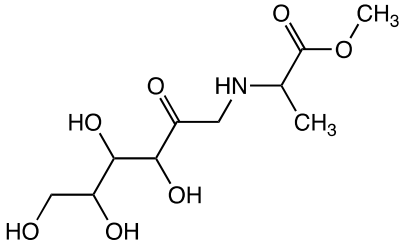	$C_{10}H_{20}NO_7$	7	38.1 ± 12.55	44.7 ± 22.75	nd
$[M + H]^+ = 266$					
$[M + H - H_2O]^+ = 248$	$C_{10}H_{18}NO_6$	10.5	64.1 ± 18.55	74.2 ± 25.8	nd
$[M + H - 2H_2O]^+ = 230$	$C_{10}H_{16}NO_5$	8	55.6 ± 21.35	50.7 ± 16.35	nd
$[M + Na]^+ = 288$	$C_{10}H_{19}NNaO_7$	0.7	22.9	0.8 ± 0.3	nd
Total Relative Intensity		26.2	180.6 ± 30.65	170.3 ± 19.7	
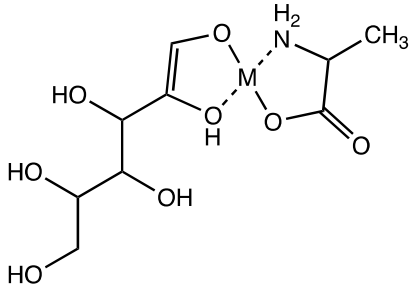	$C_9H_{18}MNO_8$	na	0.3 ± 0.05	5.2 ± 0.1	4.25 ± 1.85

$[M + H]^+$ (Fe = 324, ^{63}Cu = 331)					
$[M + H]^+$ = 333	$C_9H_{18}[^{65}Cu]NO_8$	na	0.2 ± 0.05	na	na
Total Relative Intensity			0.4 ± 0.1	5.2 ± 0.1	4.25 ± 1.85
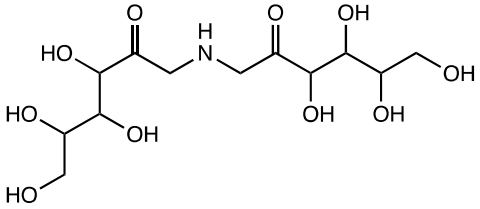	$C_{12}H_{24}NO_{10}$	3.4	0.5 ± 0.2	12.35 ± 1.75	10.5 ± 4.5
$[M + H]^+$ = 342					
$[M + H - H_2O]^+$ = 324	$C_{12}H_{22}NO_9$	1	7.4 ± 2.9	2.9 ± 0.5	2.7 ± 1.4
$[M + H - 2H_2O]^+$ = 306	$C_{12}H_{20}NO_8$	1.6	1.9 ± 0.65	3.95 ± 0.35	3.2 ± 1.5
$[M + H - 3H_2O]^+$ = 288	$C_{12}H_{18}NO_7$	0.7	2.8 ± 1.15	1.1 ± 0.1	0.6 ± 0.3
$[M + H + H_2O]^+$ = 360	$C_{12}H_{26}NO_{11}$	nd	nd	4.15 ± 0.15	0.9 ± 0.4
Total Relative Intensity		6.7	12.5 ± 4.9	24.45 ± 1.15	24.05 ± 1.95
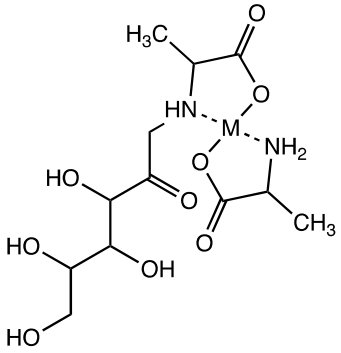	$C_{12}H_{23}MN_2O_9$	na	3.6 ± 2.95	2.6 ± 0.8	4.9 ± 2.3
$[M + H]^+$ (Fe = 395, ^{63}Cu = 402)					
$[M + H - H_2O]^+$ = 386	$C_{12}H_{21}[^{65}Cu]N_2O_8$	na	0.1	na	na

[M + Na]$^+$ (Fe = 417, ^{63}Cu = 424)	$C_{12}H_{22}MN_2NaO_9$	na	7.7	0.45 ± 0.25	0.4 ± 0.05
Total Relative Intensity			11.4 ± 2.75	3.05 ± 1.05	5.4 ± 2.35
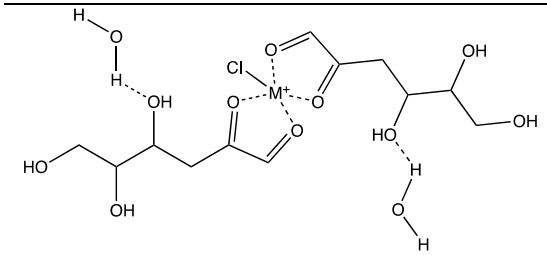	$C_{12}H_{24}[^{35}Cl]FeO_{12}$	na	nd	0.75 ± 0.15	1.1
[M + ^{35}Cl]$^+$ = 451					
[M + ^{37}Cl]$^+$ = 453	$C_{12}H_{24}[^{37}Cl]FeO_{12}$	na	nd	0.25 ± 0.05	0.4
[M + H]$^+$ = 415	$C_{12}H_{23}FeO_{12}$	na	nd	4.5 ± 1.8	5.05 ± 0.35
Total Relative Intensity		na	nd	5.5 ± 2	6.05 ± 0.35
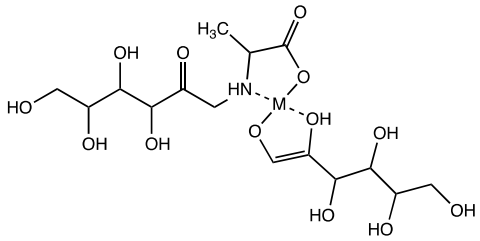	$C_{15}H_{28}MNO_{13}$	na	0.3 ± 0.1	2.45 ± 0.55	0.9 ± 0.2
[M + H]$^+$ (Fe = 486, ^{63}Cu = 493)					
[M + H]$^+$ = 495	$C_{15}H_{28}[^{65}Cu]NO_{13}$	na	0.2 ± 0.55	na	na
[M + H – H_2O]$^+$ (Fe = 468, ^{63}Cu = 475)	$C_{15}H_{26}MNO_{12}$	na	0.3	0.35 ± 0.15	0.2
Total Relative Intensity			0.7 ± 0.2	2.8 ± 0.7	1.1 ± 0.35

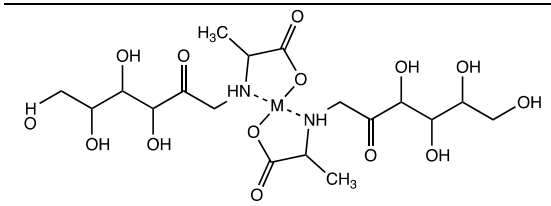	$C_{18}H_{33}MN_2O_{14}$	na	10.3 ± 1.85	3.95 ± 1.05	0.6 ± 0.1
$[\mathbf{M} + H]^+$ (Fe = 557, ^{63}Cu = 564)					
$[\mathbf{M} + H]^+ = 566$	$C_{18}H_{33}[^{65}Cu]N_2O_{14}$	na	4.6 ± 1.1	na	na
Total Relative Intensity			14.9 ± 2.95	3.95 ± 1.05	0.6 ± 0.1

[b]Error (ppm) in calculating the elemental composition

[c]$\mathbf{M}$ (with Times New Roman font): molecular mass

[d]M (with Calibri Light font): metal ion

[e]na: not available

[f]nd: not detected

[g]$[\mathbf{M} + 2]$ represents copper isotopes ^{65}Cu

[h]$[\mathbf{M} + 2]$ represents chlorine isotopes ^{37}Cl

Table S4.2. Label incorporation in Maillard reaction products obtained in the Ala/Glu/$FeCl_2$ model system in methanol

	[M+H]$^+$ (*m/z*)	Elemental Composition	Error ppm[a]	[^{13}C-U] Glu	Error ppm	[^{13}C-3] Ala	Error ppm
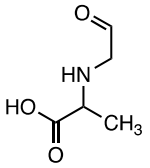 [M + H]$^+$	132.0656	$C_5H_{10}NO_3$	3.545	2	5.056	1	15.954
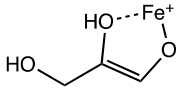 [M]$^+$	144.9585	$C_3H_5FeO_3$	2.146	3	4.566	0	– 4.87
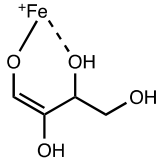 [M]$^+$	174.969	$C_4H_7FeO_4$	2.148	4	7.795	0	– 7.83
[M + ^{35}Cl]$^+$	210.9473	$C_4H_8[^{35}Cl]FeO_4$	5.94	4	– 5.43	0	– 3.54
[M + ^{37}Cl]$^+$	212.9434	$C_4H_8[^{37}Cl]FeO_4$[b]	1.42	nd[c]		0	– 2.34
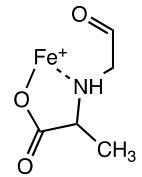 [M]$^+$	185.9848	$C_5H_8FeNO_3$	3.012	2	4.095	1	15.954

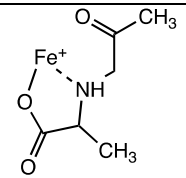 [M]+	200.001	$C_6H_{10}FeNO_3$	0.052	2	10.993	2	13.992
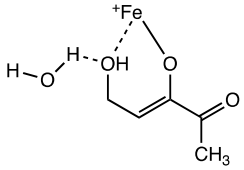 [M]+	188.9843	$C_5H_9FeO_4$	– 3.81	5	3.64	0	0.42
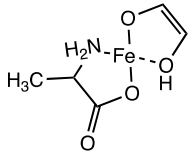 [M + H]+	203.9955	$C_5H_{10}FeNO_4$	2.803	2	7.935	1	11.609
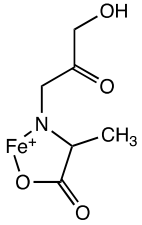 [M]+	215.9958	$C_6H_{10}FeNO_4$	0.578	3	3.148	1	12.81
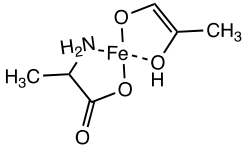 [M + H]+	218.011	$C_6H_{12}FeNO_4$	2.637	3	5.489	1	8.405

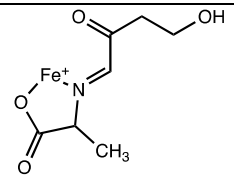 [M]$^+$	227.9968	$C_7H_{10}FeNO_4$	3.838	4	13.121	1	9.082
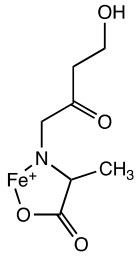 [M]$^+$	230.0117	$C_7H_{12}FeNO_4$	0.543	3	4.89	1	5.295
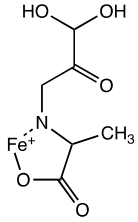 [M]$^+$	231.9913	$C_6H_{10}FeNO_5$	1.985	3	34.911	1	1.693
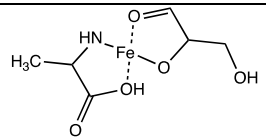 [M + H]$^+$	234.0079	$C_6H_{12}FeNO_5$	6.027	3	11.198	1	10.354
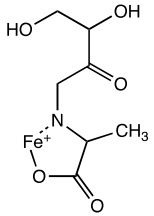 [M]$^+$	246.0064	$C_7H_{12}FeNO_5$	0.364	4	7.635	1	6.657

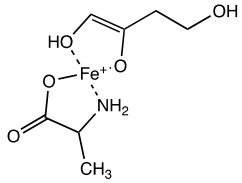 $[M + H]^+$	248.0247	$C_7H_{14}FeNO_5$	10.323	4	9.867	1	8.631
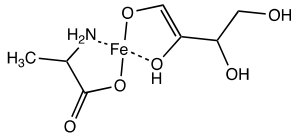 $[M + H]^+$	264.0162	$C_7H_{14}FeNO_6$	3.236	4	7.737	1	7.581
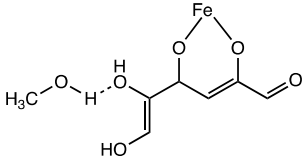 $[M + Na]^+$	268.9734	$C_7H_{10}FeNaO_6$	3.56	6	– 4.99	0	– 8.34
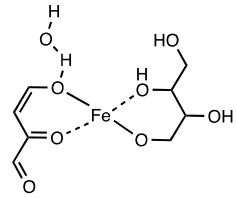 $[M + H]^+$	295.0113	$C_8H_{15}FeO_8$	1.134	8	5.192	0	6.219
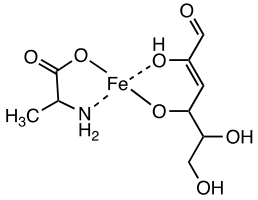 $[M + H]^+$	306.0274	$C_9H_{16}FeNO_7$	0.716	6	7.204	1	8.383
$[M - H_2O]^+$	288.0174	$C_9H_{14}FeNO_6$	1.2	6	6.405	1	10.066
$[M - 2H_2O]^+$	270.0067	$C_9H_{12}FeNO_5$	0.779	6	6.951	1	17.507

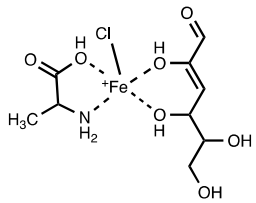	342.0044	$C_9H_{17}Fe[^{35}Cl]NO_7$	0.32	6	– 6.95	1	– 5.67
$[M + {}^{35}Cl]^+$							
$[M + {}^{37}Cl]^+$	344.0026	$C_9H_{17}Fe[^{37}Cl]NO_7$	3.66	6	– 4.03	1	– 3.18
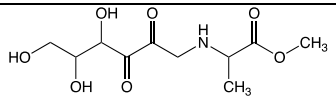	264.1085	$C_{10}H_{18}NO_7$	0.655	6	1.274	1	7.852
$[M + H]^+$							
$[M + H - H_2O]^+$	246.0979	$C_{10}H_{16}NO_6$	0.56	6	4.4	1	– 17.88
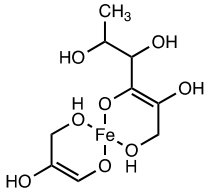	309.0278	$C_9H_{17}FeO_8$	1.69	9	19.89	0	2.98
$[M + H]^+$							
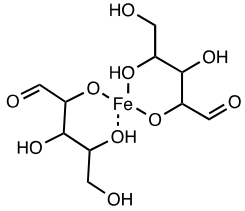	355.0327	$C_{10}H_{19}FeO_{10}$	– 0.16	10	– 2.76	0	– 5.80
$[M + H]^+$							
$[M + H - H_2O]^+$	337.0247	$C_{10}H_{17}FeO_9$	7.44	10	– 7.04	0	4.77

[a]Error (in ppm) in calculating the elemental composition

[b][M + 2] represents chlorine isotopes ^{37}Cl

[c]nd: not detected

(A)

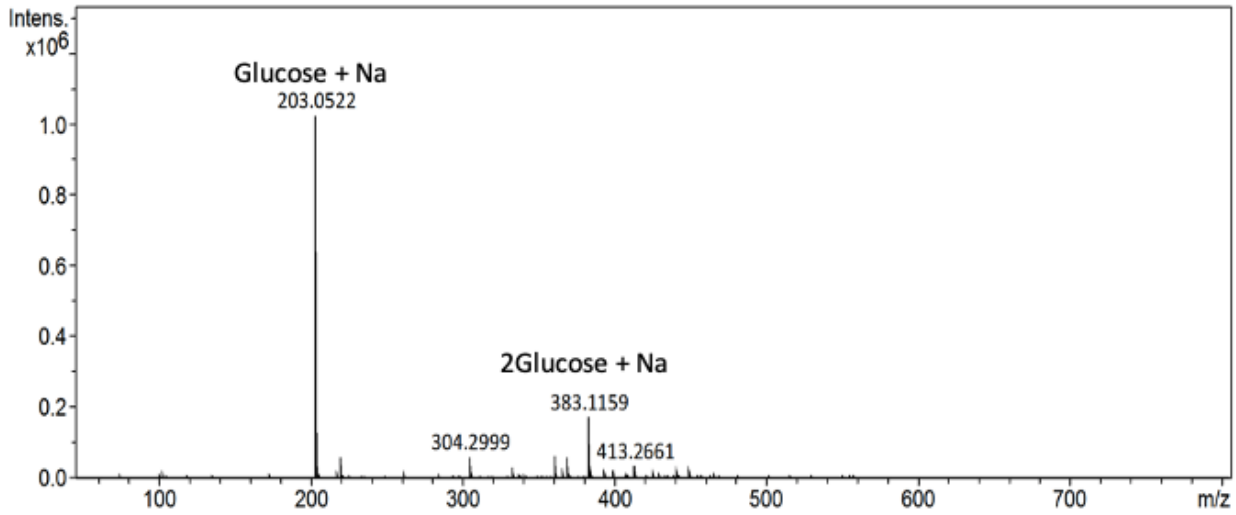

(B)

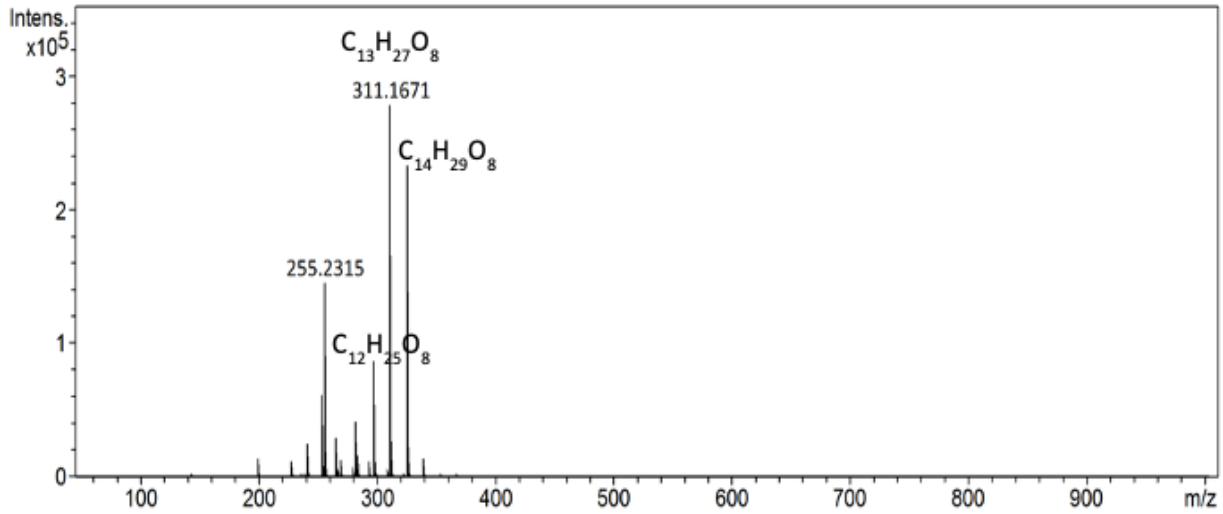

Figure S4.1. ESI/qTOF/MS spectrum of (A) heated glucose solution analyzed in positive ionization mode (B) heated glucose solution analyzed in negative ionization mode

(A)

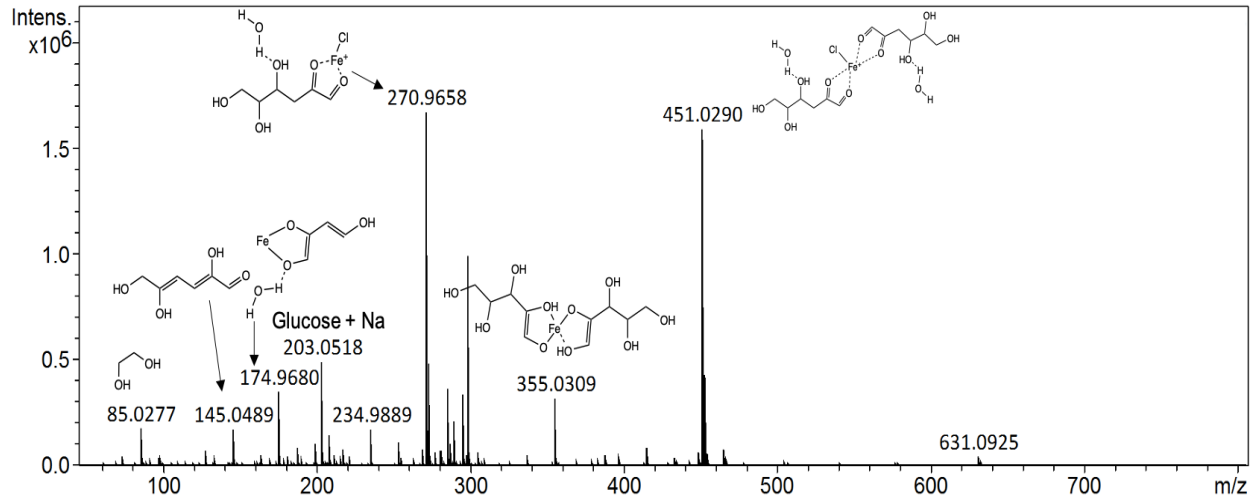

(B)

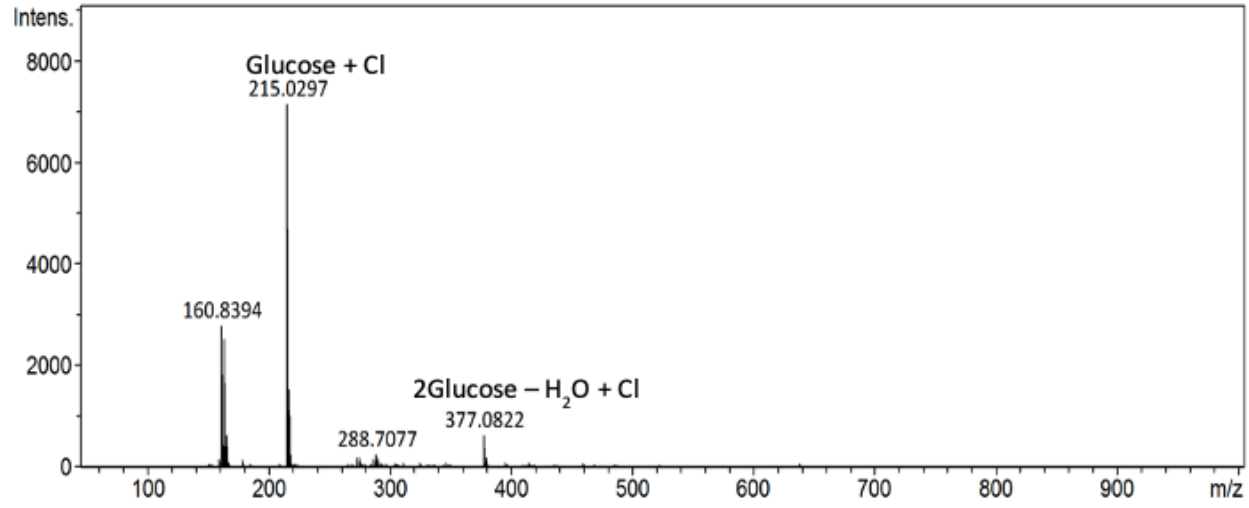

Figure S4.2. ESI/qTOF/MS spectrum of (A) heated glucose solution in the presence of $FeCl_2$ and analyzed in positive ionization mode (B) heated glucose solution in the presence of $FeCl_2$ and analyzed in negative ionization mode

CONNECTING PARAGRAPH

In **chapter 4**, we demonstrated the application of the analytical technique developed in **chapter 3** to the detection of the Maillard reaction intermediates generated in alanine/glucose mixtures. Furthermore, analysis of these mixtures have indicated that this approach allows the detection of novel and reactive Maillard reaction intermediates, such as *bis*[*N,N'*-diglycated alanine]iron(II) complexes. In **chapter 5,** we provide evidence for the possible formation of such complexes and their dissociation products, the diglycated amino acids, in glucose/alanine mixtures in the presence of $FeCl_2$ through isotope labelling technique in conjunction with electrospray ionization time-of-flight mass and tandem mass spectrometry. **Chapter 5** was published in *Food Chemistry*: Kim, E. S. and Yaylayan, V. (2022). *Bis*(alaninato)iron(II) Complexes as Molecular Scaffolds for the Generation of *N,N*-di-glycated Alanine Derivatives in the Presence of Glucose, 374(2022), 131815.

CHAPTER 5

BIS(ALANINATO)IRON(II) COMPLEXES AS MOLECULAR SCAFFOLDS FOR THE GENERATION OF *N,N*-DI-GLYCATED ALANINE DERIVATIVES IN THE PRESENCE OF GLUCOSE

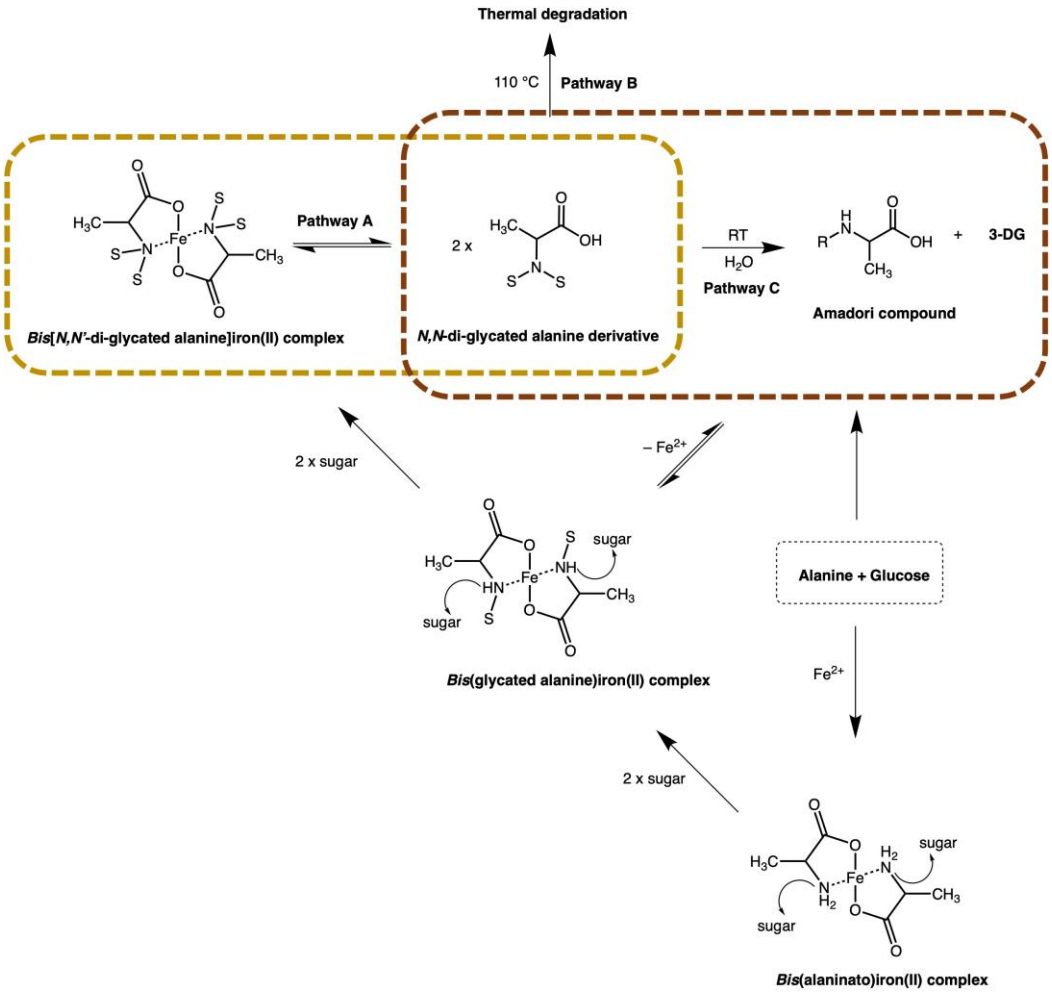

5.1. ABSTRACT

Metal ions are known to influence the course of the Maillard reaction through formation of various complexes such as *bis*(amino acids), these complexes are known to undergo more facile reaction with sugars. Due to this enhanced reactivity, the possible formation of di-glycated amino acids in glucose/alanine model systems with and without $FeCl_2$ was investigated using isotope labelling technique in conjunction with ESI/qTOF/MS/MS. Forty-eight derivatives of *bis*[*N*,*N'*-di-glycated alanine] iron(II) complexes were tentatively identified. These complexes incorporated one iron atom, two [^{13}C-3] atoms from alanine and up to twenty-four carbon atoms from glucose [^{13}C-U], were incorporated as triose (C3), tetrose (C4), pentose (C5) or hexose (C6) moieties. Furthermore, the dissociation of the above complexes released variously substituted *N*,*N*-di-glycated alanine derivatives incorporating one alanine [^{13}C-3] atom and up to twelve carbon atoms from glucose [^{13}C-U]. The MS/MS analysis of diglycated alanines indicated that they follow similar fragmentation pathways as Amadori product of alanine.

KEYWORDS: *Bis*[*N*,*N'*-di-glycated alanine]iron(II) complexes, *N*,*N*-Di-glycated alanine derivatives, Maillard reaction, Divalent iron

5.2. INTRODUCTION

The chemical transformations of sugars and amino acids during the Maillard reaction are affected by several factors such as time, temperature, pH, and most importantly, the choice and concentrations of the initial reactants (i.e., amino acids and sugars) (Rizzi, 1997; Lund and Ray, 2017). Recently, several studies have examined the role of transition metal ions in the Maillard reaction. These ions have been found to influence the formation of the Maillard reaction products (MRPs) by acting as catalysts to promote oxidative pathways and enhance their reaction rates. In addition, the formation of sugar-conjugated amino acids metal-complexes (Ramonaitytė *et al*., 2009; Nashalian and Yaylayan, 2014; 2015b) can modulate their decomposition pathways via promoting the oxidative decarboxylation of amino acids and regulating the release of important intermediates, such as Strecker aldehydes and Amadori products (Nashalian and Yaylayan, 2014;

2015a). Furthermore, it has been reported that the total volatiles and the ninhydrin-active components resulting from heating of *bis*(glycinato)copper(II)/glucose model system were formed in higher amounts than those detected in the glycine/glucose system (Nashalian and Yaylayan, 2015b). Metal cations are also known to promote the formation of 1,2-dicarbonyl compounds from glucose (Gensberger-Reigl *et al*, 2020). During thermal treatment of food, amino acids and sugars are predicted to form various complexes with transition metals. Moreover, *bis*(amino acid)metal complexes can theoretically conjugate with up to four reducing sugar moieties (Nashalian and Yaylayan, 2015b) through Amadori rearrangement and effectively generate *N*,*N*-di-glycated amino acids after dissociation (see Figure S5.1). The role of di-glycated amino acids in the Maillard reaction has not been investigated in detail. However, the available reports indicate the presence of unusually high percentage of open-chain forms of one of their sugar moieties (Feather and Mossine, 2005), and their ability to undergo hydrolysis to generate 3-deoxyglucosone (3-DG), a reactive Maillard reaction intermediate, and a free Amadori compound (Fodor and Sachetto, 1968).

Due to the enhanced reactivity of the amino acid metal complexes towards reducing sugars (Belikov *et al*., 1969), the possible formation of di-glycated alanine derivatives in alanine/glucose/$FeCl_2$ (Ala/Glu/$FeCl_2$) model systems was investigated using high-resolution electrospray ionization/quadrupole time-of-flight mass spectrometry (ESI/qTOF/MS), tandem mass spectrometry (MS/MS), and isotope labelling techniques. Alanine was chosen as a representative amino acid with simple side chain moiety.

5.3. MATERIALS AND METHODS

5.3.1. Materials and reagents

L-Alanine (98%), L-serine (98%), D-glucose, and iron(II) chloride ($FeCl_2$) (99%) were purchased from Sigma-Aldrich Chemical Co. (Oakville, Ontario, Canada). Alanine-3-^{13}C ($^{13}CH_3CH(NH_2)CO_2H$) (98%) and glucose U-^{13}C ($^{13}C_6H_{12}O_6$) (99%) were purchased from Cambridge Isotope Laboratories (Andover, MI). Liquid chromatography-mass spectrometry (LC-MS)-grade water and methanol (OmniSolv, > 99%) were obtained from VWR International (Mississauga, Ontario, Canada).

5.3.2. Sample preparation

Test model systems were prepared by adding glucose (18 mg), alanine (9 mg), and $FeCl_2$ (6.4 mg) to methanol (1 mL) and heating in stainless-steel reactors (30 mL capacity) at 110 °C for 2 h, followed by evaporation of the solvent for 30 min. The control model system was prepared similarly by heating glucose (18 mg) and alanine (9 mg) in methanol (1 mL) in stainless-steel reactors at 110 °C for 2 h in the absence of $FeCl_2$. All samples were analyzed at least in two replicates, as indicated in Table 5.1.

Table 5.1. Composition of the model systems studied[a]

	Model System
Control Model System	Alanine was added to glucose solution and heated in the absence of metal ions - **Ala/Glu**
Test Model System	Alanine was added to *bis*(serinato)iron(II) solution and heated - **$(Ser)_2Fe$/Ala** Alanine added to glucose solution heated in the presence of $FeCl_2$ - **Ala/Glu/$FeCl_2$**
Isotope Labelling Model System	[^{13}C-3] Alanine was added to glucose solution heated in the presence of - **[^{13}C-3] Ala/Glu/$FeCl_2$** Alanine added to [^{13}C-U] glucose solution heated in the presence of $FeCl_2$ - **Ala/[^{13}C-U] Glu/$FeCl_2$**

[a]All model systems were heated at 110 °C for 2 h in methanol, some test model systems were also heated in water, using a sealed stainless-steel reactor, and analyses were carried out at least in two replicates.

Synthesis of *bis*(serinato)iron(II). *Bis*(serinato)iron(II) was prepared (to study ligand exchange reaction with alanine) by dissolving serine (1.05 g) in methanol (10 mL) in the presence of KOH (0.05 g), followed by the addition of $FeCl_2$ (0.64 g). The dark reddish precipitate was filtered, washed with methanol, and dried in a vacuum oven at room temperature. The obtained solid was analyzed by ESI/qTOF/MS, which generated a major ion at $[M + H]^+ = 265.0109$ corresponding to the elemental composition of $C_6H_{13}FeN_2O_6$ with – 2.07 ppm of error.

***Bis*(serinato)iron(II) interaction with free alanine.** The *bis*(serinato)iron(II) (26.5 mg) and alanine (9 mg) were mixed in methanol or water (1 mL), and heated in a stainless-steel reactor at 110 ℃ for 2 h, followed by evaporation of the solvent for 30 min.

5.3.3. ESI/qTOF/MS analysis

The samples were dissolved in liquid chromatography (LC)-grade methanol at a 1 mg/mL concentration. The samples were then diluted 10-fold in 10% methanol prior to analysis by HR/ESI/qTOF/MS in positive ion mode. The ESI/qTOF/MS system comprised a Bruker Maxis Impact quadrupole-time-of-flight mass spectrometer (Bruker Daltonics, Bremen, Germany) operated in positive-ion mode. The samples (1 μL) were injected directly into the ESI/qTOF/MS system. Instrument calibration was performed using sodium formate clusters. The electrospray interface settings were as follows: nebulizer pressure, 0.6 bar; drying gas, 4 L/min; temperature, 180 ℃; and capillary voltage, 4500 V. The scan range was from *m/z* 100 to 1000. Molecular formulae were assigned to all the observed peaks based on their exact *m/z* values using "ChemCalc" software (Institute of Chemical Sciences and Engineering, Lausanne, Switzerland) (Patiny and Borel, 2013). ESI/qTOF/MS/MS was carried out in multiple reaction monitoring (MRM) mode for the ions at *m/z* 414, (collision energy of 5 eV), *m/z* 504 (5 eV), *m/z* 540 (10 eV), and *m/z* 298 (15 eV). The reaction intermediates were detected as singly or doubly charged ions in various ionic forms such as $[M + H^+]^+$, $[M + Fe^+ + Cl]^+$, $[M + H^+ + Cl_2]^+$, $[M + Na^+]^+$, $[M + 2Na^+]^{2+}$, $[M + 2K^+]^{2+}$, $[M + 2H^+ + Cl_2]^{2+}$, $[M + Cl_2 + Na^+ + K^+]^{2+}$, $[M + Cl_2 + 2K^+]^{2+}$, $[M + Cl_2 + 2Na^+]^{2+}$, $[M + Cl + K^+]^{2+}$, $[M + H^+ + Cl_2 + Na^+]^{2+}$, and $[M + H^+ + Cl_2 + K^+]^{2+}$ in addition to being hydrated or methanolated (see Figure S5.2). Doubly charged ions were confirmed through the observation of isotopic spacing of 0.5 amu and mono- and di-chlorinated ions were confirmed through observation of appropriate isotope abundance ratios.

5.3.4. Structural elucidation

Evidence for the proposed structures was provided through ESI/qTOF/MS analysis of their elemental composition, analysis of their MS/MS fragmentation patterns and through isotope-labelling studies using glucose [^{13}C-U] and alanine [^{13}C-3], in addition, the proposed structures were based on well-known glucose degradation products.

5.3.5. Criteria applied for tentative identification of the listed ions

Most selected ions were detected in three different reactions systems (1) unlabeled, (2) only glucose labelled, and (3) only alanine labelled systems; each analyzed in two replicates. Ions having an error up to 10 ppm level in one of the systems only were selected, if in the other two reaction systems the corresponding ion was detected in less than 5 ppm error.

5.4. RESULTS AND DISCUSSION

In the presence of metal ions, important Maillard reaction precursors, such as amino acids, sugars, sugar degradation products (SDPs), and Amadori compounds, can undergo self- or random complexations with available ligands and generate various metal-centered binary complexes (Kim and Yaylayan, 2020; 2021). Binary amino acid metal complexes have been found to influence the formation of various MRPs by acting as catalysts to promote; for example, oxidative pathways, such as the formation of glucosone, Strecker aldehydes, and amino sugars (i.e., fructosamine). Furthermore, metal complexes can enhance the rate of browning (Nashalian and Yaylayan, 2015b; Ramonaitytė *et al*., 2009), in addition to regulating or delaying the degradation of important intermediates, such as deoxy-glucosones and Amadori rearrangement products (ARPs) (Nashalian and Yaylayan, 2014; 2015a). It has also been demonstrated (Kim and Yaylayan, 2021) that in the presence of metal ions, alanine conjugated with Amadori rearrangement product, *N*-(1-deoxy-D-fructose-1-yl)-L-alanine, can exist as a binary iron complex with itself as detected at *m/z* 557.1295 ($C_{18}H_{33}FeN_2O_{14}$) and with alanine detected at *m/z* 395.0750 ($C_{12}H_{23}FeN_2O_9$) or with glucose observed at *m/z* 486.0917 ($C_{15}H_{28}FeNO_{13}$).

5.4.1. The role of metal ions in generating *bis*[*N,N'*-di-glycated alanine]iron(II) complexes

It has been demonstrated (Nashalian and Yaylayan, 2015b) that glycine/glucose model systems, when heated in the presence of $CuCl_2$, generated elevated levels of aroma compounds compared to glycine when heated with glucose in the absence of $CuCl_2$. This was attributed to the ability of amino acids to act as ligands for metal ions and generate relatively stable binary complexes of metal ions as molecular scaffolds for the further build-up of Amadori products with up to four sugar moieties (such as structure **A** in Table 5.2). The ease of Schiff base formation on the amino groups of metal complexes was attributed to the extra stabilization gained through

hyperconjugation of its π-electron system with the metals (Belikov *et al*., 1969). The subsequent release of free *N*,*N*-di-glycated amino acid derivatives (see Figure S5.1 and section 3.4) can occur through two possible pathways; one non-destructive through dissociation of the complex and the other through thermal degradation (Nashalian and Yaylayan, 2015a; Pearson and Lanier, 1964). Such *N*,*N*-di-glycated amino acids have been rarely reported in the literature, and they are known to undergo hydrolysis to generate 3-DG, a reactive Maillard reaction intermediate and a free Amadori compound (Fodor and Sachetto, 1968). Furthermore, Feather and Mossine have studied synthetic *N*,*N*-di-glycated glycine and lysine derivatives, and concluded, based on X-ray diffraction and nuclear magnetic resonance (NMR) spectroscopy (Feather and Mossine, 2005), that at least one of the sugars exists predominantly in acyclic form indicating their potential for high reactivity in the Maillard reaction systems.

Due to the importance of *N*,*N*-di-glycated amino acid derivatives as more reactive intermediates than Amadori compounds in the Maillard reaction, *bis*(alaninato)iron(II)/glucose or alanine/glucose model systems were studied in the presence and absence of $FeCl_2$ relative to their ability **(1)** to generate *bis*[*N*,*N'*-di-glycated alanine]iron(II) complexes and **(2)** to undergo subsequent dissociation to generate free *N*,*N*-di-glycated alanine derivatives.

5.4.2. Distribution of *bis*[*N*,*N'*-di-glycated alanine]iron(II) complexes in Ala/Glu/$FeCl_2$ model system

In the Ala/Glu/$FeCl_2$ model system, that was heated for 2 h at 110 °C, various reactive sugar degradation products (SDPs) can be formed, and they can subsequently react with *bis*(alaninato)iron(II) complexes formed *in situ* (Kim and Yaylayan, 2021) to generate a relatively large number of *bis*[*N*,*N'*-di-glycated alanine]iron(II) complexes. Forty-seven such proposed structures were identified and are listed in **Table S5.1.** These complexes incorporated one iron atom, two [^{13}C-3] atoms from alanine [^{13}C-3] and up to twenty-four carbon atoms from glucose [^{13}C-U], satisfying the structural requirements for *bis*[*N*,*N'*-di-glycated alanine]iron(II) complexes represented as structure **A** in Table 5.2. In structure **A**, R, R_1, R_2, and R_3 represents either hydrogen atoms or sugar moieties derived from triose (C3), tetrose (C4), pentose (C5) or hexose (C6) either in intact forms or oxidized or hydrated or dehydrated forms. The extracted ions from the high-resolution mass spectrometry (HRMS) data satisfying the above requirements are listed in Table

S1, and their distribution is summarized in Table 5.2. We identified nine groupings of *bis*[*N,N'*-di-glycated alanine]iron(II) complexes based on the total number of sugar carbon atoms incorporated in these complexes using the isotope labelling technique. Table 5.2 lists the nine groupings of *bis*[*N,N'*-di-glycated alanine]iron(II) complexes as having twelve, fourteen, fifteen, eighteen, twenty, twenty-one, twenty-two, twenty-three and twenty-four sugar carbon atoms incorporated in their structures (see Table S5.1). Some of the members of these groupings were detected in more than one ionic form, either singly or doubly charged; in Tables 5.2, S5.1, and Figure S5.2, the structures represent only one of many possible isomeric forms.

5.4.2.1. *Bis*[*N,N'*-di-glycated alanine]iron(II) complexes having twenty-four sugar carbon atoms

Theoretically, the maximum possible number of sugar carbon atoms that can be incorporated in these complexes is twenty-four, which was observed in the ions formed by incorporating four glucose moieties; two on each amino acid (see Tables S5.1 and Table 5.2). Nine such ions incorporating twenty-four carbon atoms were observed. One of the most important ions in this category was the one detected in several ionic forms such as $[M + 2H^+ + [^{35}Cl]_2]^{2+}$ at *m/z* 484.0868 $[C_{30}H_{54}Fe[^{35}Cl]_2N_2O_{25}]^{2+}$ or $[M + 2H^+ + [^{35}Cl] + [^{37}Cl]]^{2+}$ at *m/z* 485.0915 $[C_{30}H_{54}Fe[^{35}Cl][^{37}Cl]N_2O_{25}]^{2+}$, or $[M + 2H^+ + [^{37}Cl]_2]^{2+}$ at *m/z* 486.0917 $[C_{30}H_{54}Fe[^{37}Cl]_2N_2O_{25}]^{2+}$. All these ions represent glycated *bis*(alaninato)iron(II) complexed with two intact glucose moieties and two glucosone moieties (see Table S5.1). After dissociation, this complex generated one molecule of di-fructosyl alanine as observed at *m/z* 414 (see Figure 5.2 and Table S5.3) in addition to its iron complex observed at *m/z* 468.0815 and one molecule of di-glycated alanine with two glucosone moieties. The latter was observed as mono alaninato[*N,N*-diglycated]iron(II) complexed with a C3 sugar moiety, detected as $[M + H]^+$ at *m/z* 586.1057 $[C_{19}H_{32}FeN_2O_{16}]^+$, where fifteen carbon atoms from glucose [^{13}C-U] and one C-3 atom from alanine [^{13}C-3] were incorporated in the structure (Table 5.3). The remaining ions in this category represented diglycated hexoses in various redox states, as shown in Table S5.1.

Table 5.2. Distribution of the observed derivatives of *bis*[*N*,*N'*-di-glycated alanine]iron(II) complexes (Structure A) in alanine/glucose/$FeCl_2$ model system (see Table S5.1 for proposed examples)

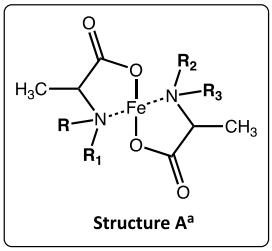

Structure A[a]

A = *Bis*[*N,N'*-di-glycated alanine]iron(II) complexes where R, R_1, R_2, and R_3 are either hydrogens or sugar moieties derived from triose (C3), tetrose (C4), pentose (C5) or hexose (C6) either intact or oxidized, methylated, hydrated, or dehydrated

Total numbers of carbon atoms incorporated from glucose in **A**	Number of ionic forms[b] detected for structure **A** in qTOF/MS	Possible sugar configurations in structure **A**
12	1	Two hexoses (2 x C6) or Four trioses (4 x C3) or Three tetroses (3 x C4), etc.
14	3	Two pentoses and one tetrose (2 x C5 + C4) or One each of hexose, pentose, and triose (C6 + C5 + C4), etc.
15	1	Three pentoses (3 x C5) or Two hexoses and one triose (2 x C6 + C3), etc.
18	2	Two hexoses and two trioses (2 x C6 + 2 x C3) or Three hexoses (3 x C6)
20	7	Three hexoses and one diose (3 x C6 + C2) or Four pentoses (4 x C4), etc.

21	3	Three hexoses and one triose (3 x C6 + C3) or One hexose and three pentoses (C6 + 3 x C5)
22	16	Three hexoses and one tetrose (3 x C6 + C4)
23	5	Three hexoses and one pentose (3 X C6 + C5)
24	9	Four hexoses (4 x C6)

[a]All the structures represented by **A** incorporated two alanine [^{13}C-3] atoms and indicated number of carbon atoms from glucose [^{13}C-U]

[b]$[M + H]^+$, $[M + Cl]^+$, $[M + H + Cl_2]^+$, $[M + Na]^+$, $[M + 2Na]^{2+}$, $[M + 2K]^{2+}$, $[M + 2H + Cl_2]^{2+}$, $[M + Cl_2 + Na + K]^{2+}$, $[M + Cl_2 + 2K]^{2+}$, $[M + Cl_2 + 2Na]^{2+}$, $[M + Cl + K]^{2+}$, $[M + H + Cl_2 + Na]^{2+}$, $[M + H + Cl_2 + K]^{2+}$, in addition to hydrated and methanolated forms

5.4.2.2. *Bis*[*N,N'*-di-glycated alanine]iron(II) complexes having twenty to twenty-three sugar carbon atoms

Bis[*N,N'*-di-glycated alanine]iron(II) complexes having twenty to twenty-three sugar carbon atoms are shown in Table S5.1 and listed in Table 5.2. Seven observed structures were associated with twenty sugar carbon incorporation as pentose or one of its oxidized forms. As to the complexes associated with twenty-one sugar carbon moieties, three such structures were observed, incorporating one tetra-oxo glucose and three tri-oxo pentoses detected as $[M + [^{35}Cl] + K]^{2+}$ at *m/z* 460.0214 $[C_{27}H_{38}Fe[^{35}Cl]N_2KO_{25}]^{2+}$, where two C-3 atom from alanine [^{13}C-3] were incorporated in the structure and $[M + [^{37}Cl] + K]^{2+}$ at *m/z* 461.0215 $[C_{27}H_{38}Fe[^{37}Cl]N_2KO_{25}]^{2+}$. In addition, hydrated deoxy-pentosone, hydrated and oxidized di-pentosone, and hydrated tri-oxo glucose conjugated with *bis*(alaninato)iron(II) complexes were detected as $[M + [^{35}Cl]_2 + 2K]^{2+}$ at *m/z* 488.9899 $[C_{27}H_{38}Fe[^{35}Cl]_2N_2K_2O_{24}]^{2+}$, and hydrated tri-oxo pentose and tri-oxo glucose conjugated with *bis*(alaninato)iron(II) complexes were detected as $[M + [^{35}Cl]_2 + 2K]^{2+}$ at *m/z*

474.9445 $[C_{27}H_{26}Fe[^{35}Cl]_2N_2K_2O_{23}]^{2+}$. Further support for their structures was provided by observing the incorporation of twenty-one carbon atoms from glucose [^{13}C-U] and two C-3 atoms from alanine [^{13}C-3]. Sixteen complexes associated with the incorporation of twenty-two sugar carbons were detected originating from variously oxidized pentoses and glucose moieties. Complexes of *bis*[*N,N'*-di-glycated alanine]iron(II) having twenty-three sugar carbon atoms were generated from glycation with various sugar derivatives such as oxidized tri-oxo pentose, glucosone, and tri-oxo glucose conjugated with *bis*(alaninato)iron(II) complexes.

5.4.2.3. *Bis*[*N,N'*-di-glycated alanine]iron(II) complexes having twelve to eighteen sugar carbon atoms

Bis[*N,N'*-di-glycated alanine]iron(II) complexes having twelve to eighteen sugar carbon atoms were detected in their various ionization forms (Figure S5.2) and listed in Table S5.1. For example, three such structures having twelve sugar carbon atoms were observed as hydrated or methanolated glyceraldehyde and diglyceraldehyde conjugated with *bis*(alaninato)iron(II) complexes. Similarly, three complexes bearing fourteen sugar carbon atoms were found as complexes formed through the conjugation of erythrose and two molecules of di-deoxy-pentosone with *bis*(alaninato)iron(II) and detected in form of $[M + [^{35}Cl]]^+$ at *m/z* 595.0667 $[C_{20}H_{28}Fe[^{35}Cl]N_2O_{13}]^+$; $[M + K]^+$ at *m/z* 622.0374 $[C_{20}H_{28}[^{63}Cu]N_2KO_{14}]^+$ and *m/z* 624.0389 $[C_{20}H_{28}[^{65}Cu]N_2KO_{14}]^+$. In addition, the complex formed through the conjugation of three sugar moities (erythrose, pentosone, and deoxypentosone) with *bis*(alaninato)iron(II) was observed as $[M + H]^+$ at *m/z* 579.1122 $[C_{20}H_{31}FeN_2O_{14}]^+$. The complex formed through the conjugation of 3-DG and two molecules of 3-deoxyerythrosone with *bis*(alaninato)iron(II) was observed as doubly charged ion $[M + 2Na^+]^{2+}$ at *m/z* 298.0627 $[C_{20}H_{34}FeN_2Na_2O_{12}]^{2+}$, where fourteen carbon atoms from glucose [^{13}C-U] and two carbon atoms from alanine [^{13}C-3] were incorporated into the structure. Only one complex having fifteen sugar carbon atoms and two complexes with eighteen sugar carbon atoms were detected in the model system.

5.4.3. Ligand exchange of *bis*(serinato)iron(II) complex with free alanine

To demonstrate the release of *N,N*-di-glycated alanine derivatives from *bis*[*N,N'*-di-glycated alanine]iron(II) complexes, a simple model system of *bis*(serinato)iron(II) complex was used to study the ability of amino acid metal complexes to undergo ligand exchange through

association/dissociation reactions at 110 ℃ for 2 h in the presence of a free amino acids such as alanine. The association and dissociation process can allow other potential ligands in a model system or in food to be configured as binary complexes replacing the existing amino acid. The half-lives corresponding to the complexes will depend on their relative stabilities and their binding kinetics, in addition to the relative concentrations of the free ligands in the model system. After heating the reaction mixture containing the *bis*(serinato)iron(II) complex and free alanine at 110 ℃ for 2 h in two different solvent systems, the reaction mixtures were cooled and analyzed using ESI/qTOF/MS, and the results are presented in Table S5.2. It was observed that the *bis*(serinato)iron(II) complex dissociated readily to release free serine and then re-associate with free alanine available in the solution to form a mixed serine/alanine iron(II) complex and *bis*(alaninato)iron(II) complex. This ligand exchange process occurred in a stepwise fashion (see Figures 5.1 and S5.3), as confirmed by the observation of the intermediate ions consisting of three amino acids: two serine and one alanine, or two alanine and one serine observed at *m/z* 354.0641 ($C_9H_{20}FeN_3O_8$), *m/z* 376.0421 ($C_9H_{19}FeN_3NaO_8$), *m/z* 338.0691 ($C_9H_{20}FeN_3O_7$), and *m/z* 360.0463 ($C_9H_{19}FeN_3NaO_7$). The relative intensities of the intermediate ions observed under ESI/qTOF/MS analysis for the $(Ser)_2Fe/Ala$ system are shown in Table S5.2, indicating that their final relative intensities were dependent on the solvent used. Free amino acids were observed to be conjugated with iron(II) as mono- and *bis* complexes in the form of $[M + H]^+$, $[M + Na]^+$, and $[M + K]^+$. Mono(alaninate)iron(II) and mono(serinate)iron(II) were detected in the form of $[M + H]^+$, the former at *m/z* 143.9744 ($C_3H_6FeNO_2$) and the latter at *m/z* 161.9847 ($C_3H_8FeNO_3$). In addition, *bis*(serinato)iron(II) was observed in three ionic forms at *m/z* 265.0112, 286.9926, and 302.9673 corresponding to $[M + H]^+$ ($C_6H_{13}FeN_2O_6$), $[M + Na]^+$ ($C_6H_{12}FeN_2NaO_6$), and $[M + K]^+$ ($C_6H_{12}FeN_2KO_6$). Furthermore, mono(alaninate) and mono(serinate)iron(II) were detected as $[M + H]^+$ at *m/z* 249.0168 ($C_6H_{13}FeN_2O_5$) and $[M + Na]^+$ at *m/z* 270.9991 ($C_6H_{12}FeN_2NaO_5$), respectively. *Bis*(alaninato)iron(II) was also observed as $[M + H]^+$ at *m/z* 233.0216 ($C_6H_{13}FeN_2O_4$) and $[M + Na]^+$ at *m/z* 255.0032 ($C_6H_{12}FeN_2NaO_4$) (Table S5.2).

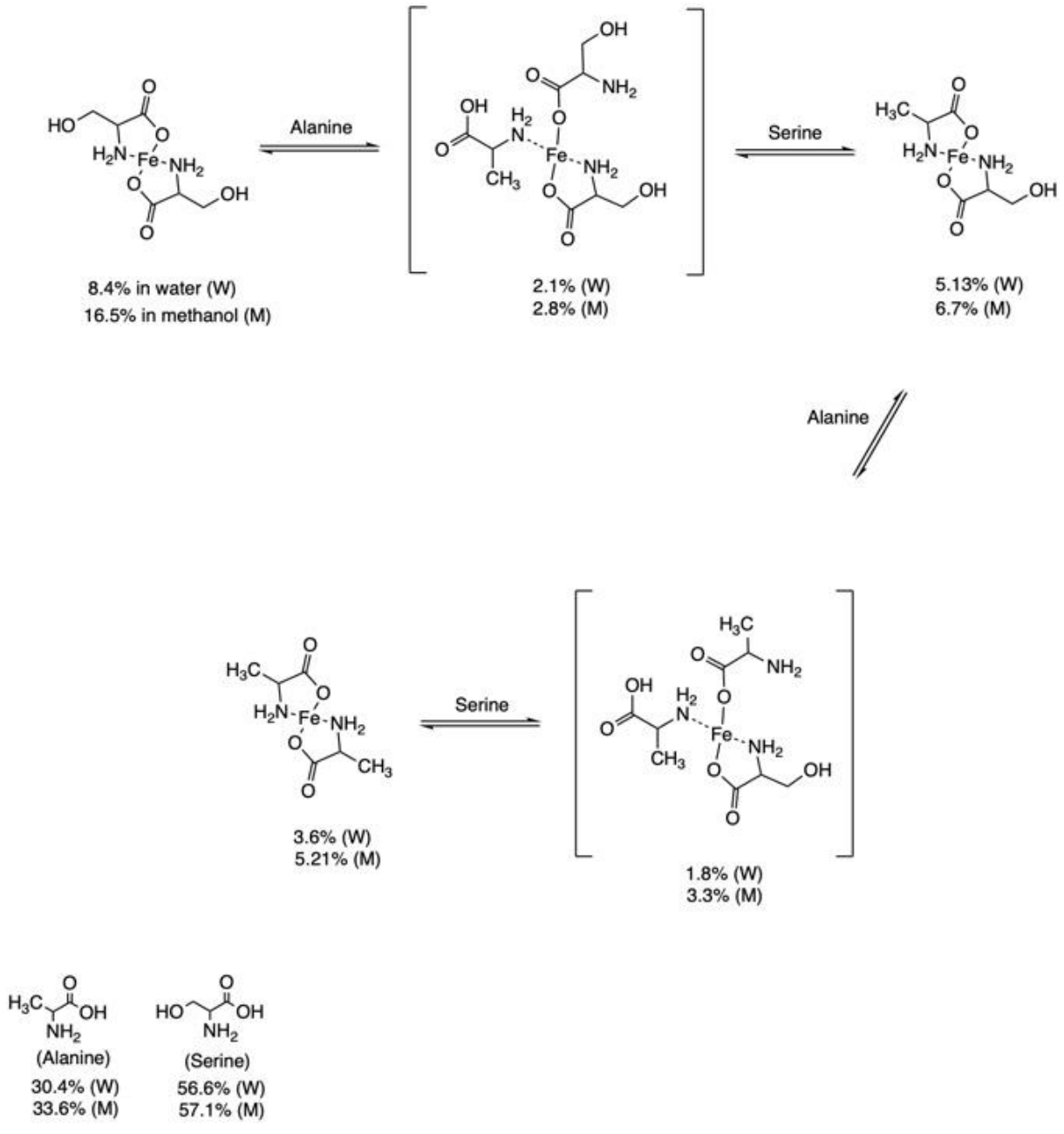

Figure 5.1. Step-by-step ligand exchange mechanism and the relative peak intensities of the intermediates after heating a mixture of synthetic $(Ser)_2Fe$ with α-alanine under Maillard reaction conditions (100 °C for 2 h) in water (W) and in methanol (M) (see also Table S5.2 and Figure S5.3)

5.4.4. Release of *N,N*-di-glycated alanine derivatives from *bis*[*N,N'*-di-glycated alanine]iron(II) complexes

Dissociation of *bis*[*N,N'*-di-glycated alanine]iron(II) complexes can release variously substituted free *N,N*-di-glycated alanine derivatives. Table 5.3 lists the observed such ions in the model system studied that incorporated one alanine [^{13}C-3] atom and up to twelve carbon atoms from glucose [^{13}C-U] as satisfying structural requirements for *N,N*-di-glycated alanine derivatives. The maximum number of sugar carbon atoms that can be incorporated is twelve. According to our data, the minimum number of carbon atoms incorporated from sugar was five, and the maximum was twelve. Inspection of Table 5.3 indicates that such alanine derivatives were formed through the reaction of dioses (C2), trioses (C3), tetroses (C4), pentoses (C5) and hexoses (C6) in their various redox states with *bis*(alaninato)iron (II) complexes consistent with the sugar incorporation data in *bis*[*N,N'*-di-glycated alanine]iron(II) complexes identified and shown in Table S5.1. Furthermore, such structures can incorporate all possible combinations of sugar fragments such as C3 + C3 or C2 + C4 for the total of six carbon atom incorporation from sugar as an example; however, only one such combination is shown in Table 5.3 for each ion. No *N,N*-di-glycated alanine derivatives were detected in the model systems lacking $FeCl_2$.

5.4.5. MS/MS fragmentations of *m/z* 414, *m/z* 504, *m/z* 540, and *m/z* 298

To provide further evidence for the proposed structures, selected ions such as *m/z* 414, 504, 540, and 298 were analyzed by ESI/qTOF/MS/MS. The ion at *m/z* 414 (Table 5.3) representing diglycated alanine with intact hexoses; the ion at *m/z* 298 in Table S5.1 representing tri-glycated *bis*(alaninato)iron complex, and two related ions at *m/z* 540 and 504 representing two diglycated alanine iron complexes having similar elemental compositions but differing only in the number of chlorine atoms, the ion observed at *m/z* 540 was di-chlorinated. The at *m/z* 504 was mono-chlorinated (see Table 5.3) as evidenced by their isotopic abundance ratios.

Table 5.3. Elemental composition and isotope incorporation in *N*,*N*-di-glycated alanine derivatives formed in Ala/Glu/$FeCl_2$ model systems

CX [a]	Structure	Ala/Glu/$FeCl_2$			Ala/Glu[^{13}C-U] /$FeCl_2$			Ala[^{13}C-3]/Glu/$FeCl_2$		
		[M+X]	Elemental Composition	Error ppm[b]	[M+X]	Elemental Composition	Error ppm	[M+X]	Elemental Composition	Error ppm
C5	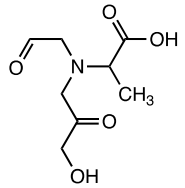	204.0859	$[C_8H_{14}NO_5]^+$	− 3.67	127.0388	$[C_3[^{13}C]_5H_{13}NNa_2O_5]^{2+}$	11.85	205.0832	$[C_7[^{13}C]H_{14}NO_5]^+$	− 33.17
C5	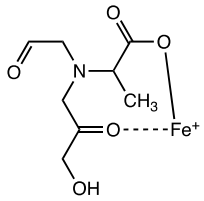	258.0068	$[C_8H_{12}FeNO_5]^+$	3.35	263.0215	$[C_3[^{13}C]_5H_{12}FeNO_5]^+$	6.706	259.008	$[C_7[^{13}C]H_{12}FeNO_5]^+$	− 4.98
C6	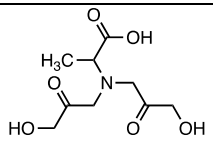	234.0976	$[C_9H_{16}NO_6]^+$	0.693	240.1161	$[C_3[^{13}C]_6H_{16}NO_6]^+$	7.46	235.0994	$[C_8[^{13}C]H_{16}NO_6]^+$	− 4.97
C6	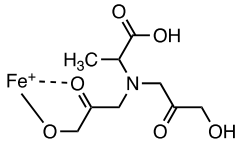	288.0174	$[C_9H_{14}FeNO_6]^+$	3.13	294.0353	$[C_3[^{13}C]_6H_{14}Fe\ NO_6]^+$	− 4.52	nd[c]		

C7	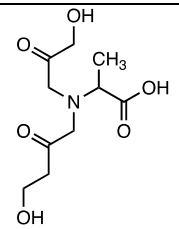	248.1133	$[C_{10}H_{18}NO_6]^+$	0.453	255.1346	$[C_3[^{13}C]_7H_{18}NO_6]^+$	− 6.85	249.115	$[C_9[^{13}C]H_{18}NO_6]^+$	7.094
C8	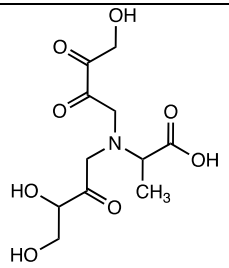	292.1019	$[C_{11}H_{18}NO_8]^+$	− 2.71	322.1212	$[C_3[^{13}C]_8H_{17}NNaO_8]^+$	30.19	293.1014	$[C_{10}[^{13}C]H_{18}NO_8]^+$	− 15.86
C8	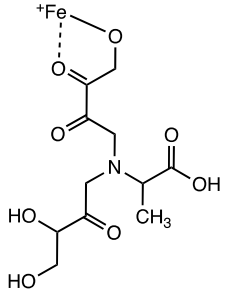	346.0194	$[C_{11}H_{16}FeNO_8]^+$	− 7.45	427.9939	$[C_3[^{13}C]_8H_{16}Fe[^{35}Cl]NKO_8]^+$	29.26	213.9851	$[C_{10}[^{13}C]H_{16}Fe[^{35}Cl]NNa_2O_8]^{2+}$	− 6.96
C8	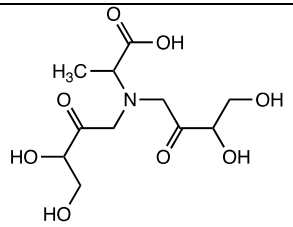	294.1191	$[C_{11}H_{20}NO_8]^+$	0.708	nd			295.1223	$[C_{10}[^{13}C]H_{20}NO_8]^+$	2.04

C8	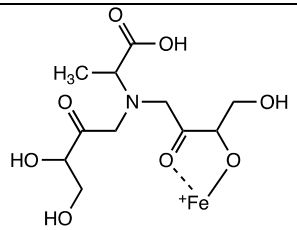	348.0403	$[C_{11}H_{18}FeNO_8]^+$	7.67	356.0667	$[C_3[^{13}C]_8H_{18}FeNO_8]^+$	6.27	349.0437	$[C_{10}[^{13}C]H_{18}FeNO_8]^+$	7.78
C9	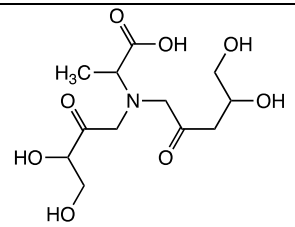	308.1331	$[C_{12}H_{22}NO_8]^+$	4.679	317.1552	$[C_3[^{13}C]_9H_{22}NO_8]^+$	30.064	347.1014	$[C_{11}[^{13}C]H_{21}NKO_8]^+$	23.54
C9	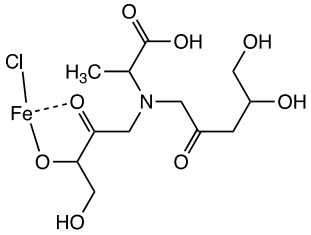	420.0183	$[C_{12}H_{20}Fe[^{35}Cl]NNaO_8]^+$	15.23	234.0055	$[C_3[^{13}C]_9H_{20}Fe[^{35}Cl]NNaKO_8]^{2+}$	12.28	nd		
C9	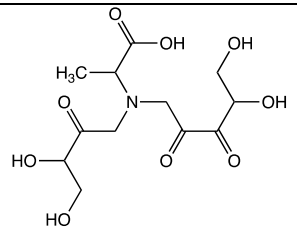	322.114	$[C_{12}H_{20}NO_9]^+$	0.602	188.0552	$[C_3[^{13}C]_9H_{19}NNa_2O_9]^{2+}$	– 11.21	nd		

C10	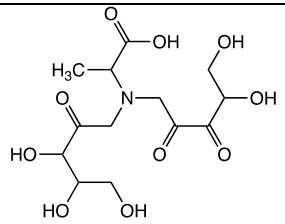	352.1245	$[C_{13}H_{22}NO_{10}]^+$	0.367	nd			353.1261	$[C_{12}[^{13}C]H_{22}NO_{10}]^+$	− 3.05
C10	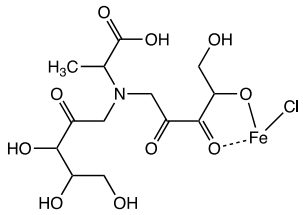	464.0044	$[C_{13}H_{20}Fe[^{35}Cl]NNaO_{10}]^+$	5.75	404.0874	$[C_2[^{13}C]_{10}H_{20}FeNO_{10}]^+$	26.59	251.9796	$[C_{12}[^{13}C]H_{20}Fe[^{35}Cl]NNaKO_{10}]^{2+}$	− 17.94
C11	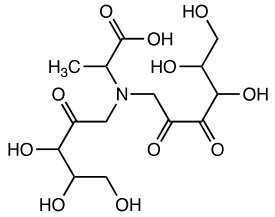	382.1349	$[C_{14}H_{24}NO_{11}]^+$	− 0.09	415.1514	$[C_3[^{13}C]_{11}H_{23}NNaO_{11}]^+$	− 4.42	405.1164	$[C_{13}[^{13}C]H_{23}NNaO_{11}]^+$	− 8.11
C11	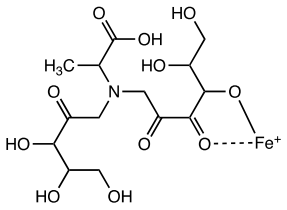	436.057	$[C_{14}H_{22}FeNO_{11}]^+$	7.63	264.0204	$[C_3[^{13}C]_{11}H_{22}Fe[^{35}Cl]NNa_2O_{11}]^+$	4.51	437.0563	$[C_{13}[^{13}C]H_{22}FeNO_{11}]^+$	− 1.67

C11	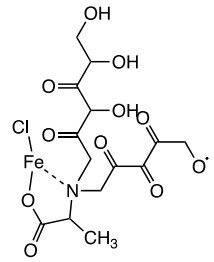	504.9473	$[C_{14}H_{17}Fe[^{35}Cl]KNO_{11}]^+$	0.38	515.9848	$[C_3[^{13}C]_{11}H_{17}Fe[^{35}Cl]NKO_{11}]^+$	1.53	467.9941	$[C_{13}[^{13}C]_1H_{18}Fe[^{35}Cl]NO_{11}]^+$	− 1.03
		506.945	$[C_{14}H_{17}Fe[^{37}Cl]KNO_{11}]^+$	1.66						
C11	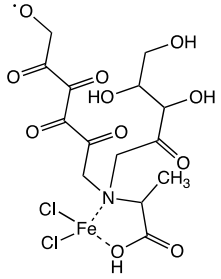	540.9262	$[C_{14}H_{18}Fe[^{35}Cl]_2KNO_{11}]^+$	0.77	515.9848	$[C_3[^{13}C]_{11}H_{17}Fe[^{35}Cl]NKO_{11}]^+$	1.53	467.9941	$[C_{13}[^{13}C]_1H_{18}Fe[^{35}Cl]NO_{11}]^+$	− 1.03
		542.9217	$[C_{14}H_{18}Fe[^{35}Cl][^{37}Cl]KNO_{11}]^+$	1.59						
		544.9203	$C_{14}H_{18}Fe[^{37}Cl]_2KNO_{11}]^+$	4.43						
C12	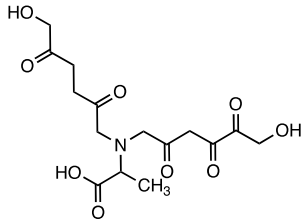	382.1161	$[C_{15}H_{21}NNaO_9]^+$	12.3	410.1272	$[C_3[^{13}C]_{12}H_{21}NKO_9]^+$	5.25	383.1144	$[C_{14}[^{13}C]_1H_{21}NNaO_9]^+$	0.5
C12		360.1313	$[C_{15}H_{22}NO_9]^+$	5.12						

C12	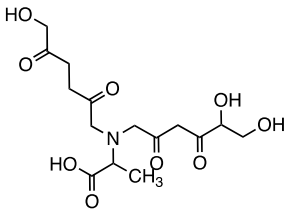	362.1452	$[C_{15}H_{24}NO_9]^+$	0.26	374.1826	$[C_3[^{13}C]_{12}H_{24}NO_9]^+$	− 5.92	385.1206	$[C_{14}[^{13}C]_1H_{23}NNaO_9]^+$	− 24.04
C12		384.1303	$[C_{15}H_{23}NNaO_9]^+$	8.46						
C12	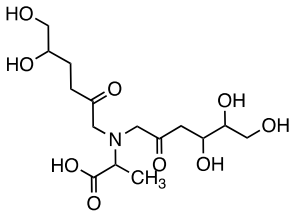	388.1587	$[C_{15}H_{27}NNaO_9]^+$	0.9	400.2097	$[C_3[^{13}C]_{12}H_{27}NNaO_9]^+$	27.71	nd		
C12	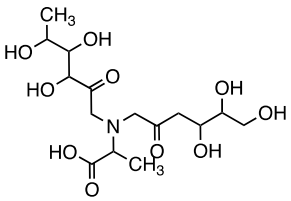	404.1566	$[C_{15}H_{27}NNaO_{10}]^+$	8.25	416.198	$[C_3[^{13}C]_{12}H_{27}NNaO_{10}]^+$	12.07	405.1557	$C_{14}[^{13}C]_1H_{27}NNaO_{10}]^+$	− 0.92
C12	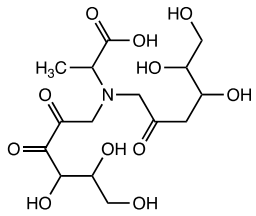	396.1522	$[C_{15}H_{26}NO_{11}]^+$	4.08	408.1886	$[C_3[^{13}C]_{12}H_{26}NO_{11}]^+$	− 4.15	419.1345	$[C_{14}[^{13}C]H_{25}NNaO_{11}]^+$	− 1.99
C12		402.1395	$[C_{15}H_{25}NNaO_{10}]^+$	4.69	392.1849	$[C_3[^{13}C]_{12}H_{26}NO_{10}]^+$	− 28.12	nd		

C12	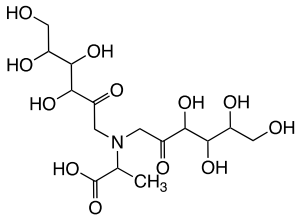	414.1625	$[C_{15}H_{28}NO_{12}]^+$	3.26	426.2021	$[C_3[^{13}C]_{12}H_{28}NO_{12}]^+$	1.623	415.1617	$[C_{14}[^{13}C]H_{28}NO_{12}]^+$	6.757
C12	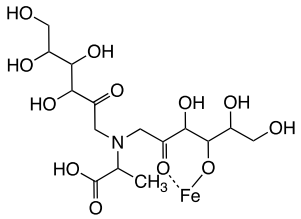	468.0815	$[C_{15}H_{26}FeNO_{12}]^+$	3.44	480.116	$[C_3[^{13}C]_{12}H_{26}FeNO_{12}]^+$	− 8.64	272.0118	$[C_{14}[^{13}C]H_{27}Fe[^{35}Cl]NKO_{12}]^{2+}$	0.96
C12	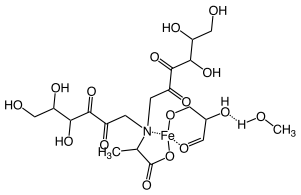	586.1057	$[C_{19}H_{32}FeNO_{16}]^+$	− 2.3	338.0549	$[C_4[^{13}C]_{15}H_{31}FeN_2NaKO_{16}]^{2+}$	7.11	323.0397	$[C_{18}[^{13}C]H_{33}Fe[^{35}Cl]NaNO_{16}]^2$	5.65

[a]Total number of carbon atoms incorporated from glucose

[b]Error (in ppm) in calculating the elemental composition

[c]nd: not detected

5.4.5.1. Ion at *m/z* 414

Based on the HRMS data, isotope labelling and MS/MS analysis, this ion represents di-glycated alanine with two intact hexoses, as shown in Figure 5.2 dissociated from the complex observed at *m/z* 484.0868. MS/MS fragmentations under 5 eV have indicated that di-glycated amino acids can release free Amadori compound as evidenced by the presence of its molecular ion at *m/z* 252 and its dehydration products at *m/z* 216 and 234 as characteristic fragmentations of the ARPs under positive ionization mode, along with its expected diagnostic ions at *m/z* 97 and 145 (Xing *et al*, 2020). As shown in Table S5.3, the isotope incorporation in the proposed fragment ions is consistent with the structures shown, providing further evidence for the origin of the proposed fragments.

5.4.5.2. Ion at *m/z* 298

Tri-glycated *bis*[alaninato]iron(II) complex was detected as doubly charged ion at *m/z* 298, as evidenced by observing its isotopic distribution at *m/z* 298.0611 (100%) and *m/z* 298.5628 (22.56%) exhibiting isotopic spacing of 0.5 amu. In addition, MS/MS fragmentations under 15 eV have generated fragments ions consistent with the proposed structure (see Table S5.6 and Figure S5.6).

5.4.5.3. Ions at *m/z* 504 & 540

The two related *N*,*N*-di-glycated alanine iron(II) complexes observed at *m/z* 504 and 540 differed only in the number of chlorine atoms. The ion at *m/z* 540 had two chlorine atoms as evidenced by the presence of related ions at 542 and 544 with the expected isotopic abundance ratio, similarly ion at *m/z* 504 with associated ion at *m/z* 506 (see Table S5.4 and Figure S5.4). Furthermore, the di-chlorinated ion at *m/z* 540 lost one and two moles of HCl to generate the ions at *m/z* 504 and *m/z* 468, respectively. In addition, retro aldol degradation of the former ion gave rise to the ions at *m/z* 444 and 446 containing the expected isotopes of chlorine ([^{35}Cl] and [^{37}Cl]) (see Figures 5.3, S5.5 and Table S5.5).

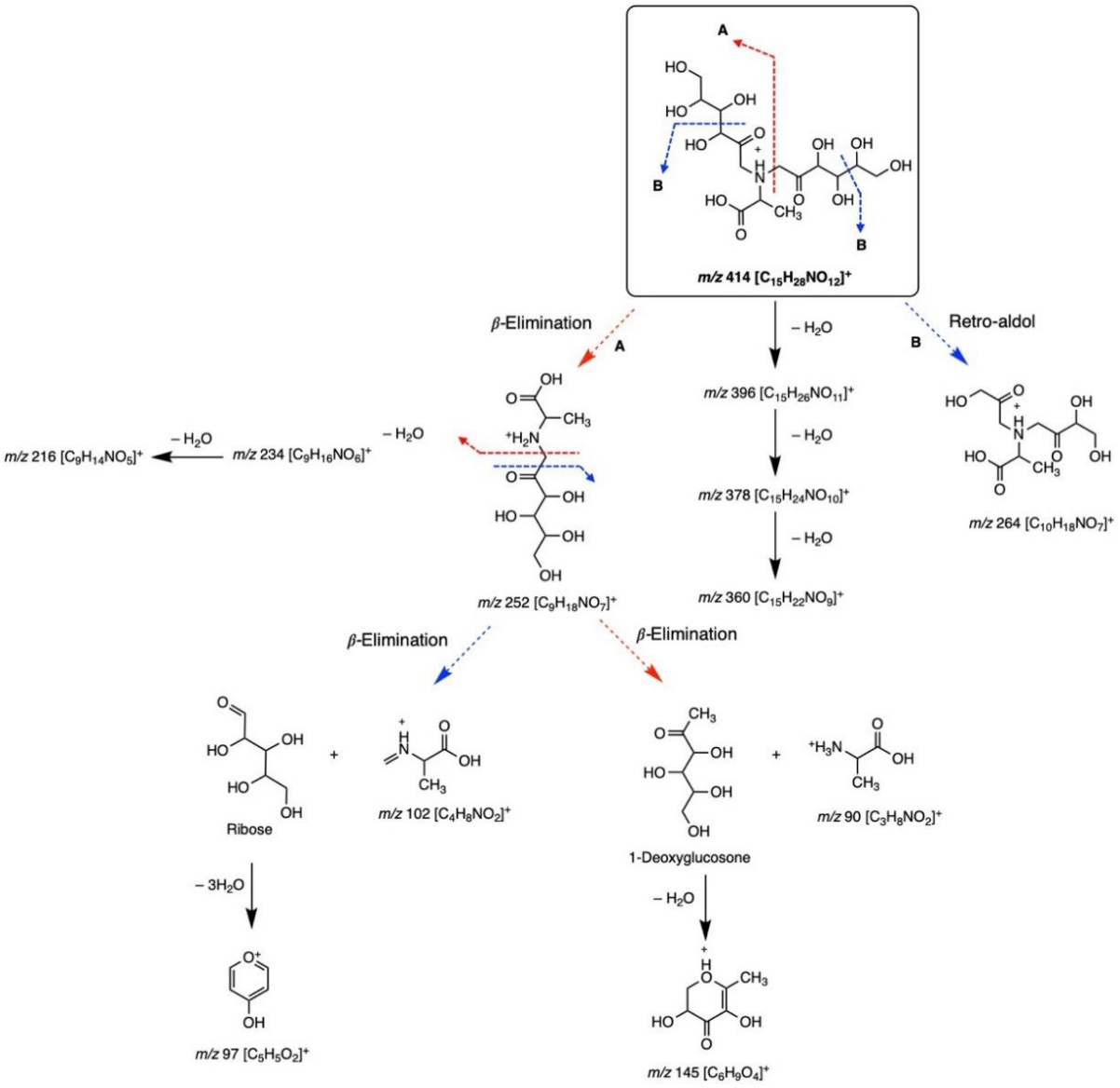

Figure 5.2. Proposed MS/MS fragmentation pathways of *m/z* 414 detected in the Ala/Glu/$FeCl_2$ model system (see Table S5.3)

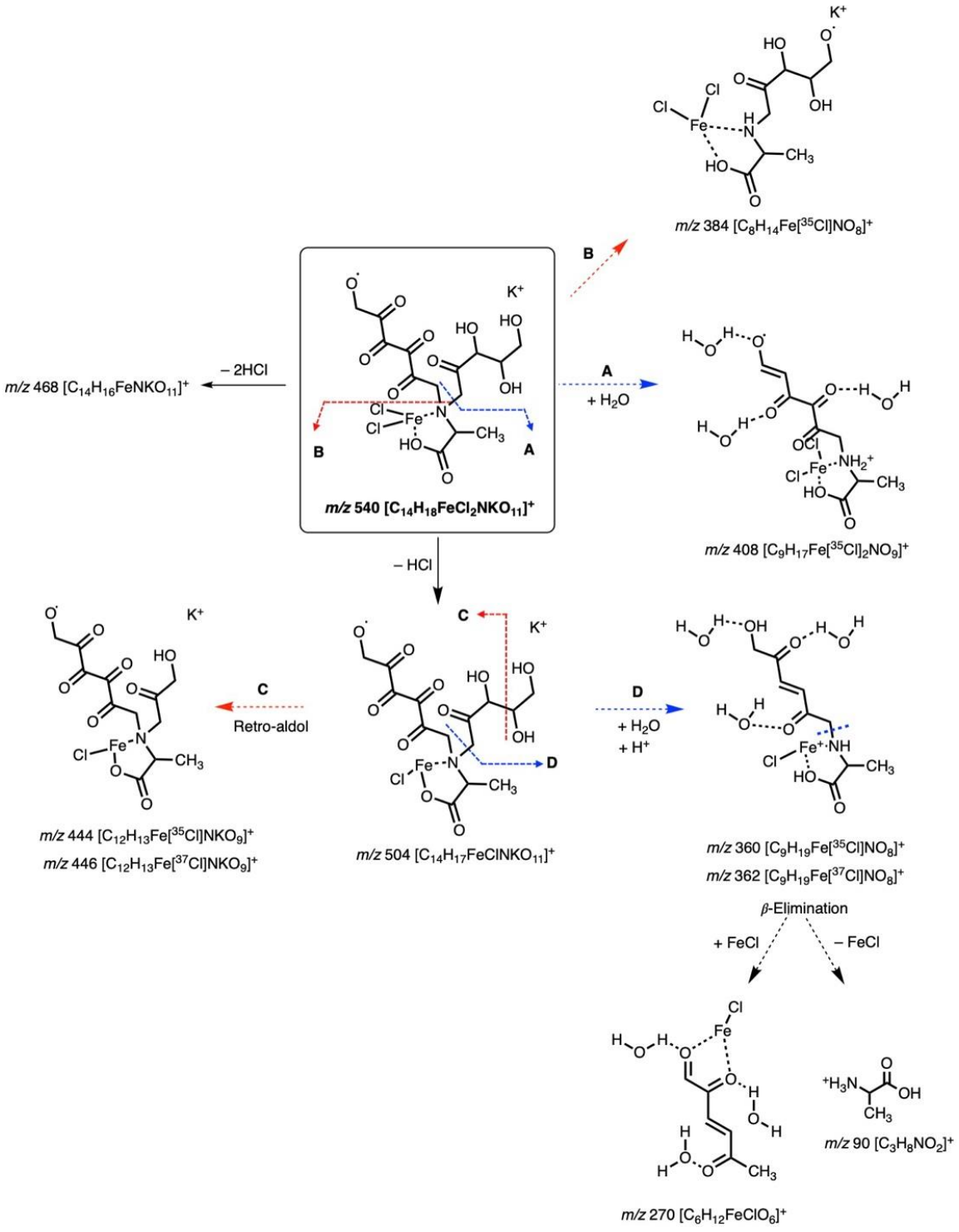

Figure 5.3. Proposed MS/MS fragmentation pathways of *m/z* 540, detected in Ala/Glu/$FeCl_2$ model system (see also Table S5.5 & Figure S5.5)

5.5. CONCLUSION

The studies conducted with glucose/alanine model systems with and without $FeCl_2$ have indicated that the addition of divalent iron to the Maillard model systems can lead to the formation of *bis*[*N*,*N'*-di-glycated alanine]iron(II) complexes with subsequent release of *N*,*N*-diglycated alanine derivatives into the reaction mixture. Such derivatives are considered to be more reactive than mono-glycated Amadori compounds and can provide the needed rationalization for the observed accelerating effect of such ions on the Maillard reaction.

5.6. REFERENCES

Belikov, V. M., Vitt, S. V., Kuznetsova, N. I., Bezrukov, M. G., Saporovskaya, M. B. (1969). Reaction of the copper complex of L-alanine with acetaldehyde and the mechanism of the Akabori reaction. *Russian Chemical Bulletin*, 18, 2371–2375.

Feather, M. S. and Mossine, V. V. (2005). Correlations between Structure and Reactivity of Amadori Compounds: the Reactivity of Acyclic Forms. *The Maillard Reaction in Foods and Medicine*, 37–42.

Fodor, G. and Sachetto, J. P. (1968). The mechanism of formation of 3-deoxy glucosulose from glucose 3-phosphate and from difructosyl glycine. *Tetrahedron Letters*, 4, pp. 401–403.

Gensberger-Reigl, S., Auditore, A., Huppert, J., and Pischetsrieder, M. (2020). Metal cations promote α-dicarbonyl formation in glucose-containing peritoneal dialysis fluids. *Glycoconjugate Journal*, 38(3), 319–329.

Kim, E. S. and Yaylayan, V. (2020). Profiling of glucose degradation products through complexation with divalent metal ions coupled with ESI/qTOF/MS/MS analysis. *Current Research in Food Science*, 3, 268–274.

Kim, E. S. and Yaylayan, V. (2021). Identification of the Maillard reaction intermediates as divalent iron complexes in alanine/glucose/FeCl2 model system using ESI/qTOF/MS/MS and isotope labelling technique. *Current Research in Food Science*, 4, pp. 287–294.

Lund, M. N. and Ray, C. A. (2017). Control of Maillard Reactions in Foods: Strategies and Chemical Mechanisms. *Journal of Agricultural and Food chemistry*, 65 (23), pp. 4537–4552.

Nashalian, O. and Yaylayan, V. A. (2014). Thermally induced oxidative decarboxylation of copper complexes of amino acids and formation of strecker aldehyde. *Journal of Agricultural and Food chemistry*, 62 (33), pp. 8518–8523.

Nashalian, O. and Yaylayan, V. A. (2015a). De novo synthesis of amino acids during the maillard reaction: qTOF/ESI mass spectrometric evidence for the mechanism of Akabori transformation. *Journal of Agricultural and Food chemistry*, 63 (1), pp. 328–334.

Nashalian, O. and Yaylayan, V. A. (2015b). Sugar-Conjugated Bis(glycinato)copper(II) Complexes and Their Modulating Influence on the Maillard Reaction. *Journal of Agricultural and Food chemistry*, 63 (17), pp. 4353–4360.

Patiny, L. and Borel, A. (2013). ChemCalc: a building block for tomorrow's chemical infrastructure. *Journal of chemical information and modeling*, 53 (5), pp. 1223–1228.

Pearson, R. G. and Lanier, R. D. (1964). Rates of rapid ligand exchange reactions by nuclear magnetic resonance line broadening studies. *Journal of the American Chemical Society*, 86, pp. 765–771.

Ramonaitytė, D. T., Keršienė, M. Adams, A., Tehrani, K. A., Kimpe, N. D. (2009). The interaction of metal ions with Maillard reaction products in a lactose–glycine model system. *Food Research International* 42 (3), pp. 331–336.

Rizzi, G. P. (1997). Chemical structure of colored maillard reaction products. *Food Reviews International*, 13 (1), pp. 1–28.

Xing, H., Mossine, V. V., Yaylayan, V. (2020) Diagnostic MS/MS fragmentation patterns for the discrimination between Schiff bases and their Amadori or Heyns rearrangement products. *Carbohydrate Research*, 491, pp. 107985–107985.

5.7. SUPPLEMENTARY DATA

Table S5.1. Elemental composition and isotope incorporation in *bis*[*N,N'*-di-glycated alanine]iron(II) complexes observed in Ala/Glu/Fe.Cl_2 model system in methanol

Structure	Ala/Glu/$FeCl_2$		Ala/Glu[^{13}C-U] /$FeCl_2$		Ala[^{13}C-3]/Glu/$FeCl_2$	
	[M+X][a] *m/z*	Elemental Composition	[M+X] *m/z*	Elemental Composition	[M+X] *m/z*	Elemental Composition
	Calc^{+c} *Calc^{2+d}*		*Calc^{+}* *Calc^{2+}*		*Calc^{+}* *Calc^{2+}*	
	Observed[e]	Error[b] (ppm)	Observed[e]	Error (ppm)	Observed[e]	Error (ppm)
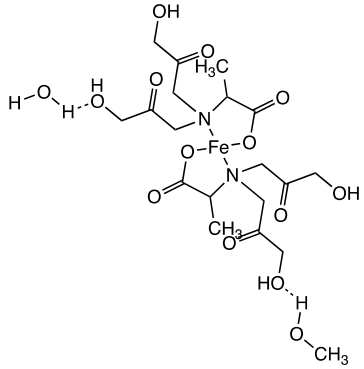	*571.1432*		*694.1005*		*573.1499*	
	–		*347.0499*		–	
	571.1434	$[C_{19}H_{35}FeN_2O_{14}]^+$	347.0533	$[C_7[^{13}C]_{12}H_{37}Fe[^{35}Cl]_2N_2KO_{14}]^{2+}$	573.1528	$[C_{17}[^{13}C]_2H_{35}FeN_2O_{14}]^+$
		– 0.64		9.53		4.06
	578.1378					
	578.1348	$[C_{19}H_{35}[^{63}Cu]N_2O_{14}]^+$				
		– 5.32				
	580.1360					
	580.1336	$[C_{19}H_{35}[^{65}Cu]N_2O_{14}]^+$				
$[M + H]^+ = 571$		– 4.26				
C12						
	595.0623		*609.1093*		*597.069*	
	595.0667	$[C_{20}H_{28}Fe[^{35}Cl]N_2O_{13}]^+$	609.1135	$[C_6[^{13}C]_{14}H_{28}Fe[^{35}Cl]N_2O_{13}]^+$	597.0737	$[C_{18}[^{13}C]_2H_{28}Fe[^{35}Cl]N_2O_{13}]^+$

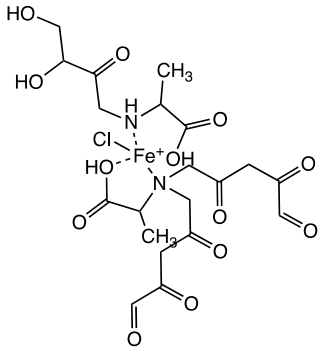 [M + Cl]$^+$ = 595	6.34		5.92		6.8	
C14						
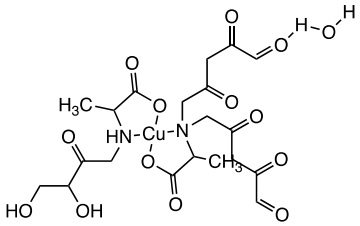 [M + K]$^+$ = 622	*622.0468*					
	622.0374	$[C_{20}H_{28}[^{63}Cu]N_2KO_{14}]^+$ – 15.13				
	624.045					
	624.0389	$[C_{20}H_{28}[^{65}Cu]N_2KO_{14}]^+$ – 9.78				
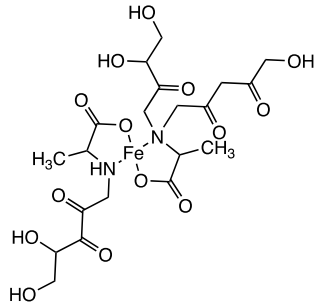 [M + H]$^+$ = 579	*579.1119* –		*704.0759* *352.0377*		*581.1186* –	
	579.1122	$[C_{20}H_{31}FeN_2O_{14}]^+$ – 0.46	352.0357	$[C_6[^{13}C]_{14}H_{33}Fe[^{35}Cl]_2N_2KO_{14}]^{2+}$ – 5.68	581.1114	$[C_{18}[^{13}C]_2H_{31}FeN_2O_{14}]^+$ – 13.38
	586.1065					
	586.1023	$[C_{20}H_{31}[^{63}Cu]N_2O_{14}]^+$ – 7.3				

C14	*588.1047*					
	588.1021	$[C_{20}H_{31}[^{65}Cu]N_2O_{14}]^+$ – 4.54				
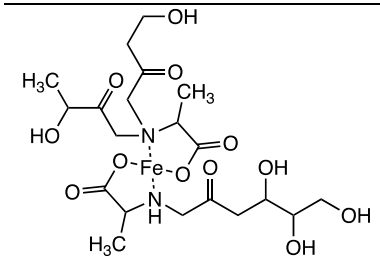 $[M + Na_2]^{2+} = 298$ **C14**	*596.1256* *298.0622*		*676.1174* *338.0584*		*598.1318* *299.0656*	
	298.0611	$[C_{20}H_{34}FeN_2Na_2O_{12}]^{2+}$ – 3.95	338.0549	$[C_6[^{13}C]_{14}H_{37}Fe[^{35}Cl]_2N_2KO_{12}]^{2+}$ 10.45	299.0668	$[C_{18}[^{13}C]_2H_{34}FeN_2Na_2O_{12}]^{2+}$ 3.91
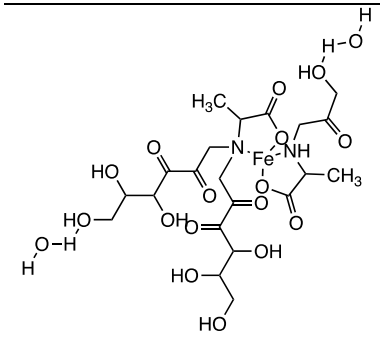 $[M + Na]^+ = 683.12$ **C15**	*683.1204*		*770.1241*		*685.1271*	
	683.1203	$[C_{21}H_{36}FeN_2NaO_{18}]^+$ – 1.05	770.1299	$[C_6[^{13}C]_{15}H_{38}Fe[^{35}Cl]_2N_2NaO_{18}]^+$ 6.76	685.1113	$[C_{19}[^{13}C]_2H_{36}FeN_2NaO_{18}]^+$ – 23.98
	683.1148 –		*704.1622* *352.0808*		*649.1448* –	
	683.1166	$[C_{24}H_{36}Fe[^{35}Cl]N_2O_{15}]^+$	352.0845	$[C_6[^{13}C]_{18}H_{35}FeN_2KO_{15}]^{2+}$	649.1427	$[C_{22}[^{13}C]_2H_{35}FeN_2O_{15}]^+$

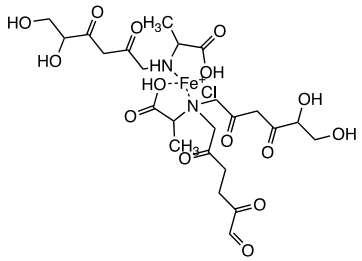 [M + Cl]$^+$ = 683.11 **C18**		1.24	10.4	– 4.14
	784.0892			
	784.0878	$[C_{24}H_{40}[^{63}Cu][^{35}Cl]_2N_2NaO_{17}]^+$	– 1.81	
	786.0874			
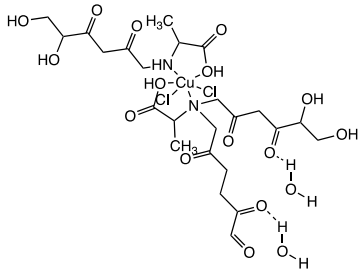 [M + Cl_2 + Na]$^+$ = 683.11 **C18**	786.0888	$[C_{24}H_{40}[^{65}Cu][^{35}Cl]_2N_2NaO_{17}]^+$	1.76	
	786.0862			
	786.0888	$[C_{24}H_{40}[^{63}Cu][^{35}Cl][^{37}Cl]N_2NaO_{17}]^+$	3.22	
	788.0846			
	788.0891	$[C_{24}H_{40}[^{65}Cu][^{35}Cl][^{37}Cl]N_2NaO_{17}]^+$	5.88	

	788.0833					
	788.0891	$[C_{24}H_{40}[^{63}Cu][^{37}Cl]_2N_2NaO_{17}]^+$ 7.33				
	930.074 *465.037*		*856.2154* *463.0763*		*800.1902* *400.0948*	
	465.0369	$[C_{25}H_{46}Fe[^{35}Cl]_2N_2NaKO_{23}]^{2+}$ – 0.38	463.0713	$[C_7[^{13}C]_{18}H_{47}Fe[^{35}Cl]_2N_2KO_{23}]^{2+}$ – 10.8	400.0909	$[C_{23}[^{13}C]_2H_{46}FeN_2O_{23}]^{2+}$ – 9.85
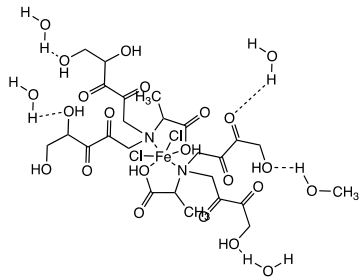 $[M + Cl_2 + Na + K]^{2+} = 465$ **C18**	*937.0693*					
	937.0492	$[C_{25}H_{46}[^{63}Cu][^{35}Cl]_2N_2NaKO_{23}]^+$ – 21.52				
	939.0675					
	939.0479	$[C_{25}H_{46}[^{65}Cu][^{35}Cl]_2N_2NaKO_{23}]^+$ – 20.93				
	939.0664					
	939.0479	$[C_{25}H_{46}[^{63}Cu][^{35}Cl][^{37}Cl]N_2NaKO_{23}]^+$ – 20.3				
	941.0646					
	941.0559	$[C_{25}H_{46}[^{65}Cu][^{35}Cl[^{37}Cl]N_2NaKO_{23}]^+$				

		– 9.25				
	941.0634					
	941.0559	$C_{25}H_{46}[^{63}Cu][^{37}Cl]_2N_2NaKO_{23}]^+$ – 8.04				
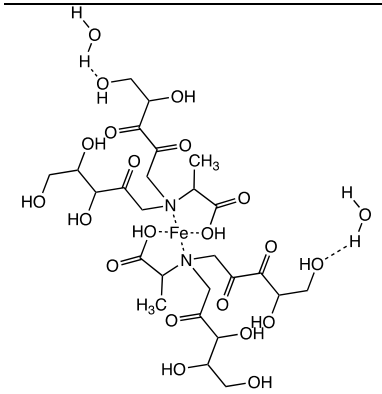 $[M + Cl_2 + Na + K]^{2+} = 463$ **C20**	*926.0797* *463.0396*		*858.2195* *429.1095*		*856.1331* *428.0663*	
	463.0392	$[C_{26}H_{46}Fe[^{35}Cl]_2N_2NaKO_{22}]^{2+}$ – 0.91	429.1061	$[C_6[^{13}C]_{20}H_{44}FeN_2Na_2O_{22}]^{2+}$ – 7.98	428.0717	$[C_{24}[^{13}C]_2H_{44}FeN_2NaKO_{22}]^{2+}$ 12.62
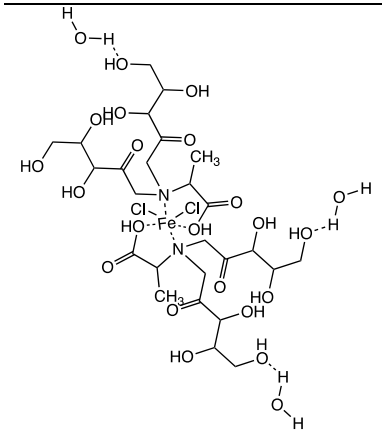	*964.0955* *482.0475*		*874.2534* *437.1264*		*878.175* *439.0872*	
	482.0497	$[C_{26}H_{52}Fe[^{35}Cl]_2N_2K_2O_{23}]^{2+}$ 4.52	437.1169	$[C_6[^{13}C]_{20}H_{51}FeN_2KO_{23}]^{2+}$ – 21.85	439.0873	$[C_{24}[^{13}C]_2H_{50}FeN_2NaKO_{23}]^{2+}$ 0.16

$[M + Cl_2 + K_2]^{2+}$ = 482

C20

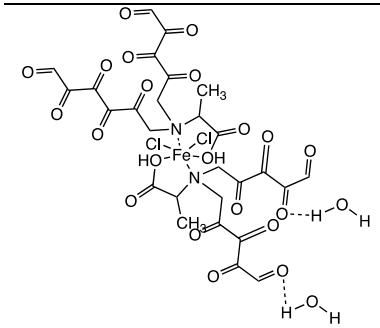	*949.8921*		*916.0249*		*840.9817*	
	474.9458		–		–	
	474.9445	$[C_{27}H_{26}Fe[^{35}Cl]_2N_2K_2O_{23}]^{2+}$	916.0401	$[C_6[^{13}C]_{21}H_{26}Fe[^{35}Cl]_2N_2NaO_{23}]^{+}$	840.9875	$[C_{25}[^{13}C]_2H_{24}FeN_2KO_{23}]^{+}$
		– 2.73		15.94		6.14

$[M + Cl_2 + K_2]^{2+}$ = 474

C21

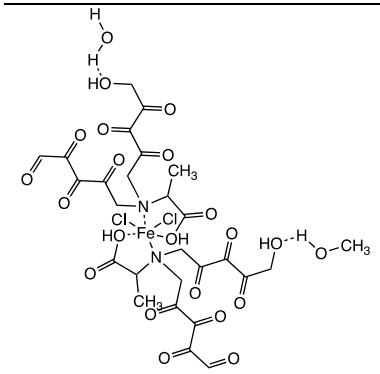	*939.9441*		*921.0475*		*866.0391*	
	469.9718		–		*433.0192*	
	469.9734	$[C_{27}H_{32}Fe[^{35}Cl]_2N_2K_2O_{22}]^{2+}$	921.0487	$[C_7[^{13}C]_{20}H_{32}Fe[^{35}Cl]_2N_2KO_{22}]^{+}$	433.0174	$[C_{25}[^{13}C]_2H_{34}FeN_2O_{22}]^{2+}$
		3.37		1.23		– 4.36

$[M + Cl_2 + K_2]^{2+}$ = 469

C20

	925.9858		*962.0269*		*868.0547*	
	462.9926		*481.0131*		*434.0271*	
	462.9927	$[C_{27}H_{34}Fe[^{35}Cl]_2N_2NaKO_{22}]^{2+}$	481.0127	$[C_7[^{13}C]_{20}H_{34}Fe[^{35}Cl]_2NK_2O_{22}]^{2+}$	434.0217	$[C_{25}[^{13}C]_2H_{36}Fe[^{35}Cl]_2N_2O_{22}]^{2+}$

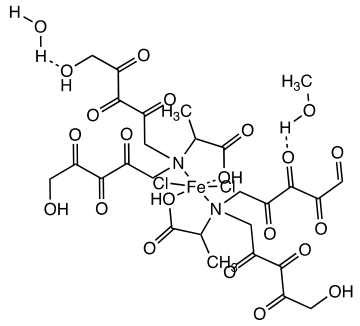		0.06		– 8.07		– 12.47
$[M + Cl_2 + Na + K]^{2+} = 462$						
C20						
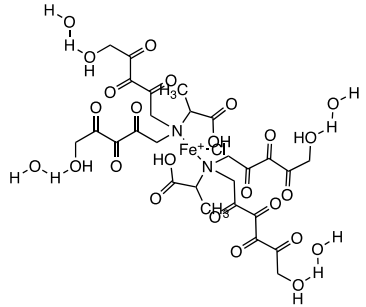	*920.0433*				*908.0552*	
	460.0213				*454.0273*	
	460.0214	$[C_{27}H_{38}Fe[^{35}Cl]N_2KO_{25}]^{2+}$	nd[f]		454.0306	$[C_{25}[^{13}C]_2H_{36}FeN_2NaKO_{25}]^{2+}$
		0.04	nd[f]			7.11
	922.0403					
	461.0199					
$[M + Cl + K]^{2+} = 460$	461.0215	$[C_{27}H_{38}Fe[^{37}Cl]N_2KO_{25}]^{2+}$				
C21		3.46				
	977.9809		*983.0774*		*904.0759*	
	488.9902		–		*452.0376*	
	488.9899	$[C_{27}H_{38}Fe[^{35}Cl]_2N_2K_2O_{24}]^{2+}$	983.0769	$[C_6[^{13}C]_{21}H_{38}Fe[^{35}Cl]_2N_2NaKO_{24}]^{+}$	452.0385	$[C_{25}[^{13}C]_2H_{40}Fe[^{35}Cl]_2N_2O_{24}]^{2+}$

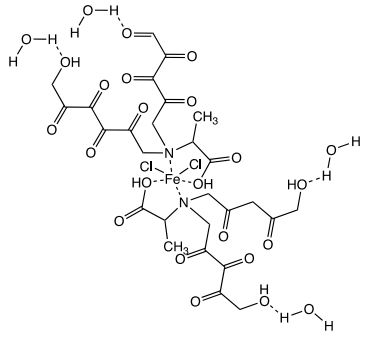 [M + Cl_2 + K_2]$^{2+}$ = 488 C21		– 0.62		– 1.14		1.82
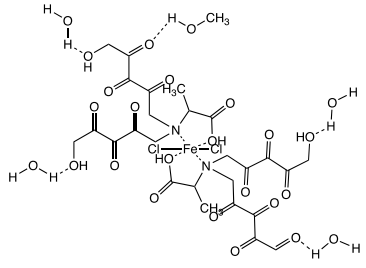 [M + Cl_2 + K_2]$^{2+}$ = 465 C20	*995.9915*		*868.1935*		*982.0242*	
	497.9954		*434.0964*		*491.0118*	
	497.994	$[C_{27}H_{40}Fe[^{35}Cl]_2N_2K_2O_{25}]^{2+}$	434.0936	$[C_7[^{13}C]_{20}H_{40}FeN_2O_{25}]^{2+}$	491.0182	$[C_{25}[^{13}C]_2H_{40}Fe[^{35}Cl]_2N_2NaKO_{25}]^{2+}$
		– 2.98		– 6.62		12.89
	997.9885					
	498.994					
	498.9911	$[C_{27}H_{40}Fe[^{35}Cl][^{37}Cl]N_2K_2O_{25}]^{2+}$				
		– 5.83				
	999.9856					
	499.9925					
	499.9933	$[C_{27}H_{40}Fe[^{37}Cl]_2N_2K_2O_{25}]^{2+}$				
		1.53				
	863.1548		*872.2142*		*865.1615*	

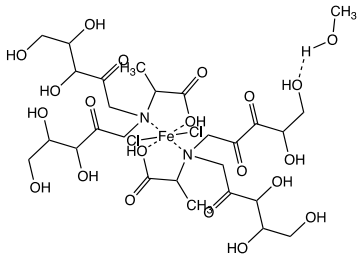	–		*436.1068*		–	
	863.1522	$[C_{27}H_{49}Fe[^{35}Cl]_2N_2O_{21}]^+$	436.102	$[C_7[^{13}C]_{20}H_{46}FeN_2Na$	865.1535	$[C_{25}[^{13}C]_2H_{49}Fe[^{35}Cl]_2N_2$
				$KO_{21}]^{2+}$		$O_{21}]^+$
		– 3.73		– 11.14		– 9.98
$[M + H + Cl_2]^+ = 863$						
C20						
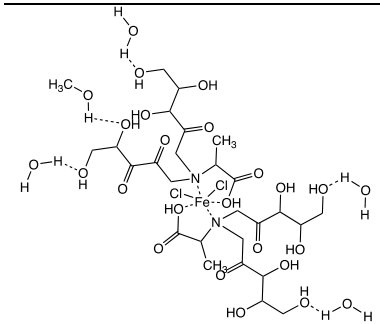	*958.1869*		*956.2356*			
	479.0931]		*478.1175*			
	479.0928	$[C_{27}H_{57}Fe[^{35}Cl]_2N_2Na$	478.1139	$[C_7[^{13}C]_{20}H_{54}Fe[^{35}Cl]N_2$	nd	
		$O_{25}]^{2+}$		$KO_{25}]^{2+}$		
		– 0.79		– 7.59		
$[M + H + Cl_2 + Na]^{2+} = 479$						
C20						
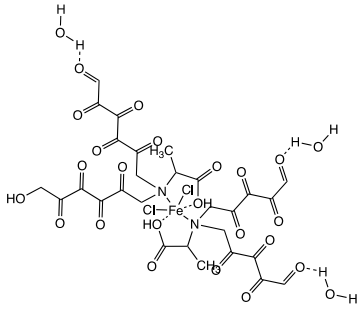	*965.9654*		*948.0337*		*887.0237*	
	482.9824		*474.0165*		–	
	482.982	$[C_{28}H_{30}Fe[^{35}Cl]_2N_2Na_2$	474.0052	$[C_6[^{13}C]_{22}H_{28}FeN_2K_2$	887.0305	$[C_{26}[^{13}C]_2H_{30}Fe[^{35}Cl]N_2$
		$O_{25}]^{2+}$		$O_{25}]^{2+}$		$O_{25}]^+$
		– 0.88		– 24.02		7.03
	967.9624					
	483.9809					
$[M + Cl_2 + Na_2]^{2+} = 482$	483.9824	$[C_{28}H_{30}Fe[^{35}Cl][^{37}Cl]N_2$				

C22		$Na_2O_{25}]^{2+}$ 3				
	969.9595 *484.9794*					
	484.9734	$[C_{28}H_{30}Fe[^{37}Cl]_2N_2Na_2$ $O_{25}]^{2+}$ – 12.52				
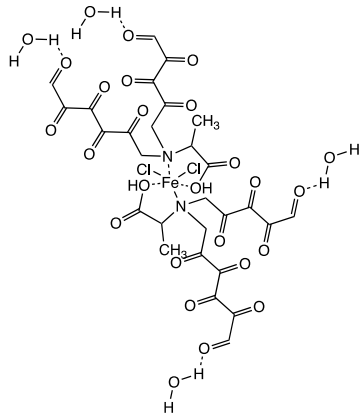 $[M + H + Cl_2 + K]^{2+} = 487$ $[M + H + Cl_2 + Na]^{2+} = 479$ C22	*975.9523* *487.9758*		*1020.008* *510.0037*		*961.985* *480.9922*	
	487.9757	$[C_{28}H_{31}Fe[^{35}Cl]_2N_2KO_{26}]^{2+}$ – 0.36	510.005	$[C_6[^{13}C]_{22}H_{30}Fe[^{35}Cl]_2$ $N_2NaKO_{26}]^{2+}$ 2.45	480.9946	$[C_{26}[^{13}C]_2H_{31}Fe[^{35}Cl]_2N_2$ $NaO_{26}]^{2+}$ 4.86
	959.9783 *479.9889*					
	479.9886	$[C_{28}H_{31}Fe[^{35}Cl]_2N_2Na$ $O_{26}]^{2+}$ – 0.64				
	961.9754 *480.9874*					
	480.984	$[C_{28}H_{31}Fe[^{35}Cl][^{37}Cl]N_2$ $NaO_{26}]^{2+}$ – 7.14				
	963.9724 *481.9859*					

	481.9814	$[C_{28}H_{31}Fe[^{37}Cl]_2N_2NaO_{26}]^{2+}$ – 9.46				
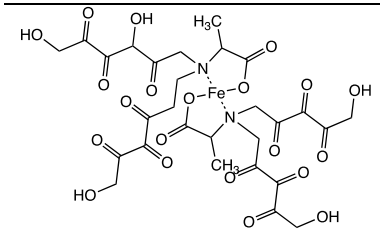 [M + H]$^+$ = 789 **C22**	*789.0919* –		*848.1502* *424.0748*		*791.0986* –	
	789.0948	$[C_{28}H_{33}FeN_2O_{21}]^+$ 2.89	424.0636	$[C_6[^{13}C]_{22}H_{35}Fe[^{35}Cl]N_2O_{21}]^{2+}$ – 26.56	791.1076	$[C_{26}[^{13}C]_2H_{33}FeN_2O_{21}]^+$ 10.58
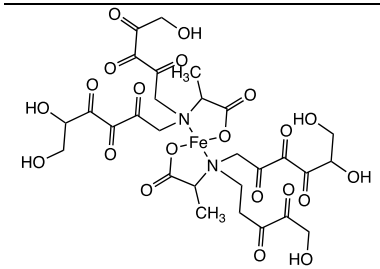 [M + H]$^+$ = 791 **C22**	*791.1076* –		*814.1892* *407.0943*		*793.1143* –	
	791.1074	$[C_{28}H_{35}FeN_2O_{21}]^+$ – 0.97	407.1011	$[C_6[^{13}C]_{22}H_{36}FeN_2O_{21}]^{2+}$ 16.58	793.1109	$[C_{26}[^{13}C]_2H_{35}FeN_2O_{21}]^+$ – 5.01
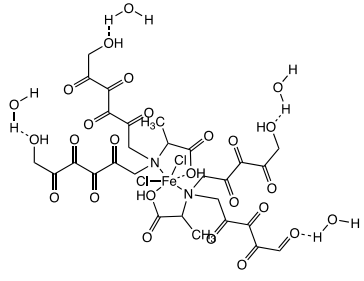	*981.9992* *490.9993*		*932.1197* *466.0595*		*1005.9879* *502.9936*	
	490.9998	$[C_{28}H_{37}Fe[^{35}Cl]_2N_2KO_{26}]^{2+}$ 0.91	466.0617	$[C_6[^{13}C]_{22}H_{35}FeN_2KO_{26}]^{2+}$ 4.55	502.9877	$[C_{26}[^{13}C]_2H_{36}Fe[^{35}Cl]_2N_2NaKO_{26}]^{2+}$ – 11.89
	983.9963					

$[M + H + Cl_2 + K]^{2+} = 490$ **C22**	*491.9978*					
	491.995	$[C_{28}H_{37}Fe[^{35}Cl][^{37}Cl]N_2KO_{26}]^{2+}$ – 5.85				
	985.9933 *492.9964*					
	493.0056	$[C_{28}H_{37}Fe[^{37}Cl]_2N_2KO_{26}]^{2+}$ 18.66				
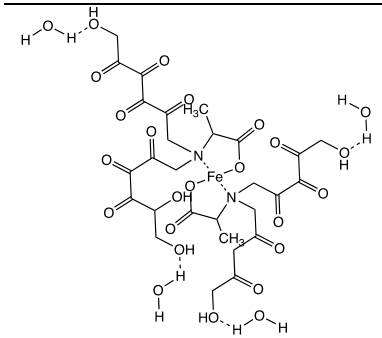 $[M + H]^{+} = 861$ **C22**	*861.1342* –				*886.1307* *443.065*	
	861.1349	$[C_{28}H_{41}FeN_2O_{25}]^{+}$ 0.14	nd		443.0681	$[C_{26}[^{13}C]_2H_{41}FeN_2NaO_{25}]^{2+}$ 6.82
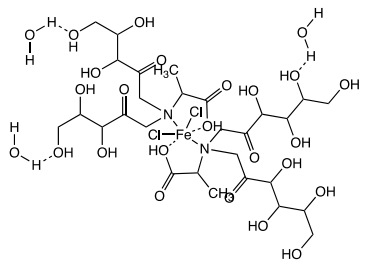 $[M + H + Cl_2 + Na]^{2+} = 485$	*970.1869* *485.0931*		*992.2607* *496.13*		*1026.1234* *513.0614*	
	485.0915	$[C_{28}H_{57}Fe[^{35}Cl]_2N_2NaO_{25}]^{2+}$ – 3.46	496.1289	$[C_6[^{13}C]_{22}H_{57}Fe[^{35}Cl]_2N_2NaO_{25}]^{2+}$ – 2.38	513.054	$[C_{26}[^{13}C]_2H_{56}Fe[^{35}Cl]_2N_2K_2O_{25}]^{2+}$ – 14.5
	972.1839 *486.0917*					

C22	486.0917	$[C_{28}H_{57}Fe[^{35}Cl][^{37}Cl]N_2$ $NaO_{25}]^{2+}$ 0				
	974.1810 *487.0902*					
	487.0934	$[C_{28}H_{57}Fe[^{37}Cl]_2N_2$ $NaO_{25}]^{2+}$ 6.51				
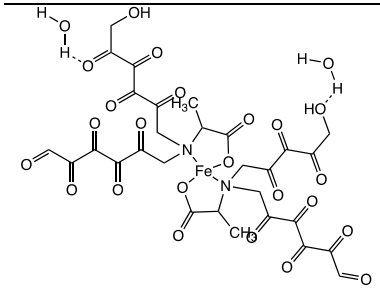 $[M + K_2]^{2+} = 468$ C23	*937.9599* *468.9796*		*1032.9904* *516.4949*		*957.9901* *478.9948*	
	468.978	$[C_{29}H_{28}FeN_2K_2O_{25}]^{2+}$ – 3.59	516.4796	$[C_6[^{13}C]_{23}H_{30}Fe[^{35}Cl]_2$ $N_2K_2O_{25}]^{2+}$ – 29.7	479.0062	$[C_{27}[^{13}C]_2H_{31}Fe[^{35}Cl]_2N_2$ $NaO_{25}]^{2+}$ 23.79
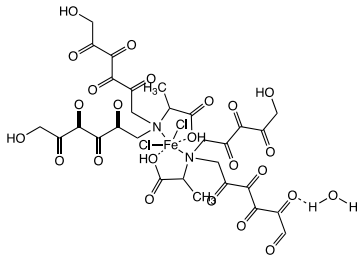 $[M + Cl_2 + Na_2]^{2+} = 480$ C23	*961.9704* *480.9849*		*904.0992* –		*907.9977* –	
	480.984	$[C_{29}H_{30}Fe[^{35}Cl]_2N_2Na_2$ $O_{24}]^{2+}$ – 2.01	904.1066	$[C_6[^{13}C]_{23}H_{30}Fe[^{35}Cl]N_2$ $O_{24}]^{+}$ 7.52	907.9948	$[C_{27}[^{13}C]_2H_{28}FeN_2NaK$ $O_{24}]^{+}$ – 3.88
	963.9675 *481.9834*					
	481.9814	$[C_{29}H_{30}Fe[^{35}Cl][^{37}Cl]N_2$				

		$Na_2O_{24}]^{2+}$ – 4.34				
	965.9645 *482.982*					
	482.982	$[C_{29}H_{30}Fe[^{37}Cl]_2N_2Na_2$ $O_{24}]^{2+}$ – 0.03				
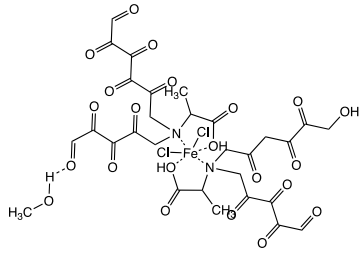 $[M + Cl_2 + Na + K]^{2+} = 472$ **C22**	*945.9545* *472.977*		*946.0464* *473.0224*			
	472.9776	$[C_{29}H_{30}Fe[^{35}Cl]_2N_2NaK$ $O_{22}]^{2+}$ 1.23	473.0224	$[C_7[^{13}C]_{22}H_{31}Fe[^{35}Cl]_2$ $N_2KO_{22}]^{2+}$ – 1.17	nd nd	
	947.9516 *473.9755*					
	473.969	$[C_{29}H_{30}Fe[^{35}Cl][^{37}Cl]_2N_2$ $NaKO_{22}]^{2+}$ – 13.81				
	955.9834 *477.9914*		*1032.9904* *516.4949*		*973.9641* *486.9817*	
	477.9925	$[C_{29}H_{31}Fe[^{35}Cl]_2N_2$ $NaO_{25}]^{2+}$ 2.19	516.4796	$[C_6[^{13}C]_{23}H_{30}Fe[^{35}Cl]_2$ $N_2K_2O_{25}]^{2+}$ – 29.7	486.977	$[C_{27}[^{13}C]_2H_{31}Fe[^{35}Cl]_2N_2$ $KO_{25}]^{2+}$ – 9.81
	957.9805					

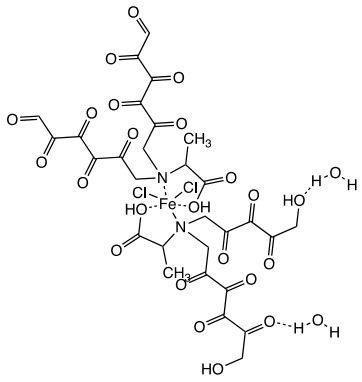 [M + H + Cl_2 + Na]$^{2+}$ = 477 **C23**	*478.9899*				
	478.9885	[$C_{29}H_{31}Fe[^{35}Cl][^{37}Cl]N_2NaO_{25}]^{2+}$ – 3.08			
	959.9775				
	479.9885				
	479.9886	[$C_{29}H_{31}Fe[^{37}Cl]_2N_2NaO_{25}]^{2+}$ 0.21			
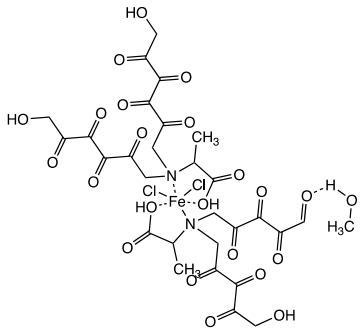 [M + Cl_2 + Na + K]$^{2+}$ = 481 **C22**	*963.9651*		*890.1244*		
	481.9823		*445.0619*		
	481.9814	[$C_{29}H_{32}Fe[^{35}Cl]_2N_2NaKO_{23}]^{2+}$ – 1.87	445.0681	[$C_7[^{13}C]_{22}H_{33}Fe[^{35}Cl]N_2O_{23}]^{2+}$ 13.81	nd
	965.9622				
	481.9808				
	482.982	[$C_{29}H_{32}Fe[^{35}Cl][^{37}Cl]N_2NaKO_{23}]^{2+}$ 2.43			
	967.9592				
	483.9793				
	483.9824	[$C_{29}H_{32}Fe[^{37}Cl]_2N_2NaKO_{23}]^{2+}$			

		6.3				
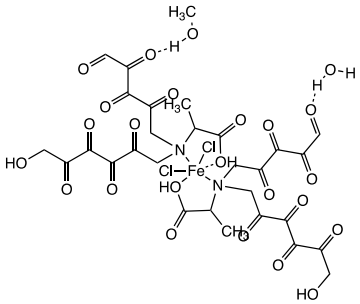 [M + H + Cl_2 + K]$^{2+}$ = 478 **C22**	*957.9781*		*1018.0078*		*959.9848*	
	478.9887		*509.0036*		*479.9921*	
	478.9885	$[C_{29}H_{33}Fe[^{35}Cl]_2N_2KO_{24}]^{2+}$	509.0004	$[C_7[^{13}C]_{22}H_{32}Fe[^{35}Cl]_2N_2K_2O_{24}]^{2+}$	479.9909	$[C_{27}[^{13}C]_2H_{33}Fe[^{35}Cl]_2N_2KO_{24}]^{2+}$
		– 0.6		– 6.35		– 2.59
	959.9751					
	479.9873					
	479.9886	$[C_{29}H_{33}Fe[^{35}Cl][^{37}Cl]N_2KO_{24}]^{2+}$				
		2.68				
	961.9722					
	480.9858					
	480.984	$[C_{29}H_{33}Fe[^{37}Cl]_2N_2KO_{24}]^{2+}$				
		– 3.82				
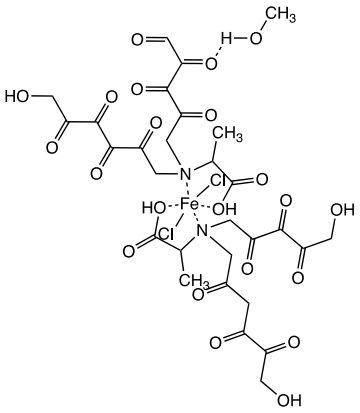	*934.0119*					
	467.0057					
	467.0052	$[C_{29}H_{34}Fe[^{35}Cl]_2N_2Na_2O_{22}]^{2+}$	457.0515	$[C_7[^{13}C]_{22}H_{34}Fe[^{35}Cl]N_2KO_{22}]^{2+}$	467.9941	$[C_{27}[^{13}C]_2H_{34}Fe[^{35}Cl]_2N_2Na_2O_{22}]^{2+}$
		– 1.07		2.71		– 31.96
	936.009					
	468.0042					
	468.003	$[C_{29}H_{34}Fe[^{35}Cl][^{37}Cl]N_2Na_2O_{22}]^{2+}$				

$[M + Cl_2 + Na_2]^{2+} = 467$ **C22**		– 2.62				
	936.0066 *468.003*		*864.1451* *432.0722*		*938.0133* *469.0063*	
	468.003	$[C_{29}H_{36}Fe[^{35}Cl]_2N_2NaKO_{21}]^{2+}$	432.0771	$[C_7[^{13}C]_{22}H_{35}FeN_2KO_{21}]^{2+}$	469.0098	$[C_{27}[^{13}C]_2H_{36}Fe[^{35}Cl]_2N_2NaKO_{21}]^{2+}$
		– 0.08		11.13		7.26
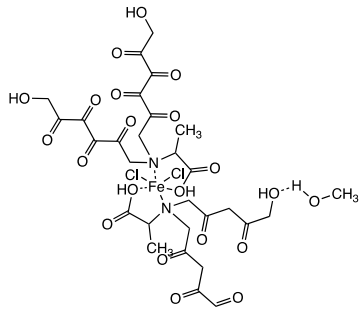 $[M + Cl_2 + Na + K]^{2+} = 468$ $[M + Cl_2 + K_2]^{2+} = 475$ **C22**	*951.9805* *475.99*					
	475.9908	$[C_{29}H_{36}Fe[^{35}Cl]_2N_2K_2O_{21}]^{2+}$ 1.67				
	953.9776 *476.9885*					
	476.9881	$[C_{29}H_{36}Fe[^{35}Cl][^{37}Cl]N_2K_2O_{21}]^{2+}$ – 0.91				
	955.9746 *477.987*					

	477.9925	$[C_{29}H_{36}Fe[^{37}Cl]_2N_2K_2O_{21}]^{2+}$ 11.39			
	983.9913 *491.9954*				
	491.995	$[C_{29}H_{36}Fe[^{35}Cl]_2N_2NaKO_{24}]^{2+}$ – 0.83	459.5775	$[C_6[^{13}C]_{23}H_{34}FeN_2Na_2O_{24}]^{2+}$ 15.57	nd
	985.9884 *492.9939*				
	493.0056	$[C_{29}H_{36}Fe[^{35}Cl][^{37}Cl]N_2NaKO_{24}]^{2+}$ 23.66			
	987.9854 *493.9924*				
	493.9989	$[C_{29}H_{36}Fe[^{37}Cl]_2N_2NaKO_{24}]^{2+}$ 13.04			
	924.0535 *462.0265*				
	462.0269	$[C_{29}H_{38}Fe[^{35}Cl]_2N_2O_{24}]^{2+}$ 0.87			
	928.0119 *464.0057*				
	464.0044	$[C_{29}H_{34}FeN_2K_2O_{24}]^{2+}$			

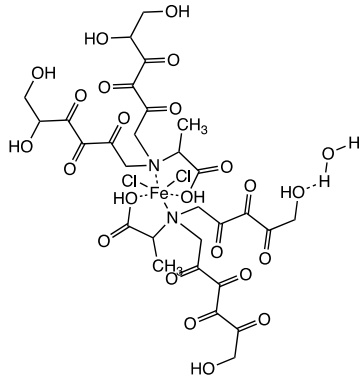

$[M + Cl_2 + Na + K]^{2+} = 491$

$[M + H_2 + Cl_2]^{2+} = 462$

$[M + K_2]^{2+} = 464$

C23

		– 2.8				
	1001.9809		*897.1637*		*950.0578*	
	500.9902		–		*475.0286*	
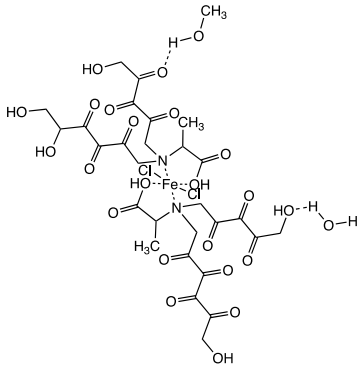	500.9876	$[C_{29}H_{38}Fe[^{35}Cl]_2N_2K_2O_{24}]^{2+}$	897.1556	$[C_7[^{13}C]_{22}H_{36}FeN_2NaO_{24}]^{+}$	475.0304	$[C_{27}[^{13}C]_2H_{39}Fe[^{35}Cl]_2N_2NaO_{24}]^{2+}$
		– 5.2		– 9.1		3.69
	1003.978					
	501.9887					
	501.9773	$[C_{29}H_{38}Fe[^{35}Cl][^{37}Cl]N_2K_2O_{24}]^{2+}$				
		– 22.77				
$[M + Cl_2 + K_2]^{2+} = 500$	*1005.975*					
C22	*502.9872*					
	502.9817	$[C_{29}H_{38}Fe[^{37}Cl]_2N_2K_2O_{24}]^{2+}$				
		– 11.04				
	974.1842		*996.2508*		*976.1909*	
	487.0918		*498.1287*		*488.0951*	
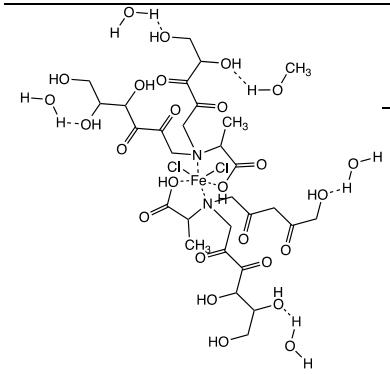	487.0934	$[C_{29}H_{56}Fe[^{35}Cl]_2N_2O_{26}]^{2+}$	498.1289	$[C_7[^{13}C]_{22}H_{56}Fe[^{35}Cl]_2N_2O_{26}]^{2+}$	488.0973	$[C_{27}[^{13}C]_2H_{56}Fe[^{35}Cl]_2N_2O_{26}]^{2+}$
		3.21		0.32		4.32
$[M + H_2 + Cl_2]^{2+} = 487$						

C22						
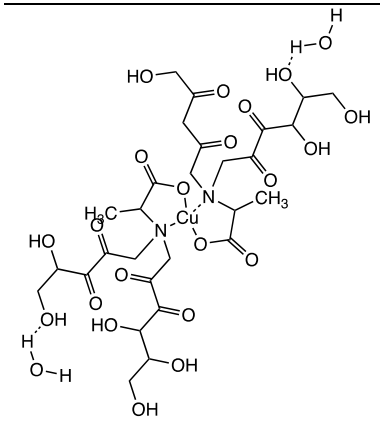 [M + K]$^{+}$ = 878 C22	*878.1262*					
	878.1322	$[C_{28}H_{44}[^{63}Cu]N_2KO_{23}]^{+}$ 6.79				
	880.1244					
	880.1302	$[C_{28}H_{44}[^{65}Cu]N_2KO_{23}]^{+}$ 6.55				
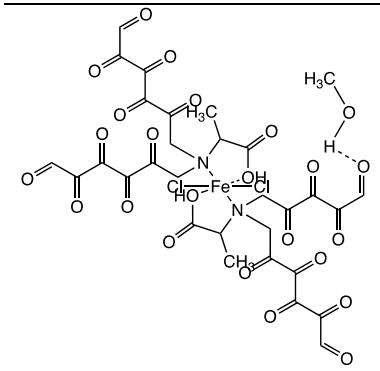 [M + Cl_2 + K_2]$^{2+}$ = 465 C23	*1001.887*		*948.0446*		*973.9615*	
	500.9432				*486.9805*	
	465.9742	$[C_{30}H_{26}Fe[^{35}Cl]_2N_2K_2O_{24}]^{2+}$ – 0.43	948.0484	$[C_7[^{13}C]_{23}H_{27}Fe[^{35}Cl]_2N_2O_{24}]^{+}$ 3.98	486.977	$[C_{28}[^{13}C]_2H_{28}Fe[^{35}Cl]_2N_2Na_2O_{24}]^{2+}$ – 7.18
	947.9362		*978.0247*		*897.9923*	
	473.9678		*489.0121*		*448.9959*	

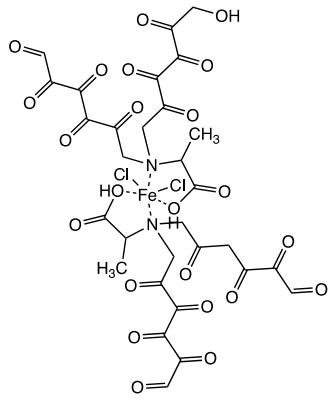 [M + H + Cl_2 + K]$^{2+}$ = 473 **C24**	473.969	$[C_{30}H_{27}Fe[^{35}Cl]_2N_2KO_{23}]^{2+}$ 2.41	489.0045	$[C_6[^{13}C]_{24}H_{26}Fe[^{35}Cl]_2N_2Na_2O_{23}]^{2+}$ – 15.58	448.9951	$[C_{28}[^{13}C]_2H_{26}Fe[^{35}Cl]N_2NaO_{23}]^{2+}$ – 1.79
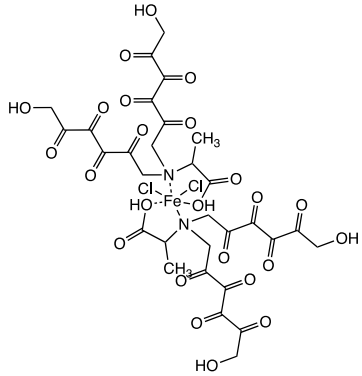 [M + H + Cl_2 + K]$^{2+}$ = 483 **C24**	*967.9624* *483.9809*		*1014.0249* *507.0121*		*969.9691* *484.9843*	
	483.9824	$[C_{30}H_{31}Fe[^{35}Cl]_2N_2KO_{24}]^{2+}$ 2.97	507.0016	$[C_6[^{13}C]_{24}H_{30}Fe[^{35}Cl]_2N_2NaKO_{24}]^{2+}$ – 20.89	484.979	$[C_{28}[^{13}C]_2H_{31}Fe[^{35}Cl]_2N_2KO_{24}]^{2+}$ – 10.96
	969.9595 *484.9794*					
	484.9734	$[C_{30}H_{31}Fe[^{35}Cl][^{37}Cl]N_2KO_{24}]^{2+}$ – 12.55				
	971.9565 *485.978*					
	485.9751	$[C_{30}H_{31}Fe[^{37}Cl]_2N_2KO_{24}]^{2+}$ – 5.99				

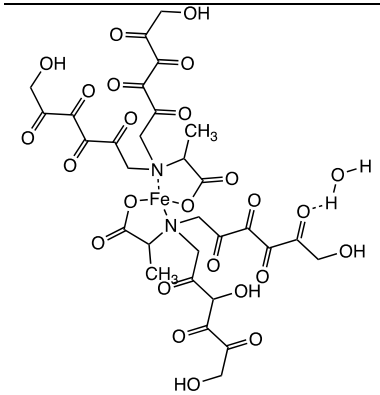	*922.0433*		*1050.025*		*1011.9773*	
	461.0214		*525.0122*		*505.9884*	
	461.0215	$[C_{30}H_{32}FeN_2Na_2O_{25}]^{2+}$	525.0161	$[C_6[^{13}C]_{24}H_{34}Fe[^{35}Cl]_2N_2K_2O_{25}]^{2+}$	505.9868	$[C_{28}[^{13}C]_2H_{34}Fe[^{35}Cl]_2N_2NaKO_{25}]^{2+}$
		0.23		7.3		– 3.16
$[M + Na_2]^{2+} = 461$						
C24						
	943.9543		*914.105*		*906.9973*	
	471.9769		*457.0522*		–	
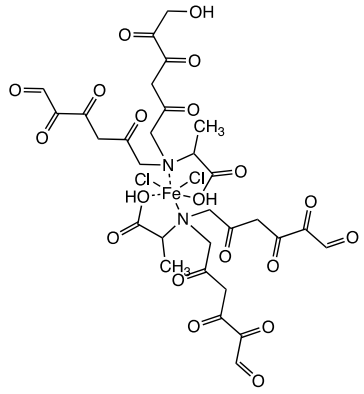	471.9758	$[C_{30}H_{32}Fe[^{35}Cl]_2N_2K_2O_{20}]^{2+}$	457.0515	$[C_6[^{13}C]_{24}H_{33}Fe[^{35}Cl]_2N_2NaO_{20}]^{2+}$	906.9962	$[C_{28}[^{13}C]_2H_{32}Fe[^{35}Cl]_2N_2KO_{20}]^{+}$
		– 2.33		– 1.64		– 1.87
	945.9514					
	472.9754					
	472.9776	$[C_{30}H_{32}Fe[^{35}Cl][^{37}Cl]N_2K_2O_{20}]^{2+}$				
		4.6				
$[M + Cl_2 + K_2]^{2+} = 471$	*947.9484*					
C24	*473.9739*					
	473.969	$[C_{30}H_{32}Fe[^{37}Cl]_2N_2K_2O_{20}]^{2+}$				
		– 10.44				

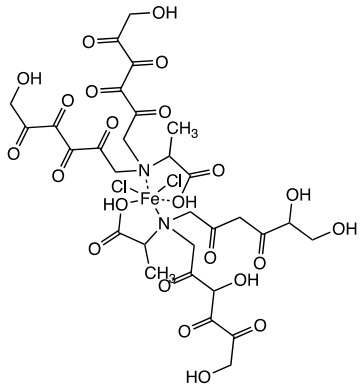 $[M + Cl_2 + Na + K]^{2+} = 489$ **C24**	*979.9964*					
	489.9979					
	489.9974	$[C_{30}H_{36}Fe[^{35}Cl]_2N_2NaKO_{23}]^{2+}$ – 1.13	458.0787	$[C_6[^{13}C]_{24}H_{34}FeN_2Na_2O_{23}]^{2+}$ 9.03	425.0563	$[C_{28}[^{13}C]_2H_{36}Fe[^{35}Cl]_2N_2O_{23}]^{2+}$ 1.37
	981.9935					
	490.9964					
	490.9998	$[C_{30}H_{36}Fe[^{35}Cl][^{37}Cl]N_2NaKO_{23}]^{2+}$ 6.77				
	983.9905					
	491.995					
	491.995	$[C_{30}H_{36}Fe[^{37}Cl]_2N_2NaKO_{23}]^{2+}$ – 0.01				
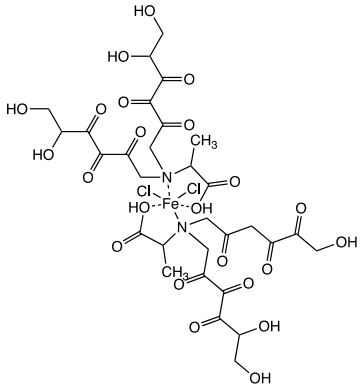 $[M + Cl_2 + K_2]^{2+} = 498$	*997.986*		*918.1653*		*984.0188*	
	498.9927		*459.0823*		*492.0091*	
	498.9911	$[C_{30}H_{38}Fe[^{35}Cl]_2N_2K_2O_{23}]^{2+}$ – 3.3	459.0778	$[C_6[^{13}C]_{24}H_{36}FeN_2Na_2O_{23}]^{2+}$ – 10	492.0105	$[C_{28}[^{13}C]_2H_{38}Fe[^{35}Cl]_2N_2NaKO_{23}]^{2+}$ 2.78
	999.983					
	499.9912					
	499.9933	$[C_{30}H_{38}Fe[^{35}Cl][^{37}Cl]N_2K_2O_{23}]^{2+}$				

C24		4.06				
	1001.9801					
	500.9898					
	500.9876	$[C_{30}H_{38}Fe[^{37}Cl]_2N_2K_2O_{23}]^{2+}$				
		– 4.38				
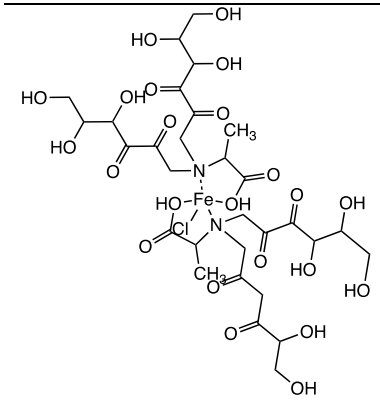	*932.116*		*942.2018*		*934.1227*	
	466.0577		*471.1006*		*467.0611*	
	466.0583	$[C_{30}H_{46}Fe[^{35}Cl]\ N_2KO_{23}]^{2+}$	471.1027	$[C_6[^{13}C]_{24}H_{44}FeN_2Na$ $KO_{23}]^{2+}$	467.0642	$[C_{28}[^{13}C]_2H_{46}Fe[^{35}Cl]N_2$ $KO_{23}]^{2+}$
		1.14		4.33	467.0642	6.59
$[M + Cl + K]^{2+} = 466$						
C24						
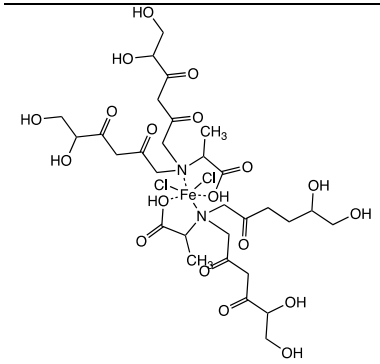	*928.1107*		*842.2819*		*914.1434*	
	464.055		*421.1407*		*457.0714*	
	464.0542	$[C_{30}H_{48}Fe[^{35}Cl]_2N_2Na$ $KO_{19}]^{2+}$	421.1491	$[C_6[^{13}C]_{24}H_{47}FeN_2$ $NaO_{19}]^{2+}$	457.0722	$[C_{28}[^{13}C]_2H_{48}Fe[^{35}Cl]_2N_2$ $Na_2O_{19}]^{2+}$
		– 1.88		19.91		1.62
$[M + Cl_2 + Na + K]^{2+} = 465$						

C24						
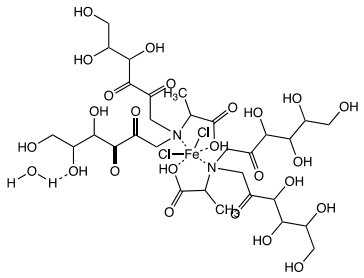 $[M + H_2 + Cl_2]^{2+} = 484$ C24	*968.1736*		*992.2541*		*970.1803*	
	484.0865		*496.1268*		*485.0899*	
	484.0868	$[C_{30}H_{54}Fe[^{35}Cl]_2N_2O_{25}]^{2+}$	496.1289	$[C_6[^{13}C]_{24}H_{54}Fe[^{35}Cl]_2N_2O_{25}]^{2+}$	485.0852	$[C_{28}[^{13}C]_2H_{54}Fe[^{35}Cl]_2N_2O_{25}]^{2+}$
		0.51		4.21		– 9.71
	970.1707					
	485.085					
	485.0915	$[C_{30}H_{54}Fe[^{35}Cl][^{37}Cl]N_2O_{25}]^{2+}$				
		– 12.55				
	972.1677					
	486.0836					
	486.0917	$[C_{30}H_{54}Fe[^{37}Cl]_2N_2O_{25}]^{2+}$				
		– 5.99				

[a]All ions (*m/z*) detected through various ionizations processes to form singly or doubly charged positive ions. Structures represent only one of many possible isomeric forms

[b]Error (ppm) in calculating the elemental composition

[c]Calculated masses (*m/z*) of singly charged ions

[d]Calculated masses (*m/z*) of doubly charged ions

[e]Observed masses (*m/z*) of *bis*[*N,N'*-di-glycated alanine]iron(II) complexes

[f]nd: not detect

Table S5.2. Free and complexed amino acids observed in the $(Ser)_2Fe/Ala$ model system (see Figures 5.1 and S5.3)

Structure	[M + X][a]	Elemental Composition[a]	Error (ppm)[b]	Relative intensities (%)	
				Water	Methanol
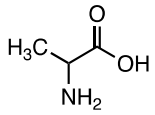	90.0549	$C_3H_8NO_2$	– 0.61	23.52 ± 0.23	31.07 ± 0.01
	112.037	$C_3H_7NNaO_2$	0.9	4.01 ± 0.71	0.96 ± 0.56
	128.0109	$C_3H_7KNO_2$	0.5	2.93 ± 0.7	1.62 ± 0.56
				30.46 ± 1.17	**33.64 ± 1.11**
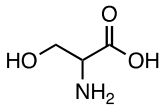	106.05	$C_3H_8NO_3$	1.23	5.35 ± 0.6	18.21 ± 4.87
	128.0318	$C_3H_7NNaO_3$	– 0.11	31.05 ± 1.29	6.41 ± 3.78
	144.0057	$C_3H_7KNO_3$	– 0.35	20.17 ± 1.72	32.5 ± 8.05
				56.57 ± 2.4	**57.17 ± 0.56**
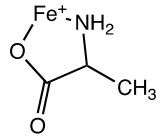	143.9744	$C_3H_6FeNO_2$	1.1	0.13 ± 0.03	0.14 ± 0.02
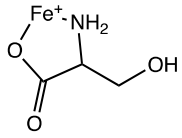	161.9847	$C_3H_8FeNO_3$	– 0.65	1.19 ± 0.04	0.62 ± 0.03
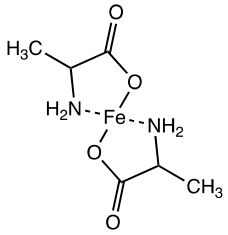	233.0216	$C_6H_{13}FeN_2O_4$	– 1.37	3.06 ± 1.6	4.29 ± 3.16
	255.0032	$C_6H_{12}FeN_2NaO_4$	– 2.6	0.54 ± 0.01	0.92 ± 0.92
				3.59 ± 1.6	**5.21 ± 4.08**
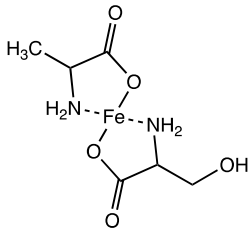	249.0168	$C_6H_{13}FeN_2O_5$	– 0.14	3.4 ± 1.67	4.72 ± 1.19
	270.9991	$C_6H_{12}FeN_2NaO_5$	1.19	1.74 ± 0.05	2.05 ± 2.05
				5.13 ± 1.62	**6.77 ± 3.24**

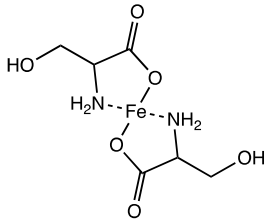	265.0112	$C_6H_{13}FeN_2O_6$	– 2.07	2.05 ± 0.4	6.18 ± 2.79
	286.9926	$C_6H_{12}FeN_2NaO_6$	– 3.91	5.56 ± 0.78	3.34 ± 0.3
	302.9673	$C_6H_{12}FeKN_2O_6$	– 1.09	0.84 ± 0.06	6.99 ± 1.68
bis(serinato)iron(II)complex					
				8.44 ± 1.23	**16.5 ± 0.81**
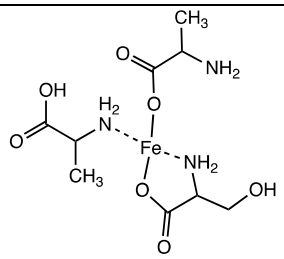	338.0691	$C_9H_{20}FeN_3O_7$	13.57	1.1	1.1
	360.0463	$C_9H_{19}FeN_3NaO_7$	– 0.44	0.7	2.2
				1.8	**3.3**
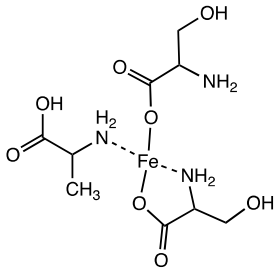	354.0641	$C_9H_{20}FeN_3O_8$	13.2	1.3	1
	376.0421	$C_9H_{19}FeN_3NaO_8$	1.94	0.8	1.8
				2.1	**2.8**

[a] All of the ions listed in Figures 5.1 and S5.3 are included in this table

[b] Error (in ppm) in calculating the elemental composition

Table S5.3. MS/MS fragment ions generated from *m/z* 414 (at 5 eV) and the number of labelled atoms incorporated in each fragment (see Figure 5.2)

m/z	Elemental composition[a]	Error (ppm)[b]	Relative Intensity (%)	Glu [^{13}C-U]	Error (ppm)	Ala [^{13}C-3]	Error (ppm)
90.0543[c]	$[C_3H_8NO_2]^{+c}$	– 7.27	82.5	0	8.922	1	9.426
97.0273	$[C_5H_5O_2]^+$	– 11.4	5.8	5	– 6.16	0	– 4.18
102.0542	$[C_4H_8NO_2]^+$	– 7.4	23.7	1	8.329	1	7.358
216.0849	$[C_9H_{14}NO_5]^+$	– 8.09	22.6	6	7.774	0	1.05
234.0967	$[C_9H_{16}NO_6]^+$	– 2.19	74.4	6	– 15.17	1	– 4.97
252.1078	$[C_9H_{18}NO_7]^+$	0.09	37.8	6	7.19	1	7.039
264.1071	$[C_{10}H_{18}NO_7]^+$	– 2.57	7.8	nd[d]		1	7.852
145.0486	$[C_6H_9O_4]^+$	– 6.45	9.3	nd		nd	
360.1279	$[C_{15}H_{22}NO_9]^+$	– 2.8	6.2	12	– 3.67	nd	
378.1409	$[C_{15}H_{24}NO_{10}]^+$	3.78	12.6	12	– 1.1	1	1.77
396.1482	$[C_{15}H_{26}NO_{11}]^+$	– 4.64	15.4	12	– 4.15	1	– 1.99
414.1617	$[C_{15}H_{28}NO_{12}]^+$	2.65	14.5	12	1.623	1	6.757

[a]All of the ions listed in Figure 5.2 are included in this table

[b]Error (in ppm) in calculating the elemental composition

[c]Base peak

[d]nd: not detected

Table S5.4. MS/MS fragment ions generated from *m/z* 504 using 5 eV collision energy (see Figure S5.4)

m/z	Elemental composition[a]	Error (ppm)[b]	Relative Intensity (%)
264.0168	$[C_7H_{14}FeNO_6]^+$	1.14	25.3
295.012	$[C_9H_{14}FeNaNO_5]^+$	2.19	16.4
324.0388	$[C_9H_{18}FeNO_8]^+$	3.61	60.9
325.0427	$[C_9H_{19}FeNO_8]^+$	– 8.47	13.6
355.0328	$[C_{12}H_{14}KNO_9]^+$	7.85	42.2
356.0366	$[C_{12}H_{15}KNO_9]^+$	– 3.48	10.5
415.055[c]	$[C_{14}H_{18}KNO_{11}]^+$	9.29	100
416.0589	$[C_{14}H_{19}KNO_{11}]^+$	– 0.16	30.3
444.9297	$[C_{12}H_{13}Fe[^{35}Cl]KNO_9]^+$	8.37	15
504.9554	$[C_{14}H_{17}Fe[^{35}Cl]KNO_{11}]^+$	16.42	14

[a]All of the ions listed in Figures S5.4 are included in this table

[b]Error (in ppm) in calculating the elemental composition

[c]Base peak

Table S5.5. MS/MS fragment ions generated from *m/z* 540 using 10 eV collision energy (see Figures 5.3 and S5.5)

m/z	Elemental composition[a]	Error (ppm)[b]	Relative Intensity (%)
90.0553	$[C_3H_8NO_2]^+$	3.83	36.8
270.9685	$[C_6H_{11}FeO_6]^+$	6.91	37.2
360.0171	$[C_9H_{19}Fe[^{35}Cl]NO_8]^+$	7.76	40.2
362.0104	$[C_9H_{19}Fe[^{37}Cl]NO_8]^+$	– 2.64	21.4
384.9098	$[C_8H_{14}Fe[^{35}Cl]_2NKO_6]^+$	– 21.07	67.6
408.9525	$[C_9H_{17}Fe[^{35}Cl]_2NO_9]^+$	– 24.27	47.8
444.9322[c]	$[C_{12}H_{13}Fe[^{35}Cl]NKO_9]^+$	13.98	100
446.9286	$[C_{12}H_{13}Fe[^{37}Cl]NKO_9]^+$	12.47	29.7
468.9765	$[C_{14}H_{16}FeNKO_{11}]^+$	12.94	22.2
504.9518	$[C_{14}H_{17}Fe[^{35}Cl]NKO_{11}]^+$	9.29	56.2

[a]All of the ions listed in Figures 5.3 and S5.5 are included in this table

[b]Error (in ppm) in calculating the elemental composition

[c]Base peak

Table S5.6. MS/MS fragment ions generated from *m/z* 298 $[M + 2Na]^{2+}$ using 15 eV collision energy (see Figure S5.6)

m/z	Elemental composition[a]	Error (ppm)[b]	Relative Intensity (%)
85.0284	$[C_4H_5O_2]^+$	– 0.07	52
90.0557	$[C_3H_8NO_2]^+$	8.27	1.6
97.0288	$[C_5H_5O_2]^+$	4.06	20.6
109.029	$[C_6H_5O_2]^+$	5.45	8.9
127.0394	$[C_6H_7O_3]^+$	3.38	24.1
145.0501	$[C_6H_9O_4]^+$	3.89	22.1
150.9692	$[C_2H_7FeO_4]^+$	2.51	13.4
163.0599	$[C_6H_{11}O_5]^+$	– 1.23	1.7
174.9693[c]	$[C_4H_7FeO_4]^+$	2.74	100
186.9695	$[C_5H_7FeO_4]^+$	3.63	15.7
192.9797	$[C_4H_9FeO_5]^+$	1.63	37.9
198.9693	$[C_5H_9FeO_5]^+$	2.41	14.2
204.9798	$[C_6H_7FeO_4]^+$	2.02	19.8
216.9799	$[C_6H_9FeO_5]^+$	2.37	20.8
234.9907	$[C_6H_{11}FeO_6]^+$	3.19	63.7
253.0014	$[C_6H_{13}FeO_7]^+$	3.5	23.7
258.991	$[C_9H_{10}FeNNaO_3]^+$	2.99	1.5
277.002	$[C_9H_{12}FeNNaO_4]^+$	4.37	19.8
295.0125	$[C_9H_{14}FeNNaO_5]^+$	3.88	13.7

[a]All of the ions listed in Figure S5.6 are included in this table

[b]Error (in ppm) in calculating the elemental composition

[c]Base peak

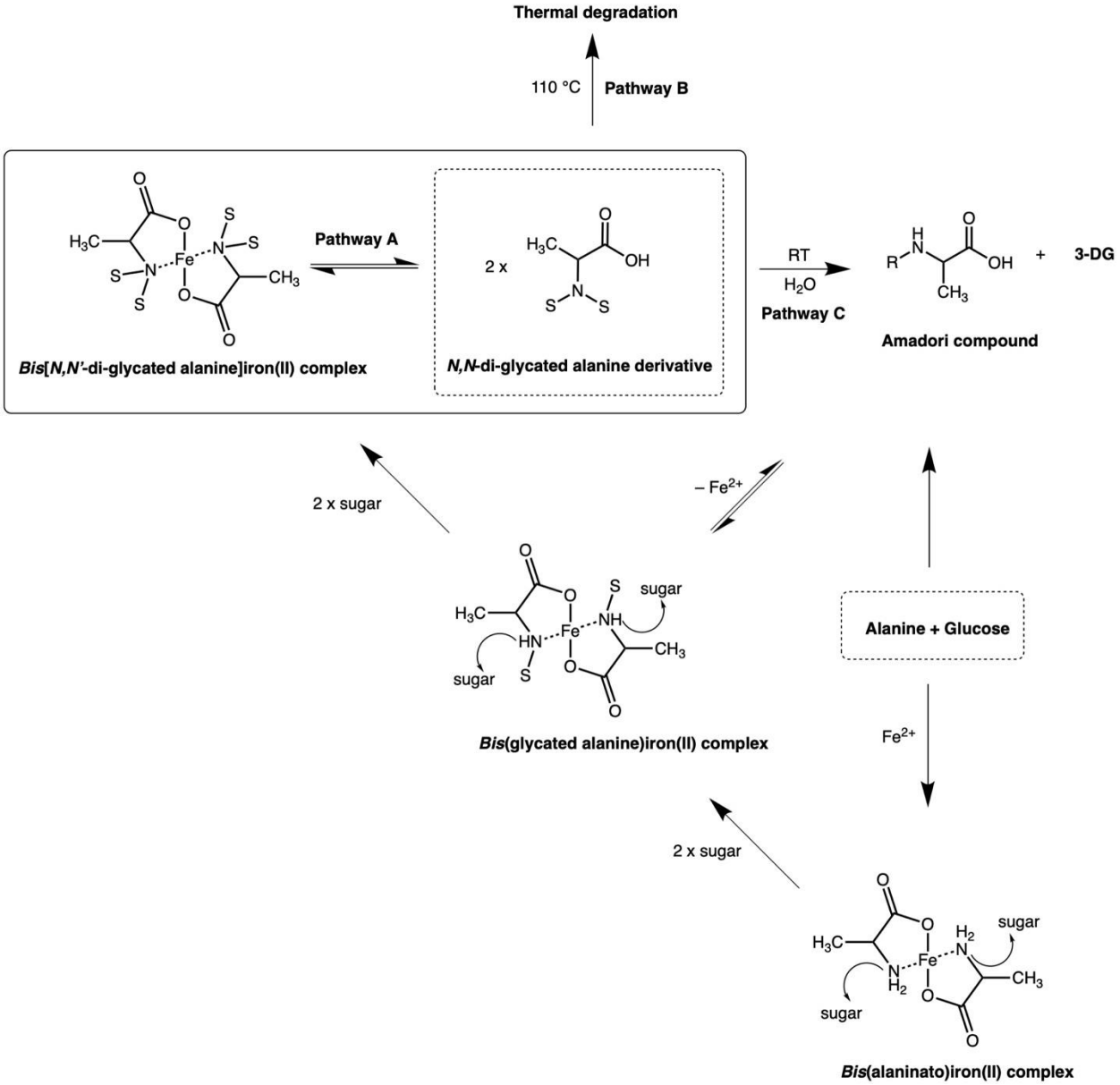

S = sugar; R= fructosyl moiety

Figure S5.1. Proposed formation and reactions of *bis*[*N,N'*-di-glycated alanine]iron(II) complexes and generation of *N,N*-di-glycated alanine derivatives. Pathway C is based on Fodor and Sachetto, 1968.

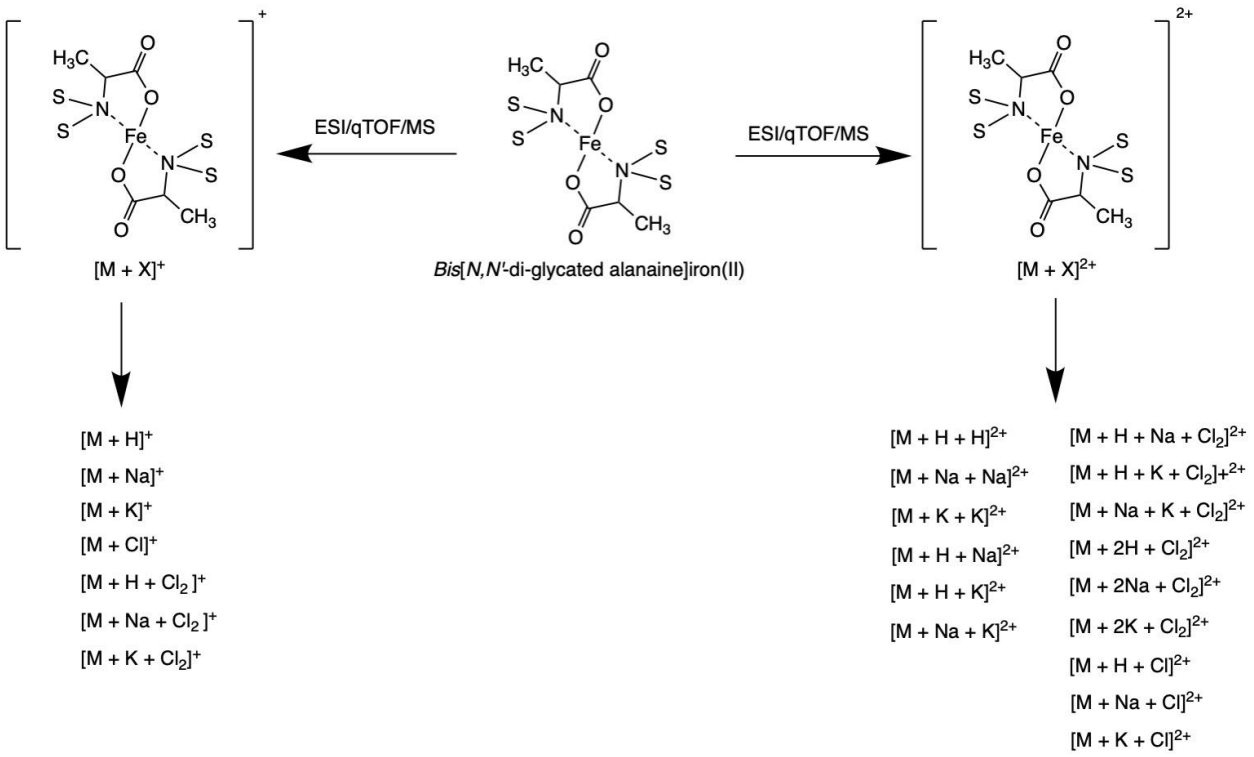

Figure S5.2. The proposed *bis*[*N,N'*-diglycated alanine]iron(II) complexes can be detected through various ionizations processes to form singly or doubly charged species, such as $[M + H^+]^+$, $[M + Fe^+ + Cl]^+$, $[M + H^+ + Cl_2]^+$, $[M + Na^+]^+$, $[M + 2Na^+]^{2+}$, $[M + 2K^+]^{2+}$, $[M + 2H^+ + Cl_2]^{2+}$, $[M + Cl_2 + Na^+ + K^+]^{2+}$, $[M + Cl_2 + 2K^+]^{2+}$, $[M + Cl_2 + 2Na^+]^{2+}$, $[M + Cl + K^+]^{2+}$, $[M + H^+ + Cl_2 + Na^+]^{2+}$, and $[M + H^+ + Cl_2 + K^+]^{2+}$

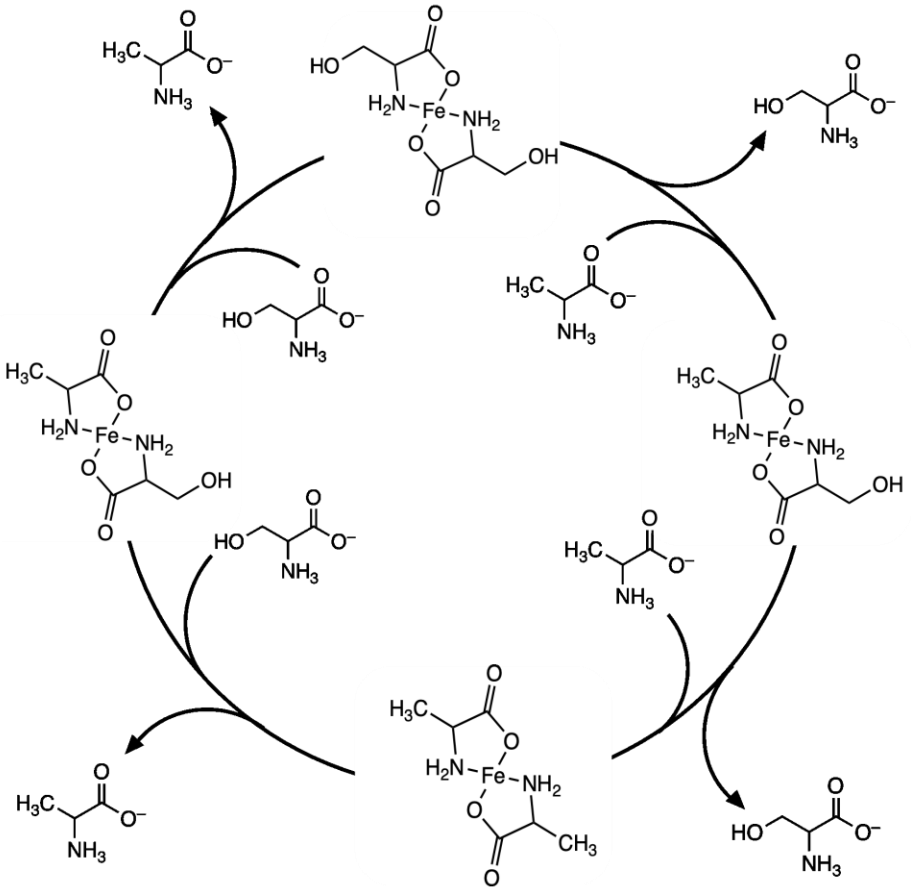

Figure S5.3. Proposed mechanism of dissociation/association of the iron(II) complexes in $(Ser)_2Fe$/Ala model system under the Maillard reaction conditions (110 °C for 2 h) (see Figure 5.1)

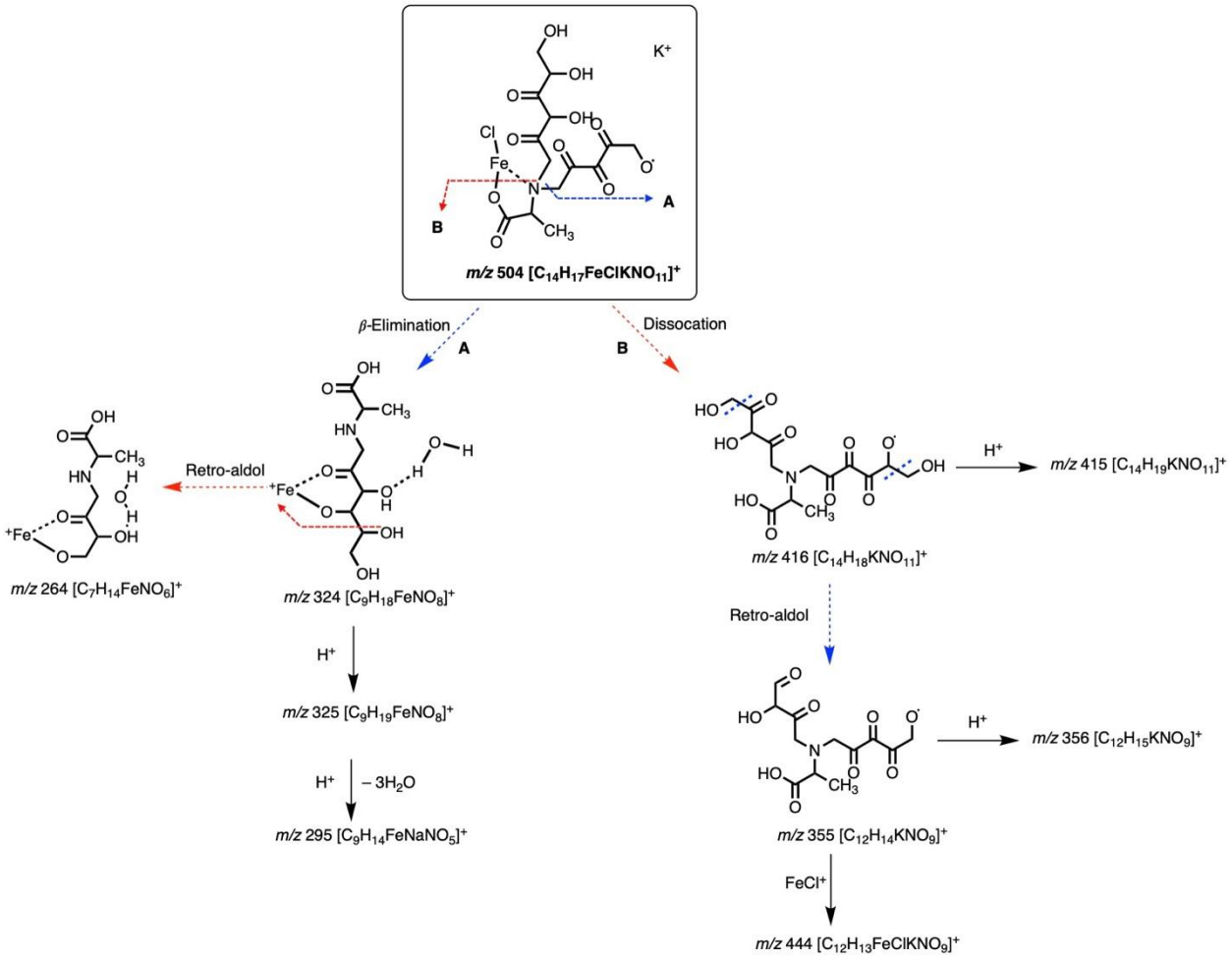

Figure S5.4. Proposed MS/MS fragmentation pathways of *m/z* 504 detected in Ala/Glu/$FeCl_2$ model system (see Table S5.4)

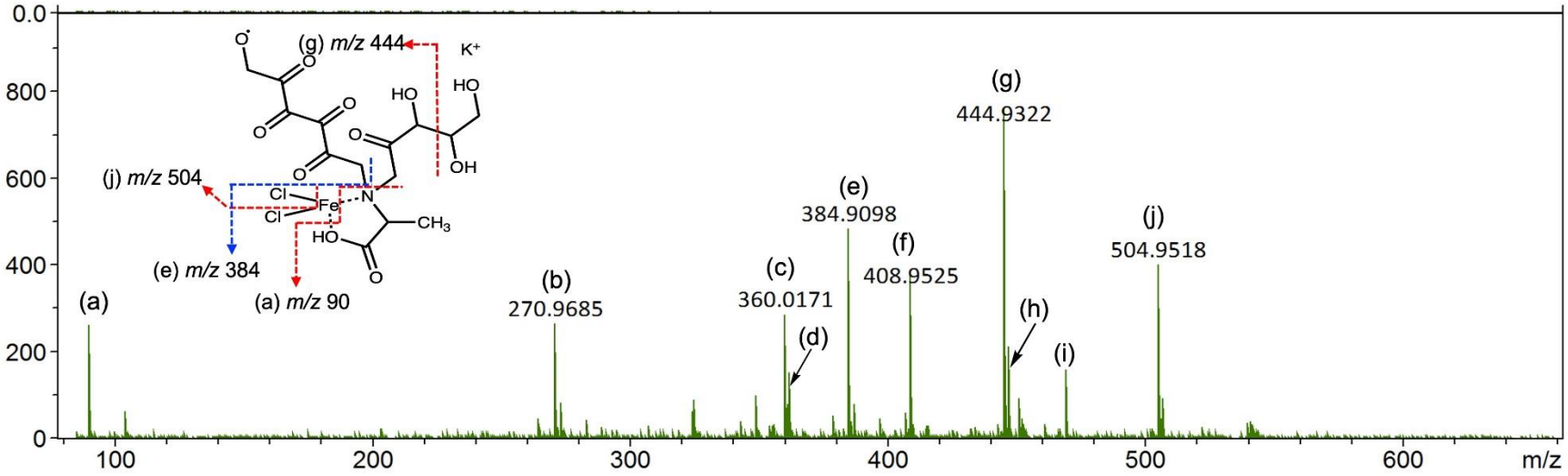

Figure S5.5. ESI/qTOF/MS/MS spectrum of *m/z* 540 detected in the Ala/Glu/$FeCl_2$ model system (see Figure 5.3 and Table S5.5)

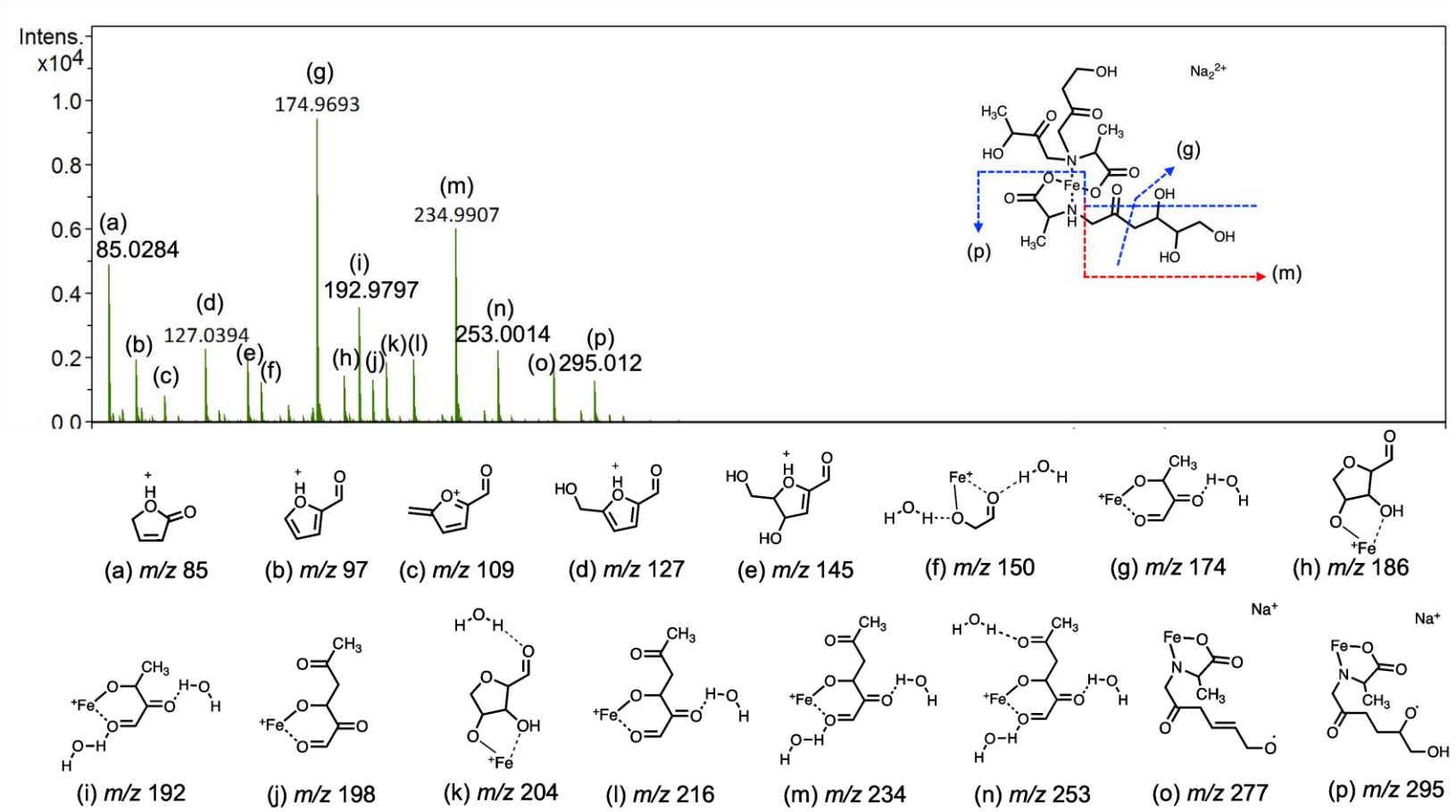

Figure S5.6. ESI/qTOF/MS/MS spectrum of *m/z* 298 $[C_{20}H_{34}FeN_2Na_2O_{12}]^{2+}$) detected in the Ala/Glu/$FeCl_2$ model system (see Table S5.6)

CONNECTING PARAGRAPH

In the previous chapter, 48 derivatives of *bis*[*N,N'*-diglycated alanine]iron(II) complexes and 17 diglycated alanine derivatives were detected in their various ionic forms as singly or doubly charged species. **In chapter 6**, we further studied the degradation products of diglycated alanine derivatives (i.e. *N,N*-diglycated alanine derivatives) and identified their various specific reactions such as intramolecular cyclization leading to oxazine and diazine derivatives. **Chapter 6** will be submitted to the journal of *Food Chemistry* under the title of "Intramolecular Cyclization of *N,N*-Diglycated Alanine Derivatives."

CHAPTER 6

INTRAMOLECULAR CYCLIZATION OF *N,N*-DIGLYCATED ALANINE DERIVATIVES

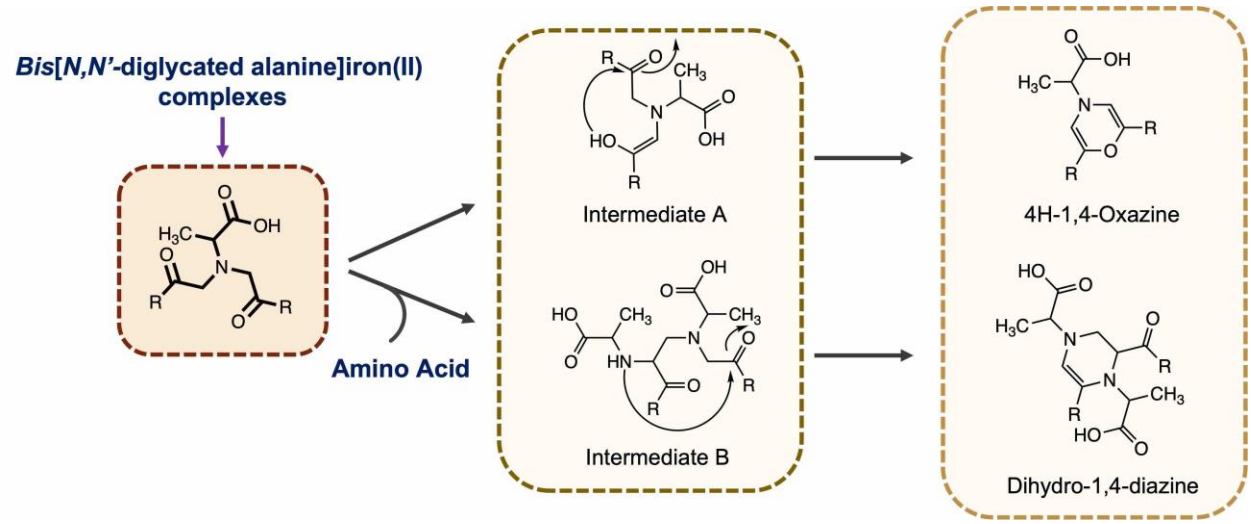

6.1. ABSTRACT

The chemistry *N*,*N*-diglycated amino acids is not well understood due to their transient nature during the Maillard reaction. Their enhanced reactivity is attributed to the presence of unusually high concentrations of open ring forms at least in one of their sugar moieties. We were able to generate *N*,*N*-diglycated alanine *in situ* through dissociation from their stable precursors *bis*[*N*,*N'*-diglycated alanine]iron(II) complexes formed in the alanine/glucose/$FeCl_2$ model system under the Maillard reaction conditions (110 °C for 2 h). Their subsequent degradations were traced using isotope-labelled reactants, such as alanine-3-^{13}C and glucose-U-^{13}C, and high-resolution electrospray ionization/quadrupole time-of-flight mass spectrometry. The *N*,*N*-diglycated alanine derivatives in the reaction mixtures were monitored through identification of ions incorporating two C-3 alanine atoms and up to 12 carbons from sugar. Through consideration of the known chemical transformations of Amadori compounds and due to the proximity of the sugar moieties to each other, two intramolecular cyclization reactions between the sugars rings are proposed; one initiated by 1,2-enolization followed by cyclization at the carbonyl group of the neighboring sugar forming 4*H*-1,4-oxazine derivatives and the second initiated by the formation of an Amadori moiety on one of the sugars and its subsequent cyclization with the carbonyl group of the adjacent sugar, leading to dihydro-1,4-diazine structures.

KEYWORDS: *N*,*N*-diglycated alanine, intramolecular cyclization, isotope labelling, Amadori compounds

6.2. INTRODUCTION

The precursors of aroma and flavour active compounds, such as Amadori and 1,2-dicarbonyl compounds, generated in the Maillard reaction during food processing, significantly influence the food quality, colour, and flavour perception. The Maillard reaction generates initial degradation products via various chemical transformations, such as redox reactions, dehydrations, and retro-aldol reactions (Vasile, 1993). In model systems or food, degradation reactions typically occur under thermal conditions and require the presence of sufficient quantities of reactive Maillard

reaction precursors, such as Schiff bases and Amadori products. In previous studies using alanine/glucose/$FeCl_2$ model systems, *bis*[*N*,*N'*-diglycated alanine]iron(II) derivatives were identified when divalent $FeCl_2$ was used in stoichiometric amounts. Furthermore, in these model systems, the dissociation of *bis*[*N*,*N'*-diglycated amino acids]iron(II) yielded free *N*,*N*-diglycated amino acid derivatives (Kim and Yaylayan, 2022), providing additional reactive precursors for the Maillard reaction. Belikov *et al*. (1969) reported that *N*,*N*-diglycated amino acids derivatives were more reactive than monoglycated amino acids owing to the formation of abundant acyclic forms in solution and solid state. In addition, literature reports regarding *N*,*N* diglycated amino acids have been limited to their chemical synthesis (Feather and Mossine, 2005; Xing and Yaylayan, 2022) or proposed as intermediates in the formation of advanced glycation end products (AGE) (Argirov *et al*., 2004) and in browning reaction (Mohsin *et al*., 2022). It is expected that *N*,*N*-diglycated amino acid intermediates to degrade similar to Amadori products during the Maillard reaction and contribute to the generation of flavours and colours. In this manuscript, we explore their degradation pathways.

6.3. MATERIAL AND METHODS

6.3.1. Materials and reagents

L-Alanine (98%), L-serine (98%), D-glucose, and iron(II) chloride ($FeCl_2$) (99%) were purchased from Sigma-Aldrich Chemical Co. (Oakville, ON, Canada). Alanine-3-^{13}C ($^{13}CH_3CH(NH_2)CO_2H$) (98%) and glucose-^{13}C-U ($^{13}C_6H_{12}O_6$) (99%) were purchased from Cambridge Isotope Laboratories (Andover, MI). Liquid chromatography–mass spectrometry (LC–MS)-grade water and methanol (OmniSolv, > 99%) were obtained from VWR International (Mississauga, ON, Canada).

6.3.2. Sample preparation

The test model systems were prepared in 1:1:0.5 molar ratios by adding glucose (18 mg), alanine (9 mg), and $FeCl_2$ (6.4 mg) to methanol (1 mL) and heating in a stainless-steel reactor at 110 °C for 2 h, followed by evaporation of the solvent for 30 min. The control model system was prepared by heating glucose (18 mg) and alanine (9 mg) in methanol at 110 °C for 2 h in the absence of metal ions. All samples were analyzed at least in two replicates, as indicated in Table S6.1.

6.3.3. ESI/qTOF/MS analysis

The samples were dissolved in liquid chromatography (LC)-grade methanol at a 1 mg/mL concentration. The samples were then diluted 10-fold in 10% methanol prior to analysis by ESI/qTOF/MS in positive-ion mode. The ESI/qTOF/MS system comprised a Bruker Maxis Impact quadrupole time-of-flight mass spectrometer (Bruker Daltonics, Bremen, Germany) operated in positive-ion mode. The samples (1 μL) were injected directly into the ESI/qTOF/MS system. Instrument calibration was performed using sodium formate clusters. The electrospray interface settings were as follows: nebulizer pressure, 0.6 bar (60,000 Pa); drying gas, 4 L/min; temperature, 180 °C; and capillary voltage, 4500 V. The scan range was from *m/z* 70 to 1000. Molecular formulas were assigned to all the observed peaks based on their exact *m/z* values using "ChemCalc" software (available online, Institute of Chemical Sciences and Engineering, Lausanne, Switzerland) (Patiny and Borel, 2013). The reaction intermediates were detected as singly or doubly charged ions in various ionic forms, such as $[M + H]^+$ and $[M + Na]^+$, in addition to being hydrated or methanolated (see Table 6.1). Mono- and dichlorinated ions were confirmed by observing appropriate isotope abundance ratios.

6.3.4. Structural elucidation

Evidence for the proposed structures was provided through high resolution ESI/qTOF/MS analysis of their elemental composition and through isotope-labelling studies using [^{13}C-U] glucose and [^{13}C-3] alanine. The proposed structures were based on well-known Maillard reaction degradation products.

6.3.5. Criteria applied for tentative identification of the listed ions

Most selected ions were detected in three different reaction systems (1) unlabelled, (2) only glucose labelled, and (3) only alanine labelled systems; each was analyzed in at least two replicates. Ions with an error in their elemental composition higher than ten ppm in only one of the above reaction systems were included if the corresponding ions in the remaining two reaction systems displayed errors with less than eight ppm. Ions detected only in the glucose/alanine/$FeCl_2$ model systems were included in Table 6.1.

6.4. RESULTS AND DISCUSSION

We have reported earlier that *bis*(alaninato)iron(II) complexes formed in alanine/glucose Maillard reaction mixtures in the presence of $FeCl_2$ (Kim and Yaylayan, 2021). Furthermore, these complexes acted as molecular scaffolds for the generation of *bis*[*N*,*N'*-diglycated]iron(II) complexes through dissociation reaction followed by released various *N*,*N*-diglycated alanine derivatives into the reaction mixture (Kim and Yaylayan, 2022). The *N*,*N*-diglycated amino acid derivatives are considered more reactive than monoglycated amino acids (Amadori intermediates) owing to their high content of acyclic forms in at least one of their carbohydrate moieties (Feather and Mossine, 2005) and undergo similar dehydration, redox, and β-elimination reactions (Kim and Yaylayan, 2022). Consequently, the *N*,*N*-diglycated alanine derivatives are expected to generate further degradation products similar to Amadori products. Identification of such degradation products can provide better insights into the Maillard reaction since the accepted mechanisms for the formation of the Maillard reaction products do not adequately account for all the observed structures in model systems or foods (Mortzfeld *et al*., 2020). Due to the lack of commercial standards of *N*,*N*-diglycated amino acids and taking advantage of the observed formation of their precursor the *bis*[*N*,*N'*-diglycated alanine]iron(II) complexes in the model systems containing $FeCl_2$, we utilized such mixtures to generate *N*,*N*-diglycated alanine *in situ* via dissociation from their stable precursor, *bis*[*N*,*N'*-diglycated alanine]iron(II) complexes, which is known to be formed in the alanine/glucose/$FeCl_2$ model system under the Maillard reaction conditions (110 °C for 2 h) (Kim and Yaylayan, 2022). The formation of *N*,*N*-diglycated alanine derivatives in the reaction mixtures were verified through identification of ions incorporating two C-3 alanine atoms and up to 12 carbon atoms from sugars (see Tables 6.1 and S6.2). Considering the known chemical transformations of Amadori compounds and due to the proximity of the sugar moieties to each other, two intramolecular cyclization reactions between the sugars were proposed. One initiated by an enolate group reacting with the carbonyl group of the neighbouring sugar and forming 4H-1,4-oxazine derivatives termed **pathway A** (see Figure 6.1). The second intramolecular cyclization reaction can occur only after the reaction of alanine with one of the sugar moieties and formation of an Amadori product as shown in Figure 6.1, the amino group of the newly formed Amadori product can undergo an intramolecular cyclization with the carbonyl group of the neighbouring sugar, leading to the formation of dihydro-1,4-diazine derivatives termed **pathway B** (Figure 6.1).

The degradation products originating from *N*,*N*-diglycated alanine derivatives observed in the reaction mixtures are reported in Figure 6.2, Tables 6.1, and S6.2.

To evaluate the formation of the proposed degradation products in the reaction mixtures, several model systems were analyzed in the presence and absence of $FeCl_2$ in glucose/alanine. The compositions of the model systems are listed in Table S6.1. The structure R = H or sugar moieties of the proposed Maillard reaction products were determined through elemental analysis using high-resolution electrospray ionization quadrupole time-of-flight mass spectrometry (HR/ESI/qTOF/MS) and isotope labelling technique. The targeted molecules were ions incorporating two C-3 alanine atoms and up to 12 carbon atoms from sugars. The extracted ions from the high-resolution mass spectrometry (HRMS) data satisfied the above requirements. Moreover, the needed precursors, such as *bis*[*N,N'*-difructosyl alanine]iron(II) complexes and *N*,*N*-diglycated alanine derivatives (Kim and Yaylayan, 2022), are listed in Table S6.2, and their distribution is summarized in Table 6.1 and Figure 6.2. The structures represent only one out of many possible isomeric forms.

Table 6.1. Elemental composition and isotope incorporation in 4*H*-1,4-oxazine, 1,4-diazine, dihydro-1,4-diazine and 1,2-disubstituted amino acids observed in alanine/glucose/$FeCl_2$ model system using methanol as solvent (see Figures 6.1 and 6.2)

Structure	Ala/Glu/$FeCl_2$			Ala/Glu[^{13}C-U] /$FeCl_2$			Ala[^{13}C-3]/Glu/$FeCl_2$		
	[M+X]	Elemental Composition	Error ppm[a]	[M+X]	Elemental Composition	Error ppm	[M+X]	Elemental Composition	Error ppm
4*H*-1,4-oxazines (pathway A)									
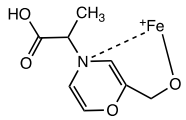 [M]$^+$	239.996	$[C_8H_{10}FeNO_4]^+$	3.87	245.0119	$[C_3[^{13}C]_5H_{10}FeNO_4]^+$	− 1.00	240.9989	$[C_7[^{13}C]H_{10}FeNO_4]^+$	0.72
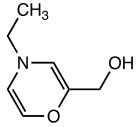 [M + H]$^+$	142.0866	$[C_7H_{12}NO_2]^+$	2.43	185.0577	$[C_2[^{13}C]_5H_{11}NKO_2]^+$	− 6.54	143.088	$[C_6[^{13}C]H_{12}NO_2]^+$	− 11.25
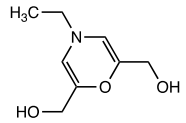 [M + H]$^+$	172.0962	$[C_8H_{14}NO_3]^+$	− 3.6	200.1001	$[C_2[^{13}C]_6H_{13}NNaO_3]^+$	3.29	195.0829	$[C_7[^{13}C]H_{13}NNaO_3]^+$	4

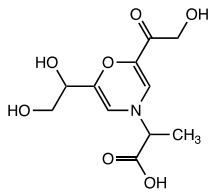 [M + H]$^+$	274.0908	$[C_{11}H_{16}NO_7]^+$	− 4.85	282.1169	$[C_3[^{13}C]_8H_{16}NO_7]^+$	− 7.33	313.0488	$[C_{10}[^{13}C]H_{15}NKO_7]^+$	− 8.19
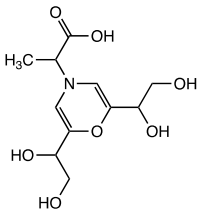 [M + H]$^+$	276.1082	$[C_{11}H_{18}NO_7]^+$	− 0.46	284.137	$[C_3[^{13}C]_8H_{18}NO_7]^+$	8.39	299.0926	$[C_{10}[^{13}C]H_{17}NNaO_7]^+$	− 1.60
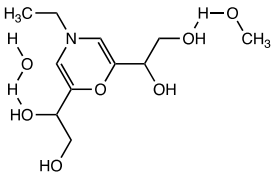 [M + Na]$^+$	304.1349	$[C_{11}H_{23}NNaO_7]^+$	− 7.63	289.1754	$[C_3[^{13}C]_8H_{23}NO_7]^+$	5.73	304.1334	$[C_{10}[^{13}C]H_{22}NNaO_7]^+$	3.94
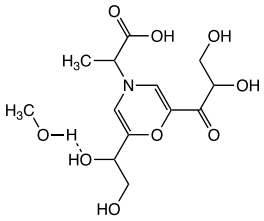 [M + H]$^+$	336.1288	$[C_{13}H_{22}NO_9]^+$	− 0.32	383.1134	$[C_4[^{13}C]_9H_{21}NKO_9]^+$	− 4.13	337.1325	$[C_{12}[^{13}C]H_{22}NO_9]^+$	0.7

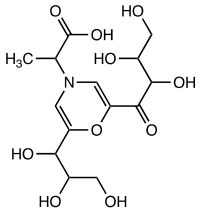 [M + H]$^+$	364.1234	$[C_{14}H_{22}NO_{10}]^+$	− 1.16	207.063	$[C_3[^{13}C]_{11}H_{22}NKO_{10}]^{2+}$	5.11	403.0835	$[C_{13}[^{13}C]H_{21}NKO_{10}]^+$	1.1
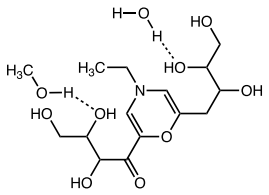 [M + H]$^+$	384.1849	$[C_{15}H_{30}NO_{10}]^+$	− 3.96	418.2189	$[C_3[^{13}C]_{12}H_{29}NNaO_{10}]^+$	24.57	385.1905	$[C_{14}[^{13}C]H_{30}NO_{10}]^+$	1.88
Intermediate B (Pathway B)									
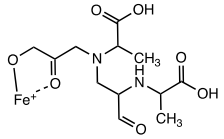 [M]$^+$	359.0547	$[C_{12}H_{19}FeN_2O_7]^+$	3.03	220.0063	$[C_6[^{13}C]_6H_{20}FeClN_2KO_7]^{2+}$	− 2.22	217.9989	$[C_{10}[^{13}C]_2H_{20}Fe[^{35}Cl]N_2KO_7]^{2+}$	− 5.41
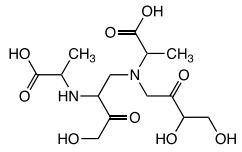	183.0817	$[C_{14}H_{26}N_2O_9]^{2+}$	1.82	373.1862	$[C_6[^{13}C]_8H_{25}N_2KO_9]^+$	10.46	405.1164	$[C_{12}[^{13}C]_2H_{24}N_2KO_9]^+$	− 4.07

$[M + 2H]^{2+}$									
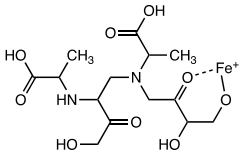 $[M +[^{35}Cl] + K]^{+}$	493.0056	$[C_{14}H_{23}Fe[^{35}Cl]N_2KO_9]^{+}$	− 3.45	485.06	$[C_6[^{13}C]_8H_{24}Fe[^{35}Cl]N_2NaO_9]^{+}$	− 0.42	229.0314	$[C_{12}[^{13}C]_2H_{25}Fe[^{35}Cl]N_2O_9]^{2+}$	− 5.69
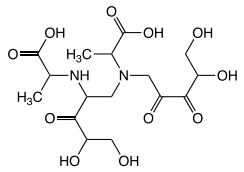 $[M + H]^{+}$	423.1637	$[C_{16}H_{27}N_2O_{11}]^{+}$	6.53	239.0831	$[C_6[^{13}C]_{10}H_{26}N_2Na_2O_{11}]^{2+}$	1.15	251.0468	$[C_{14}[^{13}C]_2H_{26}N_2K_2O_{11}]^{2+}$	13.77
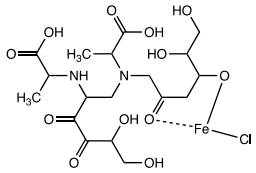 $[M +[^{35}Cl] + 2K]^{2+}$	316.9994	$[C_{18}H_{29}Fe[^{35}Cl]N_2K_2O_{12}]^{2+}$	− 5.29	304.0438	$[C_6[^{13}C]_{12}H_{30}Fe[^{35}Cl]N_2KO_{12}]^{2+}$	1.76	280.048	$[C_{16}[^{13}C]_2H_{31}Fe[^{35}Cl]N_2O_{12}]^{2+}$	− 1.97
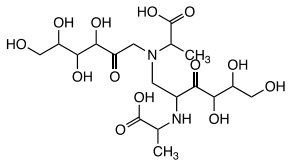 $[M + H]^{+}$	485.1997	$[C_{18}H_{33}N_2O_{13}]^{+}$	4.09	497.239	$[C_6[^{13}C]_{12}H_{33}N_2O_{13}]^{+}$	2.06	263.0842	$[C_{16}[^{13}C]_2H_{33}N_2KO_{13}]^{+}$	1.55

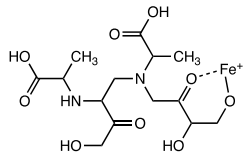 [M +[^{35}Cl] + K]$^{+}$	493.0056	$[C_{14}H_{23}Fe[^{35}Cl]N_2KO_9]^{+}$	− 3.45	485.06	$[C_6[^{13}C]_8H_{24}Fe[^{35}Cl]N_2NaO_9]^{+}$	− 0.42	229.0314	$[C_{12}[^{13}C]_2H_{25}Fe[^{35}Cl]N_2O_9]^{2+}$	− 5.69
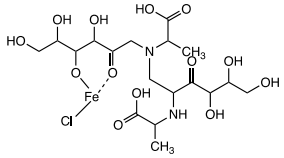 [M +[^{35}Cl] + K]$^{+}$	613.0521	$[C_{18}H_{31}Fe[^{35}Cl]N_2KO_{13}]^{+}$	4.14	551.1568	$[C_6[^{13}C]_{12}H_{31}FeN_2O_{13}]^{+}$	− 0.83	577.1011	$[C_{16}[^{13}C]_2H_{32}Fe[^{35}Cl]N_2O_{13}]^{+}$	1.23
1.2-diammino acid sugar derivatives (Pathway B_2)									
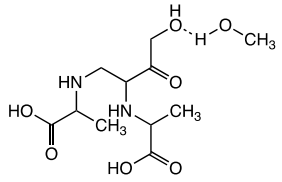 [M + Na]$^{+}$	317.1321	$[C_{11}H_{22}N_2NaO_7]^{+}$	0.56	150.085	$[[^{13}C]_4C_7H_{24}N_2O_7]^{2+}$	− 2.24	335.1119	$[[^{13}C]_2C_9H_{22}N_2O_7K]^{+}$	− 2
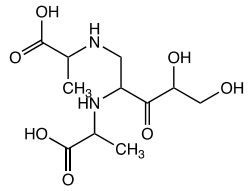	293.1379	$[C_{11}H_{21}N_2O_7]^{+}$	− 12.19	298.1517	$[[^{13}C]_5C_6H_{21}N_2O_7]^{+}$	2.01	159.0643	$[[^{13}C]_2C_9H_{21}N_2NaO_7]^{2+}$	− 5.21

$[M + H]^+$									
$[M + H - H_2O]^+$	275.1228	$[[C_{11}H_{19}N_2O_6]^+$	− 3.5	nd[b]		nd	299.1147	$[[^{13}C]_2C_9H_{18}N_2NaO_6]^+$	7.63
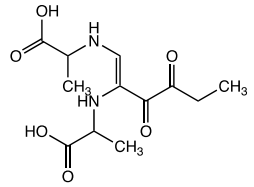 $[M + H]^+$	287.1246	$[C_{12}H_{19}N_2O_6]^+$	2.92	293.1431	$[[^{13}C]_6C_6H_{19}N_2O_6]^+$	− 2.7	327.0779	$[C_{10}[^{13}C]_2H^{18}N_2KO_6]^+$	− 25.85
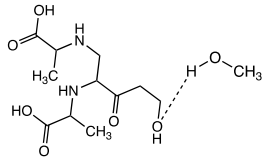 $[M + H]^+$	309.1661	$[C_{12}H_{25}N_2O_7]^+$	1.53	336.1674	$[[^{13}C]_5C_7H_{24}N_2NaO_7]^+$	9.08	178.0703	$[[^{13}C]_2C_{10}H_{24}N_2Na_2O_7]^{2+}$	− 8.15
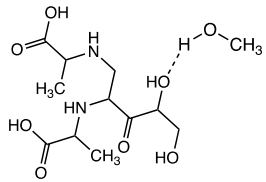 $[M + Na]^+$	347.1456	$[C_{12}H_{24}N_2NaO_8]^+$	8.97	330.1784	$[[^{13}C]_5C_7H_{25}N_2O_8]^+$	3.28	349.1459	$[[^{13}C]_2C_{10}H_{24}N_2NaO_8]^+$	− 9.44
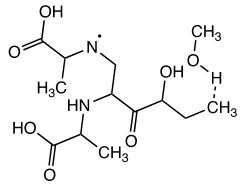 $[M + Na]^+$	344.1562	$[C_{13}H_{25}N_2NaO_7]^+$	2.33	350.1814	$[[^{13}C]_6C_7H_{25}N_2NaO_7]^+$	14.78	324.1805	$[[^{13}C]_2C_{11}H_{26}N_2O_7]^+$	1.04

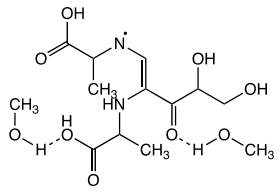 [M + K]$^+$	392.1203	$[C_{13}H_{25}N_2KO_9]^+$	2.9	359.1805	$[[^{13}C]_5C_8H_{26}N_2O_9]^+$	1.24	394.1259	$[[^{13}C]_2C_{11}H_{25}N_2KO_9]^+$	0.07
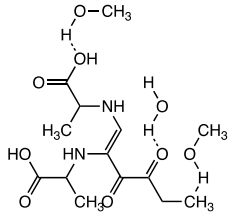 [M + Na]$^+$	391.1687	$[C_{14}H_{28}N_2NaO_9]^+$	0	375.2153	$[[^{13}C]_6C_8H_{29}N_2O_9]^+$	22.43	371.1941	$[[^{13}C]_2C_{12}H_{29}N_2O_9]^+$	1.71
[M + Na – H_2O]	373.1592	$[C_{14}H_{26}N_2NaO_8]^+$	2.85	395.1543	$[[^{13}C]_6C_8H_{26}N_2KO_8]^+$	5.31	177.0947	$[[^{13}C]_2C_{12}H_{28}N_2O_8]^{2+}$	− 2.2
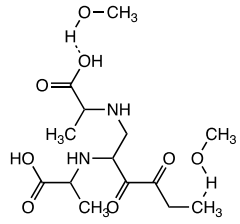 [M + H]$^+$	353.1929	$[C_{14}H_{29}N_2O_8]^+$	2.99	210.0778	$[[^{13}C]_6C_8H_{28}N_2NaKO_8]^{2+}$	-3.51	189.0939	$[[^{13}C]_2C_{12}H_{29}N_2NaO_8]^{2+}$	0.07
Dihydro-1,4-diazine and 1,4-diazine derivatives (pathway B_1)									

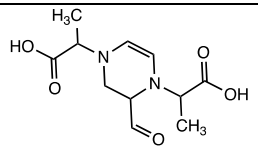 [M + H]$^+$	257.1138	$[C_{11}H_{17}N_2O_5]^+$	2.34	300.0913	$[C_6[^{13}C]_5H_{16}N_2KO_5]^+$	18.15	297.0743	$[C_9[^{13}C]_2H_{16}N_2KO_5]^+$	− 5.01
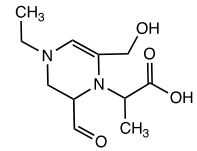 [M + Na]$^+$	265.1174	$[C_{11}H_{18}N_2NaO_4]^+$	5.74	271.1393	$[C_5[^{13}C]_6H_{18}N_2NaO_4]^+$	12.15	245.1416	$[C_9[^{13}C]_2H_{19}N_2O_4]^+$	3.9
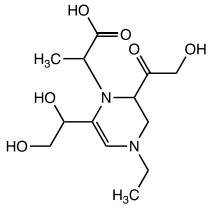 [M + Na]$^+$	325.1359	$[C_{13}H_{22}N_2NaO_6]^+$	− 3.41	333.1675	$[C_5[^{13}C]_8H_{22}N_2NaO_6]^+$	10.97	305.1597	$[C_{11}[^{13}C]_2H_{23}N_2O_6]^+$	− 6.79
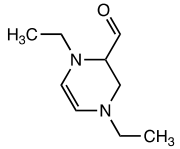 [M + Na + K]$^+$	115.0393	$[C_9H_{16}N_2NaKO]^{2+}$	− 0.18	174.1477	$[C_4[^{13}C]_5H_{17}N_2O]^+$	− 15.01	97.0647	$[C_7[^{13}C]_2H_{17}N_2NaO]^{2+}$	− 0.36

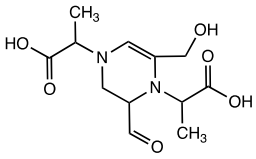 [M + H]$^{+}$	287.1238	$[C_{12}H_{19}N_2O_6]^{+}$	0.13	147.0759	$[C_6[^{13}C]_6H_{20}N_2O_6]^{2+}$	2.15	327.0779	$[C_{10}[^{13}C]_2H_{18}N_2KO_6]^{+}$	− 25.85
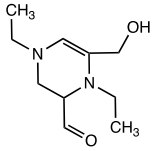 [M + 2H]$^{2+}$	100.0756	$[C_{10}H_{20}N_2O_2]^{2+}$	− 0.9	243.1252	$[C_4[^{13}C]_6H_{18}N_2KO_2]^{+}$	20.92	120.0574	$[C_8[^{13}C]_2H_{19}N_2KO_2]^{2+}$	3.45
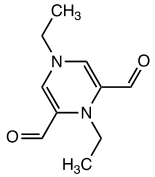 [M +2H]$^{2+}$	98.0596	$[C_{10}H_{16}N_2O_2]^{2+}$	− 4.49	223.1099	$[C_4[^{13}C]_6H_{14}N_2NaO_2]^{+}$	− 22.31	219.1027	$[C_8[^{13}C]_2H_{14}N_2NaO_2]^{+}$	5.67
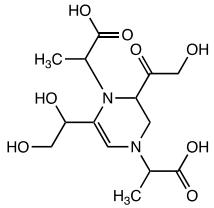 [M + H]$^{+}$	347.1457	$[C_{14}H_{23}N_2O_8]^{+}$	2.33	393.1214	$[C_6[^{13}C]_8H_{22}N_2KO_8]^{+}$	− 15.8	371.1343	$[C_{12}[^{13}C]_2H_{22}N_2Na\ O_8]^{+}$	2.03

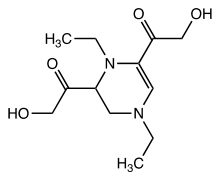 [M +H + Na]$^+$	140.07	$[C_{12}H_{21}N_2NaO_4]^{2+}$	4.27	287.1584	$[C_4[^{13}C]_8H_{20}N_2NaO_4]^+$	0.12	149.0594	$[C_{10}[^{13}C]_2H_{21}N_2KO_4]^+$	– 2.18
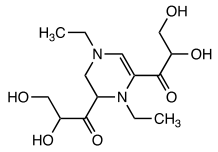 [M + Na]$^+$	339.1541	$[C_{14}H_{24}N_2NaO_6]^+$	4.25	349.1849	$[C_4[^{13}C]_{10}H_{24}N_2NaO_6]^+$	– 3.74	171.0838	$[C_{12}[^{13}C]_2H_{25}N_2NaO_6]^{2+}$	2.80
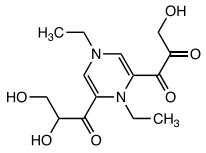 [M + Na]$^+$	335.1213	$[C_{14}H_{20}N_2NaO_6]^+$	– 0.17	323.1728	$[C_4[^{13}C]_{10}H_{21}N_2O_6]^+$	– 0.5	353.1021	$[C_{12}[^{13}C]_2H_{20}N_2KO_6]^+$	0.27
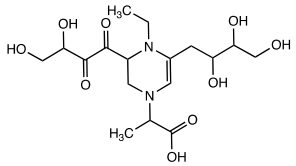 [M + Na]$^+$	427.1752	$[C_{17}H_{28}N_2NaO_9]^+$	15.21	417.2262	$[C_5[^{13}C]_{12}H_{29}N_2NaO_9]^+$	– 1.95	429.1784	$[C_{15}[^{13}C]_2H_{28}N_2NaO_9]^+$	6.96
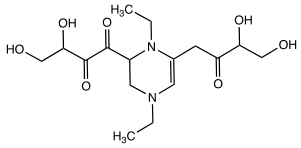	397.1378	$[C_{16}H_{26}N_2KO_7]^+$	1.61	409.1795	$[C_4[^{13}C]_{12}H_{26}N_2KO_7]^+$	5.09	nd		

$[M + K]^+$									
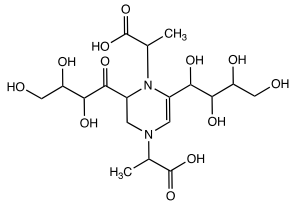 $[M + 2H]^{2+}$	234.0976	$[C_{18}H_{32}N_2O_{12}]^{2+}$	1.65	240.1167	$[C_6[^{13}C]_{12}H_{32}N_2O_{12}]^{2+}$	− 2.68	235.0994	$[C_{16}[^{13}C]_2H_{32}N_2O_{12}]^+$	− 4.97
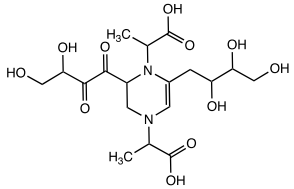 $[M + H]^+$	449.1804	$[C_{18}H_{29}N_2O_{11}]^+$	8.49	461.2181	$[C_6[^{13}C]_{12}H_{29}N_2O_{11}]^+$	2.72	451.1844	$[C_{16}[^{13}C]_2H_{29}N_2O_{11}]^+$	2.45

[a]Error (in ppm) in calculating the elemental composition

[b]nd: not detected

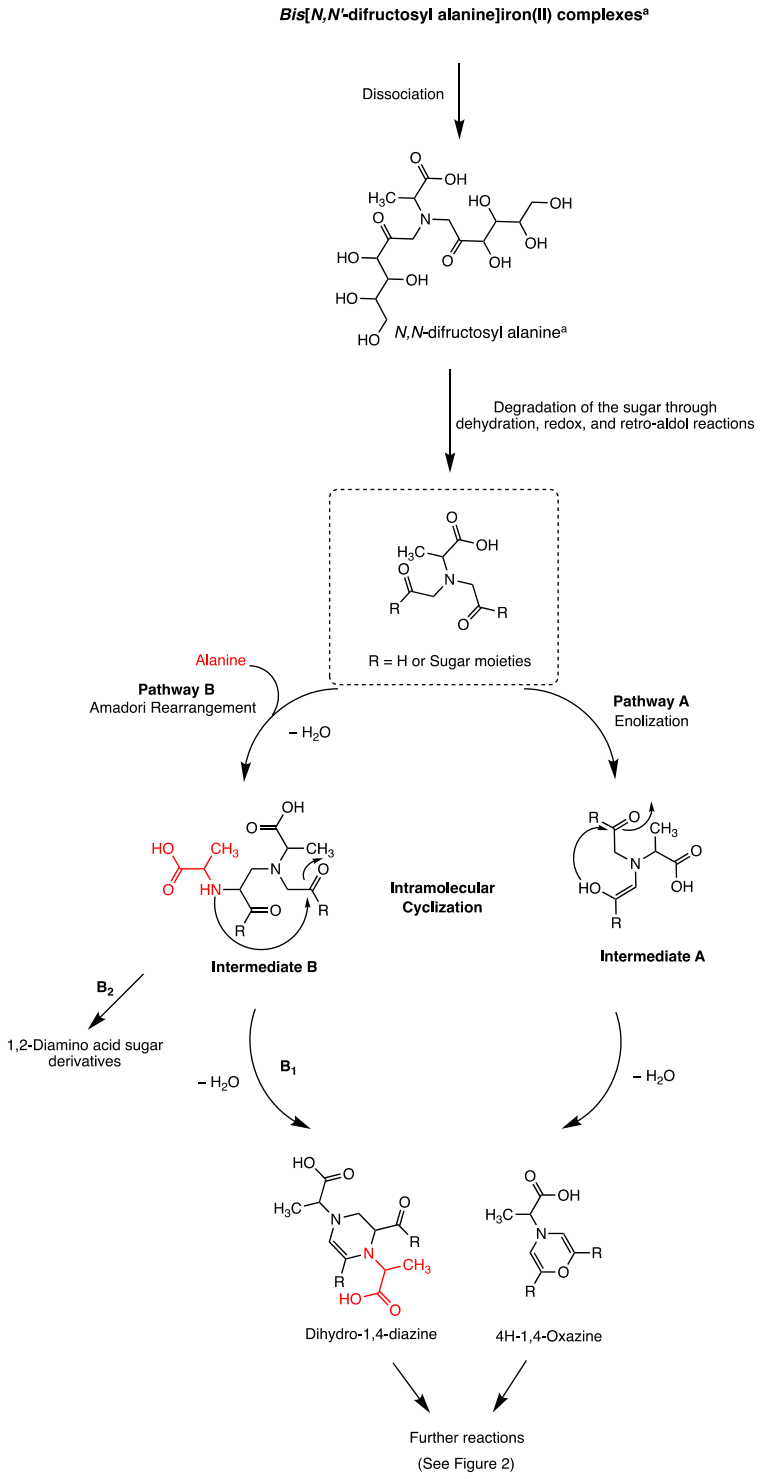

Figure 6.1. Summary of proposed initial pathways of degradation of *N*,*N*-diglycated alanine via enolization (**pathway A**) and Amadori product formation (**pathway B**). See Figure 6.2 for pathway B_2. [a]Based on Kim and Yaylayan, 2022

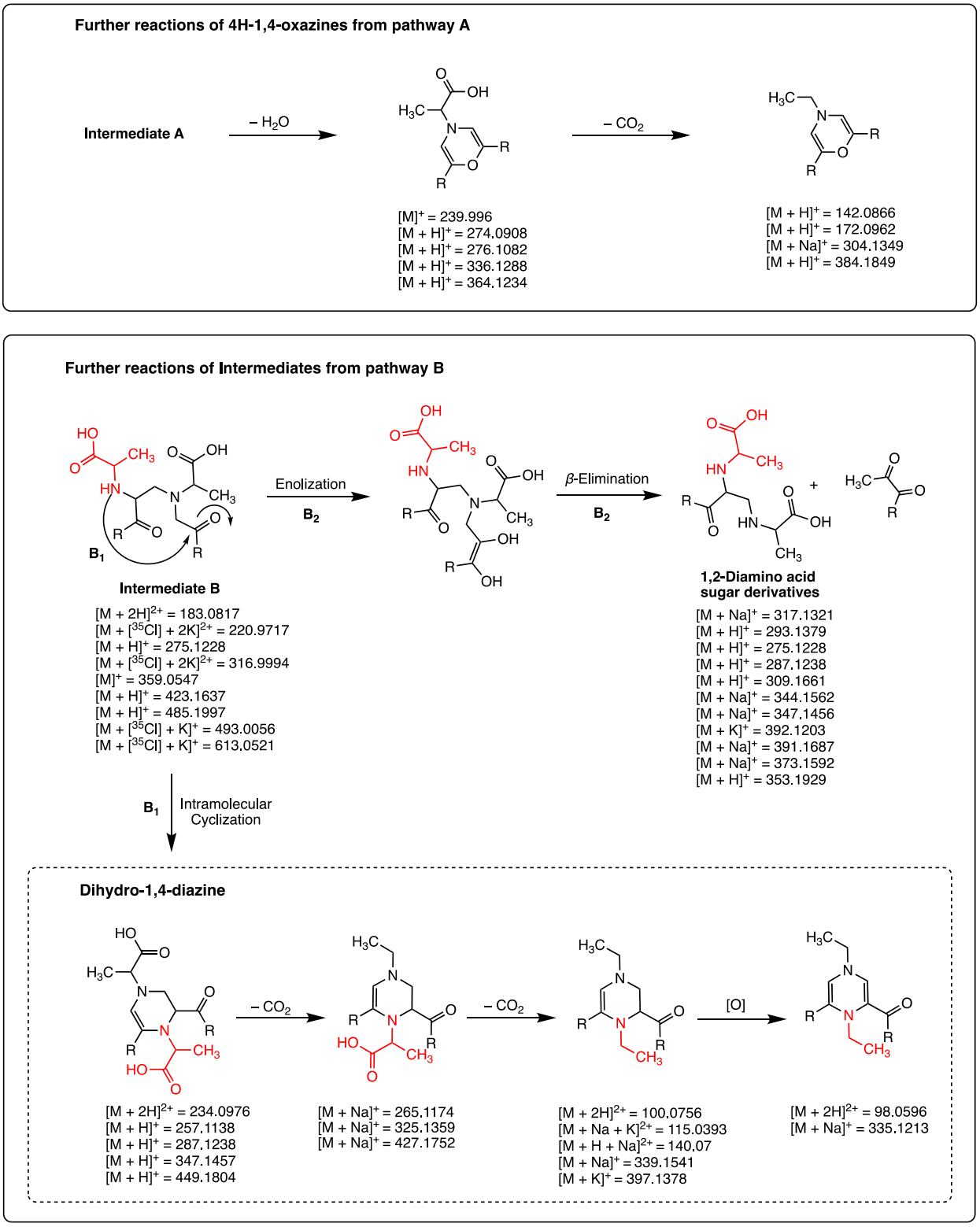

Figure 6.2. Proposed further reactions of intermediates A and B and formation of 4*H*-1,4-oxazines (**pathway A**), dihydro-1,4-diazines (**pathway B$_1$**), and 1,2-diamino sugar derivatives (**pathway B$_2$**) (see Tables 6.1 and S6.2)

6.4.1. Pathway A: formation of 4*H*-1,4-oxazine derivatives

The 1,2-enolization of one of the sugars in the *N*,*N*-diglycated alanine can lead to the formation of the intermediate A. In addition, this reaction can trigger intramolecular cyclization, followed by the formation of the proposed 4*H*-1,4-oxazine derivatives after a dehydration step, as shown in Figure 6.1. Furthermore, the initial 4*H*-1,4-oxazine can undergo decarboxylation and generate decarboxylated derivatives as shown in Figure 6.2 and the identified ions from pathway A are listed in Table 6.1. Evidence in support of the proposed structures was provided through elemental formulas as calculated from HRMS data and isotope label incorporation data from glucose and alanine, as shown in Table 6.1. A total of nine such derivatives were identified, including the decarboxylated forms as listed in Table 6.1. Theoretically, the maximum number of sugar carbon atoms that can be incorporated into 4*H*-1,4-oxazines is 12. No 4*H*-1,4-oxazine derivative incorporating two intact hexose moieties were observed; however, an ion at *m/z* 364.1234 $[C_{14}H_{22}NO_{10}]^+$ incorporating eleven carbon atoms from the sugars representing most likely glucose and pentose moieties was observed. Seven other 4*H*-1,4-oxazine derivatives containing total of five to nine sugar carbon atoms incorporated as triose (C3), tetrose (C4), pentose (C5) or their reduced/oxidized, hydrated, and methanolated counterparts were also observed. For example, the three such structures observed in the mass spectra of the 4*H*-1,4-oxazines derivatives could be generated from *N*,*N*-diglycated alanine, containing eight sugar carbon atoms, incorporating either two tetroses (or a pentose and a triose) or one of their modifications as $[M + H]^+$ at *m/z* 274.0908 $[C_{11}H_{16}NO_7]^+$ and *m/z* 276.1082 $[C_{11}H_{18}NO_7]^+$ and the decarboxylated product as $[M + H]^+$ at *m/z* 304.1349 $[C_{11}H_{23}NNaO_7]^+$. Two ions at *m/z* 172.0962 $[C_8H_{14}NO_3]^+$ and *m/z* 336.1288 $[C_{13}H_{22}NO_9]^+$ incorporated six and nine carbon atoms respectively from the sugar moieties. In addition, two ions with five carbon atoms from the sugar were incorporated in the ion observed at *m/z* 239.996 $[C_8H_{10}FeNO_4]^+$ as an iron(II) complex with an intact alanine and *m/z* 142.0866 $[C_7H_{12}NO_2]^+$ as its decarboxylated derivative. Further validation for these structures was provided by observing the incorporation of one C-3 atom from [^{13}C-3] alanine.

6.4.2. Pathway B: transformations of intermediate B and formation of dihydro-1,4-diazine and di-amino acid sugar derivatives

The HRMS data suggested that *N,N*-diglycated alanine derivatives can undergo Amadori rearrangement at one of their sugar moieties to form the intermediate B (Amadori product) as shown in Figure 6.1. The formation of Amadori product can trigger an intramolecular cyclization to form *dihydo*-1,4-diazine derivatives (**pathway B_1** in Figure 6.1). These derivatives can be traced through incorporation of two C-3 alanine atoms in their structures. Nine ions representing intermediate B (Figure 6.2) are listed in Table 6.1. In the mass spectra, the adducts corresponding to two alanines conjugated with two intact glucose moieties as intermediate B was detected as $[M + H]^+$ at *m/z* 485.1997 ($[C_{18}H_{33}N_2O_{13}]^+$) and $[M + [^{35}Cl] + K]^+$ at *m/z* 613.0521 $[C_{18}H_{31}Fe[^{35}Cl]N_2KO_{13}]^+$, respectively. In addition, an adduct with five carbon atoms from the sugar and two intact alanines was detected at *m/z* 220.9717 $[C_{11}H_{17}Fe[^{35}Cl]N_2K_2O_6]^+$ as an iron(II) complex. Similarly, the adducts incorporating eight carbon atoms from the sugar were detected at *m/z* 183.0817 $[C_{14}H_{26}N_2O_9]^{2+}$ with intact alanine and *m/z* 493.0056 $[C_{14}H_{23}Fe[^{35}Cl]N_2KO_9]^+$ as an iron(II) complex. Two adducts having a total of six and 12 carbon atoms from sugar were also observed at *m/z* 359.0547 $[C_{12}H_{19}FeN_2O_7]^+$ and *m/z* 316.9994 $[C_{18}H_{29}Fe[35Cl]N_2K_2O_{12}]^{2+}$ both with two intact alanines. Finally, an adduct having ten carbon atoms from the sugar moieties was observed at *m/z* 423.1637 $[C_{16}H_{27}N_2O_{11}]^+$with two intact alanine molecules. As shown in Figure 6.2, the initial *dihydro*-1,4-diazine moiety can undergo two decarboxylation reactions followed by oxidation to form 1,4-diazine derivatives known as *dihydro*-pyrazines. For example, intermediates B at *m/z* 485.1997 and at *m/z* 613.0521 as iron(II) complex can form after intramolecular cyclization and decarboxylation steps generating *dihydro*-1,4-diazine or 1,4-dihydropyrazines as $[M + 2H]^{2+}$ at *m/z* 234.0976 $[C_{18}H_{32}N_2O_{12}]^{2+}$.

This study identified a total of 15 unique structures with five to 12 sugar carbons incorporated as *dihydro*-1,4-diazine structures, shown in Table 6.1 and listed in Figure 6.2. The sugar moieties of these structures were either dehydrated, reduced, or oxidized incorporating two intact alanines followed by a single or double decarboxylation reactions. For instance, the HRMS results indicated the formation of four ions incorporating two hexose moieties, two of them corresponding to dihydro-1,4-diazines structures with two intact alanines observed as $[M + H]^+$ at *m/z* 449.1804 $[C_{18}H_{29}N_2O_{11}]^+$ and $[M + 2H]^{2+}$ at *m/z* 234.0976 $[C_{18}H_{32}N_2O_{12}]^{2+}$, the remaining two ions were

singly or doubly decarboxylated products detected as $[M + Na]^+$ at *m/z* 427.1752 $[C_{17}H_{28}N_2NaO_9]^+$ and $[M + K]^+$ at *m/z* 397.1378 $[C_{16}H_{26}N_2KO_7]^+$, respectively.

Adducts with a total of ten carbons from sugar and decarboxylated alanine was observed at *m/z* 335.1213 $[C_{14}H_{20}N_2NaO_6]^+$. Ions with five carbon atoms from sugar were detected as $[M + H]^+$ at *m/z* 257.1138 $[C_{11}H_{17}N_2O_5]^+$ and $[M + Na + K]^{2+}$ at *m/z* 115.0393 $[C_9H_{16}N_2NaKO]^{2+}$. On the other hand, four ions with six carbon atoms from sugar were observed as $[M + H]^+$ at *m/z* 287.1238 $[C_{12}H_{19}N_2O_6]^+$ with two intact alanines, $[M + Na]^+$ at *m/z* 265.1174 $[C_{11}H_{18}N_2NaO_4]^+$ as singly decarboxylated form, and $[M + 2H]^{2+}$ at *m/z* 100.0756 $[C_{10}H_{20}N_2O_2]^{2+}$ and $[M + 2H]^{2+}$ at *m/z* 98.0596 $[C_{10}H_{16}N_2O_2]^{2+}$ both as doubly decarboxylated form. Further validation for the proposed structures was provided by ^{13}C isotope-labelling experiments, which showed the incorporation of five to six carbon atoms of the [^{13}C-U] glucose moiety and the two C-3 atoms of [^{13}C-3] alanine into the dihydro-1,4-diazines.

Furthermore, one of the sugars in intermediate B can undergo 2,3-enolization followed by *β*-elimination (pathway B_2) to generate 1,2-diamino acid sugar derivatives (Figure 6.2); 12 such ions were detected. The HRMS results indicated that, among the 12 ions, three ions corresponded to structures incorporating six carbons from sugar in oxidized form, such as tri-oxo pentose, conjugated with two intact alanines observed as $[M + Na]^+$ at *m/z* 391.1687 $[C_{14}H_{28}N_2NaO_9]^+$, $[M + Na]^+$ at *m/z* 373.1592 $[C_{14}H_{26}N_2NaO_8]^+$and $[M + H]^+$ at *m/z* 353.1929 $[C_{14}H_{29}N_2O_8]^+$. The rest of the ions corresponded to aldose or ketose sugar moieties conjugated with two alanines, the five adducts with five carbons from sugars integrating two intact alanines were detected as $[M + H]^+$ at *m/z* 293.1379 $[C_{11}H_{21}N_2O_7]^+$, $[M + H]^+$ at *m/z* 275.1228 $[C_{11}H_{19}N_2O_6]^+$, $[M + H]^+$ at *m/z* 309.1661 $[C_{12}H_{25}N_2O_7]^+$, $[M + Na]^+$ at *m/z* 347.1456 $[C_{12}H_{24}N_2NaO_8]^+$, and $[M + K]^+$ at *m/z* 392.1547 $[C_{14}H_{29}N_2KO_8]^+$ and the adduct having four carbon atoms from sugar with two intact alanines was observed as $[M + Na]^+$ at *m/z* 317.1321 $[C_{11}H_{22}N_2NaO_7]^+$. Further validation of our proposed structures was provided by ^{13}C isotope-labelling experiments, which incorporated the C4–C6 atoms of the [^{13}C-U] glucose moiety and the two C-3 atoms of [^{13}C-3] alanine into the rearrangement products.

6.5. CONCLUSION

HRMS data have indicated that sugar moieties in *N*,*N*-diglycated alanine exhibit similar thermochemical transformations as the Amadori compounds, such as dehydration, enolization, β-elimination, redox, and retro-aldol reactions. A characteristic reaction specific to *N*,*N*-diglycated alanine was identified as intramolecular cyclization reaction generating novel 4*H*-1,4-oxazines and dihydro-1,4-diazine structure moieties.

6.6. REFERENCES

Argirov, O. K., Lin, B., Ortwerth, B. J. (2004). 2-ammonio-6-(3-oxidopyridinium-1yl)hexanoate (OP-lysine) is a newly identified advanced glycation end product in cataractous and aged human lenses. *Journal of Biological Chemistry*, *279*, 6487–6495.

Belikov, V. M., Vitt, S. V., Kuznetsova, N. I., Bezrukov, M. G., Saporovskaya, M. B. (1969). Reaction of the copper complex of L-alanine with acetaldehyde and the mechanism of the Akabori reaction. Bulletin of the Academy of Sciences of the USSR, Division of chemical science, 18, 2371–2375.

Feather, M. S. and Mossine, V. V. (2005). Correlations between structure and reactivity of Amadori compounds: the Reactivity of Acyclic Forms. In J. O' Brien, H. E. Nursten, M. J. C. Crabbe, and J. M. Ames (Eds.), *The Maillard Reaction in Foods and Medicine*, Woodhead Publishing Series in Food Science, Technology and Nutrition (pp. 37–42). Woodhead Publishing,

Kim, E. S. and Yaylayan, V. (2021). Identification of the Maillard reaction intermediates as divalent iron complexes in alanine/glucose/$FeCl_2$ model system using ESI/qTOF/MS/MS and isotope labelling technique. *Current Research in Food Science*, 4, 287–294.

Kim, E. S., and Yaylayan, V. (2022). *Bis*(alaninato)iron(II) complexes as molecular scaffolds for the generation of *N,N*-di-glycated alanine derivatives in the presence of glucose. *Food Chemistry*, 374, 131815.

Mohsin, G. F., Schmitt, F., Kanzler, C, Alzubaidi, A. K., Hornemann, A. (2022). How alanine catalyzes melanoidin formation and dehydration during synthesis from glucose. *European Food Research and Technology*, 248, 1615–1624.

Mortzfeld, F. B., Hashem, C., Vranková, K. Margit, W., Rudroff, F. (2020). Pyrazines: Synthesis and industrial application of these valuable flavor and fragrance compounds. *Biotechnology Journal*, 15(11), 2000064.

Patiny, L. and Borel, A. (2013). ChemCalc: a building block for tomorrow's chemical infrastructure. *Journal of chemical information and modeling*, 53, 5, 1223–1228.

Vasile, C. (1993). Degradation and decomposition. In C. Vasile, and R. B. Seymour (Eds.), Handbook of polyolefins: synthesis and properties. (pp. 413) Marcel Dekker Inc., New York.

Xing, H. and Yaylayan, V. (2022). Insight into Isomeric Diversity of Glycated Amino Acids in Maillard Reaction Mixtures. *International Journal of Molecular Sciences*, 23(7), 3430.

6.7. SUPPLEMENTARY DATA

Table S6.1. Composition of the model systems[a]

	Model System
Control Model System	Alanine was added to a glucose solution and heated in the absence of metal ions - **Ala/Glu**
Test Model System	Alanine was added to a glucose solution and heated in the presence of $FeCl_2$ - **Ala/Glu/$FeCl_2$**
Isotope Labelling Model System	Alanine [^{13}C-3] was added to a glucose solution and heated in the presence of $FeCl_2$ **-[^{13}C-3] Ala/Glu/$FeCl_2$**
	Alanine was added to a glucose [^{13}C-U] solution and heated in the presence of $FeCl_2$ - **Ala/[^{13}C-U] Glu/$FeCl_2$**

[a]All model systems were heated at 110 ℃ for 2 h in water or methanol using a sealed stainless-steel reactor and analyzed in at least over two replicates

Table S6.2. Proposed precursors of the reaction products observed in the alanine/glucose/$FeCl_2$ model system

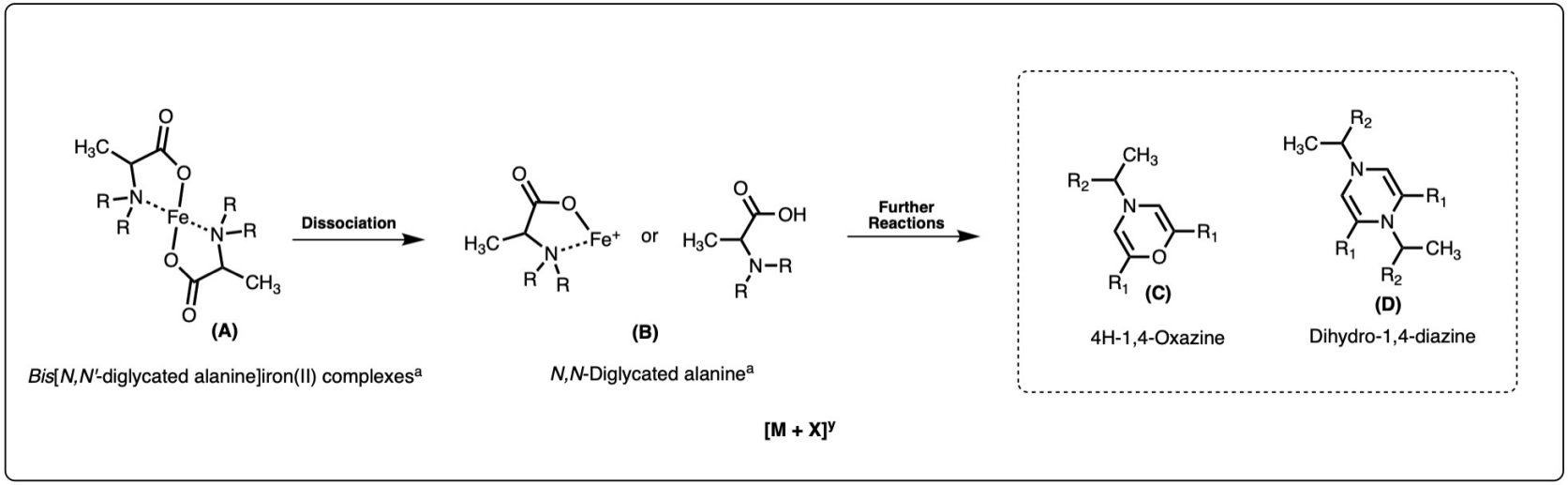

y = + or 2+

R = triose, tetrose, pentose or hexose

R_1 = $(CHOH)nCH_2OH$, where n is 1 to 4

R_2 = H or HCOOH

	Precursors (A) (see Kim & Yaylayan, 2022)	Dissociated Precursors (B) (see Kim & Yaylayan, 2022)	Reaction Products (C & D) (see Table 6.1)	
			4*H*-1,4-oxazine	1,2-Diamino acid sugar derivatives
I	$[M + Cl]^+ = 595$ $[M + H]^+ = 579$ $[M + H]^+ = 586$ $[M + Na]^+ = 683.12$	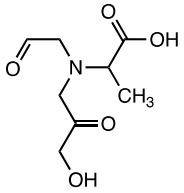 $[M + H]^+ = 204$		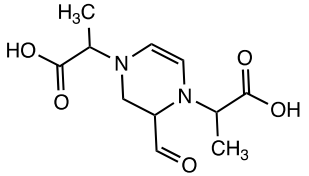 $[M + H]^+ = 257$

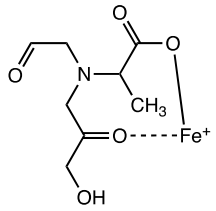

[M]$^{+}$ = 258

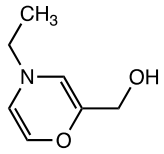

[M + H]$^{+}$ = 142

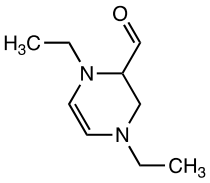

[M + Na + K]$^{2+}$ = 115

II

[M + H]$^{+}$ = 571

[M + Cl]$^{+}$ = 595

[M + H]$^{+}$ = 579

[M + H]$^{+}$ = 586

[M + Na]$^{+}$ = 683.12

[M + Cl]$^{+}$ = 683.11

[M + 2Cl + Na + K]$^{2+}$ = 465

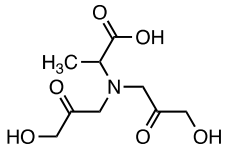

[M + H]$^{+}$ = 234

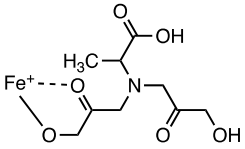

[M]$^{+}$ = 288

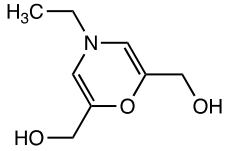

[M + H]$^{+}$ = 172

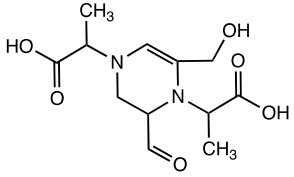

[M + H]$^{+}$ = 287

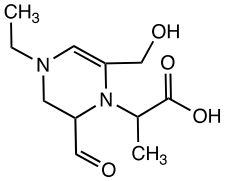

[M + Na]$^{+}$ = 265

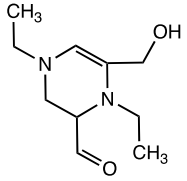

[M + 2H]$^{2+}$ = 100

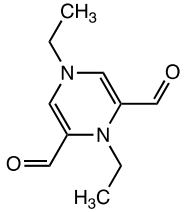

[M + 2H]$^{2+}$ = 98

III

$[M + H]^+ = 571$

$[M + Cl]^+ = 595$

$[M + H]^+ = 579$

$[M + H]^+ = 586$

$[M + Na]^+ = 683.12$

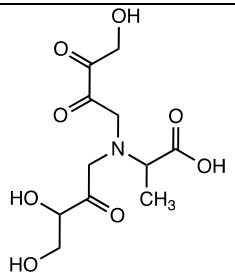

$[M + H]^+ = 292$

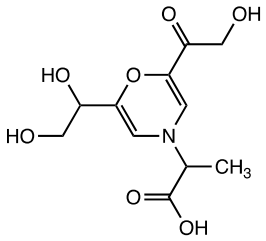

$[M + H]^+ = 274$

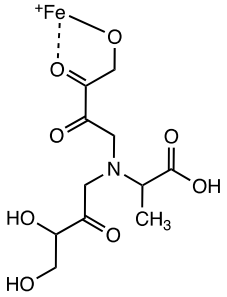

$[M]^+ = 346$

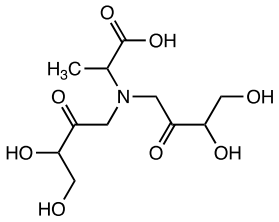

$[M + H]^+ = 294$

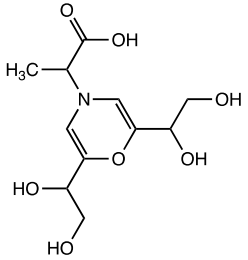

$[M + H]^+ = 276$

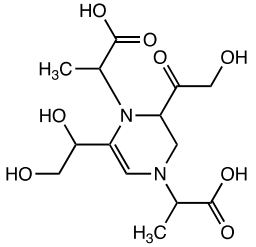

$[M + H]^+ = 347$

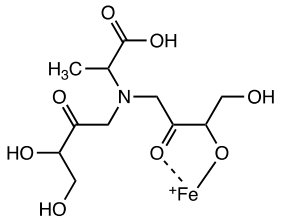

$[M]^+ = 348$

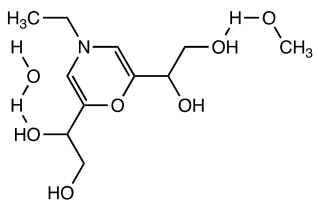

$[M + Na]^+ = 304$

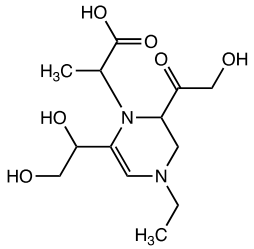

$[M + H]^+ = 325$

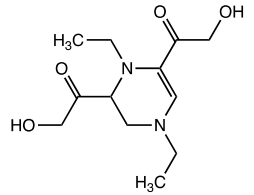

$[M + H + Na]^{2+} = 140$

IV

$[M + Cl]^+ = 595$

$[M + H]^+ = 579$

$[M + H]^+ = 586$

$[M + Na]^+ = 683.12$

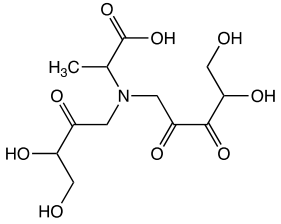

$[M + H]^+ = 322$

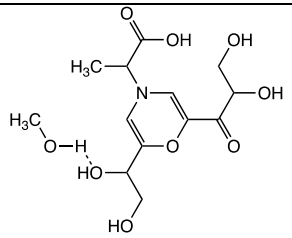

$[M + H]^+ = 336$

V

$[M + 2Cl + Na + K]^{2+} = 463$

$[M + 2Cl + 2K]^{2+} = 482$

$[M + 2Cl + 2K]^{2+} = 469$

$[M + 2Cl + Na + K]^{2+} = 462$

$[M + 2Cl + 2K]^{2+} = 465$

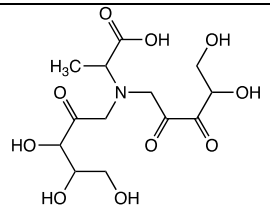

$[M + H]^+ = 352$

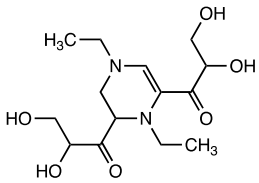

$[M + Na]^+ = 339$

[M + H + 2Cl]$^{+}$ = 863

M + H + 2Cl + Na]$^{2+}$ = 479

[M + Cl]$^{+}$ = 595

[M + H]$^{+}$ = 579

[M + H]$^{+}$ = 586

[M + Na]$^{+}$ = 683.12

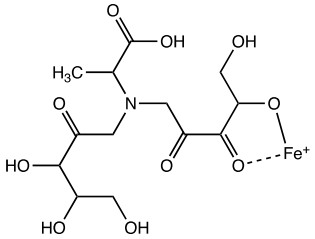

[M + Cl + Na]$^{+}$ = 464

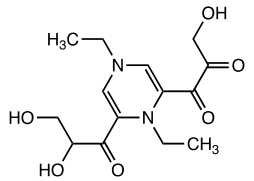

[M + Na]$^{+}$ = 335

VI

[M + Cl]$^{+}$ = 595

[M + H]$^{+}$ = 579

[M + 2Cl + 2K]$^{2+}$ = 474

[M + Cl+ K]$^{2+}$ = 460

[M + 2Cl + 2K]$^{2+}$ = 488

[M + 2K]$^{2+}$ = 468

[M + 2Cl + 2Na]$^{2+}$ = 480

[M + H + 2Cl+ Na]$^{2+}$ = 477

[M + 2Cl + Na + K]$^{2+}$ = 491

[M + 2H + 2Cl]$^{2+}$ = 462

[M + 2K]$^{2+}$ = 464

M + 2Cl + 2K]$^{2+}$ = 465

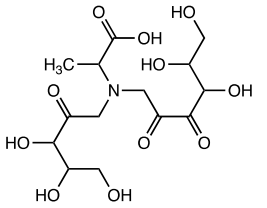

[M + H]$^{+}$ = 382

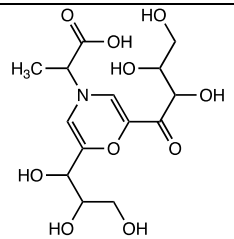

[M + H]$^{+}$ = 364

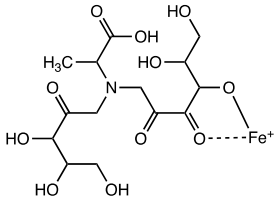

[M]$^{+}$ = 436

VII

[M + H]$^{+}$ = 586

[M + Na]$^{+}$ = 683.12

[M + Cl]$^{+}$ = 683.11

[M + 2Cl + Na + K]$^{2+}$ = 465

[M + 2Cl + Na + K]$^{2+}$ = 463

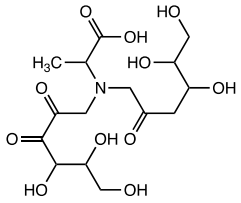

[M + H]$^{+}$ = 396

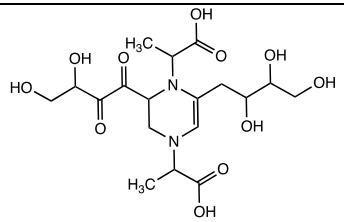

[M + H]$^{+}$ = 449

$[M + 2Cl + 2K]^{2+} = 482$

$[M + 2Cl + 2K]^{2+} = 469$

$[M + 2Cl + Na + K]^{2+} = 462$

$[M + 2Cl + 2K]^{2+} = 465$

$[M + H + 2Cl]^{+} = 863$

$M + H + 2Cl + Na]^{2+} = 479$

$[M + 2Cl + 2K]^{2+} = 474$

$[M + Cl + K]^{2+} = 460$

$[M + 2Cl + 2K]^{2+} = 488$

$[M + 2Cl + 2Na]^{2+} = 482$

$[M + H + 2Cl + Na]^{2+} = 479$

$[M + H + 2Cl + K]^{2+} = 487$

$[M + H]^{+} = 789$

$[M + H]^{+} = 791$

$[M + H + 2Cl + K]^{2+} = 490$

$[M + H]^{+} = 861$

$M + H + 2Cl + Na]^{2+} = 485$

$[M + 2Cl + Na + K]^{2+} = 472$

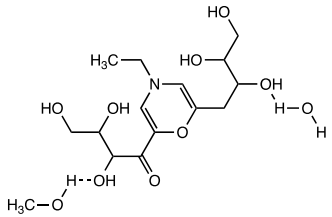

$[M + H]^{+} = 384$

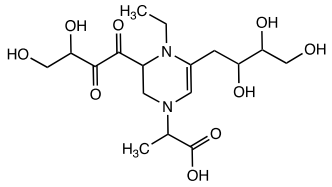

$[M + Na]^{+} = 427$

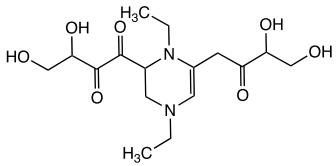

$[M + K]^{+} = 397$

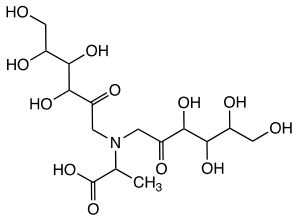

$[M + H]^{+} = 414$

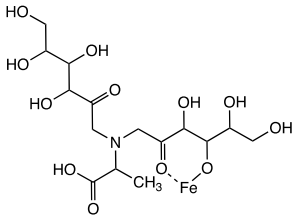

$[M]^{+} = 468$

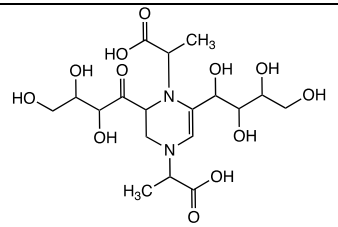

$[M + 2H]^{2+} = 234$

[a]Mechanism of the formation of *bis*[*N*,*N'*-diglycated alanine]iron(II) complexes, [*N*,*N*-diglycated alanine]iron(II) complexes, and *N*,*N*-diglycated alanine derivatives based on Kim and Yaylayan, 2022

CONNECTING PARAGRAPH

In **Chapter 6**, we explored the degradation products of *N*,*N*-diglycated alanine derivatives, indentifyng a variety of reactions. These reactions include intramolecular cyclization, which leads to the formation of oxazine and diazine derivatives. **In chapter 7,** we investigated the ability of metal ions to stabilise Schiff bases as iron complexes allowing them to be detected as cyclic oxazolidin-5-one isomers. **Chapter 7** will be submitted to the *Journal of Agriculture and Food Chemistry* under the "ESI/qTOF/MS profiling of oxazolidin-5-one derivatives in alanine/glucose/Fe^{2+} model system".

CHAPTER 7

ESI/qTOF/MS PROFILING OF OXAZOLIDIN-5-ONE DERIVATIVES IN ALANINE/GLUCOSE/FE^{2+} MODEL SYSTEM

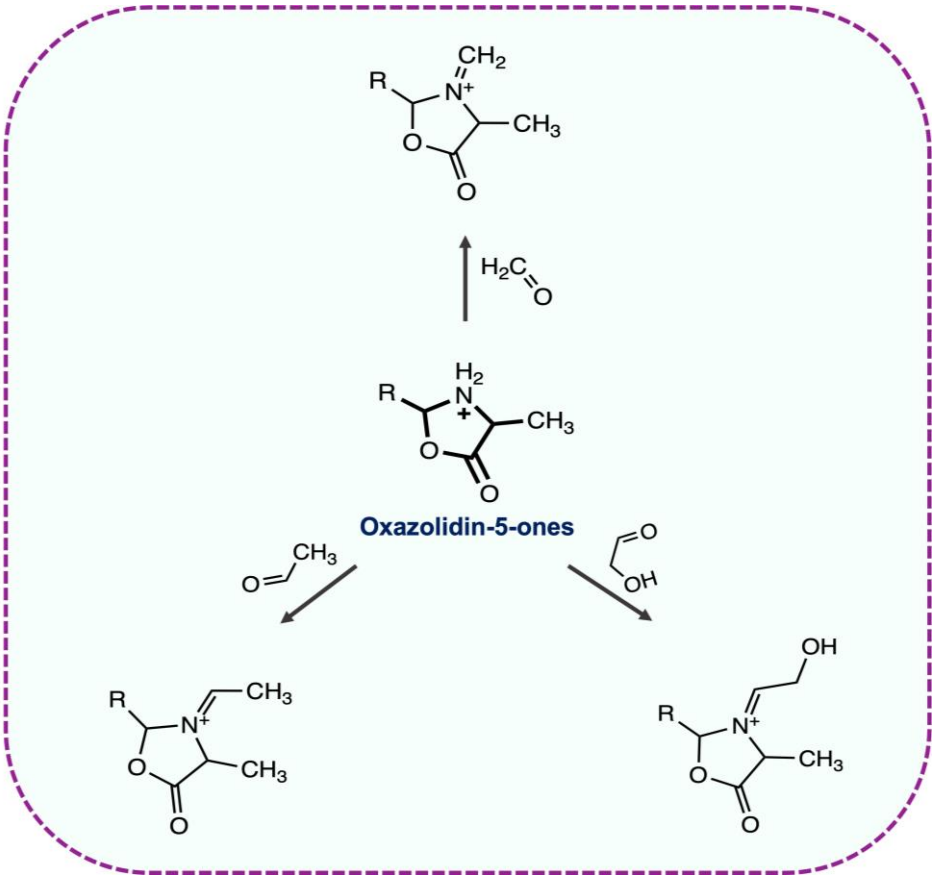

7.1. ABSTRACT

Schiff bases are typically generated by the interaction of amino groups with carbonyl compounds. They can be stabilized by various mechanisms, including Amadori rearrangement in the case of amino acids, complexation with metal ions, or through intramolecular cyclization of the carboxylate anion with the carbon atom of the imine to form a more stable cyclic isomer the oxazolidin-5-one. Unlike oxazolidin-5-ones, Schiff bases cannot be easily detected owing to their facile conversion into Amadori products, especially under acidic pH conditions. The metal ion complexation of Schiff bases enhances their stability, increasing their half-life and allowing the formation of more oxazolidin-5-one. In this chapter, high-resolution mass spectrometry and isotope labelling techniques were used to identify oxazolidin-5-one derivatives in model systems of glucose/alanine/$FeCl_2$. Spiking experiments using commonly encountered aldehydes in the Maillard reaction, such as formaldehyde, acetaldehyde, and glycolaldehyde, were used to confirm the identity of the oxazolidin-5-ones observed at *m/z* 102, *m/z* 116, and *m/z* 132, respectively. The oxazolidin-5-one derivatives, formed as stable Schiff base alternatives, can be considered as critical precursors that can enhance the flavour or browning compound generation through the Maillard reaction.

KEYWORDS: *N,N*-diglycated alanine, Amadori compounds, Intramolecular cyclization, Oxazolidin-5-one

7.2. INTRODUCTION

The generation of flavours and colours during the thermal processing of food, such as frying, roasting, and baking, is triggered by the degradation of Maillard reaction intermediates such as Schiff bases. Such degradation products include Amadori rearrangement products (ARPs) and 1,2-dicarbonyl compounds (Frank and Hofmann, 2000; Hofmann, 1998; Rizzi, 1997; Yaylayan, 2003) and their derivatives. Among the degradation products, the presence of heterocyclic aromatic compounds has been associated with an increased consumer acceptance of many processed food products. Most flavourings and colourings are currently obtained via chemical syntheses; however,

the demand for products derived from "natural" sources has been increasing (Mortzfeld *et al.*, 2020). Consequently, the food industry has shifted to using natural precursors for flavour enhancement. In food, the oxazolidin-5-ones have been proposed as critical reactive intermediates that can undergo decarboxylation to form azomethine ylides, which subsequently degrade into isomeric imines and aroma compounds. Only few studies have been reported on monitoring their generation under thermal reaction conditions using Fourier–transform infrared (FTIR) spectroscopy or high-resolution mass spectrometry (HRMS) (Chu and Yaylayan, 2008; 2009; Shimasaki *et al.*, 1993; Xing and Yaylayan, 2021). In the Maillard reaction mixtures containing metal ions, the increased ARP content was attributed to the formation of *bis*[*N*,*N'*-diglycated amino acids]iron(II) complexes. Such complexes have been observed to undergo dissociation and formation of various monoglycated amino acid (Amadori compounds) derivatives and *N*,*N*-diglycated amino acids, considered as important flavour or aroma precursors in the Maillard reaction (Kim and Yaylayan, 2020; 2021; 2022). Their further degradation products, such as 4*H*-1,4-oxazines and dihydro-1,4-diazine derivatives were reported in Chapter 6. Upon the initiation of the Maillard reaction, amino acids and reducing sugars can form Schiff bases that subsequently rearrange into ARPs or undergo intramolecular cyclization to form oxazolidin-5-one intermediates under dry conditions (Chu and Yaylayan, 2009) or during ball milling of dry sugars and amino acids (Xing and Yaylayan, 2021). This intermediate can provide an alternate pathway for sugar degradation through decarboxylation reactions. However, the subsequent chemical transformations of oxazolidin-5-one have yet to be studied in detail for flavour applications. Considering the known chemical transformations of monoglycated amino acids (Amadori compounds), *N*,*N*-diglycated amino acids, and Schiff base formation in the Maillard reaction mixtures, we investigated the possible formation of oxazolidin-5-one intermediates in alanine/glucose/$FeCl_2$ model systems under Maillard reaction conditions (110 °C for 2 h). Specifically, we employed high-resolution electrospray ionization quadrupole time-of-flight mass spectrometry (HR/ESI/qTOF/MS) and isotope labelling techniques in this study.

7.3. MATERIALS AND METHODS

7.3.1. Materials and reagents

L-Alanine (98%), D-glucose, paraformaldehyde, glycolaldehyde, acetaldehyde (99.5%), and iron(II) chloride ($FeCl_2$) (99%) were purchased from Sigma–Aldrich Chemical Co. (Oakville, ON, Canada). Alanine-3-^{13}C ($^{13}CH_3CH(NH_2)CO_2H$) (98%) and glucose-^{13}C-U ($^{13}C_6H_{12}O_6$) (99%) were purchased from Cambridge Isotope Laboratories (Andover, MA, USA). Liquid chromatography–mass spectrometry (LC–MS)-grade water and methanol (OmniSolv, >99%) were obtained from VWR International (Mississauga, ON, Canada).

7.3.2. Sample preparation

The test model systems were prepared in 1:1:0.5 molar ratios by adding glucose (18 mg), alanine (9 mg), and $FeCl_2$ (6.4 mg) to methanol (1 mL) and heating in a stainless-steel reactor at 110 °C for 2 h, followed by evaporation of the solvent for 30 min at 110 °C. The control model system was prepared by heating glucose (18 mg) and alanine (9 mg) in methanol at 110 °C for 2 h in the absence of metal ions. All samples were analyzed in at least two replicates, as shown in Table 7.1.

7.3.3. Experiments in the presence of selected Strecker aldehydes

Experiments with selected Strecker aldehydes (formaldehyde, acetaldehyde, and glycolaldehyde) were conducted using excess (~ 1:10 w/w) aldehydes relative to alanine and glucose in the presence and absence of $FeCl_2$. The relative intensities of the oxazolidin-5-one derivatives were measured using ESI/qTOF/MS spectral peaks. These experiments were performed to confirm the identity of observed oxazolidin-5-one derivatives generated in the reaction mixtures from aforementioned aldehydes by observing increases in their relative intensities. See Table 7.1

7.3.4. ESI/qTOF/MS analysis

The samples were dissolved in liquid chromatography (LC) methanol at a concentration of 1 mg/mL. The samples were then diluted 10-fold in 10% methanol prior to analysis by ESI/qTOF/MS in the positive-ion mode. The ESI/qTOF/MS system comprised a Bruker Maxis Impact quadrupole time-of-flight mass spectrometer (Bruker Daltonics, Bremen, Germany) operated in the positive-ion mode. Samples (1 μL) were injected directly into the ESI/qTOF/MS

system. Instrument calibration was performed by using sodium formate clusters. The electrospray interface settings were as follows: nebulizer pressure, 0.6 bar (60,000 Pa); drying gas, 4 L/min; temperature, 180 °C; and capillary voltage, 4500 V. The scan range was 70–1000. Molecular formulas were assigned to all observed peaks based on their exact *m/z* values using "ChemCalc" software (available online, Institute of Chemical Sciences and Engineering, Lausanne, Switzerland) (Patiny and Borel, 2013).

Table 7.1. Composition of the model systems[a]

	Model System
Control Model System	Alanine was added to a glucose solution and heated in the absence of metal ions - **Ala/Glu**
Spiked Model System	Paraformaldehyde was added to an alanine and glucose and heated in the absence of metal ions - **Ala/Glu/A** Three reactive aldehydes (paraformaldehyde:A, acetaldehyde:B, and glycolaldehyde:C) were added to an alanine and glucose solution, followed by heated in the absence of $FeCl_2$ - **Ala/Glu/A + B + C** Reactive aldehyde (paraformaldehyde:A, acetaldehyde:B, and glycolaldehyde:C) were added to an alanine and glucose solution, followed by heating in the presence of $FeCl_2$ - **Ala/Glu/$FeCl_2$/A, Ala/Glu/$FeCl_2$/B, and Ala/Glu/$FeCl_2$/C** Three reactive aldehydes (paraformaldehyde:A, acetaldehyde:B, and glycolaldehyde:C) were added to an alanine and glucose solution, followed by heated in the presence of $FeCl_2$ - **Ala/Glu/$FeCl_2$/A + B + C**
Test Model System	Alanine was added to a glucose solution and heated in the presence of $FeCl_2$ - **Ala/Glu/$FeCl_2$**
Isotope Labelling Model System	Alanine [^{13}C-3] was added to a glucose solution and heated in the presence of $FeCl_2$ -**[^{13}C-3] Ala/Glu/$FeCl_2$** Alanine was added to a glucose [^{13}C-U] solution and heated in the presence of $FeCl_2$ - **Ala/[^{13}C-U] Glu/$FeCl_2$**

[a]All model systems were heated at 110 °C for 2 h in a methanol using a sealed stainless-steel reactor and analyzed in at least over two replicates

7.3.5. Structural elucidation

Evidence for the proposed structures was provided through high-resolution ESI/qTOF/MS analysis of their elemental composition and isotope-labelling studies using [^{13}C-U] glucose and [^{13}C-3] alanine. The proposed structures are based on well-known Maillard reaction degradation products.

7.4. RESULTS AND DISCUSSION

The rationale behind divalent metal ion catalysis of oxazolidin-5-one formation (see Figure 7.1) and proposed reaction pathways of simple aldehydes with alanine are shown in Figure 7.2. According to Figure 7.2, two proposed reaction pathways can rationalize the formation of differently substituted oxazolidin-5-one derivatives observed in the reaction mixtures and promoted by metal ions. **Pathway A** involves the Schiff base formation of amino acids with simple aldehydes such as Strecker aldehydes with no α-hydroxyl functionality and therefore no possibility for Amadori rearrangement, and **pathway B** involves the Schiff base formation of amino acids with reducing sugars and simple aldehydes with an α-hydroxyl functionality such as glycolaldehyde (the Strecker aldehyde of serine). The added metal ions are predicted to stabilize the Schiff bases through complexation, as shown in Figure 7.1, prolonging their half-lives, and increasing the yield of their reaction products. The oxazolidin-5-one derivatives observed in the reaction mixtures are shown in Figures 7.2, 7.3, and Table 7.2. To evaluate the generation of the proposed oxazolidin-5-one derivatives in the reaction mixtures, spiking experiments were performed with several glucose/alanine model systems with and without added aldehydes (see Tables 7.2, S7.1, and Figure S7.1). The reaction mixtures were analyzed using HR/ESI/qTOF/MS and isotope labelling targeting ions, incorporating one alanine C-3 atom and up to four sugar carbon atoms, depending on the number and type of aldehyde moieties involved in oxazolidin-5-one formation. The extracted ions from the HRMS data satisfying these requirements are listed in Tables 7.2 and S7.1 representing only one of the many possible isomeric forms.

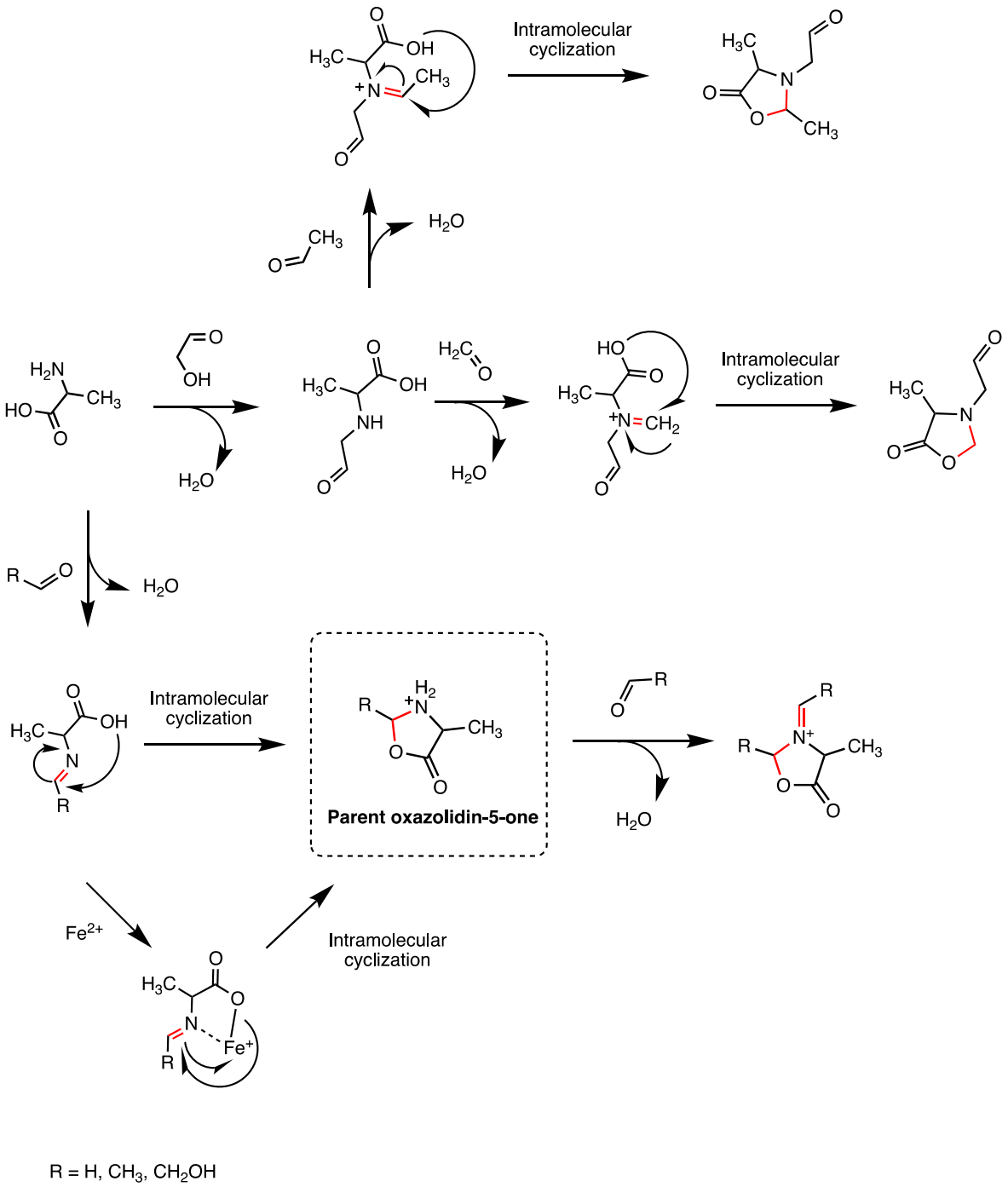

Figure 7.1. Reaction of simple aldehydes with alanine and the rationale behind divalent metal ion catalysis of oxazolidin-5-one formation (see also Figure 7.2)

7.4.1. Detection of sugar-derived aldehyde/alanine Schiff base adducts through isotope labelling

Schiff bases incorporating alanine and sugar-derived aldehydes (with up to two carbon atoms) can be observed in the Ala/Glu/$FeCl_2$ model systems using qTOF/MS analysis (see Table 7.2). We propose that these Schiff bases were detected mainly due to their existence in the more stable oxazolidin-5-one form; otherwise, they would have rapidly undergone hydrolysis before being detected. In addition, the compounds listed in Table 7.2 incorporated one ^{13}C-3 alanine atom, indicating the presence of alanine and up to four carbon atoms from glucose derived aldehydes. The incorporation of one carbon atom from glucose can indicate a formaldehyde Schiff base adduct, that of two carbon atoms can indicate acetaldehyde or glycolaldehyde, and that of three or four carbon atoms can indicate multiple addition adducts, as shown in Figures 7.1 to 7.3. Adducts incorporating formaldehyde (R = CH_2 in Figure 7.3), acetaldehyde (R = $CHCH_3$), and glycolaldehyde (R = $CHCH_2OH$) were detected in the form of $[M + H]^+$ at *m/z* 102.0548 $[C_4H_8NO_2]^+$, *m/z* 116.0706 $[C_5H_{10}NO_2]^+$, and *m/z* 132.0656 $[C_5H_{10}NO_3]^+$, respectively. Supporting evidence for the formation of Schiff bases were provided by observing the incorporation of one C-3 atom from [^{13}C-3] alanine and up to two carbon atoms from [^{13}C-U] glucose, depending on the conjugated aldehyde type. Confirmation of the formation of these adducts from the interaction of two-carbon aldehydes is provided in section 7.3.3. The initial oxazolidin-5-one adducts formed with formaldehyde (*m/z* 102), acetaldehyde (*m/z* 116), and glycolaldehyde (*m/z* 132) were observed only in the presence of $FeCl_2$ except the adduct formed with formaldehyde (Figure S7.1 and Table S7.2). According to the HRMS data, among the three initial oxazolidin-5-one compounds (Table 7.2), 4-methyl-5-oxazolidin-3-ium (*m/z* 102) was the most prominent ion, followed by acetaldehyde. These initial oxazolidin-5-one adducts can react further with similar aldehydes, forming Schiff bases as iminium ions (Figure 7.3). Examples of these ions are provided in the following section.

Table 7.2. Elemental composition and isotope incorporation in the proposed oxazolidin-5-one derivatives observed in alanine/glucose/$FeCl_2$ model system using methanol as solvent (see Figures 7.2 and 7.3)

$[M + X]^+$	Elemental Composition	Error ppm	Glu [^{13}C-U]	Elemental Composition	Error ppm	Ala [^{13}C-3]	Elemental Composition	Error ppm
102.0548	$C_4H_8NO_2$	– 1.52	103.058	$C_3[^{13}C]H_8NO_2$	– 3.01	103.0581	$C_3[^{13}C]H_8NO_2$	– 2.04
114.0549	$C_5H_8NO_2$	– 0.48	nd[b]			115.0573	$C_4[^{13}C]H_8NO_2$	– 8.78
116.0706	$C_5H_{10}NO_2$	– 0.04	118.0772	$C_3[^{13}C]_2H_{10}NO_2$	– 0.97	117.0736	$C_4[^{13}C]_1H_{10}NO_2$	– 3.07
128.0709	$C_6H_{10}NO_2$	1.98	131.0778	$C_3[^{13}C]_3H_{10}NO_2$	– 21.89	167.0321	$C_5[^{13}C]H_9KNO_2$	13.52
132.0656	$C_5H_{10}NO_3$	0.61	134.0721	$C_3[^{13}C]_2H_{10}NO_3$	– 0.96	155.0503	$C_4[^{13}C]_1H_9NaNO_3$	– 3.35
142.0866	$C_7H_{12}NO_2$	2.43	146.097	$C_3[^{13}C]_4H_{12}NO_2$	– 18.31	143.088	$C_6[^{13}C]_1H_{12}NO_2$	– 11.25
144.0655	$C_6H_{10}NO_3$	– 0.14	147.0759	$C_3[^{13}C]_3H_{10}NO_3$	2.15	183.0238	$C_5[^{13}C]H_9KNO_3$	– 5.22
155.9738	$C_4H_6FeNO_2$	– 2.83	156.9765	$C_3[^{13}C]_1H_6FeNO_2$	-6.98	nd		
158.0815	$C_7H_{12}NO_3$	2.09	nd			159.0818	$C_6[^{13}C]H_{12}NO_3$	– 17.13
169.9895	$C_5H_8FeNO_2$	– 2.3	nd			170.9924	$C_4[^{13}C]H_8FeNO_2$	– 4.95
174.0766	$C_7H_{12}NO_4$	2.96	nd			175.0794	$C_6[^{13}C]H_{12}NO_4$	– 0.22
185.9848	$C_5H_8FeNO_3$	– 0.03	187.9913	$C_3[^{13}C]_2H_8FeNO_3$	– 1.15	nd		

[a]Error (in ppm) in calculating the elemental composition

[b]nd: not detected

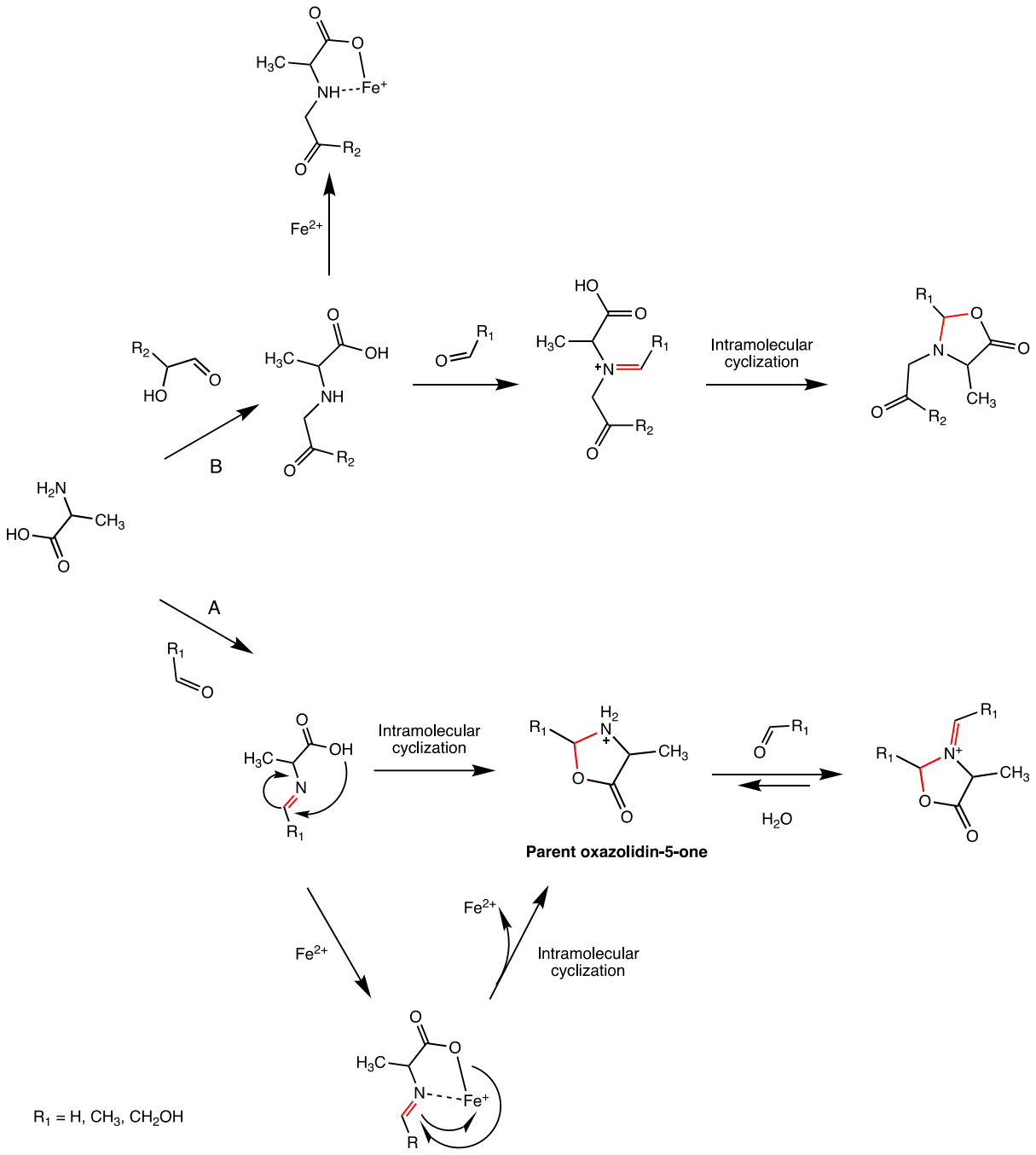

Figure 7.2. Proposed the mechanisms of the formation of oxazolidin-5-one through intramolecular cyclization of the monoglycated (pathway **A**) and diglycated (pathway **B**); Schiff bases with simple aldehydes (pathway **A**) or sugars (pathway **B**) (see also Figure 7.1)

7.4.2. Further reaction products obtained from initially formed oxazolidin-5-ones with aldehydes

The initially formed oxazolidin-5-ones are considered to be secondary amines and can further undergo Schiff base formation with available aldehydes and form iminium ions. The iminium ions that can be easily detected under positive ionization mode without protonation or sodiation (Table S7.1). Furthermore, the isotope labelling data confirmed the incorporation of multiple atoms from glucose. The oxazolidin-5-ones and their derivatives are mainly observed in the presence of metal ions during the Maillard reaction. This observation suggests that metal ions influence the formation of oxazolidin-5-one due to their ability to stabilize the Schiff bases through complexation and control the generation of *N*,*N*-diglycated amino acids (Kim and Yaylayan, 2022) and monoglycated amino acids. These glycated adducts can act as possible precursors to oxazolidin-5-ones. In the second glycation step shown in Figure 7.2, the sugars initially form a Schiff base intermediate that can undergo intramolecular cyclization initiated by the carboxylic acid moiety and form the oxazolidin-5-one isomer in equilibrium with the Schiff base. The HRMS data suggested that oxazolidin-5-one moieties with different side chains can undergo further reactions with available sugar-derived aldehydes in the reaction mixture containing metal ions (Kim and Yaylayan, 2020, 2021) to form oxazolidin-5-one derivatives (Figure 7.3). These derivatives can be traced by observing the incorporation of one alanine C-3 atom and carbon atoms from [^{13}C-U] glucose. Nine such ions representing oxazolidin-5-one derivatives are listed in Table 7.2. As shown in Figure 7.3, the initial oxazolidin-5-one adducts consisting of alanine and either formaldehyde, acetaldehyde, or glycolaldehyde can undergo further reactions with other aldehydes to form Schiff bases as iminium ions. This is reflected in the presence of signals at *m/z* 114.0549 $[C_5H_8NO_2]^+$ (alanine and formaldehyde), *m/z* 128.0709 $[C_6H_{10}NO_2]^+$ (alanine and acetaldehyde), and *m/z* 144.0655 $[C_6H_{10}NO_3]^+$ (alanine and glycolaldehyde). This observation is consistent with that of the formation of oxazolidin-5-one derivatives associated with acetaldehyde (pathway **B**) and glycolaldehyde (pathway **C**) (Figure 7.3). In pathway **B**, adducts that have reacted with acetaldehyde are observed at *m/z* 128.0709 $[C_6H_{10}NO_2]^+$ (alanine and formaldehyde), *m/z* 142.0866 $[C_7H_{12}NO_2]^+$ (alanine and acetaldehyde), and *m/z* 158.0815 $[C_7H_{12}NO_3]^+$ (alanine and glycolaldehyde). Finally, the adducts of pathway **C** have glycolaldehyde additions with $[M]^+$ at *m/z* 144.0655 $[C_6H_{10}NO_3]^+$ (alanine and formaldehyde), *m/z* 158.0815 $[C_7H_{12}NO_3]^+$ (alanine and

acetaldehyde), and *m/z* 174.0766 $[C_7H_{12}NO_4]^+$ (alanine and glycolaldehyde). As mentioned previously, further confirmation of these structures was performed by observing the incorporation of one C-3 atom from [^{13}C-3] alanine and up to four carbon atoms from [^{13}C-U] depending on the type of aldehyde (Tables 7.2 and S7.1).

7.4.3. Spiking experiments with standard aldehydes

Supporting evidence for the formation of Schiff bases with sugar derived aldehydes, spiking experiments were performed with formaldehyde, acetaldehyde, and glycolaldehyde added to the reaction mixtures. The type of substituted oxazolidin-5-one was identified based on the structure of the added aldehyde. These experiments provided further evidence that the oxazolidin-5-one derivatives were generated from various aldehydes in the system. There was a statistically significant increase in the relative intensities of the corresponding ions upon spiking with the appropriate aldehyde; these increases are shown in Table S7.2 and Figure S7.1. In addition, spiking the model system (Ala/Glu/$FeCl_2$/A) with excess formaldehyde (see Tables 1 and S2) lead to the formation of adducts incorporating not only formaldehyde (R = CH_2 in Figure 7.2), but also acetaldehyde (R = $CHCH_3$), and glycolaldehyde (R = $CHCH_2OH$). These aldehydes have been previously reported to be thermally generated from formaldehyde in the presence of metal ions through the formose reaction (Butlerov reaction) (Breslow, 1959; Breslow and Appayee, 2014).

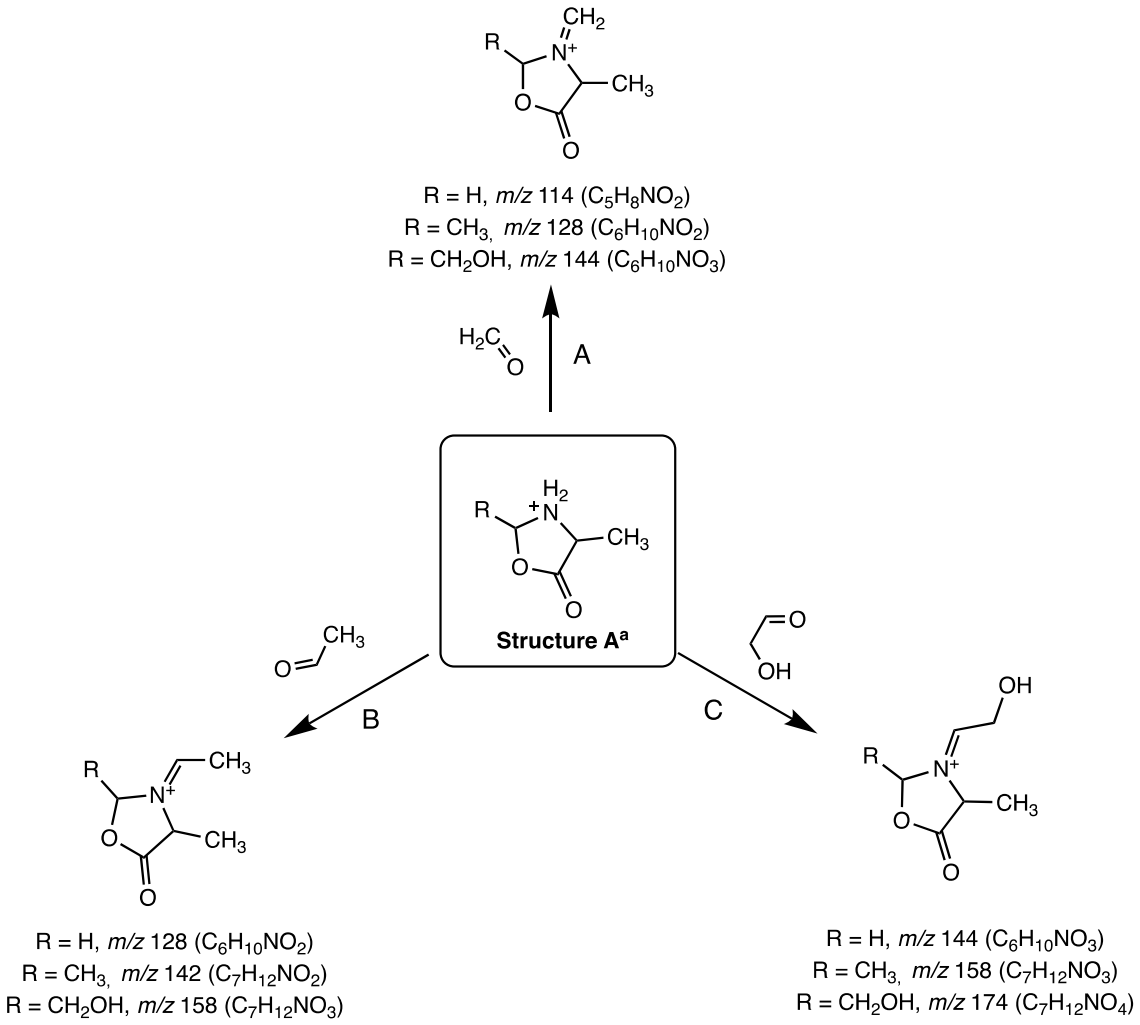

A = Parent oxazolidin-5-one derivatives, where R is H in the reaction mixture

Figure 7.3. Further reactions of parent oxazolidin-5-ones (structure A) with various aldehydes

7.5. CONCLUSION

The observed ions in this study, corresponding to Schiff base structures between alanine and short chain aldehydes, suggested the possible formation of oxazolidin-5-ones in the Maillard reaction mixtures in the presence of divalent iron and identified the previously unknown role of metal ions in the formation of flavouring and browning precursors during the Maillard reaction. Among the oxazolidin-5-one derivatives presented in Table 7.2, the ion, at *m/z* 102.0548 $[C_4H_8NO_2]^+$, associated with alanine and formaldehyde adduct, showed relatively higher intensity than that of the other oxazolidin-5-one derivatives. These results indicate that formaldehyde is the most reactive aldehyde formed in the alanine glucose mixture and that oxazolidin-5-ones can be used as indicators for both Schiff base and Strecker aldehyde formation in the Maillard reaction when divalent iron is used as a reactant.

7.6. REFERENCES

Breslow, R. (1959). On the Mechanism of the Formose Reaction. *Tetrahderon Letters*, 21, 22–26.

Breslow, R. and Appayee, C. (2014). Deuterium Studies Reveal a New Mechanism for the Formose Reaction Involvoing Hydride Shifs. *Journal of the American Chemical Society*, 136(10), 3720–3723.

Choury, M., Lopes, A B., Blond, G., Gluea, M. (2020). Synthesis of Mediaum-Sized Heterocycles by Transition-Metal-Catalyzed Intramolecular Cyclization. *Molecules*, 25(14), 3147.

Chu, F. L. and Yaylayan, V. A. (2008). Post-schiff chemistry of the Maillard reaction. *Annals of the New York Academy of Science*, 1126, 30–37.

Chu, F. L. and Yaylayan, V. A. (2009). FTIR monitoring of oxazolidinone-5-one formation and decomposition in a glycolaldehyde-phenylalanine model system by isotope labelling techniques. *Carbohydrate Research*, 344, 229–236.

Hofmann, T. (1998). Application of Site Specific ^{13}C Enrichment and ^{13}C NMR Spectroscopy for the Elucidation of the Formation Pathway Leading to a Red ^{1}H-Pyrrol-3(2H)-one during the Maillard reaction of Furna-2-carboxaldehyde and L-Alanine. *Journal of Agricultural and Food Chemistry*, 46, 941–945.

Frank, O. and Hofmann, T. (2000). Characterization of Key Chromospheres Formed by Nonenzymatic Browning of Hexoses and L-Alanine by using the Colour Activity Concept. *Journal of Agricultural and Food Chemistry*, 48, 6303–6311.

Kim, E. S. and Yaylayan, V. (2020). Profiling of glucose degradation products through complexation with divalent metal ions coupled with ESI/qTOF/MS/MS analysis. *Current Research in Food Science*, 3, 268–274.

Kim, E. S. and Yaylayan, V. (2021). Identification of the Maillard reaction intermediates as divalent iron complexes in alanine/glucose/$FeCl_2$ model system using ESI/qTOF/MS/MS and isotope labelling technique. *Current Research in Food Science*, 4, 287–294.

Kim, E. S. and Yaylayan, V. (2022). *Bis*(alaninato)iron(II) complexes as molecular scaffolds for the generation of *N*,*N*-di-glycated alanine derivatives in the presence of glucose. *Food Chemistry*, 374, 131815.

Kim, E. S. and Yaylayan, V. (Chapter 6). Intramolecular cyclization of *N*,*N*-diglycated alanine derivatives. Manuscript in preparation.

Mortzfeld, F. B., Hashem, C., Vranková, K., Winkler, M., Rudroff, F. (2020). Ryrazines: Synthesis and Industrial Application of these Valuable Flavour and Frarance Compounds. *Biotechnology Journal*, 15, 2000064.

Patiny, L. and Borel, A. (2013). ChemCalc: a building block for tomorrow's chemical infrastructure. *Journal of chemical information and modeling*, 53 (5), 1223–1228.

RjanBabu, T. V. (1991). Stereochemistry of intramolecular free-radical cyclization reaction. *Accounts of Chemical Research*, 24, 139–145.

Rizzi, G. P. (1997). Chemical structure of coloured Maillard reaction products. *Food Reviews International*, 13 (1), 1–28.

Shimasaki, C., Hirata, F, Ohta, H., Tsukurimichi, E., Yshinura, T. (1993). Thermal behavior and mass spectrometry studies of 2-oxazolidinone derivatives. *Journal of Analytical and Applied Pyrolysis*, 24(3), 291–200.

Xing, H. and Yaylayan, V. (2021). Insight into the mechnochemistry of the Maillard reaction: degradation of Schiff bases via 5-oxazolidinone intermediate. *European Food Research and Technology*. 247(15):1–12.

Yaylayan, V. A. (2003). Recent Advances in the Chemistry of Strecker Degradation and Amadori Rearrangement: Implications to Aroma and Colour Formation. *Food Science and Technology Research*, 9(1):1–6.

7.7. SUPPLEMENTARY MATERIALS

Table S7.1. Oxazolidin-5-ones having different side chains detected in the reaction mixture of alanine/glucose in the presence of divalent iron ($FeCl_2$) in methanol as the solvent. See Figure 7.3 for their formation pathways and Table 7.2 for their chemical composition

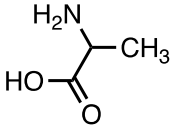 Alanine	 A = Formaldehyde	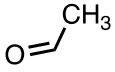 B = Acetaldehyde	 C = Glycolaldehyde

Structure[a]	[M + X]$^+$	Composition
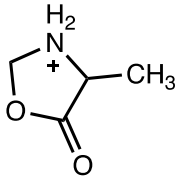	102.0548	Alanine + A
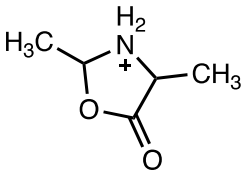	116.0706	Alanine + B
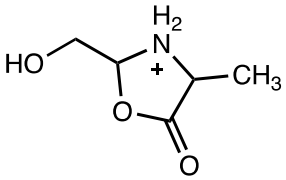	132.0656	Alanine + C
	Pathway A	
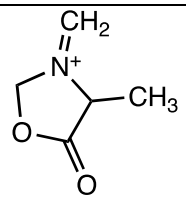	114.0549	[Alanine + A] + A
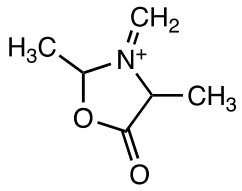	128.0709	[Alanine + B] + A

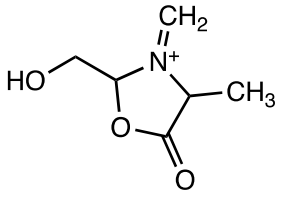	144.0655	[Alanine + C] + A
Pathway B		
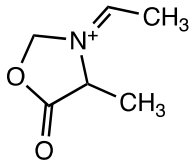	128.0709	[Alanine + A] + B
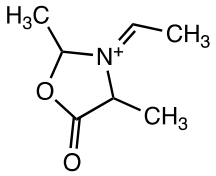	142.0866	[Alanine + B] + B
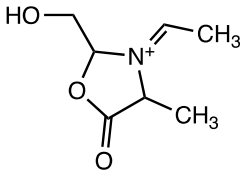	158.0815	[Alanine + C] + B
Pathway C		
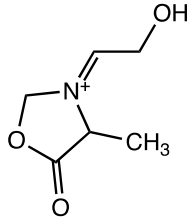	144.0655	[Alanine + A] + C
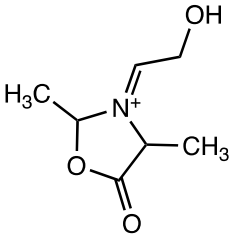	158.0815	[Alanine + B] + C
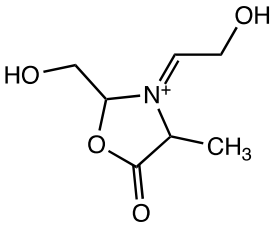	174.0766	[Alanine + C] + C

Table S7.2. Increase in intensities of the ions corresponding to the listed oxazolidin-5-ones when spiked with selected aldehydes (**A**: Formaldehyde, **B**: Acetaldehyde, and **C**: Glycolaldehyde)

	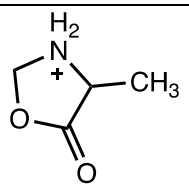	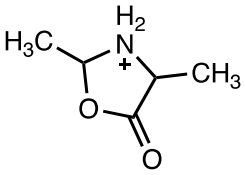	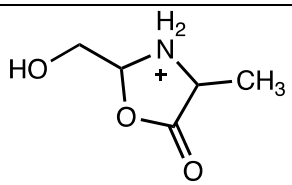
	$[M]^+$ = 102	$[M]^+$ = 116	$[M]^+$ = 132
Model system[a]			
Ala/Glu	0.6	nd[b]	nd
Ala/Glu/**A**	11.3	0.45 ± 0.07	0.45 ± 0.07
Ala/Glu/**A**+**B**+**C**	0.7	1.2	0.2
Ala/Glu/$FeCl_2$	**14.5 ± 0.98**	6.43 ± 0.32	0.83 ± 0.12
Ala/Glu/$FeCl_2$/**A**	62.35 ± 7.42	62.1 ± 6.36	3.5 ± 0.28
Ala/Glu/$FeCl_2$/**B**	10.9	8.4	0.8
Ala/Glu/$FeCl_2$/**C**	14.05 ± 0.49	2.05 ± 0.49	2.1 ± 0.14
Ala/Glu/$FeCl_2$/**A**+**B**+**C**	27.6	19.4	2.8

[a]See Table 7.1

[b]nd: not detected

(A) The mass spectrum of heated alanine and glucose in the absence of $FeCl_2$ (**Ala/Glu**)

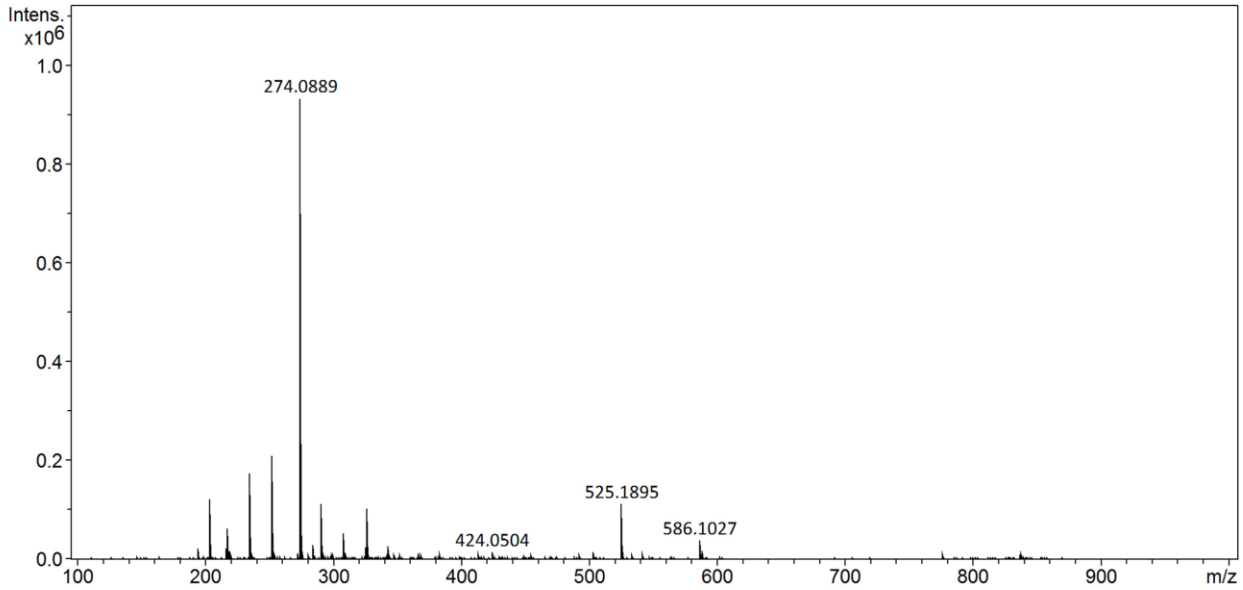

(B) The mass spectrum of heated alanine and glucose, and excess of formaldehyde in the absence of $FeCl_2$ (**Ala/Glu/A**)

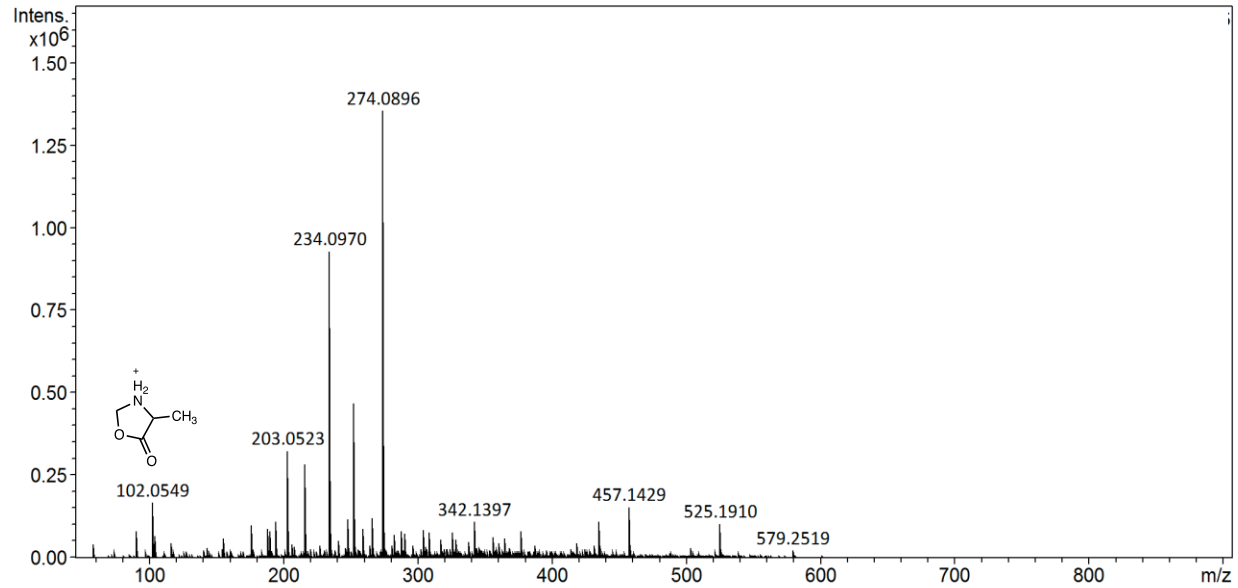

(C) The mass spectrum of heated alanine and glucose, and excess of three aldehydes (formaldehyde, acetaldehyde, and glycolaldehyde) in the absence of $FeCl_2$ (**Ala/Glu/A+B+C**)

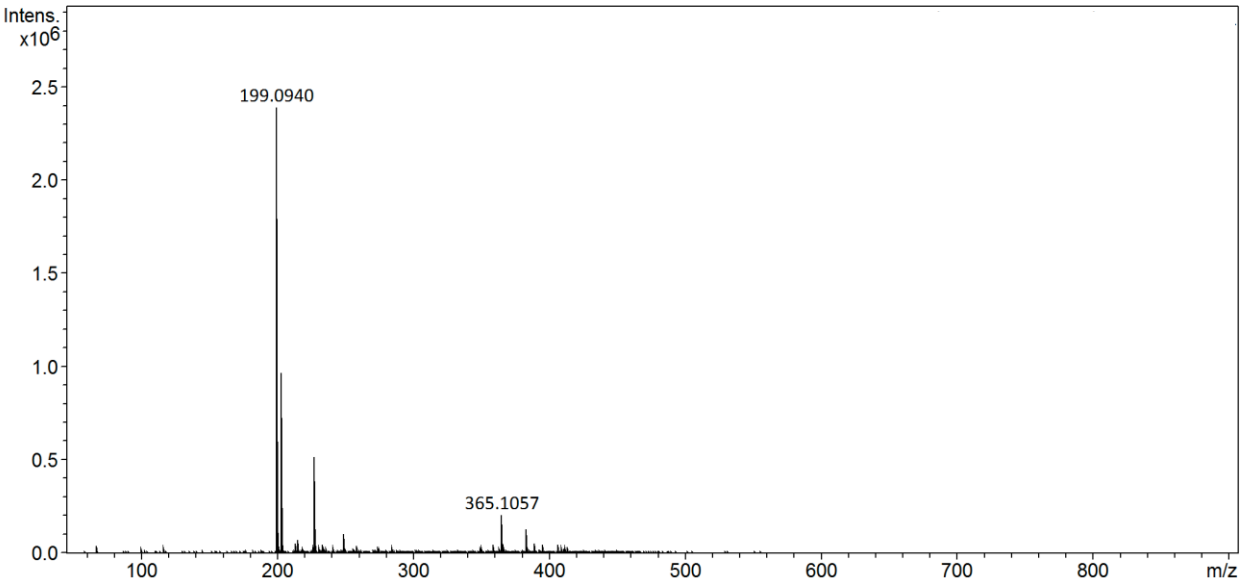

(D) The mass spectrum of heated alanine, and glucose in the presence of $FeCl_2$ (**Ala/Glu/$FeCl_2$**)

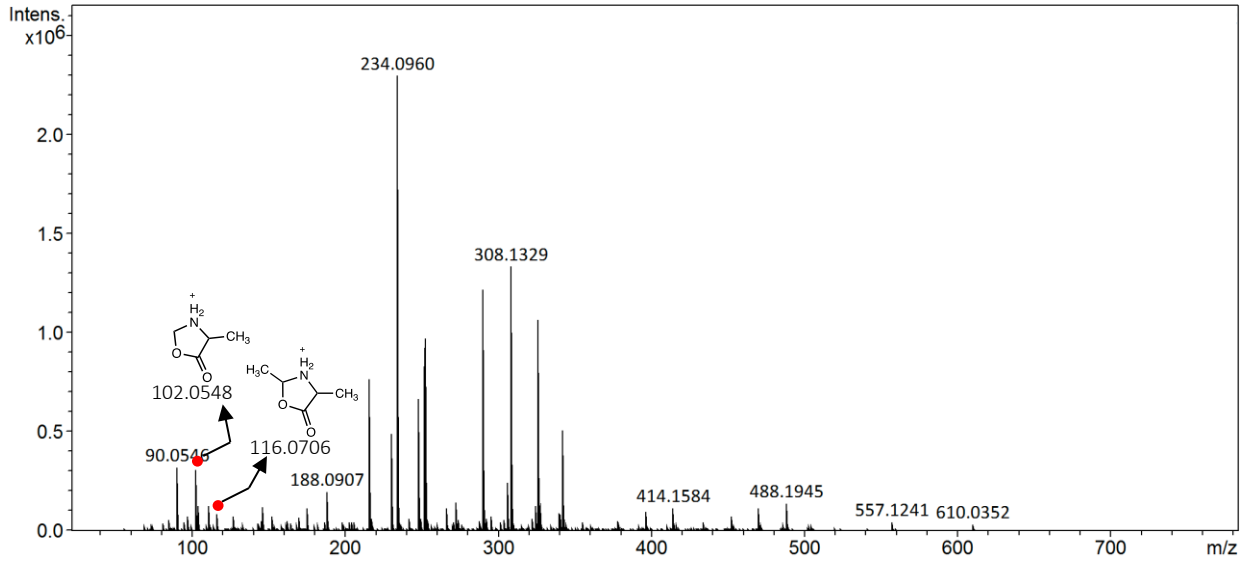

(E) The mass spectrum of heated alanine, glucose, and excess of formaldehyde in the presence of $FeCl_2$ (**Ala/Glu/$FeCl_2$/A**)

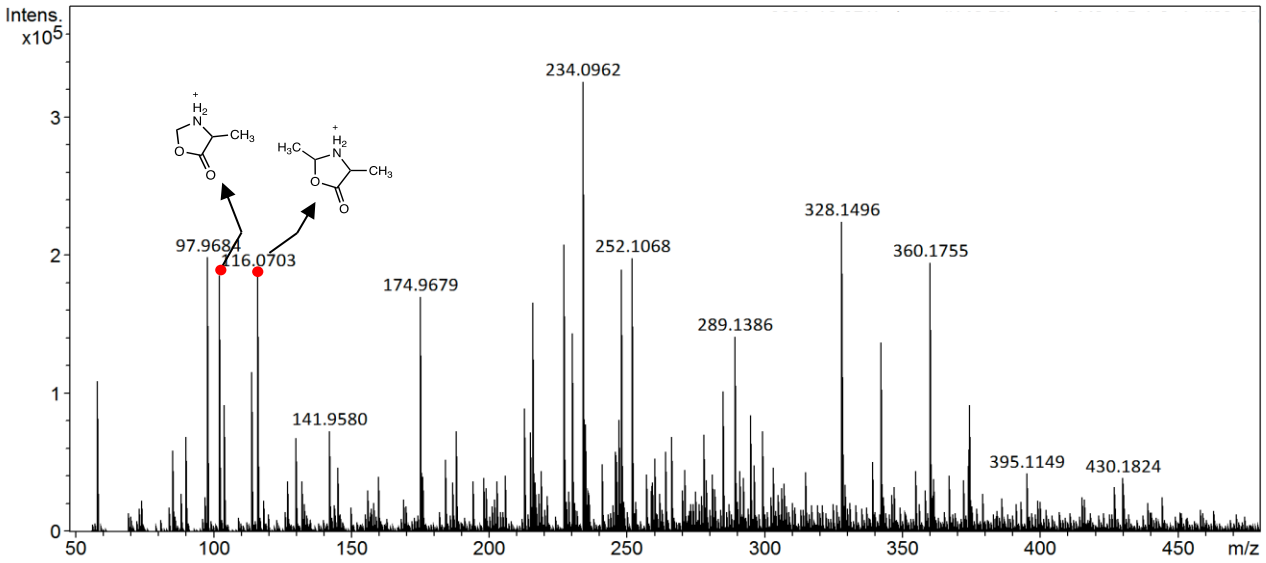

(F) The mass spectrum of heated alanine, glucose, and excess of acetaldehyde in the presence of $FeCl_2$ (**Ala/Glu/$FeCl_2$/B**)

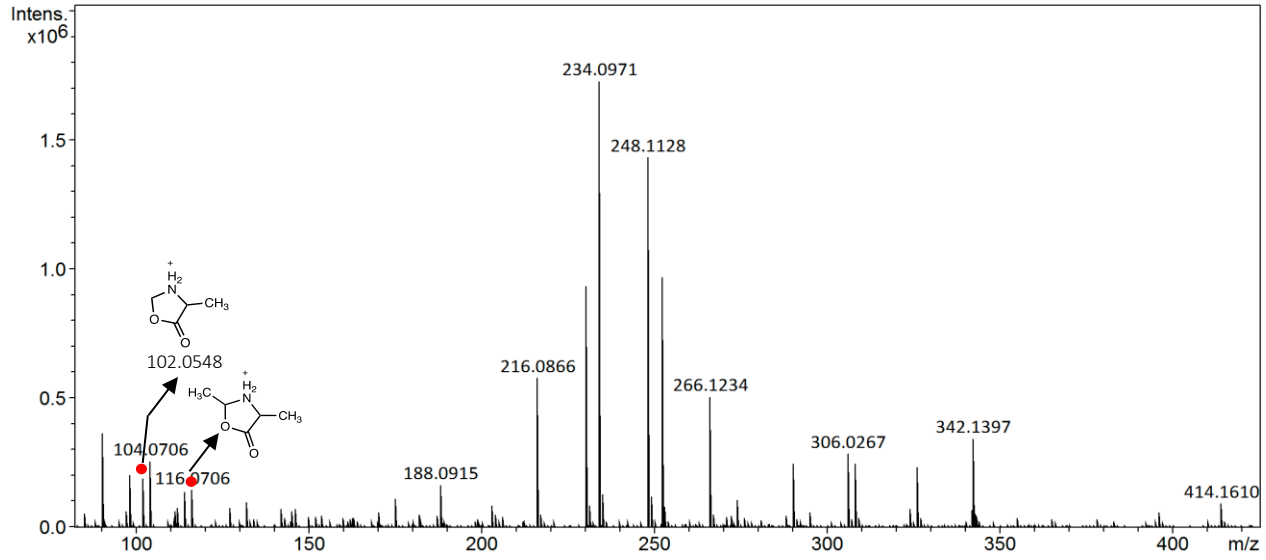

(G) The mass spectrum of heated alanine, glucose, and excess of acetaldehyde in the presence of $FeCl_2$ (**Ala/Glu/$FeCl_2$/C**)

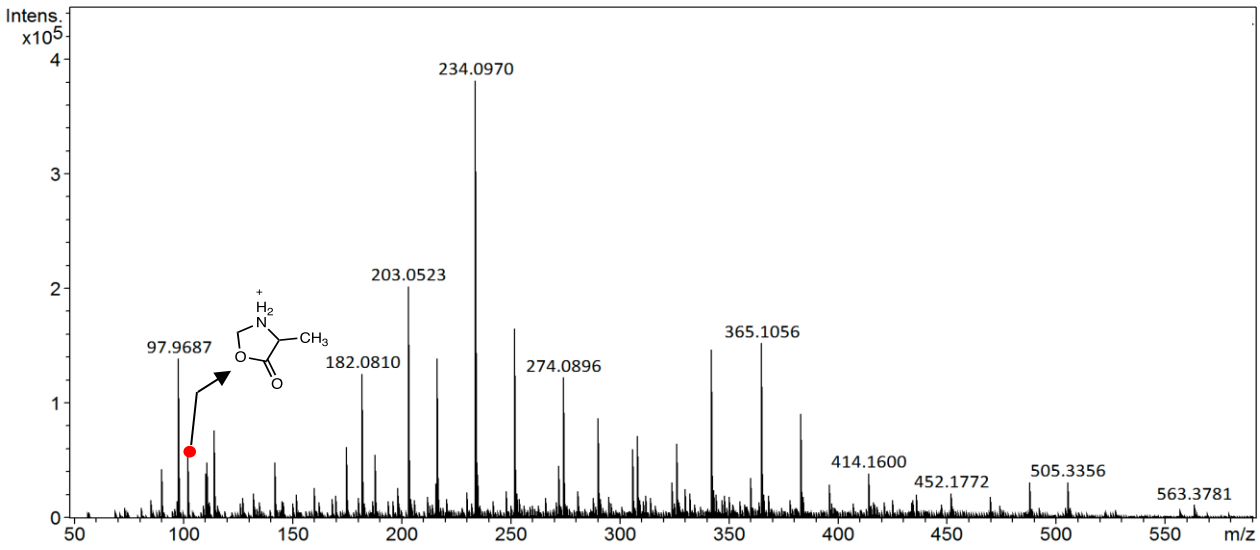

(H) The mass spectrum of heated alanine, glucose, and excess of three aldehydes (formaldehyde, acetaldehyde, and glycolaldehyde) in the presence of $FeCl_2$ (**Ala/Glu/$FeCl_2$/A+B+C)**

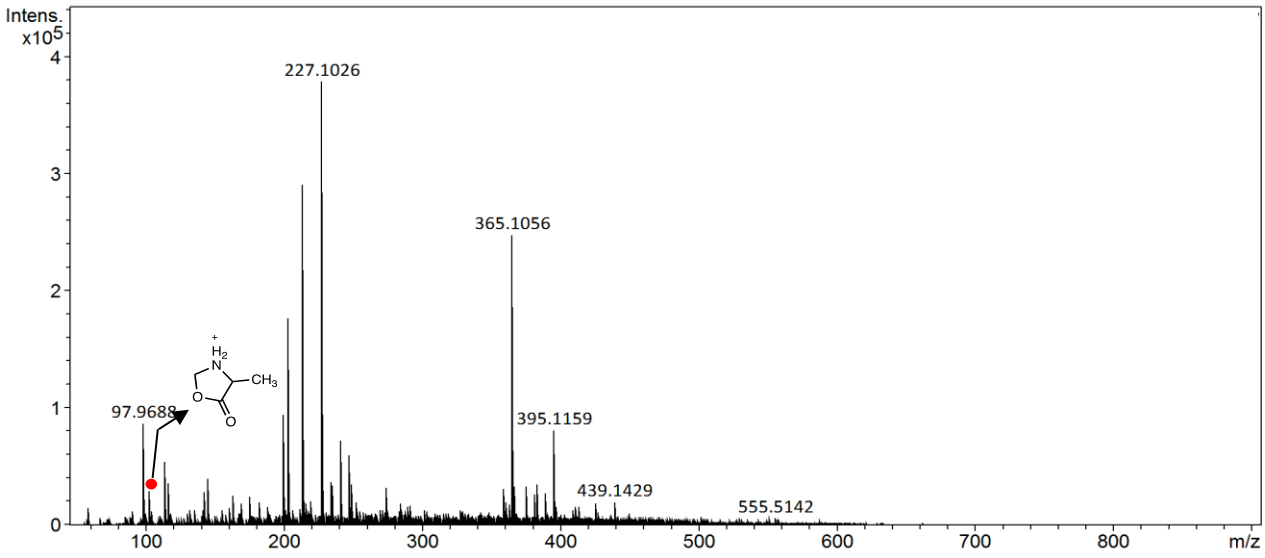

Figure S7.1. ESI/qTOF/MS spectra**: (A)** heated alanine and glucose in the absence of $FeCl_2$ (Ala/Glu), **(B)** heated alanine and glucose, and excess of formaldehyde in the absence of $FeCl_2$ (Ala/Glu/A), **(C)** heated alanine and glucose, and excess of three aldehydes (formaldehyde, acetaldehyde, and glycolaldehyde) in the absence of $FeCl_2$ (Ala/Glu/A + B + C), **(D)** heated alanine, and glucose in the presence of $FeCl_2$ (Ala/Glu/$FeCl_2$), **(E)** heated alanine, glucose, and excess of formaldehyde in the presence of $FeCl_2$ (Ala/Glu/$FeCl_2$/A), **(F)** heated alanine, glucose, and excess of acetaldehyde in the presence of $FeCl_2$ (Ala/Glu/$FeCl_2$/B), **(G)** heated alanine, glucose, and excess of acetaldehyde in the presence of $FeCl_2$ (Ala/Glu/$FeCl_2$/C), and **(H)** heated alanine, glucose, and excess of three aldehydes (formaldehyde, acetaldehyde, and glycolaldehyde) in the presence of $FeCl_2$ (Ala/Glu/$FeCl_2$/A + B + C) (see Tables 7.1 and S7.2)

CONNECTING PARAGRAPH

In **Chapter 7** we demonstrated that reactive Schiff bases in the Maillard reaction can be stabilised as their cyclic isomers in the form of oxazolidin-5-one and can be detected more easily using high-resolution electrospray ionization mass spectrometry. Due to the relatively higher stability of the oxazolidin-5-one moieties and higher concentrations, **in Chapter 8,** we explored their possible reactivity towards various aldehydes, such as formaldehyde and acetaldehyde. These aldehydes are able to interact with the amino group of oxazolidin-5-one and initiate further reactions. **Chapter 8** will be submitted to the *Journal of Agriculture and Food Chemistry* under the title "Formation of Oligomeric Oxazolidin-5-ones in Alanine/Glucose/Fe^{2+} Model System."

CHAPTER 8

FORMATION OF OLIGOMERIC OXAZOLIDIN-5-ONES IN ALANINE/GLUCOSE/FE^{2+} MODEL SYSTEM

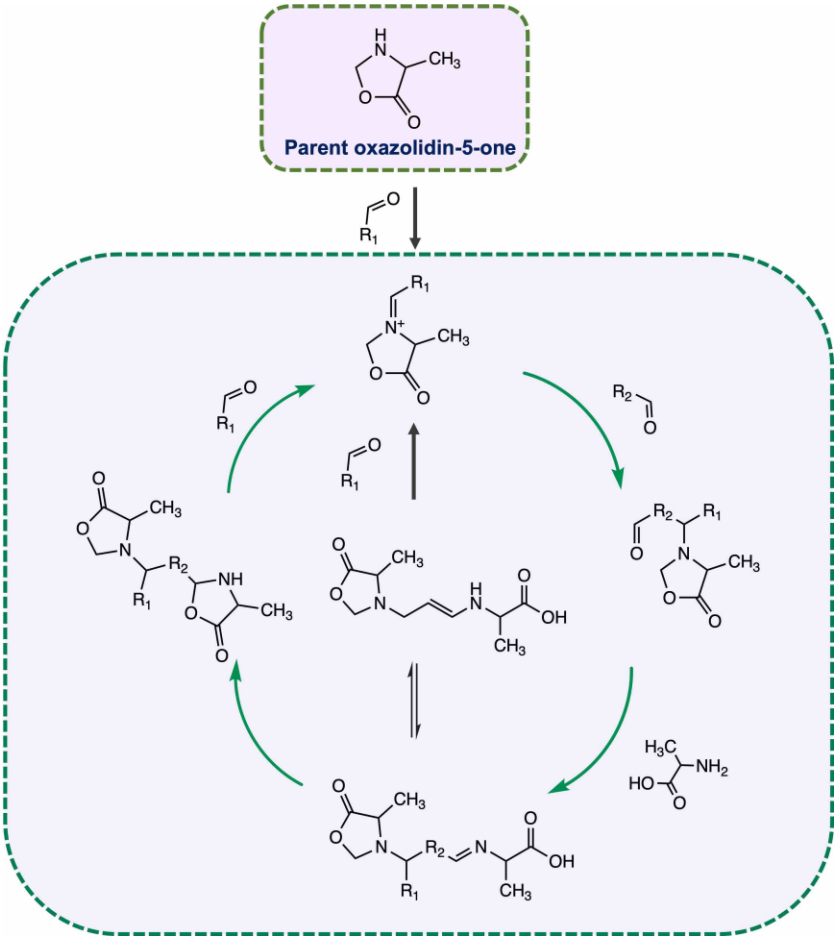

8.1. ABSTRACT

Polymerization reactions are generally unexplored in the Maillard reaction. In this chapter, we investigate the formation of oxazolidin-5-one oligomers catalyzed by divalent iron ($FeCl_2$) under Maillard reaction conditions (110 ℃ for 2 h) from alanine and glucose mixtures. Analysis of the data have indicated that initially formed 4-methyl-oxazolidin-5-one from the interaction of alanine and formaldehyde served as a molecular scaffold from which different oligomers were generated through the interaction of its amino group with three different aldehydes, such as formaldehyde, acetaldehyde, and glycolaldehyde, generating three different iminium ion derivatives of the 4-methyl-oxazolidin-5-one. Each of these derivatives served as branching point for the formation of different oligomeric structures using similar chemical transformations such as aldol type addition, Amadori rearrangement, Schiff base formation, following different sequence of reactions to form a new dimeric, trimeric or higher order oxazolidin-5-one oligomers. Twelve different reaction sequences were tentatively identified generating more than two hundred oxazolidin-5-one oligomers. Evidence from HRMS, isotope labelling using ^{13}C-3-alanine and ^{13}C-U-glucose and MS/MS data are presented in support of the proposed pathways and structures.

KEYWORDS: Oxazolidin-5-one oligomerization, Maillard reaction, $FeCl_2$, Alanine, Glucose, Stable isotope labelling, MS/MS Analysis

8.2. INTRODUCTION

Imines or Schiff bases are the initial reactive intermediates formed from the interaction of amino acids with carbonyl compounds; they can undergo various chemical transformations to be converted into more stable forms such as Amadori rearrangement products (Chu and Yaylayan, 2008), complexation with metal ions (Kim and Yaylayan, 2022), or through intramolecular cyclization of the carboxylate anion with iminium ion to form more stable cyclic isomer, the oxazolidin-5-one. The metal-ion complexation of Schiff bases enhances their stability in the reaction mixtures, increasing their half-life and allowing the formation of more oxazolidin-5-ones, as was demonstrated in chapter 7 of this dissertation. Moreover, we have identified that initial

oxazolidin-5-ones formed from short chain aldehydes and alanine such as formaldehyde (*m/z* 102) in the reaction mixture of glucose/alanine/$FeCl_2$ can serve as the precursor of further reactions involving Schiff base formation with various aldehydes followed by aldol addition and further carbonyl-amine reactions leading to intramolecular cyclization reactions and the formation of a dimeric oxazolidin-5-one moiety. Higher order oligomers can be formed in a similar sequence of reactions. In this chapter, we explored the formation of oligomeric oxazolidin-5-one structures using high-resolution mass spectrometry (HRMS), tandem mass spectrometry (MS/MS), and isotope labelling techniques.

8.3. MATERIALS AND METHODS

8.3.1. Materials and reagents

L-Alanine (98%), D-glucose, and iron(II) chloride ($FeCl_2$) (99%) were purchased from Sigma–Aldrich Chemical Co. (Oakville, ON, Canada). Alanine-3-^{13}C ($^{13}CH_3CH(NH_2)CO_2H$) (98%) and glucose-^{13}C-U ($^{13}C_6H_{12}O_6$) (99%) were purchased from Cambridge Isotope Laboratories (Andover, MA, USA). Liquid chromatography–mass spectrometry (LC–MS)-grade water and methanol (OmniSolv, >99%) were obtained from VWR International (Mississauga, ON, Canada).

8.3.2. Sample preparation

The test model systems were prepared in 1:1:0.5 molar ratios by adding glucose (18 mg), alanine (9 mg), and $FeCl_2$ (6.4 mg) to methanol (1 mL) and heating in a stainless-steel reactor at 110 °C for 2 h, followed by evaporation of the solvent for 30 min at 110 °C. The control model system was prepared by heating glucose (18 mg) and alanine (9 mg) in methanol at 110 °C for 2 h in the absence of metal ions. All samples were analyzed in at least two replicates, as shown in Table 8.1.

Table 8.1. Composition of the model systems[a]

	Model System
Control Model System	Alanine was added to a glucose solution and heated in the absence of metal ions - **Ala/Glu**
Test Model System	Alanine was added to a glucose solution and heated in the presence of $FeCl_2$ - **Ala/Glu/$FeCl_2$**
Isotope Labelling Model System	Alanine [^{13}C-3] was added to a glucose solution and heated in the presence of $FeCl_2$ - **[^{13}C-3] Ala/Glu/$FeCl_2$** Alanine was added to a glucose [^{13}C-U] solution and heated in the presence of $FeCl_2$ - **Ala/[^{13}C-U] Glu/$FeCl_2$**

[a]All model systems were heated at 110 ℃ for 2 h in water or methanol using a sealed stainless-steel reactor and analyzed in at least two replicates

8.3.3. ESI/qTOF/MS analysis

The samples were dissolved in liquid chromatography (LC) methanol at a concentration of 1 mg/mL. The samples were then diluted 10-fold in 10% methanol prior to analysis by ESI/qTOF/MS in the positive-ion mode. The ESI/qTOF/MS system comprised a Bruker Maxis Impact quadrupole time-of-flight mass spectrometer (Bruker Daltonics, Bremen, Germany) operated in the positive-ion mode. Samples (1 μL) were injected directly into the ESI/qTOF/MS system. Instrument calibration was performed by using sodium formate clusters. The electrospray interface settings were as follows: nebulizer pressure, 0.6 bar (60,000 Pa); drying gas, 4 L/min; temperature, 180 ℃; and capillary voltage, 4500 V. The scan range was 70–1000. Molecular formulas were assigned to all observed peaks based on their exact *m/z* values using "ChemCalc" software (available online, Institute of Chemical Sciences and Engineering, Lausanne, Switzerland) (Patiny and Borel, 2013).

8.3.4. Structural elucidation

Evidence for the proposed structures was provided through high-resolution ESI/qTOF/MS analysis of their elemental composition and isotope-labelling studies using [^{13}C-U] glucose and [^{13}C-3]

alanine (Tables 8.2, S8.1, and S8.2). The proposed structures based on isotope-labelling studies using [^{13}C-U] glucose and [^{13}C-3] alanine are shown in Table 8.1.

8.3.5. Criteria applied for tentative identification of the listed ions

Most selected ions were detected in three different reaction systems (1) unlabelled, (2) only glucose labelled, and (3) only alanine labelled systems; each was analyzed in at least two replicates. Ions with an error in their elemental composition higher than ten ppm in only one of the above reaction systems were included if the corresponding ions in the remaining two reaction systems displayed errors with less than eight ppm.

8.4. RESULTS AND DISCUSSION

In the Maillard reaction mixtures containing metal ions (i.e. $FeCl_2$), many of the reactive intermediates formed, such as Schiff bases, enediols, and enols can be stabilized through complexation with divalent metal ions (Kim and Yaylayan, 2022), thus increasing their half-life and facilitating their detection (Kim and Yaylayan, 2020; 2021), and in the case of Schiff bases allowing them to be readily converted into more stable oxazolidin-5-ones as was demonstrated in Chapter 7. Furthermore, it was also discovered that the nitrogen atom in the oxazolidin-5-one ring can form iminium ions with various aldehydes generated in the reaction mixture, initiating aldol-type addition with aldehydes containing α-carbons, and in the process creating various opportunities for the formation of oligomeric oxazolidin-5-one moieties as summarized in **Figure 8.1**. In this chapter, we investigate generally unexplored process in the Maillard reaction and that is of polymerization reactions using the pathways leading to the oligomerization of oxazolidin-5-one as an example (see Figure 8.1). In these studies, we used high-resolution electrospray ionization quadrupole time-of-flight mass spectrometry (HR/ESI/qTOF/MS), MS/MS, and isotope labelling techniques to provide supporting evidence for the proposed structures. In addition, the elemental compositions of the ions detected in the reaction mixtures were analyzed by HR/ESI/qTOF/MS, targeting ions that incorporated up to six ^{13}C-3 atoms from [^{13}C-3] alanine and up to 11 sugar carbon atoms from ^{13}C-U-glucose model systems. The ions extracted from the HRMS data and utilized in this chapter satisfied these requirements. HRMS analysis revealed that oxazolidin-5-one generated from alanine reaction with formaldehyde was the most predominant.

In addition, this ion played a vital role in the subsequent formation of all other observed oxazolidin-5-one derivatives. To evaluate the generation of the proposed oxazolidin-5-one derivatives, several model systems containing glucose and alanine were analyzed with and without $FeCl_2$; their compositions are listed in Table 8.2 (see also Tables S8.1 and S8.2).

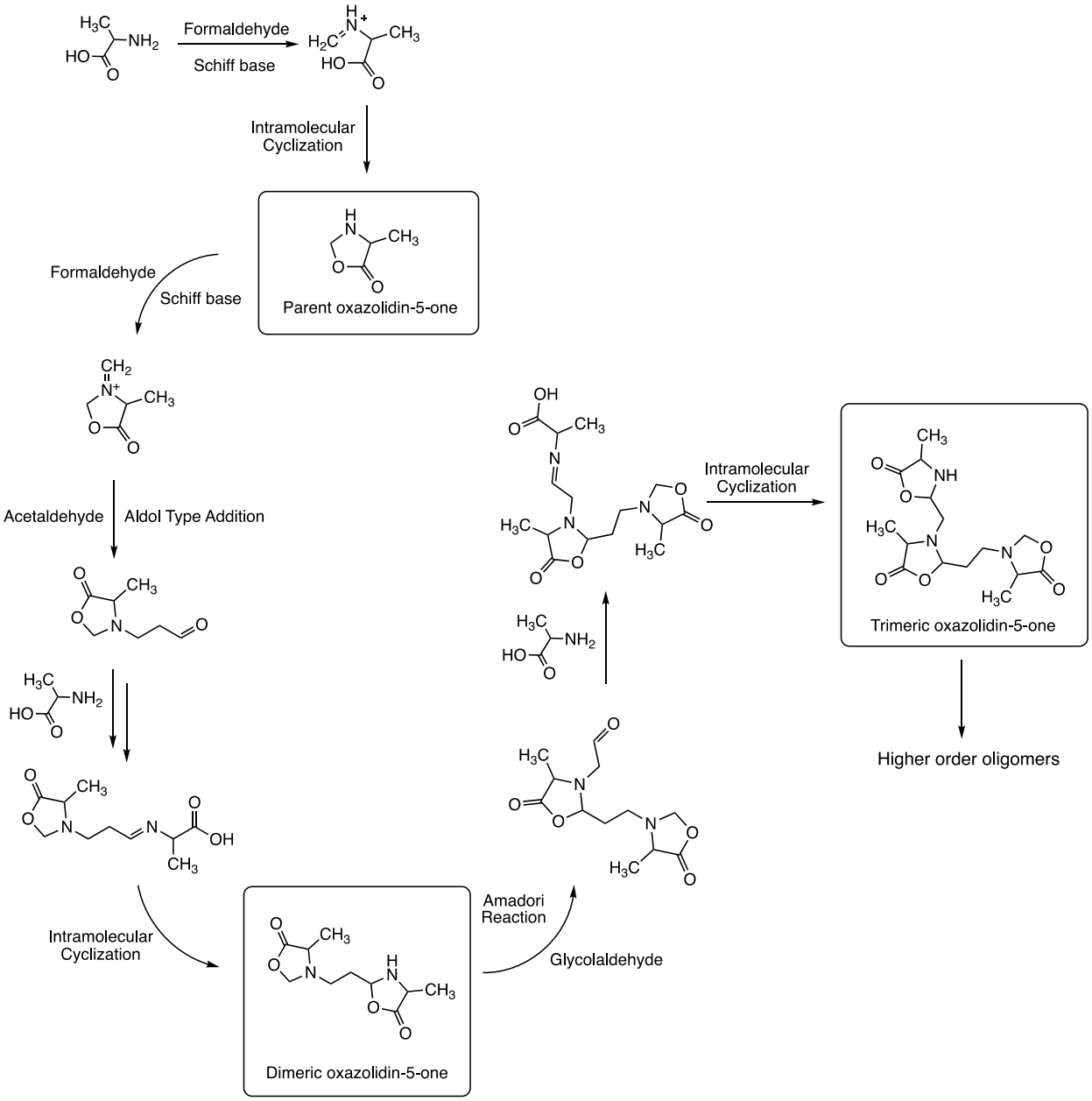

Figure 8.1. Proposed formation of oligomeric oxazolidin-5-one structures through a sequence of reactions starting from the parent 4-methyl-oxazolidin-5-one

8.4.1. Role of metal ions in the formation of oxazolidin-5-one oligomers

Heating alanine and glucose in methanolic $FeCl_2$ solution generated various peaks associated with oxazolidin-5-one structures especially with those due to the reaction of alanine with reactive small aldehydes commonly encountered in the Maillard reaction mixtures, such as formaldehyde, acetaldehyde, and glycolaldehyde; however, the ion at *m/z* 102 associated with alanine reaction with formaldehyde was relatively the most intense among the three. This initially formed 4-methyl-oxazolidinone was termed the parent oxazolidin-5-one (see Chapter 7) since it served as molecular scaffold to generate three other reactive precursors of oligomeric oxazolidin-5-one derivatives through its reaction with aldehydes such as acetaldehyde and glycolaldehyde including formaldehyde and formation of reactive iminium ions as shown in Figure 8.2. These iminium ions served as precursors leading to the formation of oligomeric structures as exemplified in Figure 8.1. When the reactions were performed in the absence of $FeCl_2$, the intensities of the ions associated with oxazolidin-5-one moieties diminished significantly, indicating the critical role of the metal ions (see also Chapter 7).

8.4.2. Formation of oxazolidin-5-one oligomers through cascade reaction

The Schiff bases of short chain aldehydes with alanine, formed in the reaction mixture containing alanine, glucose, and $FeCl_2$ in methanol heated at 110 ℃ for 2h, can undergo intramolecular cyclization to form the more stable oxazolidin-5-one structures (Figure 8.1 and Chapter 7). Analysis of the data has indicated that initially formed 4-methyl-oxazolidin-5-one from the interaction of alanine with formaldehyde was the most intense among others that termed the parent oxazolidin-5-one (Figure 8.2) since it served as a molecular scaffold, from which different oligomers were generated through the interaction of its amino group with three different aldehydes such as formaldehyde, acetaldehyde, and glycolaldehyde, generating three different iminium ion derivatives of the 4-methyl-oxazolidin-5-one shown in Figure 8.2. Each of these derivatives can branch out to different oligomeric structures undergoing a sequence of similar chemical transformations, such as aldol type additions, Amadori type rearrangement, and Schiff base formation and culminating in the final intramolecular cyclization to form new dimeric, trimeric or higher order oxazolidin-5-one oligomers as shown in Figure 8.1. Twelve different sequences of such transformations were tentatively identified (Figures S8.1–S8.12) for the formation of oxazolidin-5-one oligomers, generating a total of 229 proposed oxazolidin-5-one oligomers,

including their isomers and dehydrated forms as shown in Figures S8.1 to S8.12. The sequence of reactions depicted in Figure S8.1 or 8.3 can be considered representative of all other 12 pathways. The observed oxazolidin-5-one oligomers incorporated up to six ^{13}C-3 atoms from [^{13}C-3] alanine and up to 11 carbon atoms from [^{13}C-U] glucose at the same time, satisfying the elemental composition requirements within the error constraints stipulated under the experimental section (see Tables 8.2 and S8.2**).**

Table 8.2. Elemental composition and isotope incorporation in the proposed oxazolidin-5-one derivatives observed in alanine/glucose/$FeCl_2$ model system Monomers to tetramers of 4-methyl-5-oxazolidinone observed in alanine/glucose/$FeCl_2$ model system using methanol as solvent

$[M + X]^+$	Elemental Composition	Error ppm[a]	Glu [^{13}C-U]	Elemental Composition[c]	Error ppm	Ala [^{13}C-3]	Elemental Composition	Error ppm
102.0548	$C_4H_8NO_2$	– 1.52	103.058	$C_3[^{13}C]H_8NO_2$	– 3.01	103.0581	$C_3[^{13}C]H_8NO_2$	– 2.04
114.0549	$C_5H_8NO_2$	– 0.48	nd[b]			115.0573	$C_4[^{13}C]H_8NO_2$	– 8.78
128.0709	$C_6H_{10}NO_2$	1.98	167.0316	$C_5[^{13}C]_1H_9KNO_2$[c]	10.53	nd		
144.0655	$C_6H_{10}NO_3$	– 0.14	147.0759	$C_3[^{13}C]_3H_{10}NO_3$	2.15	183.0238	$C_5[^{13}C]H_9KNO_3$	– 5.22
158.0815	$C_7H_{12}NO_3$	2.09	nd			159.0818	$C_6[^{13}C]H_{12}NO_3$	– 17.13
170.0814	$C_8H_{12}NO_3$	1.35	175.0967	$C_3[^{13}C]_5H_{12}NO_3$	– 7.1	171.0844	$C_7[^{13}C]_1H_{12}NO_3$[d]	– 0.73
			nd			172.0881	$C_6[^{13}C]_2H_{12}NO_3$[d]	1.28
172.0972	$C_8H_{14}NO_3$	0.98	215.069	$C_3[^{13}C]_5H_{13}KNO_3$	– 2.21	195.0829	$C_7[^{13}C]_1H_{13}NO_3$	1.19
			nd			196.0815	$C_6[^{13}C]_2H_{13}NaNO_3$	– 23.06
174.0766	$C_7H_{12}NO_4$	2.96	nd			175.0794	$C_6[^{13}C]H_{12}NO_4$	– 0.22
188.092	$C_8H_{14}NO_4$	1.41	193.1078	$C_3[^{13}C]_5H_{14}NO_4$	– 3.67	189.0939	$C_7[^{13}C]H_{14}NO_4$	– 6.29
			191.0997	$C_5[^{13}C]_3H_{14}NO_4$	– 10.98	190.0982	$C_6[^{13}C]_2H_{14}NO_4$	– 1.28
227.1027	$C_{10}H_{15}N_2O_4$	0.29	231.1147	$C_6[^{13}C]_4H_{15}N_2O_4$	– 5.85	267.0579	$C_8[^{13}C]_2H_{14}KN_2O_4$	– 27.43
229.1185	$C_{10}H_{17}N_2O_4$	0.95	271.0858	$C_6[^{13}C]_4H_{16}KN_2O_4$	– 6.58	253.1076	$C_8[^{13}C]_2H_{16}NaN_2O_4$	2.62
			253.1073	$C_8[^{13}C]_2H_{16}NaN_2O_4$	1.43	254.1121	$C_7[^{13}C]_3H_{16}NaN_2O_4$	7.11
241.1186	$C_{11}H_{17}N_2O_4$	1.31	268.1112	$C_6[^{13}C]_5H_{16}NaN_2O_4$	– 21.64	265.1081	$C_9[^{13}C]_2H_{16}NaN_2O_4$	4.39
			244.1318	$C_8[^{13}C]_3H_{17}N_2O_4$	14.14	282.0858	$C_8[^{13}C]_3H_{16}KN_2O_4$	5.57
245.1135	$C_{10}H_{17}N_2O_5$	1.23	249.1313	$C_6[^{13}C]_4H_{17}N_2O_5$	18.8	285.0755	$C_8[^{13}C]_2H_{16}KN_2O_5$	– 1.01

255.1316	$C_{12}H_{18}NaN_2O_4$	2.25	283.1349	$C_6[^{13}C]_6H_{18}NaN_2O_4$	– 3.91	279.1246	$C_{10}[^{13}C]_2H_{18}NaN_2O_4$	7.21
277.1152	$C_{12}H_{18}NaN_2O_4$	– 2.45	nd			280.1204	$C_9[^{13}C]_3H_{18}NaN_2O_4$	– 19.78
			nd			281.1354	$C_8[^{13}C]_4H_{18}NaN_2O_4$	21.71
257.1141	$C_{11}H_{17}N_2O_5$	3.51	300.0913	$C_6[^{13}C]_5H_{16}KN_2O_5$	18.15	297.0743	$C_9[^{13}C]_2H_{16}KN_2O_5$	– 5.01
279.0952	$C_{11}H_{16}NaN_2O_5$	0.21						
259.1287	$C_{11}H_{19}N_2O_5$	– 0.57	302.0938	$C_6[^{13}C]_5H_{18}KN_2O_5$	– 25.5	299.0926	$C_9[^{13}C]_2H_{18}KN_2O_5$	3.88
			262.1373	$C_8[^{13}C]_3H_{18}HN_2O_5$	– 6.15	nd		
265.1151	$C_{11}H_{18}N_2NaO_4$	– 2.93	270.1288	$C_6[^{13}C]_5H_{18}NaN_2O_4$	– 14.26	245.1416	$C_9[^{13}C]_2H_{19}N_2O_4$	3.9
			nd			268.1271	$C_8[^{13}C]_3H_{18}NaN_2O_4$	4.32
			266.1148	$C_{10}[^{13}C]_1H_{18}NaN_2O_4$	– 16.66	269.1301	$C_7[^{13}C]_4H_{18}NaN_2O_4$	2.98
269.1138	$C_{12}H_{17}N_2O_5$	2.24	275.1339	$C_6[^{13}C]_6H_{17}N_2O_5$	2.08	271.1204	$C_{10}[^{13}C]_2H_{17}N_2O_5$	1.82
271.1272	$C_{12}H_{19}N_2O_5$	– 6.08	277.1504	$C_6[^{13}C]_6H_{19}N_2O_5$	5.13	311.0928	$C_{10}[^{13}C]_2H_{18}KN_2O_5$	4.37
283.1276	$C_{13}H_{19}N_2O_5$	– 4.41	290.1513	$C_6[^{13}C]_7H_{19}N_2O_5$	– 3.56	285.1355	$C_{11}[^{13}C]_2H_{19}N_2O_5$	– 0.2
			288.145	$C_8[^{13}C]_5H_{19}N_2O_5$	– 2.16	286.1381	$C_{10}[^{13}C]_3H_{19}N_2O_5$	– 2.84
287.1235	$C_{12}H_{19}N_2O_6$	– 0.92	293.1431	$C_6[^{13}C]6H_{19}N_2O_6$	– 2.7	327.0773	$C_{10}[^{13}C]_2H_{18}KN_2O_6$	– 27.68
297.1434	$C_{14}H_{21}N_2O_5$	– 3.70	327.1603	$C_6[^{13}C]_8H_{20}NaN_2O_5$	21.45	337.1064	$C_{12}[^{13}C]_2H_{20}KN_2O_5$	– 2.04
			303.1624	$C_8[^{13}C]_6H_{21}N_2O_5$	– 7.35	300.1568	$C_{11}[^{13}C]_3H_{21}N_2O_5$	7.45
			301.1579	$C_{10}[^{13}C]_4H_{21}N_2O_5$	– 0.06	339.1064	$C_{10}[^{13}C]_4H_{20}KN_2O_5$	– 21.82
299.159	$C_{14}H_{23}N_2O_5$	– 3.84	307.1859	$C_6[^{13}C]_8H_{23}N_2O_5$	– 3.54	nd		
			327.1606	$C_8[^{13}C]_6H_{22}NaN_2O_5$	– 4.96	340.125	$C_{11}[^{13}C]_3H_{22}KN_2O_5$	– 3.22
301.1401	$C_{13}H_{21}N_2O_6$	2.28	308.1594	$C_6[^{13}C]_7H_{21}N_2O_6$	– 11.35	341.0994	$C_{11}[^{13}C]_2H_{20}KN_2O_6$	– 7.63
			306.1566	$C_8[^{13}C]_5H_{21}N_2O_6$	1.35	nd		

307.1266	$C_{13}H_{20}N_2NaO_5$	0.51	314.1496	$C_6[^{13}C]_7H_{20}NaN_2O_5$	– 1.04	309.1353	$C_{11}[^{13}C]_2H_{20}NaN_2O_5$	6.95
			290.1533	$C_8[^{13}C]_5H_{21}N_2O_5$	– 27.48	nd		
			288.1525	$C_{10}[^{13}C]_3H_{21}N_2O_5$	– 7.16	313.1552	$C_9[^{13}C]_4H_{21}N_2O_5$	– 8.68
315.1557	$C_{14}H_{23}N_2O_6$	2.02	345.1629	$C_6[^{13}C]_8H_{22}NaN_2O_6$	– 2.74	317.161	$C_{12}[^{13}C]_2H_{23}N_2O_6$	– 2.44
			321.176	$C_8[^{13}C]_6H_{23}N_2O_6$	2.52	318.1671	$C_{11}[^{13}C]_3H_{23}N_2O_6$	6.2
			319.1673	$C_{10}[^{13}C]_4H_{23}N_2O_6$	– 3.7	341.1584	$C_{10}[^{13}C]_4H_{22}NaN_2O_6$	23.37
325.139	$C_{15}H_{21}N_2O_6$	– 1.27	356.1574	$C_6[^{13}C]_9H_{21}N_2O_6$	4.17	365.1041	$C_{13}[^{13}C]_2H_{20}KN_2O_6$	5.74
			332.1685	$C_8[^{13}C]_7H_{21}N_2O_6$	16.87	328.1513	$C_{12}[^{13}C]_3H_{21}N_2O_6$	5.55
328.1513	$C_{14}H_{22}N_3O_6$	3.01	333.1687	$C_9[^{13}C]_5H_{22}N_3O_6$	4.84			
349.1356	$C_{15}H_{22}N_2NaO_6$	– 4.03	358.1677	$C_6[^{13}C]_9H_{22}NaN_2O_6$	1.39	351.1417	$C_{13}[^{13}C]_2H_{22}NaN_2O_6$	– 5.74
			334.1817	$C_8[^{13}C]_7H_{23}N_2O_6$	9.44			
			332.1721	$C_{10}[^{13}C]_5H_{23}N_2O_6$	0.79	331.1768	$C_{11}[^{13}C]_4H_{23}N_2O_6$	25.12
352.1551	$C_{16}H_{22}N_3O_6$	13.6	nd			378.1457	$C_{12}[^{13}C]_4H_{22}N_3O_6$	0.06
354.1654	$C_{16}H_{24}N_3O_6$	– 1.59	361.1907	$C_9[^{13}C]_7H_{24}N_3O_6$	3.47	nd		
			359.1805	$C_{11}[^{13}C]_5H_{24}N_3O_6$	– 6.23	380.1571	$C_{12}[^{13}C]_4H_{23}NaN_3O_6$	– 11.12
361.1614	$C_{15}H_{25}N_2O_8$	2.38	370.1893	$C_6[^{13}C]_9H_{25}N_2O_8$	– 3.88	385.1437	$C_{13}[^{13}C]_2H_{24}NaN_2O_8$	– 14.27
			368.1919	$C_8[^{13}C]_7H_{25}N_2O_8$	21.39	386.149	$C_{12}[^{13}C]_3H_{24}NaN_2O_8$	– 9.2
367.1484	$C_{15}H_{24}N_2NaO_7$	2.26	352.1891	$C_8[^{13}C]_7H_{25}N_2O_7$	– 0.03	386.1258	$C_{12}[^{13}C]_3H_{24}KN_2O_7$	– 14.95
			350.1814	$C_{10}[^{13}C]_5H_{25}N_2O_7$	– 2.86	349.18	$C_{11}[^{13}C]_4H_{25}N_2O_7$	2.73
370.1615	$C_{16}H_{24}N_3O_7$	1.68	415.151	$C_9[^{13}C]_7H_{23}KN_3O_7$	25.91	nd		
			397.1607	$C_{11}[^{13}C]_5H_{23}NaN_3O_7$	2.78	396.1537	$C_{12}[^{13}C]_4H_{23}NaN_3O_7$	– 6.41
370.1992	$C_{17}H_{28}N_3O_6$	5.23	400.2097	$C_9[^{13}C]_8H_{27}NaN_3O_6$	9.13	411.1639	$C_{14}[^{13}C]_3H_{27}KN_3O_6$	1.68

			398.1974	$C_{11}[^{13}C]_6H_{27}NaN_3O_6$	– 4.86	412.167	$C_{13}[^{13}C]_4H_{27}KN_3O_6$	1.06
			396.1848	$C_{13}[^{13}C]_4H_{27}NaN_3O_6$	– 19.75	375.2157	$C_{12}[^{13}C]_5H_{28}N_3O_6$	4.43
372.1711	$C_{16}H_{26}N_3O_7$	– 4.37	379.1999	$C_9[^{13}C]_7H_{26}N_3O_7$	– 0.29	375.178	$C_{13}[^{13}C]_3H_{26}N_3O_7$	– 22.9
410.1345	$C_{16}H_{25}KN_3O_7$	5.1	415.1514	$C_{11}[^{13}C]_5H_{25}KN_3O_7$	5.34	376.1867	$C_{12}[^{13}C]_4H_{26}N_3O_7$	– 8.63
381.1069	$C_{15}H_{22}KN_2O_7$	2.73	374.1645	$C_6[^{13}C]_9H_{22}NaN_2O_7$	6.37	367.1391	$C_{13}[^{13}C]_2H_{22}NaN_2O_7$	1.28
			388.1258	$C_8[^{13}C]_7H_{22}KN_2O_7$	– 9.13	384.116	$C_{12}[^{13}C]_3H_{22}KN_2O_7$	0.2
380.1419	$C_{15}H_{23}N_3NaO_7$	– 2.42	nd			nd		
386.1955	$C_{17}H_{27}NaN_3O_7$	0.19	416.2011	$C_9[^{13}C]_8H_{27}NaN_3O_7$	0.34	389.2011	$C_{14}[^{13}C]_3H_{28}N_3O_7$	– 2.93
			414.1951	$C_{11}[^{13}C]_6H_{27}NaN_3O_7$	2.05	428.1659	$C_{13}[^{13}C]_4H_{27}KN_3O_7$	10.33
			nd			413.1909	$C_{12}[^{13}C]_5H_{27}NaN_3O_7$	0.01
392.1203	$C_{16}H_{23}N_3KO_6$	– 3.94	361.1907	$C_9[^{13}C]_7H_{24}N_3O_6$	3.47	nd		
			359.1805	$C_{11}[^{13}C]_5H_{24}N_3O_6$	– 6.23	380.1571	$C_{12}[^{13}C]_4H_{23}NaN_3O_6$	– 11.12
398.1935	$C_{18}H_{28}N_3O_7$	3.32	nd			439.1595	$C_{15}[^{13}C]_3H_{27}KN_3O_7$	3.14
436.1458	$C_{18}H_{27}KN_3O_7$	– 5.18						
			405.2124	$C_{11}[^{13}C]_7H_{28}N_3O_7$	– 8.05	nd		
			425.1943	$C_{13}[^{13}C]_5H_{27}NaN_3O_7$	8.01	403.2131	$C_{13}[^{13}C]_5H_{28}N_3O_7$	10.29
400.1714	$C_{17}H_{26}N_3O_8$	– 0.1	446.1557	$C_9[^{13}C]_8H_{25}KN_3O_8$	3.45	403.1742	$C_{14}[^{13}C]_3H_{26}N_3O_8$	– 18.12
402.1644	$C_{18}H_{25}NaN_3O_6$	2.1	389.2158	$C_9[^{13}C]_9H_{26}\ N_3O_6$	10.26	421.1482	$C_{15}[^{13}C]_3H_{25}KN_3O_6$	1.52
418.1341	$C_{18}H_{25}KN_3O_6$	– 1.38	387.201	$C_{11}[^{13}C]_7H_{26}N_3O_6$	– 10.58	384.1958	$C_{14}[^{13}C]_4H_{26}N_3O_6$	2
			385.1969	$C_{13}[^{13}C]_5H_{26}N_3O_6$	– 3.86	385.1961	$C_{13}[^{13}C]_5H_{26}N_3O_6$	– 5.94
412.1755	$C_{18}H_{26}N_3O_8$	9.85	421.2054	$C_9[^{13}C]_9H_{26}N_3O_8$	8.94	nd		
430.1801	$C_{18}H_{28}N_3O_9$	– 4.43	439.2113	$C_9[^{13}C]_9H_{28}N_3O_9$	– 2.05	nd		

442.1804	$C_{19}H_{28}N_3O_9$	– 3.63	452.2153	$C_9[^{13}C]_{10}H_{28}N_3O_9$	– 0.56			
451.1785	$C_{18}H_{28}N_4NaO_8$	– 3.18	435.2212	$C_{12}[^{13}C]_6H_{29}N_4O_8$	7.08	455.1966	$C_{14}[^{13}C]_4H_{28}NaN_4O_8$	7.13
453.1987	$C_{20}H_{29}N_4O_8$	1.57	499.185	$C_{12}[^{13}C]_8H_{28}KN_4O_8$	8.59	nd		
454.1582	$C_{18}H_{29}KN_3O_8$	– 0.93	447.2184	$C_9[^{13}C]_9H_{29}NaN_3O_8$	7.87	457.1708	$C_{15}[^{13}C]_3H_{29}KN_3O_8$	4.62
			423.2259	$C_{11}[^{13}C]_7H_{30}N_3O_8$	– 0.77	442.194	$C_{14}[^{13}C]_4H_{29}NaN_3O_8$	– 9.28
			421.2205	$C_{13}[^{13}C]_5H_{30}N_3O_8$	2.34	443.2035	$C_{13}[^{13}C]_5H_{29}NaN_3O_8$	4.6
460.1953	$C_{19}H_{30}N_3O_{10}$	5.93	470.2294	$C_9[^{13}C]_{10}H_{30}N_3O_{10}$	6.98	463.1969	$C_{16}[^{13}C]_3H_{30}N_3O_{10}$	– 12.38
464.2019	$C_{20}H_{31}N_3NaO_8$	3.37	475.2372	$C_9[^{13}C]_{11}H_{31}NaN_3O_8$	– 0.08	467.2082	$C_{17}[^{13}C]_3H_{31}NaN_3O_8$	– 4.71
			473.2256	$C_{11}[^{13}C]_9H_{31}NaN_3O_8$	– 10.42	nd		
			471.2317	$C_{13}[^{13}C]_7H_{31}NaN_3O_8$	16.72	nd		
			469.2224	$C_{15}[^{13}C]_5H_{31}NaN_3O_8$	11.27	nd		
493.1905	$C_{20}H_{30}N_4NaO_9$	0	479.2391	$C_{12}[^{13}C]_8H_{31}N_4O_9$	7.73	nd		
497.2326	$C_{22}H_{33}N_4O_9$	15.78	523.2635	$C_{12}[^{13}C]_{10}H_{33}N_4O_{10}$	20.7	nd		
519.2123	$C_{22}H_{32}N_4NaO_9$	11.85	505.2503	$C_{14}[^{13}C]_8H_{33}N_4O_9$	– 1.47	nd		
499.2325	$C_{22}H_{35}N_4O_9$	– 14.73	547.2293	$C_{12}[^{13}C]_{10}H_{34}KN_4O_9$	0.03	nd		
			nd			526.2247	$C_{17}[^{13}C]_5H_{34}NaN_4O_9$	– 26.36
			505.2579	$C_{16}[^{13}C]_6H_{35}N_4O_9$	– 4.12	527.2465	$C_{16}[^{13}C]_6H_{34}NaN_4O_9$	8.67
503.2118	$C_{22}H_{32}N_4NaO_8$	1.12	513.2424	$C_{12}[^{13}C]_{10}H_{32}NaN_4O_8$	– 4.64	nd		
			nd			524.206	$C_{17}[^{13}C]_5H_{32}KN_4O_8$	7.73
			487.2422	$C_{16}[^{13}C]_6H_{33}N_4O_8$	– 14.82	nd		
507.2047	$C_{21}H_{32}N_4NaO_9$	– 2.86	nd			489.2284	$C_{17}[^{13}C]_4H_{33}N_4O_9$	– 18.85
			523.2635	$C_{14}[^{13}C]_8H_{35}N_4O_{10}$	4.57	490.2454	$C_{16}[^{13}C]_5H_{33}N_4O_9$	9.02

515.2373	$C_{22}H_{35}N_4O_{10}$	4.91	523.2635	$C_{14}[^{13}C]_8H_{35}N_4O_{10}$	4.57	nd		
515.2217	$C_{21}H_{33}N_4O_{10}$	– 0.96	510.2533	$C_{12}[^{13}C]_9H_{33}N_4O_{10}$	7.81	505.2417	$C_{17}[^{13}C]_4H_{33}N_4O_{10}$	18.13

[a]Error (in ppm) in calculating the elemental composition

[b]nd: not detected

[c]The ions detected in Figures S8.1 to S8.12 shown various elemental composition depending on consisting of the number of acetaldehyde (see also Table S8.2)

8.4.3. A representative pathway for the oligomerization of oxazolidin-5-one

The nucleophilic nitrogen atom in the parent moiety of 4-methyl-oxazolidin-5-one observed at *m/z* 102, can initiate further reactions with reactive aldehydes, such as formaldehyde, acetaldehyde, and glycolaldehyde, generating three different reactive iminium ion derivatives shown in Figure 8.2. Each of these derivatives can undergo a specific sequence of reactions and generate different oligomeric structures; the case of formaldehyde adduct observed at *m/z* 114 is shown in Figure 8.3 can be considered as a representative example, the details of all other possible sequences are shown in Figures S8.1 to S8.12.

Generation of dimeric oxazolidin-5-one

According to Figure 8.3, oligomerization can be initiated by the reaction of the amino group of the parent 4-methyl-oxazolidin-5-one with formaldehyde and formation of a reactive iminium ion which was observed as $[M]^+$ at *m/z* 114.0554 $[C_5H_8NO_2]^+$ (see Figure 8.3). As expected, this ion incorporated two carbon atoms from [^{13}C-U] glucose and one C-3 atom from [^{13}C-3] alanine (Tables 8.2 and S8.2). Based on the analysis of the data, the iminium ion underwent an initial aldol addition reaction with acetaldehyde to form $[M + H]^+$ at *m/z* 158.0816 $[C_7H_{12}NO_3]^+$. Subsequently, this adduct formed a Schiff base with available alanine and isomerized as stable oxazolidin-5-one cyclic structure and was detected at *m/z* 229.1185 $[C_{10}H_{17}N_2O_4]$. This ion can be considered as dimeric oxzolidin-5-one oligomer shown in Figures 8.1 and 8.3. Acetaldehyde in the Maillard reaction can be generated through either sugar degradation or Strecker reaction as Strecker aldehyde and, therefore, can exist as two different isotopomeric forms in isotopically labelled reactants ([^{13}C-U] glucose or [^{13}C-3] alanine); one incorporating two labelled sugar carbon atoms and the second incorporating one ^{13}C-3 atom from alanine. Indeed, the resulting adduct observed at *m/z* 229 showed two isotopomers (see Table 8.2); one isomer incorporated four carbon atoms from [^{13}C-U] glucose and two C-3 atoms from [^{13}C-3] alanine and the other incorporated two carbon atoms from [^{13}C-U] glucose and three C-3 atoms from [^{13}C-3] alanine, consistent with the predicted origin of acetaldehyde. If all the acetaldehyde molecules in this adduct originated from alanine, we would have expected to find three C-3 atoms from [^{13}C-3] alanine and three carbon atoms from [^{13}C-U] glucose. On the other hand, if all the acetaldehyde molecules originated from sugar, the expected number of C-3 atoms would have been two from [^{13}C-3] alanine and five carbon atoms from [^{13}C-U] glucose.

Generation of trimeric oxazolidin-5-one

The dimeric oxazolidin-5-none observed at *m/z* 229.1185 can further react with a formaldehyde molecule to form a new iminium ion which was observed at *m/z* 241.1186 $[C_{11}H_{17}N_2O_4]^+$. This ion can also generate two isotopomeric structures due to the double origin of acetaldehyde. The first isomer incorporated five carbon atoms from [^{13}C-U] glucose and two C-3 atoms from [^{13}C-3] alanine; the other incorporated three carbon atoms from [^{13}C-U] glucose and three C-3 atoms from [^{13}C-3] alanine. The ion at *m/z* 241.1186 subsequently reacted with an α-carbon containing aldehyde, such as acetaldehyde or glycolaldehyde, through aldol addition and subsequently formed two new dimeric oxazolidin-5-one derivatives such as the ion $[M + Na]^+$ at *m/z* 307.1266 $[C_{13}H_{20}N_2NaO_5]^+$ formed from acetaldehyde interaction and $[M + H]^+$ at *m/z* 301.1401 $[C_{13}H_{21}N_2O_6]^+$ formed from glycolaldehyde interaction in addition to its dehydration product $[M + H]^+$ observed at *m/z* 283.1276 $[C_{13}H_{19}N_2O_5]^+$. The ion at *m/z* 301 and its dehydration product $[M + H]^+$ at *m/z* 283.1276 $[C_{13}H_{19}N_2O_5]^+$, similar to *m/z* 229.1185 needed one acetaldehyde molecules for its formation. Hence, the resulting adducts showed two isotopomers (Table 8.2). On the other hand, the ion *m/z* 307.1266 needed two acetaldehyde molecules for its formation and exhibited three isotopomers; in one isomer, all acetaldehyde molecules originated from the amino acid, and in the second, all originated from sugar, and the third had a mixed origin. (Figure S8.1 and Tables 8.2 and S8.2). The ion at *m/z* 301, following Schiff base formation with alanine and intramolecular cyclization, formed two isotopomers of trimeric oxazolidin-5-one adducts, one at *m/z* 372.1772 and the second at *m/z* 410.1345 as potassiated ion. The former incorporated seven carbon atoms from glucose and three from [^{13}C-3] alanine, and the latter five carbon atoms from glucose and four from [^{13}C-3] alanine. The dehydration product at *m/z* 354.1654 similarly displayed two isotopomers at *m/z* 361.1907 and *m/z* 359.1805.

Based on the mechanism proposed in this study, the cascade reactions generated various derivatives of oxazolidin-5-one oligomers, as evident from the HRMS and isotope labelling analyses. Furthermore, it was demonstrated that reactive aldehydes could be generated from sugar and Strecker degradation reactions. Other oxazolidin-5-one derivatives obtained through corresponding pathways are displayed in Figures S8.1 to S8.12 and analyzed in the same manner described above.

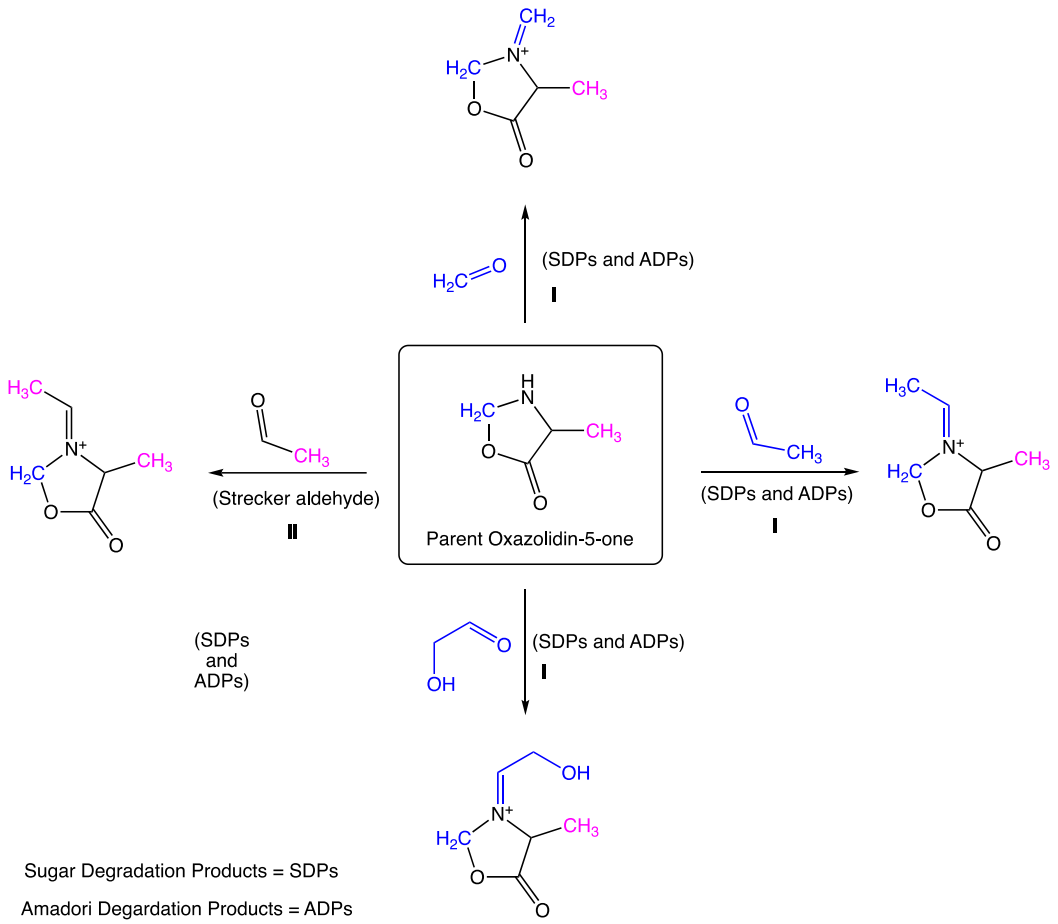

Figure 8.2. Proposed three precursors of oligomeric oxazolidin-5-ones formed from the parent compound generated from alanine and formaldehyde (Table S8.2). See also chapter 7, Figure 7.3

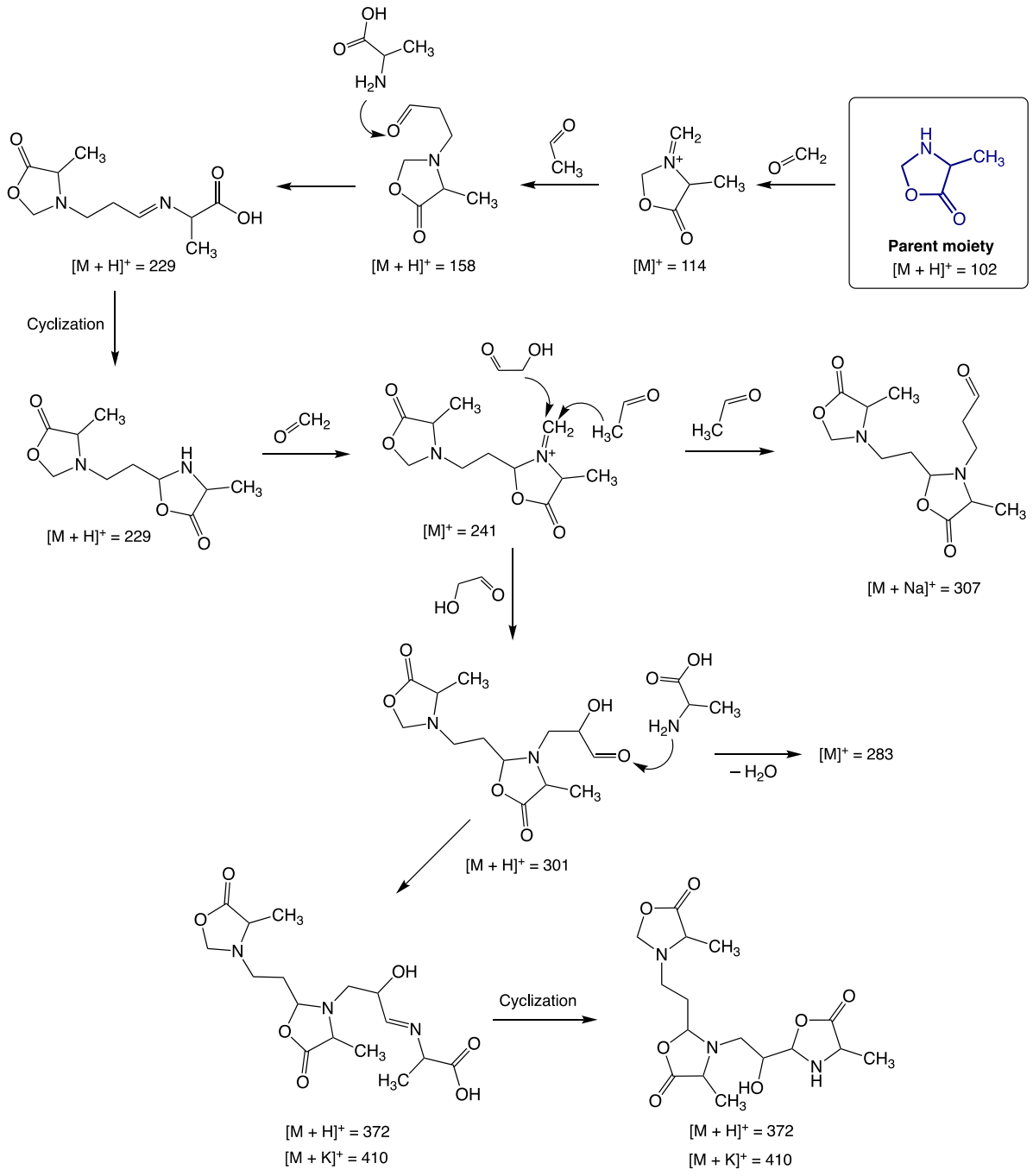

Figure 8.3. Representative detailed pathway for the formation of oxazolidin-5-one oligomers based on pathway A (see Figure S8.1)

8.4.4. MS/MS fragmentations of *m/z* 227, *m/z* 328, and *m/z* 372

To provide supporting evidence for the proposed structures, ions with high enough intensities to be analyzed by MS/MS were selected, such as *m/z* 227 representing a dimeric structure and *m/z* 328 and 372 representing trimeric structures; these ions were analyzed by high-resolution ESI/qTOF/MS/MS.

8.4.4.1. Ion at *m/z* 227 (5 eV)

Based on the HRMS data, isotope labelling and MS/MS analysis, this ion corresponded to the dehydration peak of *m/z* 245, having two oxazolidin-5-one moieties and can be formed by two different sequences of reactions generating isomeric structures such as the incorporation of two molecules of alanine and one molecule of dihydroxyacetone or by the incorporation of two molecules of alanine and one molecule each of formaldehyde and acetaldehyde as shown in Figure 8.4. In addition, MS/MS fragmentations under 5 eV have indicated that oxazolidine oligomers can undergo decarboxylation followed by the elimination of ethyl and methyl groups, as evidenced by the detection of fragments corresponding to fragment ions at *m/z* 155 and 141 (Table 8.3 and Figure 8.4). Both isomers were consistent with the MS/MS data and could not be distinguished.

Table 8.3. MS/MS fragmentations of the ions observed at *m/z* 227 using 5 eV collision energy

m/z	Elemental composition[a]	Error ppm[b]	Relative Intensity (%)
141.0651	$C_6H_9N_2O_2$	– 5.34	3
155.0808	$C_7H_{11}N_2O_2$	– 4.54	3.2
227.1016[c]	$C_{10}H_{15}N_2O_4$	– 4.55	100

[a]All of the ions listed in Figures 8.4 are included in this table

[b]Error (in ppm) in calculating the elemental composition

[c]Base peak

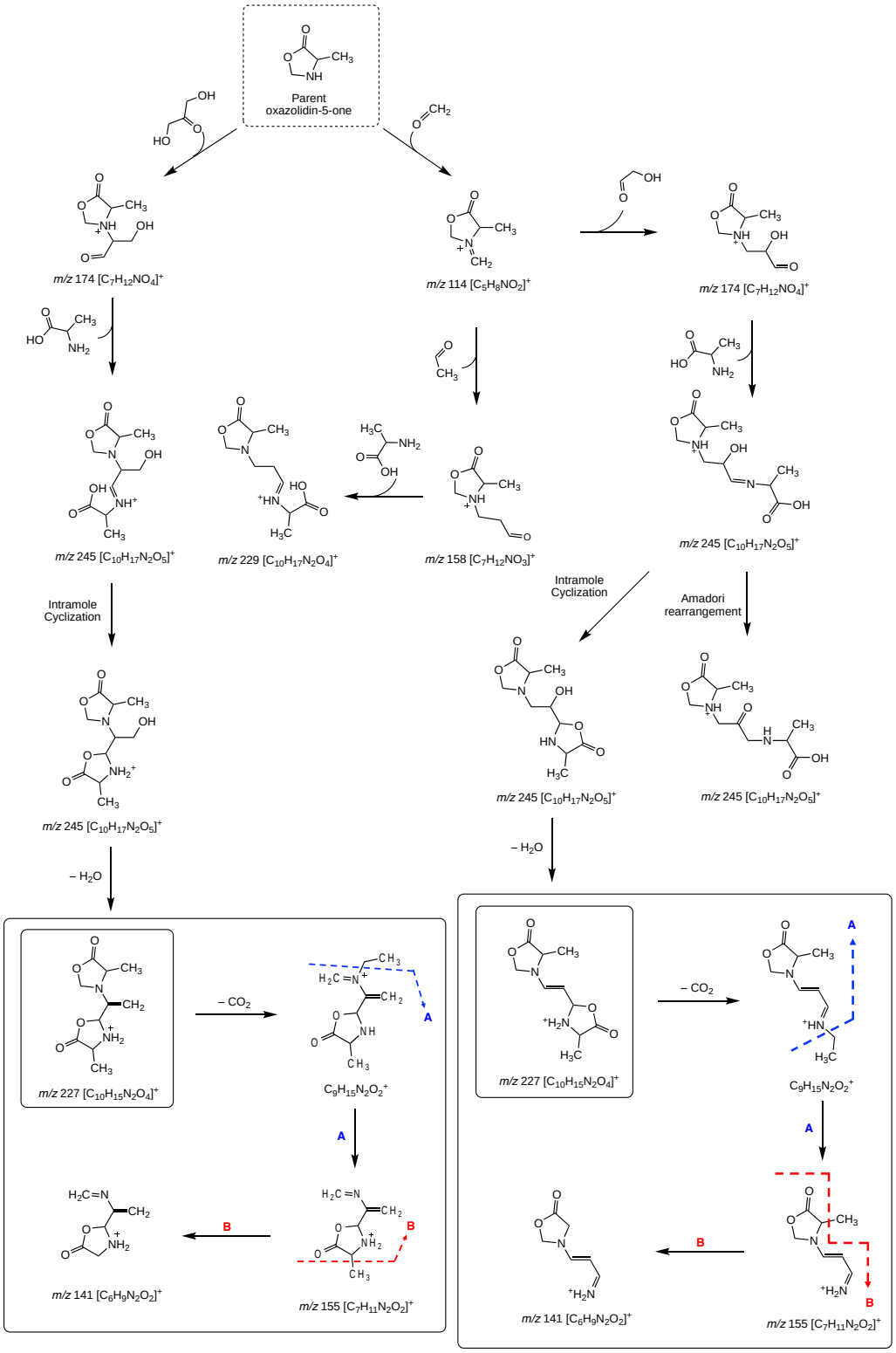

Figure 8.4. Proposed formation and MS/MS fragmentation pathways of *m/z* 227 detected in the Ala/Glu/$FeCl_2$ model system (see Table 8.3).

8.4.4.2. Ion at *m/z* 328 (10 eV)

The ion at *m/z* 328 was among the detected ions shown in Figure S8.2; this ion was observed at *m/z* 328.1513 $[C_{14}H_{22}N_3O_6]^+$ and corresponds to an oligomer having three oxazolidin-5-one moieties. The elemental composition of the MS/MS fragment ions shown in Figure 8.5 and Table 8.4 was consistent with the proposed structures and followed similar decarboxylation steps as the ion at *m/z* 227 discussed above generating several decarboxylated products such as *m/z* 284 observed as characteristic fragmentations of the oxazolidin-5-one oligomers under 10 eV (Figure 8.5 and Table 8.4).

Table 8.4. MS/MS fragmentations of the ions observed at *m/z* 328 using 10 eV collision energy

m/z	Elemental composition[a]	Error ppm[b]	Relative Intensity (%)
90.0542	$C_3H_8NO_2$	– 8.38	13.4
102.0543	$C_4H_8NO_2$	– 6.42	47
104.0699[c]	$C_4H_{10}NO_2$	– 6.77	100
116.0699	$C_5H_{10}NO_2$	– 6.07	11.9
130.0856	$C_6H_{12}NO_2$	– 5.04	4.6
139.1218	$C_8H_{15}N_2$	– 8.45	5.2
227.1013	$C_{10}H_{15}N_2O_4$	– 5.87	21.3
284.1571	$C_{13}H_{22}N_3O_4$	– 11.9	4
328.1491	$C_{14}H_{22}N_3O_6$	– 3.69	35.1

[a]All of the ions listed in Figures 8.5 are included in this table

[b]Error (in ppm) in calculating the elemental composition

[c]Base peak

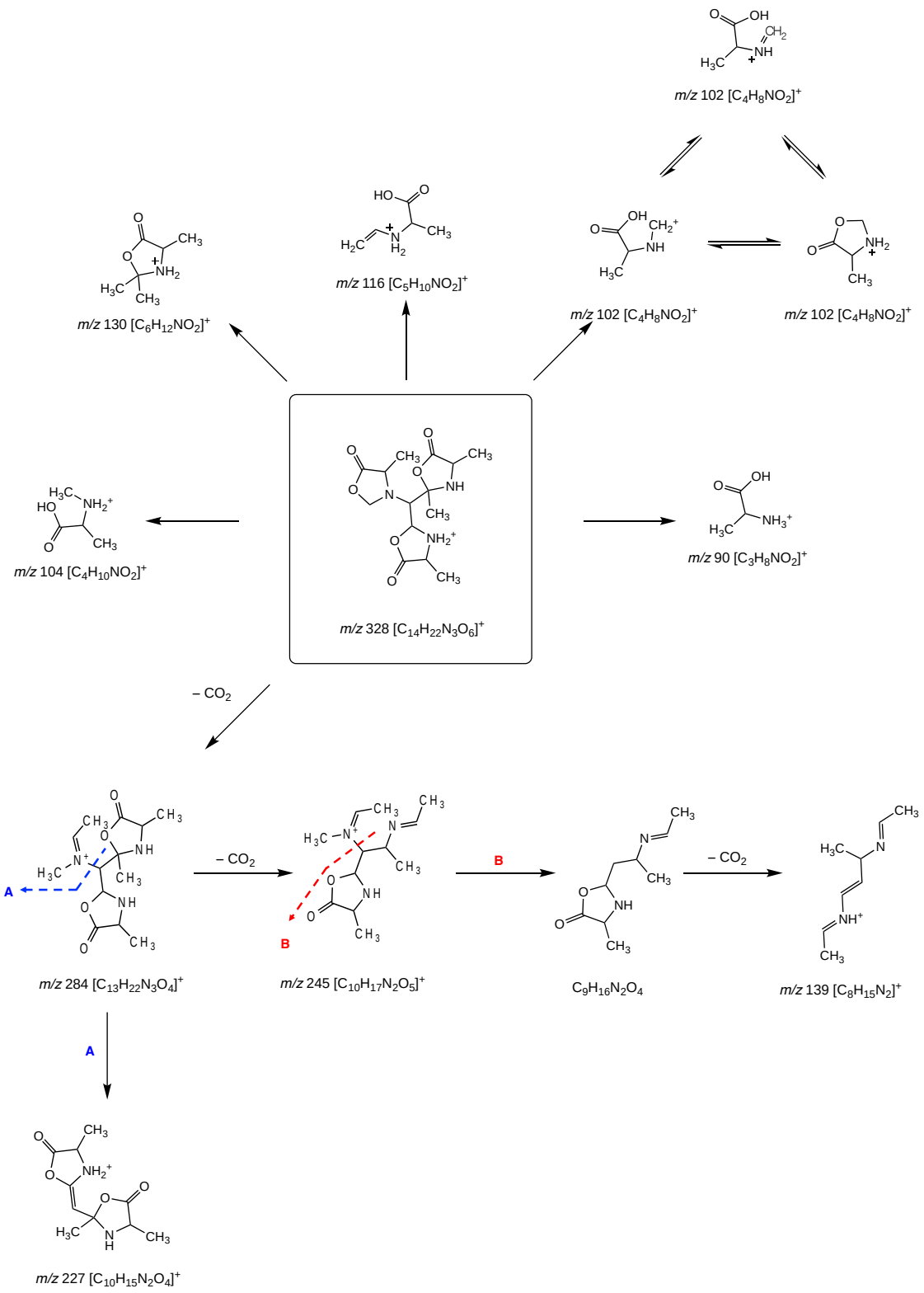

Figure 8.5. Proposed MS/MS fragmentation pathways of *m/z* 328 detected in the Ala/Glu/$FeCl_2$ model system (see Table 8.4)

8.4.4.3. Ion at *m/z* 372 (10 eV)

The formation of this trimeric oxazolidin-5-one oligomer was initiated by the parent oxazolidin-5-one, followed by several condensation reactions as shown in Figure 8.3 was observed at *m/z* 372.1711 as protonated ion and its isotopomer at *m/z* 410.1345 as potassiated ion (see section 8.4.3). As shown in the proposed MS/MS fragmentation pattern in Figure 8.6 and Table 8.5, the elemental composition of the proposed fragment ions is consistent with the proposed structures and generated the expected fragment ions at *m/z* 227, 241, 255, 271, 296, and 299 exhibiting dimeric oxazolidin-5-one moieties. The fragment ions at *m/z* 340 and 342 showed trimeric moieties. Furthermore, fragment ion having one oxazolidin-5-one unit at *m/z* 157 as characteristic fragmentations of the oxazolidin-5-one oligomer under 10 eV was also observed (Figure 8.6 and Table 8.5).

Table 8.5. MS/MS fragmentations of the ions observed at *m/z* 372 using 10 eV collision energy

m/z	Elemental composition[a]	Error ppm[b]	Relative Intensity (%)
157.096	$C_7H_{13}N_2O_2$	– 7.35	2.7
227.1012	$C_{10}H_{15}N_2O_4$	– 6.31	19
241.1177	$C_{11}H_{17}N_2O_4$	– 2.42	6.8
255.1324	$C_{12}H_{19}N_2O_4$	– 6.01	3.4
271.1275	$C_{12}H_{19}N_2O_5$	– 4.97	1.6
296.159	$C_{14}H_{22}N_3O_4$	– 5.01	1.6
299.1225	$C_{13}H_{19}N_2O_6$	– 4.22	19.4
340.1486	$C_{15}H_{22}N_3O_6$	– 5.03	5.6
342.1643	$C_{15}H_{24}N_3O_6$	– 4.86	28.2
372.175[c]	$C_{16}H_{26}N_3O_7$	– 4.1	100

[a]All of the ions listed in Figures 8.6 are included in this table

[b]Error (in ppm) in calculating the elemental composition

[c]Base peak

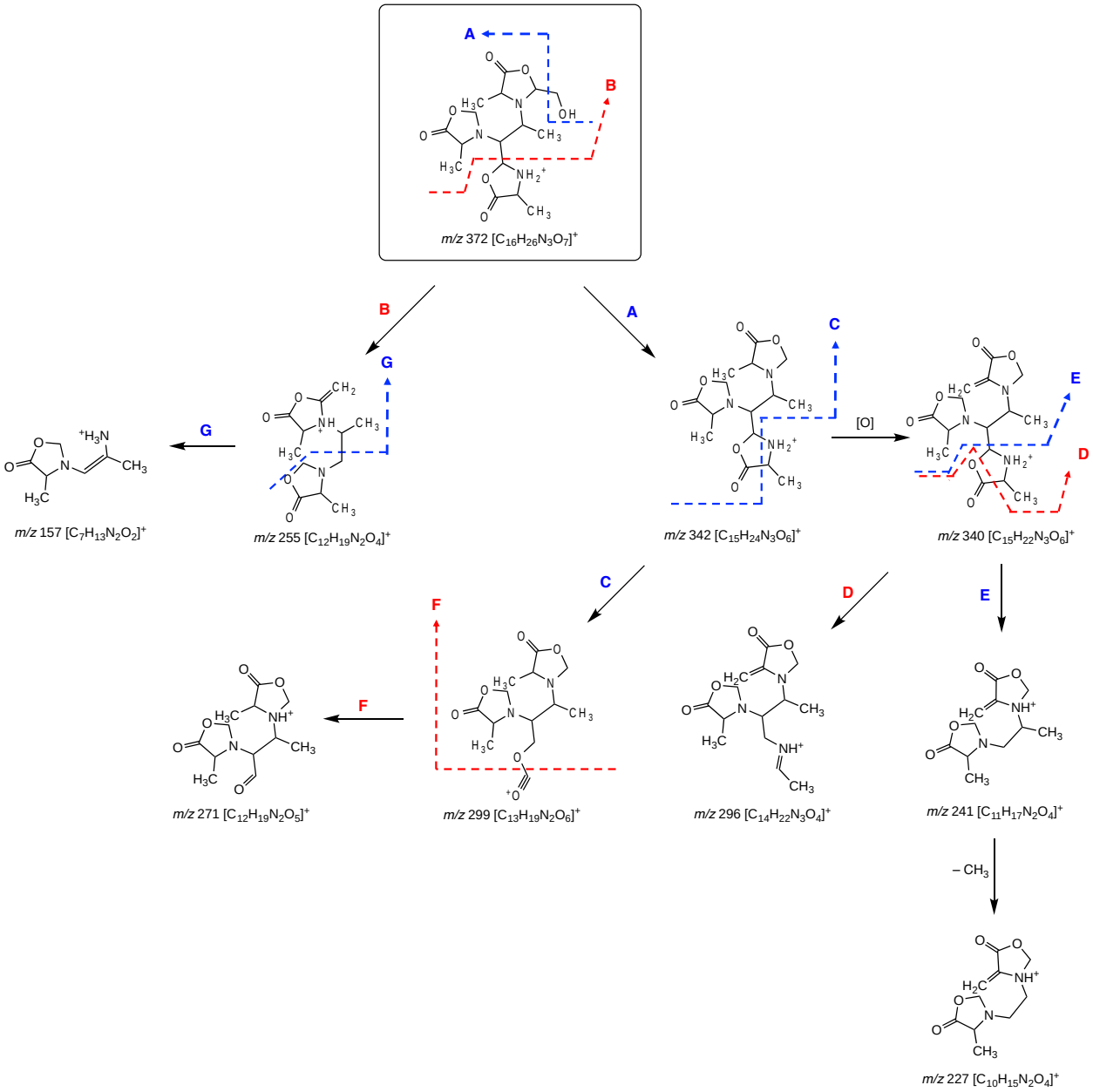

Figure 8.6. Proposed MS/MS fragmentation pathways of *m/z* 372 detected in the Ala/Glu/$FeCl_2$ model system (see Table 8.5)

8.5. CONCLUSION

The formation of oxazolidin-5-one oligomers in the Maillard reaction can be initiated by the interaction of amino acids, such as alanine, with formaldehyde, leading to the formation of 4-methyl-oxazolidin-5-one. This process can be catalyzed by divalent irons, such as Fe^{2+}. These intermediates can act as molecular scaffolds for the generation of oligomeric structures through the interaction of their amino groups with other reactive aldehydes, producing corresponding iminium ion derivatives.

These derivatives can serve as branching points for the creation of oligomeric structures, using a similar sequence of reactions, including aldol type addition, Amadori rearrangement, Schiff base formation, and culminating in intramolecular cyclization to form new and higher order oxazolidin-5-one oligomers. Oxazolidin-5-one oligomers can be considered precursors of various flavouring and browning compounds. Detailed understanding of their proposed formation pathways through HRMS, MS/MS, and isotope labelling analyses can offer further insights into the formation mechanisms of Maillard reaction products and other polymeric compounds.

8.6. REFERENCES

Chu, F. L. and Yaylayan, V. A. (2008). Post-schiff chemistry of the Maillard reaction. *Annals of the New York Academy of Science*, 1126, 30–37.

Kim, E. S. and Yaylayan, V. (2020). Profiling of glucose degradation products through complexation with divalent metal ions coupled with ESI/qTOF/MS/MS analysis. *Current Research in Food Science*, 3, 268–274.

Kim, E. S. and Yaylayan, V. (2021). Identification of the Maillard reaction intermediates as divalent iron complexes in alanine/glucose/$FeCl_2$ model system using ESI/qTOF/MS/MS and isotope labelling technique. *Current Research in Food Science*, 4, 287–294.

Kim, E. S. and Yaylayan, V. (2022). *Bis*(alaninato)iron(II) complexes as molecular scaffolds for the generation of *N*,*N*-di-glycated alanine derivatives in the presence of glucose. *Food Chemistry*, 374, 131815.

Kim, E. S. and Yaylayan, V. (Chapter 6). Intramolecular Cyclization of *N*,*N*-diglycated Alanine Derivatives. Manuscript in preparation.

Kim, E. S. and Yaylayan, V. (Chapter 7). ESI/qTOF/MS Profiling of Oxazolidin-5-one Derivatives in Alanine/Glucose/Fe^{2+} Model System.

Patiny, L. and Borel, A. (2013). ChemCalc: a building block for tomorrow's chemical infrastructure. *Journal of chemical information and modeling*, 53 (5), 1223–1228.

8.7. SUPPLEMENTARY DATA

Table S8.1. Terminal products (oxazolidin-5-one monomer to tetramer) through various pathways from A to L (see Tables 8.2, S8.2, and Figures S8.1 to S8.12)

Pathway A			
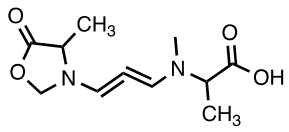	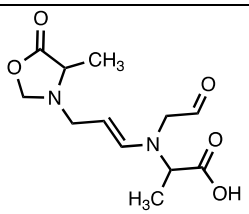	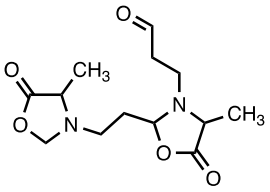	
$[M + H]^+ = 241$	$[M + H]^+ = 271$	$[M + Na]^+ = 307$	
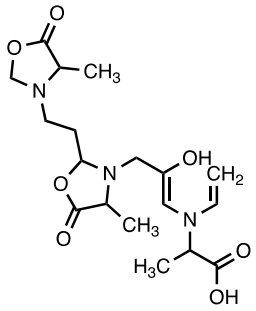		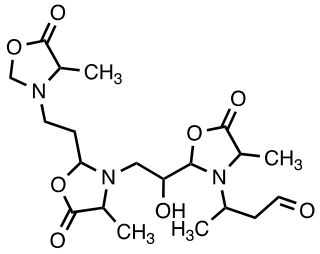	
$[M + H]^+ = 398$ $[M + K]^+ = 436$		$[M + Na]^+ = 464$	

Pathway B			
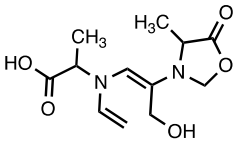	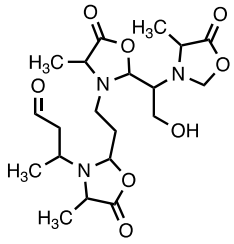	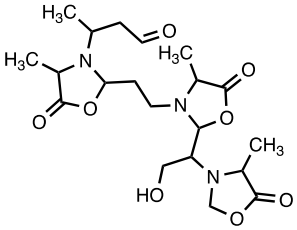	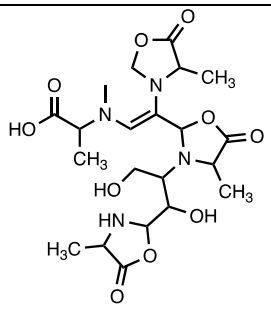
$[M + H]^+ = 271$	$[M + Na]^+ = 464$	$[M + Na]^+ = 464$	$[M + H]^+ = 515$

Pathway C

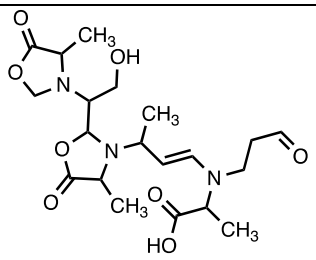

$[M + Na]^+ = 464$

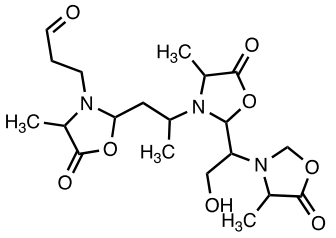

$[M + Na]^+ = 464$

Pathway D

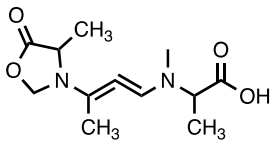

$[M + H]^+ = 255$

$[M + Na]^+ = 277$

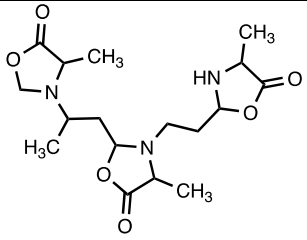

$[M + H]^+ = 370$

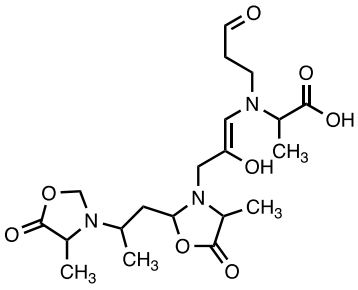

$[M + Na]^+ = 464$

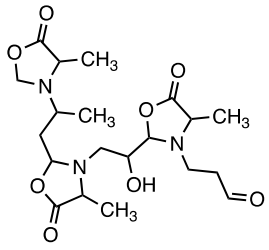

$[M + Na]^+ = 464$

Pathway E

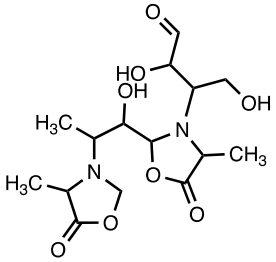

$[M + H]^+ = 361$

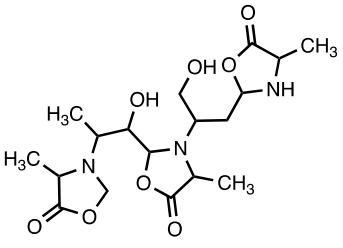

$[M + K]^+ = 454$

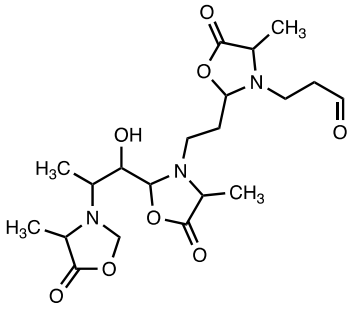

$[M + Na]^+ = 464$

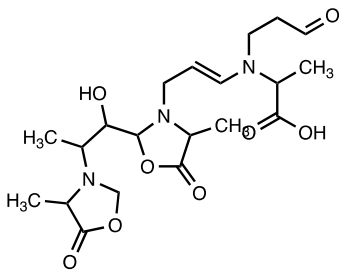

$[M + Na]^+ = 464$

Pathway F

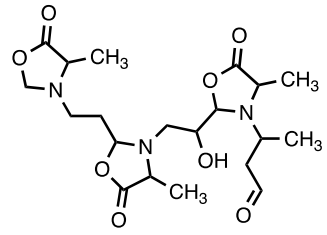

$[M + Na]^+ = 464$

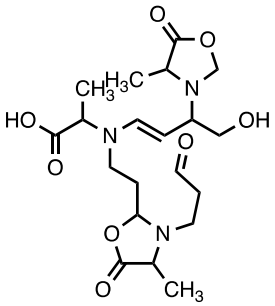

$[M + Na]^+ = 464$

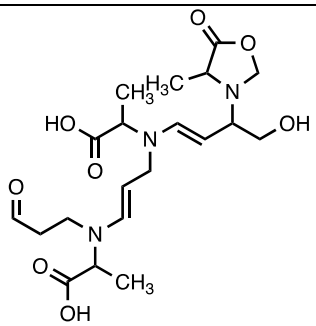

$[M + Na]^+ = 464$

Pathway G

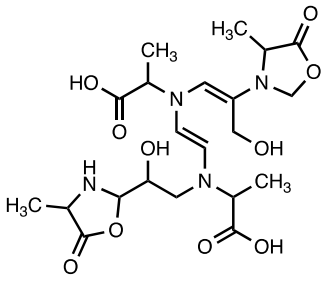

$[M + H]^+ = 515$

Pathway H

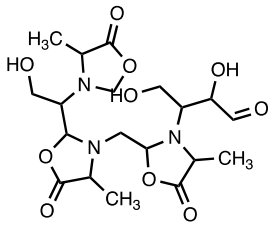

$[M + H]^+ = 460$

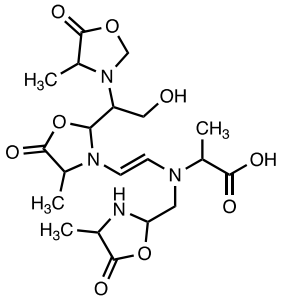

$[M + Na]^+ = 493$

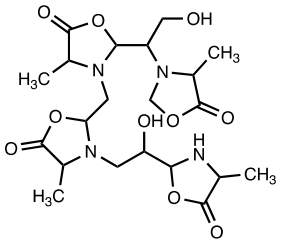

$[M + H]^+ = 515$

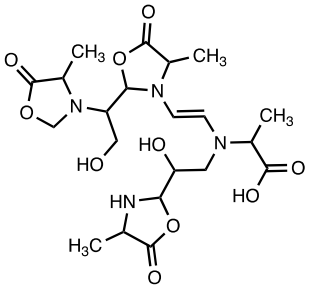

$[M + H]^+ = 515$

Pathway I

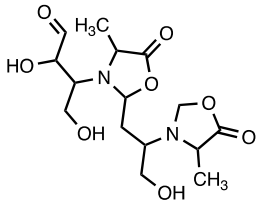

$[M]^+ = 361$

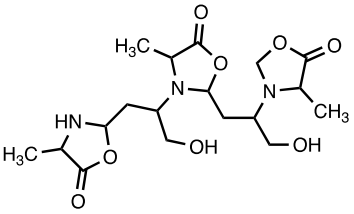

$[M + K]^+ = 454$

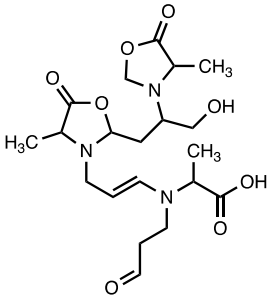

$[M + Na]^+ = 464$

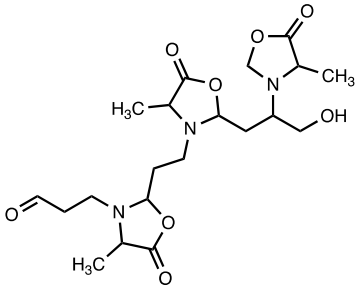

$[M + Na]^+ = 464$

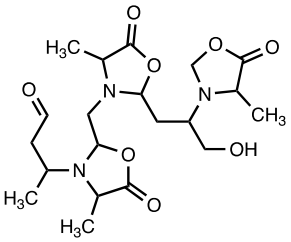

$[M + Na]^+ = 464$

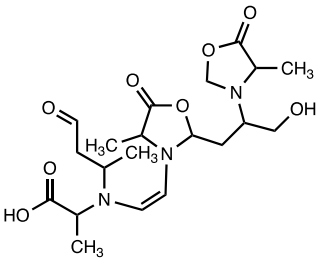

$[M + Na]^+ = 464$

Pathway J

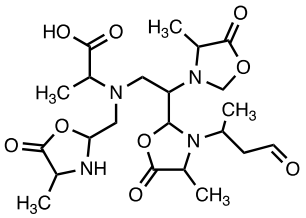

$[M + H]^+ = 499$

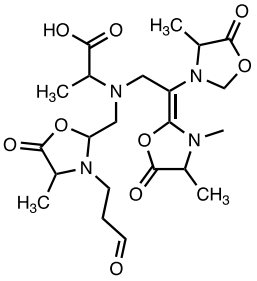

$[M + H]^+ = 497$

$[M + Na]^+ = 519$

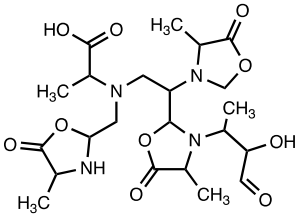

$[M + H]^+ = 515$

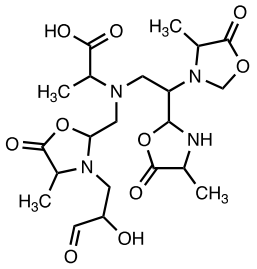

$[M + H]^+ = 515$

Pathway K

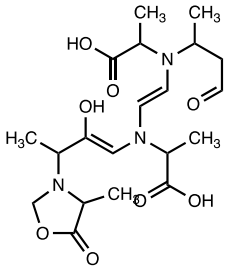

$[M + Na]^+ = 464$

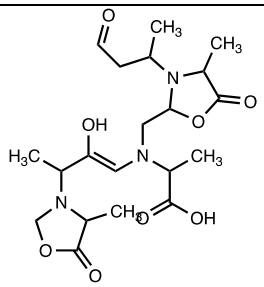

$[M + Na]^+ = 464$

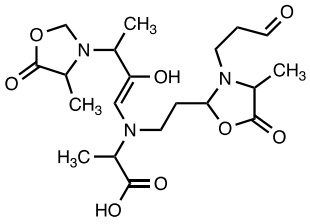

$[M + Na]^+ = 464$

Pathway L

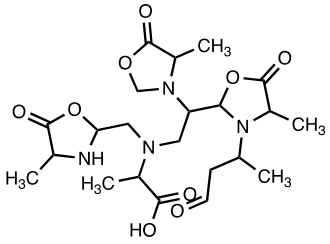

$[M + H]^+ = 499$

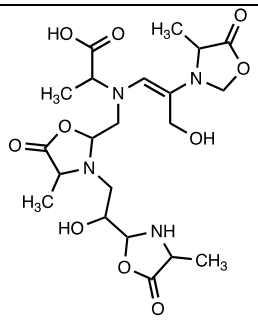

$[M + H]^+ = 515$

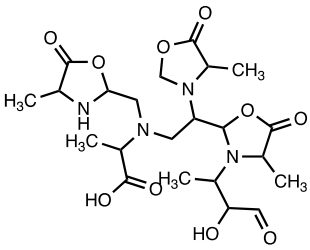

$[M + H]^+ = 515$

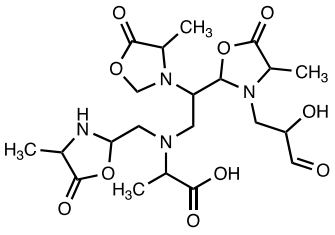

$[M + H]^+ = 515$

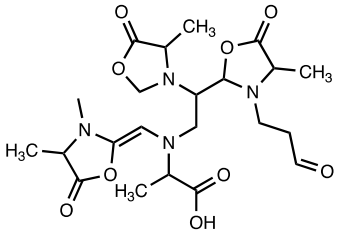

$[M + H]^+ = 497$

$[M + Na]^+ = 519$

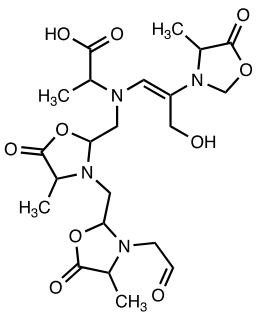

$[M + H]^+ = 499$

Table S8.2. Elemental composition and structure proposed corresponding to isotope incorporation in the oxazolidin-5-one oligomers and their isomers in alanine/glucose/$FeCl_2$ model system. Magenta coloured from [^{13}C-U] glucose and blue coloured from [^{13}C-3] alanine (see Table 8.2)

	Elemental Composition	$[M]^+/[M+X]^+$ (*m/z*)	Structure	Proposed Structure with isotope incorporation	Pathway
1	$C_4H_8NO_2$	102	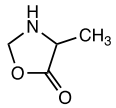	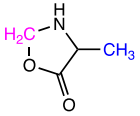	A, D, F
2	$C_5H_8NO_2$	114	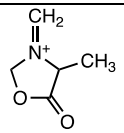	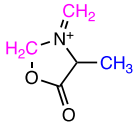	A
3	$C_6H_{10}NO_2$	128	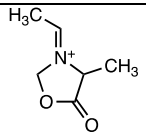	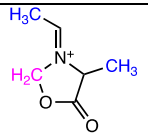	D
4	$C_6H_{10}NO_3$	144	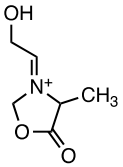	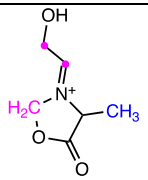	F
5	$C_7H_{12}NO_3$	158	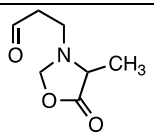	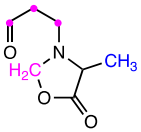	A
6	$C_8H_{14}NO_3$	172	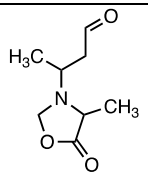	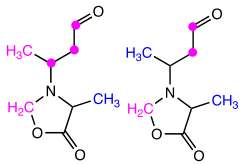	D

7	$C_7H_{12}NO_4$	174	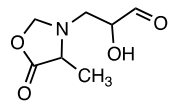	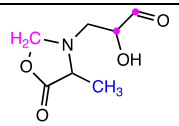	B
8	$C_8H_{14}NO_4$	188	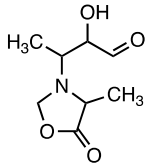	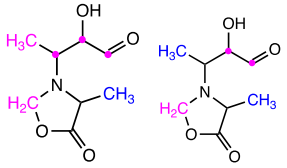	E
9	$C_8H_{14}NO_4$	188	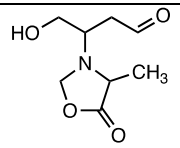	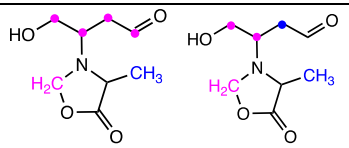	F
10	$C_{10}H_{17}N_2O_4$	229	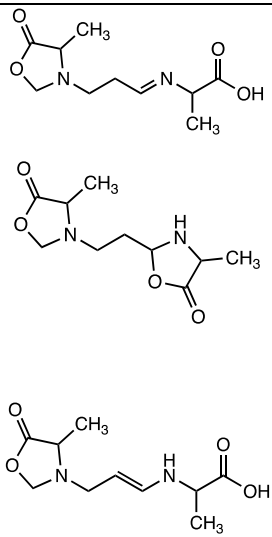	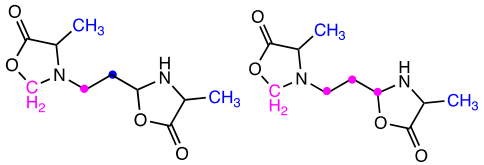	A
11	$C_{11}H_{17}N_2O_4$	241	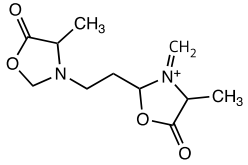	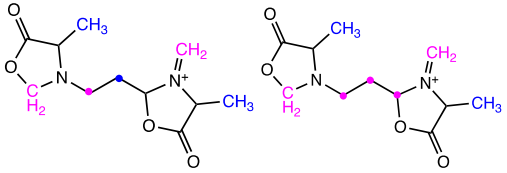	A

12	$C_{11}H_{17}N_2O_4$	241	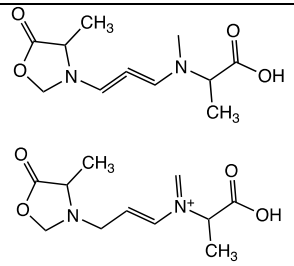	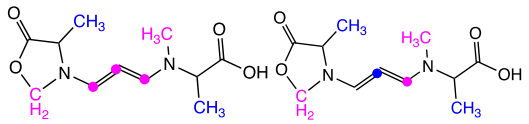	A
13	$C_{10}H_{17}N_2O_5$	245	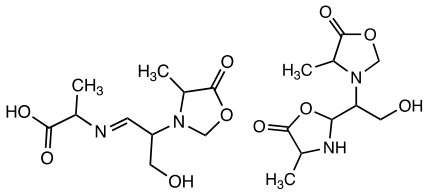	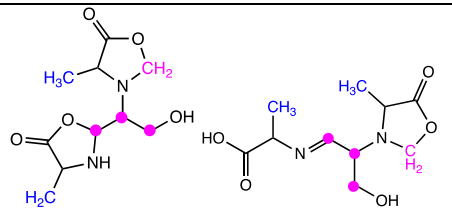	B
14	$C_{10}H_{17}N_2O_5$	245	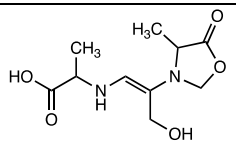	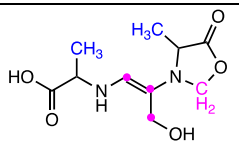	B
15	$C_{12}H_{19}N_2O_4$	255 277	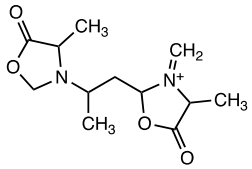	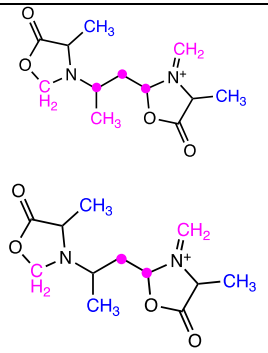	D

				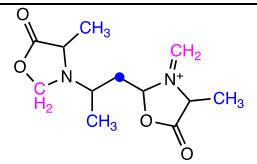	
16	$C_{12}H_{19}N_2O_4$	255 277	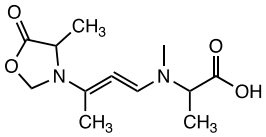	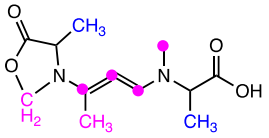 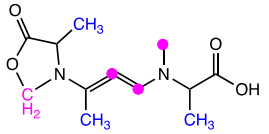	D
17	$C_{11}H_{17}N_2O_5$	257 279	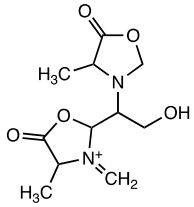	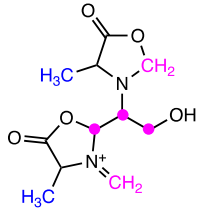	B
18	$C_{12}H_{19}N_2O_4$	257 279	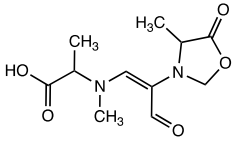	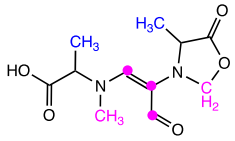	B
19	$C_{11}H_{19}N_2O_5$	259	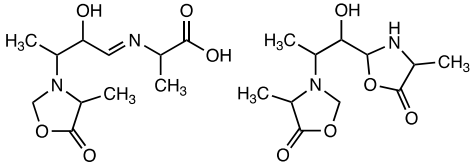	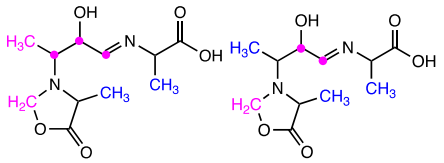	E

				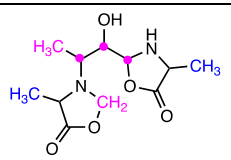 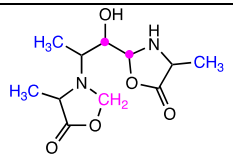	
20	$C_{11}H_{19}N_2O_5$	259	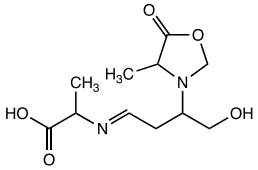	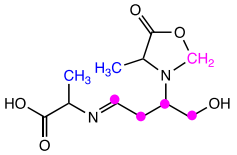 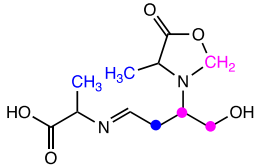	F
21	$C_{11}H_{19}N_2O_5$	259	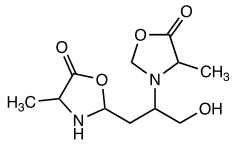	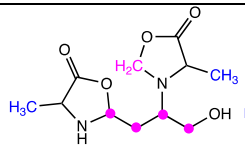 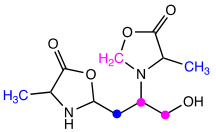	I
22	$C_{11}H_{19}N_2O_5$	259	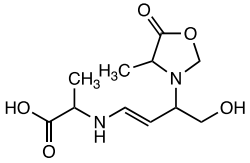	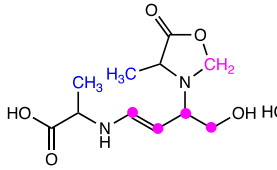 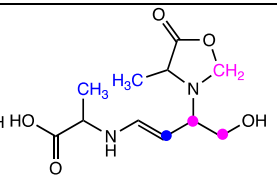	F
23	$C_{11}H_{19}N_2O_5$	259	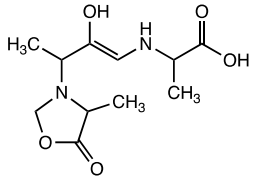	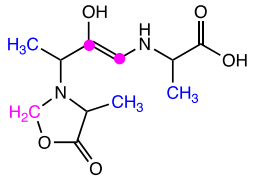 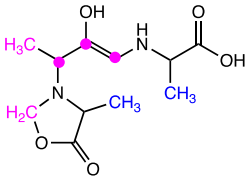	K
24	$C_{11}H_{18}N_2NaO_4$	265	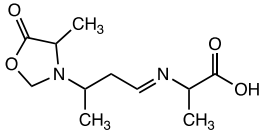 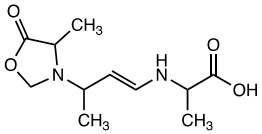	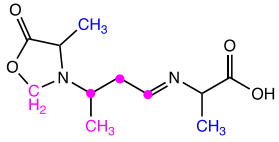 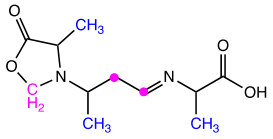 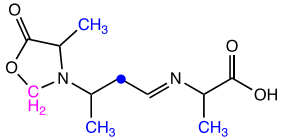	D

			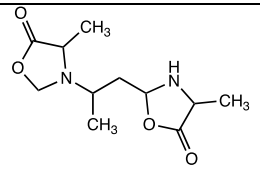	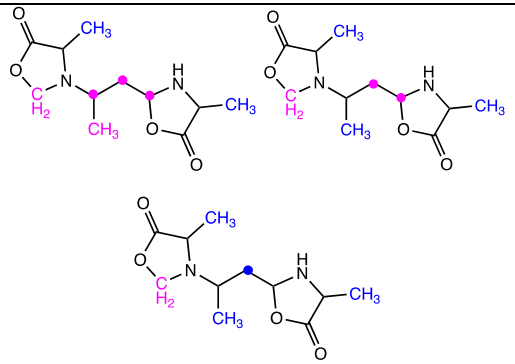	
25	$C_{12}H_{19}N_2O_5$	271	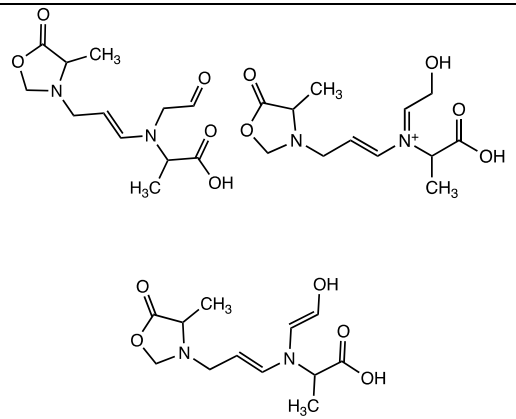	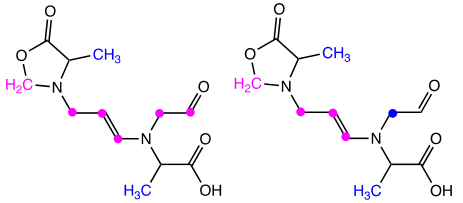	A
26	$C_{12}H_{19}N_2O_5$	271	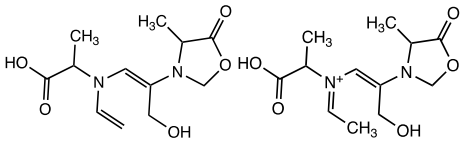	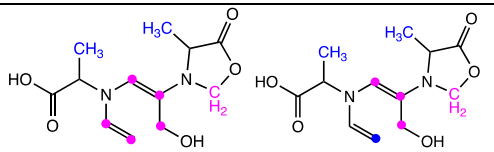	B
27	$C_{12}H_{19}N_2O_5$	271	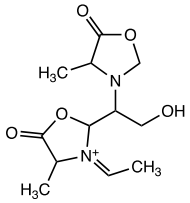	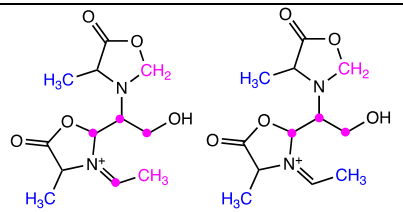	C

28	$C_{12}H_{19}N_2O_5$	271	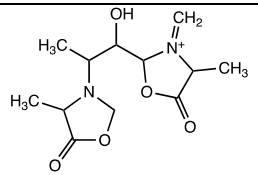	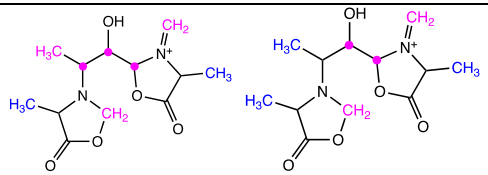	E
29	$C_{12}H_{19}N_2O_5$	271	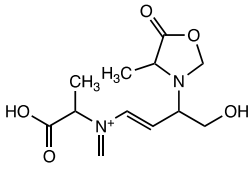	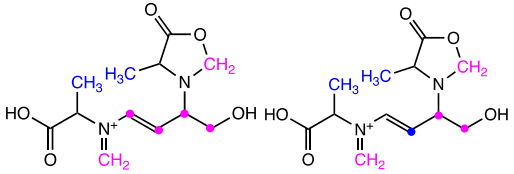	F
30	$C_{12}H_{19}N_2O_5$	271	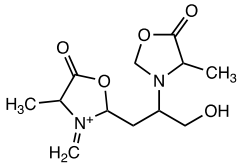	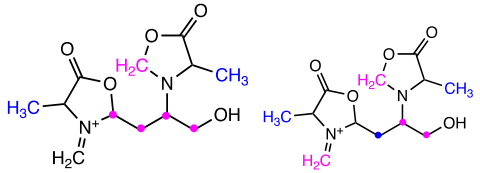	I
31	$C_{12}H_{19}N_2O_5$	271	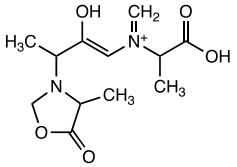	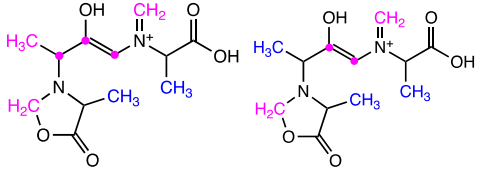	K
32	$C_{12}H_{19}N_2O_6$	287	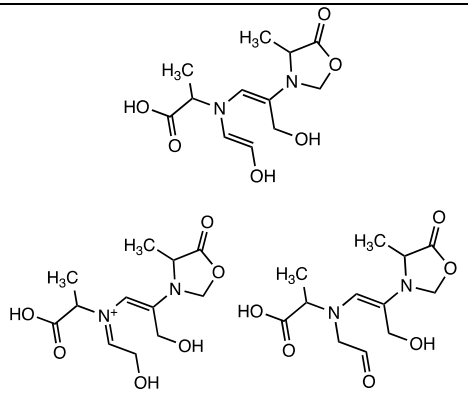	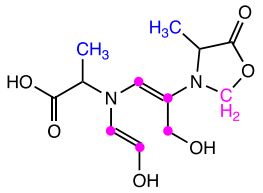	G

33	$C_{12}H_{19}N_2O_6$	287	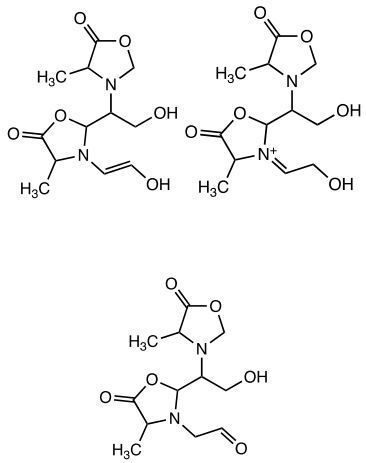	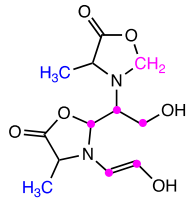	H
34	$C_{14}H_{23}N_2O_5$	299	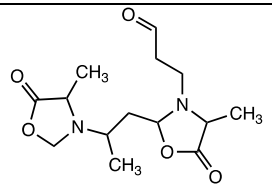	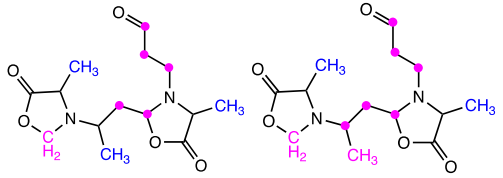	D
35	$C_{13}H_{21}N_2O_6$	301	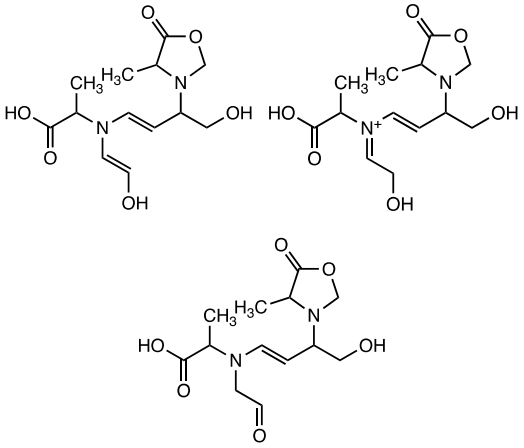	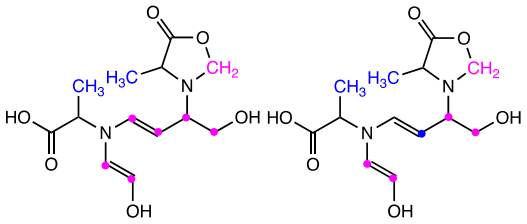	F

36	$C_{13}H_{21}N_2O_6$	301	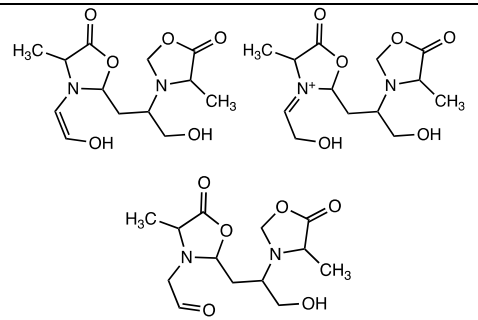	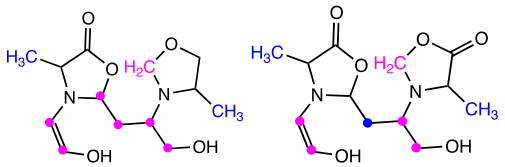	I
37	$C_{13}H_{21}N_2O_6$	301	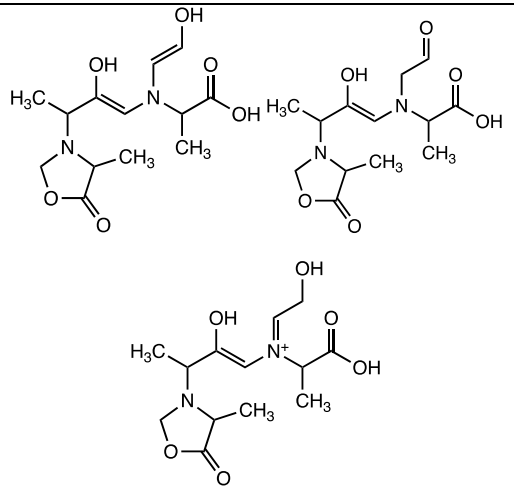	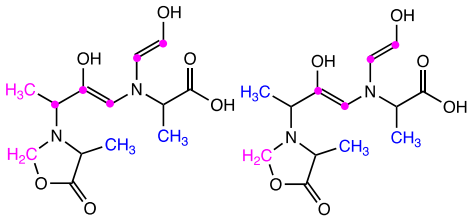	K
38	$C_{13}H_{21}N_2O_6$	301	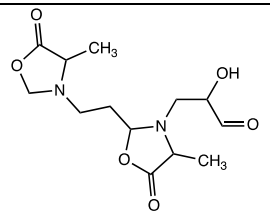	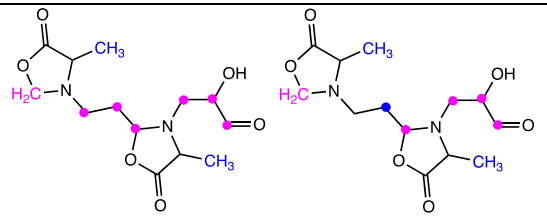	A

39	$C_{13}H_{21}N_2O_6$	301	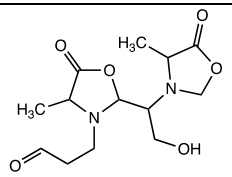	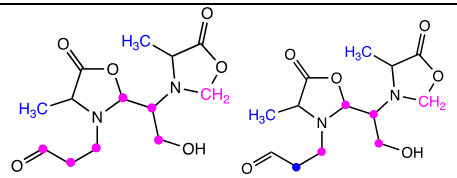	B
40	$C_{13}H_{21}N_2O_6$	301	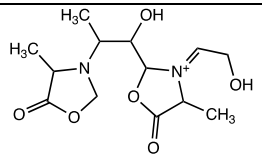	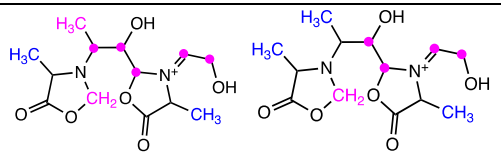	E
41	$C_{13}H_{20}N_2NaO_5$	307	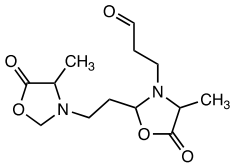	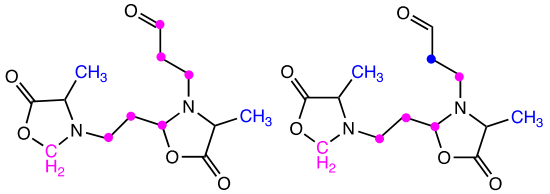	A
42	$C_{14}H_{23}N_2O_6$	315	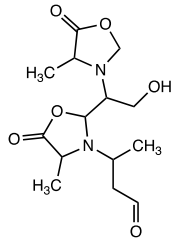	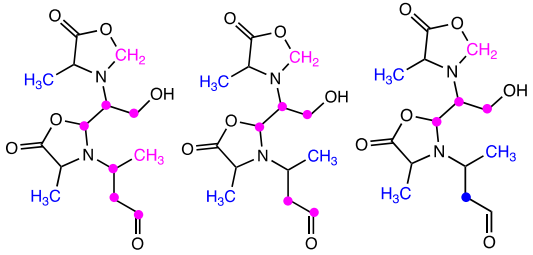	C

43	$C_{14}H_{23}N_2O_6$	315	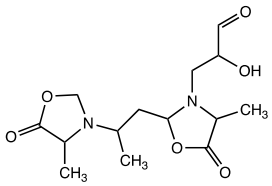	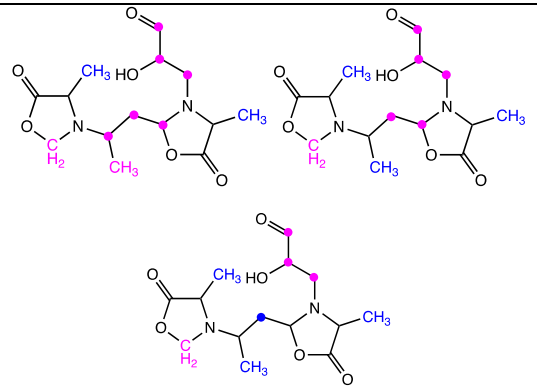	D
44	$C_{14}H_{23}N_2O_6$	315	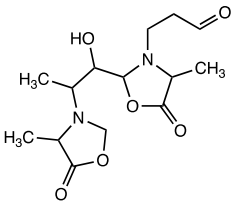	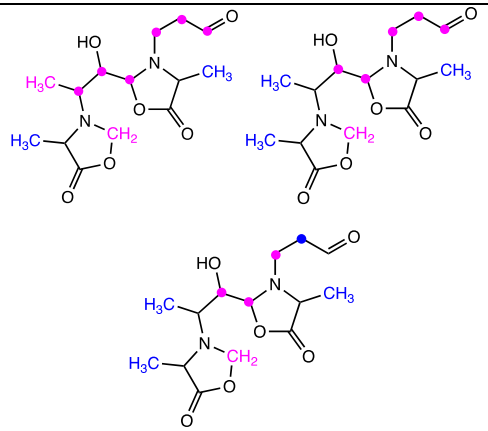	E
45	$C_{14}H_{23}N_2O_6$	315	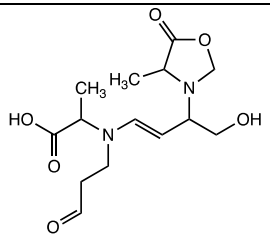	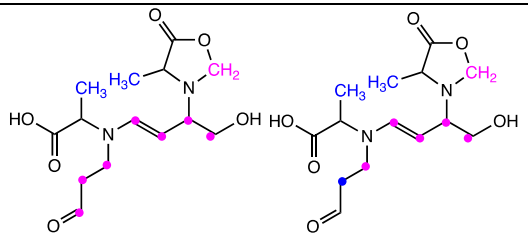	F

				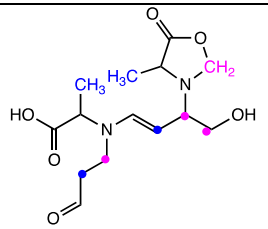	
46	$C_{14}H_{23}N_2O_6$	315	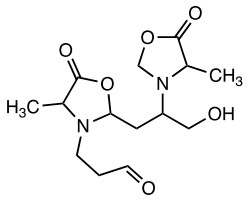	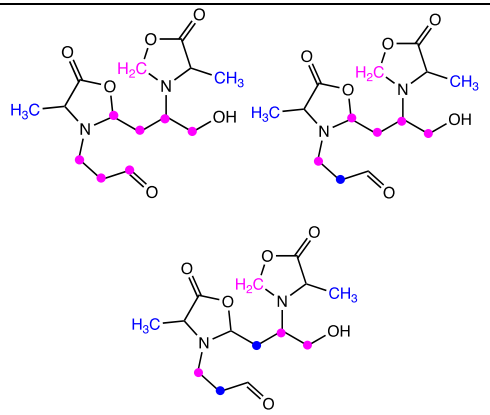	I
47	$C_{14}H_{23}N_2O_6$	315	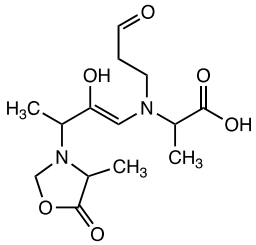	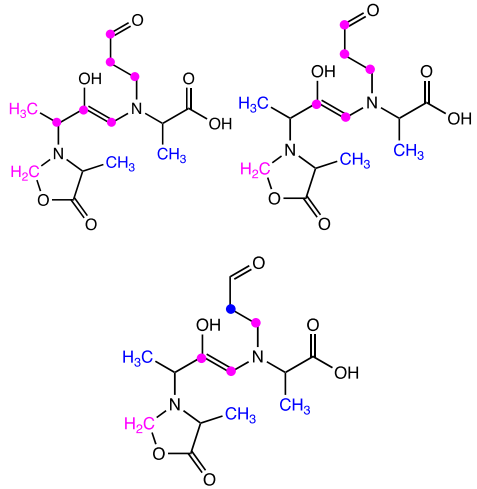	K

48	$C_{14}H_{22}N_3O_6$	328	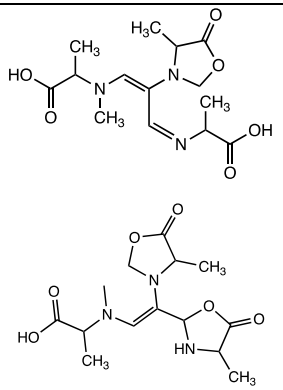	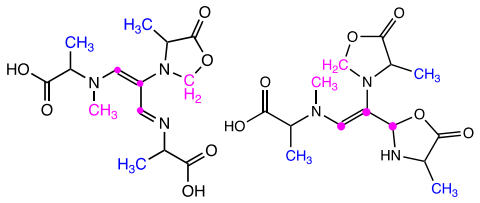	B
49	$C_{15}H_{25}N_2O_8$	361	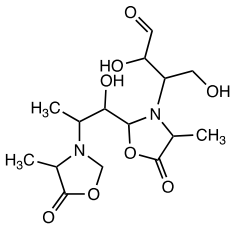	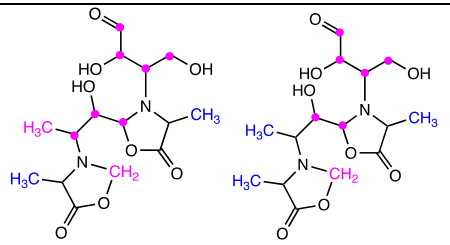	E
50	$C_{15}H_{25}N_2O_8$	361	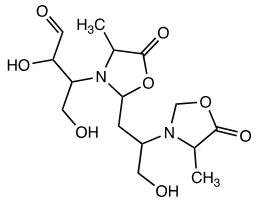	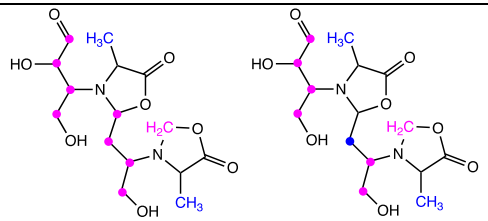	I
51	$C_{15}H_{24}N_2NaO_7$	367	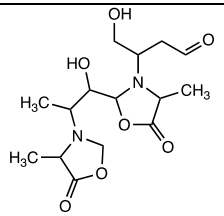	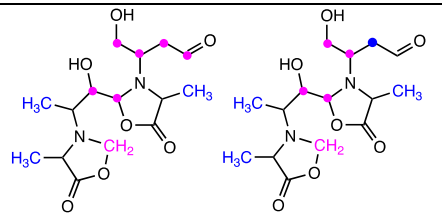	E

52	$C_{15}H_{24}N_2NaO_7$	367	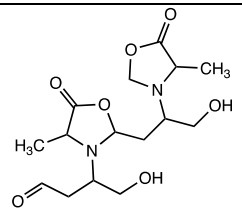	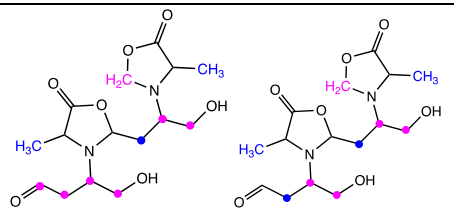	I
53	$C_{17}H_{28}N_3O_6$	370	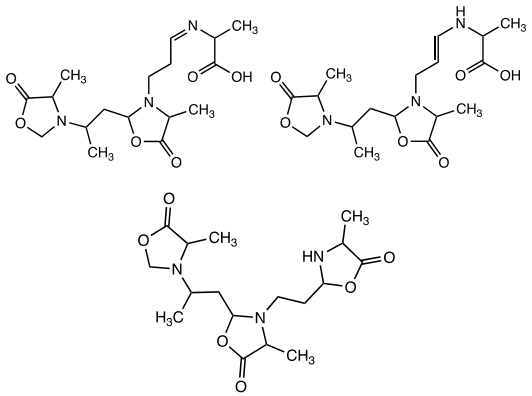	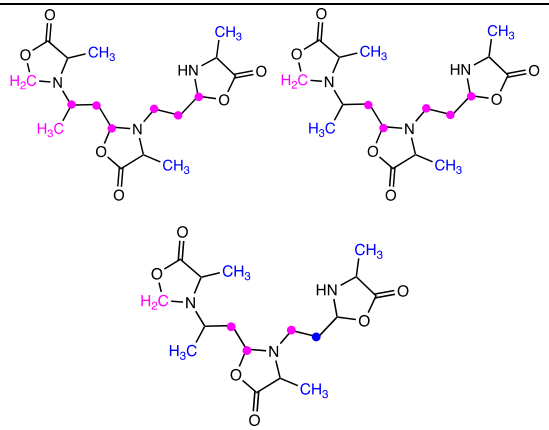	D
54	$C_{16}H_{24}N_3O_7$	370	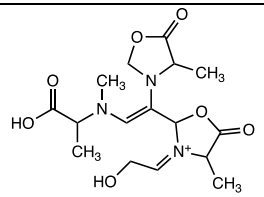	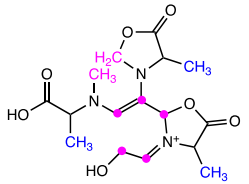	B
55	$C_{16}H_{24}N_3O_7$	370	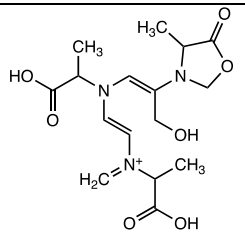	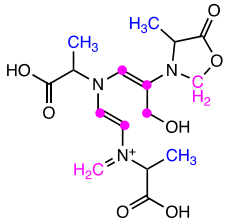	G

56	$C_{16}H_{24}N_3O_7$	370	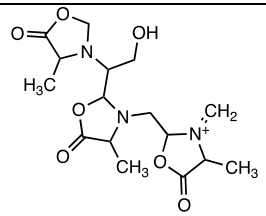	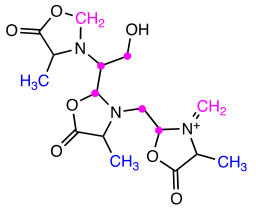	H
57	$C_{16}H_{24}N_3O_7$	370	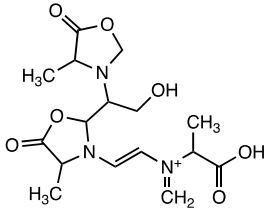	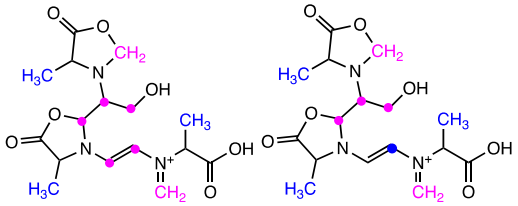	H
58	$C_{16}H_{24}N_3O_7$	370	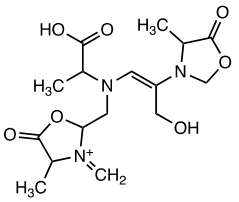	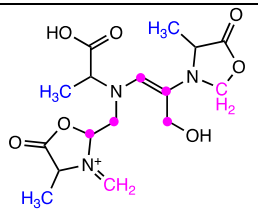	L

59	$C_{16}H_{26}N_3O_7$	372 410	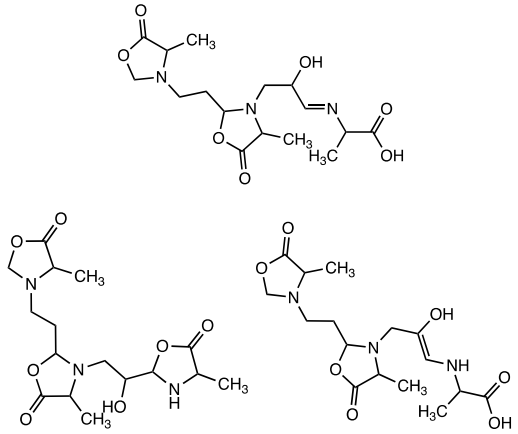	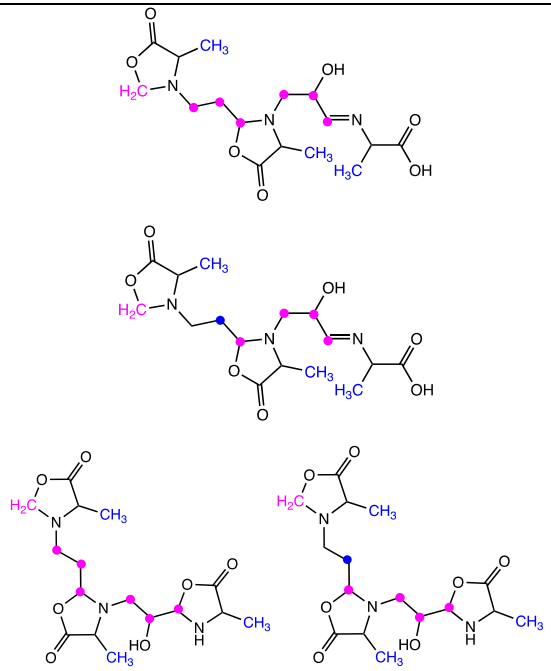	A
60	$C_{16}H_{26}N_3O_7$	372 410	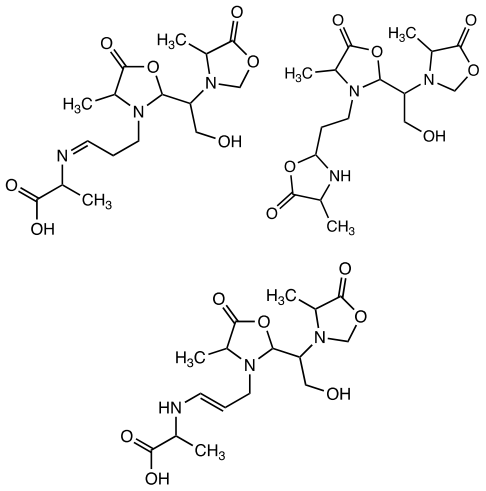	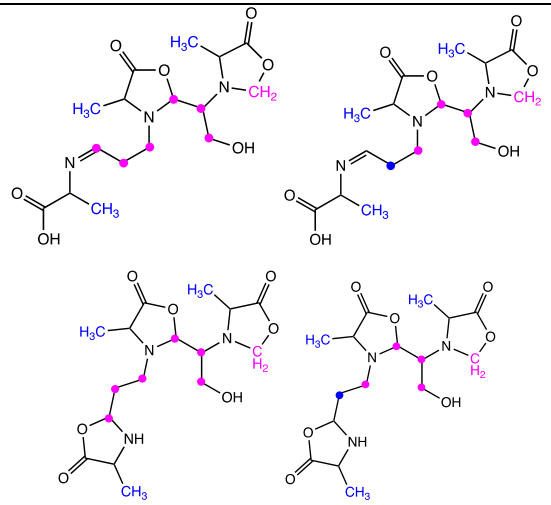	B

61	$C_{16}H_{26}N_3O_7$	372 410	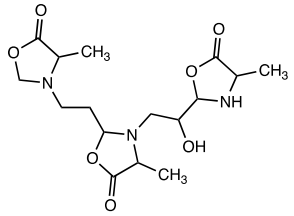	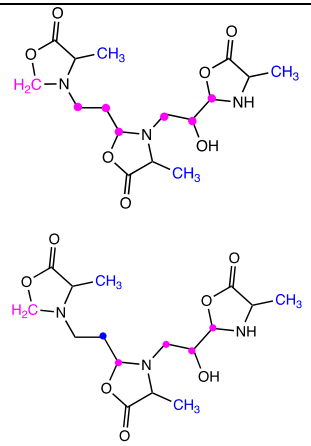	B
62	$C_{16}H_{26}N_3O_7$	372 410	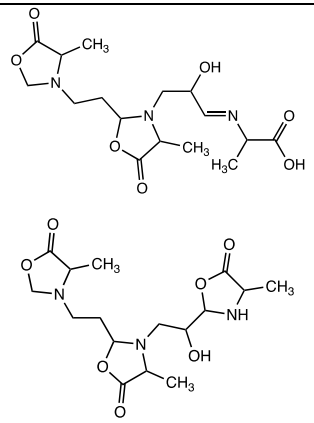	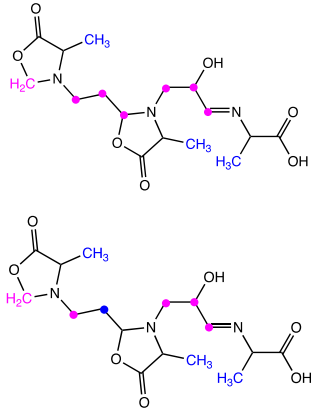	F

63	$C_{16}H_{26}N_3O_7$	372 410	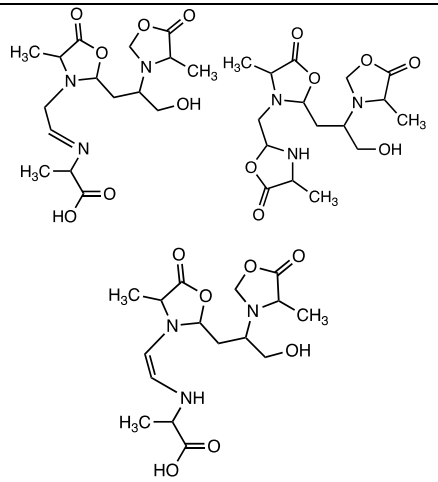	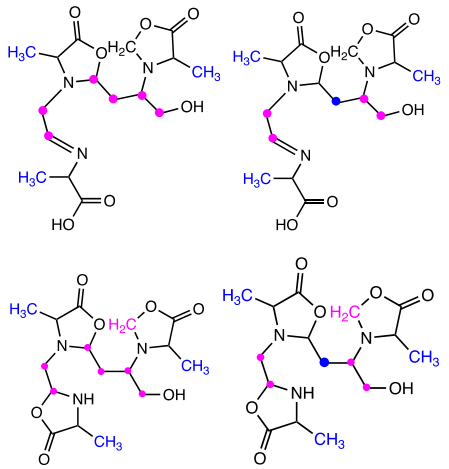	I
64	$C_{16}H_{26}N_3O_7$	410	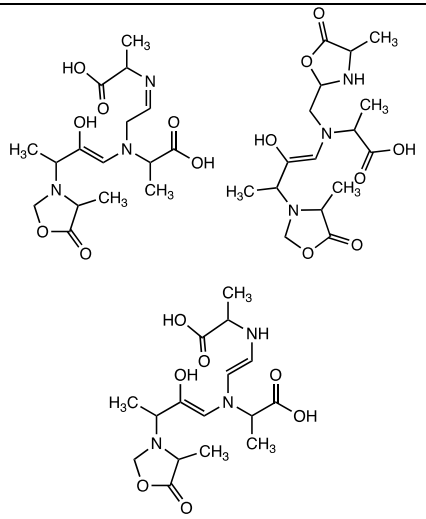	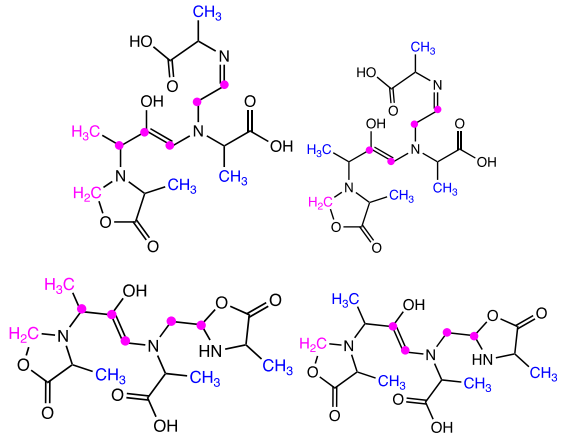	K

65	$C_{15}H_{23}N_3NaO_7$	380	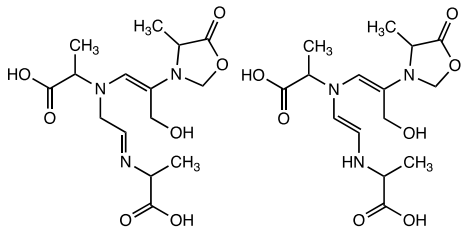	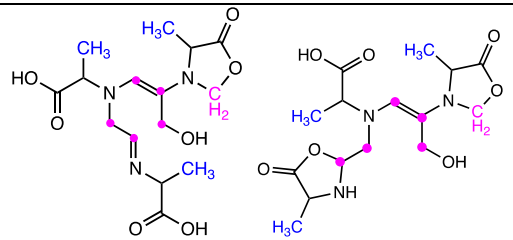	G
66	$C_{15}H_{23}N_3NaO_7$	380	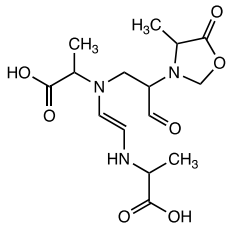	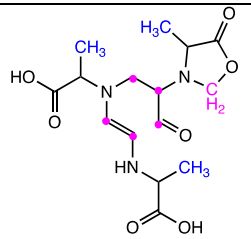	I
67	$C_{15}H_{23}N_3NaO_7$	380	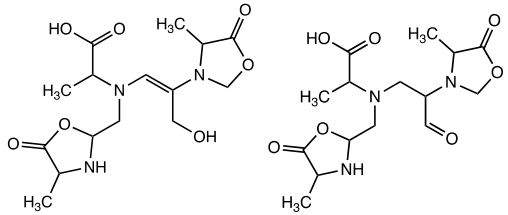	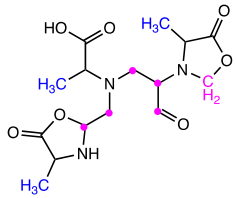	L
68	$C_{15}H_{23}N_3NaO_7$	380	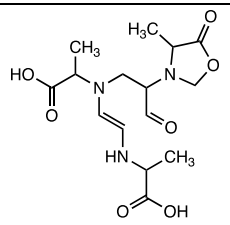	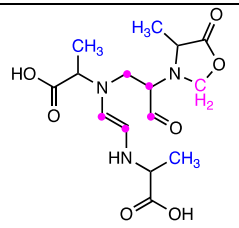	J

69	$C_{15}H_{23}N_3NaO_7$	380	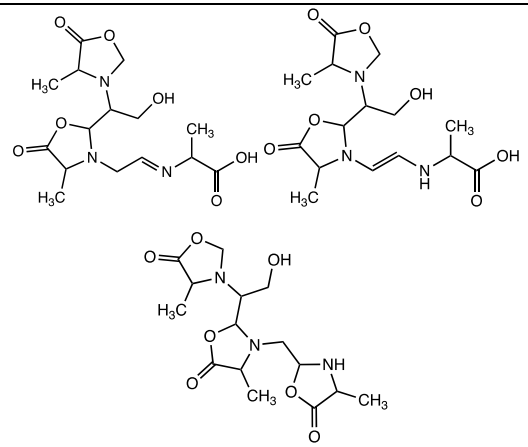	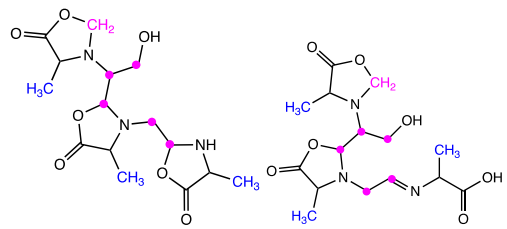	H
70	$C_{17}H_{28}N_3O_7$	386	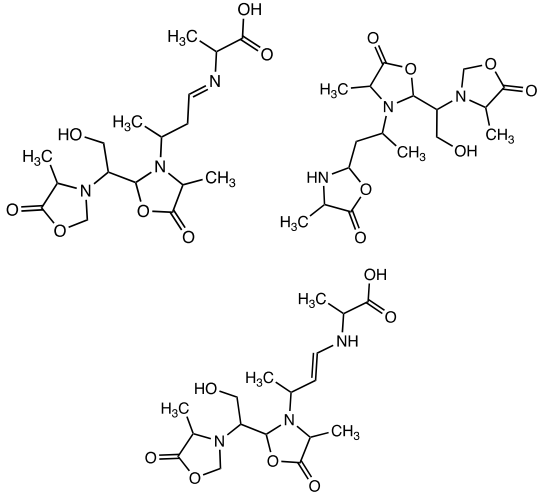	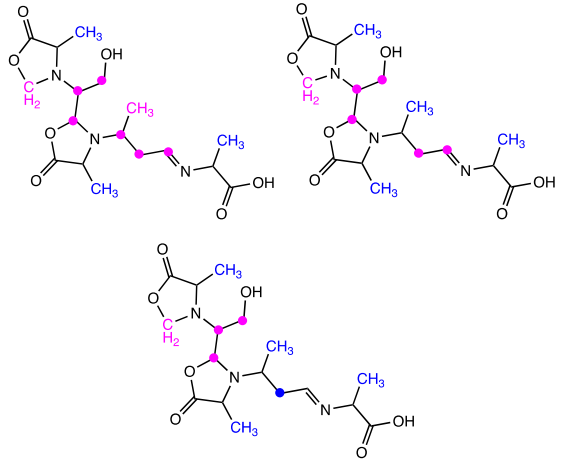	C

71	$C_{17}H_{28}N_3O_7$	386	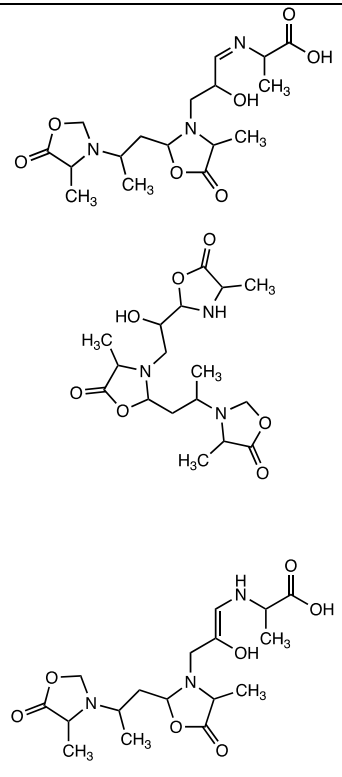	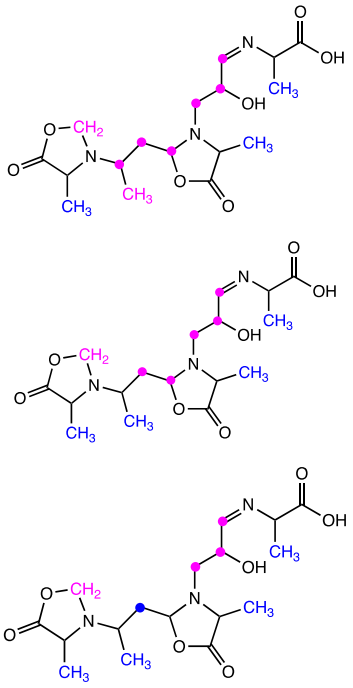	D

			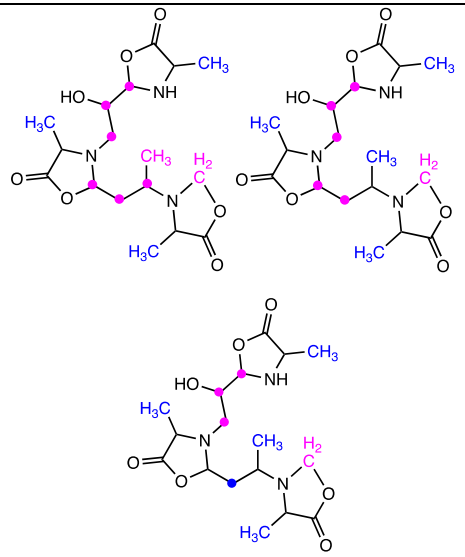		
72	$C_{17}H_{28}N_3O_7$	386	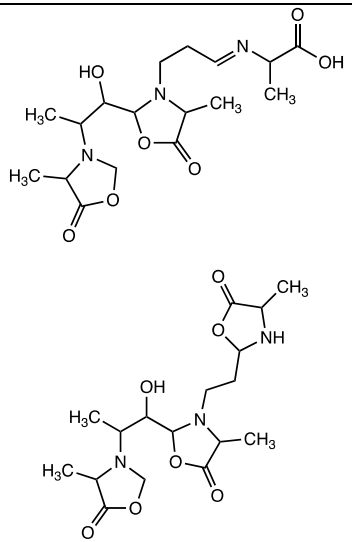	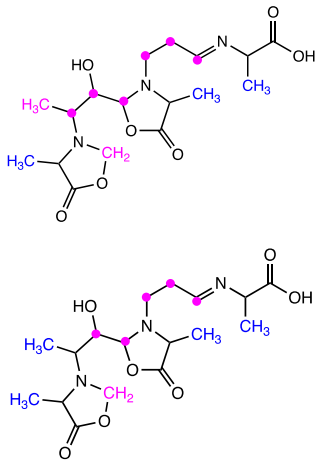	E

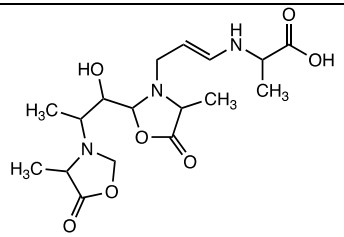

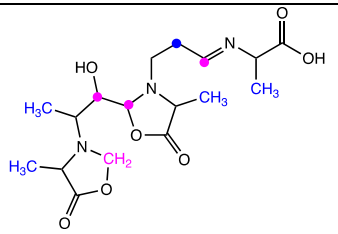

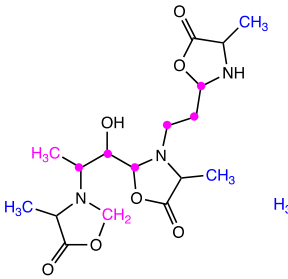

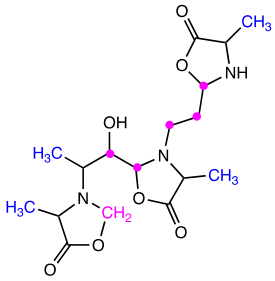

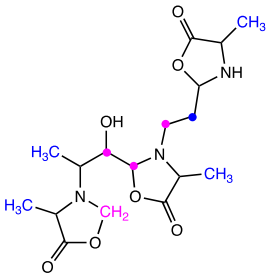

73	$C_{17}H_{28}N_3O_7$	386	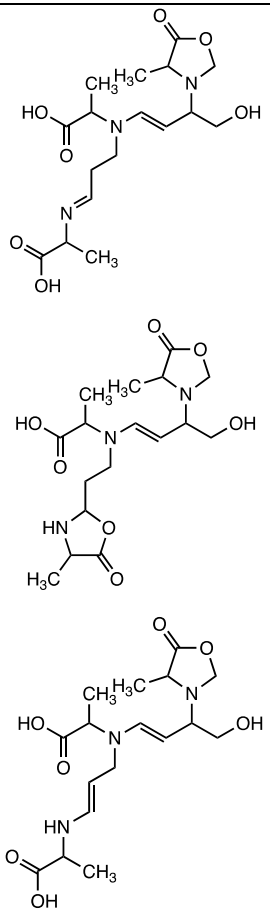	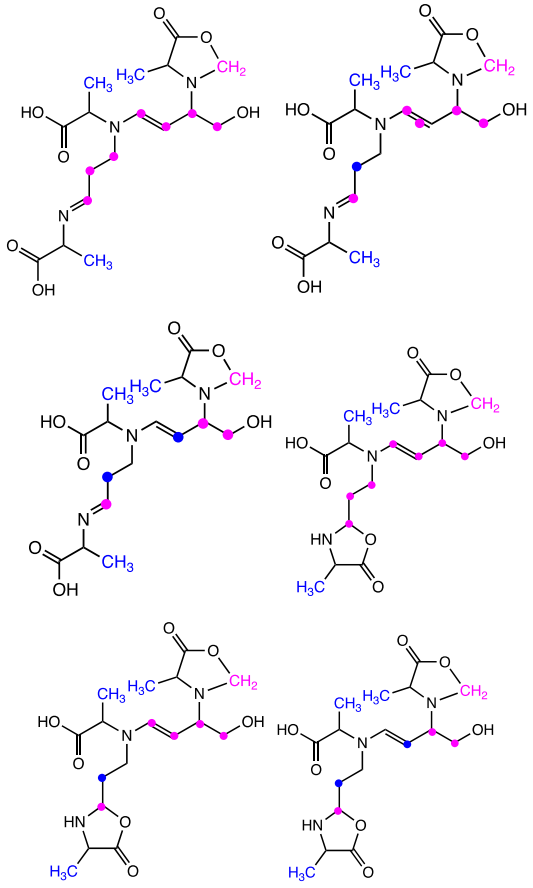	F

74	$C_{17}H_{28}N_3O_7$	386	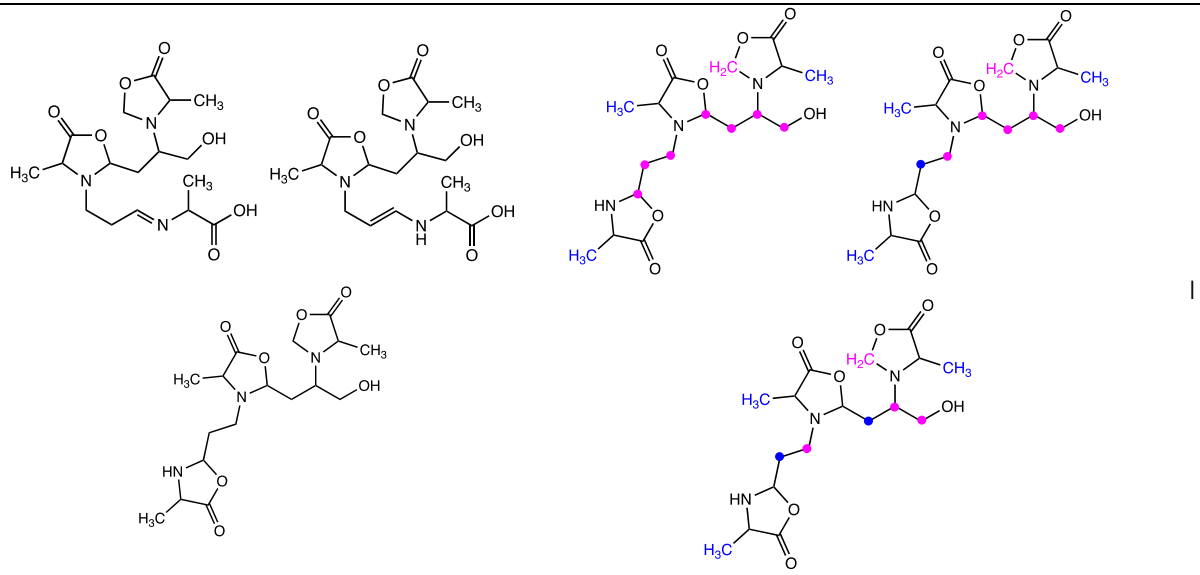	I

75	$C_{17}H_{28}N_3O_7$	386	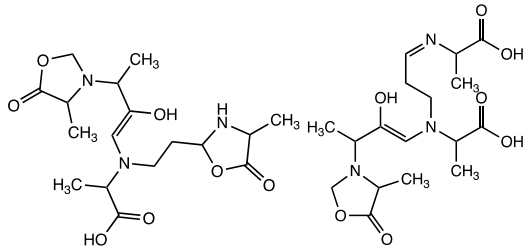	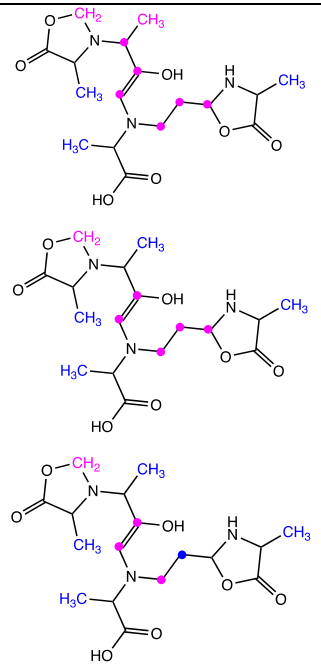	K
76	$C_{18}H_{28}N_3O_7$	398 436	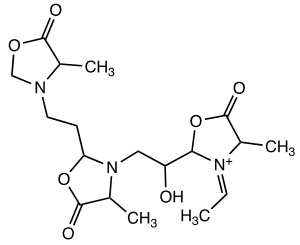	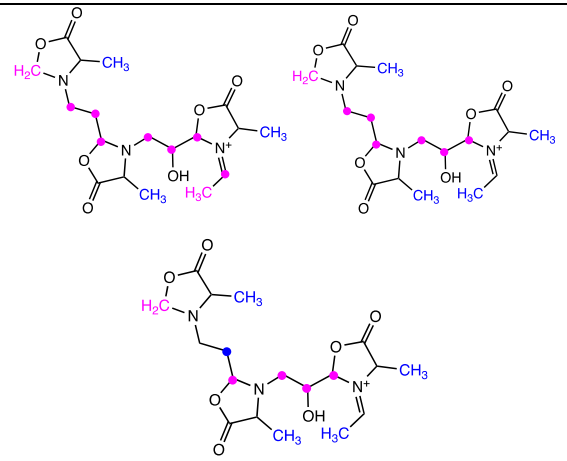	A

77	$C_{18}H_{28}N_3O_7$	398 436	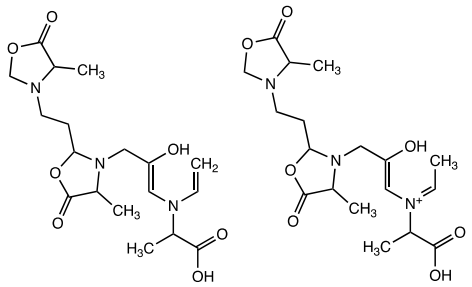	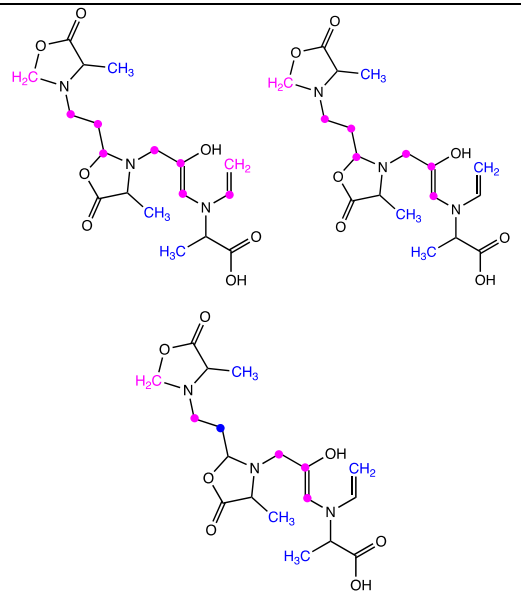	A
78	$C_{18}H_{28}N_3O_7$	398 436	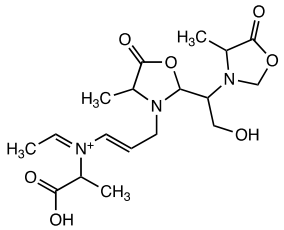	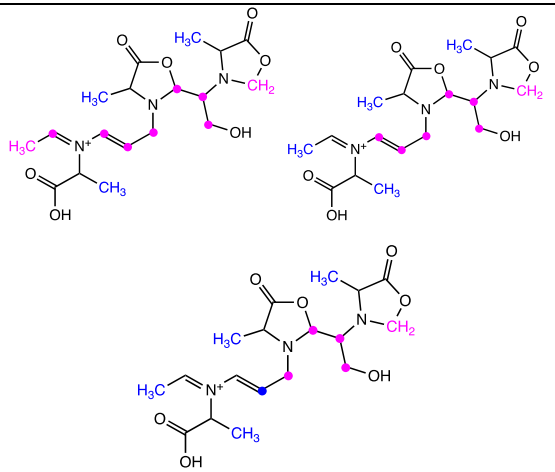	B

79	$C_{18}H_{28}N_3O_7$	398 436	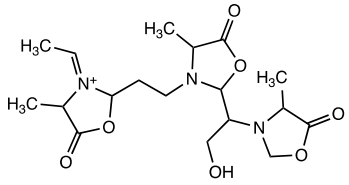	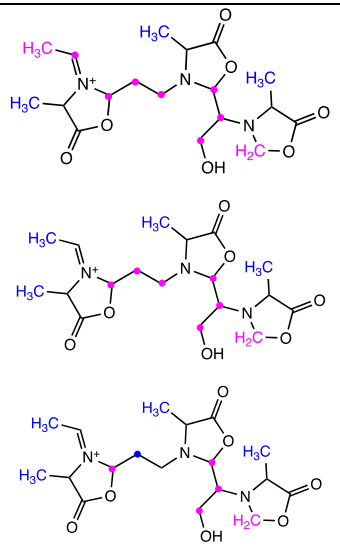	B
80	$C_{18}H_{28}N_3O_7$	398 436	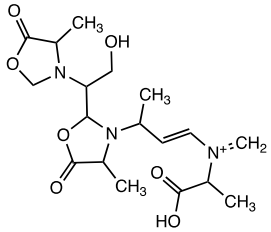	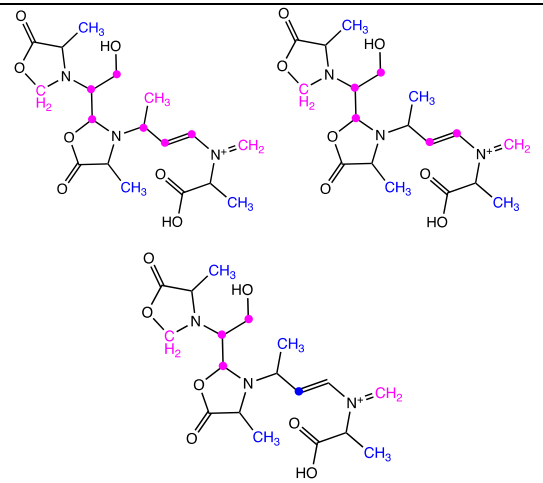	C

81	$C_{18}H_{28}N_3O_7$	398 436	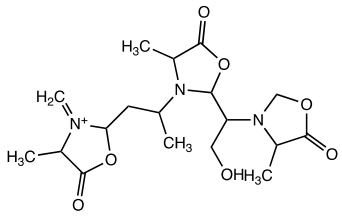	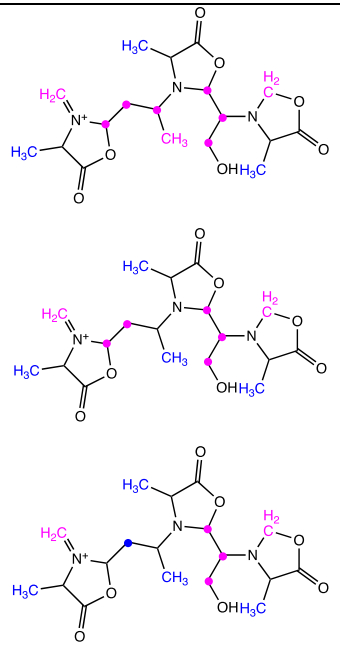	C

82	$C_{18}H_{28}N_3O_7$	398 436	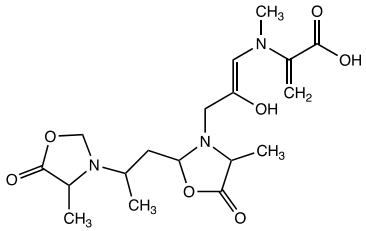	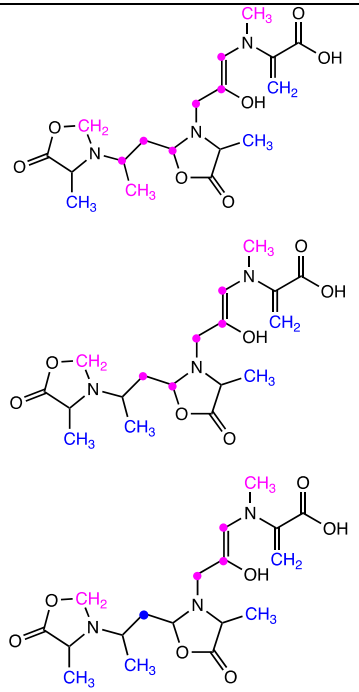	D

83	$C_{18}H_{28}N_3O_7$	398 436	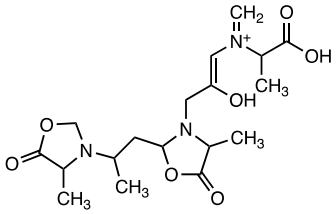	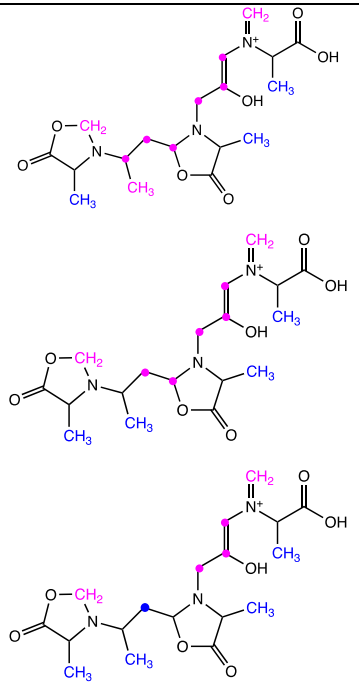	D

84	$C_{18}H_{28}N_3O_7$	398 436	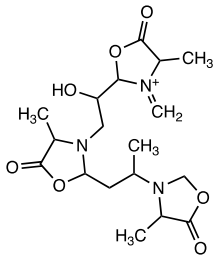	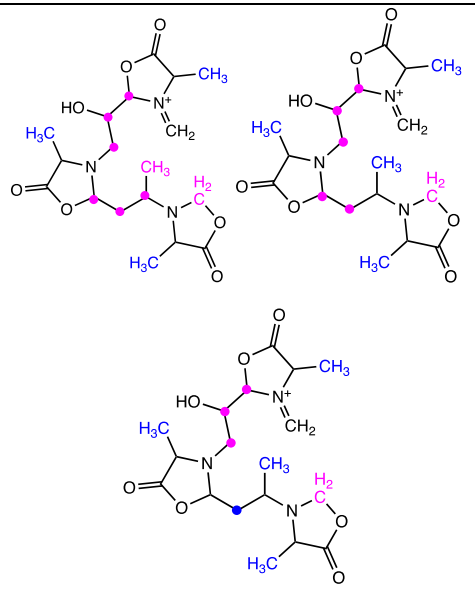	D
85	$C_{18}H_{28}N_3O_7$	398 436	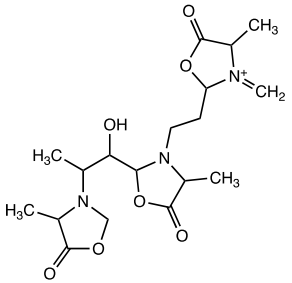	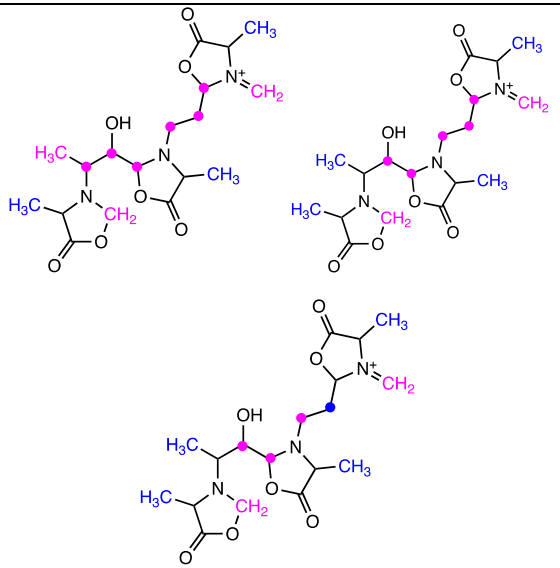	E

86	$C_{18}H_{28}N_3O_7$	398 436	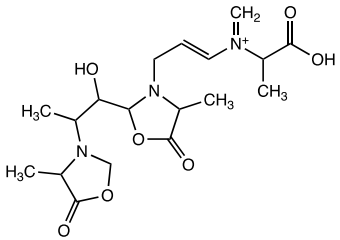	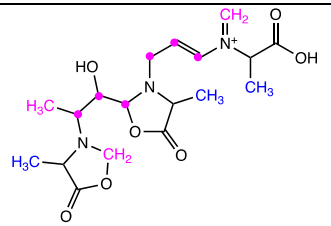 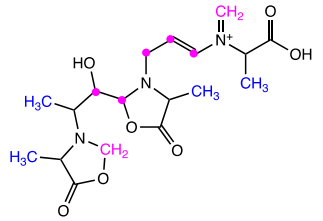 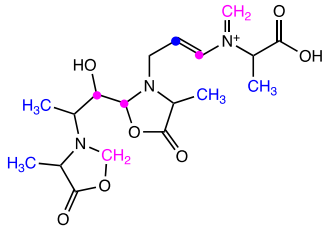	E

87	$C_{18}H_{28}N_3O_7$	398 436	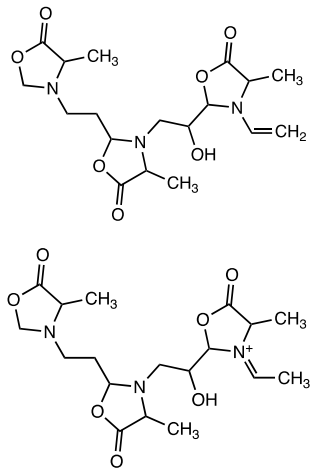	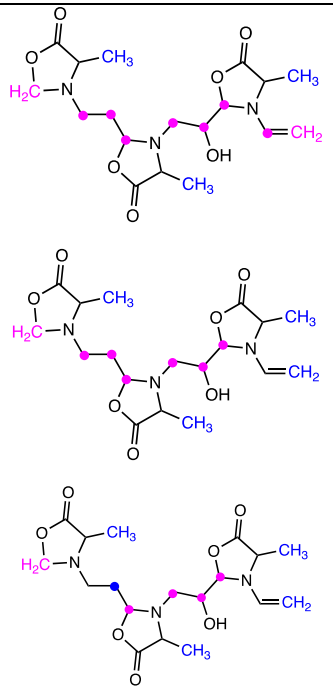	F

88	$C_{18}H_{28}N_3O_7$	398 436	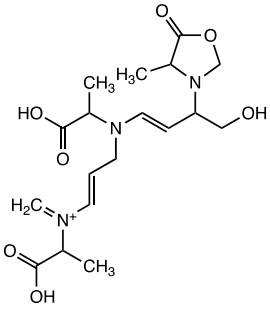	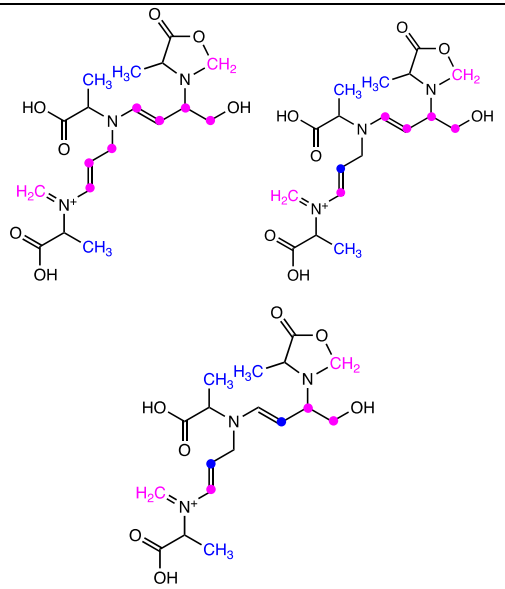	F
89	$C_{18}H_{28}N_3O_7$	398 436	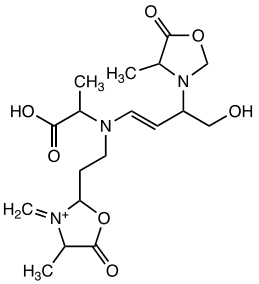	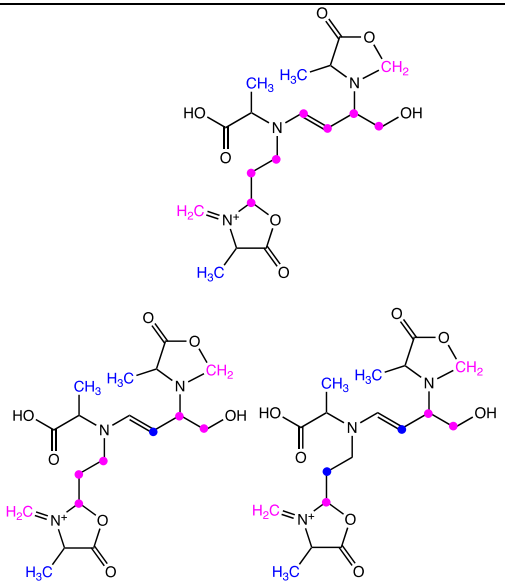	F

90	$C_{18}H_{28}N_3O_7$	398 436	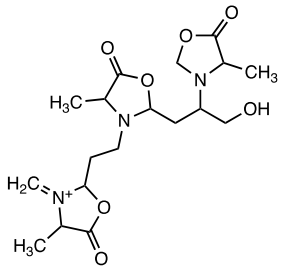	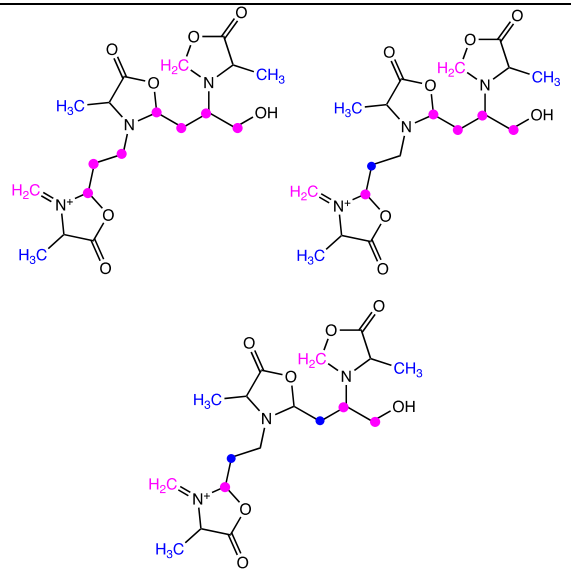	I
91	$C_{18}H_{28}N_3O_7$	398 436	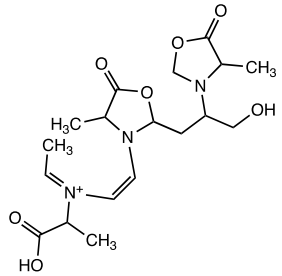	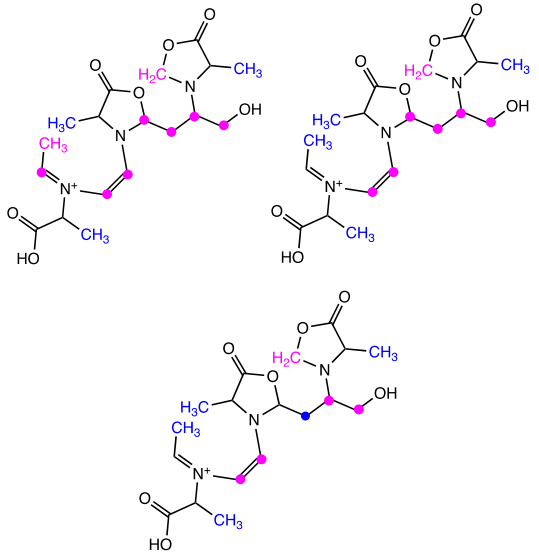	I

92	$C_{18}H_{28}N_3O_7$	398 436	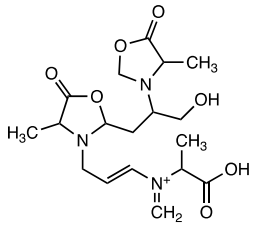	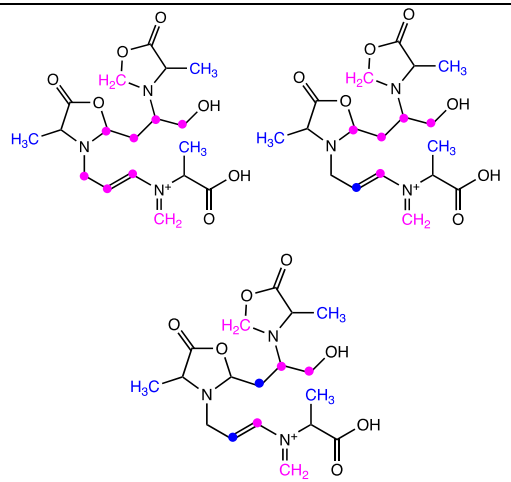	I
93	$C_{18}H_{28}N_3O_7$	398 436	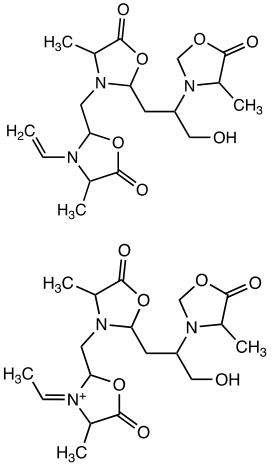	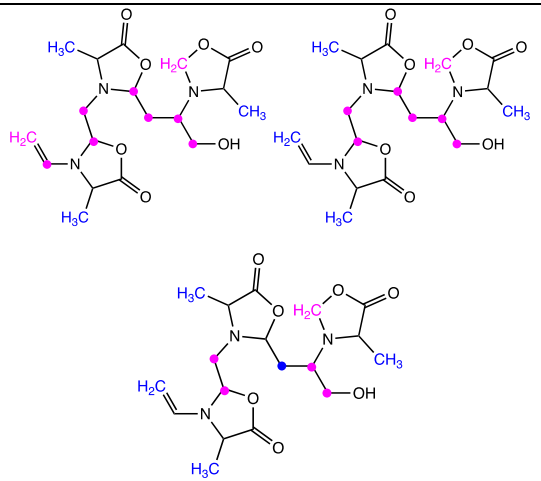	I

94	$C_{18}H_{28}N_3O_7$	398 436	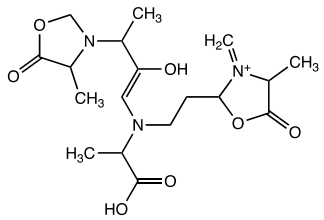	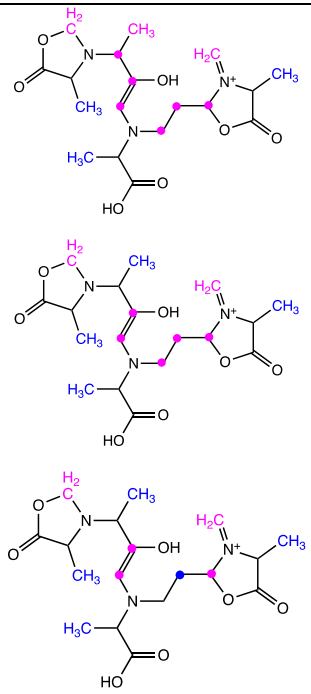	K

95	$C_{18}H_{28}N_3O_7$	398 436	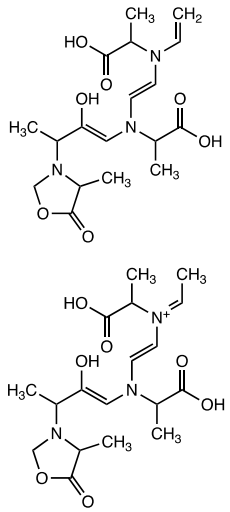	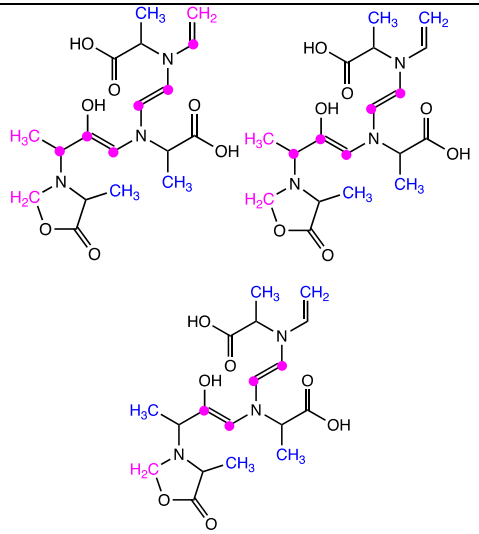	K
96	$C_{18}H_{28}N_3O_7$	398 436	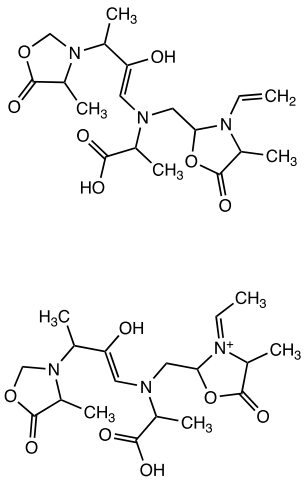	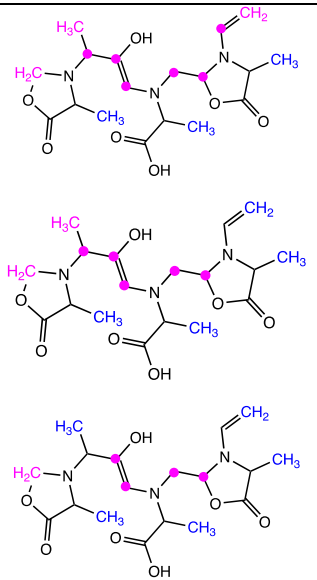	K

97	$C_{17}H_{26}N_3O_8$	400	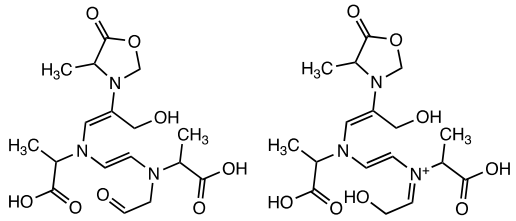	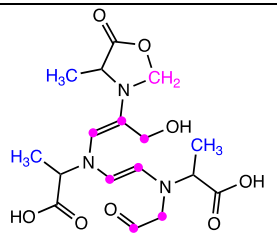	G
98	$C_{17}H_{26}N_3O_8$	400	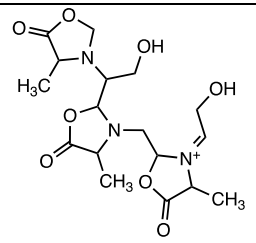	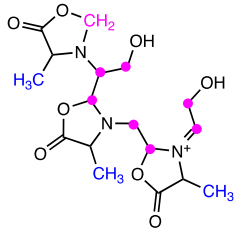	H
99	$C_{17}H_{26}N_3O_8$	400	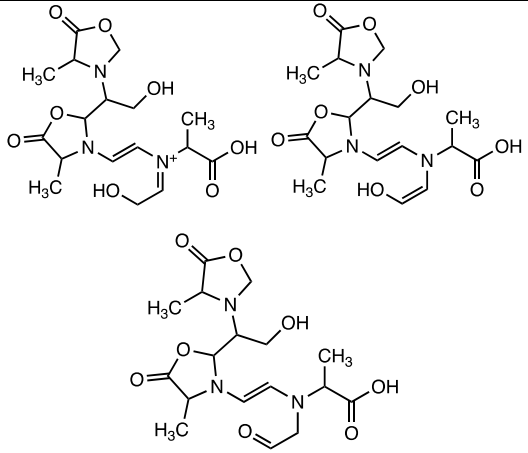	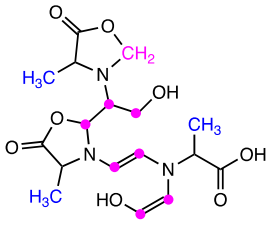	H

100		400	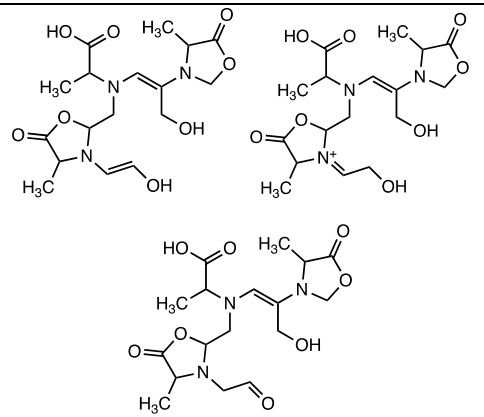	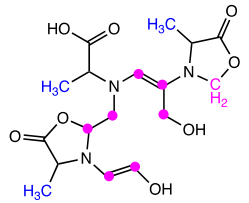	L
101	$C_{18}H_{28}N_3O_9$	430	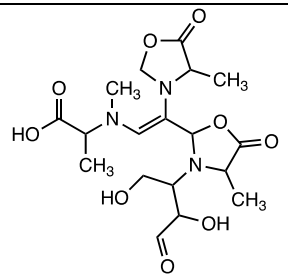	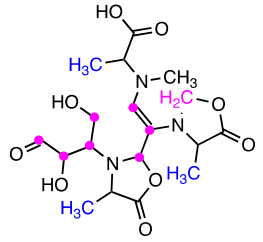	B
102	$C_{18}H_{28}N_3O_9$	430	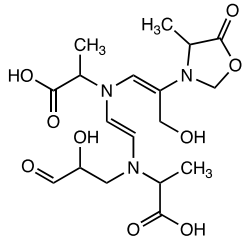	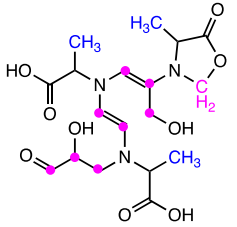	G

103	$C_{18}H_{28}N_3O_9$	430	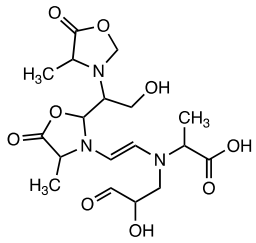	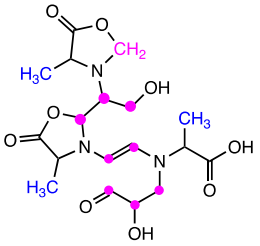	H
104	$C_{18}H_{28}N_3O_9$	430	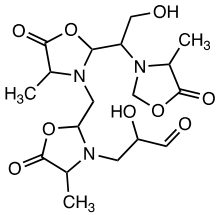	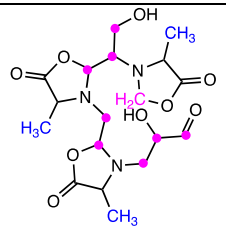	H
105	$C_{18}H_{28}N_3O_9$	430	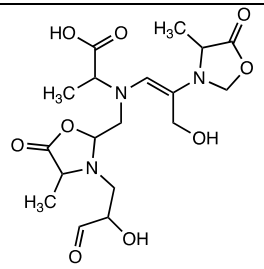	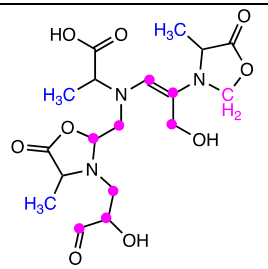	L

108	$C_{18}H_{28}N_4NaO_8$	451	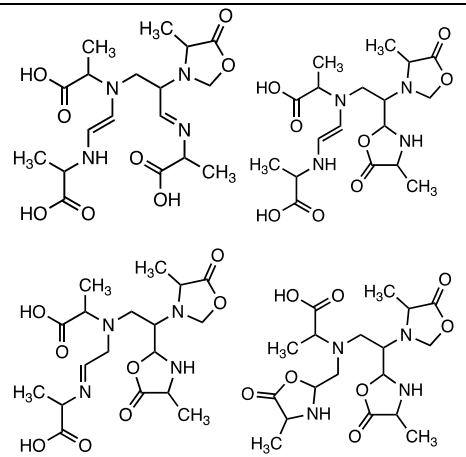	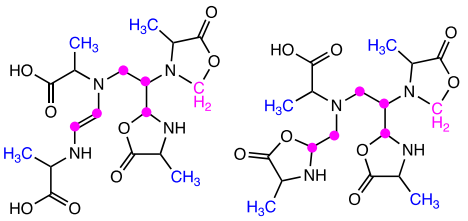	J
109	$C_{18}H_{28}N_4NaO_8$	451	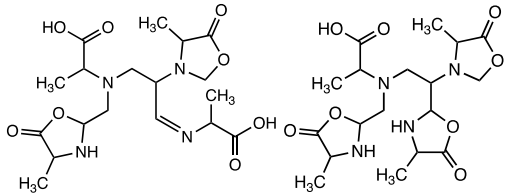	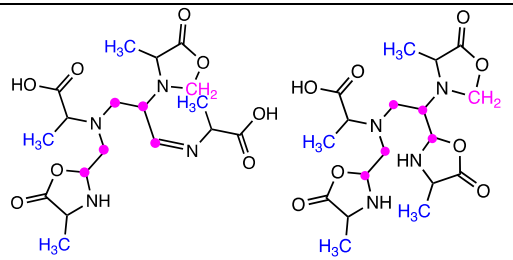	L
110	$C_{18}H_{29}KN_3O_8$	454	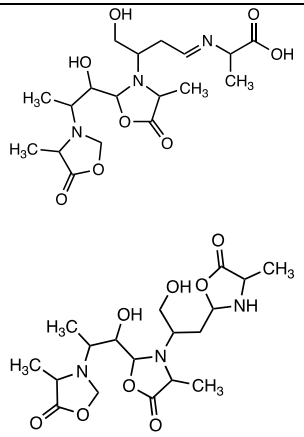	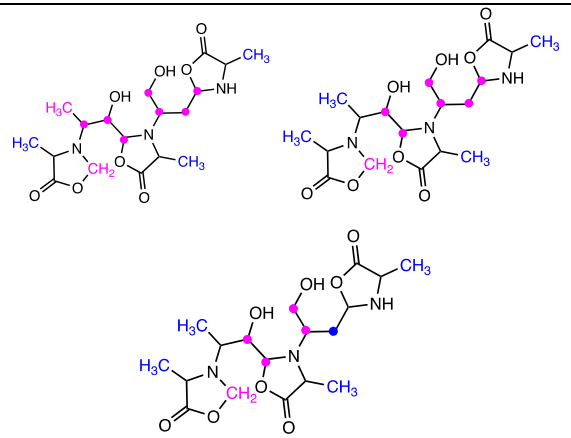	E

111	$C_{18}H_{29}KN_3O_8$	454	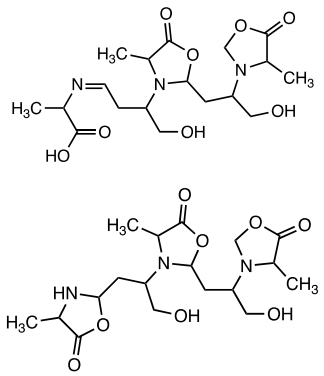	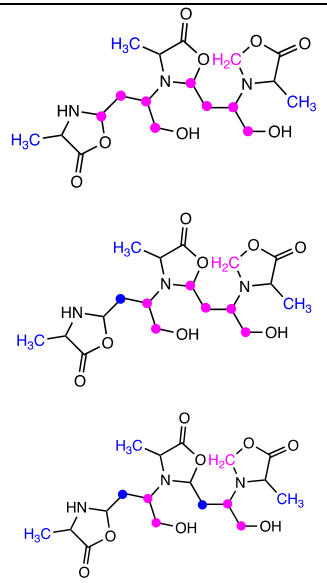	I
112	$C_{19}H_{30}N_3O_{10}$	460	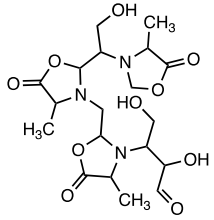	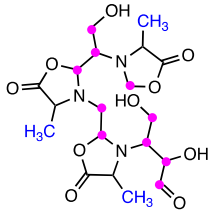	H

113	$C_{20}H_{31}N_3NaO_8$	464	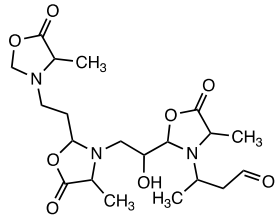	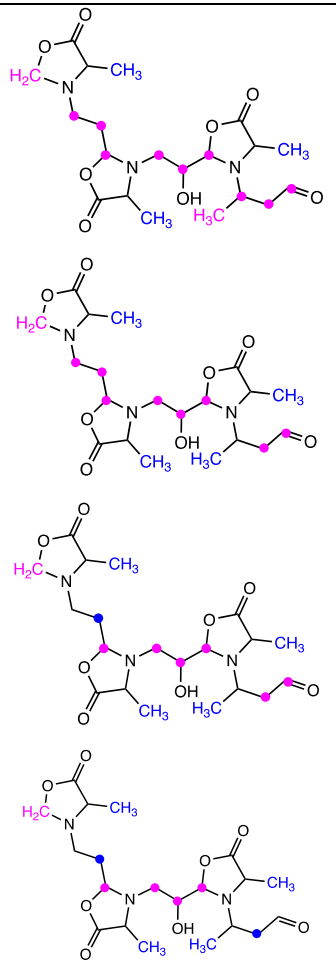	A

114	$C_{20}H_{31}N_3NaO_8$	464	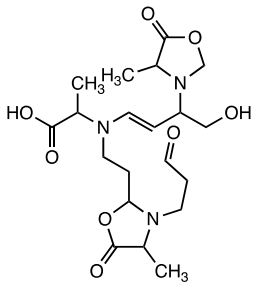	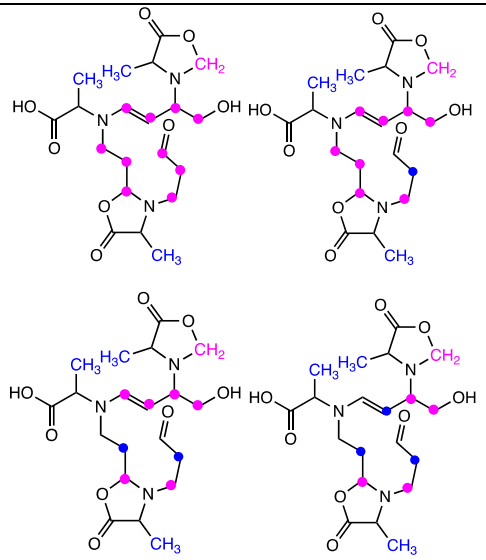	F

115	$C_{20}H_{31}N_3NaO_8$	464	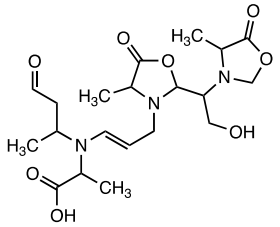	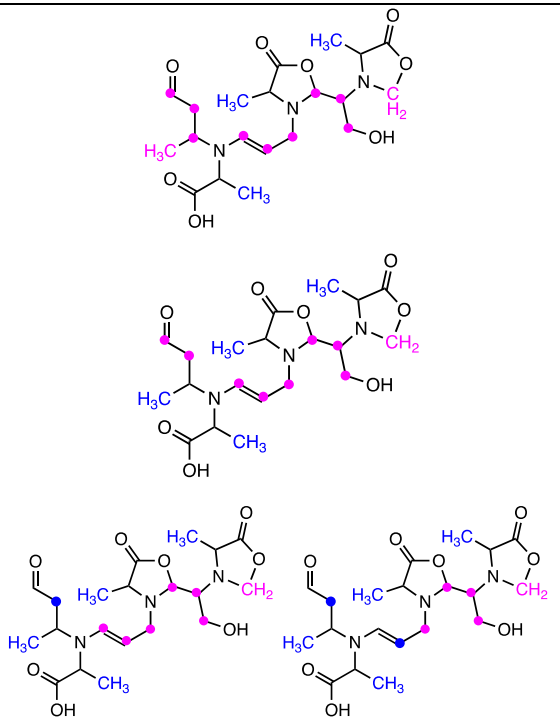	B

116	$C_{20}H_{31}N_3NaO_8$	464	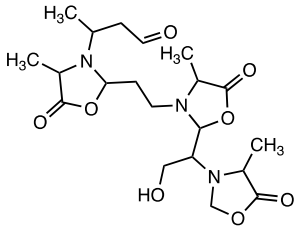	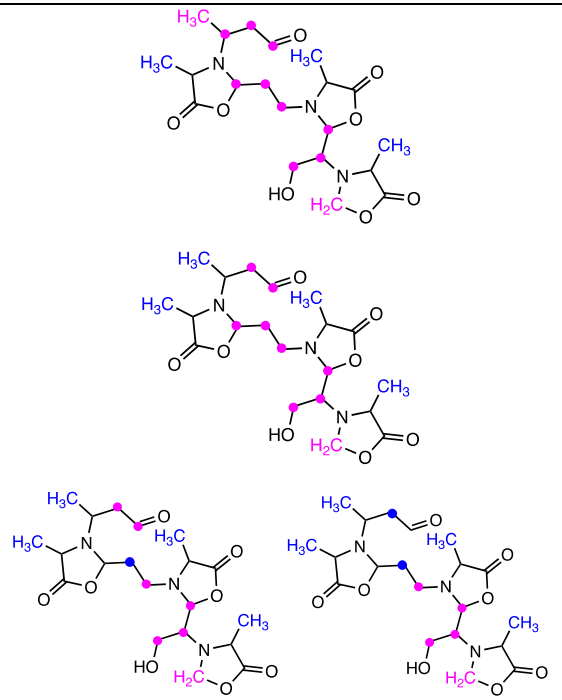	B
117	$C_{20}H_{31}N_3NaO_8$	464	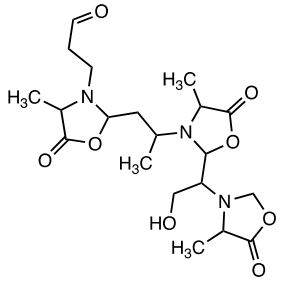	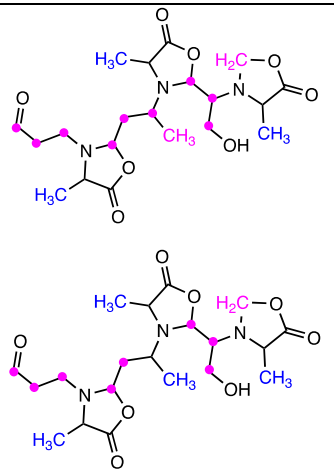	C

			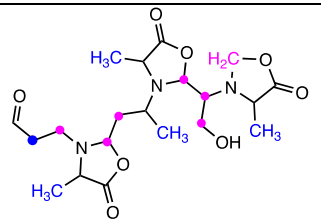		
			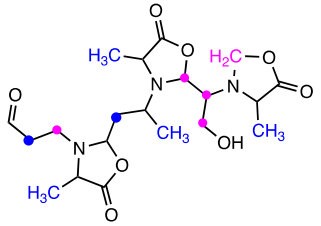		
118	$C_{20}H_{31}N_3NaO_8$	464	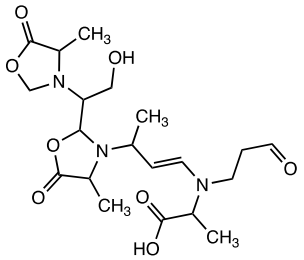	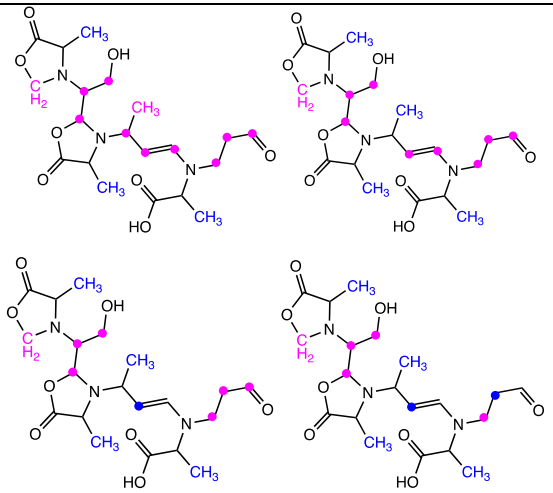	C

119	$C_{20}H_{31}N_3NaO_8$	464	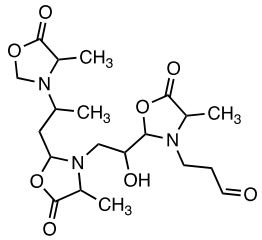	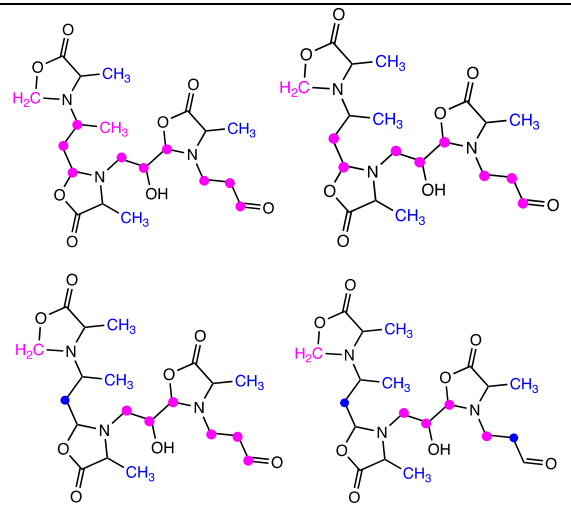	D
120	$C_{20}H_{31}N_3NaO_8$	464	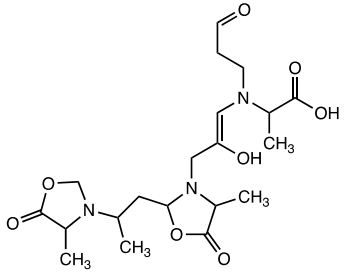	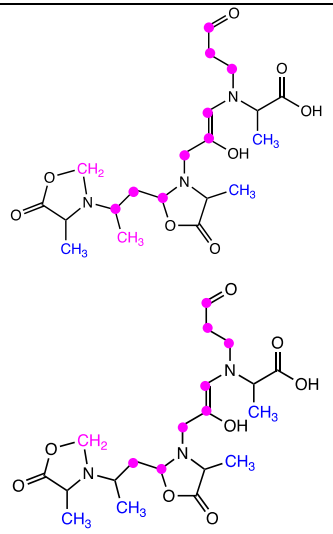	D

			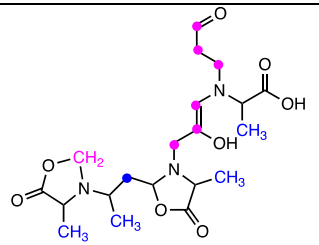 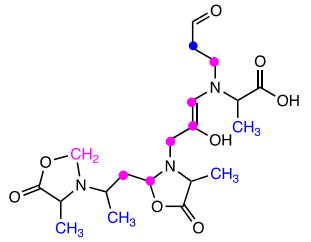	
121	$C_{20}H_{31}N_3NaO_8$	464	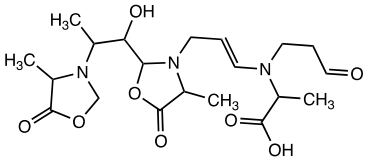	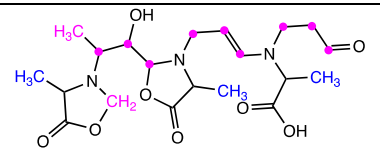 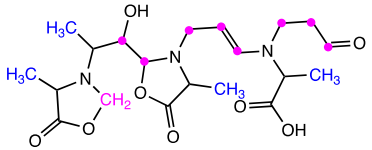 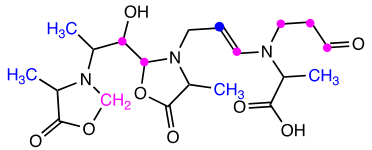 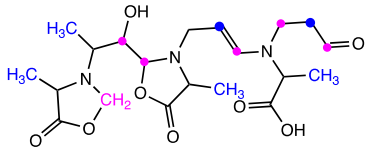 E

122	$C_{20}H_{31}N_3NaO_8$	464	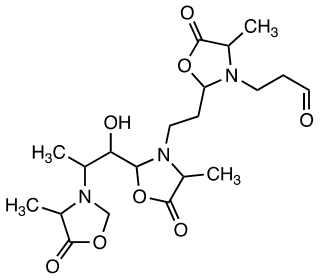	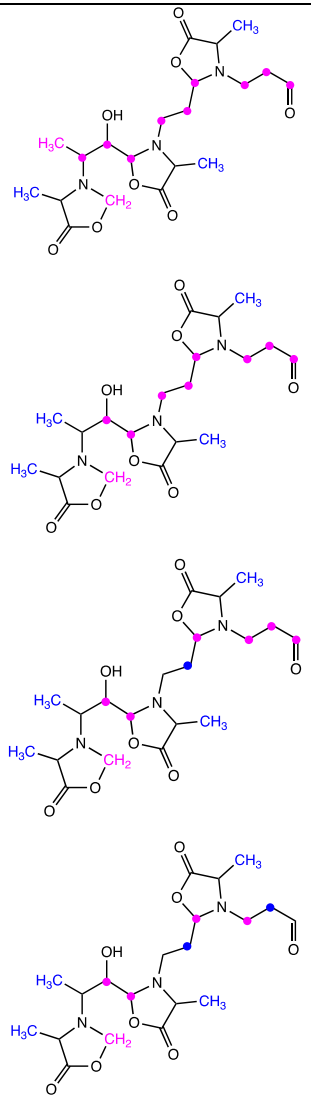	E

123	$C_{20}H_{31}N_3NaO_8$	464	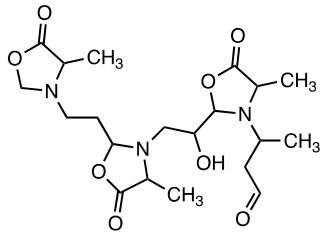	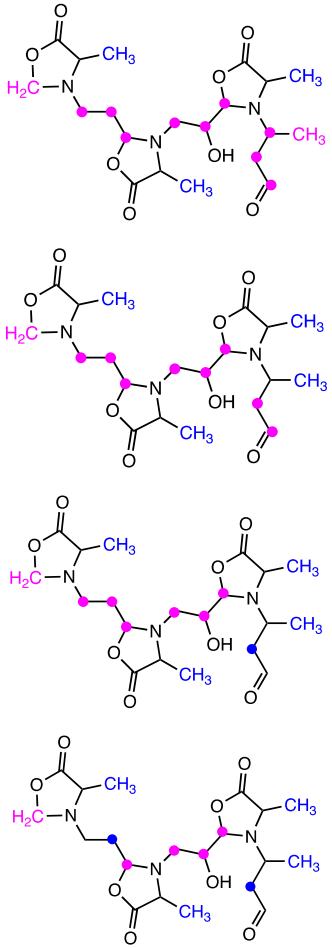	F

124	$C_{20}H_{31}N_3NaO_8$	464	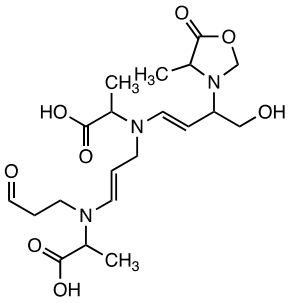	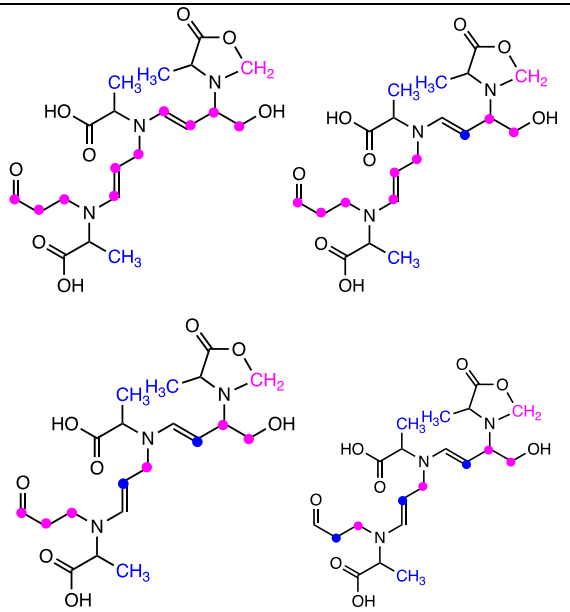	F
125	$C_{20}H_{31}N_3NaO_8$	464	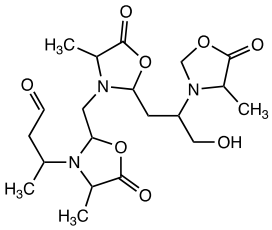	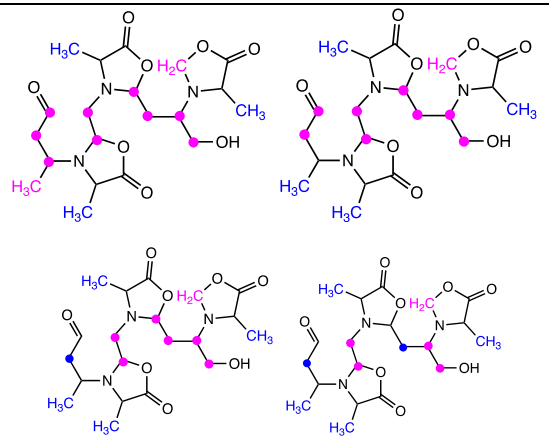	I

126	$C_{20}H_{31}N_3NaO_8$	464	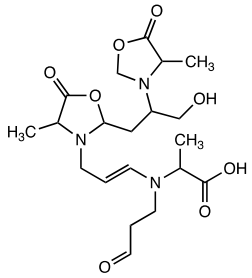	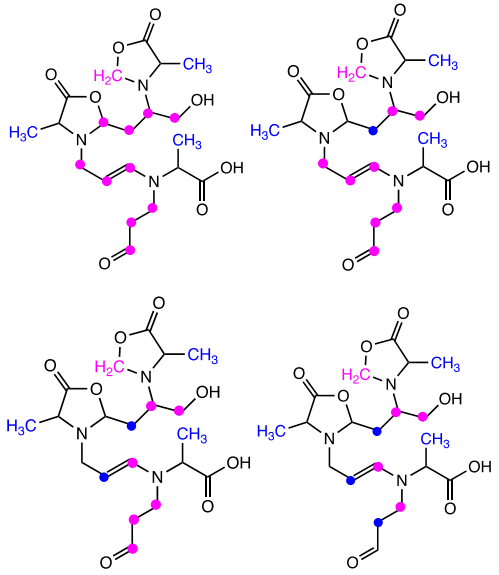	I
127	$C_{20}H_{31}N_3NaO_8$	464	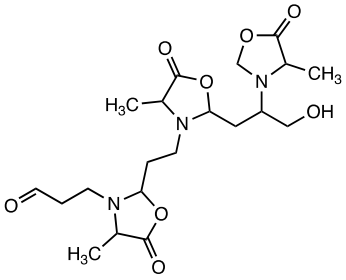	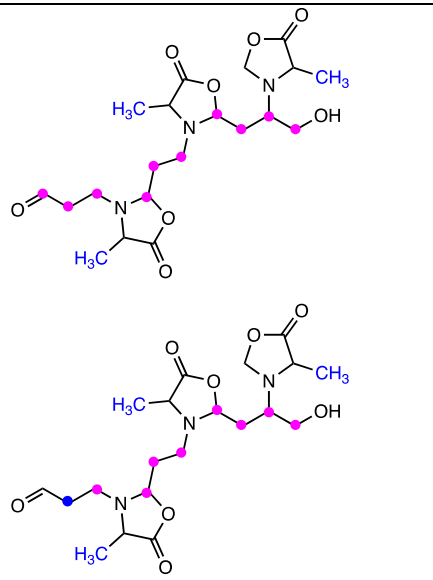	I

				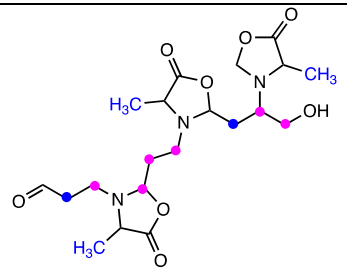 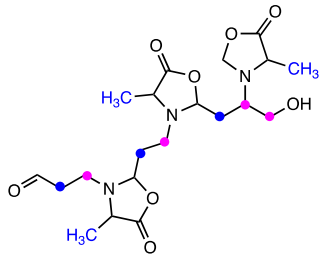	
128	$C_{20}H_{31}N_3NaO_8$	464	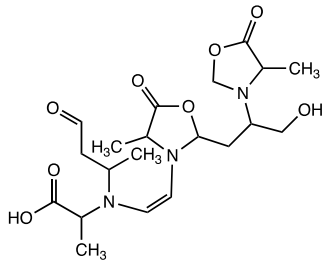	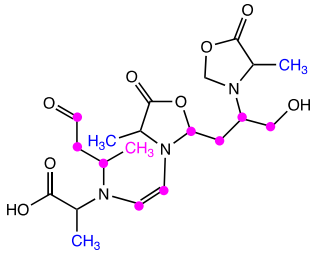 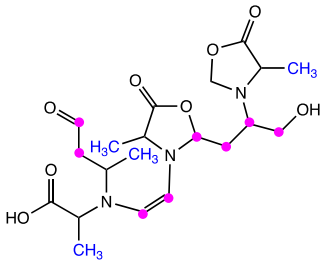	I

				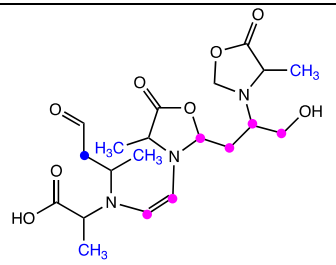 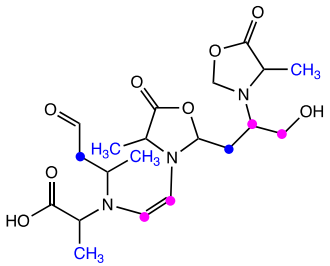	
129	$C_{20}H_{31}N_3NaO_8$	464	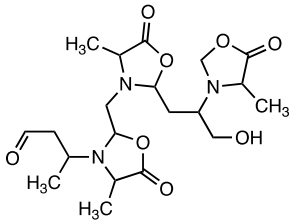	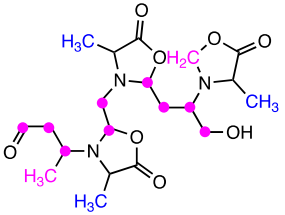 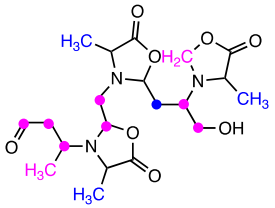	I

			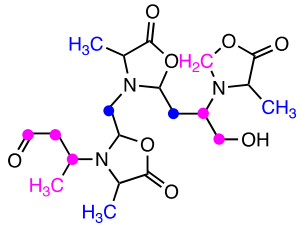 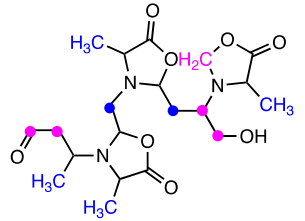		
130	$C_{20}H_{31}N_3NaO_8$	464	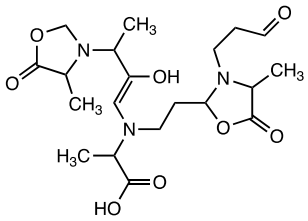	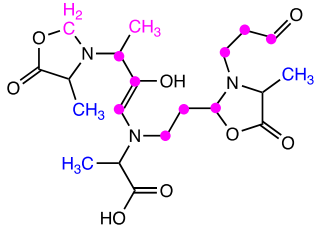 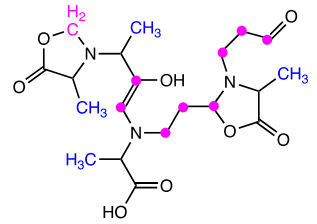	K

				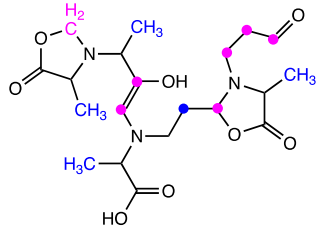 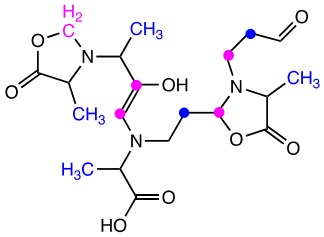	
131	$C_{20}H_{31}N_3NaO_8$	464	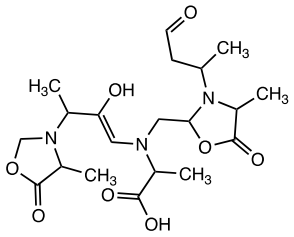	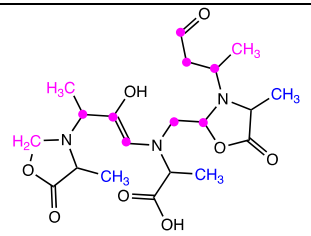 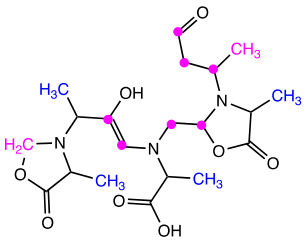	K

			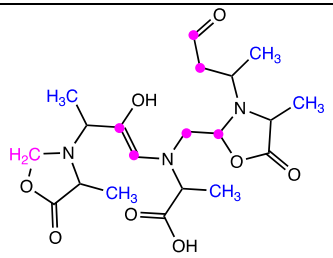 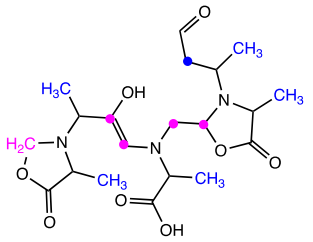		
132	$C_{20}H_{31}N_3NaO_8$	464	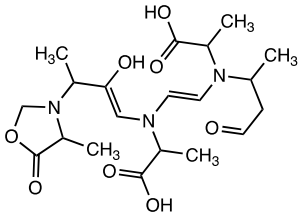	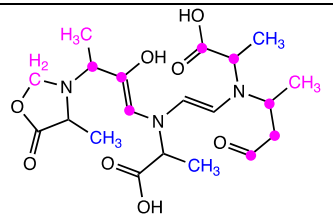 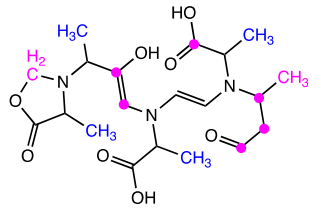	K

				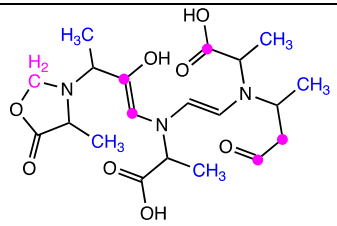 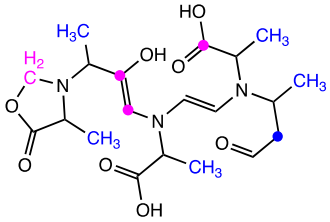	
133	$C_{20}H_{30}N_4NaO_9$	493	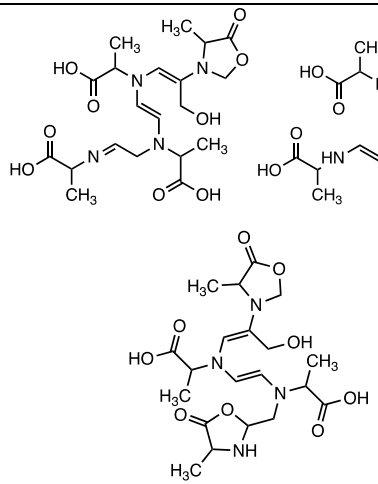	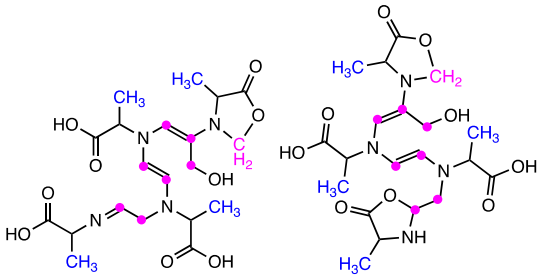	G

134	$C_{20}H_{30}N_4NaO_9$	493	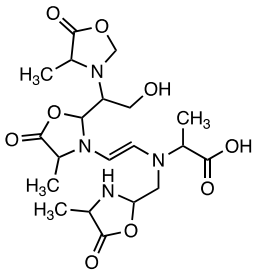	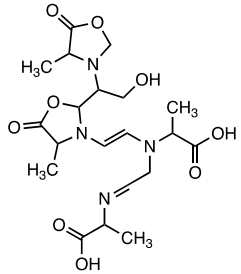	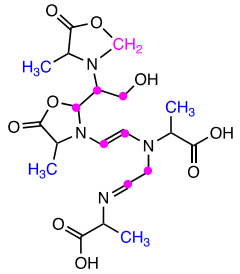	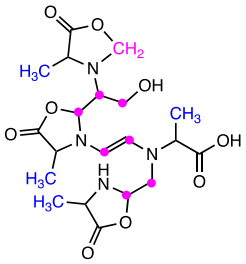	H
135	$C_{20}H_{30}N_4NaO_9$	493	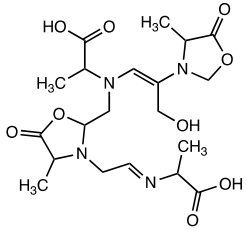	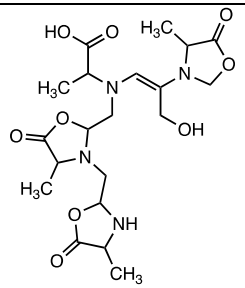	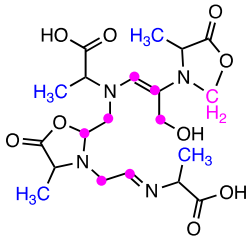	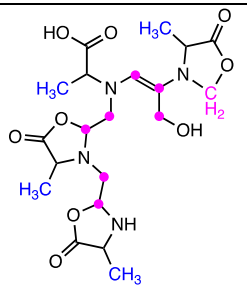	L
136	$C_{22}H_{33}N_4O_9$	497 519	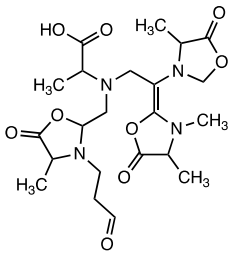	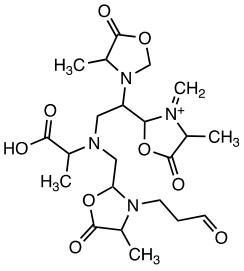	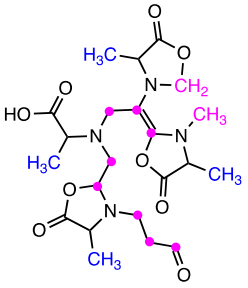	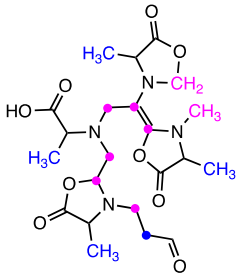	J

137		497 519	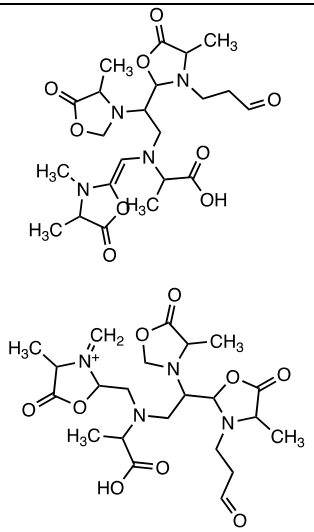	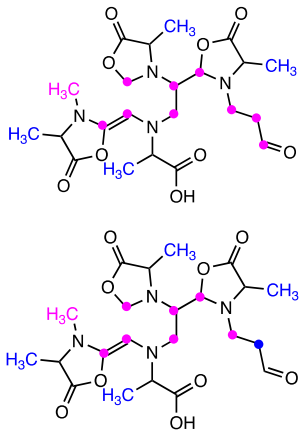	L
138	$C_{22}H_{35}N_4O_9$	499	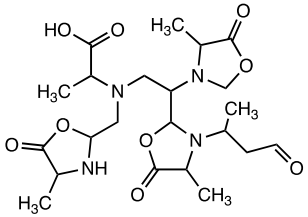	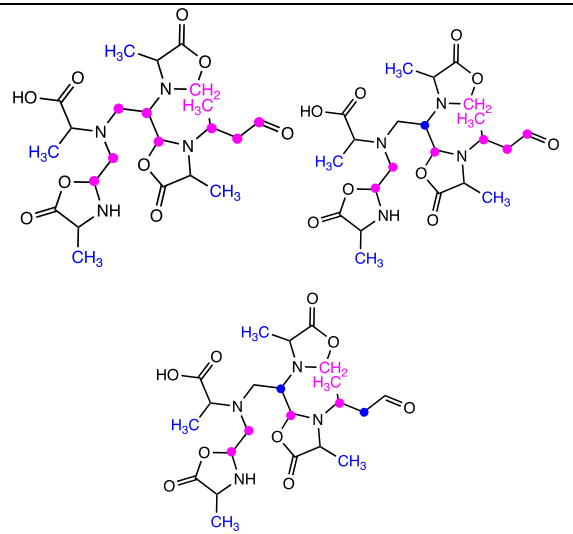	J

139	499	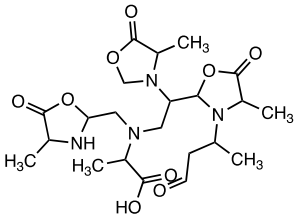	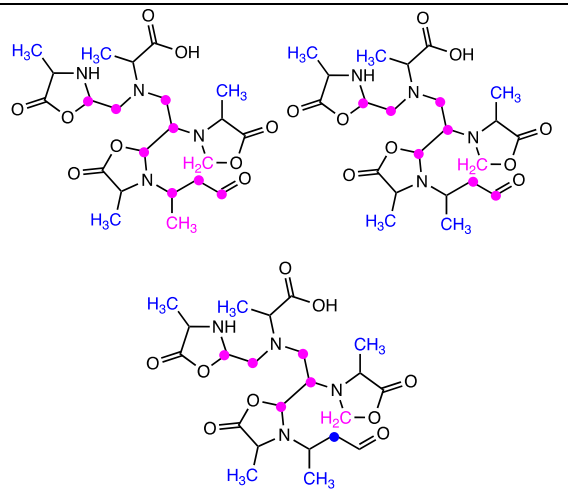	L
140	499	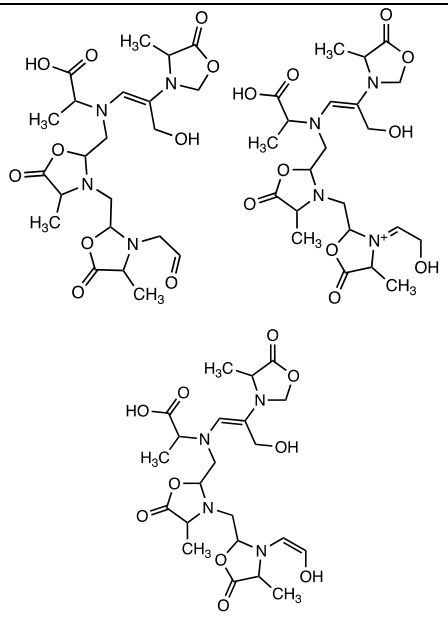	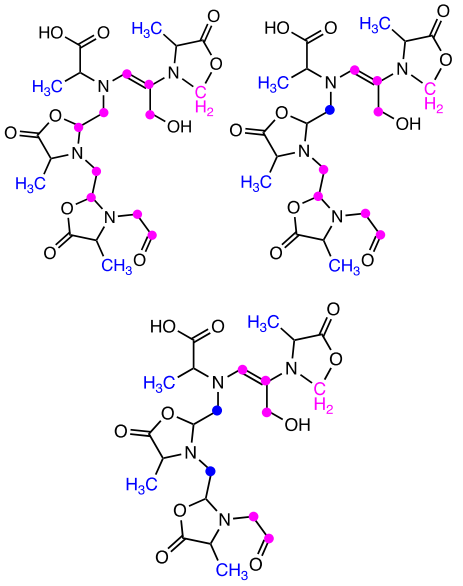	L

141	$C_{21}H_{32}N_4NaO_9$	507	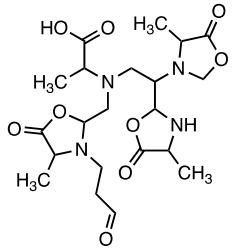	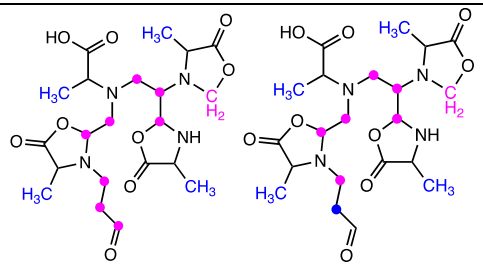	J
142	$C_{21}H_{32}N_4NaO_9$	507	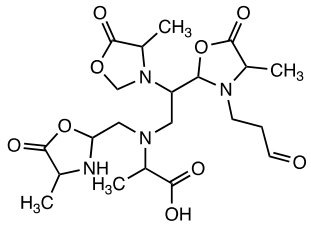	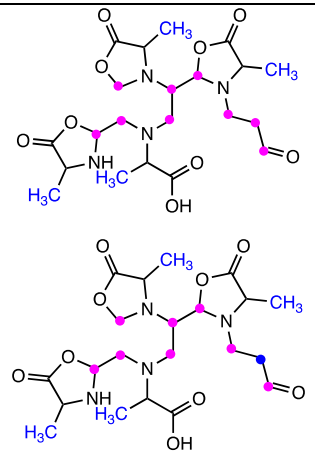	L
143	$C_{22}H_{35}N_4O_{10}$	515	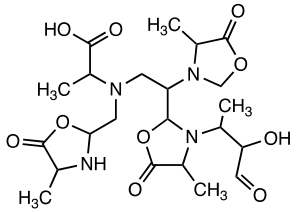	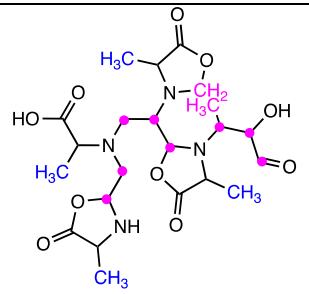	J

144	$C_{22}H_{35}N_4O_{10}$	515	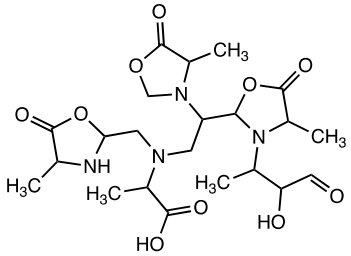	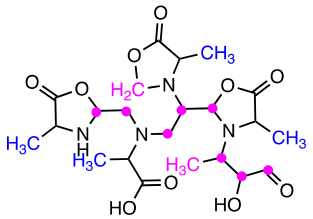	L
145	$C_{21}H_{33}N_4O_{10}$	515	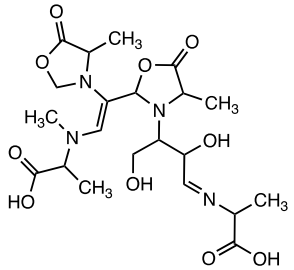 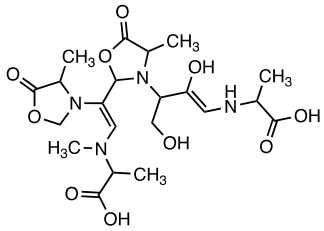 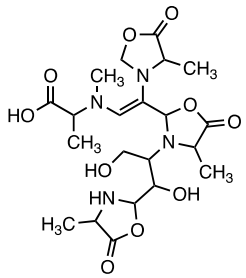	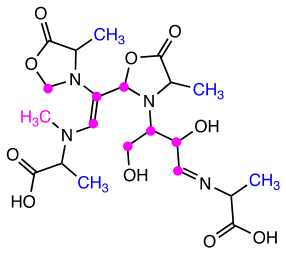 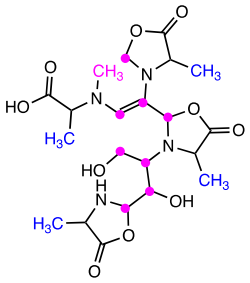	B

146	$C_{21}H_{33}N_4O_{10}$	515	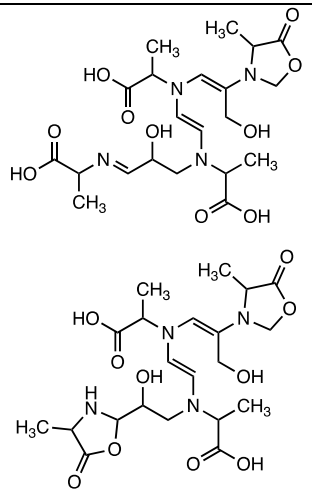	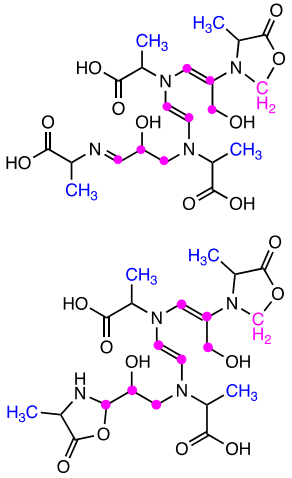	G
147	$C_{21}H_{33}N_4O_{10}$	515	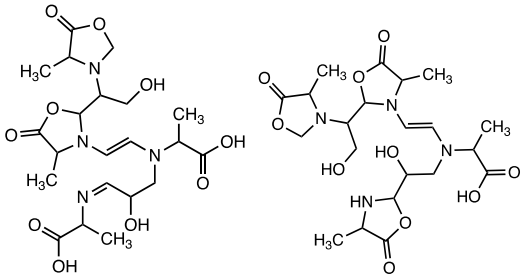	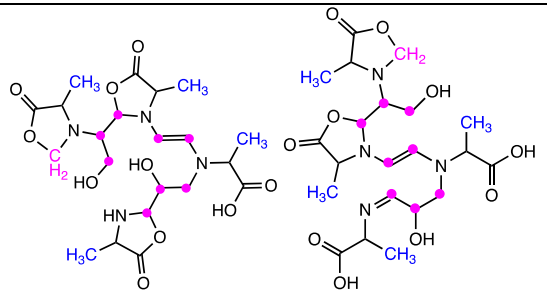	H
148	$C_{21}H_{33}N_4O_{10}$	515	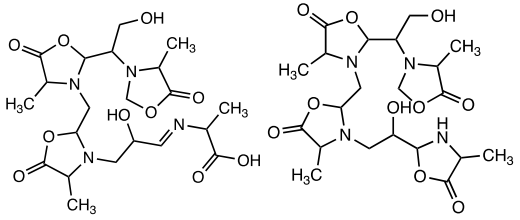	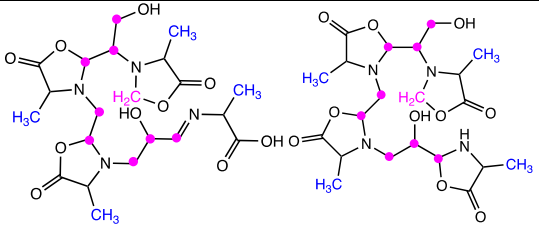	H

149	$C_{21}H_{33}N_4O_{10}$	515	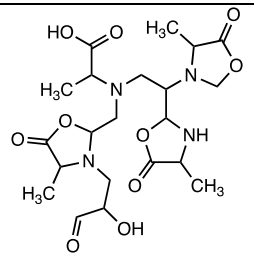	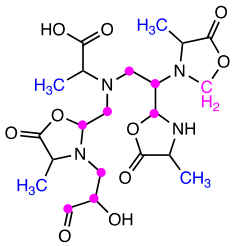	J
150	$C_{21}H_{33}N_4O_{10}$	515	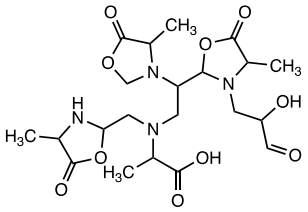	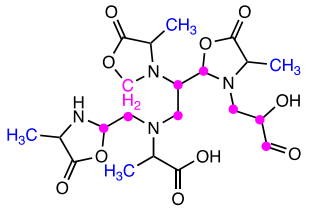	L
151	$C_{21}H_{33}N_4O_{10}$	515	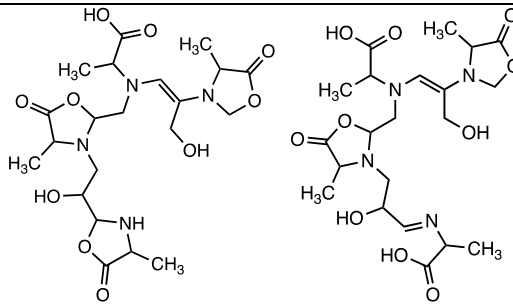	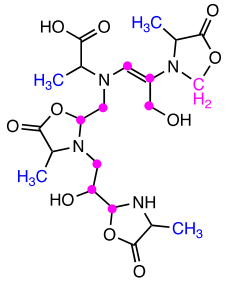	L

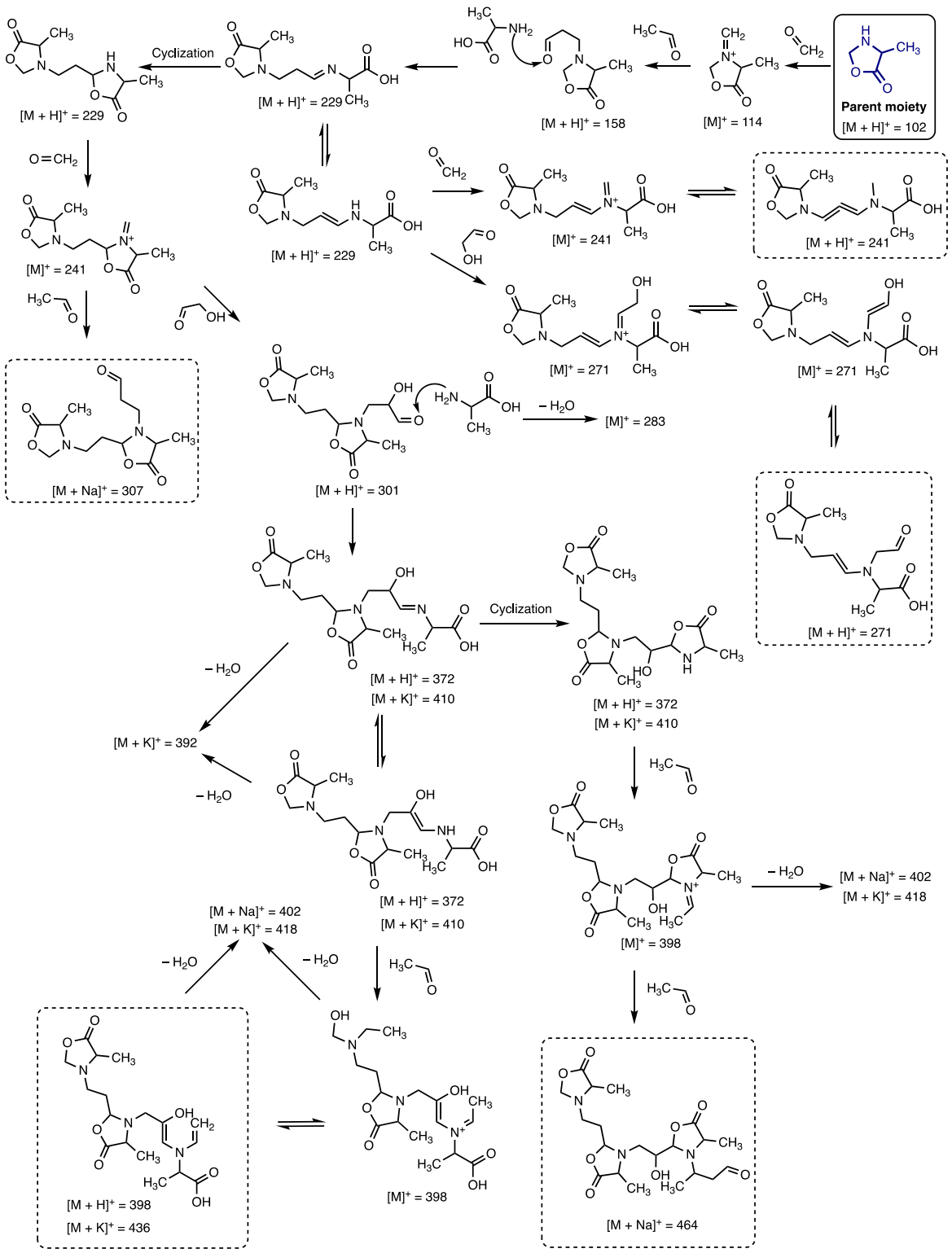

Figure S8.1. Proposed formation and reactions of oxazolidin-5-one oligomers via **pathway A** in Ala/Glu/$FeCl_2$

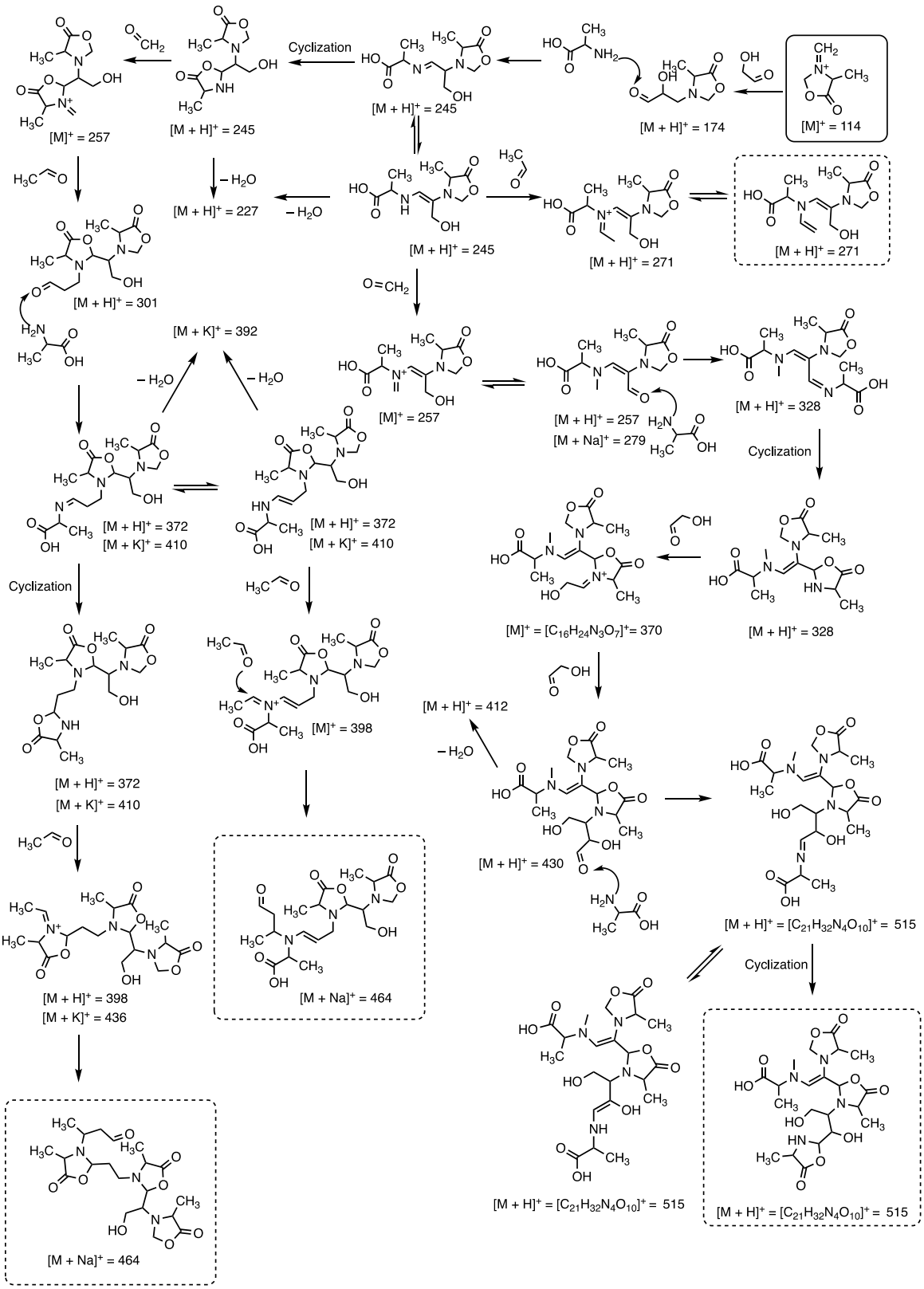

Figure S8.2. Proposed formation and reactions of oxazolidin-5-one oligomers via **pathway B** in Ala/Glu/$FeCl_2$

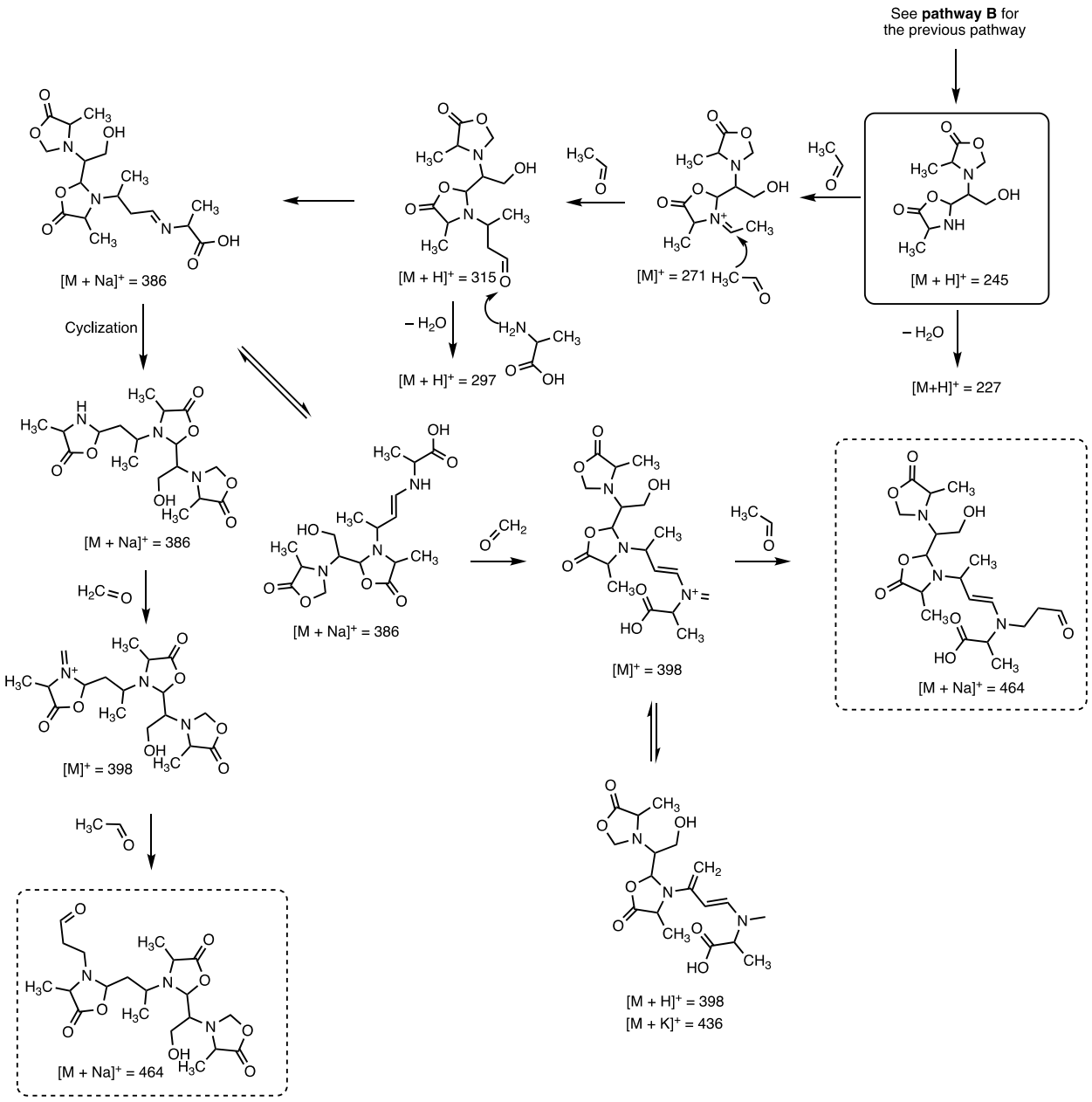

Figure S8.3. Proposed formation and reactions of oxazolidin-5-one oligomers via **pathway C** in Ala/Glu/$FeCl_2$

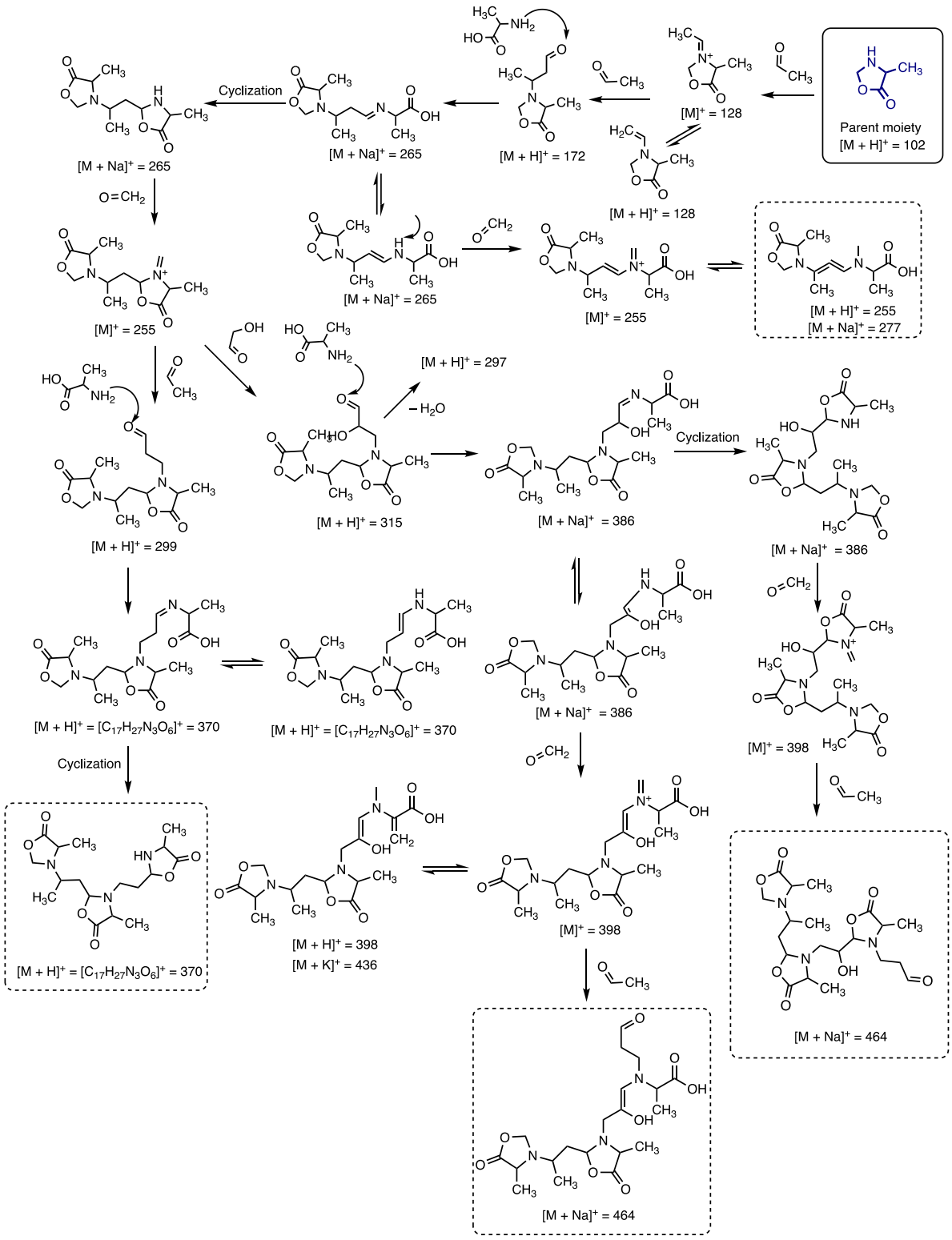

Figure S8.4. Proposed formation and reactions of oxazolidin-5-one oligomers via **pathway D** in Ala/Glu/$FeCl_2$

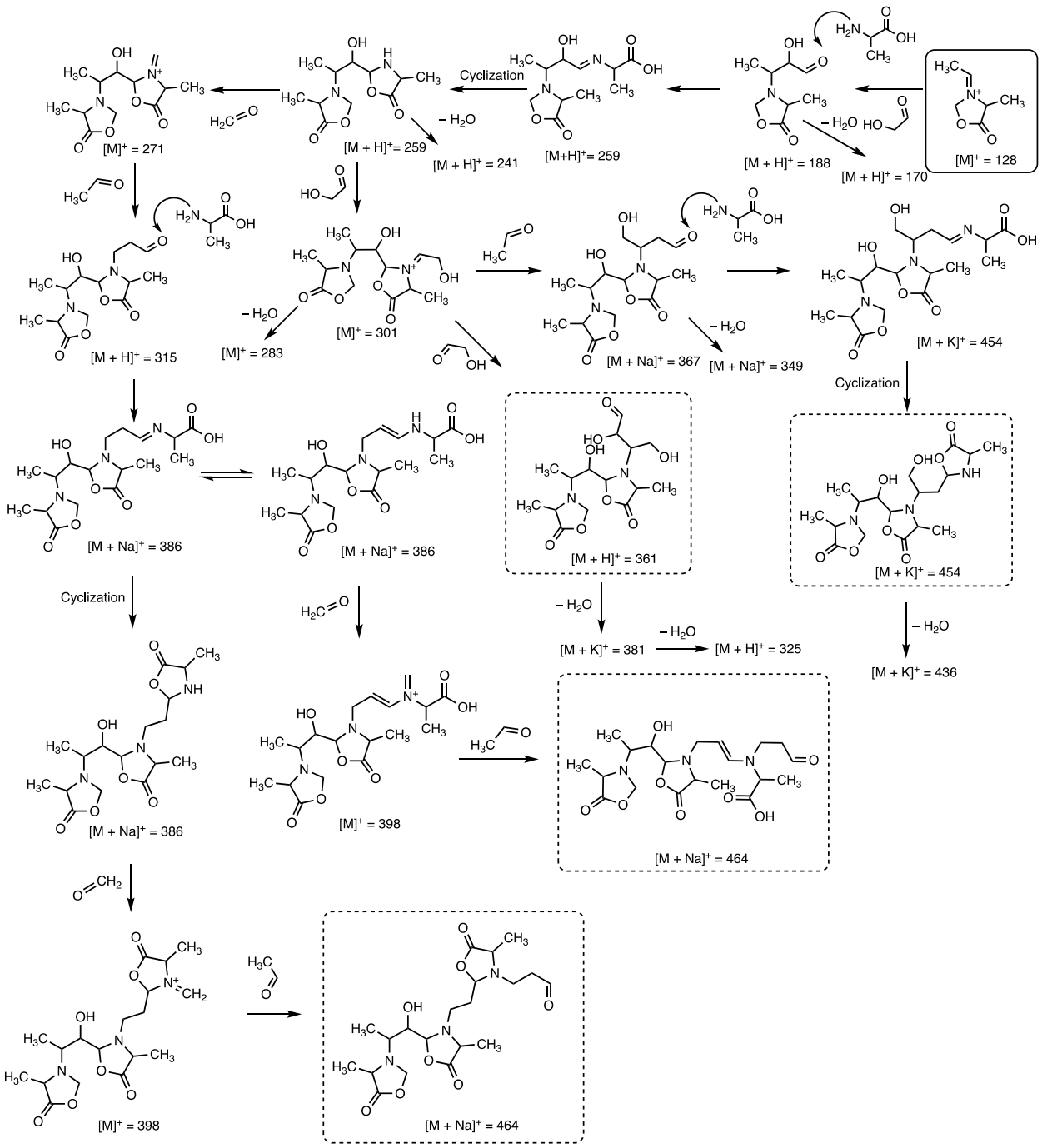

Figure S8.5. Proposed formation and reactions of oxazolidin-5-one oligomers via **pathway E** in Ala/Glu/$FeCl_2$

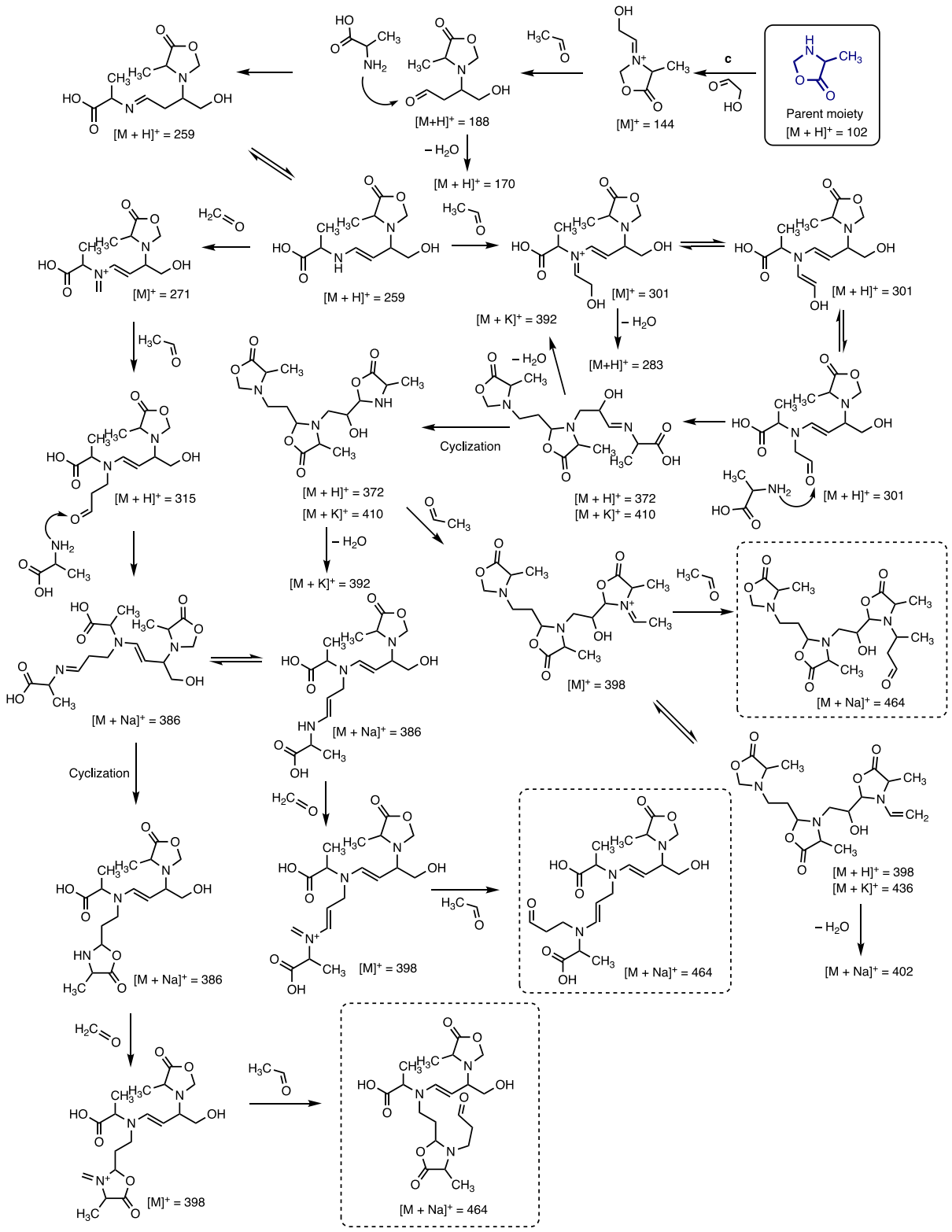

Figure S8.6. Proposed formation and reactions of oxazolidin-5-one oligomers via **pathway F** in Ala/Glu/$FeCl_2$

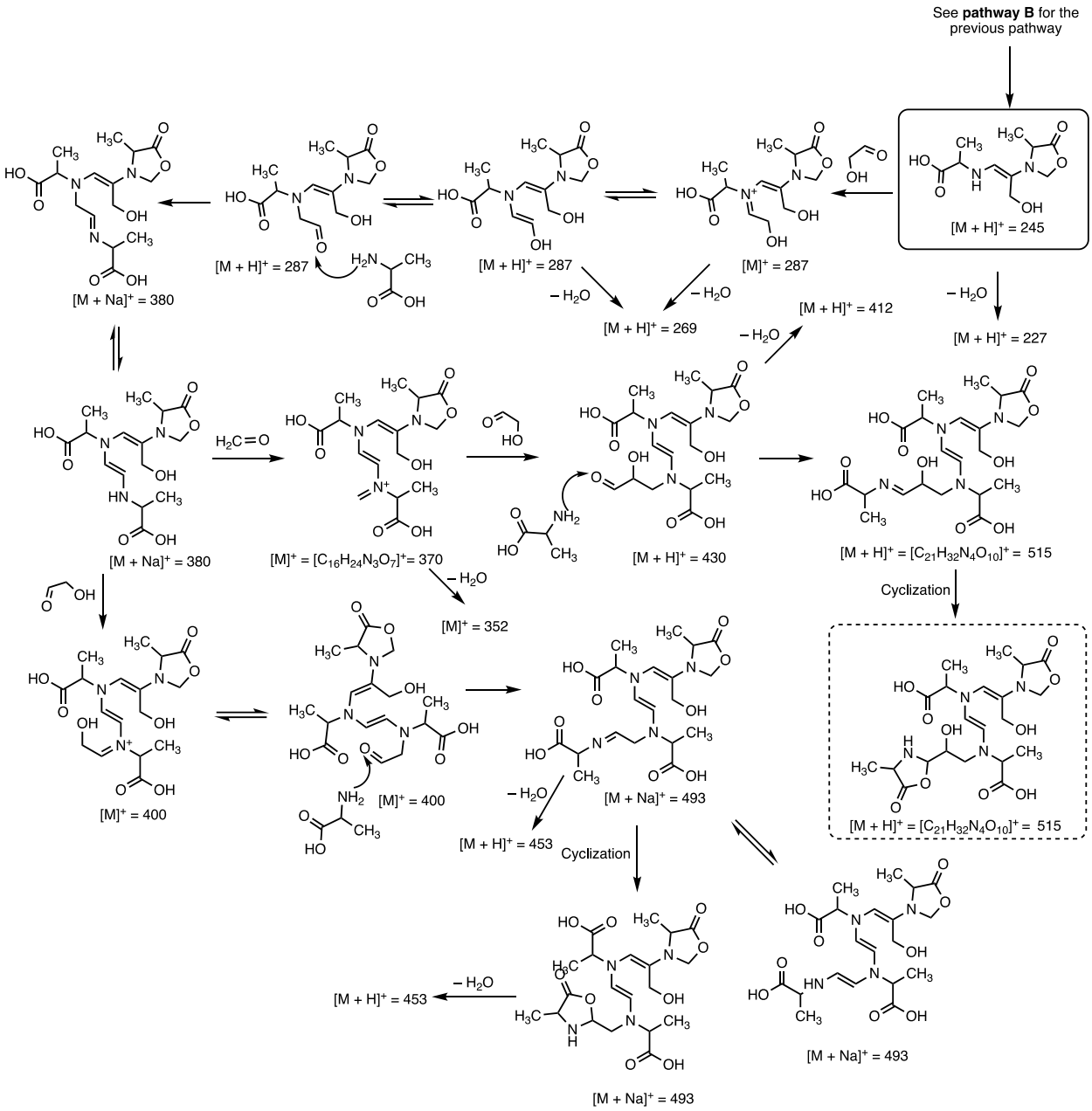

Figure S8.7. Proposed formation and reactions of oxazolidin-5-one oligomers via **pathway G** in Ala/Glu/$FeCl_2$

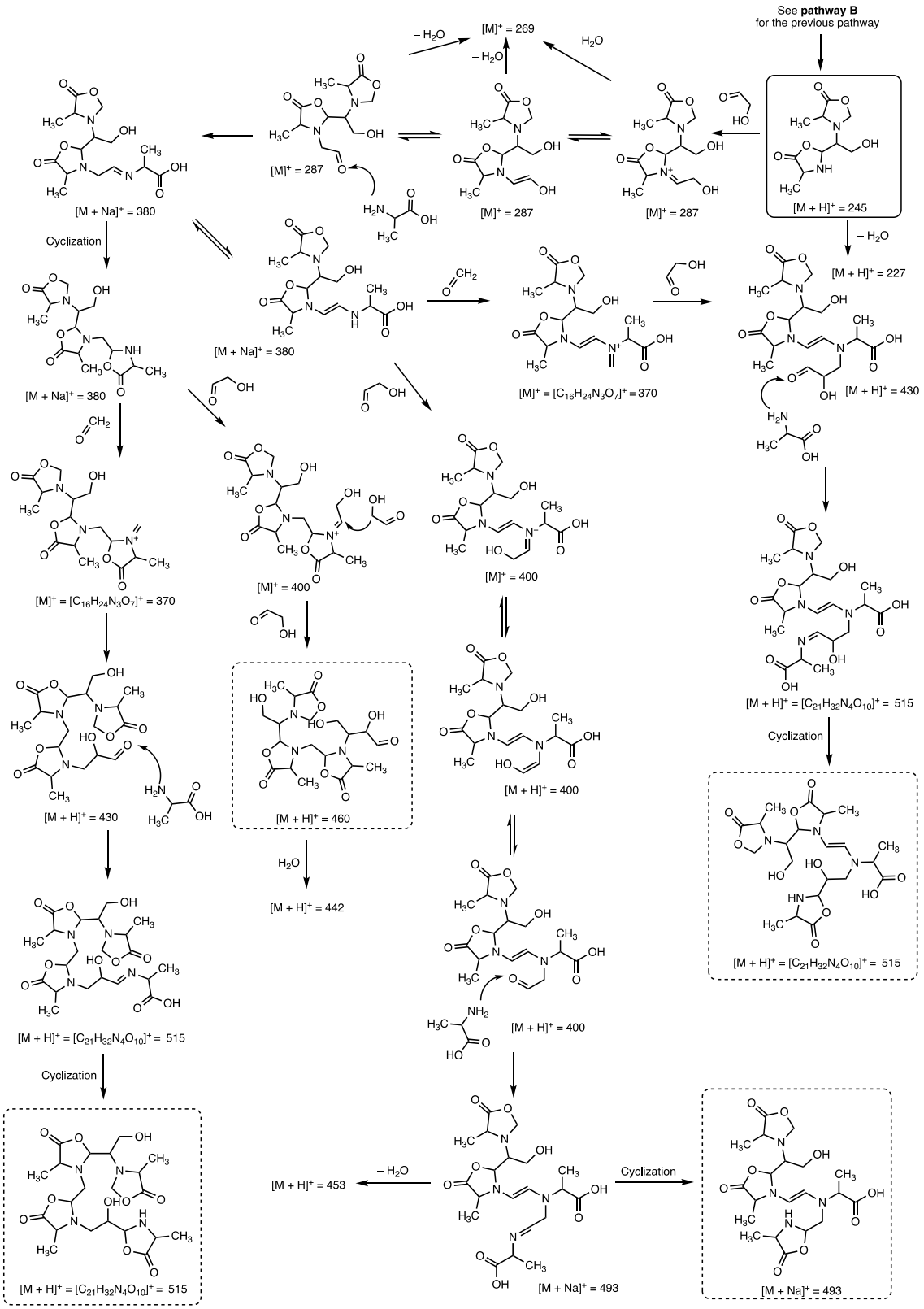

Figure S8.8. Proposed formation and reactions of oxazolidin-5-one oligomers via **pathway H** in Ala/Glu/$FeCl_2$

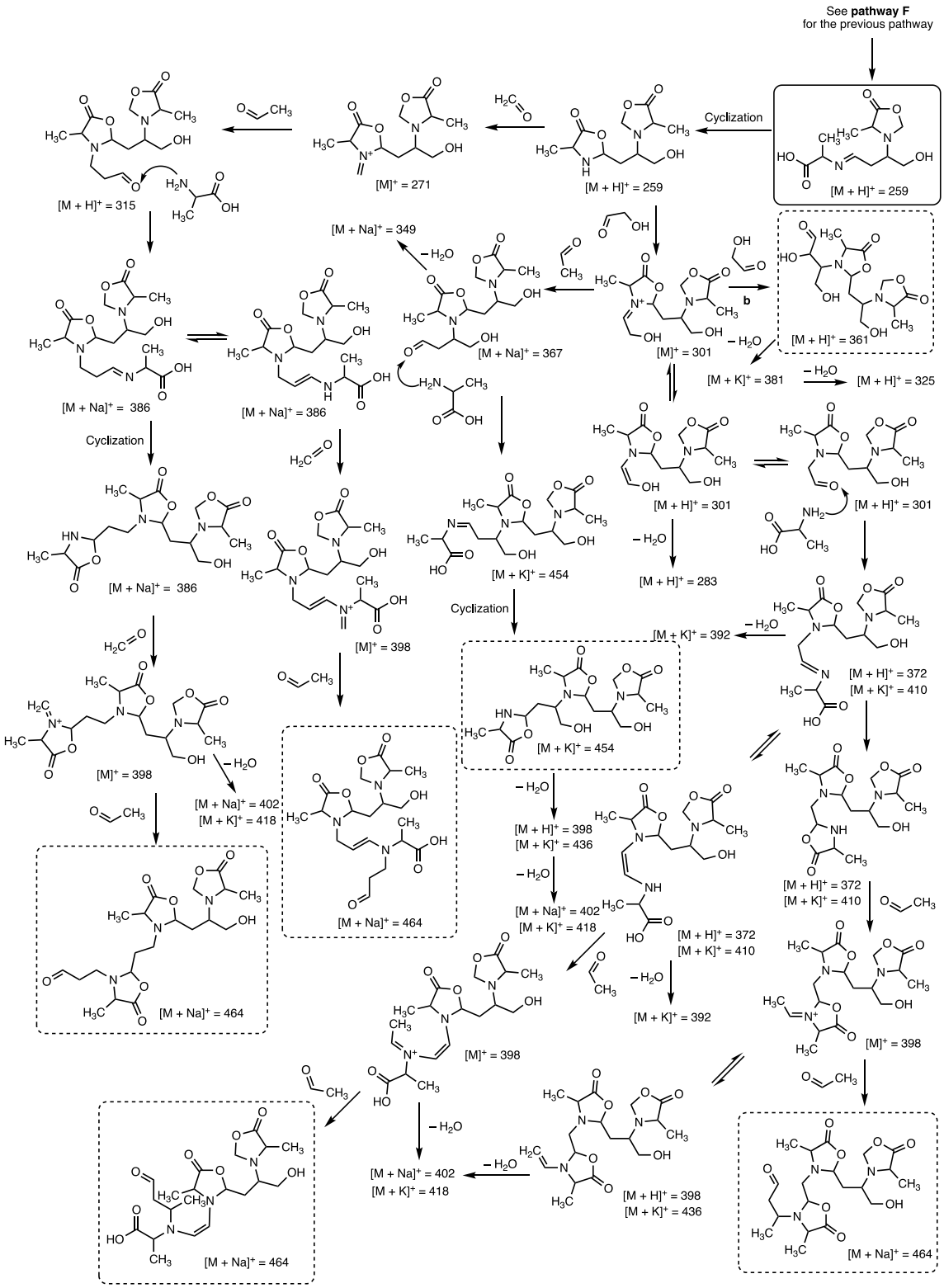

Figure S8.9. Proposed formation and reactions of oxazolidin-5-one oligomers via **pathway I** in Ala/Glu/$FeCl_2$

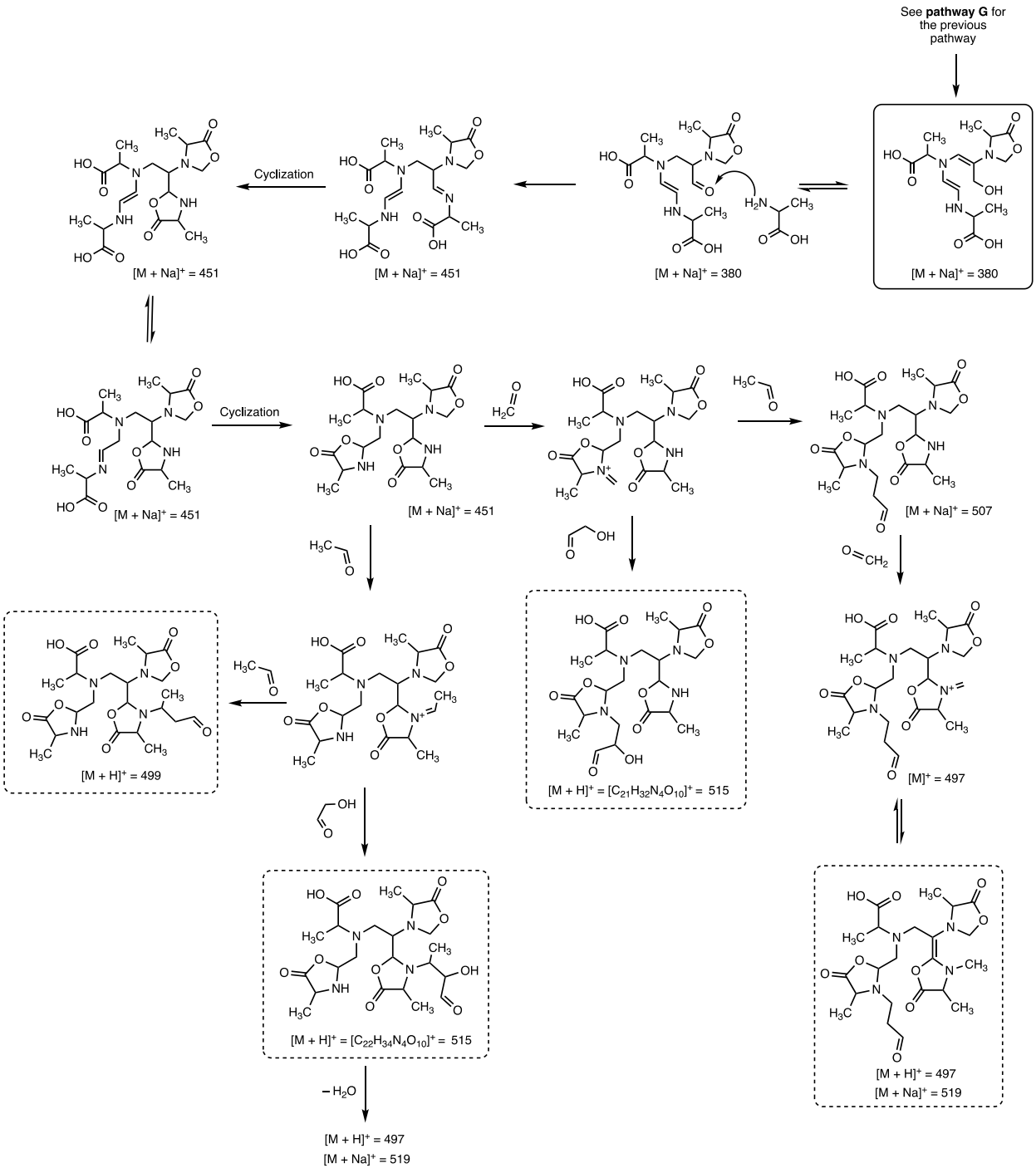

Figure S8.10. Proposed formation and reactions of oxazolidin-5-one oligomers via **pathway J** in Ala/Glu/$FeCl_2$

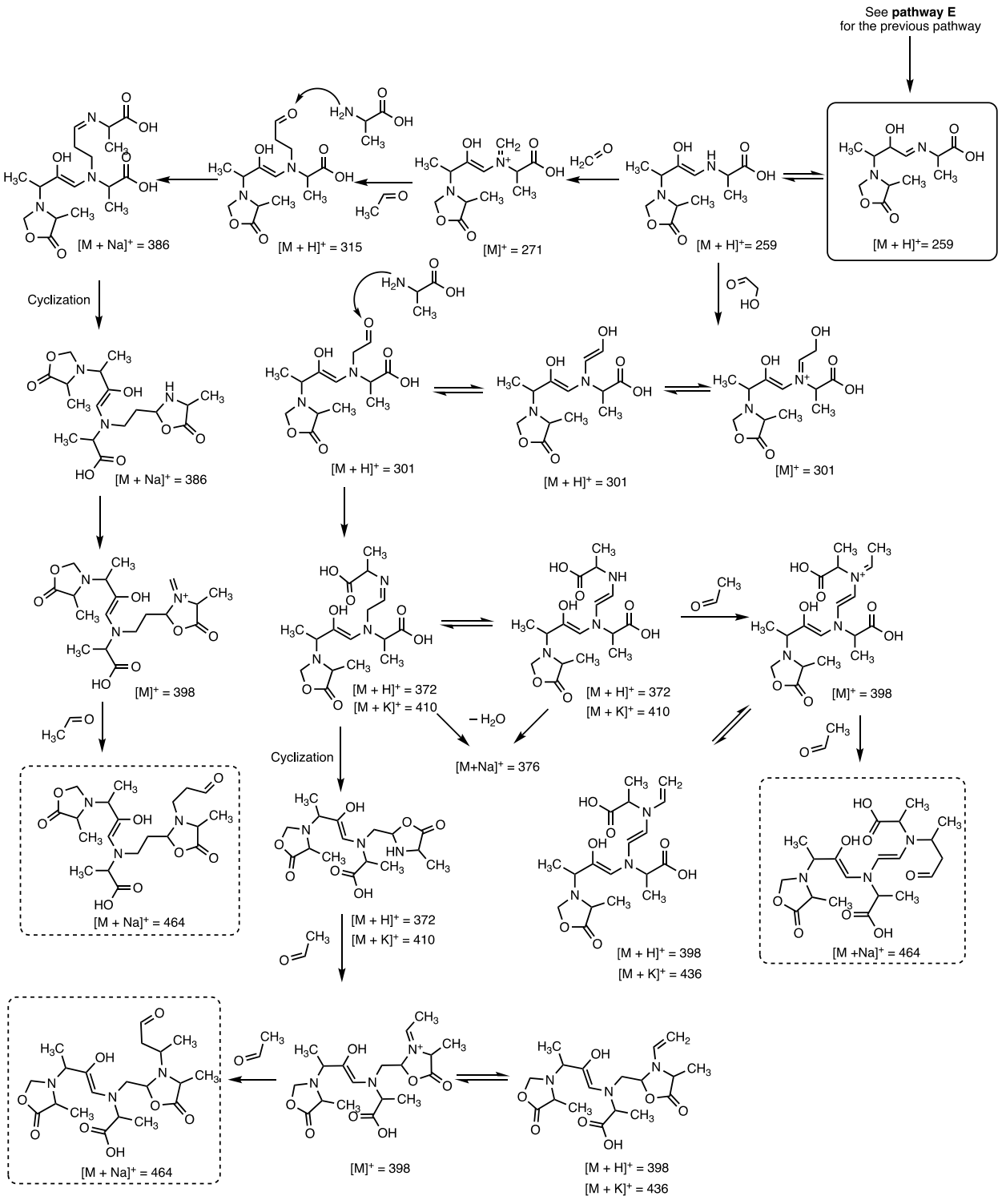

Figure S8.11. Proposed formation and reactions of oxazolidin-5-one oligomers via **pathway K** in Ala/Glu/$FeCl_2$

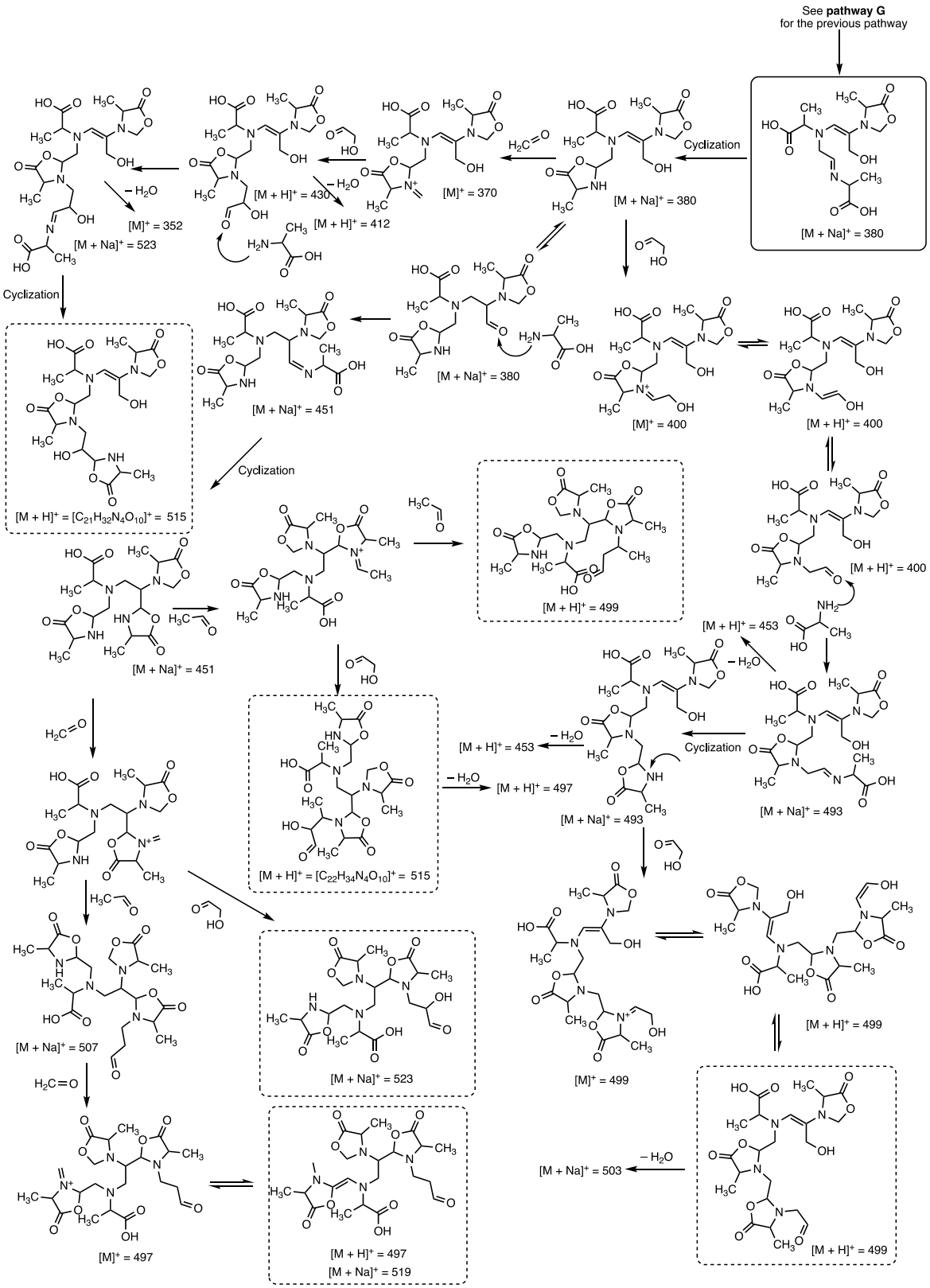

Figure S8.12. Proposed formation and reactions of oxazolidin-5-one oligomers via **pathway L** in Ala/Glu/$FeCl_2$

CHAPTER 9

GENERAL CONCLUSIONS, CONTRIBUTION TO KNOWLEDGE, AND FUTURE RESEARCH RECOMMENDATIONS

9.1. GENERAL CONCLUSIONS

In general, metal ions are used in the Maillard reaction as both reactants and catalysts. In this thesis, the role of divalent iron as an analytical reagent and a reactant was explored in model systems composed of alanine and glucose in the presence or absence of $FeCl_2$ heated for 2 h at 110 °C. This study demonstrated, for the first time, that the detection of reactive sugar degradation and Maillard reaction products can be facilitated through their complexation with metal ions in conjunction with ESI/qTOF/MS analysis. Furthermore, the unstable and reactive intermediates in the reaction mixtures were stabilized through such complexation reactions and easily detected by mass spectrometry. Various reactive sugar degradation products, considered critical precursors of flavour and browning compounds and toxicants, were conveniently profiled through complexation with divalent metal ions and ESI/qTOF/MS analysis. Many reactive sugar degradation products, acting as bidentate ligands, were converted into their stable metal complexes and subsequently detected by ESI/qTOF/MS in the positive ionization mode. Furthermore, this convenient analytical tool allowed the simultaneous detection of many critical, labile, and reactive Maillard reaction intermediates, particularly Amadori intermediates and Schiff bases. The initially formed *bis*(alaninato)iron(II) complexes were found to act as molecular scaffolds for the generation of *N*,*N*-diglycated alanine derivatives in the presence of glucose via the dissociation of *bis*[*N,N'*-diglycated alanine]iron(II) complexes. *N*,*N*-diglycated alanine derivatives are considered to be more reactive than monoglycated amino acids (Amadori products). Therefore, they may be responsible for the observed accelerating effect of the metal ions on the Maillard reaction. Furthermore, reactive *N*,*N*-diglycated alanine derivatives formed specific degradation products, such as 4*H*-1,4-oxazines, dihydro-1,4, or tetrahydropyrazines, through further reactions such as intramolecular cyclization under thermal conditions (110 °C for 2 h). On the other hand, Schiff bases are the initial interaction products of amino acids with carbonyl compounds that are very difficult to analyze due to their ease of hydrolysis. However, they can be stabilized by undergoing Amadori rearrangement or, as was demonstrated in this thesis, through complexation with metal ions and intramolecular cyclization of the carboxylate anion with the carbon atom of the imine to form more stable cyclic isomers, the oxazolidin-5-ones. Unlike oxazolidin-5-ones, Schiff bases cannot be easily detected owing to their facile conversion into Amadori products, especially under acidic pH conditions. The metal ion complexation of Schiff bases enhances their stability, increasing their half-life and allowing the formation of more oxazolidin-5-ones. One of

the critical findings of this thesis is the elucidation of the role of these intermediates as molecular scaffolds for the generation of complex oligomeric structures through the interaction of their amino groups with other reactive aldehydes generating corresponding iminium ion derivatives. These derivatives can serve as branching points for the formation of more complex oligomeric structures. Divalent metal ions, therefore, enhance the detection of reactive intermediates and promote polymerization reactions.

9.2. CONTRIBUTIONS TO KNOWLEDGE

The following novel finding was demonstrated in this thesis:

1. A convenient analytical tool, in combination with ESI/qTOF/MS/MS, was developed to profile reactive sugar degradation products in the presence of a divalent iron via complexation with sugar degradation products from both Maillard reaction model systems and food.

2. The above analytical tool was also applied for the analysis of Maillard reaction intermediates or products using previously unexplored divalent iron complexes in their various ionic forms, such as $[M + H]^+$, $[M + Cl]^+$, $[M + H + Cl_2]^+$, $[M + Na]^+$, $[M + 2Na]^{2+}$, $[M + 2K]^{2+}$, $[M + 2H + Cl_2]^{2+}$, $[M + Cl_2 + Na + K]^{2+}$, $[M + Cl_2 + 2K]^{2+}$, $[M + Cl_2 + 2Na]^{2+}$, $[M + Cl + K]^{2+}$, $[M + H + Cl_2 + Na]^{2+}$, and $[M + H + Cl_2 + K]^{2+}$.

3. The finding that *bis*[*N,N′*-diglycated alanine]iron(II) complexes can form in the presence of $FeCl_2$ and degrade upon heating, thereby releasing *N,N*-diglycated alanine derivatives as reactive precursors for aroma and browning, is reported for the first time in this study.

4. The identification of degradation products of *bis*[*N,N′*-diglycated alanine]iron(II) complexes, such as 1,4-oxazine from *N,N*-diglycated alanine derivatives or *N*-substituted Amadori products, under the condition of the Maillard reaction was demonstrated

5. The reactive Schiff bases can be detected as cyclic oxazolidin-5-ones was demonstrated for the first time.

6. A detailed mechanistic pathway for the oligomerization of oxazolidin-5-ones to form dimeric, trimeric and higher order oligomers was proposed for the first time.

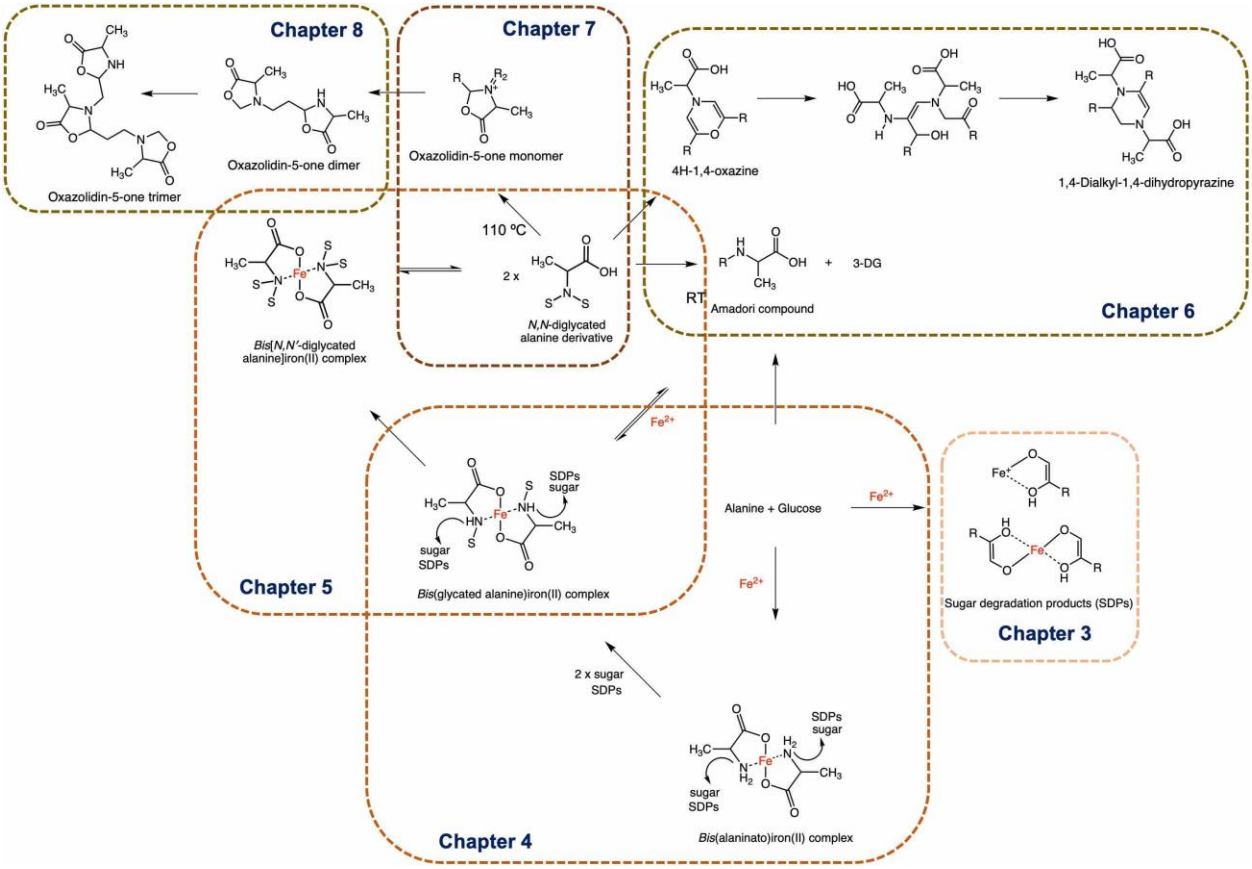

Chapter 1: Introduction

Chapter 2: Literature Review

Figure 9.1. Summary of the Maillard reaction intermediates and products in the presence of divalent iron ($FeCl_2$)

9.3. FUTURE RESEARCH

The significant discoveries in this study based on specific reactants have provided a foundation for future research on the potential effects and applications of various divalent metal ions in the Maillard reaction. Future research directions include:

1. Further investigation of the role of divalent with disaccharides and polysaccharides.

2. The exploration of the Maillard reaction chemistry of divalent metal under other reaction conditions, such as sonication, microwaves, or high-pressure processing.

3. Evaluation of the role of trivalent iron, which can also be complexed with other Maillard reaction intermediates and products, on the chemistry of the Maillard reaction.

4. Assessment of the role of other food components that can complex with metal ions, such as fatty acids, phenolics or vitamins.

5. An exploration of the role of divalent iron in the formation of characteristic flavour of cooked liver.

6. Investigation of the role of various binary complexes of Maillard reaction intermediates or products with other metals, such as Zn^{2+}, Cd^{2+}, Ca^{2+}, or Mg^{2+}.

7. Evaluation of the synergistic behaviour of a selected mixture of metal ions with specific amino acids and sugars under Millard reaction conditions.